Sarat Chandra Tripathy
Arvind Singh *Editors*

Dynamics of Planktonic Primary Productivity in the Indian Ocean

Springer

Dynamics of Planktonic Primary Productivity in the Indian Ocean

Sarat Chandra Tripathy • Arvind Singh
Editors

Dynamics of Planktonic Primary Productivity in the Indian Ocean

Springer

Editors
Sarat Chandra Tripathy
Ocean Sciences Group
National Centre for Polar and Ocean Research (NCPOR)
Ministry of Earth Sciences
Goa, India

Arvind Singh
Geosciences Division
Physical Research Laboratory (PRL)
Ahmedabad, Gujarat, India

ISBN 978-3-031-34466-4 ISBN 978-3-031-34467-1 (eBook)
https://doi.org/10.1007/978-3-031-34467-1

This Springer imprint is published by the registered company Springer Nature Switzerland AG
The registered company address is: Gewerbestrasse 11, 6330 Cham, Switzerland

Paper in this product is recyclable.

In loving memory of

Dr. Trevor Platt, FRS (12 August 1942–6 April 2020) *was a biological oceanographer who was distinguished for his fundamental contributions to quantifying primary production by phytoplankton at various scales of space and time in the ocean. He is well known for his mathematical formulation of the relationship between photosynthesis and light for phytoplankton (P–I curve). He was a fatherly figure to many scientists in the developing world through his long association with the Partnership for Observation of the Global Ocean (POGO) as its Executive Director from 2008 to 2015.*

Dr. Satya Prakash (22 September 1979–22 July 2021) *was a well-known marine scientist and a good friend. He obtained his master's degree in Applied Geology from the Indian Institute of Technology (Rorkee) and earned a Ph.D. from the Physical Research Laboratory, Ahmedabad. He was the coordinator of the Joint Project Office (JPO)–India for the Second International Indian Ocean Expedition (IIOE-2). His area of research includes biogeochemistry of the Arabian Sea and Southern Ocean using isotopes. Satya was one of the pioneers in the deployment and validation of new-generation Argo-floats with biogeochemical sensors in the Indian Ocean. He was instrumental in strengthening observational oceanographic facilities in the Indian coastal waters.*

Foreword

The Indian Ocean is unique as compared to the Atlantic and Pacific Oceans. It is characterized by highly dynamic seasonally reversing winds resulting in unique circulation and making it one of the most important regions in the world. It has been reported that the Indian Ocean is warming rapidly, in fact more rapidly than other ocean basins, but the impact of this warming is not quantified.

Despite being dynamically unique basin, the Indian Ocean still remains one of the least explored and understood ocean compared to the other major ocean basins. Some of the major expeditions such as IIOE, INDEX, JGOFS and subsequent programmes have provided valuable insights into the physical biological interactions in the Indian Ocean. Still there are knowledge gaps that needs to be filled particularly during the present era where the Indian Ocean is warming faster than the other oceans, and its impact in terms of severe cyclones, intensification of coastal and open ocean hypoxic zones and changing phytoplankton community structures probably fuelled by alteration in the nutrient stoichiometry, both the local and regional scales, needs to re-evaluated with modern tools and techniques.

Understanding the variability in phytoplankton productivity is undoubtedly one of the foremost research problems in modern oceanography. This book presents several case studies on these aspects covering a wide range of coastal/oceanic environment. The fishery, which provides livelihood to millions of people living along the coast of the Indian Ocean, is closely linked to the biogeochemical processes of the basin through its manifestation via primary and secondary productivity. Any decline, either on the local scale or on the basin scale, primary productivity will have a huge impact on the fisheries production and hence on the coastal population.

The present edited volume, titled *Dynamics of Planktonic Primary Productivity in the Indian Ocean*, comprises research carried out on phytoplankton productivity and related aspects in the Indian Oceanic region. I am sure the book will be valuable to researchers and students, who are interested in carbon dynamics in this region. Not limiting, the case studies discussed in this book would certainly provide a baseline information about phytoplankton biomass, species diversity and carbon fixation

vis-à-vis the ongoing and future climate change scenario and fisheries potential, thus would be of interest to personnel from fisheries sector, ocean managers and stakeholders who are committed to develop ways for making oceanic ecosystems sustainable.

Secretary, Ministry of Earth Sciences, Government of India, New Delhi, India M. Ravichandran

Preface

In the era of climate change, when the Indian Ocean is warming faster than other oceans, it was imperative to bring out our present understanding of this region. This also coincides with the extension of SCOR's second international Indian Ocean Expedition (IIOE-2) and the UN's decade of ocean program. There could not have been a better time to bring out this book.

Approximately one-third of humanity lives in the Indian Ocean rim countries, many of whom rely on fisheries and rain-fed agriculture and are thus most vulnerable to climate variability and extremes. Over the last two decades, the Indian Ocean alone has absorbed about a quarter of the global oceanic heat uptake, and the fate of this heat and its impact on future ocean changes is unknown. Climate models predict faster sea-level rise, more extreme monsoon rainfall, expansion of oxygen minimum zones, and decreased oceanic productivity.

The Indian Ocean remains to be least studied – partly because this region is surrounded by developing and under-developing nations. There, however, has been a great advancement in knowledge in the last couple of decades. With the advancement of the Indian Ocean Observing System (IndOOS) and its five networks, namely Research Moored Array for African-Asian-Australian Monsoon Analysis and Prediction (RAMA), Profiling floats (part of the global Argo array), Surface drifters (Global Drifter Program, GDP), Repeat temperature lines (eXpendable Bathy Thermograph (XBT) network), and tide gauges we now have a fairly good understanding about several physical and biogeochemical parameters.

Each oceanic region has different significance in influencing the global climate with their potential for drawing down atmospheric CO_2, which is the main driver of global warming. Geologically, oceanic primary productivity (PP) plays a significant role in drawing down atmospheric CO_2 and transports it to the ocean interior through 'biological pump', but its role in present climate change is not known. Thus, it is imperative to have a clear understanding of controlling mechanism(s) responsible for the PP variability in the various oceanic realms. Due to the ongoing climate change, the study of PP in relation to biogeochemical aspects in the oceanic ecosystems has

emerged as one of the foremost research problems in which the scientific fraternity across the globe is increasingly showing interest. In this context, understanding and consolidating the driving mechanisms of PP variability in diverse oceanic ecosystems has received substantial attention. The present book aims to facilitate a holistic overview of the research works carried out in this field in various oceanic realms such as Indian coastal and oceanic waters (estuaries, coastal waters, Bay of Bengal, Arabian Sea, Indian Ocean). Basically, this book attempts to compile the recent findings of Indian researchers in the field of phytoplankton productivity under one umbrella, highlights the gap areas, and suggests future research directions in this very important aspect of oceanographic research. The book contains 14 chapters that are summarized as below.

Estuaries are among the highly productive coastal ecosystems and are considered biogeochemical hotspots. In Chap. 1, Singh et al. (XIM University, Bhubaneswar) review the phytoplankton primary production in relation to environmental forcing in the Indian estuaries. Subsequently, Chap. 2 by Das and Chanda (Jadavpur University, Kolkata) compiles the knowledge gained, so far, on the phytoplankton dynamics and primary productivity in the estuarine regions and highlights the forcings that influences phytoplankton productivity in this region. In Chap. 3, Mohanty et al. (IGCAR, Kalpakkam) discuss the seasonal and interannual variations in coastal primary productivity in terms of particulate organic carbon (POC) and chlorophyll-a from Kalpakkam coast, Bay of Bengal.

Investigations on the phytoplankton productivity characteristics in the equatorial Indian Ocean (EIO) are a few, although the phytoplankton community here is diverse, and it is hypothesized that they are the principal autotrophs sustaining the possible and moderate secondary and tertiary production despite the daily low primary production. In Chap. 4, Jane Bhaskar (NCPOR, Goa) describes the variation of phytoplankton assemblages and primary productivity characteristics in the EIO during two seasons. In Chap. 5, Mitra and Leles (Cardiff University, UK) give a revised interpretation of marine primary productivity in the Indian Ocean by emphasizing the role of mixoplankton. This chapter is the first of its kind in attempting to consider the implications of the mixoplankton paradigm on marine primary productivity and ecology in the Indian Ocean.

Biological and physical dynamics in the oceans are coupled, structuring how the plankton interact with the varying environment and other organisms. To explain the processes, Smitha and Hussain (CMLRE, Kochi) describe the biophysical control on the variability in the upper layer production pattern of the north-eastern Arabian Sea in Chap. 6. Whereas, Chap. 7 by Saxena and Singh (PRL, Ahmedabad) analyses the historical records of primary productivity (assessed using ^{13}C, ^{14}C, ^{15}N, and satellite-derived chlorophyll-a data) in the northern Indian Ocean and explains the primary production and its governing factors in the northern Indian Ocean.

The ecosystem models prove to be an incredible tool that can reinforce satellite and ship-based observations to explicate the dynamics of the marine system. The modelling studies on primary productivity that has been carried out on the northern

Indian Ocean have resulted in major advances in our understanding. In this backdrop, Chap. 8 by Chakraborty et al. (INCOIS, Hyderabad) describes primary productivity dynamics in the northern Indian Ocean from an ecosystem modeling perspective. With extended satellite datasets and improved Earth system models, Modi and Koll (IITM, Pune) found that the marine primary productivity in the tropical Indian Ocean, particularly the Arabian Sea and the coastal regions of Bay of Bengal, shows a significant declining trend during 1998–2019. Their findings on past trends and future projections of marine primary productivity in the tropical Indian Ocean are described in Chap. 9.

Chapter 10 focuses on understanding primary productivity in the Indian Ocean using bio-optics and remote-sensing. Tiwari and Kolluru (King Fahd University of Petroleum and Minerals, Saudi Arabia) have briefly discussed how productivity models utilize remote sensing-based optical parameters, the difficulties and constraints associated with it, and approaches to enhance the accuracies of the productivity models. In line with this, using satellite data, Raman and Nayak (SAC, Ahmedabad) generated euphotic zone primary production maps covering the broad continental shelf, slope, and open ocean waters of Arabian Sea and computed values were validated with in situ measured rates of primary production in Chap. 11. Chapter 12 by R. K. Sarangi (SAC, Ahmedabad) attempts to encompass both the Indian satellite sensors ocean colour monitor (OCM) and scatterometer data from a single space platform for the ocean colour applications in Indian water to assess ocean algal bloom and productivity in the south-eastern Bay of Bengal.

Chapter 13 by Thomas et al. (CUSAT, Kochi) discusses the status of marine harmful algal bloom (HAB) in the tropical oceans pertaining to Indian exclusive economic zone (EEZ), including its ecological and socioeconomic influences. It also attempts to depict major algal blooms and their repercussions on productivity patterns and marine trophic structure. Primary production forms the base of marine food chain and knowing the primary production and the quantitative transfer between trophic levels, the potential production of fish in an area both first stage carnivores (zooplankton eaters) and predators, can be estimated. Chapter 14, a case study by Kumar et al. (INCOIS, Hyderabad), describes phytoplankton, primary productivity, and fishery in the northern Indian Ocean.

There are some books that describe the general processes governing the oceanic primary productivity in the global ocean and/or any particular oceanic environment. Of course, many publications in peer-reviewed journals have highlighted the causal mechanism(s) of variability in primary productivity in the oceans. However, there is no document/book that summarizes the phytoplankton productivity in the different coastal and oceanic realms surrounding the Indian continent. Several research works on phytoplankton productivity have been carried out separately in various oceanic environments, where the controlling mechanisms are not the same. Thus, combining and presenting all the observed findings in one platform is a new perspective. We

hope this book will serve as a consolidated baseline information for the future researchers who would pursue planktonic primary productivity and biogeochemistry-related research in the above-mentioned marine ecosystems and other parts of the global oceans as well.

Ocean Sciences Group, National Centre for Polar and Ocean Research (NCPOR), Ministry of Earth Sciences Goa, India — Sarat Chandra Tripathy

Geosciences Division Physical Research Laboratory (PRL) Ahmedabad, Gujarat, India — Arvind Singh

Acknowledgements

The editors thank Dr. M. Ravichandran, Secretary Ministry of Earth Sciences, and Dr. Thamban Meloth, Director National Centre for Polar and Ocean Research (NCPOR), for their encouragement and support.

We thank Mr. Aaron Schiller, Associate Editor at Springer Nature, Mr. Herbert Moses, Production Editor (Books) at Springer Nature, and Ms. Qingxin Zhang, Editorial Associate at Springer Nature, for their persistent help, guidance and encouragement throughout this project.

Inspiration from the late Prof. Jayant Kumar Mishra (Pondicherry University, Andaman) is gracefully acknowledged. The editors extend their gratitude to all the authors of this edited volume for their high-quality contributions. Support from the resource personnel Dr. Satyanarayan Panigrahi (IGCAR, Kalpakkam), Dr. Grinson George (CMFRI, Kochi), Dr. P. Sabu, Dr. Parli V. Bhaskar, Dr. Prince Prakash and Dr. Sudarsanarao Pandi of NCPOR, Goa, Dr. Rajdeep Roy (NRSC, Hyderabad), Dr. Varunan Theenathayalan (IIT, Chennai), Dr. Kunal Chakraborty and Dr. Sanjiba Kumar Baliarsingh of INCOIS, Hyderabad, Dr. Sivaji Patra (NCCR, Chennai), Dr. Surya Prkash Tiwari (King Fahd University of Petroleum and Minerals, Saudi Arabia) and Dr. Biraja Kumar Sahu (NIO, Goa) in timely reviewing the book chapters and providing constructive comments and suggestions needs a special mention. The editors appreciate everyone who facilitated directly or indirectly in producing this edited volume.

Last but not least, the production of this edited volume has been a long journey, and SCT acknowledges the relentless motivation and love received from his spouse Santosini and son Tapodipta without which the timely completion of this project would have been an arduous task.

Sarat Chandra Tripathy
Arvind Singh

Contents

About the Editors

Sarat Chandra Tripathy is a biological oceanographer and has been working as a scientist with the ocean sciences group of the National Centre for Polar and Ocean Research (NCPOR), an autonomous institution under the aegis of the Ministry of Earth Sciences, Govt. of India since 2011. He holds a Ph.D. degree in Marine Sciences from Berhampur University and D.Sc. degree in Environmental Sciences from the Nagoya University, Japan. His research interests include phytoplankton productivity, bio-optics and biogeochemistry in the oceanic realms. He has more than 60 scientific publications in peer-reviewed journals of national and international repute. He is the national representative for SCAR-SSG Life Sciences and CLIVAR/CliC/SCAR Southern Ocean Region Panel (SORP), and co-chair of Southern Ocean Indian Sector (SOIS)-regional working group of the Southern Ocean Observing System (SOOS). He is review editor of the journal *Frontiers in Marine Science* and a life member of the Ocean Society of India (OSI).

Arvind Singh is a biogeochemist and has been working as a scientist with the Geosciences Division of Physical Research Laboratory (PRL), an autonomous institution under the aegis of the Department of Space, Govt. of India since 2015. His research interests include marine nitrogen cycle and the impact of ongoing global changes on the ocean biogeochemistry. He has more than 50 scientific publications in peer-reviewed journals of national and international repute. He is an editor at *JGR-Oceans*. He is also a steering committee member of SOLAS.

Chapter 1
A Review of Phytoplankton Primary Production in Relation to Environmental Forcing in Indian Estuaries

Sambit Singh, Tamoghna Acharyya, Susmita Raulo, Bikram P. Sudatta, Chinmaya Sahoo, Suchismita Srichandan, Sanjiba Kumar Baliarsingh, and Aneesh A. Lotliker

Abstract Estuaries are among the highly productive coastal ecosystems and are considered biogeochemical hotspots. In estuaries, phytoplankton are the important primary producers that support dynamic food web. This study reviews the variability of phytoplankton primary production (PPP) in Indian estuaries by comprehensively analyzing available literature to understand the patterns of productivity and its environmental control. Only two methods have been deployed to measure PPP in Indian estuaries; among them, the oxygen evolution method (19 out of 30 studies) was way more popular than the ^{14}C incubation method (11 out of 30 studies). PPP of west coast estuaries registered a wider range of values (4–11,934 mg C m^{-3} day^{-1}) compared to east coast estuaries (24–4272 mg C m^{-3} day^{-1}). Among the riverine estuaries (RE), lagoons, and backwater, the highest PPP values were recorded from Hooghly RE (4272 mg C m^{-3} day^{-1}), Muthupet lagoon (3656 mg C m^{-3} day^{-1}), and Cochin backwater (11,934 mg C m^{-3} day^{-1}), respectively. A striking seasonality in PPP can be seen in Indian estuaries in relation to monsoon – the water column productivity driven by phytoplankton reaches its maximum during the post-monsoon season (October–December) when residence time of water parcel, light

S. Singh
Centre for Marine Living Resources and Ecology (CMLRE), Ministry of Earth Sciences, Government of India, Kochi, India

Kerala University of Fisheries and Ocean Studies (KUFOS), Kochi, Kerala, India

T. Acharyya (✉) · S. Srichandan
Department of Marine Sciences, Berhampur University, Odisha, India

S. Raulo · S. K. Baliarsingh · A. A. Lotliker
Indian National Centre for Ocean Information Services, Ministry of Earth Sciences, Government of India, Hyderabad, India

B. P. Sudatta
Heriot-Watt University, Edinburgh, United Kingdom

C. Sahoo
CSIR-National Institute of Oceanography, Regional Centre, Mumbai, India

S. C. Tripathy, A. Singh (eds.), *Dynamics of Planktonic Primary Productivity in the Indian Ocean*, https://doi.org/10.1007/978-3-031-34467-1_1

penetration, and nutrient levels reach their optimum. This is the time window when dominantly heterotrophic Indian estuaries turn autotrophic. Alternatively, in the months of monsoon (July - September), high surface runoff of refractile terrestrial detritus fuels extremely high bacterial respiration and decomposition, resulting in high CO_2 partial pressure and air-water exchange in Indian estuaries. The PPP in Indian estuaries is controlled by the complex interplay of inorganic macronutrient stoichiometry at spatial-seasonal scale. However, a general lack of interest among the scientific communities can be seen when it comes to PPP-related investigation in Indian estuaries, as the SCOPUS database retrieved only 58 research paper records during 1965 to 2021. In the context of climate change, increased anthropogenetic pressure, and coastal developments, more intensive and regular study on estimating and understanding PPP in Indian estuaries is needed.

Keywords Primary production · Phytoplankton · River · Estuaries · Monsoon · Bay of Bengal · Arabian Sea

1 Introduction

Primary production is defined as the entrapment of chemical energy within a synthesized organic compound by the living organism. The organisms responsible for the primary production are primary producers, which constitute the base of all food webs. Like terrestrial plants on land, phytoplankton act as primary producers in aquatic ecosystems. Being the photoautotrophs, phytoplankton utilize solar radiation to convert inorganic to organic carbon and supply this organic carbon to diverse heterotrophs up in the food web (zooplankton, nekton, benthos).

Primary production is allocated into net primary production (NPP) and gross primary production (GPP). GPP is the amount of carbon fixed during photosynthesis by photoautotrophs, whereas NPP, the leftover carbon available to consumers after the energy loss, occurs during catabolism and maintenance, together called respiration (R). GPP and NPP are expressed in units of mass per unit area per unit time interval (e.g., g C m^{-2} $year^{-1}$). In the euphotic zone of the upper ocean, phytoplankton account for ~94% (~50 ± 28 Pg C $year^{-1}$) of NPP (Falkowksi et al., 2004).

Estuaries, lying at the transition zone between fresh water and the marine environment of the coastal region, are highly productive ecosystems. Constant exchange and processing of matter and energy aided by tidal flushing generate a strong physico-chemical gradient which keeps a diverse range of food webs in estuaries functional. Due to high primary production and niche diversification, estuaries support various biotas such as polychaetes, nematodes, protozoans, crabs, snails, and fish. It is estimated that more than 68% of commercial fish catch takes place in estuaries of the USA (NOAA, 2022).

Estuaries act as “biogeochemical reactors” as they receive and process massive inputs of terrestrial organic matter and nutrients before passing on to the adjacent coastal ocean. Organic matter in estuaries is sourced from three different origins: (1) terrestrial detrital organic matter: refractory in nature, having low nutritive value,

and is majorly decomposed by microbes; (2) macroalgae (seaweed) and vascular plants (seagrass): 80% of organic matter from them is decomposed or exported; and (3) microalgae: organic matter present in water column, and benthic phytoplankton, which is highly labile, high in essential nutrients and hence 90% of it is rapidly recycled (Cloern et al. 2014). Most estuaries are heterotrophic (transform organic matter into the inorganic form), as the total annual ecosystem respiration exceeds gross primary production; hence, estuaries act as sources of CO_2 to the atmosphere with the global estimated budget of 0.43 Pg C $year^{-1}$ (Borges, 2005) even though estuaries cover only a small percentage area of the planet. In heterotrophic estuaries, a small temporary window of autotrophy opens when inhabitant phytoplankton "bloom" responding to conducive conditions such as low flushing time, high water clarity, optimal availability of nutrients, and low grazing pressure. This resulting transient net autotrophy is marked by CO_2 drawdown, pH shift, O_2 oversaturation, and nutrient uptake followed by increased biomass of primary (zooplankton) and secondary consumers (fish) in estuaries (Boynton et al., 1982; Cloern 2001; Cloern and Jassby 2008; Cloern et al., 2014). As noted above, the labile and high nutritional value of phytoplankton drives energy transfer to the higher trophic levels, including commercial fish (Paczkowska et al., 2020). However, excessive phytoplankton production in estuaries comes at a cost, as evidenced by the global instances of eutrophication, hypoxia, or anoxia, the shift in the biotic community, and habitat loss of seagrass, increased uptake of pollutants and heavy metals. This chapter describes the pattern of PPP in Indian estuaries, emphasizing its spatial and temporal variabilities and the key regulatory mechanisms.

2 Indian Estuaries

India encompasses an extensive total coastline of ~7500 km, and estuaries cover about 27,000 square km of area (Das & Ghosh, 2021). There are 160 minor, 45 medium, and 14 major rivers present in the Indian subcontinent, and the combined length and catchment area of all rivers are 4.5×10^4 km and 3.12×10^6 km^2, respectively (Das & Ghosh, 2021). These rivers, before opening into the adjoining ocean [the Bay of Bengal on the east coast and the Arabian Sea on the west coast], form riverine estuaries (hereafter, RE) (Fig. 1.1). Indian estuaries are characterized by high runoff during the wet Indian summer monsoon (June–September) that eventually decreases with the successive seasons, leading to striking temporal changes in salinity and velocity (Vijith et al., 2009; Acharyya et al., 2021). Due to the prevailing Indian summer monsoon (ISM), salinity fields of Indian riverine estuaries never remain in a steady state, that is, salinity ingress through tide is not balanced by salinity egress through runoff (Vijith et al., 2009). Rather during ISM, some of the major riverine estuaries such as Mahanadi, Godavari, Krishna, and Cauvery turn into a rapid flowing freshwater system with no discernible vertical salinity gradient (Sridevi, 2013). Vijith et al. (2009) referred to such estuaries as "monsoonal estuaries," which are characterized by large total runoff and episodic

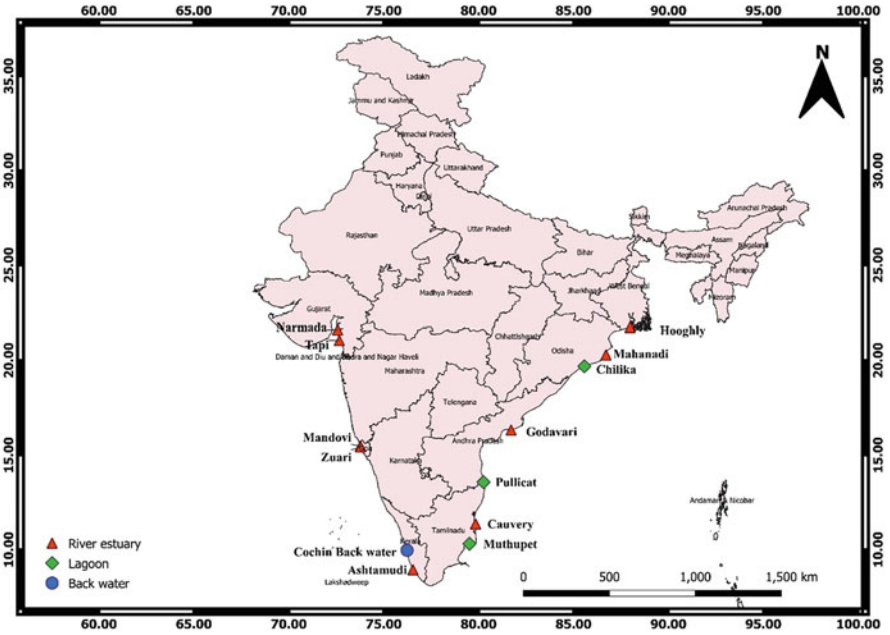

Fig. 1.1 Locations of different coastal ecosystems along the Indian coast. The triangles (red) represent the river estuaries, the diamond (green) represent coastal lagoons, and the blue (blue) represent the backwater

"highs and lulls" during the ISM. Apart from riverine estuaries, two other types of estuaries are found in India; they are coastal lagoons and backwater. Coastal lagoons are "shallow, nutrient-rich, turbulent, and light-attenuated" water bodies that run along a shoreline but remain separated from the ocean by sand bars/spits (Kjerfve 1994). On the east coast of India, some of the large and ecologically important lagoons, such as Chilika and Pullicat are situated (Singh et al., 2022). On the west coast, an extensive estuarine system of backwaters called the Cochin backwater system exists, which is known for its rich fisheries potential in the state of Kerala (Menon et al., 2000). The tidal pattern of most of the estuaries on the Indian east coast is semi-diurnal, and the west coast is a mixed type. A brief account of the estuaries both on the east coast and west coast is discussed in this chapter and detailed in Table 1.1.

Table 1.1 A detailed geographical information about the Indian estuaries along the east and west coast of India

Name of the estuary	State (east/west coast)	Latitude and longitude	Average discharge (m^3/s/day)	Area (km^2)	Coast length (km)	Type of estuary	Ecological importance	References
Hooghly estuary	West Bengal (*east coast*)	21°31″ N: 23° 30′ N-87° 45′ E:88° 45′ E		8029	295	Positive estuary Semi-diurnal type Tidal influence felt up to 290 km Coastal plain estuary Open estuary	Endowed with largest Mangroves Fishery and shrimp It forms words largest delta Sundarbans	Bulletin no. 130, CIFRI (2004)
Mahanadi estuary	Odisha (*east coast*)	20°20′19.43″ N: 20°17′ 35.20″ N-86°36′ 0.63″ E: 86°42′ 22.11″ E	2100	9	30–40	Positive estuary Semi-diurnal Tidal influence felt up to 42 km Open estuary	Mangroves Fishery Major port of India's major industries (PPL, ESSR, IFFCO, IOCL)	Acharyya et al. (2021)
Chilika lagoon	Odisha (*east coast*)	19°28′ N:19°54′ N-85° 05′ E: 85°38′ E		906–1165	64.3	Semi-diurnal Coastal lake	Largest brackish water lagoon in Asia Designated Ramsar site (in 1981) Wintering ground for migratory birds Aqua catch Dolphins, birds	Panigrahi et al. (2009)
Godavari estuary	Andhra Pradesh (*east coast*)	16°15′ N-82° 5′ E	3500	330		Semi-diurnal Tidal influence felt up to 45 to 48 km Open estuaries	Shrimp fishery Second largest area of mangroves Important nesting site for Olive Ridley turtle Important spawning ground for fin and shell fish	Bharathi et al. (2018a, b)

(continued)

Table 1.1 (continued)

Name of the estuary	State (east/west coast)	Latitude and longitude	Average discharge (m^3/s/day)	Area (km^2)	Coast length (km)	Type of estuary	Ecological importance	References
Pullicat lagoon	Tamilnadu (*east coast*)	13.33° N:13.66° N-80.23°E:80.25° E		250–450	60	Semi-diurnal Coastal lake Tidal effect is felt up to 6–10 km	Asia's second largest lagoon Mangroves Aqua culture Bird Sanctuary	Basuri et al. (2020) and Basha et al. (2012)
Cauvery estuary	Tamilnadu (*east coast*)	11°07′ N-79° 50′ E	600	800		Semi-diurnal	Main source of drinking water, irrigation, and electricity	Qasim (2003)
Muthupet estuary	Tamilnadu (*east coast*)	10.33° N-79.55° E		68		Semi-diurnal	Oyster Nursery ground for marine fishes	Gupta et al. (2006)
Cochin backwater	Kerala (*west coast*)	9° 40′ N: 10° 12′ N-76° 10′ E: 76° 30′E	634	250	113	Semi-diurnal Tidal influence felt up to 11 km	Fishery Supports well-established endemic fauna	Pranav et al. (2021) Madhu et al. (2007)
Ashtamudi estuary	Kerala (*west coast*)	8° 50′ N: 9° 5′ N-76° 30′ E: 76° 40′E	2410	51.2	16	Semi-diurnal	Designated Ramsar site Hosts many migratory birds	Saranya and Lancelet (2020)
Mandovi estuary	Goa (*west coast*)	15° 30′ N-73° 52′ E	56	1150		Semi-diurnal	Mangroves Diverse flora and fauna Nursery ground for fish, prawn, and other invertebrates	Araujo et al. (2018)

Zuari estuary	Goa (*west coast*)	15° 25′ N-73° 51′ E		550		Semi-diurnal	Mangroves Diverse flora and fauna Nursery ground for fish, prawn, and other invertebrates	Araujo et al. (2018)
Tapi estuary	Gujarat (*west coast*)	21° 20′ N-74° 30′ E	210	142.50		Semi-diurnal The tidal impact is felt up to a distance of 45 km	Fishery resource	Acharya et al. (2019)
Narmada estuary	Gujarat (*west coast*)	21° 20′ N: 22° 00′ N-72° 30′ E: 73° 20′ E	190	6346	72	Semi-diurnal	Mangrove patches	Kumar et al. (2015)

Source – River discharge: http://www.iomenvis.in/

3 An Inventory of Annual Phytoplankton Primary Production Measurements in Indian Estuaries

The bibliographic record pertaining to phytoplankton primary productivity (PPP) for the period of 2000–2021 was extracted from popular citation databases (Scopus and Google Scholar) by using the keywords "phytoplankton," "primary production," "primary productivity," "estuary," "east coast of India," "west coast of India," "chlorophyll," "GPP," and "NPP." A country filter was applied to the database to separate only India-specific investigations on PPP. A total of 212 published literature were extracted; after manual scrutiny and duplicate removal, the final number of documents came to be 58, which were specifically PPP-related studies in the Indian estuaries and were retained for extensive review. PPP investigations were mostly found in four estuaries on the east coast (Hooghly RE, Chilika lagoon, Godavari RE, Cauvery RE) and five on the west coast (Cochin backwater, Asthamudi lagoon, Mandovi RE, Zuari RE, and Muthupet lagoon). PPP studies in Indian estuaries can be traced back to 1965 which was published in the journal "Hydrobiologia" wherein water column primary productivity was measured in Hooghly and Mutlah estuaries by light and dark bottle technique (Basu, 1965). From 1965 to 1999 (34 years), the number of publications was rather low as only 8 documents were published which gradually started rising from the year 2000. The last 5 years (2018–2021) recorded 13 publications pertaining to PPP experiments in Indian estuaries; evidence of growing interest in this field. The compilation includes 30 measurements of PPP, out of which 13 are reported in terms of gross primary production (GPP), 10 as net primary production (NPP), and the rest 7 measurements reported only as "primary production." PPP was reported in various units such as mg C m^{-3} h^{-1}, mmol C m^{-2} day^{-1}, μg C L^{-1} day^{-1}, g C m^{-2} day^{-1}, mg C $m^{-3}h^{-1}$, mg C m^{-3} day^{-1}, μg C L^{-1} h^{-1}, and mmol C m^{-2} day^{-1} all of which were converted into milligram carbon per cubic meter per day expressed as mg C m^{-3} day^{-1} for ease of comparison. Likewise, all chlorophyll-*a*, and nutrient concentrations were converted into mg m^{-3} and μmol l^{-1}. Nutrient concentrations were represented as total dissolved inorganic nitrogen (DIN) and dissolved inorganic phosphate (DIP). DIN was computed by summing nitrate-nitrogen (NO_3-N), nitrite-nitrogen (NO_2-N), and ammonium-nitrogen (NH_4-N) reported in the literature. The spread and central tendency of measured productivity, nutrient, and phytoplankton biomass were represented by range and midrange. The midrange is defined as the arithmetic mean of the maximum and minimum values of the data set. Despite being sensitive to outliers, the midrange is a highly efficient estimator of the sample mean given a small sample of a sufficiently platykurtic distribution. To decipher seasonal changes in PPP, the reported sampling times in the literature were classified into pre-monsoon, monsoon, and post-monsoon as per the IMD classification wherein March–May pertains to (pre-monsoon), June–September (monsoon), and October–February (post-monsoon).

Among various in situ PPP methods, the most widely used (still in use) is the "light and dark bottle method" or oxygen evolution method developed by Gaarder

and Gran (1927). Out of the total of 30 studies on PPP, 19 studies deployed the oxygen method, and the rest 11 deployed the ^{14}C method.

Estimates of the NPP and GPP can be derived directly from changes in oxygen levels in the light and dark incubation bottles. As this method is based on Winkler's titrimetric principle of oxygen estimation, it is relatively easy for the analyst to require only a titration apparatus and is cost-effective. The major disadvantage of this method is its accuracy estimation. Furthermore, interpreting light-dark incubations and photosynthetic quotient conversion to carbon fixation magnitude is not straightforward. One of the most used methods for PPP in coastal water is the carbon radioisotope (^{14}C) method. Because of its excellent sensitivity, low sample size need, and relative ease of analysis, it has become the standard for most oceanic primary production assessments since the development of this method in 1952 by Steeman-Nielsen. However, due to the risk of radioactive material spill, particular precautions, and acquiring the necessary license for the use of radioactive materials, the practice of using this method has been discouraged in recent years (Kulk et al., 2021). In this context, the utilization of stable carbon isotopes (^{12}C and ^{13}C) method provides a better alternative. Even though this method necessitates a greater sample volume, more analytical processing, and instrumentation and is less sensitive than the ^{14}C method, it is accepted by the majority due to the absence of radioactivity. Usages of other methods to measure PPP such as oxygen/argon ratios, the isotopic composition of atmospheric and dissolved oxygen has been relatively sparse in estuarine water, even globally (Cloern et al. 2014, supplementary table). The oxygen/argon ratios method is based upon the simple stoichiometric relation between oxygen and carbon production in photosynthesis and respiration. Argon is used due to its almost similar diffusivity and solubility as oxygen without having any biological source and sinks (Hamme et al., 2019). The method of triple oxygen isotope is used to estimate GPP in some of the ocean and coastal environments (Stanley et al., 2021). But the major disadvantages are that it estimates GPP accurately in the mixed layer only and provides uncertainty in GPP rates where the role of physical transport is not accounted for properly (Nicholson et al., 2014).

4 Variabilities of Phytoplankton Primary Production and Biomass in Indian Estuaries

4.1 Phytoplankton Primary Production

The range of phytoplankton primary productivity in Indian estuaries, along with adopted analytical methods, has been synthesized in Table 1.2. PPP varies with the depth profile of an estuary; in Ashtamudi estuary, Nair et al. (1984) showed that sub-surface productivity was comparatively higher than the surface and least at the bottom. Similarly, along the estuarine salinity gradient, "mesohaline locations" with a salinity between 3 and 10 ppt (parts per thousand) are more productive (Bhavya

Table 1.2 Range of daily primary production (GPP: gross primary production) in Indian estuarine ecosystems from published literature in different periods

Ecosystem	Measure	Method	Range of primary production (mgC m^{-3} day^{-1})	References
East coast				
Hooghly estuary	GPP	O_2	37.23–4272	Choudhury and Pal (2012), Biswas et al. (2007)
Mahanadi estuary	GPP	O_2	920–2060	Pattanaik et al. (2020)
Chilika lagoon	GPP	O_2	24–376	Robin et al. (2016)
Godavari estuary	GPP	O_2	36.03–2233.99	Sarma et al. (2009)
Cauvery estuary	GPP	O_2	180–2856	Purvaja and Ramesh (2000), and Perumal et al. (2009)
Muthupet estuary	GPP	O_2	636.24–3656.4	Suganthi et al. (2018)
West coast				
Cochin backwater	GPP	O_2, ^{14}C	124–11,934	Madhu et al. (2017), Hershey et al. (2020), Praveena and Santhosh (2018), Madhu et al. (2010)
Ashtamudi estuary	GPP	O_2	636.24–3656.4	Mohamed et al. (2013)
Mandovi estuary	GPP	O_2, ^{14}C	4.56–2260.41	Krishnakumari et al. (2002), and Ram et al. (2003, 2007)
Zuari estuary	GPP	O_2, ^{14}C	4.08–1840.03	Krishnakumari et al. (2002), and Ram et al. (2003, 2007)

et al., 2017). In Indian estuaries, phytoplankton productivity is controlled by optimal light and nutrient availability, the scale of tidal exchange, magnitude, timing, and duration of freshwater flow, and geomorphological characteristics of the estuary. Most of the Indian estuaries are light-limited during the high flow period. Therefore, a strong positive correlation exists between productivity and available light or, more specifically, photosynthetically active radiation (PAR) (Parvathi et al., 2013). During the high flow period, carbon supplied from mangrove litters or surface runoff from the catchment stimulates high bacterial activity in Indian estuaries, which has been discussed in the latter section of this chapter. Usually, high PPP in estuaries is associated with increased phytoplankton biomass measured in terms of chlorophyll-*a* and phytoplankton cell numbers or biovolume (Devassy & Goes, 1989). Apart from light limitation, another strong forcing that regulates PPP in Indian estuaries is

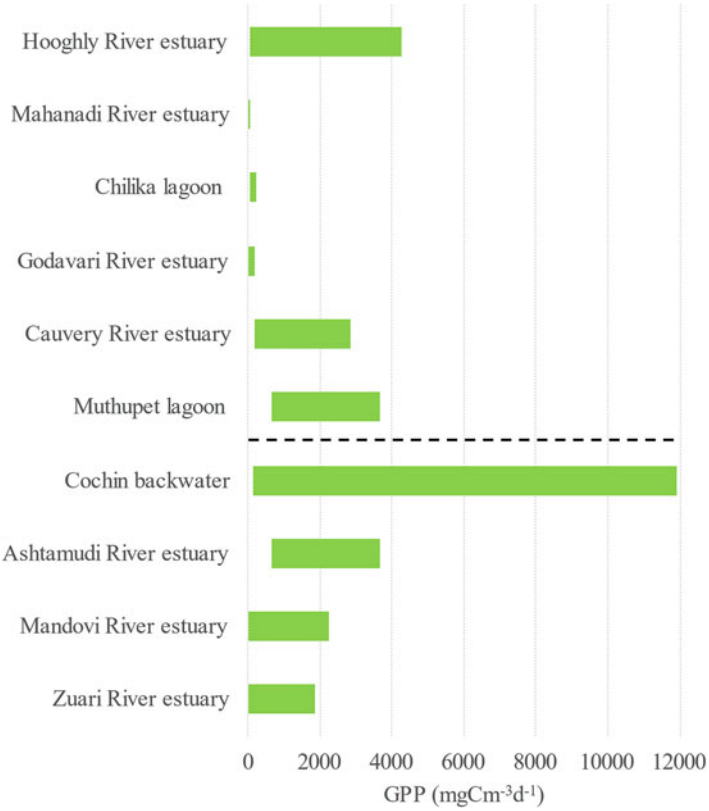

Fig. 1.2 Range of gross primary productivity (GPP) contributed by phytoplankton in Indian estuaries reported in the literature. The dashed line separates ecosystems of the east and west coast of India

the availability of nutrients in the system. Nitrogen to phosphate ratio (N:P), when stays close to 16:1, is the most ideal for PPP; however, seasonal limitation of nitrogen or phosphate often imposes restrictions on the primary production.

From the published literature, it is found that estuarine PPP on the east coast of India ranges from 24 to 4272 mg C m^{-3} day^{-1} with high spatial variability in GPP (Fig. 1.2). The details can be found in Table 1.2. Maximum recorded PPP was observed in Hooghly RE followed by heavily polluted Muthupet RE. Mahanadi and Godavari RE had similar maximum PPP values. Chilika lagoon recorded the narrowest and least PPP among the estuaries of the east coast as per the available data so far.

GPP of the Indian estuaries along the west coast ranged between 4 and 11,934 mg C m^{-3} day^{-1} (Table 1.2). Estuary-specific reported GPP values varied widely; the ranks of west coast estuaries as per the highest PPP values are Cochin backwater > Asthamudi River estuary > Mandovi River estuary > Zuari River estuary. No data on PPP were found in Narmada and Tapi estuaries on the west coast.

Variation in estuarine GPP in relation to the ISM has been reported in a few estuaries. The GPP during post-monsoon in Hooghly RE was much higher compared to pre-monsoon and monsoon (Nath et al., 2004; Biswas et al., 2007). Strong seasonality has been also reported from the estuaries in Sundarbans (offshoots of Hooghly RE), wherein GPP was the lowest in monsoon and highest in the post-monsoon period (Chaudhuri et al., 2012). The highest reported GPP in the Godavari RE was observed in the pre-monsoon when the river discharge was nil, followed by pre-monsoon when river discharge was intermediate (Sarma et al., 2009). GPP reduced to nearly one-third from pre-and post-monsoon values when freshwater discharge in the Godavari was at its peak. Robin et al. (2016) reported significantly low PPP values throughout the monsoon in Chilika lagoon due to strong light limitation driven by inputs from riverine suspended inorganic and organic matter.

Seasonal difference in GPP of west coast estuaries was not as significant as the east coast estuaries. For instance, Hershey et al. (2020) reported pre-monsoon, monsoon, and post-monsoon GPPs in Cochin backwater in the range 0.97–3.01, 1.24–3.44, and 1.35–3.85 g Cm^{-3} day^{-1}, respectively. NPP followed similar seasonal distribution pattern with slightly higher values in the post-monsoon (0.55–1.67 gCm^{-3} day^{-1}) followed by monsoon (0.61–2.49 gCm^{-3} day^{-1}) and pre-monsoon (0.45–1.45 gCm^{-3} day^{-1}).

4.2 Phytoplankton Biomass

Chlorophyll-*a* is the primary photosynthetic pigment in phytoplankton. Due to its ubiquitous presence, Chl-*a* is used as a proxy for phytoplankton biomass and their productivity. Chl-*a* in an estuarine water column is regulated by several dynamic processes such as (1) horizontal advection of phytoplankton from freshwater and marine end members, (2) washout during events of high river flow, (3) vertical mixing from the sediment, (4) sinking, (5) biomass growth, and (6) mortality that includes losses to grazers and pathogens (Brussaard, 2004).

In the estuaries along the Indian east coast, Chl-*a* ranged between 0.09 and 70.4 $mg.m^{-3}$ (Fig. 1.3). Among the riverine estuaries, the widest Chl-*a* range was reported from Godavari RE (0.6–70.4 $mg.m^{-3}$) followed by Hooghly (0.52–33.15 $mg.m^{-3}$), Cauvery (3.4–12.8 $mg.m^{-3}$), and Mahanadi RE (0.33–7.27 $mg.m^{-3}$). Chilika lagoon was richer in phytoplankton biomass than Pullicat and Muthupet lagoons (Fig. 1.3).

Except for Ashtamudi, riverine estuaries on the west coast are less populated with phytoplankton, as seen in their reported Chl-*a* values (Fig. 1.3). The highest Chl-*a* range was observed in Godavari RE (2.05–40 $mg.m^{-3}$). Chl-*a* was relatively lower in Narmada, Mandovi, and Zuari estuaries (Fig. 1.3). Cochin backwater was highly productive in terms of phytoplankton biomass (0.1–44.8 $mg.m^{-3}$). It has been designated as "one among the world's highly polluted and productive estuarine systems" (Hershey et al., 2020).

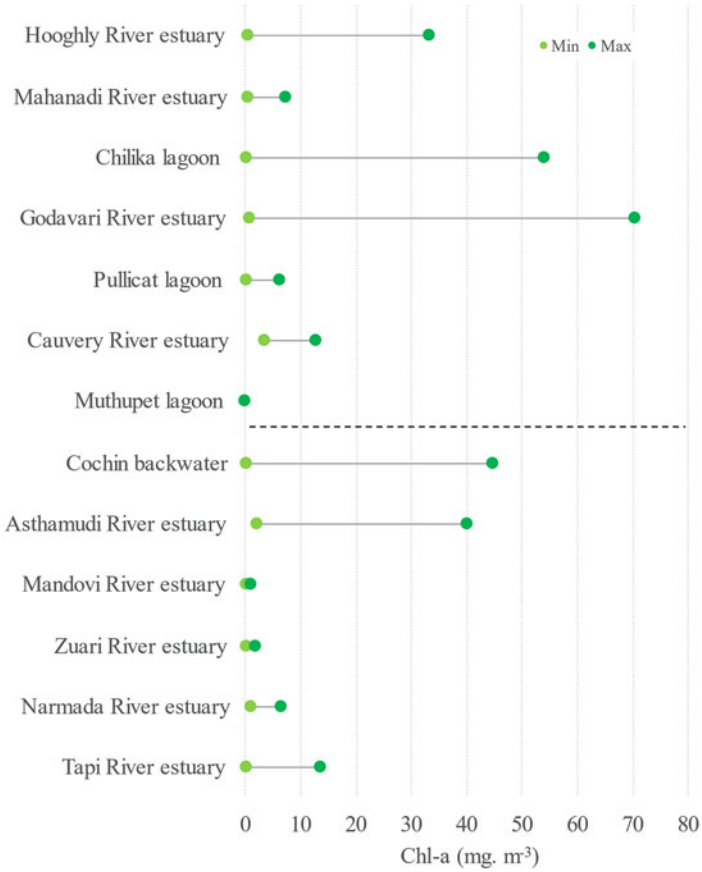

Fig. 1.3 Range of chlorophyll-*a*, a biomarker of phytoplankton biomass in Indian coastal ecosystems. The dashed horizontal line separates ecosystems of the east coast and west coast of India

4.3 Major Phytoplankton Groups Reported from Indian Estuaries

The phytoplankton diversity along Indian coastal ecosystems (estuaries, lagoons, and backwaters) is represented by the groups such as Bacillariophyta, Cyanophyta, Dinophyta, Chlorophyta, Chrysophyta, Euglenophyta, Xanthophyta, and Cryptophyta. A brief description of the phytoplankton groups can be found in Singh et al. (2022). The number of phytoplankton species reported from the Indian REs varied widely both on the east coast [365 in Hooghly, 282 in Mahanadi, 113 in Godavari, and 58 in Cauvery] and west coast [209 in Mandovi, 136 in Zuari, 35 in Narmada, 66 in Tapi]. The number of species was equally large and varied across Indian lagoons [739 in Chilika, 101 in Muthupet, 37 in Pullicat] and backwater [133

in Cochin backwaters] (Naik et al., 2009; Patil & Anil, 2011; George et al., 2012; Dey et al., 2013; Babu et al., 2013; Pednekar et al., 2014; George et al., 2015; Madhu et al., 2017; Roshith et al., 2018; Mishra et al., 2018; Bharathi et al. 2018a, b; Srichandan et al., 2019; Srichandan & Rastogi, 2020; Uthirasamy et al., 2021). Among the reported groups, Bacillariophyta has been the most abundant group among the studied riverine ecosystems (e.g., 50% of the total phytoplankton in Hooghly RE, 65% of the total phytoplankton in Godavari RE, 71% in Mandovi RE), lagoons, and backwater. Some Bacillariophytes that are abundant in Indian estuaries are *Chaetoceros* sp., *Coscinodiscus* sp., *Pleurosigma* sp., *Thalassionema* sp., and *Nitzschia* sp. Other than the Bacillariophyta, groups such as Chlorophyta, Dinophyta, Pyrrophyta, and Cyanophyta can also be found. Domination of large size phytoplankton, primarily by diatoms in the estuarine environment, has been discussed in detail by Cloern (2018). Usually, large size phytoplankton are grazed more slowly and grow faster in a nutrient-rich environment sustaining a high primary productivity that can be efficiently transferred to the consumers of higher trophic levels. As a result of the transfer of new (terrestrial) nutrients, estuaries support higher fish production akin to the coastal upwelling systems. Whether the domination of large size phytoplankton/diatoms in estuaries has been exacerbated by the anthropogenic input of nutrients is a matter of debate (Cloern, 2018); however, the global rise in temperature can possibly constrict the latitudinal distribution of diatoms and provide a selective advantage to the small size phytoplankton. A couple of recent studies in Indian backwater and lagoon based on the HPLC pigment chemo-taxonomy approach have pointed out the year-round high abundance of small size picoplankton which otherwise evade detection in microscopy due to their sheer small size (Paul et al., 2021; Srichandan et al., 2019). Paul et al. (2021) showed when the turbidity remains high, nanophytoplankton (2–20 μm) outcompete large-sized phytoplankton (>20 μm) to contribute more to PPP in Cochin backwater despite the presence of high inorganic nutrients. Since Indian estuaries turn turbid during and aftermath of the (ISM) the contribution of small size phytoplankton to primary productivity should be looked at in further detail.

5 Relationship Between Phytoplankton Production, Biomass, and Environmental Factors

5.1 Light Limitation

The phytoplankton growth rate in nutrient-rich estuaries is mainly determined by PAR, which is the amount of light available for photosynthesis in the wavelength range of 400–700 nm (Alpine & Cloern, 1988). The rate of PAR varies with incident solar irradiance, turbidity, and depth of the mixed layer (Wofsy, 1983). Many estuaries have high concentrations of mineral sediments delivered by land runoff and kept in suspension by wind induced waves and tidal currents (May et al., 2003).

Sediment-associated turbidity shrinks the photic zone to a thin layer, which leads to light limitation of photosynthesis over the estuarine water column and slow down PPP. Much of the spatial variability of PPP within some estuaries is a consequence of total suspended matter (TSM) gradients that generally decrease along the river–ocean continuum as sediments sink and their concentrations are diluted by clear ocean water. A characteristic pattern of high production near the estuary mouth and low production near the estuarine turbidity maximum (ETM) has been reported in many estuaries (Cloern et al., 2014). In ETM, the turbidity spikes due to resuspension of sediment and flocculation of particulate matter. Light availability to phytoplankton also fluctuates with wind stress that breaks down stratification and generates waves that penetrate to suspend bottom sediments in shallow estuaries.

Paul et al. (2021) suggested that water column turbidity in Cochin backwater might be one of the significant environmental factors that deter the growth of large-sized phytoplankton (>20 μm) and favor nanophytoplankton (2–20 μm). Hence, although Cochin backwater may hold significant nutrients year-round, phytoplankton size range and their contribution to the productivity are principally determined by the low available PAR (Madhu et al., 2017). A decrease in TSM has been shown to increase PPP in Hooghly RE, which presumably could influence carbon export in the adjacent Bay of Bengal (Jayaram et al., 2021). Through a microcosm study in the end member of Hooghly RE, Bhattacharyya et al. (2020) showed that this estuary becomes highly productive and a sink of CO_2 in post-monsoon which otherwise remains a significant source of CO_2. Mahanadi RE becomes net-heterotrophic during monsoon (Pattanaik et al., 2020) and in general annual mean column respiration exceeds photic zone productivity. In Godavari RE, net heterotrophy with low GPP prevailed during the peak discharge period of monsoon season (Sarma et al., 2009). Net autotrophy in the photic zone was observed only for about a couple of months in the post-monsoon period, October to November, accompanied by the rapid exhaustion of inorganic nutrients. Light limitation shifts the trophic status of the Chilika lagoon on the east coast from autotrophy to heterotrophy during the monsoon period when CO_2 air-water flux increases manifold due to enhanced bacterial metabolism (Robin et al., 2016). A similar seasonal shift in trophic status was also reported by Thottathil et al. (2008) and Hershey et al. (2020) in Cochin backwater, where the authors showed allochthonous input during freshets enhanced bacterial heterotrophic activity leading to very high pCO_2. The heterotrophic condition in Cochin backwater is stimulated by "allochthonous" input of aged and refractory phytodetritus (Renjith et al., 2013). In fact, high bacterial activity enhances bacterial productivity/primary productivity (BP/PP) ratio in estuaries, indicating that bacterioplankton consumes far more dissolved organic carbon than what is produced in situ by phytoplankton in the water column (Senthilkumar et al., 2008). Often these bacteria remain associated with the suspended particles (hence called particle-associated bacteria) supplied through allochthonous input in estuaries during high flow period fuels high bacterial production (De Souza et al., 2003). Pollutants entering from municipal sewage and industrial plants can suppress PPP by pulling down photosynthesis to respiration P/R ratio less than 1 in estuaries (Nair et al.,

1984; Purvaja & Ramesh, 2000). Human modifications of hydrologic systems have altered sediment discharge in many of the world's rivers, with downstream effects on estuarine primary producers (Cloern & Jassby, 2012).

5.2 *Nutrient Supply and Nutrient Ratio*

Nutrient concentrations and stoichiometry, specifically silicate, nitrate, nitrite, phosphate, and ammonium, act as one of the most significant determinants of phytoplankton biomass and distribution in an estuarine environment. Any shortage of nutrients causes a decrease in the photosynthetic rate in phytoplankton. The transport, transformation, retention, and export of nutrients in estuarine ecosystems are strongly influenced by estuary size (surface area), depth, volume, flushing rate, water residence time, tidal exchange, vertical mixing, and stratification (Pattanaik et al., 2021); Das & Ghosh, 2021). The source of nutrients can be both autochthonous (decomposition of organic matter, upwelling, wind-driven resuspension) and allochthonous (river discharge, weathering, atmospheric deposition). Changes in the supply of Si, N, and P and their ratios have modified phytoplankton biomass and production, especially since the mid-twentieth century (Lohrenz et al., 2008).

Based upon the reported DIN values, the riverine estuaries ranks are as follows: Ashtamudi > Tapi > Hooghly > Mahanadi > Godavari > Mandovi > Zuari > Narmada and among the lagoons: Pullicat > Chilika > Muthupet. The DIN concentration varied in the range of 0.02–170.92 μmol l^{-1} on the east coast and 0.03–293.52 44 μmol l^{-1} on the west coast. The highest DIN range was reported from Ashtamudi RE (0.07–293.52 μmol l^{-1}) and the lowest range from Muthupet lagoon (0.24–7.44 μmol l^{-1}) (Fig. 1.4). On the west coast, Asthamudi RE, Cochin backwater, and Tapi RE reported high DIN values compared to other estuaries on both coasts (Fig. 1.4).

The DIP concentrations in Indian estuaries varied in the range of 0.002–-58.10 μmol l^{-1} on the east coast and 0.01–43.17 μmol l^{-1} on the west coast. Mahanadi RE (0.01–58.10 μmol l^{-1}) and Ashtamudi RE (0.04–43.17 μmol l^{-1}) topped the list with high reported concentrations of DIP (Fig. 1.5). Among the lagoon ecosystems, Pullicat was found to have relatively higher DIP concentrations (0.95–6.00 μmol l^{-1}) compared to Chilika and Muthupet (Fig. 1.5). Low nutrient concentrations in Muthupet lagoon, Mandovi, and Zuari RE might be a limiting factor on phytoplankton biomass which can be seen from the Chl-*a* distribution (Fig. 1.3).

According to Redfield (1934), the ratio of carbon to nitrogen to phosphorus is nearly constant at 106:16:1 in both phytoplankton biomass and dissolved nutrient pools, which is called the Redfield ratio or Redfield stoichiometry. This ratio's significance is that algal production is constrained by the need for nitrogen and phosphorus in proportions of 16:1. If there is any variation in the Redfield ratio of the water column, it directly impacts the algal production in the aquatic ecosystem. The DIN: DIP ratio less than the Redfield ratio represents less abundance of

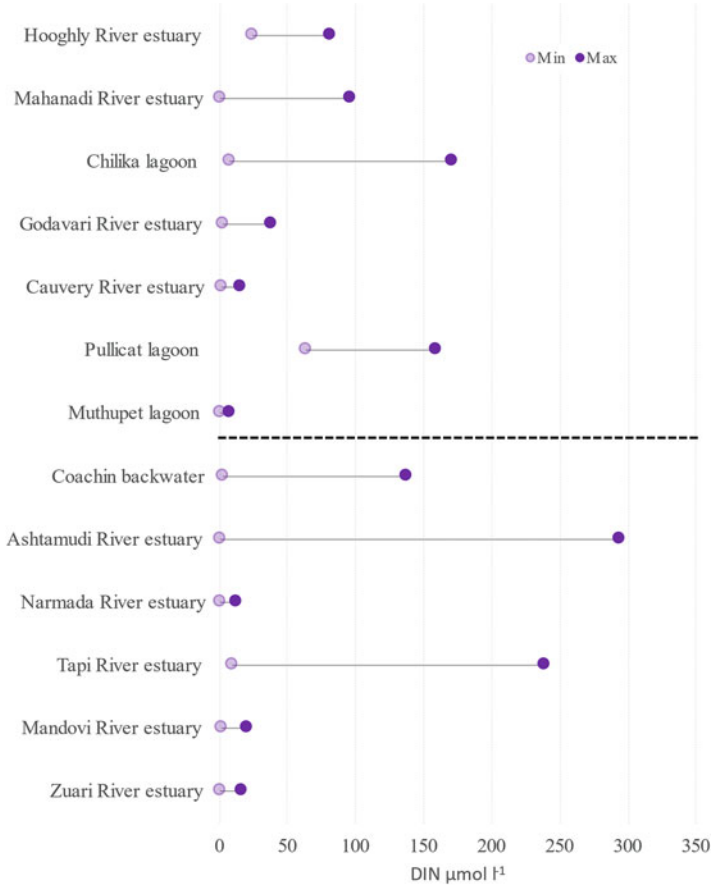

Fig. 1.4 Range of dissolved inorganic nitrogen (DIN) reported from different Indian estuaries. The dashed horizontal line segregates the ecosystems of the east and west coast of India

nitrogen, and more than the Redfield ratio represents less abundance of phosphorous. The N:P ratios are mostly regulated by the rate of river discharge, vertical mixing, atmospheric nitrogen flux, and microbial degradation in the estuaries. Significant variability in N:P ratios can be observed in REs due to marked changes in the river runoff pattern with respect to the season. For instance, Godavari RE was phosphate limited during the dry period that regulated phytoplankton biomass and productivity (Sarma et al., 2010). In contrast, Mahanadi RE exhibited nitrogen-limited conditions during the post-monsoon period when the freshwater volume in the estuary started declining (Baliarsingh et al., 2021). The N-limited nature of Mahanadi RE due to higher phosphate concentration has been further confirmed by Acharyya et al. (2021) with a large historical time-series dataset. They have shown that the nitrogen limiting condition of Mahanadi RE is maintained more by higher input of phosphate (PO_4), rather than lower input of nitrogen. In the Chilka lagoon, a high N:P ratio was

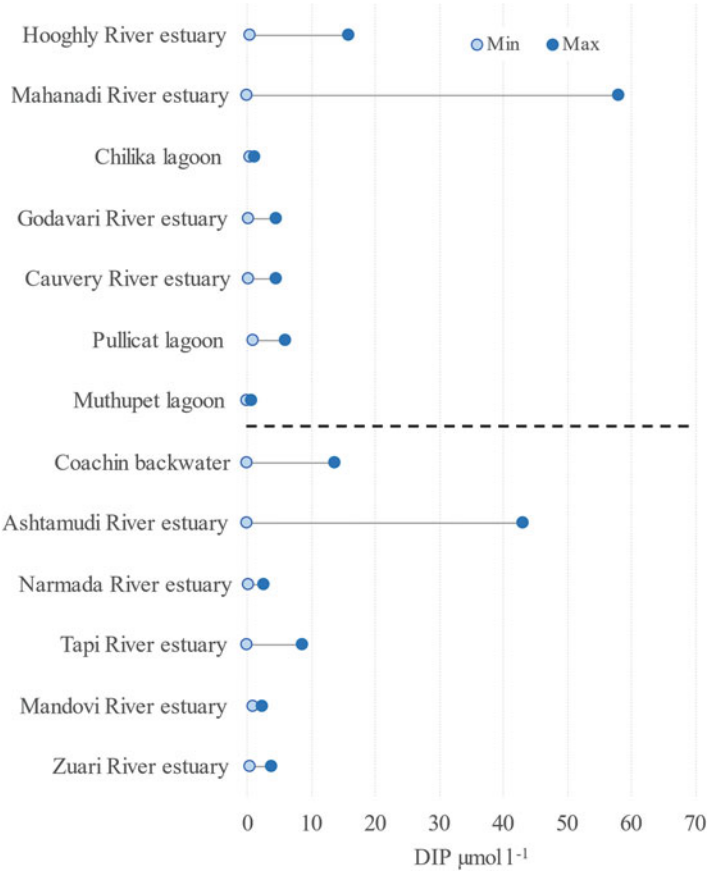

Fig. 1.5 Range of dissolved inorganic phosphate (DIP) reported from different Indian estuaries. The dashed horizontal line segregates the ecosystems of the east and west coast of India

observed during the high flow period, and the observed high ratio was due to very high concentrations of nitrogen rather than low concentrations of phosphorous (Robin et al., 2016). PPP in the Cochin backwater was influenced by the inputs of nutrients where TN:TP was close to the Redfield ratio (16:1) (Bhavya et al., 2017).

The regression plot of midrange values of GPP with DIN, DIP loading, and DIN: DIP (N:P) ratio revealed that, most of the ecosystems are productive in the lower ranges of nutrients (e.g., range of DIN: 3.84–20.19 µmol l^{-1}, DIP: 0.37–-8.12 µmol l^{-1}, N:P ratio: 1.94–12.18) (Fig. 1.6). No apparent relationship was observed between Chl-*a* and GPP, which has also been reported in previous studies. In the regression plot of DIN versus GPP, out of 10 study areas, PPP in 4 areas (Chilika lagoon, Hooghly, Mahanadi, and Ashtamudi estuary) did not increase with an increase in DIN (Fig. 1.6). From the regression between DIP and GPP, it was observed that in most areas (except Mahanadi and Ashtamudi estuary), the productivity was found to increase with the increase in DIP. In Ashtamudi and Mahanadi

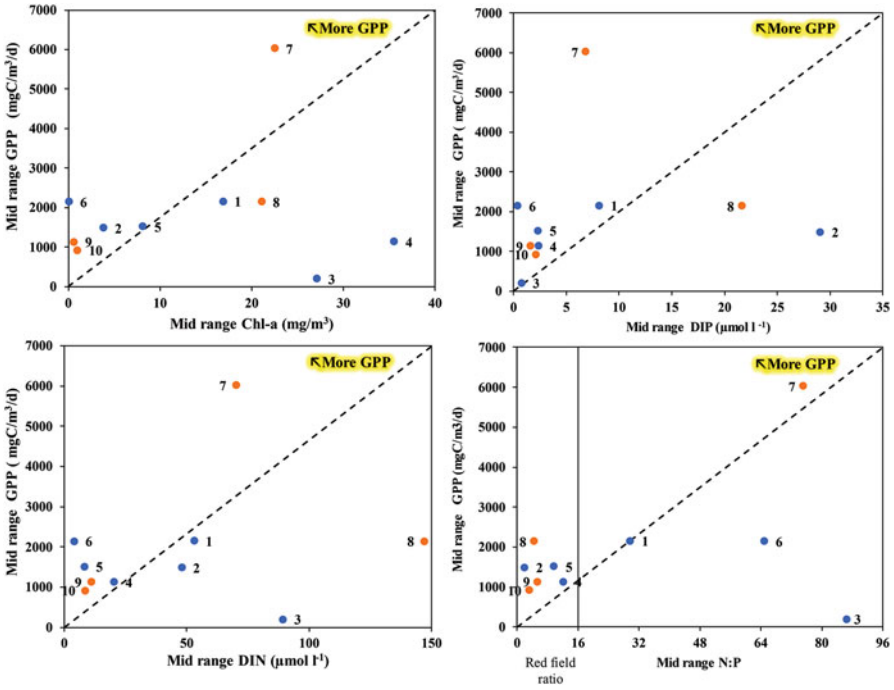

Fig. 1.6 Regression plots between midrange of chlorophyll-a (Chl-a), dissolved inorganic nitrogen (DIN), dissolved inorganic phosphate (DIP), and N:P ratio to daily phytoplankton gross primary productivity (GPP) in different ecosystems of India: (1) Hooghly RE, (2) Mahanadi RE, (3) Chilika lagoon, (4) Godavari RE, (5) Cauvery RE, (6) Muthupet lagoon, (7) Cochin backwater, (8) Ashtamudi RE, (9) Mandovi estuary, and (10) Zuari RE. The blue dots represent the ecosystems of the east coast and the orange dots the west coast. The 45° angled dashed line in each plot, which passes through the origin, is used to show the changing pattern of GPP with an increase in respective parameters. The vertical line in the plot (N:P vs. GPP) represents the red field ratio (N:P = 16)

estuary, the observed high DIP concentrations (21.60 and 29.06 µmol l^{-1}, respectively) contributed to the low N:P (<16) ratio and more GPP. The results suggest that nitrogen is more important in the regulation of PPP than phosphorous in most of the Indian estuarine ecosystems. The result also points out that except for Hooghly RE, Muthupet lagoon, Chilika lagoon, and Cochin backwater, all other estuaries clustered within the range of Redfield ratio (16), pointing out 16:1 N:P ratio is the most ideal for the phytoplankton in Indian estuaries.

5.3 Trophodynamics

Phytoplankton in natural settings are regulated by two controlling mechanisms – top-down and bottom-up. Top-down control refers to the grazing of phytoplankton

in the food chain (e.g., zooplankton and fish larvae), whereas bottom-up control refers to the availability of limiting nutrients (e.g., nitrate, phosphate, and silicate) to the phytoplankton. Microzooplankton are small size (20–200 μm) heterotrophs or mixotrophs comprising dinoflagellates, ciliates, sarcodines, and small metazoans. They are the major grazers of smaller phytoplankton (bacterioplankton, nanoplankton, and picoplankton), and owing to the fast reproduction rates, they respond quickly in tune to the phytoplankton growth. Although micro-and mesozooplankton consume most phytoplankton production in the open ocean (Calbet, 2001; Calbet & Landry, 2004), their role as grazers can be less critical in shallow estuaries and bays where benthic suspension feeders, especially bivalve mollusks, are the dominant grazers (Murrell & Hollibaugh, 1998). Bivalves are the important grazers in shallow waters because they can filter the overlying water column on timescales of days (Cloern, 1982). Microzooplankton grazing experiments were limited on the west coast of India, such as Zuari and Cochin backwaters. No experiments pertaining to the grazing impact of large filter feeders have not been conducted so far. It seems the top-down regulating mechanism of PPP in Indian estuaries is mainly unknown and offers a potential future area to study.

6 Conclusion and Future Research Direction

This chapter has synthesized phytoplankton primary production (PPP) in Indian estuaries and its dependence on nutrient inputs, light limitation, and grazing. The results, however, must be interpreted with caution as the conclusions drawn are not from experimental design or running model but based on the published literature which are most of the cases one-time observations. Range values of PPP, biomass, and nutrients in Indian estuaries reported in this chapter can potentially be affected by "outliers" warranting long-term monitoring and observation. The only estuary from where a very high-resolution PPP data (daily) was reported is Godavari RE. Other estuaries have remained under-sampled temporally. As has been shown that most of the PPP studies are confined to only nine estuaries, four from the east coast and five from the west coast, which makes the general conclusion about the productivities of Indian estuaries difficult. That too, most of the published results are from the last decade, indicating reduced effort and interest in measuring PPP in Indian estuaries. One plausible reason can be a lack of expertise on ^{14}C-based PPP measurement, which is hazardous and requires permission to conduct the experiment. Even though the oxygen evolution/light and dark bottle method of measuring PPP are not hazardous and relatively straightforward, it has its limitations. In situ incubation (mooring in the water column) in shallow Indian estuaries is fraught with logistical challenges; hence, investigators often rely on onboard or lab-based incubation, which introduces artifacts and uncertainties in the measurement due to lack of control in ambient temperature and light field. Also, primary productivity is not a popular routine water quality parameter wherein productivity or organic load of water bodies is typically reported in terms of biochemical/chemical oxygen demand

(BOD/COD) or biomass of phytoplankton (Chl-*a*). However, the current literature synthesis indicates no apparent correlation exists between Chl-*a* and PPP in Indian estuaries.

Large spatial and temporal variabilities exist in PPP and phytoplankton biomass between Indian estuaries (riverine estuaries, lagoons, and backwater). Estuaries enriched with anthropogenic organic matter such as Cochin backwater seem to be high in PPP, evidence of an overarching effect of regional water quality on the productivity of estuarine ecosystems. PPP of most Indian estuaries are strongly limited by light availability, especially during the southwest monsoon period from June to September. During this time, rapidly flowing highly turbid water breaks vertical salinity gradients, especially in riverine estuaries flushing the phytoplankton out of the estuary which were already under severe light limitation despite elevated available nutrients. Highly turbid Indian estuaries turn into net source of CO_2 during monsoon due to extremely high bacterial respiration. Water column and particle-associated bacteria have been found to rapidly decompose terrestrial (allochthonous) refractile organic matter that is brought inside the estuaries during high flow periods. In contrast, higher PPP in Indian estuaries is confined to a brief period spanning a couple of months when high freshwater runoff declines leading to a deepening of photic depth. Such transient "net autotrophy," that is, when phytoplankton production in the photic layer exceeds water-column respiration in the estuary, stimulates rapid uptake of available nutrients. Essential nutrients, such as N and P, when present in the Redfield ratio (16:1) proportion are found to be most suitable to spur the growth of phytoplankton. Most of the Indian estuaries are nitrogen-limited, but interestingly, nitrogen-limitation can also be imposed through high input of P in the system as has been shown in the Mahanadi estuary. Hence, local N or P loading, which often ends up in estuaries from agricultural runoff and industrial effluents, can play a critical role in N versus P limitation switch. This has far-reaching consequences on estuarine productivity, especially in heavily industrialized and urbanized ones, wherein such switching over can lead to altered phytoplankton community composition and size distribution. Estuaries are dominated by large size phytoplankton, typically diatoms, having larger realized niches and capable of thriving in wider salinity fluctuations. However, the role of ubiquitous picoplankton such as Synechococcus and Prochlorococcus in Indian estuaries has not been studied in detail. A new piece of evidence points out these "low-light adapted," unicellular photosynthetic bacteria contribute to a substantial proportion of primary productivity and keeps populations' pathogenic bacteria and virus under control. Besides nutrient and light limitations, the phytoplankton population, hence their primary productivity, is kept under check by intense grazing of zooplankton and benthic filter feeders. The phytoplankton clearing rate by benthic filter feeders is especially high in shallow estuaries, but no investigation has established it in Indian estuaries. Hence, the role of grazing as a regulator of PPP in Indian estuaries offers a potential future study area.

Till now, the knowledge about PPP in estuaries are almost exclusively based on "direct measurements" which is labor- and resource-intensive. PPP measurement has gained traction in recent decades due to the advent of satellite-based ocean color

radiometers to decipher potential fishing zones and other sustainable management practices at a large spatial and temporal scale. But a major drawback still confounds routine measurement of PPP in estuaries through satellite due to lack of spatial resolution, interference of high concentration of suspended sediment matter and CDOM (colored dissolved organic matter), and bottom reflectance. More efforts should be put forth in sensor calibration and validation vis-à-vis developing regional primary productivity algorithms in the coming days.

Acknowledgments The authors acknowledge the financial support received from the Coastal Monitoring Program by the Indian National Centre for Ocean Information Services (INCOIS), Ministry of Earth Sciences, Government of India. This is INCOIS contribution number 499.

References

Acharya, K. V., Dadhaniya, P., Shendage, A., Badne, A., & Chava, A. (2019). Estuarine fisheries resource of India. *International Journal of Sciences and Applied Research, 6*(1), 1–12.

Acharyya, T., Sudatta, B. P., Srichandan, S., Baliarsingh, S. K., Lotliker, A. A., Raulo, S., Singh, S., & Samanta, A. (2021). Deciphering long-term seasonal and tidal water quality trends in the Mahanadi estuary. *Journal of Coastal Conservation, 25*(6), 1–16.

Alpine, A. E., & Cloern, J. E. (1988). Phytoplankton growth rates in a light-limited environment, San Francisco Bay. *Marine Ecology Progress Series. Oldendorf, 44*(2), 167–173.

Araujo, J., Naqvi, S. W. A., Naik, H., & Naik, R. (2018). Biogeochemistry of methane in a tropical monsoonal estuarine system along the west coast of India. *Estuarine, Coastal and Shelf Science, 207*, 435–443.

Babu, A., Varadharajan, D., Perumal, N. V., Thilagavathi, B., Manikandarajan, T., Sampathkumar, P., & Balasubramanian, T. (2013). Diversity of phytoplankton in different stations from Muthupettai, South East Coast of India. *Journal of Marine Science: Research & Development, 3*(3). https://doi.org/10.4172/2155-9910.1000128

Baliarsingh, S. K., Lotliker, A. A., Srichandan, S., Roy, R., Sahu, B. K., Samanta, A., Nair, T. B., Acharyya, T., Parida, C., Singh, S., & Jena, A. K. (2021). Evaluation of hydro-biological parameters in response to semi-diurnal tides in a tropical estuary. *Ecohydrology & Hydrobiology, 21*(4), 700–717.

Basha, S. K. M., Rajya Lakshmi, E., Ratneswara Rao, B., Murthy, C. V. N., & Savithramma, N. (2012). Biodiversity and conservation of Pulicat Lake–Andhra Pradesh. *International Journal of Geology, Earth & Environmental Sciences, 2*(2), 129–135.

Basu, A. K. (1965). Observation on the probable effects of pollution on the primary productivity of the hooghly and mutlah estuaries. *Hydrobiologia, 25*(1), 302–316.

Basuri, C. K., Pazhaniyappan, E., Munnooru, K., Chandrasekaran, M., Vinjamuri, R. R., Karri, R., & Mallavarapu, R. V. (2020). Composition and distribution of planktonic ciliates with indications to water quality in a shallow hypersaline lagoon (Pulicat Lake, India). *Environmental Science and Pollution Research, 27*(15), 18303–18316.

Bharathi, M. D., Sarma, V. V., Ramaneswari, K., et al. (2018a). Influence of river discharge on abundance and composition of phytoplankton in the western coastal Bay of Bengal during peak discharge period. *Marine Pollution Bulletin, 133*, 671–683.

Bharathi, M. D., Sarma, V. V. S. S., & Ramaneswari, K. (2018b). Intra-annual variations in phytoplankton biomass and its composition in the tropical estuary: Influence of river discharge. *Marine Pollution Bulletin, 129*(1), 14–25.

Bhattacharyya, S., Chanda, A., Hazra, S., Das, S., & Das, I. (2020). Delineating CO2 and chlorophyll-a variability of an urban estuary with respect to changes in available dissolved nutrients: A microcosm study. *Indian Journal of Geo-Marine Sciences, 49*(11), 1710–1720.

Bhavya, P. S., Kumar, S., Gupta, G. V. M., & Sudheesh, V. (2017). Carbon uptake rates in the Cochin estuary and adjoining coastal Arabian Sea. *Estuaries and Coasts, 40*(2), 447–456.

Biswas, H., Mukhopadhyay, S. K., Sen, S., & Jana, T. K. (2007). Spatial and temporal patterns of methane dynamics in the tropical mangrove dominated estuary, NE coast of Bay of Bengal, India. *Journal of Marine Systems, 68*(1–2), 55–64.

Borges, A. V. (2005). Do we have enough pieces of the jigsaw to integrate CO_2 fluxes in the coastal ocean? *Estuaries, 28*(1), 3–27.

Boynton, W. R., Kemp, W. M., & Keefe, C. W. (1982). A comparative analysis of nutrients and other factors influencing estuarine phytoplankton production. In *Estuarine comparisons* (pp. 69–90). Academic Press.

Brussaard, C. P. (2004). Viral control of phytoplankton populations—A review 1. *Journal of Eukaryotic Microbiology, 51*(2), 125–138.

Calbet, A. (2001). Mesozooplankton grazing effect on primary production: A global comparative analysis in marine ecosystems. *Limnology and Oceanography, 46*(7), 1824–1830.

Calbet, A., & Landry, M. R. (2004). Phytoplankton growth, microzooplankton grazing, and carbon cycling in marine systems. *Limnology and Oceanography, 49*(1), 51–57.

Chaudhuri, K., Manna, S., Sarma, K. S., Naskar, P., Bhattacharyya, S., & Bhattacharyya, M. (2012). Physicochemical and biological factors controlling water column metabolism in Sundarbans estuary, India. *Aquatic Biosystems, 8*(1), 1–16.

Choudhury, A. K., & Pal, R. (2012). Understanding the seasonal dynamics of primary productivity in relation to phytoplankton populations from the Bhagirathi–Hooghly estuary, eastern Indian coast. *Journal of Algal Biomass Utilization, 3*(4), 80–88.

Cloern, J. E. (1982). Does the benthos control phytoplankton biomass in South San Francisco Bay. *Marine Ecology Progress Series. Oldendorf, 9*(2), 191–202.

Cloern, J. E. (2001). Our evolving conceptual model of the coastal eutrophication problem. *Marine Ecology Progress Series, 210*, 223–253.

Cloern, J. E. (2018). Why large cells dominate estuarine phytoplankton. *Limnology and Oceanography, 63*(S1), S392–S409.

Cloern, J. E., & Jassby, A. D. (2008). Complex seasonal patterns of primary producers at the land–sea interface. *Ecology Letters, 11*(12), 1294–1303.

Cloern, J. E., & Jassby, A. D. (2012). Drivers of change in estuarine-coastal ecosystems: Discoveries from four decades of study in San Francisco Bay. *Reviews of Geophysics, 50*(4), RG4001.

Cloern, J.E., Foster, S.Q., & Kleckner, A.E. (2014). Phytoplankton primary production in the world's estuarine-coastal ecosystems. *Biogeosciences, 11*(9), 2477–2501.

Das, S., & Ghosh, T. (2021). Introduction: An overview of biogeochemical cycle of estuarine system. In *Estuarine biogeochemical dynamics of the east coast of India* (pp. 1–11). Springer.

De Souza, M. J. B., Nair, S., Bharathi, P. L., & Chandramohan, D. (2003). Particle-associated bacterial dynamics in a tropical tidal plain (Zuari Estuary, India). *Aquatic Microbial Ecology, 33*(1), 29–40.

Devassy, V. P., & Goes, J. I. (1989). Seasonal patterns of phytoplankton biomass and productivity in a tropical estuarine complex (west coast of India). *Proceedings: Plant Sciences, 99*(5), 485–501.

Dey, M., Chowdhury, C., Pattnaik, A. A., Ganguly, D., Mukhopadhyay, S. K., De, T. K., & Jana, T. K. (2013). Comparison of Monsoonal change of water quality parameters between 1983 and 2008 in a tropical estuary in Northeastern India: Role of phytoplankton and community metabolism. *Marine Ecology, 34*, 14–29.

Falkowksi, P. G., Katz, M. E., Knoll, A. H., Quigg, A., Raven, J. A., Schofield, O., & Taylor, F. J. R. (2004). The evolution of modern eukaryotic phytoplankton. *Science, 305*(5682), 354–360.

Gaarder, T. (1927). Investigations of the production of plankton in the oslo fjord. Rapports et proces-verbaux des reunions. *Conseil International pour l'Exploration de la Mer, 42*, 1–48.

George, B., Kumar, J. N., & Kumar, R. N. (2012). Study on the influence of hydro-chemical parameters on phytoplankton distribution along Tapi estuarine area of Gulf of Khambhat, India. *The Egyptian Journal of Aquatic Research, 38*(3), 157–170.

George, B., Kumar, N., & Kumar, R. N. (2015). An evaluation of phytoplankton assemblage in relation to environmental variables of Narmada Estuarine Region of Gulf of Khambhat, Gujarat, India. *Applied Ecology and Environmental Research, 13*(1), 115–131.

Gupta, G. V. M., Natesan, U., Murthy, M. R., Kumar, V. S., Viswanathan, S., Bhat, M. S., Ray, A. K., & Subramanian, B. R. (2006). Nutrient budgets for Muthupet lagoon, southeastern India. *Current Science, 90*, 967–972.

Hamme, R. C., Nicholson, D. P., Jenkins, W. J., & Emerson, S. R. (2019). Using noble gases to assess the ocean's carbon pumps. *Annual Review of Marine Science, 11*(1), 75–103.

Hershey, N. R., Nandan, S. B., & Vasu, K. N. (2020). Trophic status and nutrient regime of Cochin estuarine system, India. *Indian Journal of Geo-Marine Sciences, 49*, 1395.

Jayaram, C., Patidar, G., Swain, D., Chowdary, V. M., & Bandyopadhyay, S. (2021). Total suspended matter distribution in the Hooghly river estuary and the Sundarbans: A remote sensing approach. *IEEE Journal of Selected Topics in Applied Earth Observations and Remote Sensing, 14*, 9064–9070.

Kjerfve, B. (1994). Coastal lagoons. *Coastal Lagoon Processes, 1952*, 1–8.

Krishnakumari, L., Bhattathiri, P. M. A., Matondkar, S. G. P., & John, J. (2002). Primary productivity in Mandovi-Zuari estuaries in Goa. *Journal of the Marine Biological Association of India, 44*, 1–13.

Kulk, G., Fernandez-Carrera, A., Balch, W. M., Marra, J., Neale, P., & Duhamel, S. (2021). Aquatic primary productivity field protocols for satellite validation and model synthesis. In R. A. Vandermeulen & J. E. Chaves (Eds.), *Ocean optics & biogeochemistry protocols for satellite ocean colour sensor validation, IOCCG protocol series volume 7.0*. IOCCG.

Kumar, A., Samuel, S. K., & Vyas, V. (2015). Morphometric analysis of six sub-watersheds in the central zone of Narmada River. *Arabian Journal of Geosciences, 8*(8), 5685–5712.

Lohrenz, S. E., Redalje, D. G., Cai, W. J., Acker, J., & Dagg, M. (2008). A retrospective analysis of nutrients and phytoplankton productivity in the Mississippi River plume. *Continental Shelf Research, 28*(12), 1466–1475.

Madhu, N. V., Jyothibabu, R., Balachandran, K. K., Honey, U. K., Martin, G. D., Vijay, J. G., Shiyas, C. A., Gupta, G. V. M., & Achuthankutty, C. T. (2007). Monsoonal impact on planktonic standing stock and abundance in a tropical estuary (Cochin backwaters–India). *Estuarine, Coastal and Shelf Science, 73*(1–2), 54–64.

Madhu, N. V., Balachandran, K. K., Martin, G. D., Jyothibabu, R., Thottathil, S. D., Nair, M., Joseph, T., & Kusum, K. K. (2010). Short-term variability of water quality and its implications on phytoplankton production in a tropical estuary (Cochin backwaters—India). *Environmental Monitoring and Assessment, 170*(1), 287–300.

Madhu, N. V., Martin, G. D., Haridevi, C. K., Nair, M., Balachandran, K. K., & Ullas, N. (2017). Differential environmental responses of tropical phytoplankton community in the southwest coast of India. *Regional Studies in Marine Science, 16*, 21–35.

May, D. R., Chan, A. Y., Hodges, T. D., & Avolio, B. J. (2003). Developing the moral component of authentic leadership. *Organizational Dynamics, 32*, 247–260.

Menon, N. N., Balchand, A. N., & Menon, N. R. (2000). Hydrobiology of the Cochin backwater system–A review. *Hydrobiologia, 430*(1), 149–183.

Mishra, S., Nayak, S., Pati, S. S., Nanda, S. N., Mahanty, S., & Behera, A. (2018). Spatio temporal variation of phytoplankton in relation to physicochemical parameters along Mahanadi estuary & inshore area of Paradeep coast, north east coast of India in Bay of Bengal. *Indian Journal of Geo-Marine Sciences, 47*, 1502–1517.

Mohamed, K.S., Venkatesan, V., Kripa, V., Prema, D., Joseph, M., Alloycious, P.S., Sharma, J., Valsala, K.K., Saji Kumar, K.K., Ragesh, N., Bose, J., & Mohan, A. (2013). Fishery Management Plan for Ashtamudi Lake Clam Resources. CMFRI Special Publication No: 114 48p

Murrell, M. C., & Hollibaugh, J. T. (1998). Microzooplankton grazing in northern San Francisco Bay measured by the dilution method. *Aquatic Microbial Ecology, 15*(1), 53–63.

Naik, S., Acharya, B. C., & Mohapatra, A. (2009). Seasonal variations of phytoplankton in Mahanadi estuary, East Coast of India. *Indian Journal of Marine Sciences, 38*, 184–119.

Nair, N. B., Abdul Azis, P. K., Dharmaraj, K., Arunachalam, M., Krishna Kumar, K., & Balasubramanian, N. K. (1984). Ecology of Indian estuaries: Primary productivity of the Ashtamudi estuary, south-west coast of India. *Proceedings: Animal Sciences, 93*(1), 9–23.

Nath, D., Misra, R. N., & Karmakar, H. C. (2004). *The Hooghly estuarine system-ecological flux, fishery resources and production potential. Bulletin no. 130*. Central Inland Fisheries Research Institute.

Nicholson, D. P., Stanley, R. H. R., & Doney, S. C. (2014). The triple oxygen isotope tracer of primary productivity in a dynamic ocean. *Global Biogeochemical Cycles, 28*(5), 538–552.

NOAA (2022). https://www.fisheries.noaa.gov/national/habitat-conservation/estuary-habitat accessed on April 14, 2022.

Paczkowska, J., Brugel, S., Rowe, O., Lefébure, R., Brutemark, A., & Andersson, A. (2020). Response of coastal phytoplankton to high inflows of terrestrial matter. *Frontiers in Marine Science, 7*, 80.

Panigrahi, S., Wikner, J., Panigrahy, R. C., Satapathy, K. K., & Acharya, B. C. (2009). Variability of nutrients and phytoplankton biomass in a shallow brackish water ecosystem (Chilika Lagoon, India). *Limnology, 10*(2), 73–85.

Parvathi, A., Jasna, V., Haridevi, K. C., Jina, S., Greeshma, M., Breezy, J., & Nair, M. (2013). Diurnal variations in bacterial and viral production in Cochin estuary, India. *Environmental Monitoring and Assessment, 185*(10), 8077–8088.

Patil, J. S., & Anil, A. C. (2011). Variations in phytoplankton community in a monsoon-influenced tropical estuary. *Environmental Monitoring and Assessment, 182*(1), 291–300.

Pattanaik, S., Chanda, A., & Mohapatra, P. K. (2021). Aquatic biogeochemistry of the estuarine and coastal waters of the Bay of Bengal: Impact of physical forcing and extreme atmospheric events. In *Estuarine biogeochemical dynamics of the east coast of India* (pp. 31–43). Springer.

Pattanaik, S., Chanda, A., Sahoo, R.K., Swain, S., Satapathy, D.R., Panda, C.R., Choudhury, S.B., & Mohapatra, P.R. (2020). Contrasting intra-annual inorganic carbon dynamics and air–water CO_2 exchange in Dhamra and Mahanadi Estuaries of northern Bay of Bengal, India. Limnology 21: 129–138.

Paul, M., Velappan, M. N., Nanappan, U., Gopinath, V., Velloth, R. T., Rajendran, A., Nair, M., & Peariya, A. (2021). Characterization of phytoplankton size-structure based productivity, pigment complexes (HPLC/CHEMTAX) and species composition in the Cochin estuary (south-west coast of India): Special emphasis on diatoms. *Oceanologia, 63*(4), 463–481.

Pednekar, S. M., Kerkar, V., & Matondkar, S. G. P. (2014). Spatiotemporal distribution in phytoplankton community with distinct salinity regimes along the Mandovi estuary, Goa, India. *Turkish Journal of Botany, 38*(4), 800–818.

Perumal, N. V., Rajkumar, M., Perumal, P., & Rajasekar, K. T. (2009). Seasonal variations of plankton diversity in the Kaduviyar estuary, Nagapattinam, southeast coast of India. *Journal of Environmental Biology, 30*(6), 1035–1046.

Pranav, P., Roy, R., Jayaram, C., D'Costa, P. M., Choudhury, S. B., Menon, N. N., Nagamani, P. V., Sathyendranath, S., Abdulaziz, A., Sai, M. S., & Sajhunneesa, T. (2021). Seasonality in carbon chemistry of Cochin backwaters. *Regional Studies in Marine Science, 46*, 101893.

Praveena, M., & Santhosh, S. (2018). *Monsoonal influence on water chemistry and primary productivity of Kappil backwaters, Kerala, India*. Research Department of Zoology, N. S. S. College.

Purvaja, R., & Ramesh, R. (2000). Natural and anthropogenic effects on phytoplankton primary productivity in mangroves. Chemistry and Ecology, 17(1), 41–58.

Qasim, S. Z. (2003). *Indian Estuaries*. Allied Publication Pvt. Ltd.. ISBN: 81-7764 369-X.

Ram, A. P., Nair, S., & Chandramohan, D. (2003). Seasonal shift in net ecosystem production in a tropical estuary. *Limnology and Oceanography, 48*(4), 1601–1607.

Ram, A.S.P., Nair, S., & Chandramohan, D. (2007). Bacterial growth efficiency in a tropical estuary: seasonal variability subsidized by allochthonous carbon. Microbial ecology 53: 591–599.

Redfield, A. C. (1934). *On the proportions of organic derivatives in sea water and their relation to the composition of plankton* (Vol. 1). University Press of Liverpool.

Renjith, K. R., Joseph, M. M., Ghosh, P., Habeeb Rahman, K., Kumar, R., & Chandramohanakumar, N. (2013). Biogeochemical facsimile of the organic matter quality and trophic status of a micro-tidal tropical estuary. *Environmental Earth Sciences, 70*(2), 729–742.

Robin, R. S., Kanuri, V.V., Muduli, P.R., Ganguly, D., Patra, S., Hariharan, G., & Subramanian, B.R. (2016). CO_2 saturation and trophic shift induced by microbial metabolic processes in a river-dominated ocean margin (tropical shallow lagoon, Chilika, India). Geomicrobiology Journal 33, 6: 513–529.

Roshith, C. M., Meena, D. K., Manna, R. K., et al. (2018). Phytoplankton community structure of the Gangetic (Hooghly-Matla) estuary: Status and ecological implications in relation to ecoclimatic variability. *Flora, 240*, 133–143.

Saranya, & Lancelet. (2020). Ashtamudi lake – An overview on physical characteristics. *Journal of Engineering Science, 11*(6), 398–405.

Sarma, V. V. S. S., Gupta, S. N. M., Babu, P. V. R., Acharya, T., Harikrishnachari, N., Vishnuvardhan, K., Rao, N. S., Reddy, N. P. C., Sarma, V. V., Sadhuram, Y., & Murty, T. V. R. (2009). Influence of river discharge on plankton metabolic rates in the tropical monsoon driven Godavari estuary, India. *Estuarine, Coastal and Shelf Science, 85*(4), 515–524.

Sarma, V. V. S. S., Prasad, V. R., Kumar, B. S. K., Rajeev, K., Devi, B. M. M., Reddy, N. P. C., Sarma, V. V., & Kumar, M. D. (2010). Intra-annual variability in nutrients in the Godavari estuary, India. *Continental Shelf Research, 30*(19), 2005–2014.

Senthilkumar, B., Purvaja, R., & Ramesh, R. (2008). Seasonal and tidal dynamics of nutrients and chlorophyll a in a tropical mangrove estuary, southeast coast of India. *Indian Journal of Marine Sciences, 37*, 132.

Singh, S., Acharyya, T., & Gopinath, A. (2022). Phytoplankton ecology in Indian Coastal Lagoons: a review. Coastal Ecosystems: Environmental importance, current challenges and conservation measures. 91–115.

Srichandan, S., & Rastogi, G. (2020). Spatiotemporal assessment of phytoplankton communities in the Chilika Lagoon. In C. M. Finlayson, G. Rastogi, & D. R. Mishra (Eds.), *Ecology, conservation, and restoration of Chilika Lagoon, India, Wetlands: Ecology, conservation and management* (Vol. 6, 6th ed., pp. 251–294). Springer.

Srichandan, S., Baliarsingh, S. K., Prakash, S., Lotliker, A. A., Parida, C., & Sahu, K. C. (2019). Seasonal dynamics of phytoplankton in response to environmental variables in contrasting coastal ecosystems. *Environmental Science and Pollution Research, 26*, 12025–12041.

Sridevi, B. (2013). *A comprehensive study on physical processes and their impact on biogeochemistry of Godavari estuary, India*. Doctoral dissertation, PhD thesis, Andhra University, Visakhapatnam.

Stanley, R., Juranek, L., & Nicholson, D. (2021). Aquatic primary productivity field protocols for satellite validation and model synthesis. In R. A. Vandermeulen & J. E. Chaves (Eds.), *Ocean optics & biogeochemistry protocols for satellite ocean colour sensor validation, IOCCG protocol series volume 7.0*. IOCCG.

Suganthi, A., Venkatraman, C., Bharath, B., & Perinbam, K. (2018). Influence of physio-chemical parameters on fish diversity in Muthupet estuary, southeast coast of India. *International Journal of Scientific Research in Biological Sciences, 5*, 4.

Thottathil, S. D., Balachandran, K. K., Gupta, G. V. M., Madhu, N. V., & Nair, S. (2008). Influence of allochthonous input on autotrophic–heterotrophic switch-over in shallow waters of a tropical estuary (Cochin estuary), India. *Estuarine, Coastal and Shelf Science, 78*(3), 551–562.

Uthirasamy, S., Chitra, T., Ravichandiran, S., & Kavitha, T. (2021). Phytoplankton diversity of Cauvery River in Erode, Tamil Nadu. *Recent Research Advances in Biology, 7*, 154–158.

Vijith, V., Sundar, D., & Shetye, S. R. (2009). Time-dependence of salinity in monsoonal estuaries. *Estuarine, Coastal and Shelf Science, 85*(4), 601–608.

Wofsy, S. C. (1983). A simple model to predict extinction coefficients and phytoplankton biomass in eutrophic waters 1. *Limnology and Oceanography, 28*(6), 1144–1155.

Chapter 2
Characterizing the Phytoplankton Composition and Production in the Estuarine and Oceanic Waters Along the Indian Coastline

Sourav Das and Abhra Chanda

Abstract Phytoplankton forms the base of the ecological food chain in any aquatic ecosystem and plays a crucial role in several biogeochemical processes in the marine waters that regulate the atmospheric gaseous composition. The Indian Ocean, especially the two flanks of this basin adjoining Indian landmass, the Bay of Bengal and the Arabian Sea, exhibits a unique hydrological setup. The substantial freshwater discharge from the perennial rivers flowing through the Indian peninsula stratifies the water column in the open marine waters (particularly in the Bay of Bengal). The varying salinity and nutrient profiles significantly regulate the phytoplankton species composition. The autotrophic potential of these floral communities governs the biological pump, which plays a crucial role in absorbing CO_2 from the atmosphere. Several limiting factors, such as light, nutrient concentrations, and water column stratification, govern the rate of primary productivity. Many of the Indian estuaries are highly turbid and rich in nutrients. Excessive nutrients make these waters susceptible to eutrophication, and light limitation bars the optimum productivity. Thus, the coastal waters of this region experience complicated competitive processes concerning phytoplankton productivity. The open oceanic realms in the Bay of Bengal, Arabian Sea, and the equatorial Indian Ocean exhibit significant spatiotemporal variability in species assemblage and productivity rates. Many of these regions witness harmful algal blooms. Thus, compiling the knowledge gained so far on the phytoplankton dynamics and primary productivity of this region would serve as baseline information for all future workers who would carry out specialized research in this domain.

S. Das (✉)
Department of Chemistry, Brainware University, Kolkata, West Bengal, India

School of Oceanographic Studies, Jadavpur University, Kolkata, West Bengal, India

A. Chanda
School of Oceanographic Studies, Jadavpur University, Kolkata, West Bengal, India

S. C. Tripathy, A. Singh (eds.), *Dynamics of Planktonic Primary Productivity in the Indian Ocean*, https://doi.org/10.1007/978-3-031-34467-1_2

Keywords Diatoms · Dinoflagellates · Cyanobacteria · Algal bloom · Chlorophyll-a · Primary productivity

1 Introduction

Phytoplankton forms the base of the ecological food chain in almost any surface aquatic system, and it holds for the estuaries and oceans also. These conspicuous groups of organisms can control and regulate the productivity in the upper strata of the marine ecological food chain (Waga et al., 2022). Several climatic, geomorphological, and biogeochemical processes can regulate the species assemblage, relative abundance, and biomass of the dominant phytoplankton association of a particular region over spatial and temporal scales (Rusanov et al., 2022). Nutrient levels in the estuarine water column and nearshore coastal waters play a crucial role in governing the magnitude of phytoplankton, as well as the species composition (Krishnan et al., 2022). Freshwater-marine water admixture and the consequent salinity gradient of the water bodies in the continental shelf regions tend to shape the phytoplankton species composition in these domains (Wu et al., 2022). Phytoplankton plays a decisive role in governing the marine biological carbon pump, and thus, in the present era of climate change, their dynamics have been put under the lenses (Sauterey & Ward, 2022). However, anthropogenic disturbances like excessive nutrient discharge into the marine sector have led to undesirable consequences like eutrophication, also known as harmful algal blooms, that pose deleterious impacts on marine life as a whole (Zhang et al., 2022). Thus, phytoplankton are capable of altering the biogeochemistry of the coastal and open oceanic surface water, which in turn, can have far-reaching impacts on the climate and well-being of almost the entire plethora of marine life. This is why phytoplankton and the associated primary productivity dynamics hold immense significance in the fields of oceanography and environmental science.

Indian shoreline, in this regard, offers a unique marine site that has two flanks of the Indian Ocean, namely, the Bay of Bengal and the Arabian Sea on the two sides of the peninsular region of this country. This country encompasses a coastline of almost 7500 km (including the Andaman and Nicobar Islands and Lakshadweep Islands) that exhibits substantial spatial variability in terms of both geomorphology and biogeochemistry. The eastern side of the Indian peninsula that faces the Bay of Bengal on the west has several perennial and monsoon-fed rivers. On the contrary, the Arabian Sea has much less freshwater discharge from the Indian part. These two flanks of the Indian Ocean have several contrasting characters in terms of oceanographic features (Ota et al., 2022) that give rise to diverse phytoplankton dynamics in India's periphery (Bharathi & Sarma, 2019). The anthropogenic nutrient load due to multifarious agricultural and domestic activities, as well as the freshwater discharge, varies substantially across the estuaries and the nearshore water environment in the Indian coastal periphery (Karati et al., 2021). Such variations lead to complex phytoplankton and productivity dynamics in the coastal waters of the Arabian Sea and the Bay of Bengal in the Indian coastal periphery. Besides, the biogeochemical

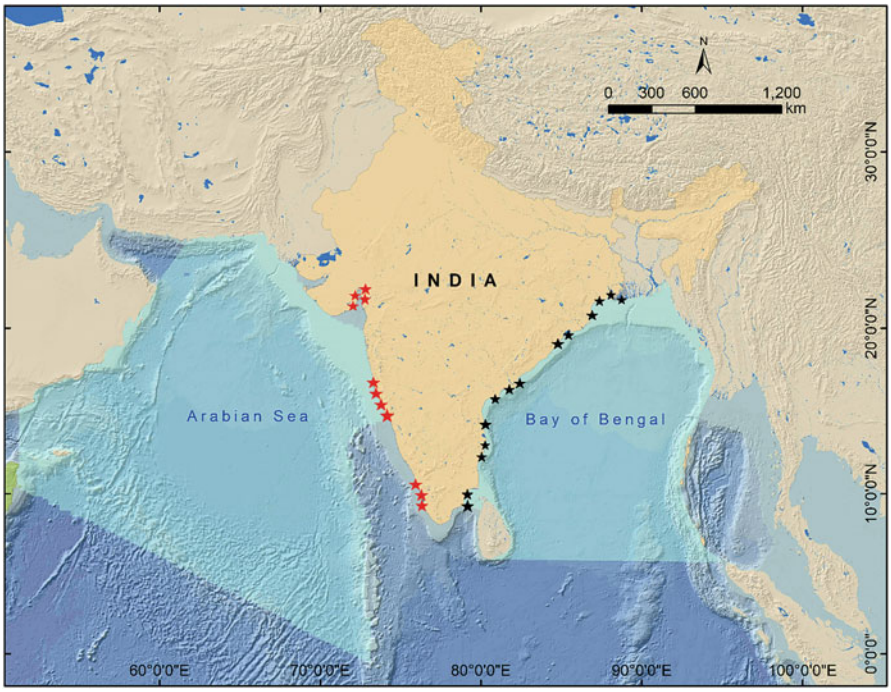

Fig. 2.1 The map showing the locations of the Arabian Sea and the Bay of Bengal. The estuaries on the east and west coasts of India that have been sampled by several researchers are indicated with black and red stars, respectively

processes of the estuaries and continental shelf waters exhibit substantial variability (Krishna et al., 2019) that again gives rise to varying scenarios of phytoplankton and primary productivity dynamics. In this regard, this chapter has collated and discussed the observations made so far on phytoplankton composition and productivity dynamics in the estuaries and continental shelf waters along the Indian coastline and the open oceanic regions of the Arabian Sea and the Bay of Bengal (Fig. 2.1).

2 Phytoplankton Species Assemblage

2.1 Estuarine Phytoplankton Dynamics

Several pieces of endeavors are reported from the Indian estuaries in this regard. The northern limit of the eastern coastline of India shelters the largest continuous mangrove forest in the world, the Sundarbans, shared by Bangladesh. The Ganges River flows into the Bay of Bengal through this region. The principal distributary

that drains the flow of the Ganges into the bay is known as the Hooghly estuary. This estuary along with several mangrove estuaries that intersperse the Sundarbans gives rise to an estuarine complex, popularly known as the Hooghly-Matla estuarine system. This estuarine complex exhibits a wide spectrum of salinity variation and hence harbors a wide variety of phytoplankton in the different water regimes of this region. Roshith et al. (2018) reported a total of 378 phytoplankton species from this estuarine complex, and they observed a predominance of diatoms, followed by blue-green algae, and dinoflagellates. Almost three decades back, De et al. (1994) recorded only 29 species from the Hooghly estuary; however, they also observed a predominance of the diatoms, namely, *Coscinodiscus radiatus* and *Coscinodiscus excentricus*. They also observed that the lack of freshwater discharge within the Sundarban estuaries has led to a comparatively higher dominance of blue-green algae. They further reported that climate change and regional sea-level rise have substantially modified the phytoplankton species composition of this region. However, Dutta et al. (2021) observed that the phytoplankton community in the estuarine water column of Sundarban plays a crucial role in CO_2 uptake in the form of dissolved inorganic carbon (DIC). Dutta et al. (2019a) inferred that respiratory activities of phytoplankton communities could be a potent source of DIC in the Hooghly-Matla estuarine complex. Similar attempts have been taken in the Mahanadi estuary by Naik et al. (2009). Unlike the Hooghly-Matla estuary, Naik et al. (2009) observed much less phytoplankton count in this region (77 species). However, the dominance of diatoms was also observed in this estuary. Contrary to many studies, Naik et al. (2009) observed that diatoms depend on the concentrations of nitrate and ammonium ions, whereas the dinoflagellates showed a significantly positive relation with nitrate and silicate concentrations. They observed that *Asterionella japonica*, *Coscinodiscus gigas*, and *Rhizosolenia alata* are some of the abundant phytoplankton species in the Mahanadi estuary. Bharathi et al. (2018), in this regard, studied the phytoplankton composition in the Godavari estuary draining into the Bay of Bengal along with the east coast of India. They reported the existence of almost 113 species of phytoplankton in this estuary. They observed that anthropogenic nutrient discharge is substantial in this estuary. Moreover, the freshwater discharge varies significantly in this estuary, especially on a seasonal scale. The monsoon-driven rainfall enhances the freshwater discharge significantly, whereas, during the dry seasons of the year, the river flow remains minimal. Bharathi et al. (2018) observed that nutrient abundance along with the stability in the water column together influences the phytoplankton abundance and composition. Acharyya et al. (2012) also observed that monsoon-driven discharge led to an intensification of phytoplankton abundance in this region. Earlier, Sarma et al. (2009) also depicted that riverine freshwater discharge modulated the metabolic rates of the existing phytoplankton composition. Like the other estuaries, diatoms were prevalent in this estuary too. However, the second dominant group that followed was blue-green algae instead of dinoflagellates. Rajkumar et al. (2009) took up a similar endeavor in the Vellar estuary adjoining the Pichavaram mangroves on the east coast of India. They recorded a total of 94 phytoplankton species in this region. Like all other east coast estuaries of India, Rajkumar et al. (2009) also

observed the predominance of diatoms, and they observed a peak in diatom counts during the pre-monsoon months of April and May. The cell counts varied between 400 and >300,000 cells l^{-1}. Rajasekar et al. (2005) carried out a similar endeavor in the Coleroon estuary of Tamil Nadu. They observed a total phytoplankton count of 84 species. Like all the other studies, they also observed dominance of the Bacillariophyceae group, and the peak cell count was observed during summer (pre-monsoon season).

The estuaries on India's west coast draining into the Arabian Sea are mostly not as large as the ones that flow along the east coast. However, there are several small to medium-sized estuaries on this coastline. Desai et al. (1984) were perhaps the first to record the phytoplankton pigments in the Mindola, Ambika, Auranga, and Purna Estuaries on the Gujarat coastline. The Narmada estuary is the most prominent one on the Gujarat coastline. George et al. (2015) studied the phytoplankton assemblages in the Narmada estuarine tract and observed the presence of 31 phytoplankton species. Contrary to the observations in many east coast estuaries of India, George et al. (2015) reported that during low freshwater discharge conditions observed in the pre-monsoon and post-monsoon seasons, the phytoplankton abundance attained its peak. They inferred that the lack of freshwater discharge enhanced the nutrient concentration in the estuarine water column of Narmada. George et al. (2012) also carried out similar endeavors in the second-most important estuary of Gujarat, that is, the Tapi estuary. They observed a total of 66 phytoplankton species in this estuary. The role of freshwater in regulating the phytoplankton abundance was the same as observed in the Narmada estuary. The post-monsoon months showed a higher abundance of phytoplankton, which coincided with the peak in nutrient concentrations. It is worth mentioning that the post-monsoon season signifies the driest season of the calendar year. Bacillariophyceae was the most dominant group followed by Cyanophyceae. The Mandovi-Zuari estuarine system is another well-studied region on India's west coast. Pednekar et al. (2011) recorded 235 phytoplankton species from this estuarine system. They observed a surge in the phytoplankton biomass concentration during the intermonsoon season associated with a sharp decline in salinity. The phytoplankton diversity was highest in the monsoon season and during the dry seasons with an increase in salinity dinoflagellates dominating over the diatoms (Table 2.1).

2.2 *Phytoplankton Dynamics in Continental Shelf Waters*

Continental shelf waters comparatively received lesser attention than inner estuarine reaches, most probably due to difficulty in year-round accessibility as a result of rough and turbulent conditions. The continental shelf waters in many of the Indian coastal peripheral regions are quite shallow, especially on the east coast of India, which reduces the ease of navigability. However, despite these factors, several studies have been carried out in such locations. Akhand et al. (2017) studied the phytoplankton abundance in the continental shelf waters adjoining the Hooghly-

Table 2.1 Crucial observations related to phytoplankton dynamics in the estuaries along the Indian shoreline

Place	Major observation	References
Hooghly-Matla estuary	378 phytoplankton species Diatoms are dominant in estuarine waters Blue-green algae are dominant in estuarine wetlands Climate change and regional sea-level rise led to changes in phytoplankton species composition	Roshith et al. (2018)
Hooghly-Matla estuary and adjoining continental shelf waters	45 phytoplankton species Close to 80% were diatoms Significant deviation from the ideal Redfield ratio	Akhand et al. (2017)
Mahanadi estuary	77 phytoplankton species Diatoms composed more than 80% of the total abundance	Naik et al. (2009)
Mahanadi estuary and adjoining continental shelf waters	116 phytoplankton species Diatoms comprised two-thirds of the total abundance all-round the year Chl-*a* ranged from 0.87 to 1.18 mg m^{-3} Phytoplankton cell count varied between 29,276 and 43,290 cells l^{-1}	Naik et al. (2020a)
Godavari estuary	113 phytoplankton species Diatoms were dominant followed by blue-green algae Freshwater discharge and anthropogenic nutrient concentration controlled the phytoplankton composition	Bharathi et al. (2018)
Vellar estuary	94 phytoplankton species Diatoms were predominant with peak values in pre-monsoon months Cell count oscillated between 400 and 3,20,000 cells l^{-1}	Rajkumar et al. (2009)
Coleroon estuary	84 phytoplankton species Bacillariophyceae group was dominant Peak cell count was observed in the summer months	Rajasekar et al. (2005)
Narmada estuary	31 phytoplankton species Highest abundance in pre-monsoon and post-monsoon seasons	George et al. (2015)
Tapi estuary	66 phytoplankton species Highest abundance in the post-monsoon season Bacillariophyceae and Cyanophyceae were the dominant groups	George et al. (2012)
Mandovi-Zuari estuary	235 phytoplankton species The species count was highest in monsoon but phytoplankton biomass was highest in the post-monsoon season Overall dominance of diatoms, however, dinoflagellates dominated in the dry seasons	Pednekar et al. (2011)

Matla estuarine complex in the northern part of the Bay of Bengal. They recorded a total of 45 phytoplankton species from this region. Close to 80% of the phytoplankton species were diatoms. *Thalassionema frauenfeldi*, *Thalassionema nitzshioides*, and *Coscinodiscus radiatus* were some of the reported species that had a high abundance in this region. They further observed a significant deviation from the ideal Redfield ratio in the waters of this region. Naik et al. (2020a, b) conducted an exhaustive survey in the estuary-to-offshore transition zone of the Mahanadi estuary. They reported a total of 116 phytoplankton species from this region. They observed that diatoms encompass more than 70% of the total phytoplankton abundance followed by dinoflagellates and blue-green algae. They observed a substantial presence of inorganic nitrogenous nutrients that exhibited a positive correlation with phytoplankton cell count that varied between 29,276 and 43,290 cells l^{-1}. The seasonality in the Indian subcontinent can be categorized as monsoon, post-monsoon, and pre-monsoon seasons. They observed peak phytoplankton count in the pre-monsoon season. Madhav and Kondalarao (2004) reported the findings from 12 cruises conducted in the coastal Bay of Bengal all along India's east coast from 1999 to 2002. They observed a total of 249 phytoplankton species in this stretch. Diatom abundance (111 species) was lower than the dinoflagellates (131). This observation was in contrast to that observed within the estuarine regions. The mean phytoplankton density was also quite low (1–367 numbers per liter) compared to that observed in the estuarine water column. The highest species abundance was during the monsoon season recording a total of 193 species. Similar endeavors are reported from the west coast. Harnstrom et al. (2009) carried out a short-term survey in the coastal Arabian Sea off the Mangalore shore and recorded 73 phytoplankton species. They observed an overall abundance of diatoms in the post-monsoon months of December and January. They also noticed a short-term variability in phytoplankton species composition with varying tidal phases. A lower species count was observed during the ebb compared to that in the flood conditions. Parab et al. (2006) carried out one of the most comprehensive monitoring of phytoplankton dynamics in selected locations parallel to the west coast of India. They observed that diatoms, dinoflagellates, and cyanobacteria exhibited a change in species composition and relative abundance with the changing seasons. During the southwest monsoon, diatoms were dominant; however, at the onset of the post-monsoon season, the cyanobacteria population acquired the oxygenated depths in these stations. An overall mixed dominance of both diatoms and dinoflagellates was reported by Parab et al. (2006). However, they noticed occasional blooms of *Trichodesmium erythraeum*, especially during the northeast monsoon phase. They concluded that the enhancing degree of anoxia in the coastal Arabian Sea can lead to an abundance of dinoflagellates over the diatoms soon.

2.3 Phytoplankton Dynamics in Open Oceanic Waters

Several studies have been conducted in the open oceanic realms of the Arabian Sea and the Bay of Bengal adjoining the Indian coastline that characterized the phytoplankton dynamics. Amol et al. (2020) studied the effects of freshwater discharge and upwelling from subsurface layers on the chlorophyll concentrations in the northern Bay of Bengal. They documented that the freshwater plumes furnish adequate nutrients into the open Bay of Bengal and stratify the water column. An apparent increase in chlorophyll levels after the monsoon took place in this region due to the furnishing of nutrient-laden freshwater discharge. However, beyond the shelf boundary, the advective transfer of nutrients from the subsurface layers played a more crucial role in enhancing the chlorophyll concentrations of the northern Bay of Bengal. Biswas et al. (2013) studied the role of copper in regulating the growth of a diatom in the northern Bay of Bengal. Cu, a heavy metal, is exploited in several biogeochemical reactions by phytoplankton; however, the same can be toxic at elevated concentrations. Biswas et al. (2013) observed that anthropogenic Cu draining through the estuaries into the northern Bay of Bengal enables the phytoplankton community to use it, especially under Fe-stressed conditions. Off the Visakhapatnam coastline, Biswas et al. (2017) considered the effect of Zn addition and enhanced CO_2 levels on the existing diatoms. They observed Zn facilitated an enhanced light absorption potential to the diatoms and enhanced CO_2 led to substantially higher primary productivity. They inferred that the increased partial pressure of CO_2 in seawater in this region could have far-reaching biogeochemical consequences.

Recent studies showed that the Arabian Sea is much more prone to bloom formation than the Bay of Bengal. Baliarsingh et al. (2018) comprehensively studied the phytoplankton in the *Noctiluca scintillans* bloom-forming and no-bloom locations in the northern part of the Arabian Sea. They reported that excessive enhancement of diatoms marked the initiation of *Noctiluca scintillans* bloom. Parab and Matondkar (2012) studied the subsurface bloom of *Trichodesmium* spp. all through the Arabian Sea. They reported that this species assemblage produced around 0.263 Tg C and 0.298 Tg N per year. Naik et al. (2020a, b) studied the latitudinal gradient of phytoplankton distribution in the Indian Ocean. They observed that the prokaryotes, dinoflagellates, and diatoms dominated the equatorial, subtropical, and polar regions, respectively. Similarly, Patil et al. (2017) studied the coccolithophore distribution across the latitudinal gradient of the Indian Ocean. They observed the highest abundance of *Emiliania huxleyi* throughout the Indian Ocean. Roy et al. (2015) analyzed the nutrient enrichment and the associated phytoplankton species assemblages in the fronts and filaments of the northeastern Arabian Sea based on which the potential fishing zones are forecasted by India. They observed that optimum nutrient-enriched zones often overlap with the SST fronts where phytoplankton growth becomes maximum. Sarma et al. (2020) suggested that eddies that form in the Bay of Bengal have a crucial role in delineating the phytoplankton species composition. Thus, several aspects have been covered in the recent pieces of research related to phytoplankton dynamics in the open marine waters of the Bay of Bengal and the Arabian Sea.

3 Primary Productivity and Chlorophyll Dynamics

Bharathi and Sarma (2019) carried out exhaustive research on the impact of monsoon on the phytoplankton biomass of the major estuaries. They recorded the chlorophyll-*a* concentrations in 28 estuaries. Figure 2.2 shows the chlorophyll-*a* variability in 26 estuaries. They observed the highest value in the Ambalayaar estuary (160 mg m^{-3}), followed by the Ponnayaar estuary (97 mg m^{-3}). In the remaining estuaries, the chlorophyll-a concentrations were less than 20 mg m^{-3}, according to Bharathi and Sarma (2019). Overall, the estuaries of the east coast exhibited significantly higher chlorophyll-a concentrations than the estuaries situated on the west coast. Akhand et al. (2016) compared the CO_2 dynamics between the freshwater-rich Hooghly estuary and the freshwater-deficient Matla estuary. They reported a chlorophyll-a range of 0.52–4.98 mg m^{-3} and 0.41–3.97 mg m^{-3} in the Hooghly and Matla estuaries, respectively. Pattanaik et al. (2020) observed the maximum chlorophyll-a concentration of 5.07 ± 1.85 mg m^{-3} and 5.29 ± 1.43 mg m^{-3} in the Mahanadi and Dhamra estuaries, respectively, during the initial months of monsoon season. Sarma et al. (2010) observed a wide range of chlorophyll-a concentrations (0.5–16 mg m^{-3}) in the Gautami-Godavari estuarine system. They observed the maximum chlorophyll-a concentration at the end of the monsoon season when the turbidity load dropped substantially. Down south on the east coast of India, the Vellar-Coleroon estuary, lying adjacent to the Pichavaram mangroves, was sampled by Senthilkumar et al. (2008). They observed a mean

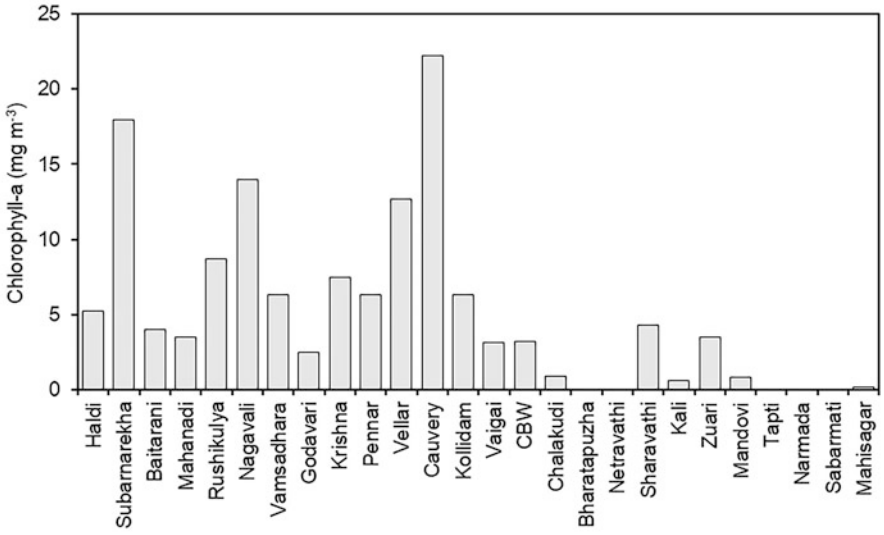

Fig. 2.2 Mean chlorophyll-a concentration observed in 26 estuaries on the Indian coastline. (Data retrieved from Bharathi and Sarma (2019))

chlorophyll-a concentration of 8.6 ± 3.4 mg m^{-3} and 11.4 ± 3.2 mg m^{-3} in the dry season and wet season, respectively. On the west coast, Lallu et al. (2014) reported a chlorophyll-a concentration range of 5.0–18.6 mg m^{-3} in the backwaters of Cochin estuary. Krishnakumari et al. (2002) reported a chlorophyll-a concentration range of 0.01–4.33 mg m^{-3} and 0.16–3.95 mg m^{-3} in the Mandovi and Zuari estuaries, respectively, draining into the Arabian Sea.

A pertinent biogeochemical parameter that is closely associated with chlorophyll-a concentration is primary productivity. The gross primary productivity reflects light on the rate of biological CO_2 uptake by the autotrophic community in the marine water column, which has far-reaching consequences and manifestations on the global climate. Overall, all the estuaries emit CO_2 toward the atmosphere and show net heterotrophic conditions. The degree of net heterotrophy varies among the estuaries. Dutta et al. (2019b) mentioned that phytoplankton productivity is one of the key mechanisms through which DIC is exported out of the estuaries to the nearshore coastal waters. Mukherjee et al. (2019), while working in the Chilika lagoon, observed that the phytoplankton community composition plays a crucial role in regulating the nitrogen uptake too from the dissolved inorganic nitrogen forms available in these water bodies. The high turbidity and light limitation in the monsoon phase led to an enhanced degree of net heterotrophy in most of the Indian estuaries. The turbid waters lead to a reduction of the photosynthetic potential of the water column. Due to such inhibition, the community respiration supersedes the gross primary production and leads to a net emission of CO_2 from these estuaries. Several studies have focused on this critical parameter in the open oceanic domain of the Bay of Bengal and the Arabian Sea. Barber et al. (2001) monitored the primary production rate in the open Arabian Sea and observed that during the southwest monsoon (123 ± 9 mmol C m^{-2} d^{-1}) and the northeast monsoon (112 ± 7 mmol C m^{-2} d^{-1}) seasons the productivity was substantially higher than the rest of the year. Böll et al. (2014) observed that during the late Holocene phase declining sea surface temperature in the Arabian Sea elevated the primary production rate. Madhupratap et al. (2003) exhaustively measured the phytoplankton primary production rate in the Bay of Bengal and reported much lower values than that observed in the Arabian Sea. Madhupratap et al. (2003) and several other studies pointed out that the Bay of Bengal though receives substantial freshwater from the perennial estuaries that drain into it, the amount of nutrients received is not high enough to promote productivity levels close to that in the Arabian sea. In the Arabian Sea, the upwelling of colder nutrient-rich water leads to an elevated degree of new autochthonous production. Bhavya et al. (2017), while working in the estuarine and offshore stations of the Cochin estuary, observed a much higher range of primary productivity within the estuarine reaches (2.5–20.4 μmol C l^{-1} h^{-1}) compared to that observed in the offshore waters of the Arabian Sea (0.007–3.1 μmol C l^{-1} h^{-1}). Krishnakumari et al. (2002) reported a GPP range of 0.012–1.31 mg C l^{-1} d^{-1} and 0.005–1.62 mg C l^{-1} d^{-1} in the Mandovi and Zuari estuaries, respectively, draining into the Arabian Sea. Pattanaik et al. (2020), while working in the adjacent Mahanadi and Dhamra estuaries draining into the Bay of Bengal, observed the highest gross

primary productivity (GPP) and net primary productivity (NPP) of 1.5 ± 0.6 mg C l^{-1} d^{-1} and 1.2 ± 0.4 mg C l^{-1} d^{-1}, respectively, in Mahanadi, and 1.6 ± 0.4 mg C l^{-1} d^{-1} and 1.3 ± 0.2 mg C l^{-1} d^{-1}, respectively, in Dhamra estuary. They observed these highest values during the summer months that almost coincided with the highest observed chlorophyll-a concentrations in their study. Akhand et al. (2021) reported a GPP range of 2.4–8.64 mg C l^{-1} d^{-1} while working in the Matla estuary. Choudhury and Pal (2012) reported a GPP range of 1.4–-5.4 mg C l^{-1} d^{-1} in the Hooghly estuary, working all around the year. The lowest productivity was observed in the monsoon months of August and the highest in the post-monsoon month of December. Sarma et al. (2009) reported a mean GPP of 33.5 mmol C m^{-2} d^{-1} in the Godavari estuary. Senthilkumar et al. (2008) observed a much lower mean GPP of 0.025 mmol C m^{-2} d^{-1} and 0.033 mmol C m^{-2} d^{-1} in the dry and wet season, respectively, in the Vellar-Coleroon estuary in the south of India's east coast. In the same Vellar estuary, Kawabata et al. (1993) reported a GPP range of 32–49 mg C m^{-3} h^{-1}; however, it is difficult to compare the two magnitudes as interconversion between these two units requires additional parameters that are absent in the reviewed literature.

4 Role of Nutrients in Governing Phytoplankton Dynamics

Availability of nutrients has an important role in the phytoplankton community structure and phytoplankton succession (Smayda, 1980). Tilman et al. (1982) described how nutrient and/or nutrient supply would be a limiting factor for the enrichment of phytoplankton in the marine system. However, in the western and central Bay of Bengal, higher nutrient concentration indicates greater phytoplankton richness (Paul et al., 2008). According to Redfield et al. (1963), for the strong flourishment of phytoplankton, the atomic N, Si, and P ratio within the cell should be about 16:16:1. Deviances from these ratios indicated nutrient-limited phytoplankton growth (Dortch & Whitledge, 1992). The limiting nutrient concentration not only varies with phytoplankton community structure but also with location and seasons (Fisher et al., 1992). Howarth (1988) described that nitrogen (N) limitation conquers most of the marine area of the World's Oceans. But Das et al. (2017) documented that the northern Bay of Bengal was phosphorus (P) limited in terms of chl-*a* abundance in the post-monsoon season. Previous studies (Parsons et al., 1961; Harrison et al., 1977; Brzezinski, 1985) indicate that when the adjoining ratios of dissolved N:P are less than 10 and the N:Si ratio is greater than 1, it indicates potential N limitation whereas N:Si is greater than 1 and Si:P ratio less than 3 are revealing of Si limitation. Therefore, N:Si:P ratios are convenient to predict the phytoplankton assemblages. Identifying the limiting nutrient acts as an important tool to understand the phytoplankton ecology. However, quantifying the N, Si, P ratios in the marine system and their influence on the phytoplankton can deliver signals for probable growth limitations.

5 Role of Freshwater Discharge in Regulating Phytoplankton Dynamics

Higher rainfall may increase the freshwater discharge to the coastal area. Increased discharge may be lowering the overall coastal water salinity. Connected discharge of dissolved organic carbon and nutrients may influence the phytoplankton dynamics or primary producers, finally altering the food web functioning (Wikner & Andersson, 2012). Most estuaries in the world including Indian estuaries are often described as net heterotrophic (Sandberg et al., 2004). Increased dissolved organic carbon may cause higher phytoplankton biomass generation (Pengerud et al., 1987; Barrera-Alba et al., 2009). Higher discharge may also affect the stratification process of the water column, causing a change in the vertical circulation of phytoplankton (Jager et al., 2008). Moreover, an increase in suspended matter and chromophoric dissolved organic matter may decrease the light availability in the water layers and result in a change in the taxonomic composition of phytoplankton assemblages (Hessen et al., 2010). Das et al. (2017) showed the higher chl-a concentration during monsoon season (higher discharge from Hugli River) in the northern Bay of Bengal.

6 Scope of Future Research

Substantial work has been done so far characterizing the species composition and the spatiotemporal variability of the phytoplankton species assemblage in the nearshore coastal waters as well as in the open Bay of Bengal and the Arabian Sea. However, increased endeavors are required to understand the probable future behavior of these phytoplankton communities under different scenarios of climate change. The marine domain of not only these two regions discussed in this study but of the entire world is experiencing and about to experience certain notable changes due to the anthropogenic effects on the overall environment of mother Earth. The sea surface temperature is expected to rise coupled with a rise in the ambient CO_2 concentration. Global warming-induced enhanced melting of polar ice caps and glaciers can bring about changes in the salinity levels too in various parts of the world. Moreover, several research endeavors in the present date have indicated that climate change induces the introduction and proliferation of alien invasive species that hampers the native ecological structure of a marine domain. The presence and functioning of these species within a natural marine ecosystem should be closely monitored and their overall effect on the ecosystem's functioning should be gauged. Thus, these future scenarios should be perceived and efforts should be taken to understand how the phytoplankton community is most likely going to respond to such changes. Most essentially, we would have to develop a solid understanding of whether these changes would provide positive or negative feedback to the ongoing climate change. Thus, mesocosm and microcosm experiments on phytoplankton communities keeping in view changing climate scenarios are perhaps the most essential needs of the hour.

7 Summary and Conclusion

A gross review of the literature indicates that the two northern flanks of the Indian Ocean have received substantial attention from the scientific community regarding the phytoplankton abundance, species assemblage, and their seasonal and spatial variability. Overall, the diatoms were dominant in the estuarine reaches; however, in the nearshore to offshore environment, dinoflagellates and blue-green algae have shown mixed dominance (Fig. 2.3). The eastern coast of India has several perennial estuaries. The northern sector of this coastline exhibited a significantly higher number of phytoplankton species than those that lie in the south. The chlorophyll-a concentrations also exhibited a marked difference between the east coast and the west coast. The east coastal estuaries had significantly higher values of chlorophyll-a than those of the west coast. Several studies indicated that the monsoon-induced freshwater discharge and frequent atmospheric physical forcing events like tropical cyclones play a crucial role in enhancing the phytoplankton abundance and simultaneously changing the species composition in the nearshore coastal waters and the estuarine reaches. More endeavors are required to study the response of the existing phytoplankton community to the changing climate scenario and growing level of pollution in the marine sector.

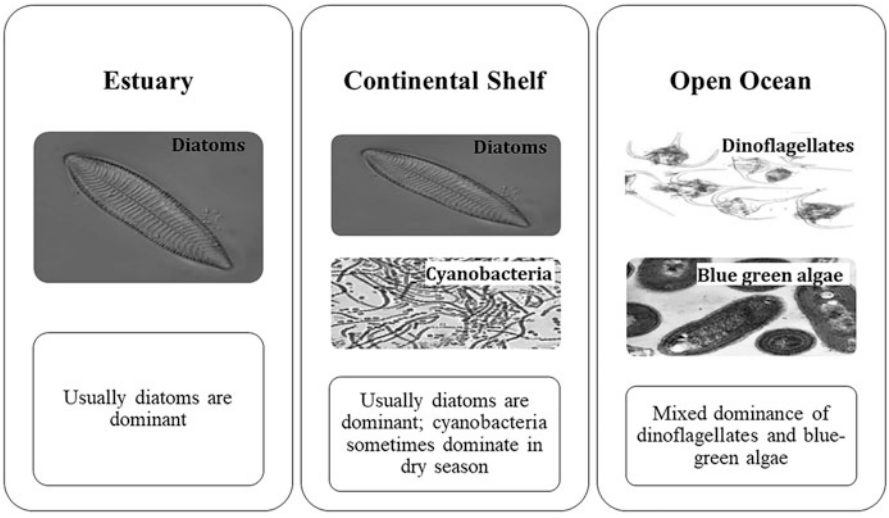

Fig. 2.3 The phytoplankton composition in the estuarine regions, continental shelves, and open oceanic regions adjoining the Indian coastline as observed from multiple studies

References

Acharyya, T., Sarma, V. V. S. S., Sridevi, B., Venkataramana, V., Bharathi, M. D., Naidu, S. A., et al. (2012). Reduced river discharge intensifies phytoplankton bloom in Godavari estuary, India. *Marine Chemistry, 132*, 15–22.

Akhand, A., Chanda, A., Manna, S., Das, S., Hazra, S., Roy, R., Choudhury, S. B., Rao, K. H., Dadhwal, V. K., Chakraborty, K., Mostofa, K. M. G., Tokoro, T., Kuwae, T., & Wanninkhof, R. (2016). A comparison of CO_2 dynamics and air-water fluxes in a river-dominated estuary and a mangrove-dominated marine estuary. *Geophysical Research Letters, 43*(22), 11–726.

Akhand, A., Chanda, A., Dutta, S., Manna, S., Giri, S., Das, S., et al. (2017). Microphytoplankton species assemblages, species-specific carbon stock, and nutrient stoichiometry in the shallow continental shelf of the northern Bay of Bengal during winter. *Indian Journal of Marine Sciences, 46*(9), 1827–1835.

Akhand, A., Chanda, A., Watanabe, K., Das, S., Tokoro, T., Hazra, S., & Kuwae, T. (2021). Reduction in riverine freshwater supply changes inorganic and organic carbon dynamics and air-water CO2 fluxes in a tropical mangrove dominated estuary. *Journal of Geophysical Research: Biogeosciences, 126*(5), e2020JG006144.

Amol, P., Vinayachandran, P. N., Shankar, D., Thushara, V., Vijith, V., Chatterjee, A., & Kankonkar, A. (2020). Effect of freshwater advection and winds on the vertical structure of chlorophyll in the northern Bay of Bengal. *Deep Sea Research Part II: Topical Studies in Oceanography, 179*, 104622.

Baliarsingh, S. K., Lotliker, A. A., Sudheesh, V., Samanta, A., Das, S., & Vijayan, A. K. (2018). Response of phytoplankton community and size classes to green Noctiluca bloom in the northern Arabian Sea. *Marine Pollution Bulletin, 129*(1), 222–230.

Barber, R. T., Marra, J., Bidigare, R. C., Codispoti, L. A., Halpern, D., Johnson, Z., et al. (2001). Primary productivity and its regulation in the Arabian Sea during 1995. *Deep Sea Research Part II: Topical Studies in Oceanography, 48*(6–7), 1127–1172.

Barrera-Alba, J. J., Gianesella, S. M. F., Moser, G. A. O., & Saldanha-Correa, F. M. (2009). Influence of allochthonous organic matter on bacterioplankton biomass and activity in a eutrophic, sub-tropical estuary. *Estuarine, Coastal and Shelf Science, 82*, 84–94.

Bharathi, M. D., & Sarma, V. V. S. S. (2019). Impact of monsoon-induced discharge on phytoplankton community structure in the tropical Indian estuaries. *Regional Studies in Marine Science, 31*, 100795.

Bharathi, M. D., Sarma, V. V. S. S., & Ramaneswari, K. (2018). Intra-annual variations in phytoplankton biomass and its composition in the tropical estuary: Influence of river discharge. *Marine Pollution Bulletin, 129*(1), 14–25.

Bhavya, P. S., Kumar, S., Gupta, G. V. M., & Sudheesh, V. (2017). Carbon uptake rates in the Cochin estuary and adjoining coastal Arabian Sea. *Estuaries and Coasts, 40*(2), 447–456.

Biswas, H., Bandyopadhyay, D., & Waite, A. (2013). Copper addition helps alleviate iron stress in a coastal diatom: Response of *Chaetoceros gracilis* from the Bay of Bengal to experimental Cu and Fe addition. *Marine Chemistry, 157*, 224–232.

Biswas, H., Shaik, A. U. R., Bandyopadhyay, D., & Chowdhury, N. (2017). CO2 induced growth response in a diatom dominated phytoplankton community from SW Bay of Bengal coastal water. *Estuarine, Coastal and Shelf Science, 198*, 29–42.

Böll, A., Lückge, A., Munz, P., Forke, S., Schulz, H., Ramaswamy, V., et al. (2014). Late Holocene primary productivity and sea surface temperature variations in the northeastern Arabian Sea: Implications for winter monsoon variability. *Paleoceanography, 29*(8), 778–794.

Brzezinski, M. A. (1985). The Si:C:N ratio of marine diatoms: Interspecific variability and the effect of some environmental variables. *Journal of Phycology, 21*, 347–357.

Choudhury, A. K., & Pal, R. (2012). Understanding the seasonal dynamics of primary productivity in relation to phytoplankton populations from the Bhagirathi–Hooghly estuary, eastern Indian coast. *Journal of Algal Biomass Utilization, 3*(4), 80–88.

Das, S., Giri, S., Das, I., Chanda, A., Ghosh, A., Mukhopadhyay, A., et al. (2017). Nutrient dynamics of northern Bay of Bengal (nBoB)—Emphasizing the role of tides. *Regional Studies in Marine Science, 10*, 116–134.

De, T. K., Choudhury, A., & Jana, T. K. (1994). Phytoplankton community organization and species diversity in the Hugli estuary, northeast coast of India. *Indian Journal of Marine Sciences, 23*, 152–156.

Desai, B. N., Ram, M. J., Abidi, S. A. H., & Nair, V. R. (1984). Distribution of phytoplankton pigments in Auranga, Ambika, Purna, and Mindola estuaries of Gujarat. *Mahasagar, 17*(2), 79–87.

Dortch, Q., & Whitledge, T. E. (1992). Does nitrogen or silicon limit phytoplankton production in the Mississippi River plume and nearby regions? *Continental Shelf Research, 12*, 1293–1309.

Dutta, M. K., Kumar, S., Mukherjee, R., Sharma, N., Acharya, A., Sanyal, P., Bhusan, R., & Mukhopadhyay, S. K. (2019a). Diurnal carbon dynamics in a mangrove-dominated tropical estuary (Sundarbans, India). *Estuarine, Coastal and Shelf Science, 229*, 106426.

Dutta, M. K., Kumar, S., Mukherjee, R., Sanyal, P., & Mukhopadhyay, S. K. (2019b). The post-monsoon carbon biogeochemistry of the Hooghly–Sundarbans estuarine system under different levels of anthropogenic impacts. *Biogeosciences, 16*(2), 289–307.

Dutta, M. K., Kumar, S., Mukherjee, R., Sharma, N., Bhusan, R., Sanyal, P., Paul, M., & Mukhopadhyay, S. K. (2021). Carbon biogeochemistry of two contrasting tropical estuarine ecosystems during premonsoon. *Estuaries and Coasts, 44*, 1916–1930.

Fisher, T. R., Peele, E. R., Ammerman, J. W., & Harding, L. W., Jr. (1992). Nutrient limitation of phytoplankton in Chesapeake Bay. *Marine Ecology Progress Series, 82*, 51–63.

George, B., Kumar, J. N., & Kumar, R. N. (2012). Study on the influence of hydro-chemical parameters on phytoplankton distribution along Tapi estuarine area of Gulf of Khambhat, India. *The Egyptian Journal of Aquatic Research, 38*(3), 157–170.

George, B., Nirmal Kumar, J. I., & Kumar, R. N. (2015). An evaluation of phytoplankton assemblage in relation to environmental variables of Narmada Estuarine Region of Gulf of Khambhat, Gujarat, India. *Applied Ecology and Environmental Research, 13*(1), 115–131.

Harnstrom, K., Karunasagar, I., & Godhe, A. (2009). Phytoplankton species assemblages and their relationship to hydrographic factors—A study at the old port in Mangalore, coastal Arabian Sea. *Indian Journal of Marine Sciences, 38*(2), 224–234.

Harrison, P. J., Conway, H. L., Holmes, R. W., & Davis, C. O. (1977). Marine diatoms in chemostats under silicate or ammonium limitation. III. Cellular chemical composition and morphology of three diatoms. *Marine Biology, 43*, 19–31.

Hessen, D. O., Carroll, J., Kjeldstad, B., Korosov, A. A., Pettersson, L. H., Pozdnyakov, D., & Sorensen, K. (2010). Input of organic carbon as determinant of nutrient fluxes, light climate and productivity in the Ob and Yenisey estuaries. *Estuarine, Coastal and Shelf Science, 88*, 53–62.

Howarth, R. W. (1988). Nutrient limitation of net primary production in marine ecosystems. *Annual Review of Ecology and Systematics, 19*, 89–110.

Jager, C. G., Diehl, S., & Schmidt, G. M. (2008). Influence of water-column depth and mixing on phytoplankton biomass, community composition, and nutrients. *Limnology and Oceanography, 53*, 2361–2373.

Karati, K. K., Ashadevi, C. R., Harikrishnachari, N. V., Valliyodan, S., Kumaraswami, M., Naidu, S. A., & Ramanamurthy, M. V. (2021). Hydrodynamic variability and nutrient status structuring the mesozooplankton community of the estuaries along the west coast of India. *Environmental Science and Pollution Research, 28*, 42477–42495.

Kawabata, Z., Magendran, A., Palanichamy, S., Venugopalan, V. K., & Tatsukawa, R. (1993). Phytoplankton biomass and productivity of different size fractions in the Vellar estuarine system, southeast coast of India. *Indian Journal of Marine Sciences, 22*, 294–296.

Krishna, M. S., Viswanadham, R., Prasad, M. H., Kumari, V. R., & Sarma, V. V. (2019). Export fluxes of dissolved inorganic carbon to the northern Indian Ocean from the Indian monsoonal rivers. *Biogeosciences, 16*(2), 505–519.

Krishnakumari, L., Bhattathiri, P. M. A., Matondkar, S. G. P., & John, J. (2002). Primary productivity in Mandovi-Zuari estuaries in Goa. *Journal of the Marine Biological Association of India, 44*, 1–13.

Krishnan, S., Patil, J. S., & Anil, A. C. (2022). Benthic-pelagic coupling assessed using phytoplankton marker pigments: A case study from the Paradip port, East Coast of India. *Environmental Science and Pollution Research, 29*, 27761–27778.

Lallu, K. R., Fausia, K. H., Vinita, J., Balachandran, K. K., Naveen Kumar, K. R., & Rehitha, T. V. (2014). Transport of dissolved nutrients and chlorophyll a in a tropical estuary, southwest coast of India. *Environmental Monitoring and Assessment, 186*(8), 4829–4839.

Madhav, V. G., & Kondalarao, B. (2004). Distribution of phytoplankton in the coastal waters of the east coast of India. *Indian Journal of Marine Sciences, 33*(3), 262–268.

Madhupratap, M., Gauns, M., Ramaiah, N., Kumar, S. P., Muraleedharan, P. M., De Sousa, S. N., et al. (2003). Biogeochemistry of the Bay of Bengal: Physical, chemical, and primary productivity characteristics of the central and western Bay of Bengal during summer monsoon 2001. *Deep Sea Research Part II: Topical Studies in Oceanography, 50*(5), 881–896.

Mukherjee, R., Kumar, S., & Muduli, P. R. (2019). Spatial variation of nitrogen uptake rates in the largest brackish water lagoon of Asia (Chilika, India). *Estuarine, Coastal and Shelf Science, 216*, 87–97.

Naik, S., Acharya, B. C., & Mohapatra, A. (2009). Seasonal variations of phytoplankton in Mahanadi estuary, east coast of India. *Indian Journal of Marine Sciences, 38*(2), 184–190.

Naik, R. K., George, J., Soares, M., Anilkumar, N., Mishra, R. K., Roy, R., et al. (2020a). Observations of surface water phytoplankton community in the Indian Ocean: A transect from tropics to polar latitudes. *Deep Sea Research Part II: Topical Studies in Oceanography, 178*, 104848.

Naik, S., Mishra, R. K., Panda, U. S., Mishra, P., & Panigrahy, R. C. (2020b). Phytoplankton community response to environmental changes in Mahanadi estuary and its adjoining coastal waters of Bay of Bengal: A multivariate and remote sensing approach. *Remote Sensing in Earth Systems Sciences, 3*(1), 110–122.

Ota, Y., Kawahata, H., Kuroda, J., Suzuki, A., Abe-Ouchi, A., Jimenez-Espejo, F. J., & Nghp, J. (2022). Millennial-scale variability of Indian summer monsoon constrained by the western Bay of Bengal sediments: Implication from geochemical proxies of sea surface salinity and river runoff. *Global and Planetary Change, 208*, 103719.

Parab, S. G., & Matondkar, S. G. P. (2012). Primary productivity and nitrogen fixation by Trichodesmium spp. in the Arabian Sea. *Journal of Marine Systems, 105*, 82–95.

Parab, S. G., Matondkar, S. P., Gomes, H. D. R., & Goes, J. I. (2006). Monsoon driven changes in phytoplankton populations in the eastern Arabian Sea as revealed by microscopy and HPLC pigment analysis. *Continental Shelf Research, 26*(20), 2538–2558.

Parsons, T. R., Stephens, K., & Stickland, J. D. H. (1961). On the chemical composition of eleven species of marine phytoplankters. *Journal of the Fisheries Research Board of Canada, 18*, 1001–1610.

Patil, S. M., Mohan, R., Shetye, S. S., Gazi, S., Baumann, K. H., & Jafar, S. (2017). Biogeographic distribution of extant Coccolithophores in the Indian sector of the Southern Ocean. *Marine Micropaleontology, 137*, 16–30.

Pattanaik, S., Chanda, A., Sahoo, R. K., Swain, S., Satapathy, D. R., Panda, C. R., Choudhury, S. B., & Mohapatra, P. K. (2020). Contrasting intra-annual inorganic carbon dynamics and air-water CO_2 exchange in Dhamra and Mahanadi estuaries of northern Bay of Bengal, India. *Limnology, 21*(1), 129–138.

Paul, J. T., Ramaiah, N., & Sardessai, S. (2008). Nutrient regimes and their effect on distribution of phytoplankton in the Bay of Bengal. *Marine Environmental Research, 66*(3), 337–344.

Pednekar, S. M., Matondkar, S. P., Gomes, H. D. R., Goes, J. I., Parab, S., & Kerkar, V. (2011). Fine-scale responses of phytoplankton to freshwater influx in a tropical monsoonal estuary following the onset of southwest monsoon. *Journal of Earth System Science, 120*(3), 545.

Pengerud, B., Skjoldal, E. F., & Thingstad, F. (1987). The reciprocal interaction between degradation of glucose and ecosystem structure. Studies in mixed chemostat cultures of marine bacteria, and bacterivorous nanoflagellates. *Marine Ecology-Progress Series, 35*, 111–117.

Rajasekar, K. T., Peramal, P., & Santhanam, P. (2005). Phytoplankton diversity in the Coleroon estuary, southeast coast of India. *Journal of the Marine Biological Association of India, 47*, 127–132.

Rajkumar, M., Perumal, P., Ashok Prabu, V., Vengadesh Perumal, N., & Thillai Rajasekar, K. (2009). Phytoplankton diversity in Pichavaram mangrove waters from south-east coast of India. *Journal of Environmental Biology, 30*(4), 489–498.

Redfield, A. C., Ketchum, B. H., & Richards, A. (1963). The influence of organisms on the composition of sea water. In M. M. Hill (Ed.), *The sea* (Vol. 2, pp. 26–77). Interscience.

Roshith, C. M., Meena, D. K., Manna, R. K., Sahoo, A. K., Swain, H. S., Raman, R. K., et al. (2018). Phytoplankton community structure of the Gangetic (Hooghly-Matla) estuary: Status and ecological implications in relation to eco-climatic variability. *Flora, 240*, 133–143.

Roy, R., Chitari, R., Kulkarni, V., Krishna, M. S., Sarma, V. V. S. S., & Anil, A. C. (2015). CHEMTAX-derived phytoplankton community structure associated with temperature fronts in the northeastern Arabian Sea. *Journal of Marine Systems, 144*, 81–91.

Rusanov, A. G., Bíró, T., Kiss, K. T., Buczkó, K., Grigorszky, I., Hidas, A., et al. (2022). Relative importance of climate and spatial processes in shaping species composition, functional structure and beta diversity of phytoplankton in a large river. *Science of the Total Environment, 807*, 150891.

Sandberg, J., Andersson, A., Johansson, S., & Wikner, J. (2004). Pelagic food web and carbon budget in the northern Baltic Sea: Potential importance of terrigenous carbon. *Marine Ecology-Progress Series, 268*, 13–29.

Sarma, V. V. S. S., Gupta, S. N. M., Babu, P. V. R., Acharya, T., Harikrishnachari, N., Vishnuvardhan, K., et al. (2009). Influence of river discharge on plankton metabolic rates in the tropical monsoon driven Godavari estuary, India. *Estuarine, Coastal and Shelf Science, 85*(4), 515–524.

Sarma, V. V. S. S., Prasad, V. R., Kumar, B. S. K., Rajeev, K., Devi, B. M. M., Reddy, N. P. C., Sarma, V. V., & Kumar, M. D. (2010). Intra-annual variability in nutrients in the Godavari estuary, India. *Continental Shelf Research, 30*(19), 2005–2014.

Sarma, V. V. S. S., Rajula, G. R., Durgadevi, D. S. L., Kumar, G. S., & Loganathan, J. (2020). Influence of eddies on phytoplankton composition in the Bay of Bengal. *Continental Shelf Research, 208*, 104241.

Sauterey, B., & Ward, B. A. (2022). Environmental control of marine phytoplankton stoichiometry in the North Atlantic Ocean. *Proceedings of the National Academy of Sciences, 119*(1), e2114602118.

Senthilkumar, B., Purvaja, R., & Ramesh, R. (2008). Seasonal and tidal dynamics of nutrients and chlorophyll a in a tropical mangrove estuary, southeast coast of India. *Indian Journal of Marine Sciences, 37*(2), 132–140.

Smayda, T. J. (1980). Phytoplankton species succession. In I. Morris (Ed.), *The physiological ecology of phytoplankton* (pp. 493–570). University of California Press.

Tilman, D., Kilham, S. S., & Kilham, P. (1982). Phytoplankton community ecology: The role of limiting nutrients. *Annual Review of Ecological Systems, 13*, 349–372.

Waga, H., Fujiwara, A., Hirawake, T., Suzuki, K., Yoshida, K., Abe, H., & Nomura, D. (2022). Primary productivity and phytoplankton community structure in surface waters of the western subarctic Pacific and the Bering Sea during summer with reference to bloom stages. *Progress in Oceanography, 201*, 102738.

Wikner, J., & Andersson, A. (2012). Increased freshwater discharge shifts the trophic balance in the coastal zone of the northern Baltic Sea. *Global Change Biology, 18*(8), 2509–2519.

Wu, Y., Guo, P., Su, H., Zhang, Y., Deng, J., Wang, M., & Zhang, X. (2022). Seasonal and spatial variations in the phytoplankton community and their correlation with environmental factors in the Jinjiang River estuary in Quanzhou, China. *Environmental Monitoring and Assessment, 194*(1), 1–13.

Zhang, C., Chu, Q., Yingchun, M., Yao, X., & Gao, H. (2022). Weakened fertilization impact of anthropogenic aerosols on marine phytoplankton—A comparative analysis of dust and haze particles. *Ecotoxicology and Environmental Safety, 230*, 113162.

Chapter 3
Seasonal and Inter-annual Variations in Primary Productivity Proxies (POC and Chlorophyll-*a*): A Study from Kalpakkam Coast, Bay of Bengal

A. K. Mohanty, Gouri Sahu, R. S. Sathishkumar, M. K. Samantara, K. D. Arunachalam, and V. Subramanian

Abstract An investigation was carried out in the Kalpakkam coastal waters, Tamilnadu, south-western Bay of Bengal mainly to find out the phytoplankton productivity and primary productivity potential of the coastal waters and its variations in terms of proxies such as chlorophyll-a (chl-a) and particulate organic carbon (POC). A long-term comparison of hydrobiological properties of the coastal waters was carried out for two data sets collected during 2006–2009 and 2019–2022. Most of the N:P values in the present study remained below 16, indicating the nitrogen limitation at this location. The ratio further decreased in recent times compared to the values a decade earlier. Chl-*a* concentrations recorded (range 0.60–4.98 mg m^{-3}) in the present study showed the following order of abundance: pre-monsoon > post-monsoon > monsoon. The two-way ANOVA clearly showed that the chl-a variations were significant with respect to seasons as well as different study periods. Concentrations of POC ranged from 92 to 275 mg m^{-3} during 2006–2009 and 108 to 229 mg m^{-3} during 2019–2022. Relatively high POC content was observed during pre-monsoon season, and low values were recorded during monsoon seasons, which followed the trend of chl-a. Its strong positive correlation with salinity and chl-a indicated that POC concentrations were mainly regulated by the phytoplankton production during the high saline months. A marginal decrease in the POC content of coastal waters at this location has been noticed in recent times as compared to the values obtained a decade earlier. Multi-dimensional scaling (MDS) with cluster overlay indicated that the two sampling periods, that is, 2006–2009 and

A. K. Mohanty (✉) · G. Sahu · M. K. Samantara · V. Subramanian
Radiological and Environmental Safety Division, Indira Gandhi Centre Atomic Research, Kalpakkam, India
e-mail: ajit@igcar.gov.in

R. S. Sathishkumar
National Center for Coastal Research, Chennai, India

K. D. Arunachalam
Centre for Environmental Nuclear Research, SRMIST, Chennai, India

S. C. Tripathy, A. Singh (eds.), *Dynamics of Planktonic Primary Productivity in the Indian Ocean*, https://doi.org/10.1007/978-3-031-34467-1_3

2019–2022 remained separated from each other with respect to the seasonal distribution of primary production. The biota-environment (BIOENV) analysis (with combinations of ten variables) indicated that a set of parameters such as pH, salinity, nitrate, ammonia, and phosphate is associated with the chl-*a* and POC. Salinity and/or nitrate were the key parameters influencing the primary productivity, as these variables were present in every combination of BEST (Bio-Env-Stepwise) results.

Keywords POC · Chlorophyll-a · Primary productivity · Coastal waters · Bay of Bengal

1 Introduction

Primary production (PP) is the process of the creation of new organic biomass from abiotic components, and the organic matter produced in this process acts as the basis of the marine food chain/web. Photosynthesis by autotrophs is generally known as PP in which light energy is utilized to synthesize chemical energy. PP in the marine environment is mainly dependent on macrophytes and phytoplankton. Though people are more familiar with the larger marine plants such as sea grasses and macro-algae (seaweeds), about 90% of marine PP is carried out by phytoplankton, the free-floating microscopic plants. It has been predicted that marine phytoplankton biomass produces 50% of the world's oxygen (Roach, 2004; Lin et al., 2003). The total quantity of organic matter produced by autotrophs is known as gross primary productivity (GP), or total production. However, a part of this synthesized organic material is consumed by the primary producers itself in the process of respiration (R). Thus, the leftover organic matter, which is utilized by the secondary and tertiary producers, is known as net production (NP) (GP-R = NP). GP is generally categorized into two parts, namely, regenerated production and new production. PP that takes place with the help of nutrients from external sources and processes, such as ocean currents and upwelling, is called new production. Whereas, regenerated production is a result of nutrient recycling within an ecosystem. Globally, oceanic productivity is comparable to terrestrial productivity. Though the autotrophic biomass accountable for PP in the marine environment is only about 1–2 billion metric tons, the net production is about 35–50 billion metric tons per year. In comparison, the terrestrial autotroph biomass of 600–1000 billion metric tons produces about 50–70 billion tons of organic matter per year (Webb, 2020). Therefore, oceanic production is almost similar to terrestrial production, albeit it is done in the marine environment with a fraction of the autotroph biomass compared to the terrestrial ecosystem. A short life span and rapid energy transfer in the marine food web as compared to the long-living plants in the terrestrial ecosystems could be the reason for such observation.

Biological production is an essential factor in any ecosystem and more so in marine environments, which determines the ecosystem functioning and controls the nutrient cycles and distribution of various elements. Single-celled phytoplankton are the chief autotrophs responsible for primary productivity which are distributed

mainly in the surface mixed layer. Among the various groups of phytoplankton, some groups, such as siliceous diatoms and calcareous coccolithophores, synthesize frustules or tests incorporating various elements. The fluxes of these siliceous frustules or calcite liths are often used as proxies for productivity measurements (Kinkel et al., 2000; Rageneau et al., 2000). During the Paleozoic and early Mesozoic periods, the marine sediment mainly originated from radiolarians known as radiolarites (Algeo et al., 2010). Formation of sediment by mineralized phytoplankton was not common until the Triassic period, and phytoplankton tests only became the major contributor to the marine sediment during the Cretaceous age (Martin, 1995; Ridgwell, 2005). Even at present, a lot of marine plankton do not have the mineralized tests and thus produce only amorphous organic matter (AOM) upon their degradation. Areas that have been dominated with non-mineralized algae, geochemical proxies such as organic phosphorus (P_{org}), total organic carbon (TOC), and biogenic barium (Ba_{bio}) have been taken to measure the productivity (Calvert & Pedersen, 2007; Tribovillard et al., 2006). PP in the ocean facilitates the fixation of atmospheric CO_2 and transportation of organic carbon from surface pelagic layers to deep oceanic waters, and this phenomenon is called biological pump. Despite numerous attempts globally, spatio-temporal variations in marine primary productivity lack a good understanding. This is mainly due to the efforts it needs to measure productivity using the current methodologies, which are cumbersome, have various limitations, and methodological errors that are difficult to avoid. Moreover, the PP proxies, such as oxygen and particulate organic carbon (POC), have to be accurately estimated to convert them to carbon production. In aquatic ecosystems, the transport, distribution, and dispersion of many elements, including carbon, takes place through an important carrier known as particulate matter. The resultant particulate organic carbon constitutes a small fraction of the ocean carbon pool that mainly involves the dissolved forms of organic and inorganic carbon. However, despite its small pool size, POC plays a significant role in the marine as well as global carbon cycle due to its sinking nature (Prentice et al., 2001). Hence, accurate POC concentration measurements are required to find out the carbon fluxes and their residence time in the oceanic environment.

Marine phytoplankton biomass has been used as an indicator of PP in the oceans. Chlorophyll-a, which is the chief pigment used for PP, is present among all the autotrophs that perform PP. Thus, it is one of the most widely used proxies for phytoplankton biomass estimation in aquatic environments. However, chl-a concentration is a biased estimator of organic carbon or the phytoplankton biomass as its content exhibits a significant cellular variation, and also its ratio with phytoplankton carbon content is inconsistent (Cullen, 1982). Accurate estimation of PP, thus, is not possible due to all these variations when chl-a is used in a PP estimation model. Compared to terrestrial environments, the factors controlling marine PP are totally different. Marine water temperature, which affects the physiology of organisms, shows lesser variations in the oceanic waters as compared to land due to the heat capacity of the seawater that causes a buffering action. In polar waters, sea ice that forms on the surface also acts as a barrier that causes an insulating effect. Among other variables, light intensity, which provides the energy to carry out

photosynthesis, and nutrients and minerals, which are essential for growth and development, play a significant part in controlling marine PP (Sigman & Hain, 2012). Presently developed theoretical models indicate that a reduction in ocean net primary productivity ranging from 3% to 10% as compared to the present scenario could take place due to the biogeochemical changes happening in recent times (Mora et al., 2013). Recent studies have reported about 60% increase in PP in the Arctic Ocean during the last two decades (Arrigo & van Dijken, 2015). The authors have attributed the same to the presence of high plankton biomass in that region. Accordingly, a hypothesis has been developed which depicts the flow of nutrients into the Arctic Ocean from other oceans, and in the future, the production levels will be higher, which could result in more carbon fixation than the present situation (Lewis et al., 2020).

The ratio between the elements carbon (C), nitrogen (N), and phosphorus (P) in exported organic matter expressed in terms of the C:N:P ratio helps determine how much atmospheric carbon sequestration has taken place in the marine environment with respect to the availability of micronutrients (Tanioka & Matsumoto, 2020). On a geologic timescale, the N:P ratios show the relative nitrate availability in comparison to phosphate concentration. Both these nutrients are supplied from external sources, such as from the atmospheric environment by nitrogen fixation and/or from the continental crust by terrestrial runoff, and their fate in the marine environment is dependent on processes such as phytoplankton uptake, organic matter degradation, and burial in the sediment sink (Redfield, 1958; Broecker, 1982; Tyrrell, 1999; Lenton & Watson, 2000). On shorter timescales, the composition of exported bulk particulate organic matter reveals the elemental stoichiometry of the primary producers (Martiny et al., 2013; Bonachela et al., 2016; Garcia et al., 2018), with added influence from the abundance of organisms, and organic matter related to zooplankton and heterotrophic bacteria. Many authors have carried out laboratory and field experiments to find out the interrelations between the C:N:P ratio of primary producers and environmental parameters. Marine phytoplankton thrives in the photic layer of seawater, where a significant spatio-temporal variation is observed in the nutrient contents, light intensity, and sea surface temperature (SST) (Tanioka & Matsumoto, 2020). Laboratory investigations indicate that these variations trigger cellular-level responses and the cells modify their resource allocation mechanisms to cope with the ambient environment (Geider & La Roche, 2002). For example, phytoplankton may modify resource distribution among the P-rich biosynthetic apparatus, N-rich light-harvesting apparatus, and C-rich energy storage reserves (Moreno & Martiny, 2018). Due to climate change and global warming, the marine environment is expected to change in the near future with respect to the availability of nutrients and light and changes in SST (Boyd et al., 2010). These abovementioned changes will possibly have significant effects on the physiology of marine phytoplankton (Van De Waal et al., 2010; Finkel et al., 2010), and studies have shown that suitable phytoplankton species can survive and adapt to future changes in SST, irradiance, and nutrient availability on decadal timescales (Irwin et al., 2015).

Though PP is the most important biological process in any ecosystem, long-term continuous data on productivity is scarce and patchy in the Indian Ocean region. The present study undertaken in the Kalpakkam coastal waters, Tamil Nadu, south-western Bay of Bengal, mainly aims to provide an insight into the phytoplankton productivity and primary productivity potential of the coastal waters and its variations in terms of proxies such as chl-*a* and POC measurements. It also aims to provide a long-term comparison of the physicochemical and biological properties of the coastal waters, measured consecutively for 3 years each during the last two decades. The first set of data was collected during 2006–2009, and the second set of data was collected during 2019–2022.

2 Materials and Methods

2.1 Study Area

Kalpakkam coast (12° 33′N and 80° 11′E), a stretch of coastal Bay of Bengal (BoB), is situated on the southeast coast of peninsular India (Fig. 3.1). As a growing strategic nuclear hub of India, Kalpakkam nuclear complex harbors various nuclear

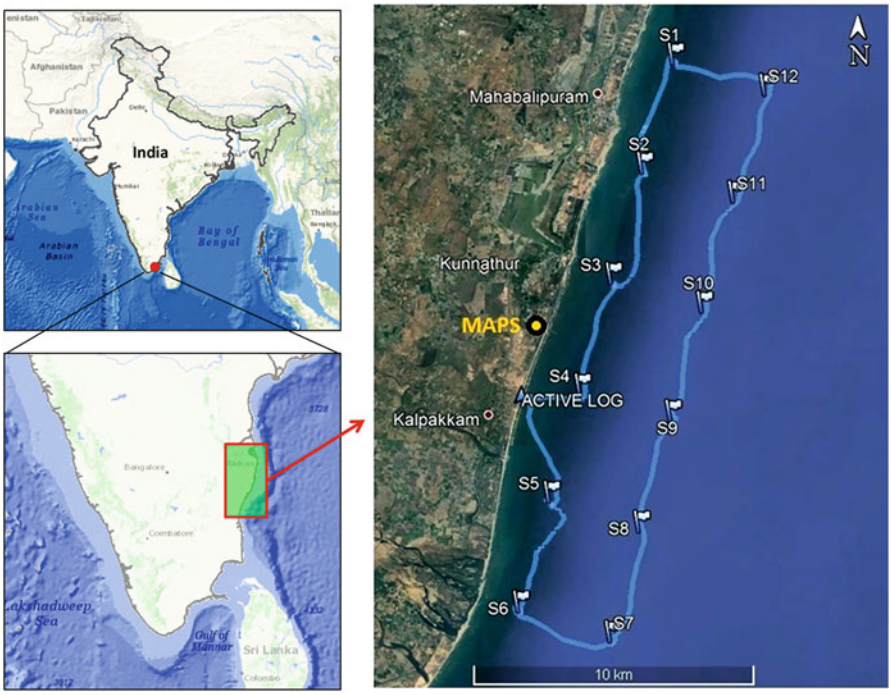

Fig. 3.1 Study area showing the sampling locations

facilities such as Madras Atomic Power Station (MAPS), a Fast Breeder Test Reactor (FBTR), a Centralized Waste Management Facility (CWMF), a Fast Reactor Fuel Cycling Facility (FRFCF), and a host of allied facilities (Rajaram et al., 2012) including the Prototype Fast Breeder Reactor (PFBR) which will be commissioned shortly. MAPS uses seawater as a condenser coolant at a rate of 35 m^3/s. The seawater is drawn through an intake well located approximately 400 m inside the sea. Until 2009, the thermal discharge ran through a canal of about 2 km to mix with the sea. The canal length varied (0.5–2 km) during different seasons, and the length variation was mainly dependent on the longshore sediment transport by coastal currents (Poornima et al., 2005). The warm water from MAPS outfall is discharged through an engineering canal of length 0.98 km with a fixed mouth and a width of about 40.1 m at the top and 25 m at the bottom. The new power plant of 500 MWe capacity, the PFBR, located about 680 m south of MAPS, will require about 29 m^3/s of seawater for cooling purposes. Similar to that of MAPS, the intake structure of the PFBR is located at about 420 m from the shoreline. The outfall water from PFBR is proposed to be discharged along with the MAPS-engineered canal parallel to the coastline formed by constructing a guided bund from PFBR outfall to that of MAPS. The combined discharge (64 m^3/s) is expected to have an elevated temperature up to 7 °C from the ambient seawater (Satpathy et al., 2006; Srinivasalu et al., 2007). Two backwaters, namely, Edaiyur and Sadras are present on the Kalpakkam coast. According to the climatology of this area, the whole year has been divided into three seasons, namely, (i) post-monsoon/summer – POM/SUM (February–May), (ii) pre-monsoon or SW monsoon – PRM/SWM (June–September), and (iii) monsoon or NE monsoon – MON/NEM (October–January). Large quantities of fresh water are discharged into the coastal region by these backwaters during the winter/northeast monsoon (NEM) and occasionally during southwest monsoon/pre-monsoon (SWM/PRM) seasons. The Buckingham Canal, an erstwhile navigation canal, runs parallel to the coast and is connected to the backwater systems. The average annual rainfall at Kalpakkam region is about 1300 mm, and a majority of it (~65%) is received during NEM.

2.2 Methods

Samples were collected from 12 different locations along the nearshore waters in Kalpakkam. Two transects parallel to the shoreline at 1.6 and 5 km inside the sea were chosen for the study (Fig. 3.1). The distance of each transect was about 20 km from north to south, and the study covered an area of approximately 100 km^2. Coastal surveys were done seasonally by motorized fiber boats in three different seasons, that is, pre-monsoon – PRM (July–September), monsoon – MON (October–January), and post-monsoon – POM (February–May). The selected sampling locations were fixed with a GPS (Global Positioning System) device

(GARMIN). The surface water samples were collected using a Niskin-Type oceanographic water sampler (2.5 L PWS, Hydro-Bios). Then the water samples were collected in polypropylene bottles and transported to the laboratory for preservation at −20 °C until analysis. The environmental parameters such as temperature, pH, salinity, dissolved oxygen (DO), and turbidity were measured on-site using a multiparameter probe (HANNA, Instruments). The collected water samples were filtered through Whatman (0.45 μm) filter paper. Filtered water samples were used to analyze dissolved micronutrients such as nitrate, orthophosphate, silicate, ammonia, total nitrogen (TN), and total phosphorus (TP). The nutrients were analyzed by using a San^{++} Continuous flow analyzer (SKALAR Analytical). Chlorophyll-*a* estimation was done by photometric method (Strickland & Parsons, 1972) using 1 L of surface water samples collected by dark polypropylene containers and preserved in an icebox and transported to the laboratory. Water sample (1 L) for chl-*a* was filtered by Whatman glass fiber (GF/F, the pore size of 0.7 μm, and a diameter of 47 mm) filter papers with the help of Millipore filtration unit. Magnesium carbonate solution (1%) was poured on the filter paper to avoid acidification of chl-*a*. The filter paper was immersed in 90% acetone and kept in the dark condition at 4 °C for 20 h. After the incubation, the extract was centrifuged at 5000 rpm for 5 min. Finally, the supernatant was taken for photometric measurement using a double-beam UV-visible spectrophotometer (Chemito Spectrascan, UV 2600). POC was estimated using the standard method EPA 440 (Zimmerman et al., 1997). A Shimadzu TOC VCP_H analyzer was used for analysis.

2.3 Data Analysis

Multivariate analyses such as multi-dimensional scaling (MDS), cluster analysis (CA), Pearson correlation matrix, two-way ANOVA, and biota-environment analysis (BIOENV) were performed using Primer 6 to find out the interrelations among the biotic and abiotic parameters, and also to find out the controlling/responsible factors influencing PP in this coastal region.

3 Results and Discussion

The results of all the physicochemical and biological parameters obtained during the study were categorized into seasonal averages (Fig. 3.2). An average seasonal value of a parameter denotes the mean value of all the samples collected, irrespective of locations, during the respective seasons. Values of all the parameters obtained during the two time periods, 2006–2009 and 2019–2022 have been compared to find out the changes over a long period.

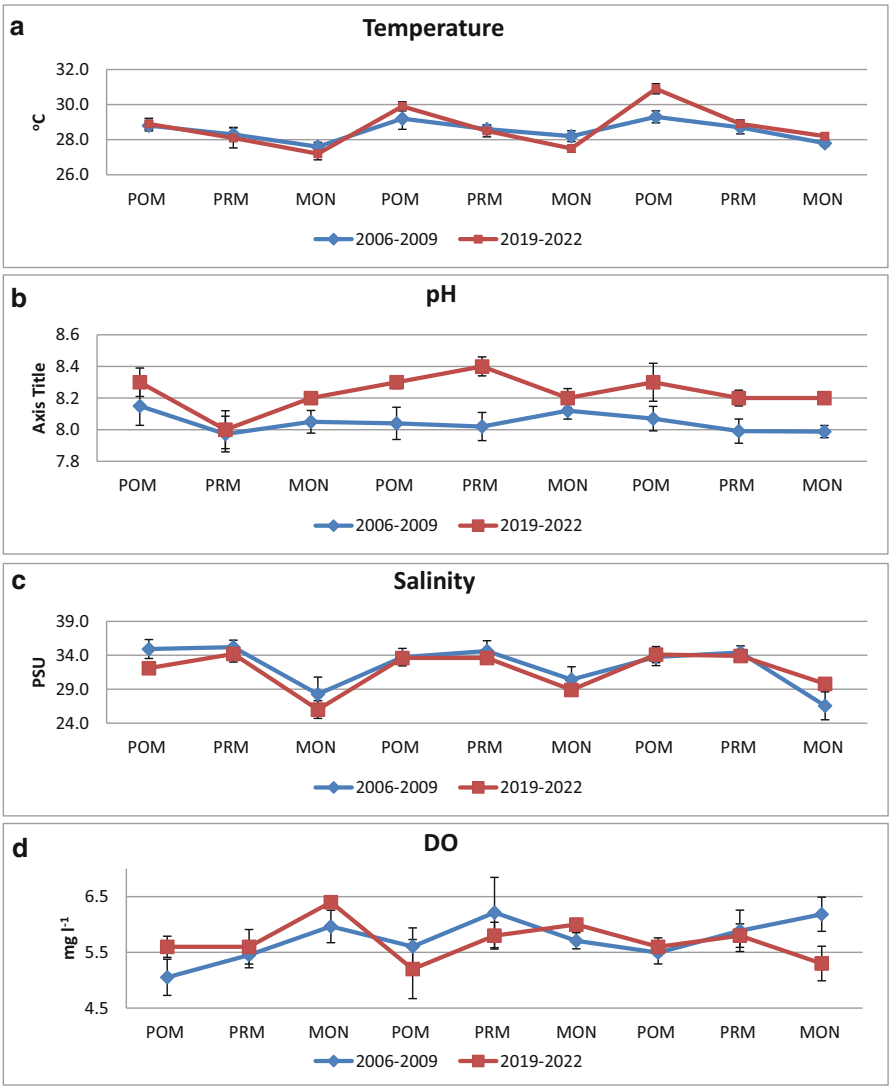

Fig. 3.2 (**a**–**d**) Variations in temperature, pH, salinity, and DO contents in the coastal waters of Kalpakkam. (**e**–**h**) Variations in turbidity, nitrate, ammonia, and total nitrogen contents in the coastal waters of Kalpakkam. (**i**–**m**) Variations in phosphate, total phosphorus, silicate, chl-a, and POC contents in the coastal waters of Kalpakkam

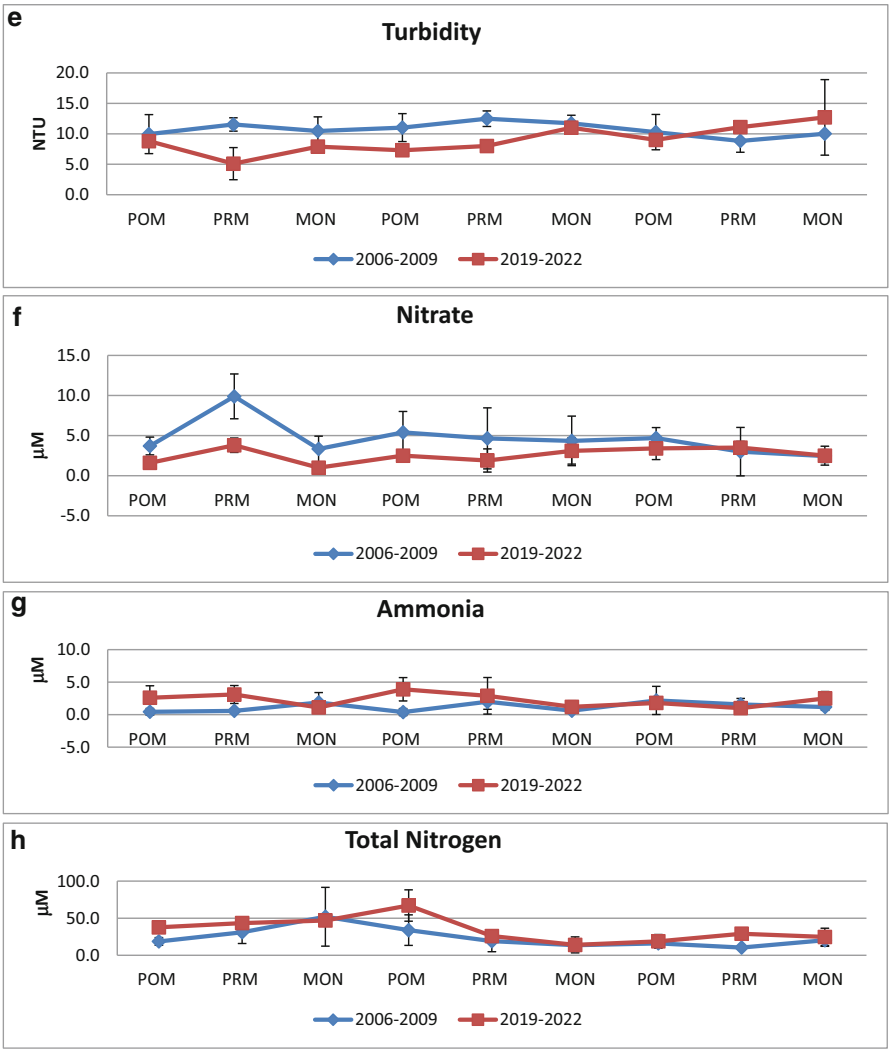

Fig. 3.2 (continued)

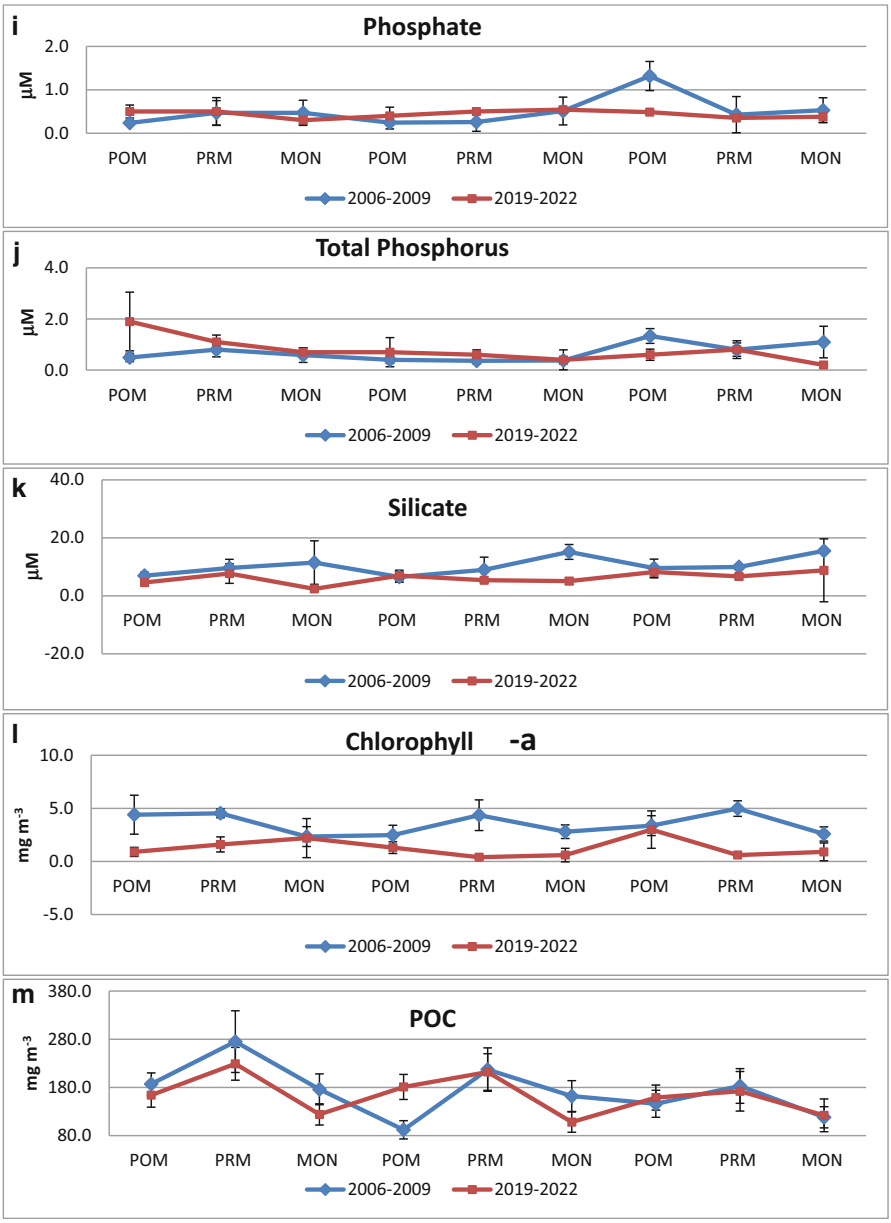

Fig. 3.2 (continued)

3.1 Water Temperature

Temperature is one of the most important physical parameters that control many physical, chemical, and biological processes in marine ecosystems (Sahu et al., 2012). It plays a significant role in marine ecosystem functioning, energy transfer, and food webs, and determines the organism's habitats and diversity. Besides, it is also a crucial parameter that induces planktonic blooms that have significance on the entire ecosystem. For example, conducive SST and water salinity are the most important parameters that trigger the cyanobacteria, mostly *Trichodesmium*, blooms (Oyeku & Mandal, 2020) in oceanic waters. Autotrophic bloom formations by various phytoplankton species are a regular phenomenon in the Kalpakkam coastal waters, which significantly impacts the nutrient cycles and plankton diversity locally (Mohanty et al., 2010; Sahu et al., 2012, 2016, 2022). Surface water temperature, in the present study, ranged between 27.6 and 29.3 °C during 2006–2009 and 27.2 and 30.9 °C during 2019–2022. Significant temporal variations in SST were recorded during both study periods. As expected, the high values were recorded during pre-monsoon (PRM) season, and the values were relatively low in the NEM seasons (Fig. 3.2a). Temperature showed a positive correlation with salinity ($r = 0.707$ and $r = 0.756$), during both study periods (Table 3.1). It showed a positive correlation with chl-a during 2006–2009, indicating the growth of phytoplankton during warmer climate. The low SST values observed during the NEM seasons could be attributed to precipitation, high cloud coverage, lower atmospheric temperature, and stronger monsoon winds. Earlier studies from the southeast coast of India have reported similar SST variations (Govindasamy et al., 2000; Satpathy et al., 2009; Damotharan et al., 2010; Vajravelu et al., 2018; Sathishkumar et al., 2021).

3.2 pH

The coastal water pH ranged from 8.0 to 8.2 and 8.0 to 8.4 during 2006–2009 and 2019–2022, respectively. Relatively high pH values were recorded during POM and PRM seasons, and lower values were recorded during the monsoon season (Fig. 3.2b). In general, anthropogenic incursions (i.e., overflows from industrial, aquaculture wastes, domestic sewage, agricultural, and freshwater runoffs) lead to short-term variations in pH, which may have long-term impact and cause harm to local marine biota. Significant variations in pH can impact the physiology of marine life, which eventually causes species migration or mass mortality in sessile organisms. In the entire study, the coastal water was alkaline, and the pH values were > 8. A number of earlier studies from the same locality have also reported similar pH variations for coastal waters (Satpathy et al., 2010, 2011; Sahu et al., 2012; Mohanty et al., 2010; Kumar et al., 2018).

Table 3.1 Correlation matrix (Pearson) of environmental variables

Variables	Temp	pH	Salinity	Turbidity	DO	Nitrate	Ammonia	TN	Silicate	Phosphate	TP	Chl-a	POC
2019–2022 ($n = 108$, Bold values are significant; $p < 0.05$)													
pH	0.432	**1**											
Salinity	**0.707**	0.123	**1**										
Turbidity	−0.306	**−0.842**	0.119	**1**									
DO	0.345	0.029	**0.661**	0.208	**1**								
Nitrate	−0.248	0.061	−0.507	−0.387	**−0.876**	**1**							
Ammonia	**−0.633**	−0.150	**−0.872**	−0.167	−0.505	0.571	**1**						
TN	0.119	−0.043	0.147	0.040	−0.183	0.436	0.190	**1**					
Silicate	−0.133	**−0.589**	−0.001	**0.833**	−0.067	−0.301	−0.250	−0.089	**1**				
Phosphate	−0.257	−0.420	0.082	**0.615**	0.127	−0.259	−0.033	0.424	0.517	**1**			
TP	0.098	−0.030	0.262	0.138	0.147	−0.192	−0.176	0.431	0.113	**0.814**	**1**		
Chl-a	**0.599**	0.031	**0.747**	0.192	**0.838**	**−0.642**	−0.462	0.221	−0.021	0.172	0.209	**1**	
POC	0.292	−0.056	**0.792**	0.365	**0.699**	−0.492	−0.533	0.424	0.067	0.443	0.379	**0.790**	**1**
2006–2009 ($n = 108$, Bold values are significant; $p < 0.05$)													
pH	0.221	**1**											
Salinity	**0.756**	0.058	**1**										
Turbidity	−0.060	0.035	0.123	**1**									
DO	−0.496	−0.567	−0.536	0.155	**1**								
Nitrate	−0.323	−0.136	−0.463	−0.045	0.246	**1**							
Ammonia	−0.038	−0.245	−0.123	−0.108	0.532	−0.187	**1**						
TN	−0.415	−0.141	−0.309	0.157	0.073	**0.675**	−0.001	**1**					
Silicate	**−0.710**	−0.115	**−0.800**	0.014	0.520	0.126	0.103	−0.136	**1**				
Phosphate	0.240	0.033	−0.086	−0.189	−0.098	−0.265	0.518	−0.196	0.214	**1**			
TP	0.079	−0.338	−0.173	−0.488	0.013	−0.306	0.423	−0.201	0.237	**0.808**	**1**		
Chlorophyll-a	0.317	−0.171	**0.758**	−0.126	−0.248	**−0.670**	0.046	−0.489	−0.419	−0.157	0.000	**1**	
POC	−0.196	−0.212	0.455	0.305	−0.139	−0.438	0.044	0.019	−0.138	−0.151	−0.123	**0.702**	**1**

3.3 Salinity

Seawater salinity ranged from 26.6 to 35.2 and 26.0 to 34.2 during 2006–2009 and 2019–2022, respectively. As expected, significant seasonal variations were recorded in salinity content (Fig. 3.2c). It considerably declined during the rainy season due to precipitation and land runoff through backwaters and canals. The Kalpakkam region receives the major bulk of rainfall during NEM (October–December) as compared to a weaker SWM, leading to a reduction in salinity levels of this coastal water. During the MON season, the discharge of freshwater from rivers results in declined surface seawater salinity, and a gradual regeneration takes place from POM to summer, during which salinity increases continuously. Along with the precipitation and land runoff, the movement of low saline water mass from northern BoB causes a reduction in coastal water salinity at this location (Varkey et al., 1996; Satpathy et al., 2010). Numerous studies have reported similar salinity variations from different regions of south-eastern parts of the Indian coast (Sulochanan & Muniyandi, 2005; Prabu et al., 2008; Damotharan et al., 2010; Manikannan et al., 2011; Mohanty et al., 2014; Kathiravan et al., 2017; Bharathi et al., 2018). A typical marine and isohaline condition prevailed during PRM and POM periods, which was most probably due to oceanic water intrusion, high solar radiation intensity, and increased wave action due to stronger northerly wind and northerly coastal water current (Varkey et al., 1996; McCreary et al., 1996; Haugen et al., 2003). Salinity exhibited a strong positive correlation with chl-a during both seasons (Table 3.1), which indicated the phytoplankton productivity at this location was relatively high during a high saline regime, that is, during POM and PRM. The strong positive correlation between salinity and POC further confirmed the above-observed increased coastal productivity during high saline conditions.

3.4 Dissolved Oxygen

The concentrations of DO fluctuated between 5.1 and 6.2 mg l^{-1} during 2006–2009 and 4.9 and 6.8 mg l^{-1} during 2019–2022. Though a specific seasonal trend was missing, DO contents showed wide variations during different seasons (Fig. 3.2d). The correlation analysis illustrated significant positive correlations of DO with chl-a and POC during 2006–2009. However, no such relations could be observed during 2019–2022. Oxygen distribution in aquatic ecosystems is significantly influenced by various factors such as photosynthetic PP organic matter degradation and re-aeration due to air-sea interactions (Granier et al., 2000). In the present investigation, the recorded occasional high concentration of DO in the coastal waters during the MON season could be attributed to the input of freshwater rich in oxygen (Das et al., 1997; Sundaramanickam et al., 2008; Damotharan et al., 2010; Manikannan et al., 2011). The positive correlation of DO with chl-a, POC, and salinity, also indicated that during high phytoplankton abundance, the photosynthetic release of DO is also a

major source of oxygen. Earlier studies from the same locality have reported similar observations in variations in DO contents in the coastal waters (Satpathy et al., 2007, 2010, 2011).

3.5 Turbidity

Water turbidity varied between 8.8 and 12.5 NTU during 2006–2009 and 5.1 and 12.7 during 2019–2022. Relatively high water turbidity was observed during the PRM season (Fig. 3.2e), which could be attributed to the strong northerly winds and northerly water current (Satpathy et al., 2011; Haugen et al., 2003). The abovementioned processes lead to low water transparency turbulence and bottom sediment re-suspension, which is relatively high during this period compared to NEM and POM seasons (Satpathy et al., 2011). The lower turbidity values were recorded during NEM seasons, which indicated that the surface runoff is not the main reason that regulated coastal water turbidity at this location; rather, re-suspension of surficial sediment due to coastal currents may be the factor responsible for it.

3.6 Nitrogenous Nutrients

Nitrate concentration ranged from 2.45 to 9.90 and 1.0 to 3.8 μ mol l^{-1} during 2006–2009 and 2019–2022, respectively. Though there was no particular seasonal pattern, higher concentrations were recorded during NEM and POM seasons, and PRM values were low (Fig. 3.2f). Nitrate showed a strong positive correlation ($p < 0.05$) with TN during 2006–2008, while a negative relation was found with chl-a during both study periods (Table 3.1). A relatively high nitrate concentration recorded during POM seasons could be due to its production from biological processes, ammonia oxidation, and from biodegradation of organic substances (Hutchinson, 1957; Govindasamy et al., 2000; Santhanam & Perumal, 2003). The nitrate enrichment during NEM could be attributed to the fact that coastal waters at this location is significantly influenced by land runoff that brings a huge quantity of nutrients from the terrestrial environment (Saravanane et al., 2000; Poornima et al., 2005). The present nitrate variations corroborated with previous observations from various Indian coasts (Vajravelu et al., 2018; Vinayachandran et al., 2002; Bharathi et al., 2017; Kathiravan et al., 2017). Similar observations have also been reported for shallow coastal ecosystems elsewhere, where river discharge, groundwater outflow, atmospheric transfer, and benthic fluxes have been considered as major sources of nutrients (Conley, 2000; Paerl, 1997; Malone et al., 1988; Nowicki & Nixon, 1985). In well-oxygenated aquatic systems, nitrate is one of the most stable forms of combined inorganic nitrogen. Fluctuations in nitrate concentrations and its reduced forms in marine waters are mainly controlled by biological activities related

to the production and decomposition of organic matter. Rapid phytoplankton assimilation and enrichment due to land runoff cause a wide variation in nitrate concentration on a spatio-temporal scale in marine ecosystems (Zepp, 1997; De Souza, 1983; Qasim, 1977). The negative correlation of nitrate with chl-a encountered in this study could be due to its biological uptake by high autotrophic biomass that thrived in that period, as reflected by the recorded relatively high chl-*a* concentration in the same season. Similar observations of nitrate content reduction and simultaneous increase in PP and plankton biomass during POM/SUM have been reported from other coastal areas of India (Prasannakumar et al., 2002).

The concentration of ammonia did not exhibit any seasonal trend, and its content in the coastal waters was in the range of 0.39–2.19 and 1.0–21.10 μ mol l^{-1}, during 2006–2009 and 2019–2022, respectively. Ammonia was negatively correlated with salinity and temperature during 2019–2022. It indicated that the ammonia concentrations were lower in the PRM period (Fig. 3.2g), which could be attributed to its uptake by the species-rich phytoplankton biomass that flourished during PRM season (Sahu et al., 2012). In general, ammonia is mostly liberated as an excretory product from aquatic animals (e.g., fishes, invertebrates, and benthic species). In certain environmental conditions, ammonia as a nutrient is also preferred by the groups of specific phytoplankters over nitrate (Dugdale et al., 2007). The abovementioned two factors mainly influence the distribution of ammonia in the marine environment (Olson, 1980; Glibert et al., 1982). Moreover, the uneven trend could also be attributed to the oxidation of ammonia to other forms and its production due to the reduction of nitrate in marine water (Sankaranrayanan & Qasim, 1969). TN concentration ranged from 10.42 to 51.96 μ mol l^{-1} and 4.70 to 67.10 μ mol l^{-1} for 2006–2009 and 2019–2022, respectively (Fig. 3.2h). In addition to the above reasons, the inflow of freshwater, decay of organic matter, water current, phytoplankton blooms, and growth of macrophytes could also have played significant roles in TN distribution (Satpathy et al., 2011). In this coastal region, the TN concentrations mostly depend on natural processes rather than anthropogenic inputs.

3.7 Phosphate and Total Phosphorus

Phosphate in the marine environment acts as a limiting factor that controls the growth of phytoplankton and subsequently affects the whole marine productivity (Cole & Sanford, 1989). Inorganic phosphate (P) and total phosphorus (TP) contents in the present study exhibited similar seasonal trends (Fig. 3.2i, j). The P concentrations ranged from 0.24 to 1.32 μM and 0.30 to 0.54 μM during 2006–2009 and 2019–2022, respectively. TP concentrations ranged from 0.36 to 1.33 and 0.40 to 1.90 for the two study periods. Various biogeochemical and physical processes, such as biological uptake, decomposition of organic matter, freshwater influx, localized upwelling, and benthopelagic coupling (Satpathy et al., 2011), influence phosphate concentration distribution in a marine ecosystem. Uptake of this nutrient by the

phytoplankton community and solubilization by the bacterial community are the two major processes that control surface water depletion. Moreover, rapid adsorption of phosphate onto fine sediment particles also acts as an important factor that controls the fate of phosphate in the marine environment (Pomeroy et al., 1965). Generally, phosphate is considered to be of marine origin unless there are contaminations from anthropogenic sources like domestic effluents that contain detergent and agricultural wastes, mostly fertilizers containing various forms of phosphate. Phosphate showed a positive correlation with turbidity during 2019–2022, indicating that either it is unutilized during the high turbidity regime (i.e., the PRM season) or its concentration is influenced by external input during monsoon season, during which turbid water enters into coastal region.

3.8 Silicate

Silicate in its dissolved form is considered to be the most important nutrient which controls the abundance and distribution of diatoms in marine waters. Silicate values ranged from 6.51 to 15.52 μM and 2.40 to 8.80 μM during 2006–2009 and 2019–2022, respectively. The correlation analysis showed a significant negative correlation with temperature and salinity and a positive correlation with turbidity (Table 3.1). It clearly indicated that silicate concentration in these coastal waters is mainly influenced by external input during monsoon rains. The seasonal trend also indicated the same (Fig. 3.2k). Various factors and processes, such as freshwater input, suspended sediment content, clay mineralogy, utilization by primary producers, and co-precipitation with humic substances, play essential roles in silicate distribution in coastal waters (Satpathy et al., 2009). In the present study, freshwater input from nearby silicate-rich backwater systems into the coast may be the reason for the high values observed. Besides, the observation of lower values may also be due to silicate adsorption by suspended sediment particles, chemical interactions with clay minerals, and bio-absorptions by primary producers, especially by silicoflagellates and diatoms (Gouda & Panigrahy, 1992; Aston, 1980).

*3.9 Chlorophyll-*a

Primary production in the marine environment depends on the principal photosynthetic pigment chl-*a*. It has long been used as the indicator of phytoplankton standing stock and primary productivity (Ediger et al., 2015). It varied from 2.35 to 4.98 mg m^{-3} during 2006–2009 and 0.60 to 3.00 mg m^{-3} during 2019–2022. Relatively high chl-*a* contents were recorded during the PRM season, and lower values were recorded during MON season (Fig. 3.2l). The correlation matrix showed a positive relation of chl-*a* with temperature, salinity, and DO, which indicated that in the summer season, during which the coastal water temperature is relatively high,

Table 3.2 ANOVA results for POC and chl-a variations

Source of variation	SS	*df*	MS	*F*	*P*-value	*F* crit
ANOVA POC						
Seasons	28,628	8	3578.5	3.643578	0.042923	3.438101
Years	401.3889	1	401.3889	0.408689	0.540505	5.317655
Error	7857.111	8	982.1389			
Total	36886.5	17				
ANOVA Chl-a						
Seasons	10.21089	8	1.276361	2.675795	0.092714	3.438101
Years	14.31838	1	14.31838	30.01743	0.000588	5.317655
Error	3.816019	8	0.477002			
Total	28.34529	17				

the primary productivity of coastal water increases at this location. The positive correlation with DO showed that the photosynthetic production of oxygen in the process of PP is one of the main contributors to this dissolved gas. Chl-*a* concentrations recorded in the study showed the following decreasing order: pre-monsoon > post-monsoon > monsoon. Relatively high phytoplankton growth and production during the pre-monsoon season could be attributed to the typical marine environmental conditions that prevailed in this region during that time (Satpathy et al., 2010). The two-way ANOVA clearly showed that the chl-a variations were significant with respect to seasons as well as different study periods (Table 3.2). Several studies have also reported similar observations from various coastal waters of India (Sarma et al., 2006; Prasannakumar et al., 2000; Madhupratap et al., 2001; Prasannakumar et al., 2002; Ganapati & Rao, 1958). Relatively high phytoplankton biomass recorded during this season has been attributed to upwelling events, a regularly occurring phenomenon in this coastal region, in which nutrient enrichment of surface water takes place by the nutrient-rich deeper water (La Fond, 1957; Murty & Varadachari, 1968). During the NE monsoon season, a visible decrease in concentrations of chl-*a* could be attributed to unfavorable circumstances such as salinity reduction and increase in turbidity content due to land drainage and precipitation. Strong positive correlation of chl-*a* with salinity further supported the above observation. During the POM season, the gradual onset of favorable phytoplankton growth conditions takes place, and it becomes more favorable during the summer/PRM season when the primary productivity levels are at maximum. A strong negative correlation was observed between Chl-*a* and nitrate. It supported the observed relatively low phytoplankton biomass during MON, as nitrate has been reported to be of external origin that enters the coastal environment through freshwater input. In contrast, the correlation also indicated that phytoplankton dynamics in these coastal waters are mainly nitrogen-dependent. The role of phosphate, which is generally of marine origin, was insignificant for the growth and production of phytoplankton at this location.

3.10 POC

Particulate organic carbon (POC), which plays a very important role in the marine carbon budget, is linked to numerous important biogeochemical processes. Concentrations of POC ranged from 92 to 275 mg m^{-3} during 2006–2009 and 108 to 229 mg m^{-3} during 2019–2022. It exhibited a similar variation pattern like chl-a with relatively high concentrations observed during PRM seasons, and low values were recorded during MON seasons (Fig. 3.2m). Its strong positive correlation with salinity and chl-a indicated that POC concentrations were mainly regulated by the phytoplankton production during the high salinity regime in these coastal waters. POC content in seawater is comprised of all organic material, that is, picoplankton, nanoplankton and microphytoplankton, heterotrophic bacteria, nanozooplankton and microzooplankton, and detritus material. Because of its significance in the oceanic productivity and food web, investigations on the POC dynamics are of paramount importance in marine environmental studies. POC, being an important fraction of marine organic carbon, plays an important role in many different biological activities, controls carbon cycles, both organic and inorganic (Liu et al., 2019), and consists of living as well as non-living materials (e.g., bacteria, phytoplankton, zooplankton, and detritus). POC is generally taken as an indicator of the production potential of the column production in the euphotic zone (Fingas, 2018). Concentrations of POC in the marine environment is influenced by phytoplankton dynamics (Fernandes et al., 2009) and various other factors, such as light intensity, salinity, temperature, nutrients, and chl-*a* concentration (Stramska, 2014). Additionally, riverine discharge (Wang et al., 2012), erosion of soil and sediment (Xu & Milliman, 2009), water current dynamics (Fan et al., 2018), environmental variations (Fan et al., 2018), tidal variations, and wind velocity (Liu et al., 2019) have been attributed to be causative factors for POC concentration variations in the marine environment. Remobilization and demineralization have also been reported to play important parts in influencing variations in POC concentration in marine hydrology (Le et al., 2017). SST is one of the most important parameters and plays a significant role in determining variations in POC content in the open oceanic environment. SST weakens the vertical mixing in the water column, leading to low nutrient concentration and phytoplankton abundance, ultimately reducing the POC content (Yu et al., 2019). However, being the chief source of POC, chl-*a* content generally shows a positive correlation with POC (Lee et al., 2020 Fernandes et al., 2009). Wind speed, which mainly determines the surface currents and water circulation in the marine environment, was positively correlated with POC content (Liu et al., 2019).

POC content in the ocean varies spatiotemporally in the surface waters as well as in the water column (Fan et al., 2018; Stramska, 2009, 2014; Yu et al., 2019). The global average of oceanic POC concentration has been reported to be in the range of 60–75 mg m^{-3} (1998–2007 meantime) (Stramska, 2009). Reported values of POC from Yellow–Bohai Sea of China were found to be relatively high in the spring season (452 ± 53.6 mg m^{-3}), and lower values were observed in the summer season

(245 ± 84.8 mg m^{-3}) (Fan et al., 2018). Seasonal variations in POC content of two riverbed estuaries in the northern Gulf of Mexico have also been reported by Le et al. (2017). To study the POC distribution pattern in different oceans (The Atlantic, Pacific, Southern), several investigations have been made (Stramska, 2014; Fan et al., 2018; Pavia et al., 2019; Zhu et al., 2011; Gardner et al., 2006; Stramska, 2009; Świrgoń & Stramska, 2015). However, information with respect to POC content in the Indian Ocean in general and from the Bay of Bengal (BoB) in particular are scarce (Bhosle et al., 1988; Radhakrishna et al., 1982). The large-scale and long-time series data available for some particular regions of the western coast of BoB are insufficient to draw any affirmative conclusion (Fernandes et al., 2009; Nandakumar et al., 1987). Recently, Sherin et al. (2018) measured the POC and chl-*a* concentration and their ratio in the BoB by quantifying the source of organic matter and nutrients that control the PP. The present values of POC more or less agree with the earlier reported values from BoB (Fernandes et al., 2009; Nandakumar et al., 1987). Though it showed a significant seasonal variation, the variations between the two study periods were insignificant (Table 3.2). However, a marginal decrease in the POC content of coastal waters at this location has been noticed recently compared to the values obtained a decade earlier.

3.11 C:N:P Ratios

The elemental composition of marine phytoplankton plays a crucial role in biogeochemical cycles globally by influencing the nutrient cycles, secondary production, and carbon budget. Although, a lot of literature is available with respect to laboratory experiments to find out the environmental drivers responsible for the elemental ratios of phytoplankton, a complete quantitative evaluation of the mechanisms is still lacking. As compared to the prokaryotic phytoplankton, the eukaryotic phytoplankton is highly sensitive to variations in nutrient compositions, perhaps due to their relatively big cell size and their quick gene expression capabilities. During the present study, N:P ratios for the years 2006–2009 ranged from 5.22 to 18.57 with an average of 11.76. Similarly, it ranged from 7.00 to 16.00, with an average of 11.04 for 2019–2022 (Table 3.3). Most of the values in the present observation remained below 16, indicating the nitrogen limitation. The ratio further decreased in recent times compared to the values a decade earlier.

The southeastern part of BoB has been reported to be nitrogen-limited (Gouda & Panigrahy, 1995; Tripathy et al., 2005; Panigrahy et al., 2006; Satpathy & Nair, 1996). The present results corroborated the earlier findings. This suggests that nitrogen was preferentially removed by phytoplankton during the abovementioned period; however, its concentration never reached below the detection limit. Therefore, the coastal system at Kalpakkam could lead to nitrogen limitation. Low N:P ratio during the abovementioned period also denotes that the nitrogen bioavailability for phytoplankton growth is less than phosphorous in this coastal water. Hence,

Table 3.3 N:P and N:Si ratios recorded in the coastal water of Kalpakkam during 2006–2009 and 2019–2022

	2006–2009			2019–2022	
	N:P	N:Si		N:P	N:Si
POM 2006	17.47	0.60	POM 2019	8.40	0.91
PRM 2006	15.63	1.09	PRM 2019	13.80	0.90
MON 2006–07	11.09	0.45	MON 2019–20	7.00	0.88
POM 2007	10.63	0.89	POM 2020	16.00	0.91
PRM 2007	18.57	0.74	PRM 2020	9.60	0.89
MON 2007–08	9.67	0.33	MON 2020–21	7.92	0.84
POM 2008	5.22	0.72	POM 2021	10.70	0.63
PRM 2008	10.70	0.46	PRM 2021	12.78	0.67
MON 2008–09	6.83	0.23	MON 2021–22	13.16	0.57

nitrogen can act as the limiting nutrient for phytoplankton growth in this setup. During the PRM seasons, the N:P ratio almost reached a value close to the Redfield ratio. Generally the southwest monsoon season (PRM in this study area) is the period of wind-driven upwelling at this location, and thus, temporary injection of nutrients into the coastal waters led to the increase of N:P ratio.

4 Inter-annual Variations in Primary Productivity and Responsible Factors

In order to find out the inter-annual variations in primary productivity, MDS with cluster overlay analysis was performed. Results indicated that the two sampling periods, that is, 2006–2009 and 2019–2022, remained separated from each other with respect to the seasonal distribution of PP (Fig. 3.3). Further, the annual variations during 2019–2022 were not similar as observed in the case of 2006–2009, and they formed two separate groups. It indicated that the primary productivity potential of this coastal water has changed over a period of 10 years. Biota-environment (BIOENV) analysis, which denotes the correlations among physicochemical and biological parameters, was performed between chl-a/POC and other environmental variables measured during the study (Table 3.4). The BIOENV analysis generally yields a group of abiotic variables that significantly influence the dynamics of biological parameters. In the present analysis, the results were truncated to five parameters. The BIOENV indicated that a set of parameters, such as pH, salinity, nitrate, ammonia, and phosphate, is associated with the biological parameters (chl-a and POC). Salinity and/or nitrate were the key parameters influencing the primary productivity, as these variables were present in every combination of BEST results. Water temperature, which generally has a significant

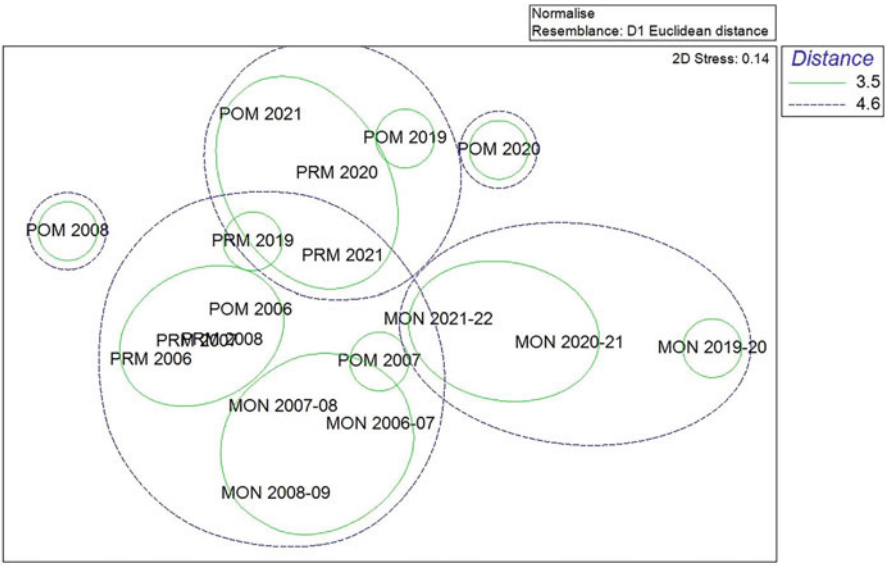

Fig. 3.3 MDS with cluster overlay showing the grouping of seasons of different study periods

Table 3.4 Best results (biota-environment analysis)

No. vars	Corr.	Selections
5	0.800	2, 3, 6, 7, 10
5	0.800	2, 3, 7, 8, 10
5	0.795	2, 3, 6, 7, 11
5	0.791	3, 4, 6, 7, 11
5	0.786	3, 4, 6, 7, 10
5	0.785	3, 4, 7, 8, 10
5	0.785	2–4, 7, 10
5	0.785	2, 6, 7, 9, 10
5	0.783	2, 4, 6, 7, 10
5	0.780	3–5, 7, 10

Variables: 1 Temp; 2 pH; 3 Salinity; 4 Turbidity; 5 DO; 6 Nitrate; 7 Ammonia; 8 TN; 9 Silicate; 10 Phosphate; 11 TP

impact on primary productivity, did not show any significant correlation with the productivity proxies used in the study. Silicate, the most important nutrient in coastal waters dominated by diatoms, did not show any impact on coastal productivity. This could be because the concentration of this nutrient in these coastal waters was never below the required limit rather, it is plentifully available throughout the year. Turbidity, which generally regulates water transparency, was not found to have any impact on coastal productivity during the study.

5 Conclusion and Future Recommendations

The present study indicated that monsoon seasons (southwest monsoon and northeast monsoon) influence the coastal characteristics at Kalpakkam. The coastal productivity at this location is nitrogen limited as most of the N:P values in the present study remained below 16. The ratio further decreased in recent times compared to the values a decade earlier. Chl-*a* concentrations recorded in the present study showed the following order of abundance: pre-monsoon > post-monsoon > monsoon. The two-way ANOVA clearly showed that the chl-a variations were significant with respect to seasons as well as different study periods. Concentrations of POC ranged from 92 to 275 mg m^{-3} during 2006–2009 and 108 to 229 mg m^{-3} during 2019–2022. Relatively high POC content was observed during pre-monsoon season, and low values were recorded during monsoon seasons, which followed the trend of chl-a. Its strong positive correlation with salinity and chl-a indicated that POC concentrations were mainly regulated by the phytoplankton production during the high salinity regime in these coastal waters. A marginal decrease in the POC content of coastal waters at this location has been noticed in recent times as compared to the values obtained a decade earlier. MDS with cluster overlay indicated that the two sampling periods, that is, 2006–2009 and 2019–2022, remained separated from each other with respect to the seasonal distribution of PP. The BIOENV (with combinations of ten variables) indicated that a set of parameters, such as pH, salinity, nitrate, ammonia, and phosphate, is associated with the biological parameters (chl-a and POC). Salinity and/or nitrate were the key parameters influencing the primary productivity, as these variables were present in every combination of BEST results.

Primary production, being the most important biological process globally, needs to be monitored continuously, especially in marine ecosystems, which is highly dynamic in nature. Unlike terrestrial ecosystems, where the primary producers are highly resilient to unfavorable conditions, phytoplankton in aquatic environments are very delicate and prone to capitulation with minor adverse conditions. Thus, a robust marine environmental monitoring program with respect to physicochemical and biological parameters is the need of this hour, especially in the era of climate change. Though the present study encompassed the proxies for primary productivity measurements, direct measurements of autotrophic production using radioisotopes, which gives a more accurate picture, will be attempted in future investigations. Such studies should be prioritized, at least near the strategic industrial locations, metropolises, and highly impacted areas, either naturally or anthropogenically, for future impact assessments.

Acknowledgments The authors would like to acknowledge the encouragement and support received from Director, SQRMG, and Director, IGCAR, to carry out the study.

References

Algeo, T. J., Hinnov, L., Moser, J., Maynard, J. B., Elswick, E., Kuwahara, K., & Sano, H. (2010). Changes in productivity and redox conditions in the Panthalassic Ocean during the latest Permian. *Geology, 38*, 187–190.

Arrigo, K., & van Dijken, G. (2015). Continued increases in Arctic Ocean primary production. *Progress in Oceanography, 136*, 60–70. https://doi.org/10.1016/j.pocean.2015.05.002

Aston, S. R. (1980). Nutrients dissolved gasses and general biochemistry in estuaries. In E. Olausson & I. Cato (Eds.), *Chemistry and biogeochemistry of estuaries* (pp. 233–262). Wiley.

Bharathi, M. D., Patra, S., Sundaramoorthy, S., Madeswaran, P., & Sundaramanickam, A. (2017). Elucidation of seasonal variations of physicochemical and biological parameters with statistical analysis methods in Puducherry coastal waters. *Marine Pollution Bulletin, 122*(1–2), 432–440.

Bharathi, M. D., Patra, S., Sundaramoorthy, S., Madeswaran, P., Chandrasekar, D., & Sundaramanickam, A. (2018). Seasonal variability in plankton food web composition in Tuticorin coastal waters, south east coast of India. *Marine Pollution Bulletin, 137*, 408–417.

Bhosle, N. B., Dhople, V. M., & Wagh, A. B. (1988). Distribution of particulate organic carbon in the central Arabian Sea. *Proceedings of the Indian Academy of Sciences – Earth and Planetary Sciences, 97*, 35–47. https://doi.org/10.1007/BF02861625

Bonachela, J. A., Klausmeier, C. A., Edwards, K. F., Litchman, E., & Levin, S. A. (2016). The role of phytoplankton diversity in the emergent oceanic stoichiometry. *Journal of Plankton Research, 38*(4), 1021–1035. https://doi.org/10.1093/plankt/fbv087

Boyd, P. W., Strzepek, R., Fu, F., & Hutchins, D. A. (2010). Environmental control of open-ocean phytoplankton groups: Now and in the future. *Limnology and Oceanography, 55*(3), 1353–1376. https://doi.org/10.4319/lo.2010.55.3.1353

Broecker, W. S. (1982). Ocean chemistry during glacial time. *Geochimica et Cosmochimica Acta, 46*(10), 1689–1705. https://doi.org/10.1016/0016-7037(82)90110-7

Calvert, S. E., & Pedersen, T. F. (2007). Elemental proxies for palaeoclimatic and palaeoceanographic variability in marine sediments: Interpretation and application. In C. Hillaire-Marcel & A. De Vernal (Eds.), *Proxies in late cenozoic paleoceanography* (Developments in Marine Geology) (Vol. 1, pp. 567–644). Elsevier.

Cole, C. V., & Sanford, R. L. (1989). Biological aspects of the phosphorus cycle. In *Proceedings of international symposium on phosphorous requirements for sustainable agriculture in Asia and Oceania*. SCOPE/UNEP.

Conley, D. J. (2000). Biogeochemical nutrient cycles and nutrient management strategies. *Hydrobiologia, 410*, 87–96.

Cullen, J. J. (1982). The deep chlorophyll maximum: Comparing vertical profiles of chlorophyll a. *Canadian Journal of Fisheries and Aquatic Sciences, 39*, 791–803.

Damotharan, P., Perumal, N. V., Arumugam, M., Vijayalakshmi, S., & Balasubramanian, T. (2010). Seasonal variation of physicochemical characteristics in point calimere coastal waters south east coast of India. *Middle-East Journal of Scientific Research, 6*(4), 333–339.

Das, J., Das, S. N., & Sahoo, R. K. (1997). Semidiurnal variation of some physico-chemical parameters in the Mahanadi estuary, east coast of India. *Indian Journal of Marine Sciences, 26*, 323–326.

De Souza, S. N. (1983). Study on the behaviour of nutrients in the Mandovi estuary during premonsoon. *Estuarine, Coastal and Shelf Science, 16*, 299–308.

Dugdale, R. C., Wilkerson, F. P., Hogue, V. E., & Marchi, A. (2007). The role of ammonium and nitrate in spring bloom development in San Francisco Bay. *Estuarine, Coastal and Shelf Science, 73*(1–2), 17–29.

Ediger, D., Polat Beken, Ç., Feyzioğlu, M., Şahin, F., & Tan, İ. (2015). Establishing boundary classes for the quality classification of southeastern Black Sea using phytoplankton biomass. *Turkish Journal of Fisheries and Aquatic Sciences, 15*, 1–10.

Fan, H., Wang, X., Zhang, H., & Yu, Z. (2018). Spatial and temporal variations of particulate organic carbon in the Yellow-Bohai Sea over 2002-2016. *Scientific Reports, 8*, 7971. https://doi.org/10.1038/s41598-018-26373-w

Fernandes, L., Bhosle, N. B., Matondkar, S. G. P., & Bhushan, R. (2009). Seasonal and spatial distribution of particulate organic matter in the Bay of Bengal. *Journal of Marine Systems, 77*, 137–147.

Fingas, M. (2018). Remote sensing for marine management. In *World seas: An environmental evaluation* (pp. 103–119). Elsevier. https://doi.org/10.1016/b978-0-12-805052-1.00005-x

Finkel, Z. V., Beardall, J., Flynn, K. J., Quigg, A., Rees, T. A. V., & Raven, J. A. (2010). Phytoplankton in a changing world: Cell size and elemental stoichiometry. *Journal of Plankton Research, 32*, 119–137. https://doi.org/10.1093/plankt/fbp098

Ganapati, P. N., & Rao, D. V. S. (1958). Qualitative studies of plankton off Lawson's Bay, Waltair. *Proceedings of Indian Academy of Science, 48*, 189–209.

Garcia, C. A., Baer, S. E., Garcia, N. S., Rauschenberg, S., Twining, B. S., Lomas, M. W., & Martiny, A. C. (2018). Nutrient supply controls particulate elemental concentrations and ratios in the low latitude eastern Indian Ocean. *Nature Communications, 9*(1), 4868. https://doi.org/10.1038/s41467-018-06892-w

Gardner, W. D., Mishonov, A. V., & Richardson, M. J. (2006). Global POC concentrations from in-situ and satellite data. *Deep-Sea Research Part II: Topical Studies in Oceanography, 53*, 718–740. https://doi.org/10.1016/j.dsr2.2006.01.029

Geider, R., & La Roche, J. (2002). Redfield revisited: Variability of C:N:P in marine microalgae and its biochemical basis. *European Journal of Phycology, 37*, 1–17. https://doi.org/10.1017/S0967026201003456

Glibert, P. M., Biggs, D. C., & McCarthy, J. J. (1982). Utilization of ammonium and nitrate during austral summer in the Scotia Sea. *Deep Sea Research Part A. Oceanographic Research Papers, 29*(7), 837–850.

Gouda, R., & Panigrahy, R. C. (1992). Seasonal distribution and behavior of silicate in the Rushikulya estuary, east coast of India. *Indian Journal of Marine Sciences, 24*, 111–115.

Gouda, R., & Panigrahy, R. C. (1995). Seasonal distribution and behaviour of nitrate and phosphorous in Rushikulya esuary, east coast of India. *Indian Journal of Marine Sciences, 24*, 233–235.

Govindasamy, C., Kannan, L., & Azariah, J. (2000). Seasonal variation in physic-chemical parameters properties and primary production in the coastal water biotopes of Coromandel Coast, India. *Journal of Environmental Biology, 21*, 1–7.

Granier, C., Pétron, G., Müller, J. F., & Brasseur, G. (2000). The impact of natural and anthropogenic hydrocarbons on the tropospheric budget of carbon monoxide. *Atmospheric Environment, 34*(29–30), 5255–5270.

Haugen, V. E., Vinayachandran, P. N., & Yamagata, T. (2003). Comment on Indian Ocean: Validation of the Miami isopycnic coordinate ocean model and ENSO events during 1958-1998. *Journal of Geophysical Research, 108*(C6), 3179.

Hutchinson, G. E. (1957). *A treatise on limnology* (Vol. 1, p. 243). Wiley.

Irwin, A. J., Finkel, Z. V., Müller-Karger, F. E., & Troccoli Ghinaglia, L. (2015). Phytoplankton adapt to changing ocean environments. *Proceedings of the National Academy of Sciences, 112*(18), 5762–5766. https://doi.org/10.1073/pnas.1414752112

Kathiravan, K., Natesan, U., & Vishnunath, R. (2017). Spatio-temporal variability of hydrochemical characteristics of coastal waters of Gulf of Mannar Marine Biosphere Reserve (GoMMBR), South India. *Applied Water Science, 7*(1), 361–373.

Kinkel, H., Baumann, K.-H., & Cepek, M. (2000). Coccolithophores in the equatorial Atlantic Ocean: Response to seasonal and Late Quaternary surface water variability. *Marine Micropaleontology, 39*(1–4), 87–112. https://doi.org/10.1016/S0377-8398(00)00016-5

Kumar, S. B., Mohanty, A. K., Padhi, R. K., Selvanayagam, M., & Satpathy, K. K. (2018). Coastal water characteristics along Tamil Nadu, east coast of India during pre-northeast monsoon period. *Indian Journal of Geo-Marine Sciences, 47*(2), 308–318.

La Fond, E. C. (1957). Oceanographic studies in the Bay of Bengal. *Proceedings of Indian Academy of Science, 46*, 1–46.

Le, L., Lehrter, J. C., Hu, C., MacIntyre, H., Beck, M. W. (2017). Satellite observation of particulate organic carbon dynamics in two river-dominated estuaries. *Journal of Geophysical Research: Oceans, 122*, 555–569, https://doi.org/10.1002/2016JC012275

Lee, D., Son, S., Joo, H., Kim, K., Kim, M. J., Jang, H. K., Yun, M. S., Kang, C.-K., & Lee, S. H. (2020). Estimation of the particulate organic carbon to chlorophyll-a ratio using MODIS-Aqua in the East/Japan Sea, South Korea. *Remote Sensing, 12*, 840. https://doi.org/10.3390/rs12050840

Lenton, T. M., & Watson, A. J. (2000). Redfield revisited: 1. Regulation of nitrate, phosphate, and oxygen in the ocean. *Global Biogeochemical Cycles, 14*(1), 225–248. https://doi.org/10.1029/1999GB900065

Lewis, K. M., van Dijken, G. L., & Arrigo, K. R. (2020). Changes in phytoplankton concentration now drive increased Arctic Ocean primary production. *Science, 369*(6500), 198–202. https://doi.org/10.1126/science.aay8380

Lin, I., Liu, W. T., Wu, C.-C., Wong, G. T. F., Hu, C., Chen, Z., Wen-Der, L., Yang, Y., & Liu, K.-K. (2003). New evidence for enhanced ocean primary production triggered by tropical cyclone. *Geophysical Research Letters, 30*(13), 1718.

Liu, D., Bai, Y., He, X., Tao, B., Pan, D., Chen, C. T. A., Zhang, L., Xu, Y., & Gong, C. (2019). Satellite estimation of particulate organic carbon flux from Changjiang River to the estuary. *Remote Sensing of Environment, 223*, 307–319. https://doi.org/10.1016/j.rse.2019.01.025

Madhupratap, M., Nair, K. N. V., Gopalakrishnan, T. C., Haridas, P., Nair, K. K. C., Venugopal, P., & Gauns, M. (2001). Arabian Sea oceanography and fisheries off the west coast of India. *Current Science, 81*, 355–361.

Malone, T. C., Crocker, L. H., Pike, S. E., & Wendler, B. W. (1988). Influences of river flow on the dynamics of phytoplankton production in a partially stratified estuary. *Marine Ecology Progress Series, 48*, 235–249.

Manikannan, R., Asokan, S., & Ali, A. H. M. S. (2011). Seasonal variations of physico-chemical properties of the Great Vedaranyam Swamp, Point Calimere Wildlife Sanctuary, South-east coast of India. *African Journal of Environmental Science and Technology, 5*(9), 673–681.

Martin, R. E. (1995). Cyclic and secular variation in microfossil biomineralization: Clues to the biogeochemical evolution of Phanerozoic oceans. *Global and Planetary Change, 11*(1), 1–23.

Martiny, A. C., Pham, C. T. A., Primeau, F. W., Vrugt, J. A., Moore, J. K., Levin, S. A., & Lomas, M. W. (2013). Strong latitudinal patterns in the elemental ratios of marine plankton and organic matter. *Nature Geoscience, 6*(4), 279–283. https://doi.org/10.1038/ngeo1757

McCreary, J. P., Han, W., Shankar, D., & Shetye, S. R. (1996). Dynamics of the East India coastal current 2: Numerical solutions. *Journal of Geophysical Research, 101*, 13993–14010.

Mohanty, A. K., Satpathy, K. K., Sahu, G., Hussain, K. J., Prasad, M. V. R., & Sarkar, S. K. (2010). Bloom of Trichodesmium erythraeum (Ehr.) and its impact on water quality and plankton community structure in the coastal waters of southeast coast of India. *Indian Journal of Marine Sciences, 39*(3), 323–333.

Mohanty, A. K., Sahu, G., Bramha, S. N., Samantara, M. K., & Satpathy, K. K. (2014). Assessment of temporal variation in coastal water characteristics through multivariate statistics-A case study at southwestern Bay of Bengal, India. *Indian Journal of Geo-Marine Science, 3*(9), 1718–1731.

Mora, C., et al. (2013). Biotic and human vulnerability to projected changes in ocean biogeochemistry over the 21st century. *PLOS Biology, 11*(10), e1001682. https://doi.org/10.1371/journal.pbio.1001682

Moreno, A. R., & Martiny, A. C. (2018). Ecological stoichiometry of ocean plankton. *Annual Review of Marine Science, 10*, 43–69. https://doi.org/10.1146/annurev-marine-121916-063126

Murty, C. S., & Varadachari, V. V. R. (1968). Upwelling along the east coast of India. *Bulletin National Institute of Science, India, 36*, 80–86.

Nandakumar, K., Venkat, K., & Bhosle, N. B. (1987). Distribution of particulate organic carbon in the central Bay of Bengal. *Proceedings of the Indian Academy of Sciences – Earth and Planetary Sciences, 96*(2), 189–193.

Nowicki, B. L., & Nixon, S. W. (1985). Benthic nutrient remineralization in a coastal lagoon ecosystem. *Estuaries, 8*, 182–190.

Olson, R. J. (1980). Nitrate and ammonium uptake in Antarctic waters. *Limnology and Oceanography, 26*, 1064–1074.

Oyeku, O. G., & Mandal, S. K. (2020). Historical occurrences of marine microalgal blooms in Indian peninsula: Probable causes and implications. *Oceanologia, 63*, 51. https://doi.org/10.1016/j.oceano.2020.08.008

Paerl, H. W. (1997). Coastal eutrophication and harmful algal blooms: Importance of atmospheric deposition and groundwater as "new" nitrogen and other nutrient sources. *Limnology and Oceanography, 42*, 1154–1165.

Panigrahy, R. C., Mishra, S., Sahu, G., & Mohanty, A. K. (2006). Seasonal distribution of phytoplankton in the surf waters off Gopalpur, east coast of India. *Journal of the Marine Biological Association of India, 48*, 156–160.

Pavia, F. J., Anderson, R. F., Lam, P. J., Cael, B. B., Vivancos, S. M., Fleisher, M. Q., Lu, Y., Zhang, P., Cheng, H., & Lawrence Edwards, R. (2019). Shallow particulate organic carbon regeneration in the South Pacific Ocean. *Proceedings of the National Academy of Sciences of the United States of America, 116*, 9753–9758. https://doi.org/10.1073/pnas.1901863116

Pomeroy, C. R., Smith, E. E., & Grant, C. M. (1965). The exchange of phosphate between estuarine water and sediments. *Limnology and Oceanography, 10*, 167–172.

Poornima, E. H., Rajadurai, M., Rao, T. S., Anupkumar, B., Rajamohan, R., Narasimhan, S. V., & Venugopalan, V. P. (2005). Impact of thermal discharge from a tropical coastal power plant on phytoplankton. *Journal of Thermal Biology, 30*(4), 307–316.

Prabu, V. A., Rajkumar, M., & Perumal, P. (2008). Seasonal variations in physico-chemical characteristics of Pichavaram mangroves, southeast coast of India. *Journal of Environmental Biology, 29*(6), 945–950.

Prasannakumar, S., Madhupratap, M., Dileep Kumar, M., Gauns, M., Muraleedharan, P. M., Sarma, V. V., & De Souza, S. N. (2000). Physical control of primary productivity on a seasonal scale in central and eastern Arabian Sea. *Proceedings of Indian Academy of Science, 109*, 433–441.

Prasannakumar, S., Muralidharan, P. M., Prasad, T. G., Ganus, M., Ramaiah, N., De Souza, S. N., et al. (2002). Why Bay of Bengal is less productive during summer monsoon compared to the Arabian Sea? *Geophysical Research Letter, 29*, 88.1–88.4.

Prentice, I., Farquhar, G., Fasham, M., Goulden, M., Heimann, M., Jaramillo, V., Kheshgi, H., Le Quéré, C., Scholes, R., Wallace, D. W. R., et al. (2001). The carbon cycle and atmospheric carbon dioxide. In J. T. Houghton, Y. Ding, D. J. Griggs, M. Noguer, P. J. van der Linden, X. Dai, K. Maskell, & C. A. Johnson (Eds.), *Climate change 2001: The scientific basis* (pp. 185–237). Cambridge University Press.

Qasim, S. Z. (1977). Biological productivity of the Indian Ocean. *Indian Journal of Marine Sciences, 6*, 122–137.

Radhakrishna, K., Thiri, P. M. A., & Devassy, V. P. (1982). Chlorophyll a, phaeopigments and particulate organic carbon in the Northern and Western Bay of Bengal. *Indian Journal of Marine Sciences, 11*, 278–291.

Rageneau, O., Tréguer, P., Leynaert, A., Anderson, R. F., Brzezinski, M. A., DeMaster, D. J., Dugdale, R. C., Dymond, J., Fischer, G., François, R., Heinze, C., MaierReimer, E., Martin-Jézéquel, V., Nelson, D. M., & Quéguiner, B. (2000). A review of the Si cycle in the modern ocean: Recent progress and missing gaps in the application of biogenic opal as a paleoproductivity proxy. *Global and Planetary Change, 26*, 317–365.

Rajaram, S., Brindha, J. T., Sreedevi, K. R., & Hegde, A. G. (2012). Efficiency as a function of MEQ-CWT for large area germanium detectors using LLNL phantom. *Radiation Protection Dosimetry, 148*(1), 121–125.

Redfield, A. C. (1958). The biological control of chemical factors in the environment. *American Scientist, 46*(3), 205–221, 230A.

Ridgwell, A. (2005). A Mid Mesozoic Revolution in the regulation of ocean chemistry. *Marine Geology, 217*(3), 339–357.

Roach, J. (2004, June 7). Source of half earth's oxygen gets little credit. *National Geographic News*. Retrieved 4 April 2016.

Sahu, G., Satpathy, K. K., Mohanty, A. K., & Sarkar, S. K. (2012). Variations in community structure of phytoplankton in relation to physicochemical properties of coastal waters, southeast coast of India. *Indian Journal of Geo-Marine Sciences, 41*(3), 223–241.

Sahu, G., Mohanty, A. K., Sarangi, R. K., Bramha, S. N., & Satpathy, K. K. (2016). Upwelling initiated algal bloom event in the coastal waters of Bay of Bengal during post northeast monsoon period. *Current Science, 10*, 979–981.

Sahu, G., Mohanty, A. K., Sarangi, R. K., & Satpathy, K. K. (2022). Asterionellopsis glacialis (Family:Fragilariaceae; Class: Bacillariophyceae; Phylum: Ochrophyta) bloom and its impact on plankton dynamics at Kalpakkam (Bay of Bengal, Southeast coast of India). *Oceanologia, 64*(1), 145–159.

Sankaranrayanan, V. N., & Qasim, S. Z. (1969). Nutrients of the Cochin Backwaters in relation to environmental characteristics. *Marine Biology, 2*, 236–247.

Santhanam, P., & Perumal, P. (2003). Diversity of zooplankton in Parangipettai coastal waters, southeast coast of India. *Journal of the Marine Biological Association of India, 45*(2), 144–151.

Saravanane, N., Nandakumar, K., Durairaj, G., & Nair, K. V. K. (2000). Plankton as indicators of coastal water bodies during southwest to northeast monsoon transition at Kalpakkam. *Current Science, 78*, 173–176.

Sarma, V. V., Sadhuram, Y., Sravanthi, N. A., & Tripathy, S. C. (2006). Role of physical processes in the distribution of chlorophyll-*a* in the Northwest Bay of Bengal during pre- and post-monsoon seasons. *Current Science, 91*, 1133–1134.

Sathishkumar, R. S., Sundaramanickam, A., Sahu, G., Mohanty, A. K., Ramesh, T., & Ajmal Khan, S. (2021). Intense bloom of the diatom Hemidiscus hardmanianus (Greville) in relation to water quality and plankton communities in Tuticorin coast, Gulf of Mannar, India. *Marine Pollution Bulletin, 163*, 111757. https://doi.org/10.1016/j.marpolbul.2020.111757

Satpathy, K. K., & Nair, K. V. K. (1996). Occurrence of phytoplankton bloom and its effect on coastal water quality. *Indian Journal of Marine Sciences, 25*, 145–147.

Satpathy, K. K., Mohanty, A. K., Prasad, M. V. R., Bhaskar, S., Jebakumar, K. E., & Natesan, U. (2006). Impact of biofouling community on the cooling water quality with special emphasis on its nutrient content. In *Proceedings of the international conference on recent advances in marine antifouling technology* (pp. 326–337). Allied Publishers.

Satpathy, K. K., Mohanty, A. K., Sahu, G., Prasad, M. V. R., Venkatesan, R., Natesan, U., & Rajan, M. (2007). On the occurrence of Trichodesmium erythraeum (Ehr.) bloom in the coastal waters of Kalpakkam, east coast of India. *Indian Journal of Science and Technology, 1*(2), 1–9.

Satpathy, K. K., Sahu, G., Mohanty, A. K., Prasad, M. V. R., & Panigrahy, R. C. (2009). Phytoplankton community structure and its variability during southwest to northeast monsoon transition in the coastal waters of Kalpakkam, east coast of India. *International Journal of Oceans and Oceanography, 3*, 43–74.

Satpathy, K. K., Mohanty, A. K., Natesan, U., Prasad, M. V. R., & Sarkar, S. K. (2010). Seasonal variation in physicochemical properties of coastal waters of Kalpakkam, east coast of India with special emphasis on nutrients. *Environmental Monitoring and Assessment, 164*(1–4), 153–171.

Satpathy, K. K., Mohanty, A. K., Sahu, G., Sarguru, S., Sarkar, S. K., & Natesan, U. (2011). Spatio-temporal variation in physicochemical properties of coastal waters off Kalpakkam, southeast coast of India, during summer, pre-monsoon and post-monsoon period. *Environmental Monitoring and Assessment, 180*(1–4), 41–62.

Sherin, C. K., Sarma, V. V. S. S., Rao, G. D., Viswanadham, R., Omand, M. M., & Murty, V. S. N. (2018). New to total primary production ratio (f-ratio) in the Bay of Bengal using isotopic composition of suspended particulate organic carbon and nitrogen. *Deep Sea Research Part I: Oceanographic Research Papers, 139*, 43–54. https://doi.org/10.1016/j.dsr.2018.06.002

Sigman, D. M., & Hain, M. P. (2012). The biological productivity of the ocean. *Nature Education Knowledge, 3*(6), 1–16. Retrieved 1 June 2015. The deep chlorophyll maximum (DCM) occurs at the contact where there is adequate light for photosynthesis and yet significant nutrient supply from below.

Srinivasalu, S., Thangadurai, N., Switzer, A. D., Mohan, V. R., & Ayyamperumal, T. (2007). Erosion and sedimentation in Kalpakkam (N Tamil Nadu, India) from the 26th December 2004 tsunami. *Marine Geology, 240*(1–4), 65–75.

Stramska, M. (2009). Particulate organic carbon in the global ocean derived from SeaWiFS ocean color. *Deep Sea Research Part I: Oceanographic Research Papers, 56*, 1459–1470. https://doi.org/10.1016/j.dsr.2009.04.009

Stramska, M. (2014). Particulate organic carbon in the surface waters of the North Atlantic: Spatial and temporal variability based on satellite ocean colour. *International Journal of Remote Sensing, 35*, 4717–4738. https://doi.org/10.1080/01431161.2014.919686

Strickland, J. D. H., & Parsons, T. R. (1972). *A practical handbook of seawater analysis* (Fisheries Research Board of Canada Bulletin) (Vol. 167, 2nd ed., pp. 261–310). Fisheries Research Board of Canada.

Sulochanan, B., & Muniyandi, K. (2005). Hydrographic parameters off Gulf of Mannar and Palk Bay during an year of abnormal rainfall. *Journal of the Marine Biological Association of India, 47*(2), 198–200.

Sundaramanickam, A., Sivakumar, T., Kumaran, R., Ammaiappan, V., & Velappan, R. (2008). Comparative study of physico-chemical investigation along Parangipettai and Cuddalore Coast. *Journal of Environmental Science and Technology, 1*(1), 1–10.

Świrgoń, M., & Stramska, M. (2015). Comparison of in situ and satellite ocean color determinations of particulate organic carbon concentration in the global ocean. *Oceanologia, 57*, 25–31. https://doi.org/10.1016/j.oceano.2014.09.002

Tanioka, T., & Matsumoto, K. (2020). A meta-analysis on environmental drivers of marine phytoplankton C:N:P. *Biogeosciences, 17*(11), 2939–2954. https://doi.org/10.5194/bg-17-2939-2020

Tribovillard, N., Algeo, T. J., Lyons, T. W., & Riboulleau, A. (2006). Trace metals as paleoredox and paleoproductivity proxies: An update. *Chemical Geology, 232*, 12–32.

Tripathy, S. C., Ray, A. K., Patra, S., & Sarma, V. V. (2005). Water quality assessment of Gautami-Godavari mangrove estuarine ecosystem of Andhra Pradesh, India during September 2001. *Journal of Earth System Science, 114*, 185–190.

Tyrrell, T. (1999). The relative influences of nitrogen and phosphorus on oceanic primary production. *Nature, 400*(6744), 525–531. https://doi.org/10.1038/22941

Vajravelu, M., Martin, Y., Ayyappan, S., & Mayakrishnan, M. (2018). Seasonal influence of physico-chemical parameters on phytoplankton diversity, community structure and abundance at Parangipettai coastal waters, Bay of Bengal, south east coast of India. *Oceanologia, 60*(2), 114–127.

Van De Waal, D. B., Verschoor, A. M., Verspagen, J. M. H., Van Donk, E., & Huisman, J. (2010). Climate-driven changes in the ecological stoichiometry of aquatic ecosystems. *Frontiers in Ecology and the Environment, 8*(3), 145–152. https://doi.org/10.1890/080178

Varkey, M. J., Murty, V. S. N., & Suryanaryan, A. (1996). Physical oceanography of the Bay of Bengal and Andaman Sea. In A. D. Ansell, R. N. Gibson, & M. Barnes (Eds.), *Oceanography and marine biology* (Vol. 34, pp. 1–70). UCL Press.

Vinayachandran, P. N., Murty, V. S. N., & Ramesh Babu, V. (2002). Observations of barrier layer formation in the Bay of Bengal during summer monsoon. *Journal of Geophysical Research: Oceans, 107*(C12), SRF-19.

Wang, X., Ma, H., Li, R., Song, Z., & Wu, J. (2012). Seasonal fluxes and source variation of organic carbon transported by two major Chinese Rivers: The Yellow River and Changjiang (Yangtze) River. *Global Biogeochemical Cycles, 26*(2), GB2025. https://doi.org/10.1029/2011GB004130

Webb, P. (2020). *Introduction to oceanography*. https://LibreTexts.org

Xu, K., & Milliman, J. D. (2009). Seasonal variations of sediment discharge from the Yangtze River before and after impoundment of the Three Gorges Dam. *Geomorphology, 104*, 276–283. https://doi.org/10.1016/j.geomorph.2008.09.004

Yu, J., Wang, X., Fan, H., & Zhang, R. H. (2019). Impacts of physical and biological processes on spatial and temporal variability of particulate organic carbon in the North Pacific Ocean during 2003–2017. *Scientific Reports, 9*, 1–15. https://doi.org/10.1038/s41598-019-53025-4

Zepp, R. G. (1997). Interactions of marine biogeochemical cycles and the photodegradation of dissolved organic carbon and dissolved organic nitrogen. In A. Gianguzza, E. Pelizzetti, & S. Sammarkano (Eds.), *Marine chemistry* (pp. 329–352). Kluwer Academic Plublication.

Zhu, G. H., Liu, Y. L., Chen, L. H., Yu, P. S., Jin, M., & Liu, Z. L. (2011). Studies on phytoplankton and particulate organic carbon in the Southern Ocean. *Applied Mechanics and Materials, 137*, 344–352. https://doi.org/10.4028/www.scientific.net/amm.137.344

Zimmerman, C. F., Keefe, C. W., & Bashe, J. (1997). *Method 440.0 determination of carbon and nitrogen in sediments and particulates of estuarine/coastal waters using elemental analysis* (EPA/600/R-15/009). U.S. Environmental Protection Agency.

Chapter 4
Variation of Phytoplankton Assemblages and Primary Productivity Characteristics in the Equatorial Indian Ocean During Two Seasons

Jane Theophline Bhaskar

Abstract The Equatorial Indian Ocean (EIO) is considered to be a highly oligotrophic marine regime. The nutrients, chlorophyll *a* (chl *a*), phytoplankton abundance, community structure, and production along 83°E from 1°N to 5°S in the EIO for northeast monsoon (NEM; February 2003) and southwest monsoon (SWM; July–August 2003) were studied. Nutrient concentrations, chl *a*, and phytoplankton productivity (<25 mg C m^{-2} d^{-1}) did not vary much, but cell abundances and taxonomic composition were different between the seasons. Subsurface chlorophyll maxima (~60–80 m) coincided with higher nutrient concentrations (≥2 μM) during both periods. Column (0–100 m depth) chl *a* ranged between 12.4 and 18.8 mg m^{-2} (NEM) and 3.4 and 19.29 mg m^{-2} (SWM). Integrated phytoplankton abundance ranged from 7.2 to 60.8 × 10^3 cells m^{-2} (NEM) and 9.6 to 26 × 10^3 cells m^{-2} (SWM). Overall, diatoms formed 87% and 84%, and dinoflagellates constituted 13% and 16% of the phytoplankton communities during NEM and SWM, respectively. Investigations on the primary or phytoplankton productivity characteristics in the EIO are few, although the phytoplankton community here is diverse, and it is hypothesized that they are the principal autotrophs sustaining the possible and moderate secondary and tertiary production despite the daily low primary production.

Keywords Central Indian Ocean · Chlorophyll · Diatoms · Dinoflagellates · Phytoplankton · Productivity

J. T. Bhaskar (✉)
National Centre for Polar and Ocean Research, Ministry of Earth Sciences, Headland Sada, Vasco-da-Gama, Goa, India

S. C. Tripathy, A. Singh (eds.), *Dynamics of Planktonic Primary Productivity in the Indian Ocean*, https://doi.org/10.1007/978-3-031-34467-1_4

1 Introduction

Phytoplankton form the base of the marine food web and play an important role in the global biogeochemical cycles and are thus important driving forces of global climate (Falkowski et al., 1998). Phytoplankton are primary producers that are highly diverse, comprising eukaryotic algal cells, namely, diatoms, dinoflagellates, and coccolithophorids to prokaryotes like cyanobacteria and many picoplanktonic forms are ecologically very important, sensitive to changing environmental conditions and regulate the global carbon dioxide levels by means of primary production. Most resilient, ecologically versatile phytoplankton communities adjust their position in the water column of most marine regions to achieve optimal growth and reproduction. They thus integrate a range of hydro-meteorological conditions and may act as indicators of natural or anthropogenically induced environmental changes (Reid et al., 2003). In the oceanic regimes, they can be found in the upper 200 m, and their productivity is estimated to be ca 200 g C m^{-2} y^{-1} (Dawes, 1998). Investigations on phytoplankton community structure are thus important as such studies allow us to observe their responses to environmental changes.

In general, the Indian Ocean is considered more productive than the Atlantic and Pacific (Kabanova, 1968). However, the oligotrophic equatorial Indian Ocean (EIO) with a deep euphotic (~100 m) zone and generally low nutrients has been scantily investigated. Aside from the earlier reports of the International Indian Ocean Expedition (IIOE) on phytoplankton assemblages (Taylor, 1973; Durairatnam, 1964), recent investigations from these waters are sparse despite a large number of investigations under the aegis of JGOFS in the Arabian Sea during the 1990s (Anon, 2002). Though the IIOE covered the Indian Ocean extensively (Zeitzschel, 1973) and reported 237 different phytoplankton taxa (Thorrington-Smith, 1971), thereon, the taxonomic studies on phytoplankton from the EIO, however, are quite a few (Taylor, 1973; Durairatnam, 1964; Gnanasoundari, 1987; Liu et al., 2021). However, in comparison, some recent studies have reported on the primary production from the southwest tropical Indian Ocean (Roxy et al., 2016; Tripathy et al., 2020).

Hydrological conditions in the Indian Ocean depend largely on the monsoonal winds, which change direction with the seasons (Kabanova, 1968), thus affecting the currents in the surface layers. As a consequence of these seasonal variations, greater than 90% of rainfall over the Indian subcontinent occurs during the southwest monsoon (SWM) which occurs between June and September and the northeast monsoon (NEM) that occurs during December to March (Ruma & Shaji, 2019).

Chlorophyll production is usually low during intermonsoon seasons. Most of the biological studies carried out in the Indian Ocean have focused on primary production along the coastal regions of Kenya (Kromkamp et al., 1997), Somalia (Veldhuis et al., 1997; Smith et al., 1998), Northern Arabian Sea (Qasim, 1982; Bhattathiri et al., 1996), and Bay of Bengal (Radhakrishna et al., 1978, Bhattathiri et al., 1980, Anon., 2002, Madhupratap et al., 2003; Madhu et al., 2006). A recent study has been carried out describing the physical and biogeochemical processes in the coastal

regions of the Indian Ocean (Vinaychandran et al., 2021). However, there are no recent investigations on the general productivity characteristics, species composition, and distribution of phytoplankton from the EIO. In this study, we examined the microplankton distribution and composition, its biomass (chlorophyll *a*), and primary productivity during SWM and NEM across the equator from 1°N to 5°S along 83°E.

2 Methods

2.1 Study Site

Sampling for this study was carried out onboard Russian Research Vessel *A. A. Sidorenko* during the northeast monsoon (NEM; January 27–February 23, 2003) and southwest monsoon (SWM; July 8–August 12, 2003) seasons. The ship embarked on a 30-day cruise from Mormugao port, Goa, India, and returned to the same port after the sampling during both seasons. Water samples were collected for measuring concentrations of nutrients and chlorophyll, and for enumerating and identification of phytoplankton from 7 stations (Fig. 4.1) located at 1°N (S1), Equator (S2), 1°(S3), 2°(S4), 3°(S5), 4°(S6), and 5°S(S7) along 83°E. Water depth at these stations ranged from 2000 to 2200 m; however, the water samples collected for this study were restricted up to the top 120 m. Samples were collected from the surface, 10 m, 20 m, and thereafter at 20 m intervals till 100 or 120 m using Niskin samplers fixed on a hydrocast during NEM and CTD rosette during SWM.

2.2 Nutrients

Nitrate (using Cadmium column) and nitrite were determined by the Moris and Riley method (Grasshoff, 1983) and measured at 543 nm. Phosphate was measured at 880 nm, as described by Murphy and Riley (1962). Dissolved silicates were analyzed as described in Grasshoff (1983) and measured at 810 nm spectrophotometrically.

2.3 Biological Parameters

Chlorophyll *a* (chl *a*) concentrations were determined fluorometrically (Turner Designs, USA, 10 AU) by filtering two replicates of 1 L water samples from each depth using GF/F filters and extracting overnight in 10 ml of 90% acetone at 4 °C in a refrigerator (Fernandes et al., 2007).

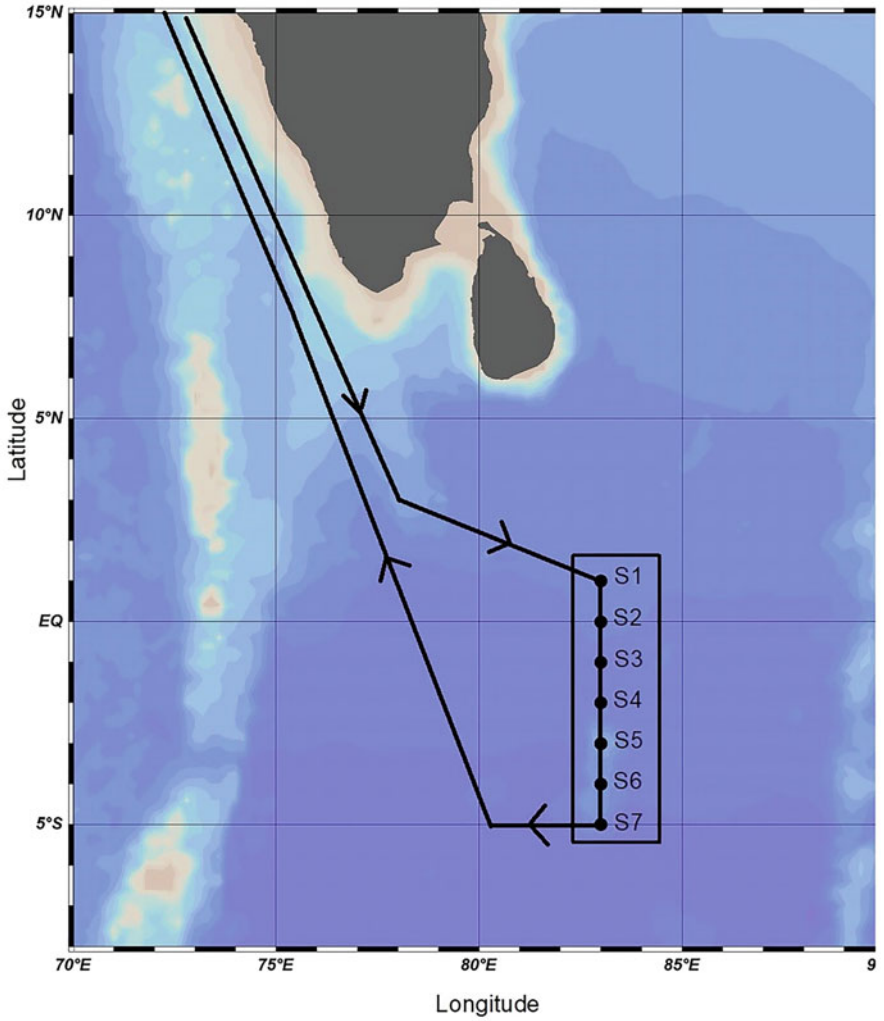

Fig. 4.1 Study map depicting the sampling stations along the equatorial Indian Ocean during two different seasons

For primary production (PP) measurements, water samples were drawn from the abovementioned seven or eight depths at predawn as per the JGOFS protocols (UNESCO, 1994) and were collected in three 300 ml polycarbonate bottles (Nalgene, Germany). One ampoule of $NaH^{14}CO_3$ was added to each bottle (two light and one dark bottle at each depth) and incubated in situ using a mooring system (Fernandes et al., 2007) for 12 hours from just before sunrise to a half-hour past sunset following the JGOFS protocols (UNESCO, 1994). Incorporation of ^{14}C was

determined by filtering 100 ml sample from each bottle through GF/F filters (25 mm diameter, 0.7 μm pore size, Whatman, USA). The filters were transferred to scintillation vials individually and exposed overnight to HCl (0.5 N) fumes in a closed container. A 5 ml liquid scintillation cocktail (Sisco Research Laboratory, Mumbai) was added to each vial, and the radioactivity was measured in a scintillation counter (Wallac 1409DSA, Perkin Elmer, USA). The PP rate was expressed as mg C m^{-3} d^{-1}, as per JGOFS protocols (UNESCO, 1994) for discrete depths, and as mg C m^{-2} d^{-1} for column-integrated (trapezoid) values (Fernandes et al., 2007).

For analyzing phytoplankton cell counts and composition, water samples from each depth were fixed in Lugol's iodine (1% w/v) and 3% formaldehyde and stored in the dark until taken out for analyses. A natural settling (for 24 hours in 1 L jars set on a table in the dark) and siphoning procedure was followed to concentrate samples from 250 to 20 ml. Enumeration and identification of phytoplankton (>5 μm) population up to the genus and, in certain cases, species level, were carried out in duplicates. One ml of the concentrated samples was loaded onto a Sedgewick rafter plankton counting chamber and examined microscopically at 200× & 400× magnification. Genus and species identification followed the keys of Subramanyan (1946, 1968), Subramanyan and Sarma (1961), Lebour (1978), Desikachary and Ranjithadevi (1986), Desikachary and Prema (1987), Desikachary et al. (1987), Constance et al. (1985a, b), and Tomas (1997). In some cases, an oil immersion objective at 100× on a Zeiss (Axioskop, 2plus, Germany) microscope was also used to confirm identification.

3 Results

3.1 Hydrography

The sea surface temperature did not show large-scale differences between the seasons. It ranged from 28.2 °C at 1°N to 27.4 °C at 5°S during NEM. Similarly, it decreased slightly from 28.7 °C at 1°N to 28.1 °C at 5°S during SWM. Surface salinity was lower in NEM (33.6–33.63) than during SWM, where it ranged from 34.8 to 35.05 and maintained a mean of approximately 34.5 in the deep (up to 300 m) during SWM (Fernandes et al., 2007).

In the PP stations (S2, S5, and S7), the average temperature ranged from 25.3 °C (S7) to 27.2 °C (S2) and 26.8 °C (S5) to 27.1 °C (S2) during NEM and SWM, respectively (Table 4.1). However, the average salinity was lower in NEM and ranged from 32.27 (S7) to 34.75 (S5) during NEM and 34.80 (S2) to 34.84 (S7) during SWM.

Table 4.1 The mean temperature and salinity during northeast monsoon (NEM) and southwest monsoon (SWM) at the primary productivity stations

	NEM		SWM	
Station	Temp	Salinity	Temp	Salinity
S2	27.19 (18.9–29.2)	34.74 (34.05–34.99)	27.10 (19.9–28.2)	34.80 (34.83–34.75)
S5	26.41 (21–28.3)	34.75 (32.85–35.64)	26.8 (20.0–28.5)	34.8 (34.75–34.83)
S7	25.29 (17.75–28.4)	32.27 (28.89–34.02)	26.9 (21.0–28.4)	34.84 (34.78–35.05)

Ranges are given in parentheses

3.2 Nutrients

The surface total nitrate (TN) concentrations ranged from 0.09 to 10.92 μM during NEM. TN concentrations were ≥3 μM at three of the six stations covered (Fig. 4.2). Surface TN concentrations during SWM, ranged from 0 to 0.65 μM (Fig. 4.3), while concentrations ≥6 μM were observed at 100 m and below. TN concentrations generally increased with increasing depths. The nitracline (>2 μM) was deeper during NEM and existed below 80 m, whereas during SWM, it existed below 60 m. The surface TN concentrations were relatively high at three locations (1°S (S3), 2°S (S4), 3°S (S5), along 83°E during NEM. At the other locations (equator (S2), 4°S (S6), and 5°S (S7)), low concentrations persisted almost up to 80 m (Fig. 4.2).

Surface phosphate ranged from 0.04 to 0.25 μM and 0.15 to 0.34 μM during NEM and SWM, respectively (Fig. 4.2). The highest surface concentration of 0.3 μM was observed at 1°S during SWM (Fig. 4.3). At most of the stations, phosphate concentrations showed an increasing trend from 80 m during both the seasons increasing to about 1 μM at 100 m at most sampled locations during NEM.

Seasonal differences in the surface SiO_4 concentrations were not pronounced either (Fig. 4.2). Surface silicate ranged from 0.06 to 1.93 μM in the NEM, while it ranged from 0.12 to 1.67 μM in the SWM (Fig. 4.3). Its concentrations were higher at greater depths during both the seasons.

3.3 Chlorophyll Distribution

The surface chl *a* concentration was generally less than 0.1 mg m^{-3} during both seasons except for a relatively high concentration (0.19 mg m^{-3}) at the equator during SWM (Fig. 4.4). There was pronounced subsurface chlorophyll maximum (SCM) around 80 m at all stations during the NEM, and the peaks fluctuated between 40 and 80 m during SWM. The 0–100 m column values ranged from 12.4 mg m^{-2} (S2) to a high value of 18.7 mg m^{-2} (S6) during NEM, and during SWM, the chl *a* values reduced from north to south of the equator with the minimum of 3.47 mg m^{-2} observed at S5 (Fig. 4.7).

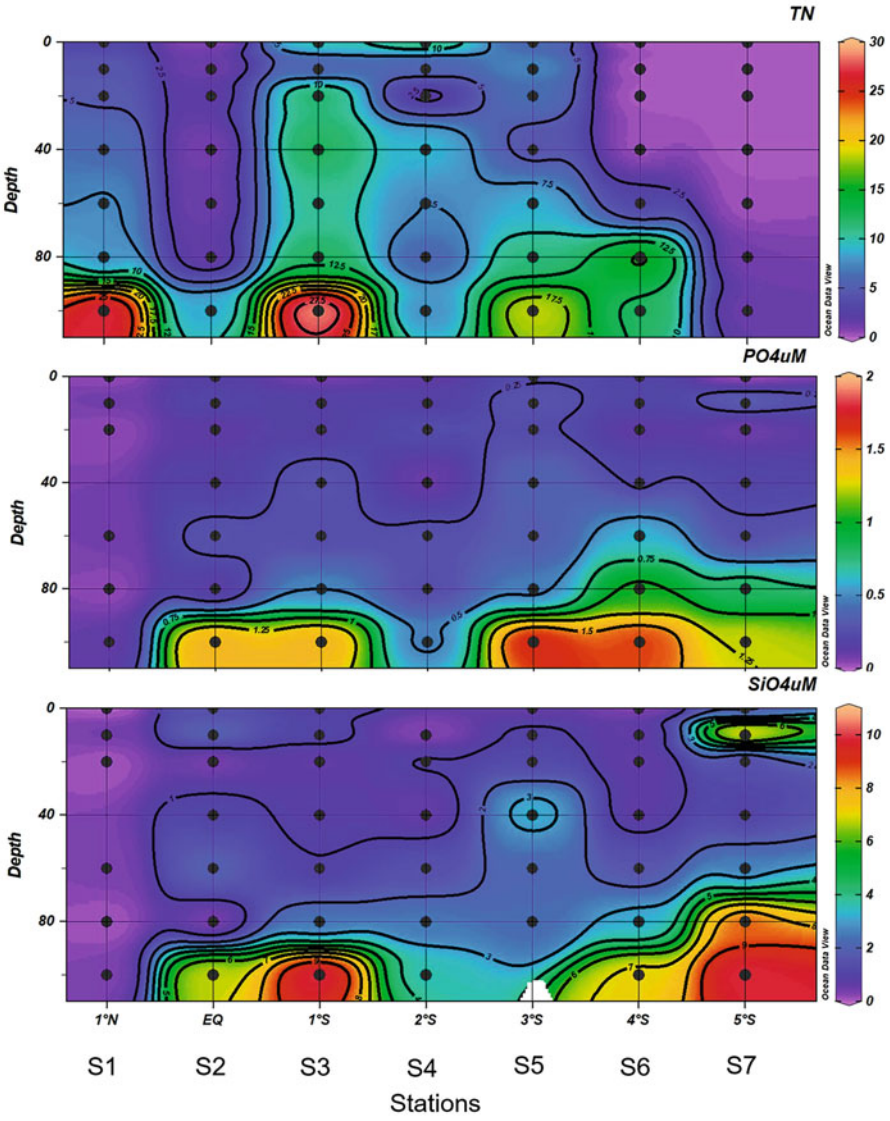

Fig. 4.2 Distribution of total NO_3-N (TN; μM), phosphate (PO4; μM), and silicate (SiO_4; μM) concentrations along the equatorial Indian Ocean during northeast monsoon (NEM)

3.4 Primary Production

Primary production during both season was highest in the surface and decreased with depth. Primary productivity ranged from 0.01 to 2.14 mg C m^{-3} d^{-1} in the NEM and 0.01 to 0.73 mg C m^{-3} d^{-1} in the SWM (Fig. 4.5), increasing from the equator to the south stations (5°S). In general, the surface primary productivity was higher at all

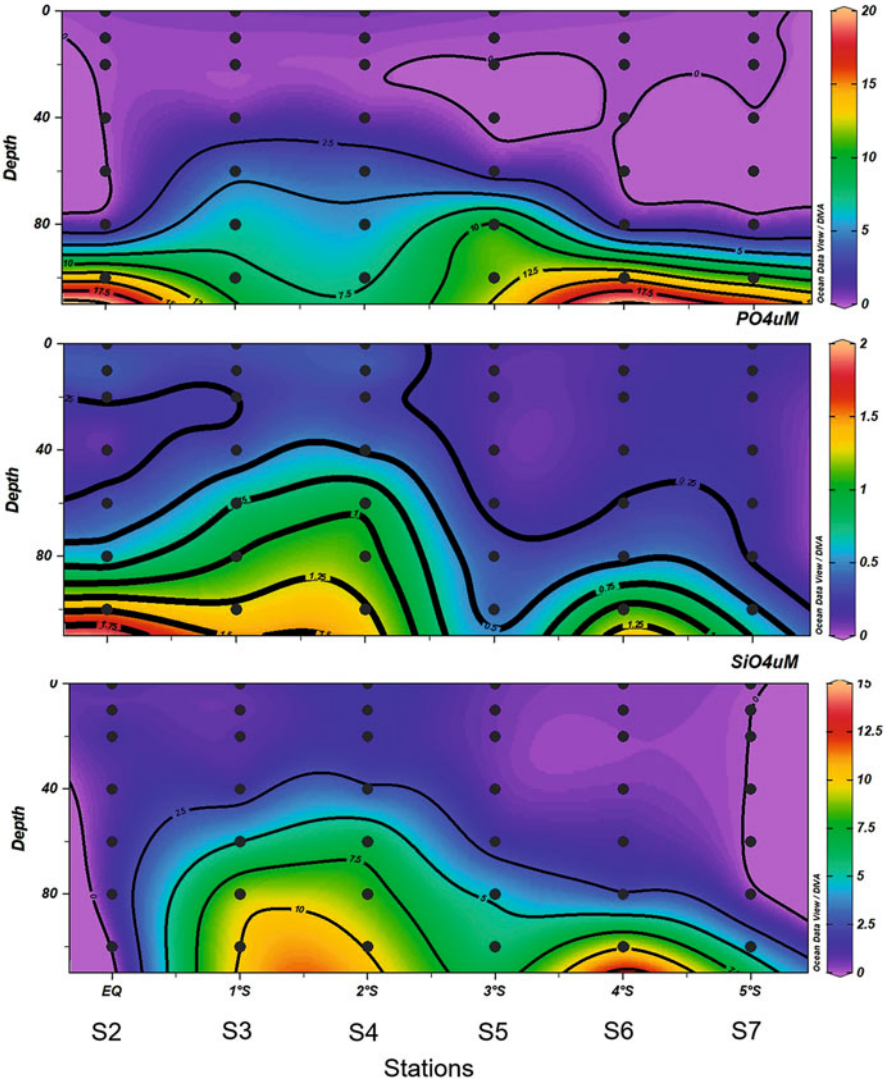

Fig. 4.3 Distribution of total NO_3-N (TN; μM), phosphate (PO4; μM), and silicate (SiO_4; μM) concentrations along the equatorial Indian Ocean during southwest monsoon (SWM)

stations (S2, S5, S7) during NEM as compared to SWM. However, at the equator (S2), below 10 m the production rates were almost negligible during NEM, whereas the production rates were higher from 20 m and reached a maximum at 60 m during SWM. At station S5, the productivity rates decreased from the surface to a depth of 40 m and thereafter increased slightly more than what was observed at S2 during NEM. The primary production rates showed a similar pattern in SWM too with

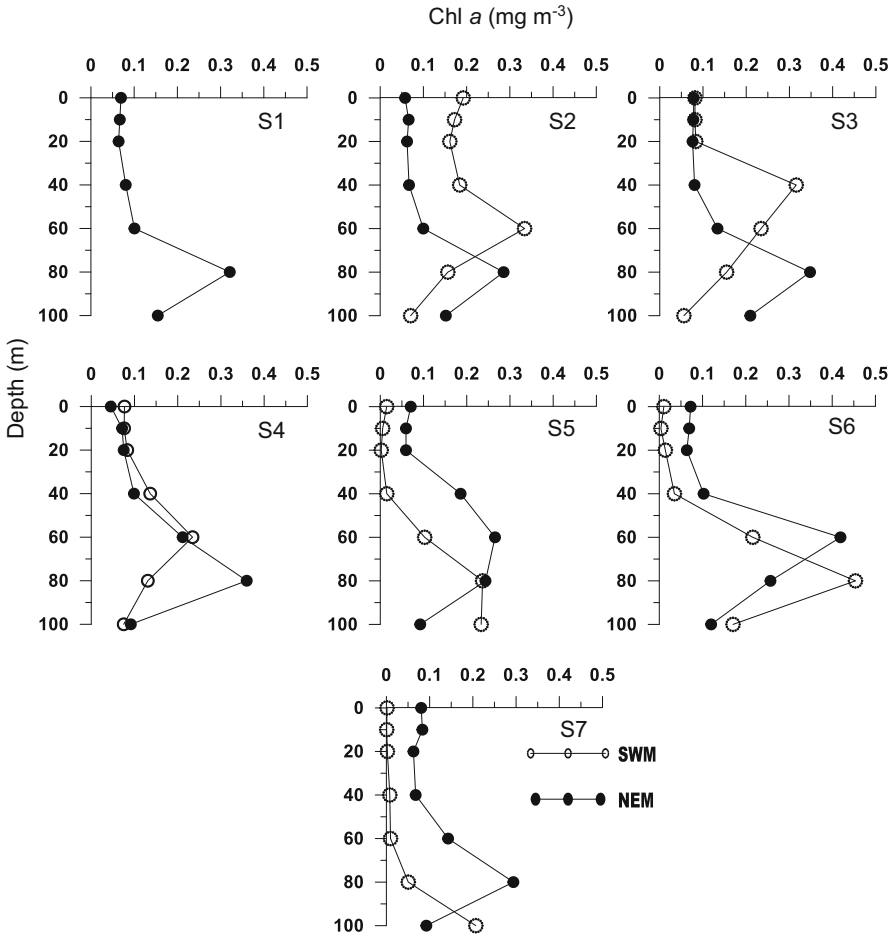

Fig. 4.4 Vertical profiles of chlorophyll *a* (mg m^{-3}) in the Equatorial Indian Ocean along 83°E during southwest monsoon (SWM) and northeast monsoon (NEM)

slightly higher concentrations at 20–40 m depth as compared to NEM. During NEM, at the southernmost station (S5), maximum productivity was observed as compared to S2 and S3 throughout the water column whereas during SWM minimum production was observed. The column-integrated production ranged from 4.85 to 39.79 and 10.36 to 19.91 mg C m^{-2} d^{-1} during NEM and SWM, respectively (Fig. 4.7). The average column production was observed to be higher during the NEM (20 mg C m^{-2} d^{-1}) than the SWM (16 mg C m^{-2} d^{-1}).

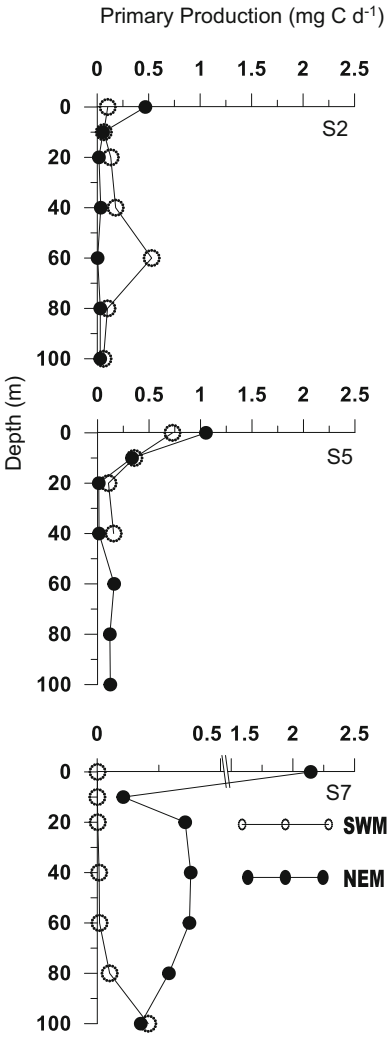

Fig. 4.5 Primary production (mg C m^{-3} d^{-1}) in the Central Indian Ocean (83°E) during northeast monsoon (NEM) and southwest monsoon (SWM). Samples from three depths at 3°S 83°E were lost during the SWM due to entangling in a fishing net from a vessel nearby

3.5 Phytoplankton Distribution and Assemblages

In general, the overall phytoplankton abundance was observed to be higher in NEM as compared to SWM. During NEM, the highest phytoplankton abundance (approximately 1280 cells l^{-1}) was seen at 60 m at S6 (4°S 83°E). Column phytoplankton cell counts ranged from 7 to 61 × 10^3 cells m^{-2}, increasing from north to south of the equator (S5, S6, and S7) with a maximum abundance observed at S6. Diatoms contributed (87%) greater than dinoflagellates (13%) to the total abundance (Fig. 4.8) with the greatest abundance of diatoms observed at S5 and dinoflagellates at S6 (4°S 83°E).

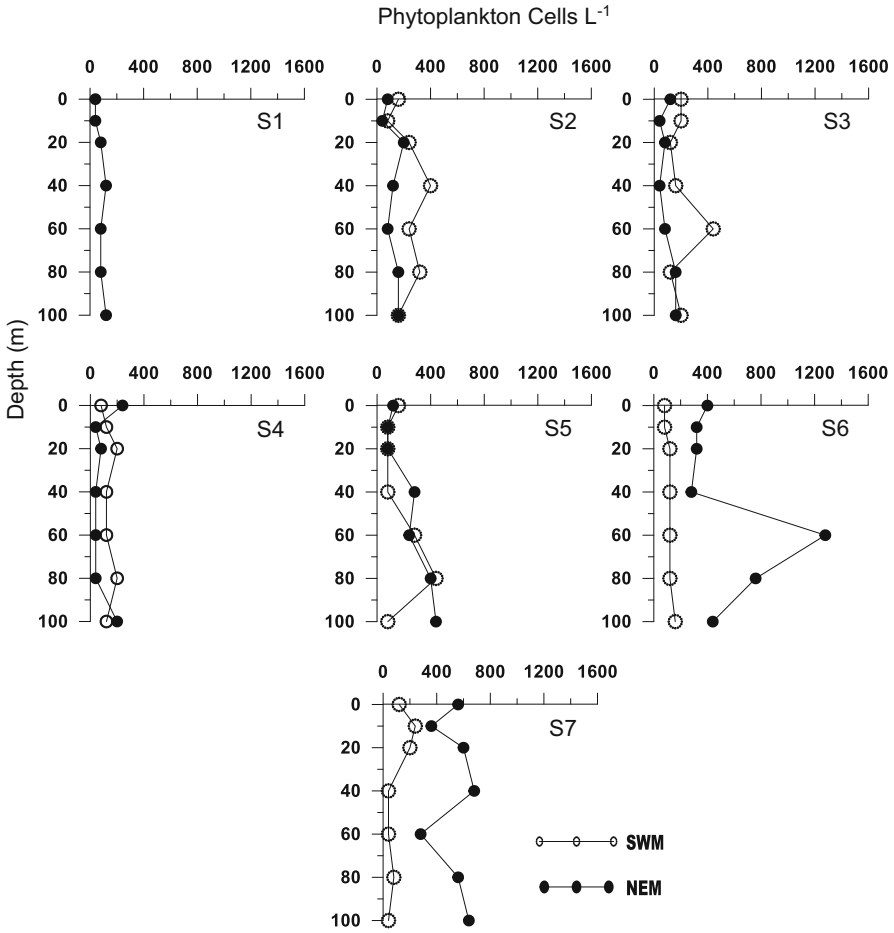

Fig. 4.6 Vertical profiles of phytoplankton cell counts (cells L^{-1}) in the Equatorial Indian Ocean along 83°E during southwest monsoon (SWM) and northeast monsoon (NEM)

During SWM, the highest abundance was seen between 60 and 80 m at locations S3 (1°S) and S5 (3°S) (Fig. 4.6). The integrated phytoplankton cell counts ranged from 10 to 26 × 10^3 cells m^{-2} (Fig. 4.7) and the maximum abundance was at the equator (S2) and least at S7. Diatoms and dinoflagellates constituted 83% and 16% of the total counts during SWM, respectively (Fig. 4.8). *Dictyocha crux* was the only Silicoflagellate that was observed during SWM. The largest numbers of diatoms were observed at S3 (1°S 83°E), and high numbers of dinoflagellates were seen at the equator (S2) during SWM (Table 4.2). Shannon–Weaver (H′) diversity indices were 4.5 during NEM and 4.3 during SWM.

Nineteen species of centric diatoms were identified during NEM. While 15 centric diatoms were observed during the SWM, their diversity did not vary much between the seasons. However, the pennales were dominant during NEM with as many as

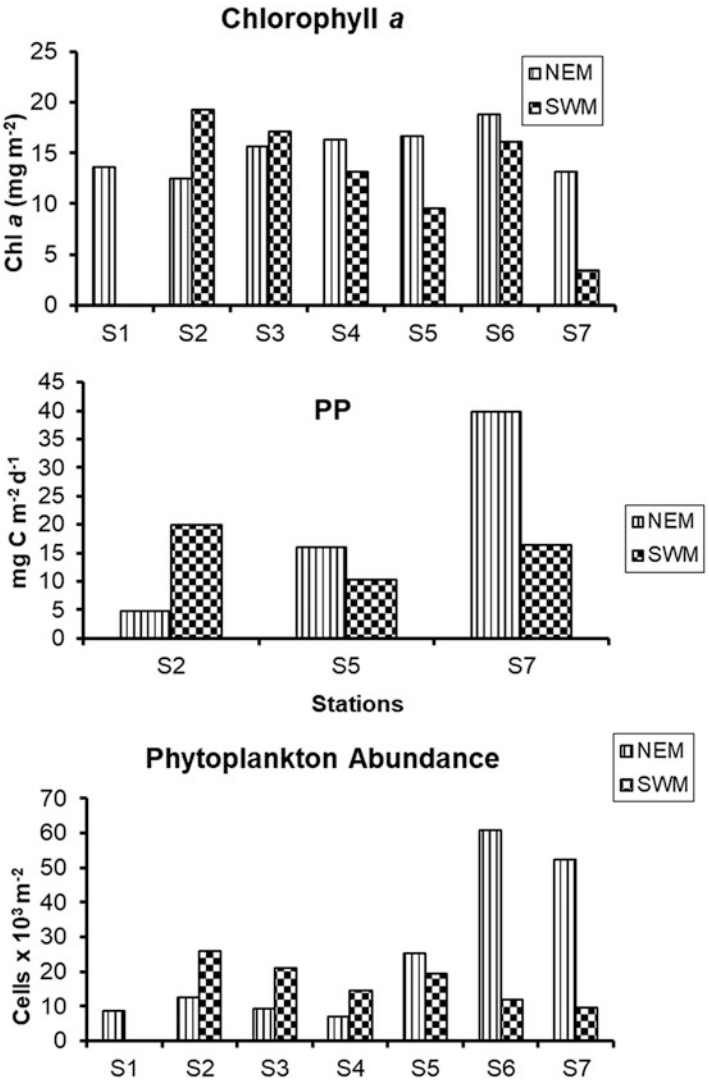

Fig. 4.7 The column-integrated (trapezoidal) values of (**a**) chl *a* (mg m^{-2}), (**b**) phytoplankton cell counts (cells m^{-2}), and (**c**) production (mg C m^{-2} d^{-1}) in the Equatorial Indian ocean during the northeast monsoon (NEM) and southwest monsoon (SWM)

20 species against a low of 8 species recorded during SWM. *Navicula* spp. were the most abundant (approximately 20% of the total diatoms), followed by *Pseudonitzschia* spp. (15%), *Thalassionema nitzschioides* (6%) and *Coscinodiscus* sp. (5%) during the NEM. Species of *Navicula* were abundant throughout the 1°N to 5°S transect, while *Pseudonitzschia* spp., *Thalassionema nitzschioides,* and *Coscinodiscus* sp. were mostly preponderant in the southern stations. When

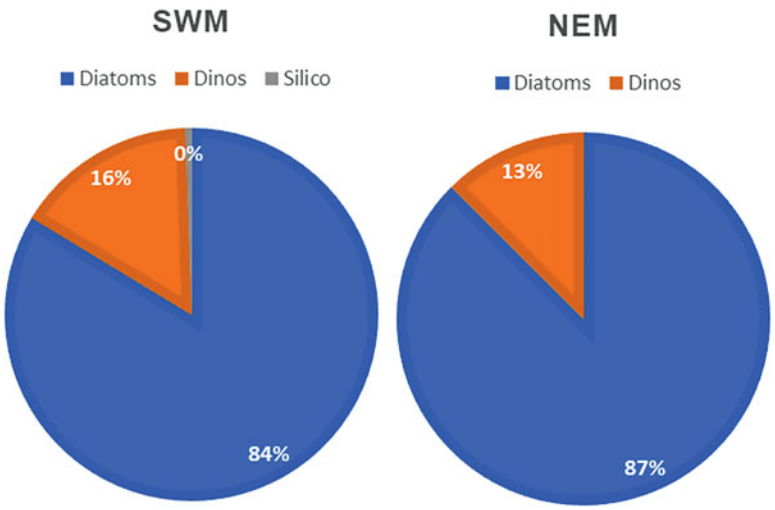

Fig. 4.8 Percent contribution of diatoms and dinoflagellates to the phytoplankton assemblages during northeast monsoon (NEM) and southwest monsoon (SWM)

compared with the other locations, dinoflagellates were the highest at S6 (4°S) with *Podolampus palmipes* (3.70%) and *Oxytoxum* sp. (3.03%) being the most abundant. During the SWM too, *Navicula* spp. (39%) were more abundant forming of the total diatoms, followed by *Coscinodiscus* spp. (10%) and *Navicula distans* (5%). Among the dinoflagellates, *Oxytoxum* sp. (6%) followed by *Ceratium furca* (3%) were abundant during this season.

Coscinodiscus sp., *Navicula directa*, *Navicula* sp., and *Pseudonitzschia* sp. during the NEM and *Coscinodiscus* sp. and *Navicula* spp. during the SWM were the ubiquitous species found at all depths. *Chaetoceros didymus*, *Chaetoceros coarctatus*, *Chaetoceros eibenii, Chaetoceros lorenzianus*, *Rhizosolenia* sp., *Hemidiscus hardmanius*, *Centrodinium*, *Nitzschia closterium*, *Grammatophora serpentina*, *Striatella punctata*, and *Corythrodinium tesselelatum* were observed in deeper waters (100–120 m) during NEM, while there were no particular species that was exclusively observed in deeper waters during SWM.

4 Discussion

The Equatorial Indian Ocean is subjected to a complex system of surface currents driven by monsoon winds (Shetye et al., 1994; Smith et al., 1998). During May–September (southwest monsoon, SWM), the winds accelerate the East African Coastal Current (EACC) to >200 cm s^{-1}, while wind reversal takes place from November to March (northeast monsoon, NEM) (Kromkamp et al., 1997). During NEM, the Somali current moves south-eastward and merges with the EACC, which

Table 4.2 List of phytoplankton and percent contribution of each species/taxon observed in the Equatorial Indian Ocean (EIO) along 83°E during the southwest monsoon (SWM) and northeast monsoon (NEM) of 2003

	% Contribution	
Phytoplankton species	NEM	SWM
Diatoms	%	%
Centric diatom		
Actinomonas mirabilis	0.34	–
Amphora sp.	0.34	–
Asteromphalus marylandicus	1.01	–
Bacteriastrum elongatum	4.04	–
Biddulphia alterans	–	0.54
Centrodinium	0.34	–
Chaetoceros coarctatus	1.35	1.63
Chaetoceros didymus	1.01	1.09
Chaetoceros eibenii	1.35	1.63
Chaetoceros sp.	1.35	–
Chaetoceros lorenzianus	1.68	–
Coscinodiscus jonesianus	–	0.54
Coscinodiscus radiatus	–	0.54
Coscinodiscus sp.	5.72	10.33
Coscinodiscus sp1	–	0.54
Cylindrotheca closterium	2.69	–
Ditylum brightwelli	0.67	2.72
Hemiaulus haukii	1.35	2.72
Hemidiscus hardmanianus	0.34	–
Leptocylindrus sp.	0.34	–
Planktoniella sol	1.01	–
Rhizosolenia imbricata	–	1.09
Rhizosolenia cylindrus	0.67	3.26
Rhizosolenia sp.	0.34	–
Rhizosolenia styliformis	–	3.26
Thalassiosira subtilis	–	0.54
Thalassiosira sp.	–	2.17
Pennate diatom		
Fragilaria doliolus	0.67	4.89
Grammatophora serpentina	0.34	–
Grammatophora undulata	0.67	–
Navicula directa	4.04	–
Navicula delicatula	0.67	–
Navicula braarudii	1.01	–
Navicula distans	4.04	5.43
Navicula sp.	20.88	14.67
Navicula sp. 1	1.35	6.52
Navicula sp. 2	–	12.50

(continued)

Table 4.2 (continued)

Phytoplankton species	% Contribution	
	NEM	SWM
Diatoms	%	%
Navicula sp. 3	–	2.72
Navicula sp. 4	–	2.72
Nitzschia closterium	0.34	–
Nitzschia lanceolata	0.34	–
Nitszschia obtusa	0.34	–
Nitzschia sp.	1.35	–
Pleurosigma sp.	1.01	–
Pseudonitzschia sp.	15.15	–
Striatella punctata	0.67	–
Synedra ulna	1.01	–
Synedra sp.	0.34	–
Thalassionema nitzschioides	6.06	1.09
Thalassiothrix longisimma	0.34	–
Dinoflagellates		
Ceratium dens	0.34	–
Ceratium extensum	0.34	–
Ceratium furca	1.35	3.26
Ceratium kofoidii	0.34	–
Ceratium longicuris	1.01	–
Ceratium trichoceros	–	1.09
Corythodinium tesselatum	0.34	–
Peridinium sp.	0.67	0.54
Podopampus palmipes	3.70	2.72
Protoperidinium sp.	1.35	–
Pyrocystis lunula	–	1.09
Pyrophacus stenii	–	0.54
Oxytoxum sp.	3.03	6.52
Cyanobacteria		
Trichodesmium sp.	0.34	–
Silicoflagellates		
Dictyocha crux	–	0.54
Unidentifiable	0.67	0.54
Total phytoplankton cells L^{-1}	**11,840**	**7360**

– Denotes absence

later feeds the Equatorial Counter Current (ECC; Düng et al., 1980; McClanahan, 1988; Swallow et al., 1991; Burkill et al., 1993). This ECC moves eastward south of 2°S (Ruma & Shaji, 2019). Also, along 5–15°S and approximately 50–80°E exists the upwelling region called the Seychelles-Chagos-Thermocline Ridge (SCTR) (Vinaychandran et al., 2021). In this region, during NEM, currents move eastward from the upwelling SCTR region, bringing in more nutrients into the EIO at 5°S.

This is also reflected in our study wherein higher concentrations of silicate and phosphate are observed at S7 (5°S). However, the direction of currents is westward along the south of 2°S during SWM, and the surface winds are toward the north-western direction (Ruma & Shaji, 2019).

The meteorological and hydrographical parameters play a critical role in determining the ideal growth conditions of the phytoplankton (Krey, 1973). The present study was done during two major wind reversal periods, NEM and SWM. Seasonal chl *a* concentration during NEM (0.01–0.42 mg m^{-3}) and SWM (0.001–0.45 mg m^{-3}) was within the range (0.05–0.5 mg m^{-3}) (Figs. 4.4 and 4.7) reported for the same region (Krey, 1973; Liu et al., 2021). The column-integrated chl *a* concentration also did not vary much. The subsurface chlorophyll maxima (SCM) were observed deeper than 60 m in EIO, which coincided with higher nutrient levels at these depths. In the subsurface layers below 50 m, the SCM might be mostly due to microphytoplankton (e.g., *Coscinodiscus* sp., *Rhizosolenia* sp., and *Fragilaria* sp.), which benefit from the higher concentrations of TN at such depths. During SWM, relatively higher microphytoplankton abundance was seen at S5 (3°S; 60 and 80 m) and S7 (5°S; surface–20 m). Averages of the integrated phytoplankton abundance were higher (25×10^3 cells m^{-2}) during NEM south of the equator (S5–S7) as against SWM (17×10^3 cells m^{-2}). However, Gnanasoundari (1987) reported higher phytoplankton counts south of the equator during SWM.

Deep SCMs were usually observed coinciding with the thermocline during this study (Murty et al., 2000). High values of PP were also earlier reported from the deep SCM layers along the equator during NEM (Liu et al., 2021). It is also well known that phytoplankton tend to settle in the stable zone of the seasonal thermocline rather than in the surface mixed layer (Pingree et al., 1978). The stability of the water column (Fasham et al., 1985; Catalano et al., 1997) is a potential factor controlling the phytoplankton distribution and hence the PP in the ocean. The EIO does not experience upwelling, thereby affecting the surface nutrient concentrations. The euphotic zones, estimated by Secchi disk depths, were fairly deeper than 80 m during both seasons, coinciding with higher concentrations of nutrients below 50 m in the SWM and very low at the surface. This is clearly reflected in the low chlorophyll and PP in the surface waters. In addition, as all three nutrients are far lower at the surface (Krey & Babenerd, 1976; Tripathy et al., 2020), it is unlikely that the advection of nutrients through the prevalent equatorial currents into the study area is effective enough for enhancing PP.

The deep SCMs observed during both seasons were similar to those reported by Tripathy et al. (2020) in the EIO. The deep SCM could also be attributed to the rapid nutrient turnover in the top 50 m by picoplankton as observed in other oligotrophic regions (Campbell & Vaulot, 1993; Burkill et al., 1993). However, along 5°N 55°E, the picoplankton abundance was recorded to be 4.7×10^4 cells cm^{-3} (Reckermann & Veldhuis, 1997), and it is likely that the influence of picophytoplankton in the daily production might be only to a tune of <25% of total PP. Around 25% contribution of picoplankton was also reported during the SWM from the same region (Tripathy et al., 2020). However, picoplankton abundance was not estimated in this study; hence, their contribution to the PP and biomass could not be ascertained.

A total of 51 taxa were identified during NEM (39 species of diatoms and 10 of dinoflagellates, 1 of cyanobacteria), it appears that this season supports many more species than those recorded during SWM, wherein only a total of 32 taxa were observed (23 diatoms and 7 dinoflagellates, a single species of silicoflagellate; Fig. 4.8). These numbers of taxa are fewer compared to those reported by Durairatnam (1964) and Gnanasoundari (1987). We observed subsurface maxima during both seasons in the number of species (Table 4.3), phytoplankton cell abundance, and chl *a* around 60–80 m. The phytoplankton cell counts in the strata of chlorophyll maxima accounted for over 70% of the 100 m column total. This also coincided with deeper SCM during both seasons. Gnanasoundari (1987) and Durairatnam (1964), however, observed a decrease in the number of species with increasing depth. It is likely that the concentrations of TN, SiO_4, and PO_4 might have been different during these years.

Nutrient-rich waters are dominated by diatoms, whereas dinoflagellates dominate in nutrient-impoverished oceanic waters (Qasim & Kureishy, 1986). Overall, in this study, the contribution of diatoms in the total water column was 84% and 87% during SWM and NEM, respectively. This was contrary to the observation by Gnanasoundari (1987), who reported that the standing crop of dinoflagellates exceeded that of diatoms between 2°S and 6°S along 59–60°E. Higher diatoms abundance (SWM:46%; NEM:49%) was observed below 40 m during this study, whereas higher dinoflagellate abundance was observed in the surface (SWM: 9%; NEM: 7%) as compared to deeper depths (SWM: 7%; NEM: 4%). Higher abundance of diatoms to dinoflagellates in the top 50 m could be attributed to their ability to tolerate higher insolation (Gnanasoundari, 1987). Recent reports too have observed the diatoms and dinoflagellates to be abundant in the surface, and deeper layers, with a contribution of 66% and 33% to the total mean abundance, respectively (Liu et al., 2021). Along the equatorial Pacific also, higher diatoms and dinoflagellates abundance was observed in the surface and the top 60 m, respectively (Iriarte & Fryxell, 1995). Our observation coincided with a recent study (Liu et al., 2021) that reported a maximum abundance of dinoflagellates (105 cells L^{-1}) at the surface and which decreased with depth. With the exception of *Gonyaulax polyedra,* which maintained maximum numbers at the surface during noon other species such as *Ceratium furca*, *Gymnodinium*, *Ceratium dens*, and *Prorocentrum micans* are all concentrated lower in the water column (Blasco, 1978). Hasle (1950) and Dodge and Hart-Jones (1977) have also noted that some dinoflagellates avoid surface waters during daylight hours. Since our sample collections were mostly done in the early mornings before sunrise, our observation of higher dinoflagellates at surface could be attributed to the time of collection of the samples.

The column PP rates in the study area (NEM: 20 mg C m^{-2} d^{-1}; SWM: 16 mg C m^{-2} d^{-1}; Fernandes et al., 2007) were far lower than the minimum of 113 mg C m^{-2} d^{-1} during NEM (Liu et al., 2021) and 176 mg C m^{-2} d^{-1} during SWM (Tripathy et al., 2020) along EIO. However, the study area reported by Liu et al. (2021) included not only the EIO but also the Bay of Bengal and Sumatra region, and Tripathy et al. (2020) included the upwelling regions in the Tropical Indian Ocean. During NEM, maximum productivity was observed at the southernmost station S7,

Table 4.3 Seasonal differences in the vertical distribution of the number of species of diatoms and dinoflagellates in the Equatorial Indian Ocean along 83°E during 2003

		1°N		Equator		1°S		2°S		3°S		4°S		5°S	
Depth (m)		NEM	SWM	NEM	SWM	NEM	SWM	NEM	SWM	NEM	SWM	NEM	SWM	NEM	SWM
0	Diatoms	1	[a]	1	4	2	4	3	1	2	3	6	1	2	2
	Dinoflagellates	–		1	–	–	–	1	1	1	–	1	1	–	1
10	Diatoms	1		–	1	1	5	–	2	2	2	5	1	3	3
	Dinoflagellates	–		1	1	–	–	1	–	–	–	1	1	2	1
20	Diatoms	2		2	4	1	2	1	3	1	1	5	2	6	2
	Dinoflagellates	–		1	–	–	1	1	2	–	1	1	1	1	–
40	Diatoms	2		3	6	1	3	1	3	4	–	3	2	5	1
	Dinoflagellates	–		–	1,1[b]	–	1	–	–	2	2	1	1	2	–
60	Diatoms	2		2	**2**	1	**6**	1	**2**	**4**	3	**9**	1	2	1
	Dinoflagellates	–		–	**3**	1	**2**	–	–	**2**	1	**2**	2	–	–
80	Diatoms	**1**		**1**	4	**3**	3	**1**	2	3	**5**	9	**2**	**6**	1
	Dinoflagellates	**1**		–	1	–	–	–	–	–	–	1	1	–	1
100	Diatoms	3		2	2	4	3	3	1	6	1	5	2	3	**1**
	Dinoflagellates	–		–	1	–	–	2	–	1	–	1	–	–	–
120	Diatoms	–		–	–	–	5	–	1	–	2	–	2	–	1
	Dinoflagellates	–		–	–	–	–	–	1	–	–	–	–	–	–

Figures in bold to indicate the zone of sub chlorophyll maxima

[a]Sampling was not carried out during SWM

[b]Silicoflagellate

which could be due to the proximity of the S7 station to the SCTR region, which is a permanently upwelling region in the Indian Ocean (Vinaychandran et al., 2021). The currents occurring during the NEM brings in nutrients to this station as evidenced by higher concentrations of nutrients at this station (Fig. 4.2) as compared to the other two PP stations. This coincided with the maximum phytoplankton abundance and chlorophyll too. Higher PP values at 5°S were also earlier reported to be due to the effect of South Equatorial Current and relatively low sea level anomaly during NEM (Liu et al., 2021). Spatially, the contribution of diatoms was highest (92%) as compared to dinoflagellates (7%) at S7 during NEM. At this station, the dominant species were *Navicula* sp. (26%), *Pseudonitzschia* spp. (20%), *Chaetoceros* spp. (12%), *Thalassionema nitzschioides* (5.43%), and *Coscinodiscus* sp. (5.43%).

During SWM, least PP was observed at S7, and it coincided with very low phytoplankton cell numbers and biomass. This could be due to the reversal of the currents which move westward toward the SCTR getting in low nutrient waters from the eastern part of the Indian Ocean. This is also reflected in the low nutrient levels observed in the water column during this period (Fig. 4.3). At this station, the dominant species were *Navicula* sp. (50%), *Rhizosolenia styliformis* (15%), with overall very less abundance as compared to that observed during NEM at the same station. Our study corroborates with earlier studies wherein the phytoplankton biomass, composition, and production have been linked to the upwelling and equatorial circulation patterns in the equatorial Pacific (Chavez et al., 1990) and the Indian Ocean regions (Vinaychandran et al., 2021). In the Equatorial Pacific regions, changes in the abundance of pennate diatoms resulted in the variability of phytoplankton biomass and PP (Chavez et al., 1990). Apparently, despite the generally lower cell counts, the diversity of phytoplankton assemblages in the equatorial waters is appreciable, as also observed earlier (Durairatnam, 1964; Gnanasoundari, 1987). While competitive exclusion is the general norm in most habitats, the physiological adaptations of these phytoplankton assemblages in such oligotrophic environs are worth investigating to delineate their potential growth rates.

5 Conclusion

The total abundance, the biomass, and the primary production in the EIO is largely affected by the currents and wind pattern existing during the time of sampling. Although the phytoplankton abundance was slightly more during the NEM than the SWM, the maximum abundance reported in this study were far lower than those reported previously for the same region. The higher abundance during NEM is also reflected in the PP rates, despite similar TN and phosphate concentrations. During NEM, high silicate entrainment at S7 supported chain-forming and centric diatoms. Even in open oligotrophic waters, the centric diatoms show a preference for high nutrient regions (Kobayashi & Takahasi, 2002); this explains their predominance in the subsurface layers during NEM wherein the nutrient concentrations were higher.

The pennates such as *Navicula* sp., which was predominant in this study, have higher surface-to-volume ratio and extremely low sinking rates, thrive in the least upwelling regions/low nutrient concentrations (Pace et al., 1986), and may influence the PP. Primary production is governed by a variety of biotic (community composition, age of the cells, grazing pressure, etc.) and abiotic (macro- and micro-nutrient limitation, MLD, insolation, etc.) factors. The dominance of centric diatoms at S7 and by pennates like *Navicula* sp. at other stations may have influenced the PP in these stations. The contribution of pennates to the PP rates is reported to be relatively lower than larger diatoms (Chavez et al., 1990). However, there is no such study comparing the PP rates within the phytoplankton community from the EIO. In view of a warming Indian Ocean, changes in the community structure of the phytoplankton may be expected, which may impact the PP rates, grazing community, and carbon flow through the food web in these waters. Therefore, the estimation of PP rates of various dominant phytoplankton groups and their contribution to the gross PP in these waters needs to be addressed at the earliest. Such a study shall help in assessing the future response of the phytoplankton community to a rapidly warming Indian Ocean and its impact on fisheries.

6 Future Directions

The phytoplankton form the base of the aquatic food web, and therefore their composition shapes the grazer population such as the mesozooplankton and the planktivorous fishes. The IIOE atlases suggest moderate to high zooplankton biomass in the sampling region, thus translate into noticeable tertiary production. As observed during this study, the spatio-temporal differences in phytoplankton composition are not high and do not show strong seasonal differences, and their biomass is concentrated mostly below the depth of the nitracline. A diatom-dominated system will have a shorter food pyramid as against the non-diatom-dominated system. Recent studies have observed that the Indian Ocean is warming, which will lead to alterations in the phytoplankton community structure, biomass, and rate of production; this will lead to cascading effects in the higher organisms, thereby disrupting the marine food web. A model study on the marine net primary production (mNPP) has projected a drop in the mNPP in the range of 4–8% by the year 2080 in the Indian Ocean regions (Krumhardt et al., 2017). In many ways, the EIO is not really akin to the more productive Equatorial Pacific with high nutrient low chlorophyll regions and therefore the studies in the EIO should not be restricted to only the biomass but more understanding of the contribution of the phytoplankton community to the primary production and the drivers of food web in this region of low productivity need to be addressed both for ecological and sustainable living resource harnessing purposes.

Acknowledgments The author wishes to thank Director, NCPOR, for providing opportunity; Dr. S. R. Shetye, ex-Director, NIO, and Dr. V. K. Banakar, retired scientist, NIO for facilities and encouragement, Dr. N. Ramiah, guide and retired Scientist, NIO, and Dr. S. C. Tripathy. Prof N. Anand at the University of Madras gave numerous technical advice on phytoplankton identification to JTB during the work. This work was supported by the Department of Ocean Development, New Delhi, under the Cobalt crust Programme.

References

Anon. (2002). *Report of Indian Ocean Synthesis Group on Arabian Sea Process Study*. JGOFS Report No. 35. SCOR and JGOFS International Office. ISSN:1016-7331.

Bhattathiri, P. M. A., Devassy, V. P., & Radhakrishana, K. (1980). Primary production in the Bay of Bengal during southwest monsoon of 1978. *Mahasagar, 13*, 315–323.

Bhattathiri, P. M. A., Pant, A., Sawant, S., Gauns, M., Matondkar, S. G. P., & Mohanraju, R. (1996). Phytoplankton production and chlorophyll distribution in the eastern and central Arabian Sea in 1994–1995. *Current Science, 71*, 857–862.

Blasco, D. (1978). Observations on the diel migration of marine dinoflagellates off the Baja California coast. *Marine Biology, 46*, 41–47.

Burkill, P. H., Mantoura, R. F. C., & Owens, N. J. P. (1993). Biogeochemical cycling in the northwestern Indian Ocean: A brief overview. *Deep-Sea Research Part II, 40*, 643–649.

Campbell, L., & Vaulot, D. (1993). Photosynthetic picoplanktonic community structure in the subtropical North Pacific Ocean near Hawaii (station ALOHA). *Deep Sea Research Part I, 40*, 2043–2060.

Catalano, G., Povero, P., Fabiano, M., Benedettis, F., & Goffart, A. (1997). Nutrient utilization and particulate organic matter changes during summer in the upper mixed layer. *Deep Sea Research Part I, 44*, 97–112.

Chavez, F. P., Buck, K. R., & Barber, R. T. (1990). Phytoplankton taxa in relation to primary production in the Equatorial Pacific. *Deep Sea Research Part A, 37*, 1733–1752.

Constance, A. S., Carroll, S. E., Hillman, N. S., Janal, M. J., & Vancouvering, J. A. (1985a). Catalogue of diatoms. In *The Ellis and Messina catalogues of micropaleontology, Book 1*. Micropaleontology Press.

Constance, A. S., Carroll, S. E., Hillman, N. S., Janal, M. J., & Vancouvering, J. A. (1985b). Catalogue of diatoms. In *The Ellis and Messina catalogues of micropaleontology, Book 2*. Micropaleontology Press.

Dawes, C. J. (1998). *Marine botany* (2nd ed.). Wiley.

Desikachary, T. V., & Prema, P. (1987). Diatoms from the Bay of Bengal. In *Atlas of diatoms*. Madras Science Foundation.

Desikachary, T. V., & Ranjithadevi, K. A. (1986). Marine fossil diatom from India and Indian Ocean Region. In *Atlas of diatoms*. Madras Science Foundation.

Desikachary, T. V., Gowthaman, S., & Latha, Y. (1987). Diatom Flora of some sediments from the Indian Ocean Region. In *Atlas of diatoms*. Madras Science Foundation.

Dodge, J. D., & Hart-Jones, B. (1977). The vertical and seasonal distribution of dinoflagellates in the North Sea. *Botanica Marina, 20*, 307–311.

Düng, W., Molinari, R. L., & Swallow, J. C. (1980). Somalia current: Evolution of surface flow. *Nature, 209*, 588–590.

Durairatnam, M. (1964). Vertical distribution of phytoplankton in an area near Cocos- Keeling Island, Indian Ocean. *Information Bulletin on Planktology in Japan, 11*, 1–6.

Falkowski, P. G., Barber, R. T., & Smetacek, V. (1998). Biogeochemical controls and feedbacks on ocean primary production. *Science, 281*, 200–206.

Fasham, M. J. R., Platt, T., Irwin, B., & Jones, K. (1985). Factors affecting the spatial pattern of the deep chlorophyll maximum in the region of the Azores front. In J. Crease, W. J. Gould, & P. M. Saunders (Eds.), *Progress in oceanography* (pp. 129–165). 1985, Pergamon Press.

Fernandes, V., Rodrigues, V., Ramaiah, N., & Paul, J. T. (2007). Relevance of bacterioplankton abundance and production in the oligotrophic equatorial Indian Ocean. *Aquatic Ecology, 42*, 511–519.

Gnanasoundari, B. (1987). Studies on phytoplankton from the western equatorial Indian Ocean. *Seaweed Research and Utilisation, 10*, 53–65.

Grasshoff, K. (1983). In M. Ehrhardt & K. Kremling (Eds.), *Methods of sea water analysis* (2nd revised and extended ed., p. 419). Verlag Chemie.

Hasle, G. R. (1950). Phototactic vertical migration in marine dinoflagellates. *Oikos, 2*, 162–175.

Iriarte, J. L., & Fryxell, G. A. (1995). Micro-phytoplankton at the equatorial Pacific (140°W) during the JGOFS EqPAC Time Series studies: March to April and October 1992. *Deep-Sea Research Part II, 42*, 559–583.

Kabanova, Y. G. (1968). Primary production of the northern part of the Indian Ocean. *Oceanology, 8*, 214–225.

Kobayashi, F., & Takahasi, K. (2002). Distribution of diatoms along equatorial transect in the western and central Pacific during La Nina conditions. *Deep Sea Research Part II, 49*, 2801–2821.

Krey, J. (1973). Primary Production in the Indian Ocean I. In: (Zeitzschel, B, eds) The Biology of the Indian Ocean, Ecological Studies, Analysis and Synthesis (Vol 3). Springer-Verlag, Berlin, pp.115–130.

Krey, J., & Babenerd, B. (1976). Environmental conditions. In *Phytoplankton production: Atlas of the International Indian Ocean Expedition* (pp. 15–16).

Kromkamp, J., De Bie, M., Goosen, N., Peene, J., Van Rijswijk, P., Sinke, J., & Duineveld, G. C. A. (1997). Primary production by phytoplankton along the Kenyan coast during the SE monsoon and November intermonsoon 1992 and the occurrence of Trichodesmium. *Deep-Sea Research Part II, 44*, 1195–1212.

Krumhardt, K. M., Lovenduski, N. S., Long, M. C., & Lindsay, K. (2017). Avoidable impacts of ocean warming on marine primary production: Insights from the CESM ensembles. *Global Biogeochemical Cycles, 31*, 114–133.

Lebour, M. (1978). *The plankton diatoms of northern seas* (Vol. 244). Otto Koeltz Science Publishers.

Liu, H., Song, Y., Zhang, X., Zhang, G., Wu, C., Wang, X., Thangaraj, S., Wang, D., Chen, J., & Sun, J. (2021). Spatial variation in primary production in the Eastern Indian Ocean. *Frontiers in Marine Science, 8*, 757529. https://doi.org/10.3389/fmars.2021.757529

Madhu, N. V., Jyothibabu, R., Maheswaran, P., Gerson, V. J., Gopalakrishnan, T., & Nair, K. (2006) Lack of seasonality in phytoplankton standing stock (chlorophyll a) and production in the western Bay of Bengal. *Continental Shelf Research, 26*, 1868–1883.

Madhupratap, M., Gauns, M., Ramaiah, N., Prasanna Kumar, S., Muraleedharan, P. M., De Sousa, S. N., Sardesai, S., & Muraleedharan, U. (2003). Biogeochemistry of the Bay of Bengal: Physical, chemical and primary productivity characteristics of the central and western Bay of Bengal during summer monsoon 2001. *Deep-Sea Research Part II, 50*, 881–896.

McClanahan, T. R. (1988). Seasonality in East Africa's coastal waters. *Marine Ecology Progress Series, 44*, 191–199.

Murphy, J., & Riley, J. P. (1962). A modified single solution method for the determination of phosphate in natural waters. *Analytica Chimica Acta, 27*, 31–36.

Murty, V. S. N., Gupta, G. V. M., Sarma, V. V., Rao, B. P., Jyothi, D., Shastri, P. N. M., & Supraveena, Y. (2000). Effect of vertical stability and circulation on the depth of the chlorophyll maximum in the Bay of Bengal during May–June, 1996. *Deep Sea Research Part I, 47*, 859–873.

Pace, D. R., Yoneshique, Y., & Jacob, S. A. (1986). Phytoplankton mass culture in discontinuously upwelling water. *Aquaculture, 58*, 123–132.

Pingree, R. D., Holligan, P. M., & Mardell, G. T. (1978). The effects of vertical stability on phytoplankton distribution in the summer on the north-west European shelf. *Deep Sea Research Part I, 25*, 1011–1028.

Qasim, S. Z. (1982). Oceanography of the Northern Arabian Sea. *Deep Sea Research Part I, 29*, 1041–1068.

Qasim, S. Z., & Kureishy, T. W. (1986). Biological productivity in the seas around India: Present status and major threats. *Proceedings of the Indiana Academy of Sciences, 44B*, 1–17.

Radhakrishna, K., Bhattathiri, P. M. A., & Devassy, V. P. (1978). Primary productivity of the Bay of Bengal during August–September 1976. *Indian Journal of Marine Sciences, 7*, 94–98.

Reckermann, M., & Veldhuis, M. J. W. (1997). Trophic interactions between pico-phytoplankton and micro- and nanozooplankton in the western Arabian Sea during the NE monsoon 1993. *Aquatic Microbial Ecology, 12*, 263–273.

Reid, P. C., Colebrook, J. M., Matthews, J. B. L., Aiken, J., & Continuous Plankton Recorder Team. (2003). The continuous plankton recorder: Concepts and history, from plankton indicator to undulating recorders. *Progress in Oceanography, 58*, 117–173.

Roxy, M. K., Modi, A., Murtugudde, R., Valsala, V., Panickal, S., Prasanna Kumar, S., Ravichandran, M., Vichi, M., & Levy, M. (2016). A reduction in marine primary productivity driven by rapid warming over the tropical Indian Ocean. *Geophysical Research Letters, 43*, 826–833. https://doi.org/10.1002/2015gl066979

Ruma, S., & Shaji, C. (2019). Seasonal variability and long-term trends of the surface and subsurface circulation features in the Equatorial Indian Ocean. *Environmental Monitoring and Assessment, 191*, 810. https://doi.org/10.1007/s10661-019-7707-6

Shetye, S. R., Gouveia, A. D., & Shenoi, S. S. C. (1994). Does winter cooling lead to subsurface salinity minimum off Saurashtra, India? In B. N. Desai (Ed.), *Oceanography of the Indian Ocean* (pp. 617–625). Oxford and IBH Publishing Co. Pvt.Ltd.

Smith, S. L., Codispoti, L. A., Morrison, J. M., & Barber, R. T. (1998). The 1994–1996 Arabian Sea Expedition: An integrated, interdisciplinary investigation of the response of the northwestern Indian Ocean to monsoonal forcing. *Deep-Sea Research Part II, 45*, 1905–1915.

Subramanyan, R. (1946). A systematic account of the marine plankton diatoms off the Madras Coast. *Proceedings/Indian Academy of Sciences, 24*(B), 85–197.

Subramanyan, R. (1968). The Dinophyceae of the Indian Sea. In *Special volume of Marine Biological Association of India, Mandapam Camp* (pp. 1–118).

Subramanyan, R., & Sarma, A. H. (1961). Studies on the phytoplankton of the West Coast of India. *The Indian Journal of Fisheries, 7*, 307–336.

Swallow, J. C., Schott, F., & Fieux, M. (1991). Structure and transport of the East African coastal current. *Journal of Geophysical Research, 96*, 22 245–22 257.

Taylor, F. J. R. (1973). General features of dinoflagellate material collected by the "Anton Bruun" during the International Indian Ocean Expedition. In B. Zeitzschel (Ed.), *The biology of the Indian Ocean, ecological studies, analysis and synthesis* (Vol. 3, pp. 155–169). Springer.

Thorrington-Smith, M. (1971). West Indian Ocean phytoplankton: A numerical investigation of phytohydrographic regions and their characteristic phytoplankton associations. *Marine Biology, 9*, 115–137.

Tomas, C. R. (Ed.). (1997). *Identifying marine phytoplankton* (p. 857). Academic Press Limited.

Tripathy, S. C., Sabu, P., Patra, S., Naik, R. K., Sarkar, A., Venkataramana, V., Kerkar, A. U., & Sudarsanarao, P. (2020). Biophysical control on variability in phytoplankton production and composition in the south western tropical Indian Ocean during monsoon 2014. *Frontiers in Marine Science, 7*, 515. https://doi.org/10.3389/fmars.2020.00515

UNESCO. (1994). *Protocols for the Joint Global Ocean Flux Study (JGOFS) core measurements, IOC manuals and guides 29* (p. 170). UNESCO.

Veldhuis, M. J. W., Kraay, G. W., Bleijswijk, J. D. L. V., & Baars, M. A. (1997). Seasonal and spatial variability in phytoplankton biomass, productivity and growth in the northwestern Indian Ocean: The southwest and northeast monsoon, 1992-1993. *Deep-Sea Research Part I, 44*, 425–449.

Vinaychandran, P. N., Masumoto, Y., Roberts, M. J., Huggett, J. A., Halo, I., Chatterjee, A., Amol, P., Gupta, G. V. M., Singh, A., Mukherjee, A., et al. (2021). Review and syntheses: Physical and biogeochemical processes associated with upwelling in the Indian Ocean. *Biogeosciences, 18*, 5967–6029.

Zeitzschel, B. (1973). *The biology of the Indian Ocean. ecological studies, analysis and synthesis* (Vol. 3, p. 549). Springer.

Chapter 5
A Revised Interpretation of Marine Primary Productivity in the Indian Ocean: The Role of Mixoplankton

Aditee Mitra and Suzana Gonçalves Leles

Abstract Traditional interpretations of marine plankton ecology, such as that in the Indian Ocean, mirror the plant-animal dichotomy of terrestrial ecology. Thus, single-celled phytoplankton produce food consumed by single-celled zooplankton, and these are in turn consumed by larger zooplankton through to higher trophic levels. Our routine monitoring surveys, research, models, and water management protocols all reflect this interpretation. The last decade has witnessed the development of an important revision of that traditional vision. We now know that the phytoplankton-zooplankton dichotomy represents, at best, a gross simplification. A significant proportion of the protist plankton at the base of the oceanic food-web can photosynthesise (make food 'like plants') and ingest food (eat 'like animals'), thus contributing to both primary and secondary production simultaneously in the same cell. These protists are termed 'mixoplankton', and include many species traditionally labelled as 'phytoplankton' (a term now reserved for phototrophic microbes that are incapable of phagocytosis) or labelled as 'protist zooplankton' (now reserved for protist plankton incapable of phototrophy). Mixoplankton include various harmful algal species, most likely all the phototrophic dinoflagellates, and even iconic exemplar 'phytoplankton' such as coccolithophorids (which can consume bacteria). Like all significant revisions to ecology, the mixoplankton paradigm will take time to mature but to ignore it means that we fail to properly represent plankton ecology in teaching, science, management, and policy. This chapter introduces the mixoplankton functional groups and provides the first insight into the biogeography of these organisms in the Indian Ocean. A first attempt to consider the implications of the mixoplankton paradigm on marine primary productivity and ecology in the Indian Ocean is also given.

A. Mitra (✉)
School of Earth and Environmental Sciences, Cardiff University, Park Place, Cardiff, Wales, UK
e-mail: MitraA2@Cardiff.ac.uk

S. G. Leles
Department of Marine and Environmental Biology, University of Southern California, Los Angeles, CA, USA

S. C. Tripathy, A. Singh (eds.), *Dynamics of Planktonic Primary Productivity in the Indian Ocean*, https://doi.org/10.1007/978-3-031-34467-1_5

Keywords Indian Ocean · Biogeography · Mixoplankton · Mixotrophy · Phytoplankton · Primary production

1 Reassessing Primary Production in the Indian Ocean

The Indian Ocean covers ~30% of the global ocean area (74.92 million km^2, latitude: 25°N–40°S, longitude: 45°E–115°E), has a coastline of ~66,526 km shared by 38 countries and supports, socioeconomically, >30% of the global human population (Wafar et al., 2011). The Indian Ocean (henceforth IO) comprises nine large marine ecosystems and is home to various keystone species; for example, >30% of the global coral population are IO inhabitants (Wafar et al., 2011; Roxy et al., 2016, 2020). The IO also makes a substantial contribution to global fish production through small-scale as well as commercial fisheries; it is one of the top producers of tuna, and ~13% of the global wild-fish catch come from the IO (FAO, 2020; Dalpadado et al., 2021). However, research attention on the IO has been significantly below that applied to the Atlantic and Pacific Oceans. In part, this may be attributed to the complexities and variabilities in the oceanographic and atmospheric conditions (Krey, 1973; Hood et al., 2009), as well as the geopolitics of the area. To advance out knowledge in understanding primary productivity in the IO, it is important to rethink how we perceive the microbial food-web. The subject of this chapter, mixoplankton – protist plankton that photosynthesise and eat, is one that has evaded mainstream oceanography for over a century. As the IO is explored, it is only right for studies of mixoplankton, as contributors to marine primary production, to be embedded in that process with all due haste.

A core component of IO research involves quantification of the primary production, which ultimately supports fisheries as well as biodiversity. Phytoplankton, prokaryotic cyanobacteria and eukaryotic protists, are the primary producers that employ photo-autotrophy to fix carbon. This production is then transferred to fish via their consumers, the zooplankton (Mitra et al., 2014a; Fig. 5.1a). More recently, there has been an increased emphasis on understanding the impact of various climate change stressors on primary productivity. There have been concerns that increasing sea surface temperatures in conjunction with increasing oxygen minimum zones in the IO will lead to a decline in primary productivity and shifts in the dominance of the organisms that drive it. Such a decline will, in turn, impact fish stocks and, thence, regional and global food security (Gomes et al., 2014; Dalpadado et al., 2021).

The study of primary production in any ecosphere needs to take into account the development of paradigms, and this applies equally to the IO. If we do not get the fundamentals underpinning the functioning of an ecosphere correct, then everything else collapses. During various instances, in the past decades, marine science has had cause to reconsider the key foundations of marine ecology (reviewed by Glibert & Mitra, 2022). In the late 1970s, marine ecology saw the advent of the 'microbial loop' introduced by Pomeroy (1974), and more formally described by Azam et al. (1983). This led to the food chain description of microbial components of marine

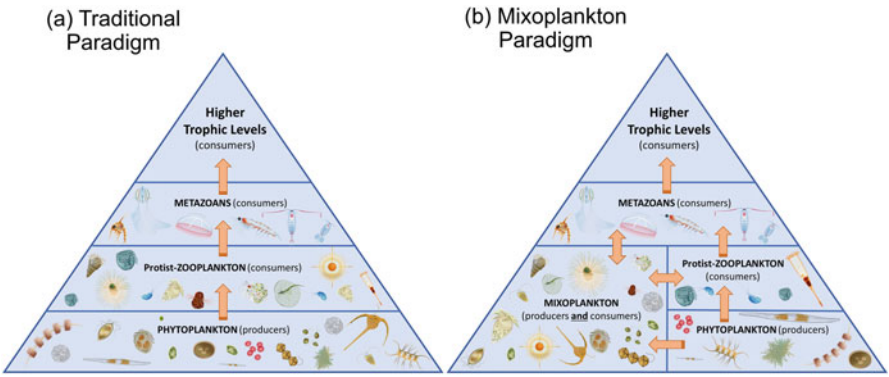

Fig. 5.1 (**a**) Traditional versus (**b**) mixoplankton paradigms for the structure of the Indian Ocean marine food-web. Arrows indicate transfer of energy. Mixoplankton can consume microbial plankton as well as metazoan grazers. Plankton images not to scale. See also Table 5.1 for definitions of the functional groups

ecology to be reimaged as a 'web'. In this web, bacteria play a major role as consumers of dissolved organic matter as well as decomposers of particulate organic matter. The activities of bacteria, and those of their grazers, regenerate nutrients to support primary production, especially in regions where upwellings are of low significance. Nearly two decades after the formalisation of the microbial loop, enhanced understanding of the importance of viruses and processes by which viruses facilitate the movement of nutrients from organisms to pools of dissolved and particulate organic matter led to the concept of the 'viral shunt' (Wilhelm & Suttle, 1999; Jiao et al., 2010). The microbial loop and viral shunt together further enhanced our understanding of how these microbial communities aid the transformation of labile dissolved organic carbon to more recalcitrant forms – important sources of sequestered oceanic carbon – via the 'microbial carbon pump' (Jiao et al., 2010, 2014).

At present, we stand at a point when we need to reconsider something that is arguably more fundamental in marine ecology. It transpires that science did not get the description of the functionalities of the organisms at the base of the plankton food-web correct. Over the last decade, a new paradigm in marine ecology has emerged – a paradigm that reimages the base of all marine food-webs. This is the 'mixoplankton paradigm'.

2 The Mixoplankton Paradigm

Understanding mechanisms that drive life in the single largest ecosystem of our planet, the Ocean, remains a pivotal research theme in natural sciences. About half of Earth's carbon fixation and oxygen production are attributed to the activities of

microscopic marine plankton. Marine systems, and indeed humans, are thus ultimately dependent on the activities of these microscopic plankton. Traditionally the planktonic communities have been considered to occupy clear niches in the ecosystem as phototrophic primary producers (phytoplankton), heterotrophic primary consumers (protist-zooplankton), and remineralisers (bacterioplankton). In this marine food-web structure, the food-producing phytoplankton, comprising prokaryotic cyanobacteria and eukaryotic protist plankton, are consumed by the protist-zooplankton (primary consumers). These zooplankton are then consumed by metazoan plankton (e.g. copepods, krill), which in turn provide food and energy to the higher trophic levels (HTLs; e.g. fish, cetaceans). This traditional view of the marine food-web, following a plant-animal dichotomy, is analogous to the pyramidal structure of the terrestrial food-web (Fig. 5.1a; Mitra et al., 2014a; Glibert & Mitra, 2022).

Over the last decade, there has been an increasing awareness that protist plankton engaging in 'mixotrophy' via photo-autotrophy and phago-heterotrophy are important members of the marine food-web communities (Flynn et al., 2013). Mixotrophy is not new to marine ecology. Indeed, in primary producing phytoplankton, mixotrophy has long been recognised as an important nutritional strategy, especially for harmful algal bloom (HAB) species (Burkholder et al., 2008). Typically, 'mixotrophy' in marine microalgae refers to photo(auto)trophy plus osmo(hetero)-trophy; mixotrophy through phago(hetero)trophy has traditionally been considered to be of relatively minor importance for microalgae (see Table 5.1 for definitions of forms of nourishment). However, various exemplar 'phytoplankton' are now recognised to be capable of consumption of prey; examples include the iconic coccolithophorid *Emiliania huxleyi* (Avrahami & Frada, 2020); the cosmopolitan ecosystem disruptive *Phaeocystis globosa* (Koppelle et al., 2022); the ecologically important *Tripos furca* (Bockstahler & Coats, 1993); the diverse bacterivorous phytoflagellates of the microbial carbon pump (Unrein et al., 2014); toxin-producing HABs *Alexandrium* spp. and *Dinophysis* spp. whose blooms result in shellfish contamination and harvesting closures (Jeong et al., 2005; Reguera et al., 2014). Likewise, over a third of the traditionally labelled 'protist-zooplankton' species, consumers of microalgae, have been found to be capable of engaging in acquired phototrophy through kleptoplastidy (e.g. *Laboea strobila*, Stoecker et al., 2009) or endosymbiosis (e.g. various species of Foraminifera, Bé et al., 1977; Gast & Caron, 1996).

The protist plankton thus includes photosynthetic micro-plankton that also eat, and predatory micro-plankton that also photosynthesise. The base of the oceanic food-web, therefore, does not follow the typical plant-animal dichotomy concept akin to terrestrial systems; textbook and modelling descriptions of marine food-webs are, for the most part, incorrect. This recognition where most oceanic primary producers cannot be analogised as 'miniature plants' and their primary consumers as 'miniature animals' has led to a paradigm shift in the understanding of marine ecology (Mitra et al., 2016; Flynn et al., 2019; Glibert & Mitra, 2022; Fig. 5.1b). To help emphasise the shift in categorisation of plankton functional type and in the usage of the term 'mixotroph' (noting that mixotrophy does not have to involve

Table 5.1 Glossary to terms describing forms of nourishment and functional groups (types) of microbial plankton; terminologies and definitions collated from Flynn et al. (2019), Glibert & Mitra (2022) and Mitra et al. (2023b).

Forms of nourishment	**Definitions**	
Autotrophy	Nutrition involving the synthesis of complex organic substances using photosynthesis (phototrophy) or chemosynthesis. Typically associated with the use of inorganic nutrients.	
Heterotrophy	Nutrition involving the consumption and interconversions of sources of organic carbon; this includes osmotrophy and phagotrophy.	
Mixotrophy	Nutrition involving both autotrophy and heterotrophy. Autotrophy may be via photosynthesis or chemosynthesis. Heterotrophy may be via osmotrophy and/or phagotrophy.	
Osmotrophy	A mode of heterotrophy involving the uptake and consumption of dissolved organic compounds; includes auxotrophy (uptake of vitamins). Also referred to as osmo(hetero)trophy.	
Phagotrophy	A mode of heterotrophy involving the engulfment of particles (often whole organisms) into a phagocytic vacuole in which digestion occurs. Also referred to as phago(hetero)trophy.	
Phototrophy	A mode of autotrophy involving the fixation of CO_2 using energy derived from light. Also referred to as photo(auto)trophy.	
Plankton functional groups (types)	**Abbreviations**	**Definitions**
Bacteria	–	Prokaryote plankton acquiring nourishment via osmo(hetero)trophy, and some also via chemo (auto)trophy (rendering them mixotrophic).
Constitutive Mixoplankton	CM	Mixoplankton with an inherent capacity for photo(auto)trophy (cf. NCM) in addition to osmo(hetero)trophy.
Cyanobacteria	–	Prokaryote members of the phytoplankton acquiring nourishment via photo(auto)trophy and osmo(hetero)trophy rendering them mixotrophic.
endosymbiotic Specialist Non-Constitutive Mixoplankton	eSNCM	SNCM that acquire their capacity for photo (auto)trophy through harbouring photosynthetic endosymbionts (cf. pSNCM).
Generalist Non-Constitutive Mixoplankton	GNCM	NCM that acquire their capacity for photo (auto)trophy from general (i.e. from a range of potential non-specific) phototrophic prey (cf. SNCM).
Mixoplankton	M	Plankton protists capable of obtaining nourishment via photo(auto)trophy *and* osmo(hetero)-trophy *and* phago(hetero)trophy; that is, they are photo-osmo-phago-mixotrophic (cf. phytoplankton and protist-zooplankton).
Non-Constitutive Mixoplankton	NCM	Mixoplankton that acquire the capability for photo(auto)trophy from consumption (via phago(hetero)trophy) of phototrophic prey. There are three functional forms of NCM: GNCM, pSNCM, and eSNCM (cf. CM).

(continued)

Table 5.1 (continued)

Phytoplankton	P	Plankton obtaining nourishment via photo (auto)trophy and osmo(hetero)trophy rendering them mixotrophic. They are incapable of phago (hetero)trophy. Exemplars include the eukaryotic diatoms and prokaryotic cyanobacteria (cf. mixoplankton and protist-zooplankton).
Protist	–	Single-celled eukaryotic organism. These include 6 functional types of plankton: pZ, GNCM, pSNCM, eSNCM, CM, and P.
Protist-Zooplankton	pZ	Protist zooplankton obtaining nourishment via heterotrophy (phagotrophy and osmotrophy). They cannot engage in autotrophy. (cf. phytoplankton and mixoplankton).
plastidic Specialist Non-Constitutive Mixoplankton	pSNCM	SNCM that acquire their capacity for photo (auto)trophy from sequestration of photosynthetic apparatus and nuclear material from specific phototrophic prey (cf. eSNCM).
Specialist Non-Constitutive Mixoplankton	SNCM	NCM that acquire their capacity for photo (auto)trophy from specific phototrophic prey. There are two functional types of SNCM: pSNCM and eSNCM (cf. GNCM).

predation, Table 5.1), Flynn et al. (2019) coined the term 'mixoplankton' to describe planktonic protists that engage in photo(auto)trophy *plus* osmo(hetero)trophy *plus* phago(hetero)trophy. This distinguishes them from the non-phagotrophic phytoplankton (e.g. diatoms) and the non-phototrophic protist-zooplankton (e.g. tintinnids). The descriptor 'phytoplankton' is thus now reserved for phototrophs (both protists and cyanobacteria) that are incapable of phagotrophy though capable of mixotrophy through osmotrophy (Flynn et al., 2019; Glibert & Mitra, 2022, Table 5.1).

A widespread role for mixotrophy through osmotrophy is demonstrated by many decades of research illustrating the use of sugars, amino acids, and other dissolved organics (Antia et al., 1981; Flynn & Butler, 1986; Meyer et al., 2022). The term 'mixotroph' and 'mixotrophy' are often used indiscriminately to refer to traits and ecological implications of the mixotrophic phytoplankton as well as of the mixoplankton. While all mixoplankton are mixotrophs by virtue of their ability to engage in photo-osmo-phago-trophy, all mixotrophs are not mixoplankton (see Table 5.1 for definitions of microbial plankton functional types). Photo-osmo-mixotrophy (of phytoplankton) versus photo-osmo-phago-mixotrophy (of mixoplankton) has very different implications for ecology and biogeochemical cycling. A mixoplankter actively removes a wide range of competitors (bacteria to metazoans) from the ecosystem through hunting, killing, and eating (Fig. 5.1b). For example, the HAB-forming mixoplankton *Karlodinium armiger* have been observed to predate on metazoans (e.g. copepods; Berge et al., 2012); within the traditional marine food-web, metazoan grazers are categorised as predators of the microalgae

K. armiger. We thus see a reversal of the traditional trophic 'role' with mixoplanktonic activity directly impacting the food-web dynamics. Further, the processes of prey digestion and assimilation by mixoplankton results in the release of a range of different end products – dissolved and particulate organics – through excretion and defecation (voiding), potentially contributing towards the biological and/or microbial carbon pumps (Mitra et al., 2014b; Glibert & Mitra, 2022). In contrast, the photo-osmo-mixotrophy employed by phytoplankton neither removes any prey, competitors, or grazers from the food-web nor does this type of mixotrophy lead to the production of any defecated particulate matter that further structures the plankton food-web.

Another aspect of mixoplankton that is often confused in discussions on the topic is the evolutionary lineage of protist evolution. The ancestral protist was phagotrophic (Raven et al., 2009) and would have retained at least a level of the osmotrophic capabilities present in the earliest microbes, if only to recover leaked metabolites (Flynn & Berry, 1999). From these, ancestral mixoplankton evolved by the integration of photosystems from their prey (originally cyanobacteria-like species; Ponce-Toledo et al., 2017; Sánchez-Baracaldo et al., 2017). What are now (sensu Flynn et al., 2019) termed 'phytoplankton protists' then evolved from the loss of phagotrophy. Mixoplankton did not, therefore, evolve through combining traits from protist zooplankton and protist phytoplankton; the latter evolved by loss of an important trait for protist evolution, namely, phagotrophy (Mitra et al., 2023a).

3 Mixoplankton in the Indian Ocean

Mixoplankton comprise a diverse group of protist plankton which can be functionally divided between those with a constitutive ability to photosynthesise (constitutive mixoplankton; CM), and those which need to acquire phototrophic capabilities (non-constitutive mixoplankton; NCM) (Flynn et al., 2019; Mitra et al., 2023b). NCM acquire their phototrophic potential by stealing photosynthetic machinery from (i) many prey types (generalists: GNCM; e.g. *Laboea strobila*, McManus & Fuhrman, 1986; Stoecker et al., 1987; *Strombidinium conicum*, Stoecker et al., 1988/89), (ii) from only specific prey (plastidic specialists: pSNCM; e.g. *Mesodinium rubrum*, Gustafson et al., 2000; Johnson et al., 2016; *Dinophysis acuminata*, Jacobson & Andersen, 1994; Park et al., 2006), or, (iii) by harbouring endosymbionts (endosymbiotic specialists: eSNCM; e.g. green *Noctiluca scintillans*, Subrahmanyan, 1954; Wang et al., 2016; foraminiferans such as *Globigeria bulloides*, *Orbulina universa*, Spindler & Hemleben, 1980; Gastrich, 1987). Accordingly, marine protist plankton can be broadly divided into six functional groups (types), with the phago-heterotrophic protist-zooplankton and the photo-osmo-mixotrophic phytoplankton occupying the two ends of the trophic spectrum (Mitra et al., 2016; Flynn et al., 2019; Mitra et al., 2023b). Figure 5.2 provides a key to this plankton functional group (type) classification specifically providing examples from the IO plankton communities; this has been modified from Mitra et al. (2016), Mitra

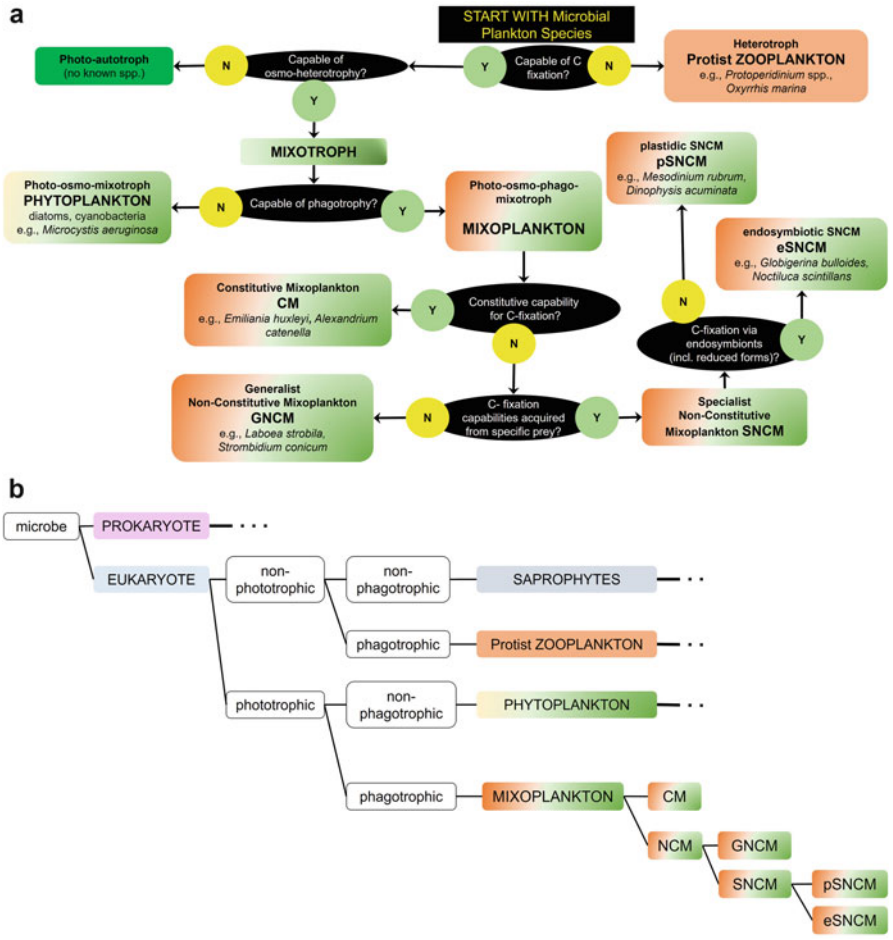

Fig. 5.2 Classification of the Indian Ocean marine microbial plankton under the mixoplankton paradigm. (**a**) Functional group classification key for marine microbial plankton. N no, Y yes. (Modified from Mitra and Flynn et al. (2021) and Mitra et al. (2023b)). (**b**) Marine microbial plankton traits tree leading to mixoplankton. Dash-dotted lines indicate additional tree branches. (Modified from Mitra et al. (2023b)).

and Flynn (2021) and Mitra et al. (2023b), to take into account the coining of the term 'mixoplankton'. Figure 5.3 provides a schematic of the physiological processes associated with the different forms of nourishment employed by the different protist plankton functional groups; this has been modified from Mitra et al. (2023a). Functional group descriptions are commonly used by scientists to partition the numerous taxonomic classes into categories more relevant to ecology; it is also referred to as 'functional type' especially in modelling studies (Mitra et al., 2016). Accordingly, in this chapter, we will use the terminologies 'functional group' and 'functional type' synonymously.

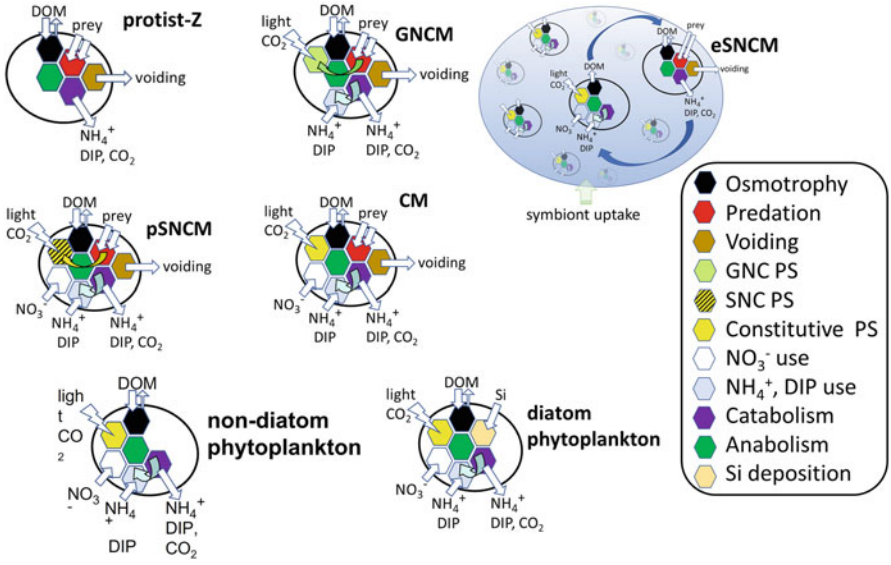

Fig. 5.3 Schematic representations of the six protist functional type configurations under the mixoplankton paradigm. Physiological functions of each functional group are indicated by the hexagons. The six protist functional groups are: zooplankton (with no phototrophy; pZ), generalist non-constitutive mixoplankton (with acquired phototrophy; GNCM), plastidic specialist non-constitutive mixoplankton (with acquired phototrophy from specialist prey; pSNCM), endosymbiotic specialist non-constitutive mixoplankton (with symbionts for acquired phototrophy; eSNCM), constitutive mixoplankton (inherent phototrophic capability; CM) and phytoplankton (with no phagotrophy). All protist types can use dissolved organic matter (DOM); phytoplankton are thus mixotrophs by combining photo(auto)trophy with osmo(hetero)trophy. See also Table 5.1 for definitions of the functional groups and nutritional strategies. Schematics are not to scale; see Table 5.2 for size ranges of IO mixoplankton. (Figure modified from Mitra et al. (2023a)

3.1 Mixoplankton Biogeography in the Indian Ocean

Different mixoplankton functional groups have diverse spatial and temporal distributions (Leles et al., 2017, 2019; Faure et al., 2019), but collectively include representatives with global significance throughout the wide size range of protist plankton (Flynn et al., 2019; Mitra et al., 2023b). The size range is extensive, ranging from some of the smallest CM of a few micrometre diameter (e.g. *Florenciella* sp., Li et al., 2020) to single-celled Rhizaria exceeding 1 cm (e.g. *Orbulina universa*, Spindler & Hemleben, 1980; Gastrich, 1987). Here we present, a biogeographic study of the different mixoplankton functional groups that occur in the IO.

In order to undertake this study, we aligned the mixoplankton species listed in 'The Mixoplankton Database' (Mitra et al., 2023b) to those reported in the Ocean Biogeographic Information System database (OBIS; http://www.iobis.org/) for the IO. For this purpose, data from OBIS were oriented by the division of the global

ocean into subsets defined by 54 biogeographic provinces according to Longhurst (2007). We considered the following Longhurst biogeographic provinces (LP) to encompass the IO: North-western Arabian Coastal Upwelling (ARAB), Archipelago Deep Basins Oligotrophic Gyres (ARCH), Australia-Indonesia Coastal Seas (AUSW), Eastern Africa Coastal Seas (EAFR), Eastern India Coastal Seas (INDE), Western India Coastal Seas (INDW), Red Sea and Persian Gulf Coastal Seas (REDS), Indian South Subtropical Gyres (ISSG), Indian Monsoon Gyres (MONS), Sunda-Arafura Shelves (SUND), parts of Subantarctic Water Ring (SANT), and parts of South Subtropical Convergence province (SSTC). This division of the IO was similar to that employed by Dalpadado et al. (2021). At least one record was necessary to assume the occurrence of mixoplankton in any province. Grids corresponding to Longhurst's provinces used in the maps were obtained from http://www.marineregions.org/.

Figure 5.4 shows the biogeographic distribution of the different mixoplankton functional types in the IO. The constitutive mixoplankton species (CM) would all have been traditionally labelled as 'phytoplankton' and, therefore, identified only as primary producers with no role in predation. The species within the three non-constitutive mixoplankton groups (GNCM, pSNCM, eSNCM) would have been traditionally considered to be 'protist-zooplankton'. Their food-web activity would have been labelled as 'consumers' of primary producers and prey for metazoan grazers (secondary consumers), with no consideration of their contribution towards primary production.

3.2 Mixoplankton Traits

The biogeography data revealed that 150 mixoplankton species have been recorded within the OBIS database for the IO. Of these, 58 species are constitutive mixoplankton (CM), and 92 species are non-constitutive mixoplankton (NCM) (Fig. 5.5a; see also Table 5.2 and Mitra et al. (2023b)). Of those 150 species, 33 species are recorded as HABs in the IOC-UNESCO harmful algal bloom database (https://marinespecies.org/hab/). Ten of the HAB species belong to the plastidic specialist NCM (pSNCM) functional group, while the remaining species belong to the CM functional group.

The size range of the observed mixoplankton species in the IO is highly diverse between and within each functional type (Fig. 5.5b). The CM species encompass pico to micro size ranges (e.g. *Florenciella* sp.: ESD 0.6 µm, Li et al., 2020; *Tripos furca*: 150 µm × 50 µm, Mitra et al., 2023b), while the sizes of pSNCM and eSNCM species range from nano to meso (e.g. pSNCM *Pfiesteria piscicida* ESD: 10–20 µm, Parrow & Burkholder, 2004; eSNCM *Dinothrix paradoxa* ESD: 12–20 µm, Pascher, 1914; eSNCM *Globigerina bulloides*: ~200 µm, Bé et al., 1977). Only two GNCM plastidic ciliates (*Laboea strobila*, *Strombidium conicum*) are reported as present in the OBIS database for the IO, and the sizes of these range between 40 and 150 µm (Stoecker et al., 1988/89; McManus & Fuhrman, 1986). An analysis of the size

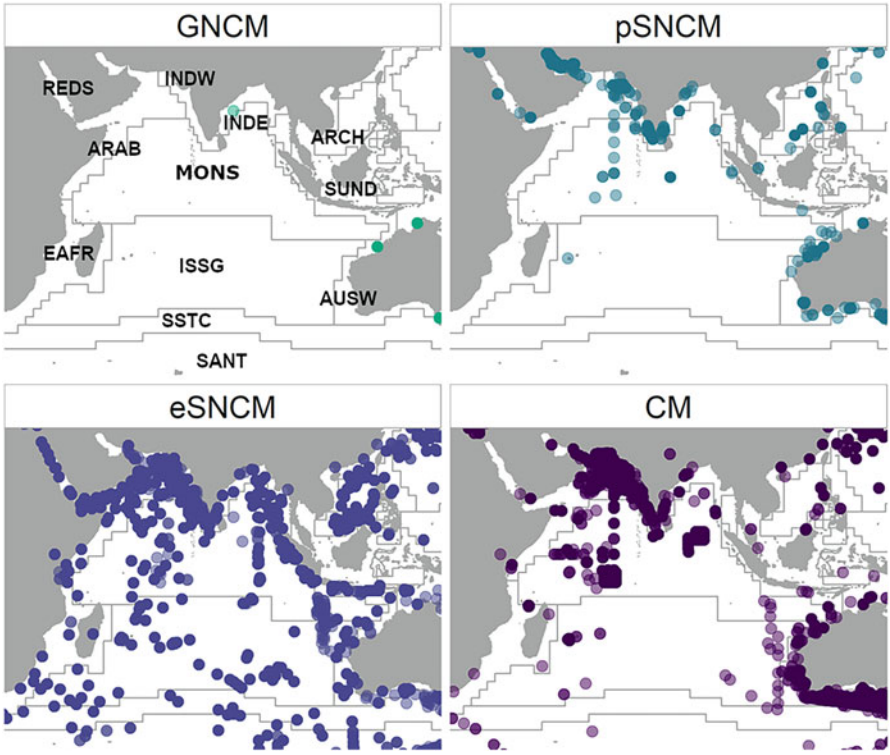

Fig. 5.4 Occurrence of mixoplankton across the Indian Ocean. The number of records are derived from the OBIS database and plotted according to Longhurst's biogeographic provinces of the IO (Longhurst, 2007). Outputs are provided for each of the four mixoplankton functional groups: generalist non-constitutive mixoplankton (GNCM), plastidic specialist non-constitutive mixoplankton (pSNCM), endosymbiotic specialist non-constitutive mixoplankton (eSNCM), and constitutive mixoplankton (CM). See also Fig. 5.2 and Tables 5.1 and 5.2. The IO and neighbouring IO provinces are indicated in the panel showing GNCM distribution

relationship between the mixoplankton predator and their prey also shows the diverse size range of prey ingested by these different mixoplankton functional groups (Fig. 5.5c). This is indicative of the role that mixoplankton must play in the plankton dynamics of the IO.

Analysis of the mixoplankton taxonomic groups revealed Dinoflagellata to be the most observed taxonomic group in the IO (Fig. 5.6a), while the most frequently and highest recorded species belong to the Foraminifera taxonomic group (Table 5.2). Indeed, the top 10 species recorded from the IO all belong to the Formanifera, and 60% of these species were observed in all of the IO Longhurst provinces. Within the specialist non-constitutive mixoplankton types, eSNCM showed greater diversity in their ability to acquire phototrophy compared to pSNCM (Fig. 5.6b vs. Fig. 5.6c).

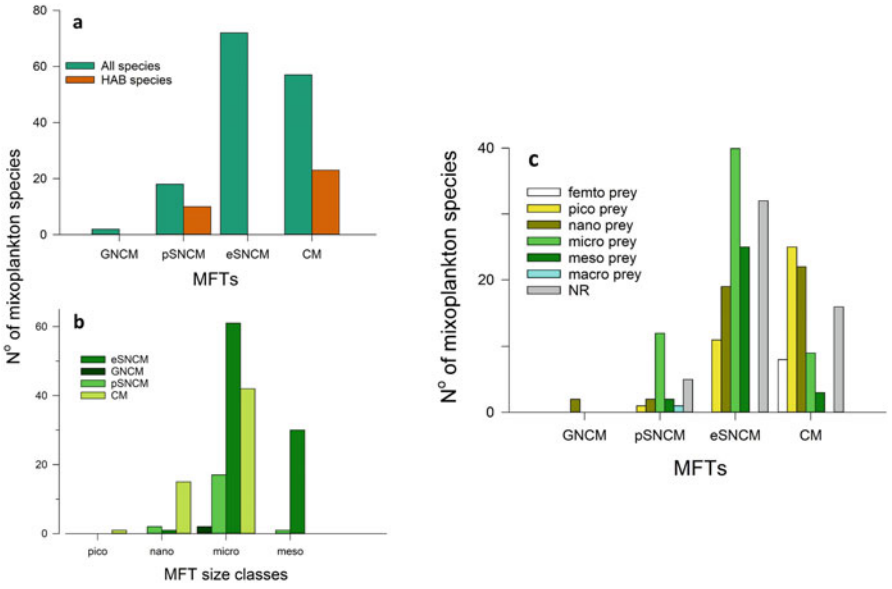

Fig. 5.5 Diversity of the IO mixoplankton species and their prey. (**a**) Species categorised according to mixoplankton functional types (MFT). (**b**) Size class distribution of the species within each MFT. (**c**) Relationship between prey size class and mixoplankton size class for each of the MFTs: generalist non-constitutive mixoplankton (GNCM), plastidic specialist non-constitutive mixoplankton (pSNCM), endosymbiotic specialist non-constitutive mixoplankton (eSNCM), and constitutive mixoplankton (CM). NR indicates not recorded. See also Table 5.1 and Fig. 5.3

3.3 Primary Production and Bacterial Farming by Mixoplankton

An obvious question that arises is as follows: what are the implications of the mixoplankton paradigm for primary production? One of the 'common' taxonomic prey groups associated with the top 30 IO species in the OBIS database (Table 5.2) are the prokaryotic Bacteria and Cyanobacteria. These prokaryotes have been shown to be resilient to multi-stressors (Oliver et al., 2014), with evidence that climate change is seeing an up-shift in the abundance of these picoplankton at the expense of the larger, protist, primary producers across the global Ocean (Morán et al., 2010, 2015).

Mitra et al. (2014b) explored the importance of accounting for the mixoplankton-prokaryote predator-prey interactions in marine systems. In that study, the 'traditional paradigm' configuration considered the simple plant-animal dichotomy where primary production was a function of phytoplankton (diatoms and cyanobacteria) activity (phototrophy + osmotrophy), and remineralisation was due to bacteria. The phytoplankton and bacteria were consumed by protist-zooplankton (phagotrophy), which in turn were consumed by metazoan grazers. In this system, the

Table 5.2 Top 30 frequently recorded species from the Indian Ocean in the OBIS database

#	MFT	Species	Taxonomy	HABs	OBIS	#LP	% LP	Size	Example prey taxonomy
1	eSNCM	*Globigerina bulloides*	Foraminifera	No	9953	11	100	Micro-meso	Bacteria, Copepoda, Sarsostraca
2	eSNCM	*Globigerinoides ruber*	Foraminifera	No	8581	11	100	Micro-meso	Ciliophora, Copepoda
3	eSNCM	*Globigerinita glutinata*	Foraminifera	No	8336	10	91	Micro-meso	Bacteria, Ciliophora, Copepoda
4	eSNCM	*Orbulina universa*	Foraminifera	No	6916	11	100	Micro-meso	Ciliophora, Copepoda
5	eSNCM	*Trilobatus sacculifer*	Foraminifera	No	6756	9	82	Micro-meso	Bacteria, Copepoda, Sarsostraca
6	eSNCM	*Globigerinella siphonifera*	Foraminifera	No	6364	11	100	Micro-meso	Bacteria, Copepoda, Sarsostraca
7	eSNCM	*Globorotalia menardii*	Foraminifera	No	5665	10	91	Micro-meso	Diatomeae, Ochrophyta
8	eSNCM	*Neogloboquadrina dutertrei*	Foraminifera	No	5514	11	100	Micro-meso	Diatomeae
9	eSNCM	*Globigerina falconensis*	Foraminifera	No	4751	10	91	Micro-meso	Bacteria, Copepoda, Sarsostraca
10	eSNCM	*Pulleniatina obliquiloculata*	Foraminifera	No	4265	11	100	Micro-meso	Ochrophyta
11	eSNCM	*Globigerinoides conglobatus*	Foraminifera	No	3490	9	82	Micro-meso	Bacteria, Copepoda, Sarsostraca
12	eSNCM	*Globorotalia tumida*	Foraminifera	No	1833	10	91	Micro-meso	Ciliophora, Copepoda
13	CM	*Emiliania huxleyi*	Haptophyta	No	1668	8	73	Nano	Bacteria
14	eSNCM	*Globoquadrina conglomerata*	Foraminifera	No	1289	7	64	Micro-meso	Bacteria, Copepoda, Sarsostraca
15	CM	*Phaeocystis globosa*	Haptophyta	Yes	1278	3	27	Nano	Bacteria
16	CM	*Tripos furca*	Dinoflagellata	No	1175	9	82	Micro	NR◆
17	eSNCM	*Globorotalia hirsuta*	Foraminifera	No	1137	8	73	Micro-meso	Bacteria, Copepoda, Sarsostraca
18	eSNCM	*Noctiluca scintillans*	Dinoflagellata	No	971	8	73	Meso	Diatomeae, Dinoflagellata
19	CM	*Tripos fusus*	Dinoflagellata	No	905	7	64	Micro	NR◆
20	CM	*Tripos muelleri*	Dinoflagellata	No	901	7	64	Micro	NR◆
21	CM	*Gonyaulax spinifera*	Dinoflagellata	Yes	820	7	64	Micro	Cyanobacteria
22	eSNCM	*Candeina nitida*	Foraminifera	No	807	7	64	Meso	Bacteria, Copepoda, Sarsostraca
23	CM	*Heterocapsa rotundata*	Dinoflagellata	No	647	1	9	Nano	Bacteria, Diatomeae

(continued)

Table 5.2 (continued)

#	MFT	Species	Taxonomy	HABs	OBIS	#LP	% LP	Size	Example prey taxonomy
24	CM	*Protoceratium reticulatum*	Dinoflagellata	Yes	594	7	64	Micro	NR◆
25	eSNCM	*Turborotalita humilis*	Foraminifera	No	589	9	82	Micro-meso	Bacteria, Copepoda, Sarsostraca
26	pSNCM	*Mesodinium rubrum*	Ciliophora	No	492	3	27	Nano-micro	Cryptophyceae
27	CM	*Gymnodinium catenatum*	Dinoflagellata	Yes	474	3	27	Micro	Cyanobacteria, Cryptophyceae, Dinoflagellata
28	CM	*Calcidiscus leptoporus*	Haptophyta	No	336	5	45	Nano	Bacteria
29	pSNCM	*Dinophysis acuminata*	Dinoflagellata	Yes	288	3	27	Micro	Ciliophora
30	CM	*Prorocentrum micans*	Dinoflagellata	No	222	7	64	Micro	Cyanobacteria,Diatomeae, Cryptophyceae, Dinoflagellata, Haptophyta, Ochrophyta

Data obtained from Mitra et al. (2023b)

Species classified according to mixoplankton functional groups/types (MFT): constitutive mixoplankton (CM), and non-constitutive mixoplankton (NCM); NCM species classified according to source of acquired phototrophy (generalists: GNCM; plastidic specialists: pSNCM; endosymbiotic specialists: eSNCM). 'HABs' indicates whether the mixoplankton is recorded as a harmful algal bloom species in the IOC-UNESCO HABs list. 'OBIS' indicates total number of observations per species recorded in the OBIS database. #LP indicate number of Longhurst provinces where ≥5 observations have been reported for the species while %LP indicates % occurrence of the mixoplankton species in the 11 Longhurst provinces in the Indian Ocean. femto, <0.2 μm; pico, 0.2–2 μm; nano, 2–20 μm; micro, 20–200 μm; meso, 200 μm–20 mm. *NR*◆ prey not recorded; mixoplankton activity evidenced through presence of food vacuoles

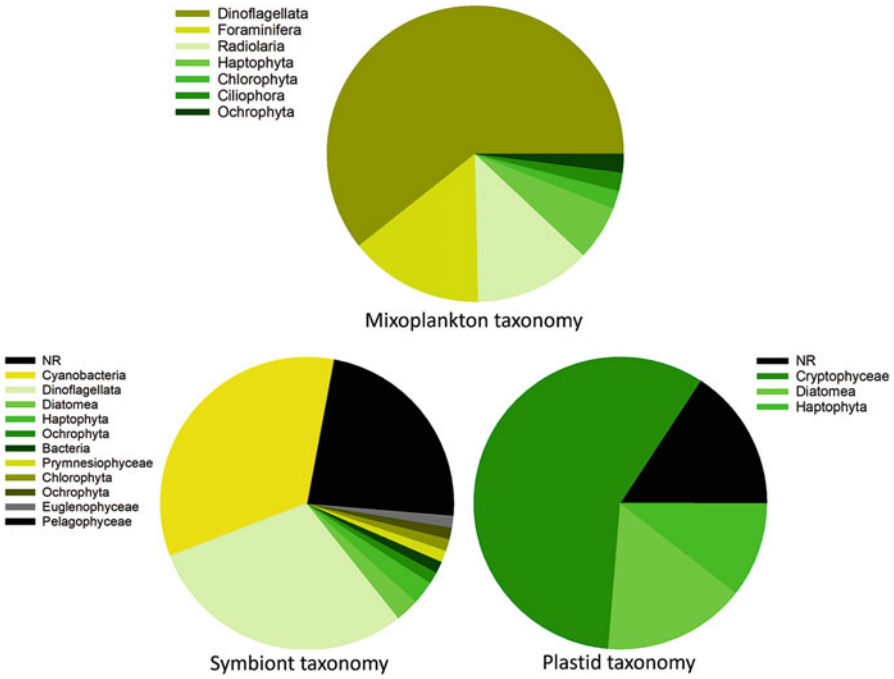

Fig. 5.6 Diversity of IO mixoplankton species and the sources of acquired phototrophy for the IO specialist non-constitutive mixoplankton (SNCM). Symbiont taxonomy, sources of endosymbionts for acquired phototrophy in endosymbiotic specialist non-constitutive mixoplankton (eSNCM). Plastid taxonomy, taxonomic groups contributing photosynthetic material to plastidic specialist non-constitutive mixoplankton (pSNCM). NR indicates not recorded. See also Fig. 5.3 and Table 5.1

phytoplankton and bacteria thus competed for dissolved inorganic nutrients (Fig. 5.7a). Within the 'mixoplankton paradigm', the protist 'phytoplankton' functional group was replaced with a 'constitutive mixoplankton' (CM) group. CM preyed upon cyanobacteria and bacteria (via phagotrophy) as well as engaged in C-fixation (via phototrophy). Thus, in this configuration, the CM are not competing with the prokaryote community for nutrients, rather the CM-bacterial activities were argued to be akin to 'farming' of the bacterial prey supported by the release of dissolved organics by the mixoplankton (Fig. 5.7b). Mixoplanktonic activity resulted in higher C-fixation due to enhanced nutrient feedbacks (Fig. 5.7c). This study thus showed that consideration of mixoplankton in food-web studies could have profound impacts on the ecosystem dynamics.

Ecosystem functioning has been shown to depend crucially on the description of the plankton functional types (phytoplankton vs. CM vs. NCM) with open ocean plankton dynamics. Description of the food-web organisms under the mixoplankton paradigm could potentially have a more stable equilibrium resulting in higher production rates due to variable (enhanced) nutrient feedbacks (e.g. Mitra et al., 2016; Leles et al., 2018). Leles et al. (2021) further demonstrated the importance of

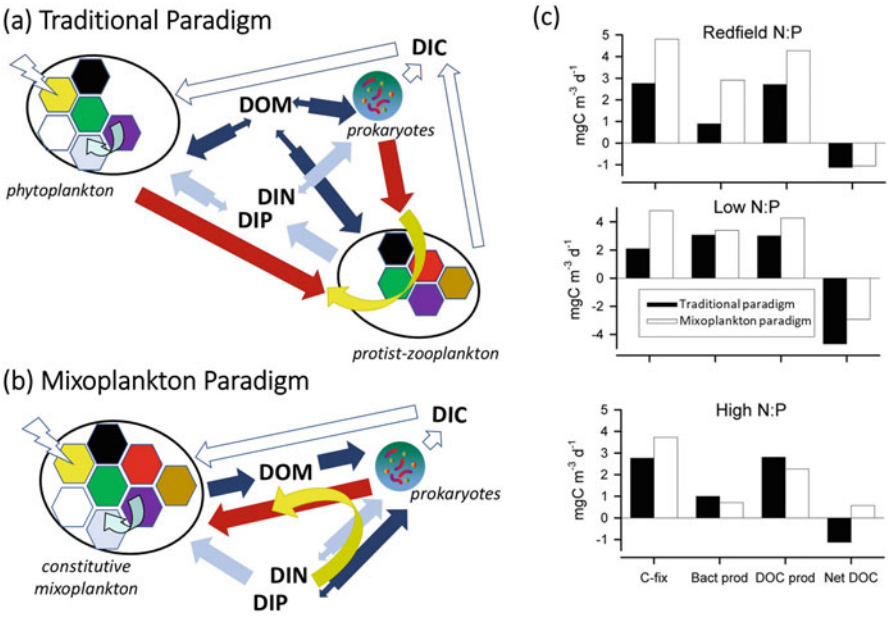

Fig. 5.7 Impact of 'Bacterial farming' on primary production under the mixoplankton paradigm. Schematic showing the detailed involvement of bacteria and DOM for the supply of nutrients to support primary production (yellow arrows) in (**a**) the traditional paradigm versus (**b**) the mixoplankton paradigm. Red arrows indicate predatory links. (**c**) Results from in silico experiments conducted under the traditional versus mixoplankton paradigms. Cfix, rates of primary production; Bact prod, bacterial production; DOC prod, production of dissolved organic carbon (from all sources, including voiding of material by grazers and primary production leakage), and Net DOC = biological production of DOC – bacterial uptake of DOC (negative value indicates reliance of bacteria on DOC in part from outside of the mixed layer). The inorganic nutrient regimes (all with an inorganic N input of 1 μM) are in Redfield N: P (molar ratio 16), low N: P (molar ratio 4), or high N: P (molar ratio 64). (Figures and results modified from Mitra et al. (2014b)). See also Fig. 5.3 and Table 5.1 for plankton functional group physiology and definitions

different mixoplankton functional types coupled with different sizes to plankton bloom dynamics and, thence primary production. For example, within the European regional seas' ecosystem model, the magnitude of the spring bloom differed when micro-phytoplankton were replaced by micro-mixoplankton; further, the timing of nano-plankton bloom altered when considered under the mixoplankton paradigm.

4 Discussion

The term 'mixoplankton' is relatively new, but the activities of these organisms are not new. Yet even after decades of marine research, species of the mixoplankton communities still remain enigmatic. Studies of the base of the oceanic food-web still follow the false plant-animal dichotomy (Fig. 5.1a) with primary production

focussing solely on phytoplankton (diatoms and cyanobacteria) activity. The mixoplankton paradigm sees a major shift in our understanding of the ecosystem functioning of various protist plankton (Fig. 5.1b); consumers of primary producers are now also contributing to carbon fixation (Glibert & Mitra, 2022). It is important to reflect on why and how science managed to miss this important community of marine ecology for so long; there are a few key reasons that warrant reflection.

4.1 Sampling Bias in Monitoring

From microscopic analyses to molecular data, ocean colour, and ecosystem models, all share one common aspect – these approaches are traditionally rooted in the phytoplankton-zooplankton paradigm, and thus neglect the mixoplankton communities. Current field monitoring methods do not reflect the complexity of the marine food-web under the mixoplankton paradigm, where different mixoplankton functional groups play a diverse and important role (Fig. 5.1b; Mitra et al., 2014b; Leles et al., 2021; Glibert & Mitra, 2022). Routine field sampling techniques are also based on the plant-animal phytoplankton-zooplankton dichotomy. Critically, such techniques are not well adapted to provide quantitative data for mixoplankton where phototrophy and phagotrophy are concurrent and synergistic processes (Mitra & Flynn, 2010). Research is too often conducted by experts in phytoplankton or zooplankton, with separate sampling and measurement approaches. For example, the presence of chlorophyll is typically used as an indicator of phytoplankton biomass and, thence, carbon fixation in surveys and ecosystem monitoring. However, chlorophyll is actually not just an indicator of the presence of phytoplankton; it may also indicate the presence of mixoplankton, which are not just primary producers, but also consumers, and include harmful species (Fig. 5.1b, Mitra & Flynn, 2021). It is thus important that plankton monitoring programmes take into account the mixoplankton communities. Their proliferation is not driven solely by light and inorganic nutrients as that of phytoplankton communities; therefore, they have a much wider and diverse impact on marine trophic dynamics (Anschütz et al., 2022; Larsson et al., 2022).

Traditional sampling protocols, based on microscopic identification and quantification, are commonly biased towards certain taxonomic groups or size classes of protists. In our interrogation of the OBIS database for the IO, we found ca. 70% of the species to belong to the Dinoflagellata group (Fig. 5.6); previous studies on mixoplankton biogeography in global oceans (Faure et al., 2019; Leles et al., 2019) have observed a similar bias towards this group. Such a bias towards dinoflagellates can be attributed to a focus on global HAB events due to their deleterious impact on aquaculture and fisheries (Al Shehhi et al., 2014; Reguera et al., 2014; Kudela et al., 2015; Harrison et al., 2017); we found records of dinoflagellates in 27–64% of the Longhurst provinces within the IO (Table 5.2).

The IO biogeography data show a wide range of functional diversity within the mixoplankton community (Fig. 5.5). While species of sizes ranging from pico-meso (1–800 μm) have been recorded across the different mixoplankton functional groups (Table 5.2), the majority of the recorded species fall within the micro (20–200 μm) size range (Fig. 5.5b). Previous studies have suggested that sampling bias adversely affects investigations of small mixoplankton, occurring within the pico- and nano-plankton size spectrum (Leles et al., 2019), as well as the larger (>600 μm) mixoplankton (Leles et al., 2017). Microscopy still remains the primary and best methodology for identification of organisms to species level. However, that approach is problematic for smaller (pico- and nano-) mixoplankton.

Protist species have been traditionally defined based on morphological differences, but this is compounded by the presence of cryptic species with very similar body forms but different physiologies, particularly among nanoplankton (Lie et al., 2018). While DNA sequence information has been proposed as a potential tool to address such shortcomings in the detection of protistan diversity (De Vargas et al., 2015), it should be noted that estimates from DNA sequences are strongly dependent on primer choice, amplification protocols, and sequencing and can also be biased towards certain groups (Caron & Hu, 2019; Strzepek et al., 2022). The study by Faure et al. (2019), for instance, identified a gap in sequence data in the GNCM and pSNCM groups compared to the CM and eSNCM groups. At best, sequences provide semi-quantitative data only. We need quantitative data for presence and for vital rates of not just mixoplankton but also their prey and predators to understand ecosystem functioning – 'omics cannot provide such data (Strzepek et al., 2022).

Various rhizarian taxa, including eSNCM Foraminifera and Radiolaria, occur within the 'larger' meso-plankton (>500 μm) size category. However, when considering plankton within the meso size range, sampling and monitoring studies typically focus on the metazoan planktonic grazers (e.g. copepods) (Leles et al., 2017). Yet, imaging surveys have revealed that nearly 30% of total zooplankton biomass across the oceans are rhizarians, most of which are eSNCM (Biard et al., 2016). Within routine monitoring surveys, these meso- mixoplankton are typically under-represented because their cells are severely damaged by plankton nets and also because they slowly dissolve during attempts to preserve samples (Biard et al., 2016). We found the most frequently recorded mixoplankton species in the IO to be the eSNCM rhizarian Formanifera occurring in all the Longhurst biogeographic provinces (Table 5.2; Fig. 5.4). A recent study reports that mixoplanktonic rhizarians dominate the oligotrophic waters of the IO (110°E, Davies et al., 2022; i.e. comprising parts of the AUSW, MONS, ISSG Longhurst provinces, Longhurst, 2007). This important group would traditionally be labelled as predatory protist-zooplankton, and therefore, their potentially significant contributions towards primary production in the IO through carbon fixation would be ignored.

4.2 Challenges for Aquaculture and Fisheries

Over 80% of the world's human population lives within 100 km of the coast, and the IO coastline is ~66,526 Km, shared by 38 countries (Wafar et al., 2011). The majority of the coastal zone belts of the IO are densely populated, with the Ocean playing a substantial socioeconomic role in the provision of ecosystem services to these communities (De Young, 2006). The Sustainable Development Goals of the United Nations highlight the importance of ocean health and sustainability, especially under climate change (Arora & Mishra, 2019). This, in turn, highlights the need for revision of the ocean health indicators in line with the mixoplankton paradigm. In marine systems, chlorophyll is typically used as a proxy for measuring phytoplankton productivity, including for fisheries and aquaculture management. This is because chlorophyll and its analogues in remote sensing or ocean colour provide a ready and sensitive monitor of 'phytoplankton' (see Sect. 3.3 above). The concept that, on occasions, this signature is due to organisms other than strict phototrophs creates a challenge. This is especially important for predictions of algal blooms and their impacts on aquaculture and fisheries (Jeong et al., 2005; Reguera et al., 2014). Various HAB species are mixoplanktonic (Mitra & Flynn, 2021), and the growth of these HABs is not controlled simply by light and dissolved organics and inorganics (i.e. nutrients that support phototrophy and osmotrophy). Competitors and even grazers could provide food for the proliferation of HABs (Berge et al., 2012).

New types of ecosystem disruptive mixoplankton blooms are also appearing in the IO – such as the eSNCM dinoflagellate green *Noctiluca scintillans* (Gomes et al., 2014) and the mucosphere-producing CM dinoflagellate *Prorocentrum* cf. *balticum* and *P. cordatum* (Larsson et al., 2022; Tillmann et al., 2023) – and are expanding across coastal oceans with climate change. In the Arabian Sea sector of the IO, green *N. scintillans* blooms are leading to the collapse of the traditional phytoplankton-zooplankton-fisheries link in the food-web with severe food security and socioeconomic hardships to a population of over 140 million people (Goes et al., 2018). Other mixoplankton blooms affect recreational activities, and the property market – discolouration of water caused by *Karlodinium veneficum* blooms have been known to result in a decrease in prices of highly sought-after waterside properties; this species has been recorded (in OBIS) as occurring in the INDE and INDW Longhurst provinces of the IO.

There is also a potential interaction with aquaculture, as fish farms release both the nutrients needed for photosynthesis, but also the organic matter used directly or indirectly (via support of prey species) by mixoplankton. Algal blooms are a major issue for aquaculture all around the globe, and the IO supports a range of different aquacultures such as sea cucumbers, seaweeds, and shell- and fin-fisheries (De Young, 2006; FAO, 2020). Studies on fisheries and aquaculture without considering mixoplanktonic activity leave gaps in our understanding of what controls the many algal blooms that impact these ecosystem services.

4.3 Primary Production in Ecosystem and Climate Change Models

Carbon fixation through primary production is one of the cornerstone processes in marine ecology and oceanography; in the IO, primary production studies have been focussed mainly in the Arabian Sea and the 110°E sections (Krey, 1973; Hood et al., 2009). Modelling is a widely used tool to study the impact of climate change on primary productivity. However, the traditional split between 'phytoplankton' and 'zooplankton' still defines the means by which plankton are structured within climate change models, with a few exceptions (Ghyoot et al., 2017; Leles et al., 2018, 2021; Li et al., 2022). The majority of global models of primary productivity thus ignore the diverse strategies adopted by protist plankton, leaving us largely ignorant of how photo-osmo-phago-trophy of mixoplankton affect the competitive outcomes within protist communities. Modellers generally avoid complexity, and mixoplankton are complex; they are more than merged 'phytoplankton' and 'zooplankton' (Flynn & Mitra, 2009; Mitra & Flynn, 2010; Mitra et al., 2023a). Introducing mixoplankton to models is thus an uphill battle. The challenge in embedding the well-established microbial loop and virus shunt descriptions in models (both are typically absent from models) perhaps warns us of the challenge ahead. However, the absence of mixoplankton in models is more than just another simplification, for it also reflects a flawed description of the organisms that are currently included in the models and labelled as 'phytoplankton' and 'zooplankton'.

Biogeochemical models, particularly 3D models, tend to compare simulations against ocean colour data due to the availability of continuous global estimates of surface Chl-a concentrations (Bracher et al., 2017; Dalpadado et al., 2021). However, such data do not capture the diversity of forms and functions among phototrophic taxa, including phytoplankton and mixoplankton. From the 1990s, increasing efforts have been applied to developing algorithms that can retrieve information on the composition and size structure of phototrophic communities from ocean colour (Sathyendranath, 2014). These methods utilise information from (presumed) phytoplankton abundance, cell size, and bio-optical properties such as pigment composition, absorption, and backscattering (reviewed in Bracher et al., 2017). Most algorithms provide information about the dominance or the presence/absence of a particular group, or the fraction of Chl-a associated with three different size classes (pico-, nano-, and micro-plankton). Such information is not, however, easily transferable to the plankton functional types within biogeochemical models, and the situation will be more complex when considering mixoplankton as the 'colour' in those organisms could be due to acquired phototrophy or ingested prey.

There are various other challenges with acquiring and using remote sensing data. For example, biogeochemical models are typically biomass-based (e.g. carbon, nitrogen); currently, there is no reliable algorithm to convert chlorophyll data to carbon biomass as the Chl:C ratio varies significantly under different environmental conditions (as does the C:N ratio) and with different species. There are limitations

with acquiring data using remote sensing as the methodology can be applied to the ocean surface only, while plankton are distributed throughout the vertical water column. This limitation is further compounded in coastal areas – the most important areas for ecosystem services and thus primary productivity, and the habitat for many mixoplankton – due to the presence of c-DOM and particulate matter (Flynn & McGillicuddy Jr, 2018; Flynn et al., 2021).

An argument voiced for ignoring mixoplankton in the ecosystem and climate change models is a paucity of data. However, given the new lines of evidence for the global ubiquity of the different mixoplankton functional types (Leles et al., 2017, 2019) and their not in-substantial impact on primary production (Fig. 5.7; Ghyoot et al., 2017; Leles et al., 2021), this argument can no longer be considered to be justifiable. The data labelled as 'phytoplankton' or 'zooplankton', are not just representative data for those functional groups, but they are confused by the presence of data for mixoplankton.

5 Conclusions and Future Directions

There is as yet no definitive answer to the most profound question, '*what is the significance of mixoplanktonic activities?*'. This applies equally to the IO as to any other oceanic area. The available data and metrics are insufficient to determine the actual contribution of mixoplanktonic species. Indeed, there is very little quantitative knowledge that is holistic on these ubiquitous but often cryptic species. Thus, no synthesis or consensus exists for how to best estimate the contribution of mixoplankton to primary and secondary productivities, to biogeochemical cycling, to the microbial carbon pump, or how these important plankton may react to climate change events such as ocean acidification (Flynn & Mitra, 2023). A major problem in attaining holistic quantitative data is attributed to the methodologies used in routine oceanographic science; field and laboratory methodologies for protist physiology are designed for phototrophy or phagotrophy – for mixoplankton both are required simultaneously.

One important challenge is that neither traditional sampling protocols nor high-throughput sequencing captures the presence of mixoplankton and/or indicate their potential activity, while analyses of metabarcoding data must rely on previous experimental evidence to classify the operational taxonomic units as mixoplankton (Faure et al., 2019; Leles et al., 2019). Even though not a common practice, it is relatively simple to quantify the biomass of non-constitutive mixoplankton versus that of their heterotrophic counterparts. Mixoplanktonic ciliates (e.g. GNCM *Laboea strobila*, *Strombidium conicum* in IO), for example, are easily identifiable from the heterotrophic ones through the examination of samples under epifluorescence microscopy or with a FlowCAM (e.g. Stoecker et al., 2014; Haraguchi et al., 2018). The same does not apply to CM because these are not necessarily actively feeding at all times. Constitutive mixoplankton smaller than 20 μm are usually distinguished from their phytoplanktonic counterparts by experiments on measuring

rates of bacterivory. Such experiments are limited by a series of assumptions, including that community ingestion rates can be approximated from ingestion rates measured in a few individuals (Safi & Hall, 1999; Anderson et al., 2017). In reality, feeding varies over the diel cycle, and only a proportion of the total mixoplankton assemblage will be actively feeding at any time during an experiment (e.g. Avrahami & Frada, 2020; Koppelle et al., 2022; Mitra & Flynn, 2023). Paradoxically, most bacterivory studies do not provide information on protistan diversity (Unrein et al., 2014; Beisner et al., 2019). Without quantifying mixoplankton activity, we cannot have a clear understanding of the impact of mixoplankton on primary production, plankton trophodynamics, and global biogeochemical cycles.

Climate change is impacting the biodiversity and the food-web structure of the IO (Gomes et al., 2014). Given the socioeconomic importance of the IO, it is important that the mixoplankton paradigm is integrated into studies of ocean productivity from research through to monitoring and management (e.g., of aquaculture and fisheries). Various methods have been developed or repurposed to isolate and culture mixoplankton for laboratory and fieldwork to gain a quantitative understanding of their functionality (Hansen et al., 2021; Flynn et al., 2021; Mitra et al. 2021a, b, c). While suggestions have been made for the need to develop high-end research methodologies (e.g. single-cell transcriptomics, 'nanoSIMS') for in situ mixoplankton identification (Beisner et al., 2019 but cf. Strzepek et al., 2022), such methods are too expensive for regular monitoring of food-web dynamics not only in the IO but in coastal seas and oceans globally. There is thus a need to repurpose or develop more cost-effective in situ methods. For example, a recent study has demonstrated how the 'dilution technique', traditionally used to study zooplankton predator-prey dynamics, can be repurposed for quantification of mixoplankton predator-prey interactions (Duarte Ferreira et al., 2021).

Now science (belatedly) recognises the presence and importance of different mixoplankton. At the very least, all future plankton research and monitoring programmes need to caveat their work as being incomplete unless mixoplankton are explicitly studied. What is really needed, however, is to make mixoplankton studies as routine as studies of phytoplankton. To do otherwise not only ignores mixoplankton but it damages the value of 'phytoplankton' science by contaminating it with information on non-phytoplankton species.

Acknowledgements The authors thank Kevin J. Flynn for comments on an earlier version of this chapter. This work was supported by the European Commission funded H2020-MSCA-ITN Project MixITiN 766327, the Sêr Cymru II WEFO ERDF Programme MixoHUB 82372, UKRI NERC Funded Global Partnerships Grant NocSym (NE/W004461/1) and the Brazilian government programme Science Without Borders (232845/2014-0) through CNPq (Conselho Nacional de Desenvolvimento Científico e Tecnológico). The plankton images in Fig. 5.1 were prepared by Nick Cox (hello@nickcox.uk). This is a contribution to SCOR WG #165 MixONET which is supported by grant OCE-214035 from the National Science Foundation to the Scientific Committee on Oceanic Research (SCOR) and contributions from SCOR National Committees. This is Cardiff EARTH CRediT contribution 6.

References

Al Shehhi, M. R., Gherboudj, I., & Ghedira, H. (2014). An overview of historical harmful algae blooms outbreaks in the Arabian Seas. *Marine Pollution Bulletin, 86*, 314–324.

Anderson, R., Jürgens, K., & Hansen, P. J. (2017). Mixotrophic phytoflagellate bacterivory field measurements strongly biased by standard approaches: A case study. *Frontiers in Microbiology, 8*, 1398. https://doi.org/10.3389/fmicb.2017.01398

Anschütz, A. A., Flynn, K. J., & Mitra, A. (2022). Acquired phototrophy and its implications for bloom dynamics of the *Teleaulax-Mesodinium-Dinophysis*-Complex. *Frontiers in Marine Science, 8*, 799358. https://doi.org/10.3389/fmars.2021.799358

Antia, N. J., Harrison, P. J., & Oliveira, L. (1981). The role of dissolved organic nitrogen in phytoplankton nutrition, cell biology and ecology. *Phycologia, 30*, 1–89.

Arora, N. K., & Mishra, I. (2019). United Nations Sustainable Development Goals 2030 and environmental sustainability: Race against time. *Environmental Sustainability, 2*, 339–342.

Avrahami, Y., & Frada, M. J. (2020). Detection of phagotrophy in the marine phytoplankton group of the coccolithophores (Calcihaptophycidae, Haptophyta) during nutrient-replete and phosphate-limited growth. *Journal of Phycology, 56*, 1103–1108.

Azam, F., Fenchel, T., Field, J. G., Gray, J. S., Meyer-Reil, L. A., et al. (1983). The ecological role of water-column microbes in the sea. *Marine Ecology Progress Series, 10*, 257–263.

Bé, A. W., Hemleben, C., Anderson, O. R., Spindler, M., Hacunda, J., et al. (1977). Laboratory and field observations of living planktonic foraminifera. *Micropaleontology, 23*, 155–179.

Beisner, B. E., Grossart, H. P., & Gasol, J. M. (2019). A guide to methods for estimating phago-mixotrophy in nanophytoplankton. *Journal of Plankton Research, 41*, 77–89.

Berge, T., Poulsen, L. K., Moldrup, M., Daugbjerg, N., & Hansen, P. J. (2012). Marine microalgae attack and feed on metazoans. *The ISME Journal, 6*, 1926–1936.

Biard, T., Stemmann, L., Picheral, M., Mayot, N., Vandromme, P., et al. (2016). In situ imaging reveals the biomass of giant protists in the global ocean. *Nature, 532*, 504–507.

Bockstahler, K. R., & Coats, D. W. (1993). Spatial and temporal aspects of mixotrophy in Chesapeake Bay dinoflagellates. *The Journal of Eukaryotic Microbiology, 40*, 49–60.

Bracher, A., Bouman, H. A., Brewin, R. J. W., Bricaud, A., Brotas, V., et al. (2017). Obtaining phytoplankton diversity from ocean color: A scientific roadmap for future development. *Frontiers in Marine Science, 4*, 1–15.

Burkholder, J. M., Glibert, P. M., & Skelton, H. M. (2008). Mixotrophy, a major mode of nutrition for harmful algal species in eutrophic waters. *Harmful Algae, 8*, 77–93.

Caron, D. A., & Hu, S. K. (2019). Are we overestimating protistan diversity in nature? *Trends in Microbiology, 27*, 197–205.

Dalpadado, P., Arrigo, K. R., van Dijken, G. L., Gunasekara, S. S., Ostrowski, M., et al. (2021). Warming of the Indian Ocean and its impact on temporal and spatial dynamics of primary production. *Progress in Oceanography, 198*, 102688.

Davies, C. H., Beckley, L. E., & Richardson, A. J. (2022). Copepods and mixotrophic Rhizaria dominate zooplankton abundances in the oligotrophic Indian Ocean. *Deep Sea Research Part II, 202*, 105136. https://doi.org/10.1016/j.dsr2.2022.105136

De Vargas, C., Audic, S., Henry, N., Decelle, J., Mahé, F., et al. (2015). Eukaryotic plankton diversity in the sunlit ocean. *Science, 348*, 1–11.

De Young, C. (Ed.). (2006). *Review of the state of world marine capture fisheries management: Indian Ocean (No. 488)*. Food & Agriculture Organisation.

Duarte Ferreira, G., Romano, F., Medić, N., Pitta, P., Hansen, P. J., et al. (2021). Mixoplankton interferences in dilution grazing experiments. *Scientific Reports, 11*, 1–16.

FAO. (2020). *The state of world fisheries and aquaculture 2020. Sustainability in action*. FAO. https://doi.org/10.4060/ca9229en

Faure, E., Not, F., Benoiston, A. S., Labadie, K., Bittner, L., et al. (2019). Mixotrophic protists display contrasted biogeographies in the global ocean. *The ISME Journal, 13*, 1072–1083.

Flynn, K. J., & Berry, L. S. (1999). The loss of organic nitrogen during marine primary production may be significantly overestimated when using 15N substrates. *Proceedings of the Royal Society of London. Series B, 266*, 641–647.

Flynn, K. J., & Butler, I. (1986). Nitrogen sources for the growth of marine microalgae; role of dissolved free amino acids. *Marine Ecology Progress Series, 34*, 281–304.

Flynn, K. J., & McGillicuddy, D. J., Jr. (2018). Modeling marine harmful algal blooms; current status and future prospects. In S. E. Shumway, J.-A. M. Burkholder, & S. Morton (Eds.), *Harmful algal blooms: A compendium desk reference*. Wiley Science Publishers.

Flynn, K. J., & Mitra, A. (2009). Building the "perfect beast": Modelling mixotrophic plankton. *Journal of Plankton Research, 31*, 965–992.

Flynn, K. J., Stoecker, D. K., Mitra, A., Raven, J. A., Glibert, P. M., et al. (2013). Misuse of the phytoplankton–zooplankton dichotomy: The need to assign organisms as mixotrophs within plankton functional types. *Journal of Plankton Research, 35*, 3–11.

Flynn, K. J., Mitra, A., Anestis, K., Anschütz, A. A., Calbet, A., et al. (2019). Mixotrophic protists and a new paradigm for marine ecology: Where does plankton research go now? *Journal of Plankton Research, 41*, 375–391.

Flynn, K. J., Mitra, A., Glibert, P., & Smyth, T. (2021). *Mixoplankton international workshop report*. Zenodo. https://doi.org/10.5281/zenodo.5521009

Flynn, K.J., & Mitra, A. (2023). Feeding in mixoplankton enhances phototrophy increasing bloom-induced pH changes with ocean acidification. *Journal of Plankton Research*, https://doi.org/10.1093/plankt/fbad030

Gast, R. J., & Caron, D. A. (1996). Molecular phylogeny of symbiotic dinoflagellates from planktonic foraminifera and radiolaria. *Molecular Biology and Evolution, 13*, 1192–1197.

Gastrich, M. D. (1987). Ultrastructure of a new intracellular symbiotic alga found within planktonic foraminifera. *Journal of Phycology, 23*, 623–632.

Ghyoot, C., Flynn, K. J., Mitra, A., Lancelot, C., & Gypens, N. (2017). Modeling plankton mixotrophy: A mechanistic model consistent with the shuter-type biochemical approach. *Frontiers in Ecology and Evolution, 5*, 1–16.

Glibert, P. M., & Mitra, A. (2022). From webs, loops, shunts, and pumps to microbial multitasking: Evolving concepts of marine microbial ecology, the mixoplankton paradigm, and implications for a future ocean. *Limnology and Oceanography, 67*, 585–597.

Goes, J. I., Gomes, H. D. R., Al-Hashimi, K., & Buranapratheprat, A. (2018). Ecological drivers of green *Noctiluca* blooms in two monsoonal-driven ecosystems. In *Global ecology and oceanography of harmful algal blooms* (pp. 327–336). Springer.

Gomes, H. D. R., Goes, J. I., Matondkar, S. P., Buskey, E. J., Basu, S., et al. (2014). Massive outbreaks of *Noctiluca scintillans* blooms in the Arabian Sea due to spread of hypoxia. *Nature Communications, 5*, 1–8.

Gustafson, D. E., Stoecker, D. K., Johnson, M. D., Van Heukelem, W. F., & Sneider, K. (2000). Cryptophyte algae are robbed of their organelles by the marine ciliate *Mesodinium rubrum*. *Nature, 405*, 1049–1052.

Hansen, P. J., Flynn, K. J., Mitra, A., Calbet, A., Saiz, E., et al. (2021). *A manual for isolation and culture of mixoplankton to support experimental studies*. Zenodo. https://doi.org/10.5281/zenodo.5520864

Haraguchi, L., Jakobsen, H. H., Lundholm, N., & Carstensen, J. (2018). Phytoplankton community dynamic: A driver for ciliate trophic strategies. *Frontiers in Marine Science, 5*, 1–16.

Harrison, P. J., Piontkovski, S., & Al-Hashmi, K. (2017). Understanding how physical-biological coupling influences harmful algal blooms, low oxygen and fish kills in the sea of Oman and the Western Arabian Sea. *Marine Pollution Bulletin, 114*, 25–34.

Hood, R. R., Wiggert, J. D., & Naqvi, S. W. A. (2009). Indian Ocean research: Opportunities and challenges. *Geophysical Monograph Series, 185*, 409–428.

Jacobson, D. M., & Andersen, R. A. (1994). The discovery of mixotrophy in photosynthetic species of *Dinophysis* (Dinophyceae): Light and electron microscopical observations of food vacuoles in *Dinophysis acuminata*, *D. norvegica* and two heterotrophic dinophysoid dinoflagellates. *Phycologia, 33*, 97–110.

Jeong, H. J., Park, J. Y., Nho, J. H., Park, M. O., Ha, J. H., et al. (2005). Feeding by red-tide dinoflagellates on the cyanobacterium *Synechococcus*. *Aquatic Microbial Ecology, 41*, 131–143.

Jiao, N., Herndl, G. J., Hansell, D. A., Benner, R., Kattner, G., et al. (2010). Microbial production of recalcitrant dissolved organic matter: Long-term carbon storage in the global ocean. *Nature Reviews Microbiology, 8*, 593–599.

Jiao, N., Robinson, C., Azam, F., Thomas, H., Baltar, F., et al. (2014). Mechanisms of microbial carbon sequestration in the ocean–future research directions. *Biogeosciences, 11*, 5285–5306.

Johnson, M. D., Beaudoin, D. J., Laza-Martinez, A., Dyhrman, S. T., Fensin, E., et al. (2016). The genetic diversity of *Mesodinium* and associated cryptophytes. *Frontiers in Microbiology, 7*, 2017. https://doi.org/10.3389/fmicb.2016.02017

Koppelle, S., López-Escardó, D., Brussaard, C. P., Huisman, J., Philippart, C. J., et al. (2022). Mixotrophy in the bloom-forming genus *Phaeocystis* and other haptophytes. *Harmful Algae, 117*, 102292. https://doi.org/10.1016/j.hal.2022.102292

Krey, J. (1973). Primary production in the Indian Ocean I. In *The biology of the Indian Ocean* (pp. 115–126). Springer.

Kudela, R., Berdalet, E., Bernard, S., Burford, M., Fernand, L., et al. (2015). *Harmful algal blooms. A scientific summary for policy makers*. IOC/UNESCO, Paris (IOC/INF-1320).

Larsson, M. E., Bramucci, A. R., Collins, S., Hallegraeff, G., Kahlke, T., et al. (2022). Mucospheres produced by a mixotrophic protist impact ocean carbon cycling. *Nature Communications, 13*, 1–15.

Leles, S. G., Mitra, A., Flynn, K. J., Stoecker, D. K., Hansen, P. J., et al. (2017). Oceanic protists with different forms of acquired phototrophy display contrasting biogeographies and abundance. *Proceedings of the Royal Society B: Biological Sciences, 284*, 20170664.

Leles, S. G., Polimene, L., Bruggeman, J., Blackford, J., Ciavatta, S., et al. (2018). Modelling mixotrophic functional diversity and implications for ecosystem function. *Journal of Plankton Research, 40*, 627–642.

Leles, S. G., Mitra, A., Flynn, K. J., Tillmann, U., Stoecker, D., et al. (2019). Sampling bias misrepresents the biogeographical significance of constitutive mixotrophs across global oceans. *Global Ecology and Biogeography, 28*, 418–428.

Leles, S. G., Bruggeman, J., Polimene, L., Blackford, J., Flynn, K. J., et al. (2021). Differences in physiology explain succession of mixoplankton functional types and affect carbon fluxes in temperate seas. *Progress in Oceanography, 190*, 102481.

Li, Q., Edwards, K. F., Schvarcz, C. R., Selph, K. E., & Steward, G. F. (2020). Plasticity in the grazing ecophysiology of *Florenciella* (Dichtyochophyceae), a mixotrophic nanoflagellate that consumes *Prochlorococcus* and other bacteria. *Limnology and Oceanography, 66*, 47–60.

Li, M., Chen, Y., Zhang, F., Song, Y., Glibert, P. M., et al. (2022). A three-dimensional mixotrophic model of *Karlodinium veneficum* blooms for a eutrophic estuary. *Harmful Algae, 113*, 102203.

Lie, A. A. Y., Liu, Z., Terrado, R., Tatters, A. O., Heidelberg, K. B., et al. (2018). A tale of two mixotrophic chrysophytes: Insights into the metabolisms of two *Ochromonas* species (Chrysophyceae) through a comparison of gene expression. *PLoS One, 13*, 1–20.

Longhurst, A. (2007). *Ecological geography of the sea*. Academic Press.

McManus, G. B., & Fuhrman, J. A. (1986). Photosynthetic pigments in the ciliate *Laboea strobila* from Long Island Sound, USA. *Journal of Plankton Research, 8*, 317–327.

Meyer, N., Rydzyk, A., & Pohnert, G. (2022). Pronounced uptake and metabolism of organic substrates by diatoms revealed by pulse-labeling metabolomics. *Frontiers in Marine Science, 9*. https://www.frontiersin.org/article/10.3389/fmars.2022.821167

Mitra, A., & Flynn, K. J. (2010). Modelling mixotrophy in harmful algal blooms: More or less the sum of the parts? *Journal of Marine Systems, 83*, 158–169.

Mitra, A., & Flynn, K. J. (2021). HABs and the mixoplankton paradigm. In B. Reguera & E. Bresnan (Eds.), *UNESCO harmful algae news No. 67*. Zenodo. https://doi.org/10.5281/zenodo.5109703

Mitra, A., Castellani, C., Gentleman, W. C., Jónasdóttir, S. H., Flynn, K. J., et al. (2014a). Bridging the gap between marine biogeochemical and fisheries sciences; configuring the zooplankton link. *Progress in Oceanography, 129*, 176–199.

Mitra, A., Flynn, K. J., Burkholder, J. M., Berge, T., Calbet, A., et al. (2014b). The role of mixotrophic protists in the biological carbon pump. *Biogeosciences, 11*, 995–1005.

Mitra, A., Flynn, K. J., Tillmann, U., Raven, J. A., Caron, D., et al. (2016). Defining planktonic protist functional groups on mechanisms for energy and nutrient acquisition: Incorporation of diverse mixotrophic strategies. *Protist, 167*, 106–120.

Mitra, A., Hansen, P. J., & Flynn, K. J. (Eds.). (2021a). *Seasonal distribution of non-constitutive mixoplankton across arctic, temperate and mediterranean coastal waters*. Zenodo. https://doi.org/10.5281/zenodo.5055708

Mitra, A., Gypens, N., Hansen, P. J., & Flynn, K. J. (Eds.). (2021b). *A guide for field studies and environmental monitoring of mixoplankton populations*. Zenodo. https://doi.org/10.5281/zenodo.5054916

Mitra, A., Flynn, K. J., Konstantinos, A., Joost, M., Ferreira Guilherme, D., & Calbet, A. (Eds.). (2021c). *Novel approaches for investigating marine planktonic mixotrophy. Zenodo*. https://doi.org/10.5281/zenodo.5148500

Mitra, A., Flynn, K.J., Stoecker D.K., & Raven, J.A. (2023a) Trait trade-offs in phagotrophic microalgae: the mixoplankton conundrum. *European Journal of Phycology*, https://doi.org/10.1080/09670262.2023.2216259

Mitra, A., Caron, D.A., Faure, E., Flynn, K.J., Leles, S.G., Hansen, P.J., McManus, G.B., Not, F., Gomes, H.R., Santoferrara, L.F., Stoecker, D.K., & Tillmann, U. (2023b). The Mixoplankton Database (MDB): Diversity of photo-phago-trophic plankton in form, function, and distribution across the global ocean. *The Journal of Eukaryotic Microbiology, 70,* e12972. https://doi.org/10.1111/jeu.12972

Mitra, A., & Flynn, K.J. (2023). Low rates of bacterivory enhances phototrophy and competitive advantage for mixoplankton growing in oligotrophic waters. *Scientific Reports*, *13,* 6900. https://doi.org/10.1038/s41598-023-33962-x

Morán, X. A. G., López-Urrutia, Á., Calvo-Díaz, A., & Li, W. K. (2010). Increasing importance of small phytoplankton in a warmer ocean. *Global Change Biology, 16*, 1137–1144.

Morán, X. A. G., Alonso-Sáez, L., Nogueira, E., Ducklow, H. W., González, N., et al. (2015). More, smaller bacteria in response to ocean's warming? *Proceedings of the Royal Society B, 282*, 20150371.

Oliver, A. E., Newbold, L. K., Whiteley, A. S., & van der Gast, C. J. (2014). Marine bacterial communities are resistant to elevated carbon dioxide levels. *Environmental Microbiology Reports, 6*, 574–582.

Park, M. G., Kim, S., Kim, H. S., Myung, G., Kang, Y. G., et al. (2006). First successful culture of the marine dinoflagellate *Dinophysis* acuminata. *Aquatic Microbial Ecology, 45*, 101–106.

Parrow, M. W., & Burkholder, J. (2004). The sexual life cycles of *Pfiesteria piscicida* and Cryptoperidiniopsoids (Dinophyceae). *Journal of Phycology, 40*, 664–673.

Pascher, A. (1914). Über Flagellaten und Algen. *Berichte. Deutsche Botanische Gesellschaft, 32*, 136–160.

Pomeroy, L. R. (1974). The ocean's food web, a changing paradigm. *Bioscience, 24*, 499–504.

Ponce-Toledo, R. I., Deschamps, P., López-García, P., Zivanovic, Y., Benzerara, K., et al. (2017). An early-branching freshwater cyanobacterium at the origin of plastids. *Current Biology, 27*, 386–391.

Raven, J. A., Beardall, J., Flynn, K. J., & Maberly, S. C. (2009). Phagotrophy in the origins of photosynthesis in eukaryotes and as a complementary mode of nutrition in phototrophs: Relation to Darwin's insectivorous plants. *Journal of Experimental Botany, 60*, 3975–3987.

Reguera, B., Riobó, P., Rodríguez, F., Díaz, P. A., Pizarro, G., et al. (2014). *Dinophysis* toxins: Causative organisms, distribution and fate in shellfish. *Marine Drugs, 12*, 394–461.

Roxy, M. K., Modi, A., Murtugudde, R., Valsala, V., Panickal, S., et al. (2016). A reduction in marine primary productivity driven by rapid warming over the tropical Indian Ocean. *Geophysical Research Letters, 43*, 826–833.

Roxy, M. K., Gnanaseelan, C., Parekh, A., Chowdary, J. S., Singh, S., et al. (2020). Indian ocean warming. In *Assessment of climate change over the Indian region*. Springer.

Safi, K. A., & Hall, J. A. (1999). Mixotrophic and heterotrophic nanoflagellate grazing in the convergence zone east of New Zealand. *Aquatic Microbial Ecology, 20*, 83–93.

Sánchez-Baracaldo, P., Raven, J. A., Pisani, D., & Knoll, A. H. (2017). Early photosynthetic eukaryotes inhabited low-salinity habitats. *PNAS, 114*, E7737–E7745.

Sathyendranath, S. (Ed.). (2014). Phytoplankton functional types from Space. In *Reports of the International Ocean Color Coordinating Group* (p. 156). IOCCG.

Spindler, M., & Hemleben, C. (1980). Symbionts in planktonic foraminifera (Protozoa). In W. Schwemmier & S. HEA (Eds.), *Endocytobiology endosymbiosis and cell biology*. Walter de Gruyter & Co.

Stoecker, D. K., Michaels, A. E., & Davis, L. H. (1987). Large proportion of marine planktonic ciliates found to contain functional chloroplasts. *Nature, 326*, 790–792.

Stoecker, D. K., Silver, M. W., Michaels, A. E., & Davis, L. H. (1988/89). Enslavement of algal chloroplasts by four *Strombidium* spp. (Ciliophora, Oligotrichida). *Marine Microbial Food Webs, 3*, 79–100.

Stoecker, D. K., Johnson, M. D., de Vargas, C., & Not, F. (2009). Acquired phototrophy in aquatic protists. *Aquatic Microbial Ecology, 57*, 279–310.

Stoecker, D. K., Weigel, A. C., Stockwell, D. A., & Lomas, M. W. (2014). Microzooplankton: Abundance, biomass and contribution to chlorophyll in the Eastern Bering Sea in summer. *Deep Sea Research Part II, 109*, 134–144.

Strzepek, R. F., Nunn, B. L., Bach, L. T., Berges, J. A., Young, E. B., et al. (2022). The ongoing need for rates: Can physiology and omics come together to co-design the measurements needed to understand complex ocean biogeochemistry? *Journal of Plankton Research, 44*, 485–495.

Subrahmanyan, R. (1954). A new member of the Euglenineæ, *Protoeuglena Noctilucæ* gen. et sp. nov., occurring in *Noctiluca miliaris suriray*, causing green discoloration of the sea off Calicut. In *Proceedings of the Indian Academy of Sciences-Section B* (Vol. 39, pp. 118–127). Springer India.

Tillmann, U., Mitra, A., Flynn, K.J., & Larsson, M.E. (2023). Mucus-Trap-Assisted Feeding Is a Common Strategy of the Small Mixoplanktonic *Prorocentrum pervagatum* and *P. cordatum* (Prorocentrales, Dinophyceae). *Microorganisms, 11*, 1730. https://doi.org/10.3390/microorganisms11071730

Unrein, F., Gasol, J. M., Not, F., Forn, I., & Massana, R. (2014). Mixotrophic haptophytes are key bacterial grazers in oligotrophic coastal waters. *The ISME Journal, 8*, 164–176.

Wafar, M., Venkataraman, K., Ingole, B., Ajmal Khan, S., & LokaBharathi, P. (2011). State of knowledge of coastal and marine biodiversity of Indian Ocean countries. *PLoS One, 6*, e14613.

Wang, L., Lin, X., Goes, J. I., & Lin, S. (2016). Phylogenetic analyses of three genes of *Pedinomonas noctilucae*, the green endosymbiont of the marine dinoflagellate *Noctiluca scintillans*, reveal its affiliation to the order Marsupiomonadales (Chlorophyta, Pedinophyceae) under the reinstated name *Protoeuglena noctilucae*. *Protist, 167*, 205–216.

Wilhelm, S. W., & Suttle, C. A. (1999). Viruses and nutrient cycles in the sea: Viruses play critical roles in the structure and function of aquatic food webs. *Bioscience, 49*, 781–788.

Chapter 6
Biophysical Control on the Variability in the Upper Layer Production Pattern of the North-Eastern Arabian Sea

B. R. Smitha and Midhun Shah Hussain

Abstract Understanding the dynamic interplay between physical and biological processes is a major challenge in ocean-related studies, especially to develop predictive capabilities and while addressing the climate change impacts. Biological and physical dynamics in the oceans are coupled, and primary producers being the most important element in an ecosystem, the subject is vastly explored, in terms of the chaotic interactions between various elements of the ecosystem in different spatiotemporal scales. Fluid (ocean) properties are a key factor interacting with plankton behaviour, driving the biological processes and their spatiotemporal patterns. The present chapter is on the role of density gradient in determining the vertical profile of chlorophyll-a in a warm/stratified region, the north-eastern Arabian Sea (NEAS), during the winter-spring season. The dynamics of the recurring bloom (green *Noctiluca*), one of the important regional ecosystem issues, is explained for initial, peak, and withdrawal stages based on in situ observations. The Bio-Argo and conductivity-temperature-depth (CTD) profiler-based analysis for 2003–2019 shows the early onset of the spring bloom and intensification in the subsurface chlorophyll maxima (SCM) in the NEAS since the recent past. The empirical orthogonal teleconnection (EOT) is effectively utilised to explain the surface-subsurface interaction in maintaining the upper layer production pattern and the adaptive strategies of the phytoplankton in respect of the buoyancy control.

Keywords Arabian Sea · Chlorophyll · Stratification · Subsurface chlorophyll maxima · EOT

B. R. Smitha (✉)
Centre for Marine Living Resources and Ecology, Ministry of Earth Sciences, Kochi, India
e-mail: smitha@cmlre.gov.in

M. S. Hussain
School of Marine Sciences, Cochin University of Science and Technology, Kochi, India

S. C. Tripathy, A. Singh (eds.), *Dynamics of Planktonic Primary Productivity in the Indian Ocean*, https://doi.org/10.1007/978-3-031-34467-1_6

1 Introduction

Oceans and their resources are essential to human well-being and social and economic development worldwide. Oceans provide livelihoods, subsistence, and benefits from immense resources, including fisheries, tourism, energy, fuel, and other sectors. Their conservation and sustainable use are central to achieve the Sustainable Development Goals especially for the developing countries. In addition to these, the oceans regulate the global ecosystem by absorbing heat and carbon dioxide (CO_2) from the atmosphere. However, oceans and resources are extremely vulnerable to changes especially due to the climate change impacts, both natural and as a matter of man-made effects. Effects of anthropogenic carbon emissions in our oceans include unprecedented warming, acidification, declining oxygen concentrations, and changes in nutrient cycling (IPCC, 2019). These physical and chemical changes are shifting the distribution, phenology, abundance, composition, and trophic interactions of phytoplankton (IPCC, 2019). This is likely to have ecosystem-wide consequences, as phytoplankton undertake 50% of the world's photosynthesis (Field et al., 1998; Falkowski and Oliver, 2007; Falkowski et al., 2017) underpinning the role of ocean productivity (Lewis et al., 1983; Falkowski et al., 2004; Doney, 2006; Richardson & Poloczanska, 2008) in maintaining the carbon budget of the Earth. Considering the significance of these tiny organisms in the global carbon sequestration processes, especially in the tropical region, the present work is framed to explore the influential changes of warming in these organisms, how the fluid properties influence plankton assemblage/distribution and the biological interactions adjust these changes.

The warming impacts in an ecosystem are complex, and amongst this, the biophysical coupling in various degrees of scales is preferred here to explore the impacts as this is a key indicator of change that is traceable. The general impacts of warming include the biomechanics of plankton swimming and feeding (Guasto et al., 2012), particle aggregation and sedimentation, variations in chemical signals, temporal dynamics in the phytoplankton, turbulence-plankton interactions, etc. Strong seasonality and, as a result, the temporal (seasonal and sub-seasonal) variation in the phytoplankton dynamics evince the vulnerability levels of an organism to sustain in extreme conditions (especially due to warming) they experience. Northeastern Arabian Sea (NEAS) is selected to discuss the issues pertaining to this topic, because of its unique characteristics like year-long (except during mid-February to May) productive nature, presence of open ocean upwelling, mesoscale eddies, convective mixing, the recurring occurrence of harmful algal blooms (HABs) during mid-Feb to March, intense oxygen minimum zones (OMZ) in the column (150–1000 m), etc. The regional sea surface temperature (SST) varies between 24 and 28.5 °C and the sea surface salinity between 35.2 and 36.8 psu. The upper layers are well mixed during winter monsoon (WM) and summer monsoon (SM) with mixed layer depth (MLD) in the range of 20–120 m. Taking into

consideration these peculiar seasonal dynamics of the NEAS, the present chapter attempts to explore the possible warming impacts in the upper layer phytoplankton dynamics. In view of the above, the present work addresses the (1) physical properties of the ocean and the floating plankton, (2) relevance/scope of NEAS to address the impact studies as a natural laboratory, and (3) phytoplankton spatial heterogeneity and interactions in the vertical scale in a stratified warming system.

2 Data, Methods, and Approach

Present analysis has enormously used the Argo profiles (temperature, salinity, and chlorophyll (Chl-a)), satellite data sets, results from the in situ observations (CTD system (SBE 911 Plus) equipped with auxiliary dissolved oxygen sensors, fluorescence, and PAR measured onboard *FORV Sagar Sampada*), and numerical expressions adopting various empirical relations and ecological concepts. Source of surface Chl-a and SST is Aqua MODIS (level III products) which was developed by NASA Goddard Space Flight Center, Ocean Ecology Laboratory, Ocean Biology Processing Group. Also, time series Chl-a was obtained from European Space Agency-Ocean Colour Climate Change Initiative (ESA-OCCCI). The globally distributed potential density (0–100 m depth) was obtained from Argo products of APDRC for the period 2001 to 2020 in 1 × 1 monthly averaged bin. The data is validated with the density values from CTD and Bio-Argo floats which are extracted/processed using the package *Ponman*.

2.1 Empirical Orthogonal Teleconnections

The empirical orthogonal teleconnection (EOT) (Van Den Dool et al., 2000) was used to unwind the relationships between the surface-subsurface interaction based on the temporal variations in sigma-t and the interaction between two layers (here surface and subsurface). The data sets used are raster maps of monthly average Chl-*a* from 2005 to 2019. For the subsurface a new layer is defined referring the SCM peaks. EOTs refer to a correlation-based approach by interpreting the extracted modes, and the analysis is done using the package '*remote*' in R. EOTs carry a quantitative meaning in the form of explained variance, thus enabling an intuitive interpretation of the results. In this case, the temporal variability of one domain (predictor) was analysed with regard to the explained variance of the temporal dynamics of another domain (response). Apart from similarity in the temporal dimension (i.e., identical amount of data points over time), the algorithm can be applied to any two domains without further requirements such as identical spatial resolution or physical units of the data, which was used to exploit for this analysis.

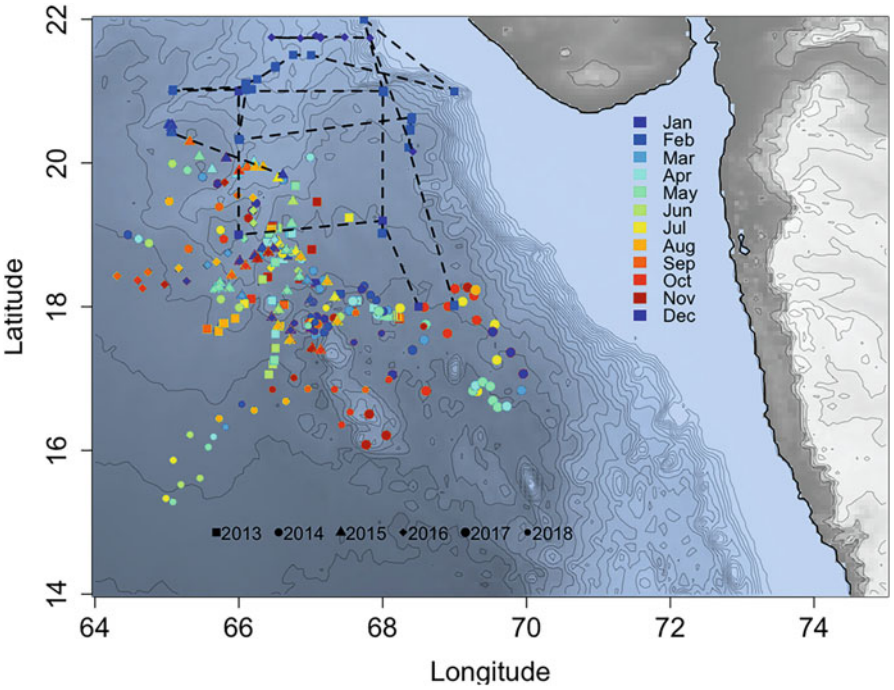

Fig. 6.1 Map showing the profile locations, for CTD and Bio-Argo profiles. The black dotted lines with blue dots are the CTD transects utilised in the study which are measured onboard FORV Sagar Sampada; the coloured points are Bio-Argo locations for different months. The profiles during 2013–2018 and the profiles (3 or more per month) are gridded to get the monthly mean

Here the predictor domain is the surface layer of the study area, whereas the response domains are various depth layers. Besides, the analysis aids to find a time series of EOT throughout the months as shown below (Fig. 6.1).

The approach adopted in discussing this chapter is interdisciplinary, focusing the biology and physics and the coupling between these two. These types of multidisciplinary studies have improved our understanding of marine plankton ecology significantly in the recent past. The newly developed methodologies as well as the increased focus in the area have rapidly advanced the study of planktonic biophysical interactions across spatial and temporal scales. Improved resolution and advanced instrumentation have resulted in sampling in smaller scales than previously possible; also, the recent developments in ocean observing systems and updated remote sensing and other technologies/methods have brought out advanced views of plankton and physical processes at large scales. Recent studies mostly emphasise the importance of behaviour and physics in shaping both plankton distributions and the surrounding environment.

3 Physical Properties of the Ocean and the Floating Plankton

The response of the vast ocean to the various forces acting on it is related to the physical properties of the water, which shows significant variability in time and space. Due to the low molecular weight, the water is relatively dense and viscous and is a barely compressible fluid with a relatively high melting and boiling point. This is attributed to the asymmetric molecular structure and the polarity of the water molecule. These properties of water on Earth make it an essential commodity for life, especially the physical properties which act on the ocean surface. The most abundant and responsive (to climatic variations) tiny microscopic organisms mostly prefer sunlit layers for effective photosynthesis and adopt multiple strategies to maintain buoyant at ocean surface. Biophysical processes relevant to plankton ecology range between scales; for example, microscale turbulence influences planktonic growth and grazing at millimetre scales, whereas features such as fronts and eddies can shape larger-scale plankton distributions (Prairie et al., 2012). Most of the research in this field focuses on specific processes and thus is limited to a narrow range of spatial scales.

Phytoplankton are tiny microscopic organisms at the base of the food web and directly or indirectly support all marine life. They are categorised as the primary producers critical to maintaining biodiversity and supporting fisheries in the global ocean. Due to their high turnover rates and sensitivity to changes in environmental conditions, phytoplankton are considered the indicators of changing oceanographic conditions, climate, and deterioration in water quality (Davies et al., 2016). There are about 5000 species of marine phytoplankton reported world over (Righetti et al., 2020). The phytoplankton controls buoyancy by optimising the ionic concentration phenotypic plasticity by controlling the biovolume and regulating respiration and metabolism (Gemmell et al., 2016). The sinking rate of the organism in static fluids (neutrally buoyant) can be best explained by Stokes equation (Stokes, 1851; Bach et al., 2012). The buoyant phytoplankton having similarity to a particle in the fluid move through the water column in response to g ($= 9.8\ m/s^2$), and the settlement of these particles is referred to as Stokes relation of particle settling. Whereas, in a dynamic system with complex mixing processes due to upwelling, convective mixing, eddies, currents, etc., the simulation of settling velocity based on Stokes equation will be unrealistic due to the complex or chaotic interaction between different components. As mentioned in the famous quote by Lewis F Richardson (1921), the major flows compensated by return currents at depth and a wide spectrum of intermediate eddies of diminishing sizes and of progressively smaller scales of turbulent diffusivity, ulimately in molecular viscosity.

> Big whorls have little whorls
> That feed on their velocity,
> And little whorls have lesser whorls
> And so on to viscosity

The tiny floating organisms are highly responsive to these forces in various scales, from viscosity to big whorls. Phytoplankton cells control their density by increasing its own hydrodynamic resistance or decreasing its density with respect to that of seawater to reduce their sinking rate (Shah et al., 2020). To maintain buoyant at the surface, one of the strategies adopted by certain taxa is the departure from the spherical form through the provision of additional surface area by shape attenuation. Chain or needle-like forms or flattered plate-like structures are often observed in respect of various taxonomic groups. Lewis (1976) represented these modifications through maximum linear dimension of the unit against the organism's surface-volume ratio. These adaptations help in maintaining the buoyancy strategies rather than enabling the effective exchange of gases, nutrients, and other solutes across the cell surface.

To survive and grow, phytoplankton rely on nutrient uptake by diffusion, which is strongly dependent on the fluid motion/turbulence. The organisms perceive turbulence according to their size relative to the Kolmogorov length scale (a few millimetres in general), which is a measure of kinematic viscosity and the turbulent kinetic energy dissipation rate (Thorpe, 2005). Nutrient uptake and lack of flow at the cell surface result in a region of reduced nutrients around the cell, which is known as the 'concentration boundary layer' (Nishihara & Ackerman, 2009). Microscale turbulence cause thinning of the concentration boundary layers (Arin et al., 2002; Peters et al., 2006), which increases flow adjacent to the organism (Karp-Boss et al., 1996; Kiorboe et al., 2001) in addition to sinking or swimming. These processes can significantly increase nutrient uptake and phytoplankton growth.

The vertical distribution and the dynamics of phytoplankton become more complex in turbulent conditions. In general, the parameterisation is done in terms of the eddy diffusion to incorporate the effect due to diffusive and advective processes. The heterogeneous upper layer of the ocean with eddies, filaments, meanders, etc., in various shapes, intensities, and sizes, play a key role as drivers in determining the growth, survival, and distribution pattern of the phytoplankton. Other than the buoyancy control on an organism, turbulent mixing results in aggregation and patchy distribution of the phytoplankton in the water column (Jennifer et al., 2012; Prairie et al., 2011; Durham et al., 2013). The study based on a general water column model indicates sinking phytoplankton cells manage to persist at intermediate levels of turbulence irrespective of the critical depth (Huisman et al., 1999; Huisman & Sommeijer, 2002a, b). Inflows associated with convergence and, in lower velocities, cells accumulate in the centre of the vortex resulting in the formation of a retention zone, trapping the sinking particles, hence inhibiting sedimentation (Stommel, 1949).

Considering the adaptational strategies of the marine phytoplankton and as these species being a major sequestrator of CO_2, it is clear that a strong understanding of the dynamics and its complex response to the varying climate is of utmost importance. The climatic response being heterogeneous in various spatiotemporal domains is chaotic, and so the development of predictive capabilities towards this is challenging with the present understanding. In similar attempts to understand the

regional differences in processes that drive bloom phenological shifts, Yamaguchi et al. (2022) estimate the relative contributions of these processes to phenological shifts and show the dominant contributions within the biomass considered. The same approach is adopted in the present study, and of the six marine ecosystems delineated in the Indian waters, NEAS is considered, which is crucial in terms of the unique physical and biogeochemical processes, recurring algal blooms in the oceanic region, intensification in OMZ, and related ecosystem threats of the time.

4 Relevance/Scope of North-Eastern Arabian Sea (NEAS) to Address the Impact Studies as a Natural Laboratory

The NEAS bordering 16–24°N latitude and 62–74°E longitude is under the direct influence of the summer monsoon (SM) low-level jet (*Findlater jet*) from the south-west and winter monsoon (WM) cold dry continental dry air from the north-east (Kumar & Prasad, 1996; Kushwaha et al., 2022). The annual average primary productivity (PP) in NEAS (0.776 tonne C/km^2/day) is relatively higher (Sanjeevan et al., 2011) both during the SM and WM seasons when compared to the south-eastern Arabian Sea (SEAS) and Lakshadweep Sea ecosystems (LSE). The NEAS is maintained dynamically active and is experienced with strong vertical mixing during both SM and WM, whereas the intermittent SIM and FIM (fall inter-monsoon) are relatively quiescent in terms of the upper layer mixing. During SM the vertical mixing is accelerated due to the open ocean upwelling/Ekman divergence north of the Findlater jet/low-level jet and through large-scale horizontal advection of upwelled waters from the northern and western Arabian Sea (Kumar Prasanna et al., 2001; Wiggert et al., 2000). During WM, enhanced evaporation and, as a result, convective mixing (Madhupratap et al., 1996; Banse & McClain, 1986; Wiggert et al., 2000) trigger and maintain the high biological production (Banse, 1984; Kumar Prasanna et al., 2001). In addition to these seasonal basin-scale processes, NEAS offshore is characterised by eddies/meanderings and irregular flow patterns.

As per various reports on the marine living resources program (MLRP), more than 450 species of microalgae have been observed from the eastern Arabian Sea so far, of which 86 were bloom-forming and about 45 were toxic species. The centennial changes in these algal blooms show that their occurrences increased significantly post-industrial growth (Padmakumar et al., 2012). Extensive blooms of green *Noctiluca* are recurrently observed during winter/spring inter-monsoon seasons in the north-eastern Arabian Sea. The high-performance liquid chromatography (HPLC) based analysis and interpretations made using *Chemtax*, revealed the dominance of diatoms in the coastal waters of the EAS basin in general (Anil Kumar et al., 2021). While, a closer evaluation of the physical processes and nutrient dynamics of the offshore regions revealed that the entrainment of nutrients into the sunlit upper column through convective mixing supported the dominant cyanobacterial population in the NEAS (Anil Kumar et al., 2021). Extensive algal

blooms dominated by diatoms, dinoflagellates, or by mixed algal groups are peculiarities of the region (Madhu et al., 2012; Dwivedi et al., 2015; Gomes et al., 2014). The drivers of the biological production and the formation and spread of blooms in NEAS during WM/SIM are based on convective mixing (Lotliker Aneesh et al., 2018), iron enrichment (Banerjee & Prasanna Kumar, 2014), land-based nutrient enrichment, etc. and due to the mesoscale processes like cold/warm core eddies and meanders (Smitha et al., 2021). For the open ocean waters during winter-spring, the observations record numerical abundance/standing stock of the phytoplankton (average value) as 4×10^5 cells/L (Lathika, 2015). Amongst these, diatoms form the predominant group, taking advantage of the rapid pumping of nutrients due to convective mixing, while the same is shifted to a dinoflagellate-dominant system during early SIM.

NEAS is addressed in a number of studies, especially on the biological responses during winter and spring, due to the potential impact and emerging issues associated with the region, viz., the HAB and the OMZ. Being a stratified period and as evinced in the regime shifts and altered trends (Roxy et al., 2016; Shah et al., 2020; Smitha et al., 2021), the present section also focuses on the same time span to explain the biophysical coupling. The physical driving force that results in vertical mixing and biological interactions that promote and sustain the high productivity pockets (here the spring *Noctiluca* blooms) in the offshore/deep-sea waters of NEAS during the SIM season (Smitha et al., 2021) is mostly associated with warm core eddies (convergence, clockwise circulatory flow pattern). With the onset of the WM, several cold and warm core eddies appear in NEAS, and as the season progresses, turbulent mixing inside these convergence zones intensifies, pushing the MLDs to 100 m or deeper. Deep mixing limits primary production (PP), conserving nutrients (Dufois et al., 2016). With the advent of spring inter-monsoon (SIM; mid-Feb), wind gets weaker, and as a result, SST increases to record values >27 °C leading to strong surface stratification and reduced turbulent mixing, which is a favourable condition for the blooming of green *Noctiluca* inside these warm core eddy regions (Fig. 6.2).

The mesoscale features that occur with a uniformly distributed available potential energy (APE), manifested by the perturbations in the density surfaces relative to the horizontal level that is available for conversion into kinetic energy (Kumar Prasanna et al., 1992) and which is irregular in energy pattern, harbour different biological responses. The existence of a relatively weaker APE region within an eddy prefers to harbour dinoflagellates green *Noctiluca scintillans* with cell numbers reaching 5.8×10^6/l (observation during March 2013) and contributing as much as 97.8% of the microalgae standing stock (Smitha et al., 2021). Cold core eddies with uniform APE are, in general, the sites of mixed algal blooms dominated by diatoms, whereas the eddies with non-uniform APE promote intense blooms of the green *Noctiluca scintillans* on its relatively calm fronts. With the onset of SIM, during mid-February, the deep MLD associated with the warm core eddy begins to shallow, becomes less turbulent, and promotes the proliferation and blooming of green *Noctiluca* utilising the nutrients conserved inside the eddy. These blooms are sustained till April through regenerated production. April onwards, the oligotrophic surface waters of NEAS are transported southwards by the West India Coastal Current where the SST

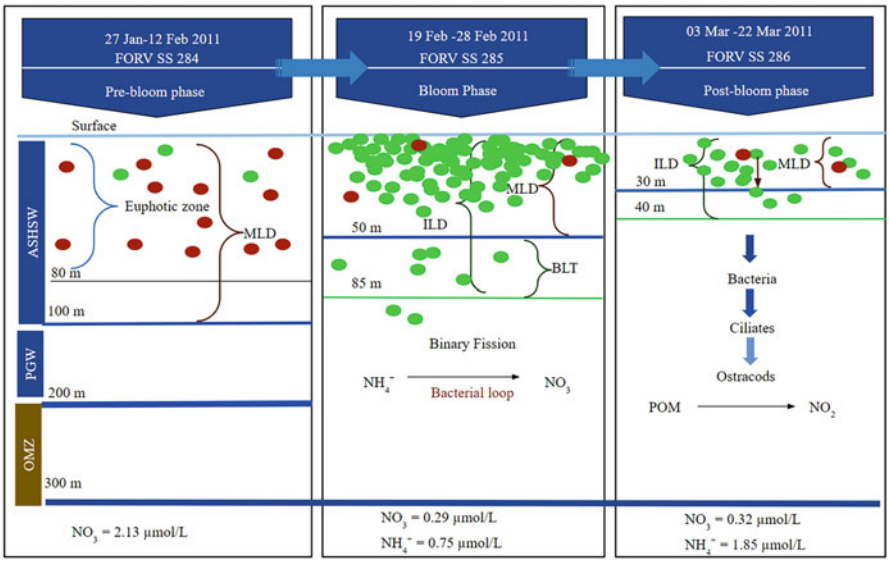

Fig. 6.2 Different stages of the bloom (green *Noctiluca*) in the NEAS during winter-spring are given in the schematic representation. The green circles denote *Noctiluca* cells. Brick red circles are for diatom cells. The picturisation is done referring to the FORV SS observations during 2011 and the secondary information from the available literature. (Figure reproduced from Smitha et al. (2021))

is higher, and the surface waters contain more iron. Under these conditions, the cyanobacteria *T. erythraeum* undertakes diazotrophy and forms extensive blooms (Padmakumar et al., 2010). Intense blooms of *T. erythraeu*m have been reported from Ratnagiri (17°N), Goa, Mangalore, up to Kochi (10°N) areas during April and May (Padmakumar et al., 2010). An analysis of the long-term trends in the sea surface height anomaly (SSHA) of NEAS (1993–2019) indicates a positive trend that suggests strengthening in stratification and, as a result, enhanced *Noctiluca* blooms (Smitha et al., 2021).

Considering the alarming need for regular monitoring of the HABs of the region, a species-specific satellite algorithm for *Noctiluca*, diatom, and mixed bloom occurrence was developed based on satellite measurements (Dwivedi et al., 2015), as part of the MLRP. The model detects bloom-forming algae *Noctiluca scintillans* and its discrimination from diatoms using Moderate Resolution Imaging Spectroradiometer (MODIS) Aqua data in a mixed-species environment using in situ remote sensing reflectance spectra (Satlantic hyperspectral radiometer) for the bloom and non-bloom waters and linking to the spectral shapes of the reflectance spectra for different water types. The method developed is a useful tool for the monitoring and assessment of the *Noctiluca* bloom and its variability, which is a crucial ecosystem element in the NEAS dynamics, and the analysis of long-term trends depicts a clear indication of the intensification of blooms (Dwivedi et al., 2016) as indicated in Smitha et al. (2021).

5 Phytoplankton Spatial Heterogeneity and Interactions in the Vertical Scale in a Warming/Stratified System

The major impact of warming is stratification, and hence we restrict further explanations of the impact on the primary production in the context of stratification and where there is a significant positive trend in the intensification (Righetti et al., 2019). In the tropics, thermal stratification (during warm conditions) contributes to a shallowing of the mixed layer above the nutricline and a reduction in the transfer of nutrients to the surface sunlit layers, ultimately limiting phytoplankton growth.

As explained in the above sections, warming in the NEAS has a multitude of responses, such as altered production patterns (Roxy et al., 2016), OMZs, stratifications, and frequent blooming (HABs), which is on its increasing trend in intensity and spread (Dwivedi et al., 2015). In this regard, stratification elicits visible biological implications such as poor ventilations, low nutrient mixing, and prominent subsurface chlorophyll maxima (SCM). A recent study on SCM in the NEAS (Shah et al., 2020) established the influence of stratified waters on sinking phytoplankton groups. The relations have a wider future scope on SCM occurrence and intensification in tropical/subtropical systems as the warming strengthens the upper ocean stratification (Capotondi et al., 2012), which may further result in an altered production pattern. The Bio-Argo profiles indicate that the depth of SCM is close to the isopycnal layers of 23.8–23.9 kg/m^3 in the 40–60-m-depth range. An increase in temperature is a key factor determining the density gradient, and thus SCM is a strong indicator of warming seas. High SCM values (1.518–3.892 mg/m^3) in the present observations substantiate the fact that the SCM is strengthening progressively with warming. Overall, it is put forward that the warming, associated density gradient, and strong subsurface-surface coupling are instrumental in regulating the upper layer production pattern.

The NEAS has experienced remarkable warming in recent decades (Roxy et al., 2014); however, there is a significant disparity in trend between seasons. The Dec-Feb wind in the NEAS for long term records strengthening in the wind (Narvekar et al., 2017), while the Jan-Mar wind shows a weakening trend (Goes et al., 2020). The effects of warming are reflected in the fluid dynamics properties of the NEAS, resulting in strong stratification and changing the community of primary producers. It is well-known that bloom formation is positively related to a warm climate. This relationship appears to be linked to enzyme kinetics (Boscolo-Galazzo et al., 2018) and associated metabolic rates (Paerl & Huisman, 2008). Studies by Iversen and Ploug (2013) in subpolar waters show the influence of surface water and thermocline temperatures (15° and 4 °C) on the sinking rate of diatom aggregates and bacterial carbon-specific respiration rate. The study shows that community respiration rates in aggregates are lower at 4 °C than at 15 °C due to lower cell-specific activities. These ambient temperatures were found to be required for remineralisation of organic matter by the microbiota. However, re-stratification by warming after winter convections creates the optimum bloom condition. In most tropical systems, the spring bloom follows the same pattern (Sarma et al., 2019;

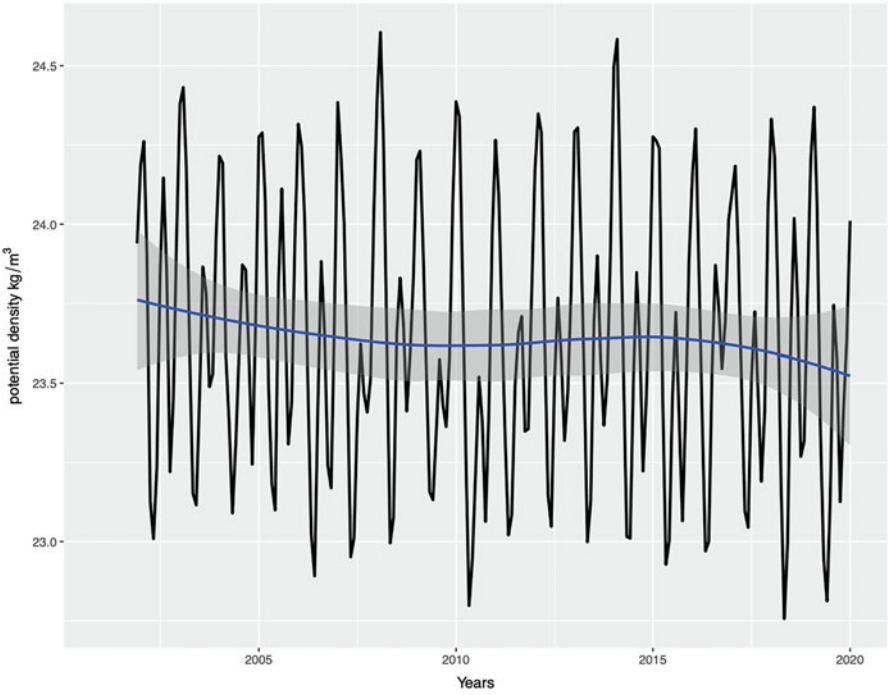

Fig. 6.3 The decadal trends show a lowering of potential density

Sverdrup, 1953). The time series of potential density in NEAS shows (Fig. 6.3) a decreasing trend (23.75 to 23.5 kg/m^3) at a rate of 0.238 kg/m^3 per 20 year, indicating the effects of warming and showing almost similar changes in the magnitude of the decrease in potential density in the tropics (24.24 to 24.18 kg/m^3) globally. In addition to the changes in potential density, the settling velocity simulations for the upper 100 m above in NEAS shed light on the vertical dynamics of surface Chl-a, which explains the changes in response to the density changes (Shah et al., 2020). The density changes associated with the onset of stratification are critical for triggering the bloom. The sequel of winter convective mixing in winter to stratified SIM is the general seasonal pattern in the region where bloom phases begin in the transition phase of the season.

The stratified system generally supports surface blooms by utilising nutrients taken up by winter convective mixing (Madhupratap et al., 1996) and mesoscale eddies (Smitha et al., 2021). The SST time series suggests that the onset of warming/stratification or the withdrawal of seasonal winter mixing is early in NEAS, indicating a gradual shift since 2000 (Shah et al., 2020). The early onset of bloom in the first week of February, which was in the first week of March before the year 2003, coincides with the change in surface density in this region since 2003 (Fig. 6.4). The peak Chl-a values at the surface and the shallowing pycnoclines have overlapping signals in most of the years considered for analysis. The significant observation is

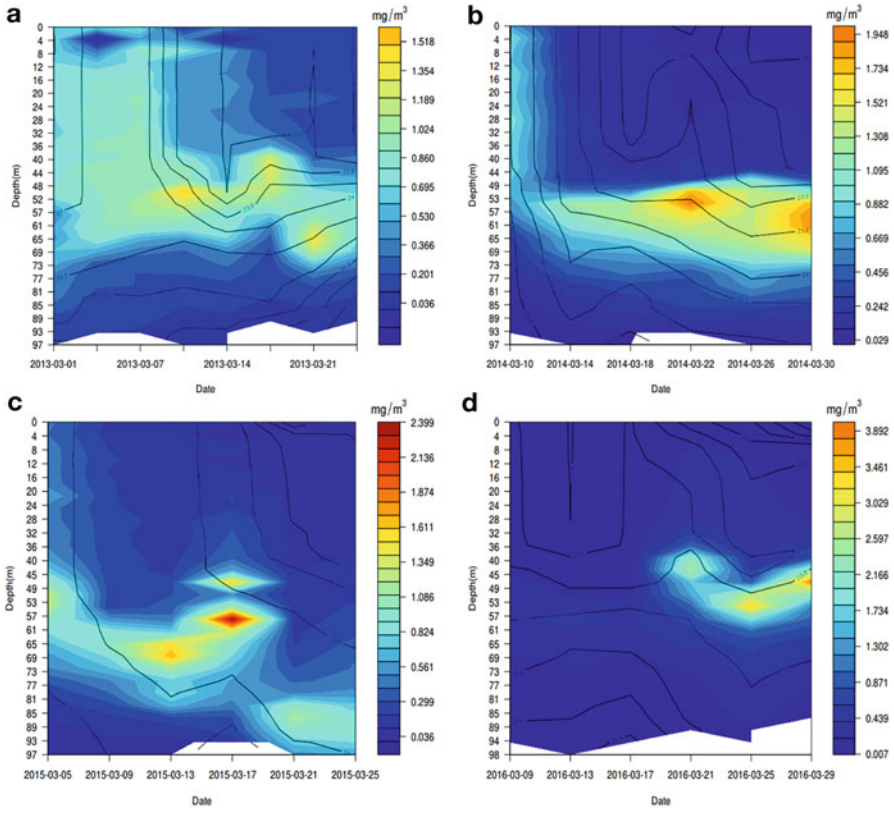

Fig. 6.4 The vertical profiles on chlorophyll-a which are shown with surface and subsurface maxima in primary production in the near past, during March 2013–2016. The profiles are Argo derived and **a**, **b**, **c**, and **d** chronologically represent years 2013, 2014, 2015, and 2016

that the majority of the signals of stratification and the associated impacts shift towards February; the temporal shift resulting altered pattern is attributed to the change in magnitude and duration of the regional, seasonal wind; however, the same is to be addressed in detail to explore the key dynamics of this change.

Analysis of long-term data sets from Chl-a and SST shows dramatic changes in phytoplankton production and distribution in the NEAS. In the physical setting, stratification, a major result of global warming, plays a significant role in these changes. Changes in the pycnocline have increased submerged production, coinciding with extreme events such as ENSO (Vidya & Kurian, 2018). The changing production pattern is also reflected in the distribution of the newly emerging mixotrophic *Noctiluca* bloom, which is expanding its range northwards globally, where the ocean is getting warmer (Harrison et al., 2011).

6 Surface-Subsurface Interaction Based on EOT

The EOT proposes a new variance for calculating functions empirically and orthogonally from a given space-time data set. EOTs are used in explaining the teleconnection between different surfaces/domains (van den Dool, 2007) considering the pixel-to-pixel correlations. The data is first simplified to a time series, identifying a point in the domain through linear regression between the two domains of interest. EOTs are explained based on a multiple linear regression-based approach that allows straightforward interpretation of the extracted modes, and internal EOTs are used to explain teleconnections between the spatiotemporal domains. The present analysis was done on a set of two different temporal domains of Chl-a profiles (2005–2019), each season of SIM and WM, which are spatially separated by surface and subsurface. In the first set of WM (Fig. 6.5), the temporal profiles of each pixel of the subsurface of December (predictor domain) are regressed against the profiles of all pixels in the surface of January and February (being the peak winter months, the January-February average values are considered for the response domain). From the calculation of coefficients of determination and its sum, the highest variance in the response domain was considered as a base point. The first EOT modes are the variations in fitting between base point and raster bands, where the residuals of fits are used to calculate the next EOT. The same procedures were run on the set of SIM

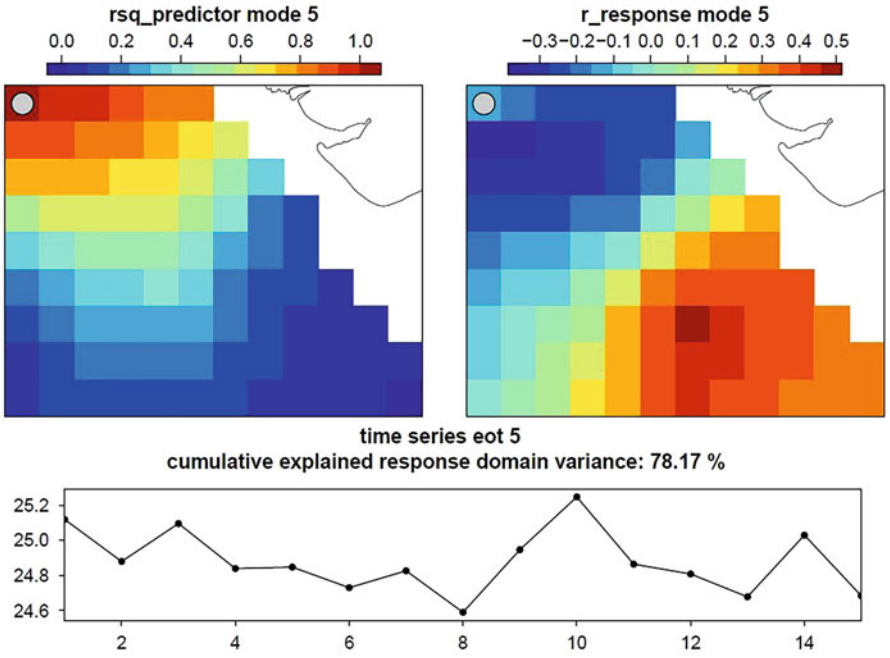

Fig. 6.5 EOT explained for the WM, explaining the subsurface-to-surface interaction

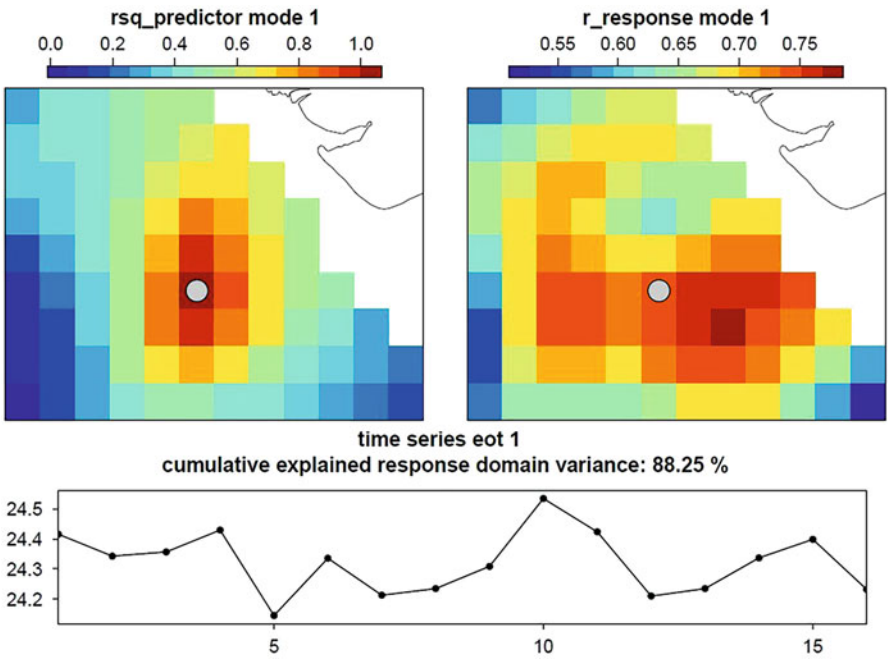

Fig. 6.6 EOT explained for the SIM, explaining the surface to subsurface interaction

(Fig. 6.6), but here the predictor domain is the surface of January-February, and the response domain is the subsurface of March, where the strongest SCM occurred. Three EOT modes were developed for SIM and nine for WM. The EOT modes derived are according to the optimum number, which could better explain the variability of the response field. The quality of modes was determined according to the level of variance, as well as the correlation coefficient on the response domain.

The EOTs derived based on the sigma-t from monthly average Chl-*a* convey that, apart from the evenly distributed anomalistic surface processes, there are strong interactions between surface and subsurface (Figs. 6.5 and 6.6) levels. The first three modes of SIM themselves explain about 88.5% of the variance, whereas the first nine modes explain the 78.17% variances in WM. According to the analysis, the SIM shows strong surface-subsurface interactions in terms of sigma-t and is very much visible in the first mode with a correlation coefficient of 0.75. By the way, the WM suggests reciprocal interactions on the first mode, but very significant interactions on mode 5 with a correlation coefficient of 0.5. These spatial relations were found to be very insightful when considering convective mixing as well as sinking during spring stratification and correlate well with the observed shift in the Chl-a maxima between surface and subsurface.

The EOTs derived for the SIM months suggest that the surface waters of January-February sink down to the subsurface till March, and these signals are prominent in all three EOT modes. This observation complements the prominent subsurface

maxima that persist in this month. This emphasises that phytoplankton lost its buoyancy support from the denser layer of the surface and began to sink (Shah et al., 2020). This disintegrates the blooms from the surface and results in an oligotrophic environment. In contrast to this, the turbulent months don't show such a positive change in sigma-t; instead, the values are very close to zero.

There have been a number of studies explaining the biophysical interactions in the microscales, the scale of centimetres and less where individual plankton interact with each other and with the surrounding environment. Understanding of the interaction between microscale fluid motion and its effects on plankton is limited due to methodological limitations, which were largely explained earlier by theory and experimental studies. Recent advances in technology have allowed novel research in both the laboratory and the field, expanding our understanding of plankton-fluid interactions. Hence it is important to assess how small-scale turbulence can affect plankton growth, species abundance/diversity, and prey-predator relations, as well as how plankton can influence their physical environment by changing the local viscosity, inducing the small-scale fluid motion, which is a major gap in the understanding on the biophysical coupling in the phytoplankton dynamics in the Indian marine ecosystems.

7 Conclusion and Future Perspectives

The sustainable development strategies towards implementing blue economy and ecosystem-based management demand a thorough understanding of the marine ecosystem. The impacts, as experienced, vary in time and space and can be linear, predictive, chaotic, and even random or stochastic. The primary consumers or the phytoplankton would prefer to be in the upper sunlit layers, and the plankton adapt to maintain buoyant at levels appropriate to utilise adequate light. Studies on phytoplankton in the context of warming usually are limited to the community shifts or eco-physiological plasticity of the organisms. But immediate changes of warming are well observed in fluid dynamics rather than the community shifts and plasticity. This is well evident in the lowlight adaptations of vertically sinking phytoplankton groups. The present chapter summarises the biophysical coupling based on the observations and evidences in a warming/stratified oceanic region winter-spring NEAS, which can be treated as a natural laboratory to attempt these kinds of impact studies. In addition to the recent regime shift, the early onset of the recurring green *Noctiluca* bloom, strengthening in the subsurface chlorophyll concentration, the strong coupling between the surface and subsurface, and the predominant role of density gradients in the Chl-*a* vertical profile are discussed. What is lacking in this compilation is the behavioural pattern or impact of the phytoplankton in energy flows, associated turbulence, and with the major circulation patterns/eddies, which are dissipated through cascades of smaller and finer circulatory structures. Explanation of the impact of these small-scale disturbances still remains unanswered for the

Indian ecosystems. This envisages future research plans comprising more in situ observations with emphasis on microscale variations and appropriate coupling of these observations with experimental and modelling outputs to explain the dynamics in a large spatiotemporal domain.

Acknowledgement The authors are grateful to the secretary, Ministry of Earth Sciences (MoES), and the present and past directors of CMLRE for supporting the work and for providing facilities onboard FORV Sagar Sampada for in situ measurements. All the fellow participants of the cruises considered in the present compilation are thankfully acknowledged. In situ data from earlier cruises are obtained from FORV Data Centre in CMLRE. Vertical Argo profiles of chlorophyll used for the study are received from ESSO-INCOIS, Hyderabad, India.

References

IPCC, 2019: IPCC Special Report on the Ocean and Cryosphere in a Changing Climate [H.-O. Pörtner, D.C. Roberts, V. Masson-Delmotte, P. Zhai, M. Tignor, E. Poloczanska, K. Mintenbeck, A. Alegría, M. Nicolai, A. Okem, J. Petzold, B. Rama, N.M. Weyer (eds.)]. Cambridge University Press, Cambridge, UK and New York, NY, USA, 755 pp. https://doi.org/10.1017/9781009157964

Iversen, M. H., & Ploug, H. (2013). Temperature effects on carbon-specific respiration rate and sinking velocity of diatom aggregates – potential implications for deep ocean export processes. *Biogeosciences, 10*(6), 4073–4085.

Arin, L., Marrasé, C., Maar, M., et al. (2002). Combined effects of nutrients and small-scale turbulence in a microcosm experiment. I. Dynamics and size distribution of osmotrophic plankton. *Aquatic Microbial Ecology, 29*(1), 51–61. https://doi.org/10.3354/ame029051

Anil Kumar Vijayan, B. Bikram Reddy, V. Sudheesh, Prachi Hemant Marathe, Vishnu N. Nampoothiri, N.V. Harikrishnachari, P. Kavya, G.V.M. Gupta, M.V. Ramanamurthy. (2021). Phytoplankton community structure in a contrasting physico-chemical regime along the eastern Arabian Sea during the winter monsoon, *Journal of Marine Systems, 215*, 103501, ISSN 0924-7963. https://doi.org/10.1016/j.jmarsys.2020.103501

Bach, L. T., Riebesell, U., Sett, S., et al. (2012). An approach for particle sinking velocity measurements in the 3–400 μm size range and considerations on the effect of temperature on sinking rates. *Marine Biology, 159*(8), 1853–1864. https://doi.org/10.1007/s00227-012-1945-2

Banerjee, P., & Prasanna Kumar, S. (2014). Dust induced episodic phytoplankton blooms in the Arabian Sea during winter monsoon. *Journal of Geophysical Research: Oceans, 119*, 7123–7138. https://doi.org/10.1002/2014JC010304

Banse, K. (1984). Overview of the hydrography and associated biological phenomena in the Arabian Sea, Off Pakistan. In J. D. Milliman & B. H. Haq (Eds.), *Marine geology and oceanography of Arabian Sea and Coastal Pakistan* (pp. 217–303). Van Nostrand Reinhold/ Scientific and Academic Editions.

Banse, K., & McClain, C. R. (1986). Winter blooms of phytoplankton in the Arabian Sea as observed by the coastal zone color scanner. *Marine Ecology Progress Series, 34*, 201–211.

Boscolo-Galazzo, F., Crichton, K. A., Barker, S., et al. (2018). Temperature dependency of metabolic rates in the upper ocean: A positive feedback to global climate change? *Global and Planetary Change, 170*, 201–212.

Capotondi, A., Alexander, M. A., Bond, N. A., et al. (2012). Enhanced upper ocean stratification with climate change in the CMIP3 models. *Journal of Geophysical Research: Oceans, 117*(4). https://doi.org/10.1029/2011JC007409

Davies, C., Coughlan, A., Hallegraeff, G., et al. (2016). A database of marine phytoplankton abundance, biomass and species composition in Australian waters. *Scientific Data, 3*, 160043. https://doi.org/10.1038/sdata.2016.43

Doney, S. C. (2006). Oceanography – Plankton in a warmer world. *Nature, 444*, 695–696. https://doi.org/10.1038/444695a

Dufois, F., Hardman-Mountford, N. J., et al. (2016). Anticyclonic eddies are more productive than cyclonic eddies in sub-tropical gyres because of winter mixing. *Science Advances*, (2), e1600282. https://doi.org/10.1126/sciadv.1600282

Durham, W., Climent, E., Barry, M., et al. (2013). Turbulence drives microscale patches of motile phytoplankton. *Nature Communications, 4*, 2148. https://doi.org/10.1038/ncomms3148

Dwivedi, R., Rafeeq, M., Smitha, B. R., et al. (2015). Species identification of mixed algal bloom in the Northern Arabian Sea using Remote Sensing techniques. *Environmental Monitoring and Assessment, 87*, 51. https://doi.org/10.1007/s10661-015-4291-2

Dwivedi, R., Priyaja, P., Rafeeq, M., et al. (2016). MODIS-Aqua detects *Noctiluca scintillans* and hotspots in the central Arabian Sea. *Environmental Monitoring and Assessment, 188*, 50. https://doi.org/10.1007/s10661-015-5041-1

Falkowski, P., & Oliver, M. (2007). Mix and match: How climate selects phytoplankton. *Nature Reviews. Microbiology, 5*, 813–819. https://doi.org/10.1038/nrmicro1751

Falkowski, P. G., Katz, M. E., et al. (2004). The evolution of modern eukaryotic phytoplankton. *Science, 305*, 354–360. https://www.science.org/doi/10.1126/science.1095964

Falkowski, P. G., Lin, H., & Gorbunov, M. Y. (2017). What limits photosynthetic energy conversion efficiency in nature? Lessons from the oceans. *Philosophical Transactions of the Royal Society B: Biological Sciences, 372*(1730), 20160376. https://doi.org/10.1098/rstb.2016.0376

Field, C. B., Behrenfeld, M. J., Randerson, J. T., et al. (1998). Primary production of the biosphere: Integrating terrestrial and oceanic components. *Science, 281*(5374), 237–240. https://doi.org/10.1126/science.281.5374.237

Gemmell, B. J., Oh, G., Buskey, E. J., & Villareal, T. A. (2016). Dynamic sinking behaviour in marine phytoplankton: Rapid changes in buoyancy may aid in nutrient uptake. *Proceedings. Biological Sciences, 283*(1840), 20161126. https://doi.org/10.1098/rspb.2016.1126

Goes, J. I., Hongzhen, T., do Rosario Gomes, H., et al. (2020). Ecosystem state change in the Arabian Sea fuelled by the recent loss of snow over the Himalayan-Tibetan Plateau region. *Scientific Reports, 10*, 7422. https://doi.org/10.1038/s41598-020-64360-2

Gomes, H. D. R., Goes, J. I., & Matondkar, S. G. P. (2014). Massive outbreaks of Noctiluca scintillans blooms in the Arabian Sea due to spread of hypoxia. *Nature Communications, 5*, 4862. https://doi.org/10.1038/ncomms5862

Guasto J, S., Rusconi, R., & Stocker, R. (2012). Fluid mechanics of planktonic microorganisms. Annual Review of Fluid Mechanics, 44, 373–400. https://doi.org/10.1146/annurev-fluid-120710-101156

Harrison, P. J., Furuya, K., Glibert, P. M., et al. (2011). Geographical distribution of red and green Noctiluca scintillans. *Chinese Journal of Oceanology and Limnology, 29*, 807–831. https://doi.org/10.1007/s00343-011-0510-z

Huisman, J., & Sommeijer, B. (2002a). Population dynamics of sinking phytoplankton in light-limited environments: Simulation techniques and critical parameters. *Journal of Sea Research, 48*, 83–96. https://doi.org/10.1016/S1385-1101(02)00137-5

Huisman, J., & Sommeijer, B. (2002b). Maximal sustainable sinking velocity of phytoplankton. *Marine Ecology-Progress Series, 244*, 39–48. https://www.jstor.org/stable/24866361

Huisman, J., van Oostveen, P., & Weissing, F. J. (1999). Critical depth and critical turbulence: Two different mechanisms for the development of phytoplankton blooms. *Limnology and Oceanography, 44*, 1781–1787. https://doi.org/10.4319/lo.1999.44.7.1781

Jennifer, C., Prairie Kelly, R., Sutherland Kerry, J., et al. (2012). Biophysical interactions in the plankton: A cross-scale review. *Limnology and Oceanography: Fluids and Environments*, 121–145. https://doi.org/10.1215/21573689-1964713

Karp-Boss, L., Boss, E., & Jumars, P. A. (1996). Nutrient fluxes to planktonic osmotrophs in the presence of fluid motion. *Oceanography and Marine Biology, 34*, 71–108.

Kiorboe, T., Plough, H., & Thygesen, U. (2001). Fluid motion and solute distribution around sinking aggregates. I. Small scale fluxes and heterogeneity of nutrients in the pelagic environment. *Marine Ecology Progress Series, 211*, 1–13. https://doi.org/10.3354/meps211001

Kumar Prasanna, S., Babu, M. T., & Rao, D. P. (1992). Energy and generating mechanism of a subsurface, cold core eddy in the Bay of Bengal. *Indian Journal of Marine Sciences, 21*, 140–142.

Kumar Prasanna, S. P., Ramaiah, N., Gauns, M., et al. (2001). Physical forcing of biological productivity in the Northern Arabian Sea during the Northeast Monsoon. *Deep Sea Research Part II: Topical Studies in Oceanography, 48*, 1115–1126. https://doi.org/10.1016/S0967-0645(00)00133-8

Kushwaha, V. K., Prasanna Kumar, S., Feba, F., et al. (2022). Findlater jet induced summer monsoon memory in the Arabian Sea. *Scientific Reports, 12*, 13037. https://doi.org/10.1038/s41598-022-17025-1

Kumar, P, S., & Prasad, T. G. (1996). Winter Cooling in Northern Arabian Sea. *Current Science, Special Section: JGOFS (INDIA), 71* (11).

Lathika, C. T. (2015). Microphytoplankton community structure along the North Eastern Arabian Sea during Winter monsoon. Ph.D Thesis. Cochin University of Science and Technology, p. 218. http://dyuthi.cusat.ac.in/purl/4985

Lewis, W. M. J. (1976). Surface/volume ratio: Implications for phytoplankton morphology. *Science, 192*, 885–887. https://doi.org/10.1126/science.192.4242.885

Lewis, M. R., Cullen, J. J., & Platt, T. (1983). Phytoplankton and thermal structure in the upper ocean: Consequences of nonuniformity in chlorophyll profile. Journal of Geophysical Research, 88(C4), 2565. https://doi.org/10.1029/JC088iC04p02565

Lotliker Aneesh, A., Baliarsingh, S. K., Trainer Vera, L., et al. (2018). Characterization of oceanic Noctiluca blooms not associated with hypoxia in the Northeastern Arabian Sea. *Harmful Algae, 74*, 46–57. https://doi.org/10.1016/j.hal.2018.03.008

Madhu, N. V., Jyothibabu, R., Maheswaran, P. A., et al. (2012). Enhanced chlorophyll a and primary production in the northern Arabian Sea during the spring intermonsoon due to green Noctiluca scintillans bloom. *Marine Biology Research, 8*, 182–188. https://doi.org/10.1080/17451000.2011.605143

Madhupratap, M., Prasanna Kumar, S., Bhattathiri, P. M. A., et al. (1996). Mechanism of the biological response to winter cooling in the north-eastern Arabian Sea. *Nature (London), 384*, 549–552. https://doi.org/10.1038/384549a0

Narvekar, J., D'Mello, J. R., Prasanna Kumar, S., et al. (2017). Winter-time variability of the estern Arabian Sea: A comparison between 2003 and 2013. *Geophysical Research Letters, 44*. https://doi.org/10.1002/2017GL072965

Nishihara, G., & Ackerman, J. D. (2009). Diffusive boundary layers do not limit the photosynthesis of the aquatic macrophyte, Vallisneria americana, at moderate flows and saturating light levels. *Limnology and Oceanography, 54*(6), 1874–1882. https://doi.org/10.4319/lo.2009.54.6.1874

Padmakumar, K. B., Smitha, B. R., Thomas, L. C., et al. (2010). Blooms of Trichodesmium erythraeum in the South Eastern Arabian Sea during the onset of 2009 summer monsoon. *Ocean Science Journal, 45*, 151–157. https://doi.org/10.1007/s12601-010-0013-4

Paerl, H. W., & Huisman, J. (2008). Blooms like it hot. *Science, 320*(5872), 57–58. https://doi.org/10.1126/science.1155398

Peters, F., Arin, L., Marrasé, C., et al. (2006). Effects of small-scale turbulence on the growth of two diatoms of different size in a phosphorus-limited medium. *Journal of Marine Systems, 61*(3−4), 134–148. https://doi.org/10.1016/j.jmarsys.2005.11.012

Prairie, J. C., Franks, P. J. S., Jaffe, J. S., et al. (2011). Physical and biological controls of vertical gradients in phytoplankton. *Limnology and Oceanography: Fluids and Environments, 1*, 75–90. https://doi.org/10.1215/21573698-1267403

Prairie, J. C., Sutherland, K. R., Nickols, K. J., et al. (2012). Biophysical interactions in the plankton: A cross-scale review. *Limnology and Oceanography: Fluids and Environments, 2*(1), 121–145. https://doi.org/10.1215/21573689-1964713

Padmakumar, K. B., Menon, N. R.and Sanjeevan, V. N. (2012). Is Occurrence of Harmful Algal Blooms in the Exclusive Economic Zone of India on the Rise? 2012. Volume 2012 Article ID 263946. https://doi.org/10.1155/2012/263946

Richardson, L. F., (1921). Some measurements of atmospheric turbulence. *Philosophical Transactions of the Royal Society of London. Series A, Containing Papers of a Mathematical or Physical Character, 221*, 1–28.

Richardson, A. J., & Poloczanska, E. S. (2008). Ocean science – Under-resourced, under threat. *Science, 320*, 1294–1295. https://doi.org/10.1126/science.1156129

Righetti, D., Vogt, M., Gruber, N., et al. (2019). Global patterns of phytoplankton diversity driven by temperature and environmental variability. *Science Advances, 5*, eaau6253. https://doi.org/10.1126/sciadv.aau6253

Righetti, D., Vogt, M., Zimmermann, N. E., Guiry, M. D., & Gruber, N. (2020). PhytoBase: A global synthesis of open-ocean phytoplankton occurrences. *Earth System Science Data, 12*, 907–933. https://doi.org/10.5194/essd-12-907-2020

Roxy, M. K., Ritika, K., Terray, P., et al. (2014). The curious case of Indian Ocean warming. *Journal of Climate, 27*(22), 8501–8509. https://doi.org/10.1175/JCLI-D-14-00471.1

Roxy, M. K., Modi, A., Murtugudde, R., et al. (2016). A reduction in marine primary productivity driven by rapid warming over the tropical Indian Ocean. *Geophysical Research Letters, 43*, 826–833. https://doi.org/10.1002/2015GL066979

Shah, M. H., Smitha, B. R., & Mohamed Hatha, A. A. (2019). Ponman: A method for exploratory analysis of ocean depths using Bio-Arg. *The Indian Ocean Bubble, International Indian Ocean Expedition, 2*(10), 10–12. Algorithm.

Shah, M, H., Smitha, B. R., Mohamed Hatha, A. A., et al. (2020). Subsurface chlorophyll maxima in the North Eastern Arabian Sea: Simulation on impact of warming. *Ecological Indicators, 110*. https://doi.org/10.1016/j.ecolind.2019.105858

Sanjeevan, V. N., Smitha, B. R., Asha Devi, C. R., et al. (2011). *Revalidation of potential yield from Indian EEZ. A trophodynamic approach. Report of the Working Group for Revalidating the Potential of Fishery Resources in the Indian EEZ* (pp. 50–60). Ministry of Agriculture.

Sarma, V. V. S. S., Patil, J. S., Shankar, D., et al. (2019). Shallow convective mixing promotes massive *Noctiluca scintillans* bloom in the northeastern Arabian Sea. *Marine Pollution Bulletin, 138*, 428–436. https://doi.org/10.1016/j.marpolbul.2018.11.054

Smitha, B. R., Sanjeevan, V. N., Padmakumar, K. B., et al. (2021). Role of mesoscale eddies in the sustenance of high biological productivity in North Eastern Arabian Sea during the winter-spring transition period. *Science of the Total Environment, 809*. https://doi.org/10.1016/j.scitotenv.2021.151173

Stokes, G. G. (1851). On the effect of the internal friction of fluids on the motion of pendulums. *Transaction of the Cambridge Philosophical Society, 9*, 8–106.

Stommel, H. (1949). Trajectories of small bodies sinking slowly through convective cells. *Journal of Marine Research, 8*, 24–29.

Sverdrup, H. U. (1953). On conditions for the vernal blooming of phytoplankton. *ICES Journal of Marine Science, 18*(3), 287–295.

Thorpe, S. (2005). *The Turbulent Ocean*. Cambridge University Press.

van den Dool, H. M. (2007). *Empirical methods in short-term climate prediction*. Oxford University Press.

Van Den Dool, H. M., Saha, S., & Johansson, Å. (2000). Empirical orthogonal teleconnections. *Journal of Climate, 13*(8), 1421–1435. https://doi.org/10.1175/1520-0442(2000)013<1421:EOT>2.0.CO;2

Vidya, P. J., & Kurian, S. (2018). Impact of 2015–2016 ENSO on the winter bloom and associated phytoplankton community shift in the northeastern Arabian Sea. *Journal of Marine Systems, 186*, 96–104. https://doi.org/10.1016/j.jmarsys.2018.06.005

Vijayan, A. K., Reddy, B. B., Sudheesh, V., et al. (2021). Phytoplankton community structure in a contrasting physico-chemical regime along the eastern Arabian Sea during the winter monsoon. *Journal of Marine Systems, 215*(103501), 15p. https://doi.org/10.1016/j.jmarsys.2020.103501

Wiggert, J. D., Jones, B. H., Dickey, T. D., et al. (2000). The northeast Monsoon's impact on mixing, phytoplankton biomass and nutrient cycling in the Arabian Sea. *Deep-Sea Research Part II, 47*, 1353–1385. https://doi.org/10.1016/S0967-0645(99)00147-2

Yamaguchi, R., Rodgers, K. B., Timmermann, A., et al. (2022). Trophic level decoupling drives future changes in phytoplankton bloom phenology. *Nature Climate Change, 12*, 469–476. https://doi.org/10.1038/s41558-022-01353-1

Chapter 7
Primary Production and Its Governing Factors in the Northern Indian Ocean

Himanshu Saxena and Arvind Singh

Abstract Were it not for the oceans, our Earth would have suffered much more warming because of industrial pollution. The oceans moderate our climate because of their large thermal inertia. They absorb about one-quarter of the atmospheric carbon dioxide (CO_2), a potent greenhouse gas, which has increased from 277 parts per million (ppm) to 407 ppm during the last ~250 years due to increasing human use of fossil fuels. Our ability to predict future climate is hampered because of limited data on CO_2 drawdown by the oceans, both by dissolution and photosynthesis by marine phytoplankton. In this chapter, we discuss historical records of primary productivity (assessed using ^{13}C, ^{14}C, ^{15}N, and satellite-derived chlorophyll *a* and net primary productivity data) in the northern Indian Ocean. The Arabian Sea and the Bay of Bengal, the twin basins of the northern Indian Ocean, are biologically nonidentical basins due to the differences in phenomenon and strength of the wind-induced physical processes, such as upwelling, convective mixing, and eddies. Historical records of measurements indicate that most of the primary productivity experiments in the Arabian Sea are spread out all over its region, while in the Bay of Bengal, they lie in the central Bay of Bengal and along the east coast of India. The Arabian Sea has approximately two and a half times the primary productivity of the Bay of Bengal. While the Arabian Sea displays vast spatial and temporal variability in biological productivity due to replenishment of nutrients in the summer and winter monsoon, the Bay of Bengal largely remains unaffected due to stratification and thus oligotrophic throughout the different seasons.

Keywords Primary production · New production · Monsoon · Chlorophyll · Indian Ocean

H. Saxena (✉)
Physical Research Laboratory, Department of Space, Ahmedabad, Gujarat, India
e-mail: himanshu@prl.res.in

A. Singh
Geosciences Division, Physical Research Laboratory (PRL), Ahmedabad, Gujarat, India

S. C. Tripathy, A. Singh (eds.), *Dynamics of Planktonic Primary Productivity in the Indian Ocean*, https://doi.org/10.1007/978-3-031-34467-1_7

1 Introduction

Our Earth would have suffered much more warming owing to industrial pollution if the ocean was not there to do us a favor. The global ocean regulates the Earth's climate because of its large thermal inertia. It has absorbed about 30% (~34 Pg C) of the excess atmospheric carbon dioxide (CO_2) gas (~110 Pg C) added by human activities between the period 1994 and 2007 (Gruber et al., 2019). Although CO_2 is an essential greenhouse gas, its excess is leading to an increase in the Earth's tropospheric temperature. The human usage of fossil fuels has increased atmospheric CO_2 concentration from ~277 parts per million (ppm) in 1750 to ~407 ppm in 2018 (Joos & Spahni, 2008; Dlugokencky & Tans, 2018), which our planet has not experienced for at least last 2 million years (Hönisch et al., 2009). Our ability to predict future climate is hampered because of limited data available on CO_2 draw-down by the ocean, by both physical phenomenon—through CO_2 dissolution (solubility pump)—and biological phenomenon—through photosynthesis by marine phytoplankton (biological pump).

The solubility pump is a physical process in which CO_2 dissolves in surface waters and sinks to the ocean's interior. The solubility of gasses is more in colder waters than warmer waters, and also, through thermohaline circulation, which is driven by the formation of deep water at high latitudes where seawater is usually colder and denser, CO_2 is pumped from the atmosphere into the ocean's interior. The global oceanic CO_2 sink is about 2 Pg C $year^{-1}$ from 1994 to 2007 (DeVries, 2022). The sinking flux of CO_2 is approximately balanced by the diffusive upward flux of CO_2 into warmer, tropical surface waters. Phytoplankton—the world's smallest primary producers—establish the marine food web. The energy they translate from the Sun into biochemical compounds via the process of photosynthesis gets passed to the food chain and thereby sustains life of all sizes. Phytoplankton convert dissolved inorganic forms of C (i.e., CO_2, HCO_3^- and CO_3^{2-}) to their organic matter using light as an energy source, a process known as primary production or C fixation. In the ocean, phytoplankton inhabits the well-lit upper layer of the ocean, called the euphotic zone. Model estimates of the global ocean primary production results in the net assimilation of 45–57 Pg C $year^{-1}$, which account for half of the net assimilation by photosynthetic organisms on the Earth's surface (Field et al., 1998). Much of the inorganic C that is fixed through photosynthesis is respired back to CO_2 in the surface ocean through microbial degradation/remineralization processes (Turner, 2015). This respired CO_2 is again fixed to organic matter or released to the atmosphere. But a fraction (5–25%) of the product of primary production sinks as dead organisms and particles (Rocha & Passow, 2007), where some of it is respired in the intermediate layers and can remain sequestered for years to centuries (DeVries et al., 2012) and some of it is exported to the deep ocean (Rocha & Passow, 2007). This vertical transfer of organic matter is more efficient at high latitudes than at low-latitude regions owing to the relative abundance of large-sized, rapidly sinking particles and the slower rate of remineralization at high latitudes (Dinauer et al., 2022). Through this process, called the biological C pump, CO_2 is sequestered in the

interior of the ocean for long periods of time (centennial to millennial timescales), during which it does not influence the climate (Siegenthaler & Sarmiento, 1993). Changes in the magnitude of the biological pump have been hypothesized for variations in atmospheric CO_2 levels during glacial and interglacial periods (Sigman & Boyle, 2000). Conclusively, the biological pump plays a crucial role in controlling atmospheric CO_2.

The element C forms the backbone of life. Next to C, the element nitrogen (N) plays a fundamental role in budding and nourishing life components (Schindler, 1975; Smith, 1984), since all the major cellular components, such as genetic materials (e.g., deoxyribonucleic acid (DNA) and ribonucleic acid (RNA)), proteins, and energy carrier molecules (e.g., adenosine triphosphate (ATP)), stemmed from these elements. The requirement of C and N for life is enormous. For every 100 atoms of C assimilated into the cell, around 2–20 atoms of N are required, depending on the organism (Sterner & Elser, 2002). C in the form of CO_2 is usually abundant enough not to limit primary production. In fact, its concentration in the atmosphere has relentlessly increased and almost doubled during the last 250 years (Friedlingstein et al., 2020). Instead, the scarcity of N often limits the growth and productivity of phytoplankton in most surface oceans (Falkowski et al., 1998; Moore et al., 2013), even on geological timescales (Falkowski, 1997). Though the most abundant form of N, i.e., dinitrogen gas (N_2), is over 400 μmol L^{-1} in seawater, it is inaccessible to most of the phytoplankton. Analogically, it is the same situation as rhymed by Samuel Taylor Coleridge in his poem The Rime of the Ancient Mariner for a thirsty mariner surrounded by seawater—*water, water everywhere but not a drop to drink*. Likewise, the majority of Phytoplankton are unable to assimilate N_2 but requires the bioaccessible or reactive forms of N (N_r), such as ammonium (NH_4^+), nitrate (NO_3^-), nitrite (NO_2^-), and dissolved organic N (DON). Notably, a specialized group of free-living and symbiotic prokaryotes, termed diazotroph, is capable of N_2 fixation—a process of breaking the highly stable triple bond in the N_2 molecule and converting (or fixing) it to NH_4^+. N_2 fixation fuels the cellular N-needs of phytoplankton by providing a natural fertilizer (Falkowski et al., 1998; Tyrrell, 1999) and can sustain up to 50% of primary production in some of the oceanic regions (Karl et al., 1997). The additional sources of N_r to the surface ocean include atmospheric deposition, riverine input, upwelling, and eddies. The primary production supported by these new N_r to the euphotic zone is widely known as new primary production (Fig. 7.1), which is equivalent to the losses through the sinking of organic matter out of the euphotic zone over annual timescales (Eppley & Peterson, 1979). Other than N_r, nutrients such as phosphate (PO_4^{3-}) and iron (Fe) are important in regulating primary production. Therefore, the availability of nutrients, especially the N_r macronutrient, drives the efficiency of the biological pump.

The northern Indian Ocean is one of the most biologically productive regions of the global ocean as a result of unique forcings by the Asian monsoon system. In this chapter, we have compiled primary production data in the northern Indian Ocean (above the equator) from a series of cruise expeditions conducted between the period of 1986 and 2021 during the winter and summer monsoon and inter-monsoon

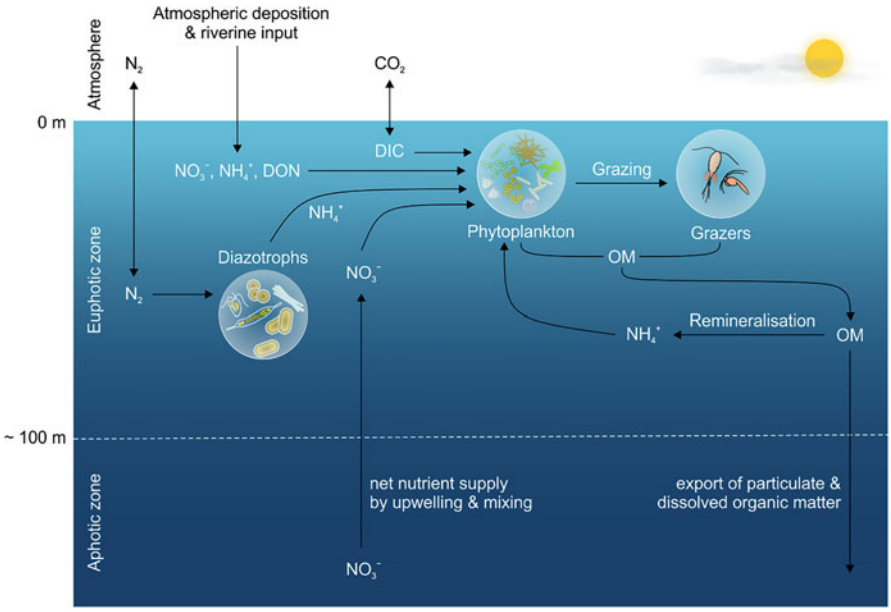

Fig. 7.1 Schematic showing primary production and its sources of nitrogenous nutrients. (DIC, dissolved inorganic carbon; OM, organic matter) (The schematic of diazotrophs is inspired and modified from Zehr and Capone (2020))

periods. This chapter presents and discusses historical ^{13}C-, ^{14}C-, and ^{15}N-based primary productivity data, where ^{15}N-based total N uptake rates are converted to primary productivity via Redfield equivalents, assuming photoautotrophs require 1 mol N to fix 6.6 mol C (Redfield, 1958). Satellite-derived chlorophyll *a* and net primary productivity data are additionally being used to assess phytoplankton dynamics.

2 Trends in Primary Productivity in the Northern Indian Ocean

The northern Indian Ocean consists of twin nonidentical basins, the Arabian Sea and the Bay of Bengal, located to the west and the east of the Indian subcontinent, respectively (Fig. 7.2). Both the basins are biogeochemically distinct owing to the influence of physical processes. During the monsoon, the winds over the northern Indian Ocean blow from the northeast between November and February (known as the northeast or winter monsoon) and reverse from the southwest direction (known as the southwest or summer monsoon) between June and October (Fig. 7.2). The transition period between these monsoons, which occur from March to May, is

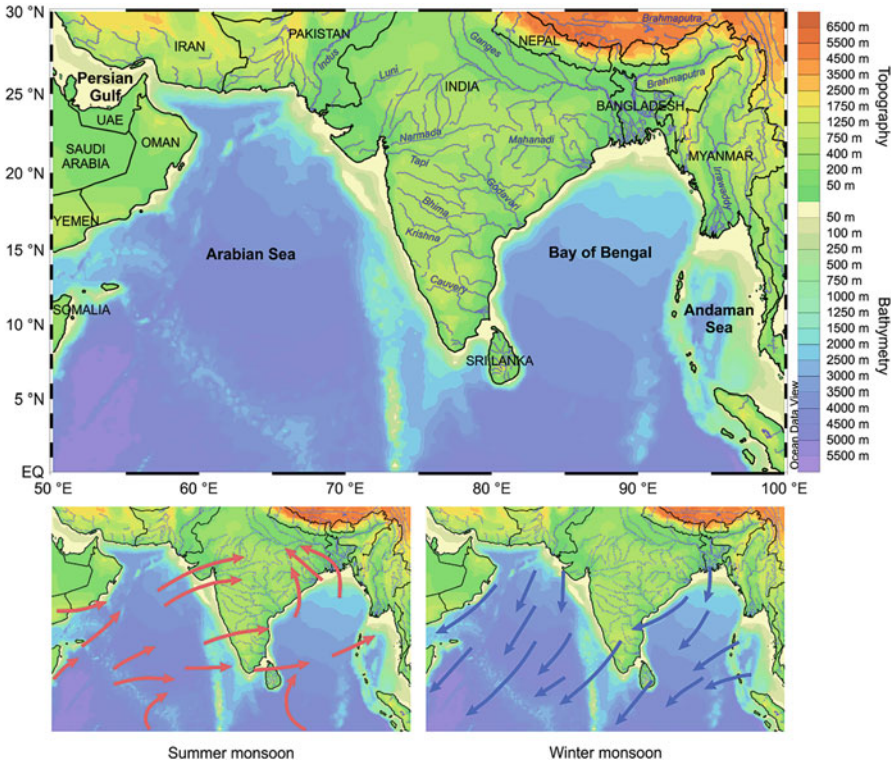

Fig. 7.2 Map showing the rivers draining into the twin basins of the northern Indian Ocean, the Arabian Sea and the Bay of Bengal. The bottom two panels indicate the reversal of wind direction during summer and winter monsoon

known as the inter-monsoon. The seasonal variability in biological activity alternates from being highly productive during monsoons to relatively less productive during the inter-monsoon period in the northern Indian Ocean (Figs. 7.3 and 7.4).

The Arabian Sea is one of the most productive regions of the global ocean. It displays vast seasonal variation in biological productivity due to the seasonal reversal of monsoonal winds. During the summer monsoon, in the Arabian Sea, which possesses one of the major western boundary upwelling regions (McCreary & Kundu, 1985), strong coastal upwelling as a result of alongshore southwesterly winds injects nutrient-rich subsurface waters to the nutrient-poor surface waters along Oman, Yemen, and Somalia (Findlater, 1969; Wyrtki, 1973), resulting in massive phytoplankton blooms (Fig. 7.3). The upwelled waters, along with phytoplankton blooms, extend far and wide from the western region, causing large-scale nutrient fertilization of the surface waters and, thus, inducing phytoplankton blooms (Fig. 7.3). The upwelling along the west coast of India begins at its southern tip during April–May, intensifies and propagates northward as the summer monsoon progresses, and ends during September–October (Shah et al., 2018). The coastal

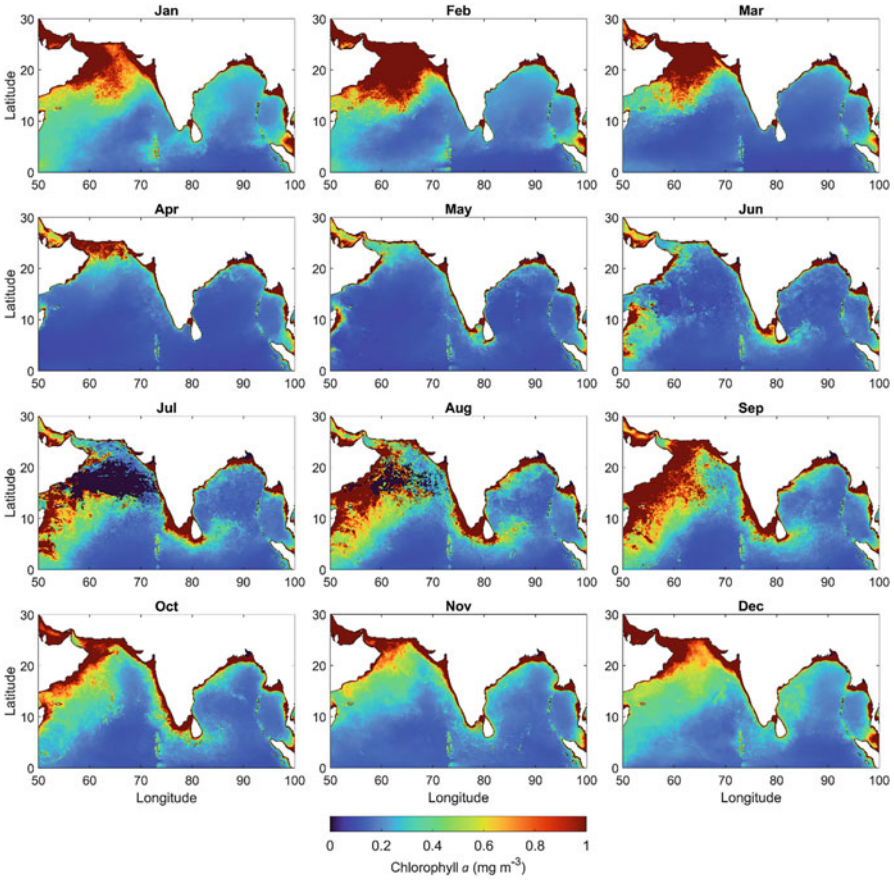

Fig. 7.3 Monthly mean climatology (2002–2021) of surface chlorophyll *a* concentration illustrating seasonal variability of phytoplankton biomass in the northern Indian Ocean (monthly climatological 4 km resolution data obtained from Aqua/MODIS for 2002–2021)

dynamics and the resulting influence on biological activity differ substantially between the eastern and western boundary system of the Arabian Sea and even between the northern and southern parts of the eastern Arabian Sea (Figs. 7.3 and 7.4). While the upwelling in the western Arabian Sea was a consequence of wind-driven upwelling system, the upwelling along the eastern Arabian Sea (particularly in the southeastern Arabian Sea) is a combined result of wind-driven eastern boundary upwelling system, alongshore wind stress, coastally trapped Kelvin waves, offshore propagating Rossby waves, the horizontal divergence of currents, and by the propagation of coastally trapped waves (Smitha et al., 2008; Shah et al., 2019). In the north of the eastern Arabian Sea, coastal upwelling is weak due to weak wind stress (Smitha et al., 2008). The biological response to these variations in upwelling intensity and extension during the summer monsoon also varies

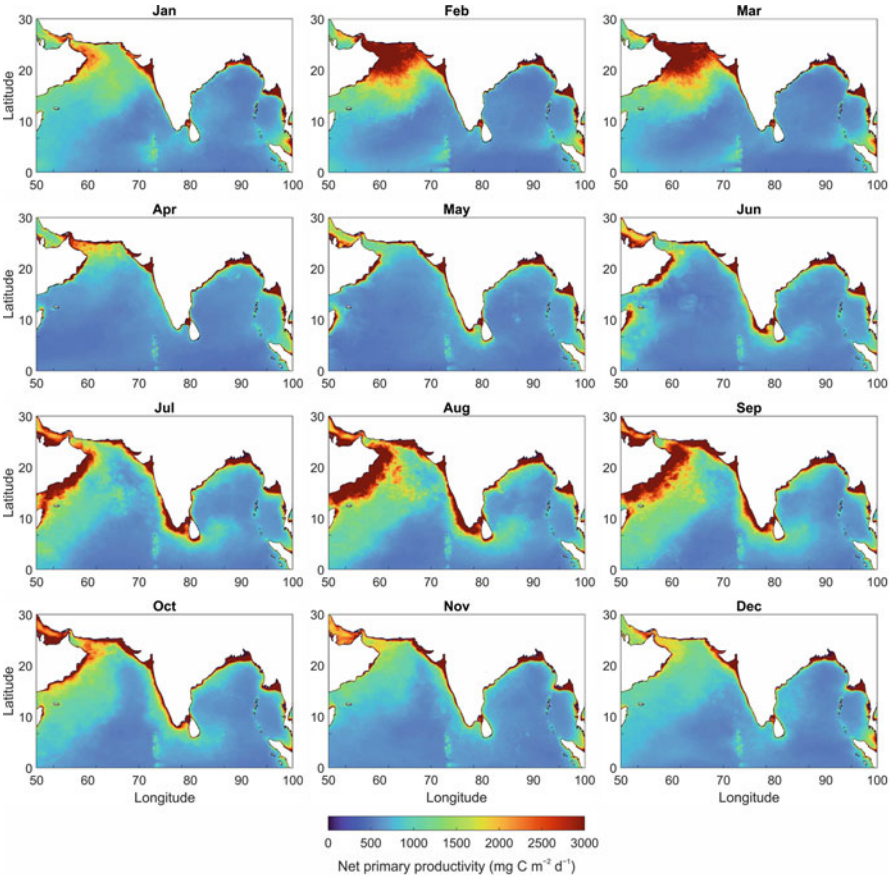

Fig. 7.4 Monthly mean climatology (2002–2021) of net primary productivity illustrating seasonal variability in biological productivity in the northern Indian Ocean, with more pronounced spatial and temporal variability in biological activity in the Arabian Sea than in the Bay of Bengal. The net primary productivity is based on MODIS chlorophyll, MODIS sea surface temperature, MODIS photosynthetically active radiation, and temperature-dependent photosynthetic efficiency using the "Eppley" version of the vertically generalized production model (*Eppley*-VGPM) (Behrenfeld & Falkowski, 1997)

significantly, ranging from largely extended phytoplankton blooms in the western Arabian Sea to moderately extended blooms in the eastern Arabian Sea (Fig. 7.3). During the winter monsoon, the Arabian Sea water densifies due to excess evaporation over precipitation and net heat loss due to the prevalence of cool and dry northeasterly winds (Madhupratap et al., 1996). This causes convective mixing (particularly north of 10°N), which replenishes the surface waters with nutrient-rich subsurface waters. This causes an increase in phytoplankton biomass and productivity in the central Arabian Sea during the winter monsoon that lasts till March (Figs. 7.3 and 7.4). Additionally, the open ocean upwelling, wind-driven

mixing, and lateral advection of nutrient-rich waters make the central Arabian Sea more productive (Bauer et al., 1991; Brock et al., 1991; McCreary et al., 1996; Prasanna Kumar et al., 2001). These highly biologically active summer and winter monsoon periods are intervened by the inter-monsoon season, during which due to calm, stratified, and oligotrophic conditions (Smith et al., 1998; Vimal Kumar et al., 2008), the Arabian Sea becomes relatively less productive than during the peak monsoons (Figs. 7.3 and 7.4). In contrast, the Bay of Bengal, which is similarly landlocked in the north and situated at the same latitude as the Arabian Sea, largely remains oligotrophic and less productive. The Bay of Bengal experiences lesser seasonal variability in biological productivity, with the variability of lesser intensity mostly confined to the west coast of the Bay of Bengal during the summer and winter monsoon (Figs. 7.3 and 7.4).

Most of the primary productivity measurement experiments in the Arabian Sea are spread out all over its region, while in the Bay of Bengal, they lie in the central Bay of Bengal and along the east coast of India. The water column-integrated primary productivity varied from 117 to 4126 mg C m^{-2} day^{-1} (average: 514 mg C m^{-2} day^{-1}) in the Bay of Bengal, while that in the Arabian Sea varied from 4 to 7659 mg C m^{-2} day^{-1} (average 1268 mg C m^{-2} day^{-1}) (Tables 7.1, 7.2, and 7.3), a 1.5-fold higher primary productivity in the Arabian Sea in comparison to the Bay of Bengal. The highest productivity was mostly observed off Oman and the northeastern Arabian Sea (Table 7.1). The primary productivity in the Arabian Sea is higher than in the Bay of Bengal during all the seasons, with a strong difference during the summer monsoon but a more or less similar difference during the winter monsoon and the inter-monsoon periods (Table 7.3).

3 Factors Governing Differences in Primary Productivity

After sunlight, the availability of nutrients controls primary productivity. Though fundamentally different physical mechanisms, upwelling during the summer monsoon and convective mixing during the winter monsoon are the primary cause for the replenishment of nutrients in surface layers of the northern Indian Ocean (particularly the Arabian Sea), resulting in large and long-lasting phytoplankton blooms. The monsoon-mediated seasonal changes in nutrient availability are responsible for the spatial and temporal variability of phytoplankton blooms. Both basins receive nutrients through river runoff, atmospheric deposition, and eddy. The Indian subcontinent possesses a rich river system, where most of the rivers discharge their waters into the Arabian Sea (0.3×10^{12} m^3 $year^{-1}$) or the Bay of Bengal (1.6×10^{12} m^3 $year^{-1}$) (Subramanian, 1993). Most of the nutrients associated with agricultural and nonagricultural activities in northern India drain into the river system. The major riverine input of N_r in both the basins (~81% in the case of the Arabian Sea and ~96% in the case of the Bay of Bengal) is consumed during its course within rivers and estuaries (Kumar et al., 2004; Singh & Ramesh, 2011). The coastal region of the Bay of Bengal receives ~0.38 Tg N $year^{-1}$ (1 Tg = 10^{12} g) and

Table 7.1 Historical record of water column-integrated primary productivity (mg C m^{-2} day^{-1}) in the Arabian Sea (AS). (NE, Northeast)

Region	Period	^{14}C based	^{13}C based	^{15}N based	Reference
Winter monsoon					
Somali basin	Jan–Feb 1993	200			Veldhuis et al. (1997)
Central AS	Nov–Dec 1994	560.3			Savidge and Gilpin (1999)
Off Oman to central AS	Nov–Dec 1994			657.4	Watts and Owens (1999)
Off Oman to central AS	Jan 1995			2041.8	McCarthy et al. (1999)
Off Oman to central AS	Jan 1995	1918			Barber et al. (2001)
Central and NE AS	Feb 1995	568			Madhupratap et al. (1996)
Central AS	Feb 1995	473.3			Gauns et al. (2005)
Coastal NE AS	Feb 1995	200			Gauns et al. (2005)
Off Oman to central AS	Nov 1995			860.1	McCarthy et al. (1999)
Off Oman to central AS	Dec 1995	1232			Barber et al. (2001)
Central AS	Feb 1997	955			Naqvi et al. (2002)
NE AS	Nov–Jan 2000	1114.2			Balachandran et al. (2008)
NE AS	Nov–Dec 2001	1114			Jyothibabu et al. (2004)
NE AS	Nov 2001	21.1			Matondkar et al. (2006)
NE AS	Jan 2003	3356.7			Matondkar et al. (2006)
NE AS	Jan 2003			689.0	Kumar et al. (2010)
NE AS	Feb 2003	219.1			Matondkar et al. (2006)
NE AS	Dec–Feb 2003, 2004	4.3			Parab and Matondkar (2012)
Central AS	Feb–Mar 2004			818.6	Prakash et al. (2008)
NE AS	Dec 2004	7343.3			Matondkar et al. (2006)
Central AS	Nov–Dec 2009		388.2		Shiozaki et al. (2014)
Coastal NE AS	Nov 2010		79.2		Singh et al. (2019)
NE AS	Feb 2013	4–76.4			Ahmed et al. (2017)
Coastal NE AS	Dec 2019		135.4		Saxena et al. (2022)
Central AS	Dec 2019		208.0		Saxena et al. (2022)
Inter-monsoon					
Central and NE AS	Apr–May 1994	210			Madhupratap et al. (1996)
Central AS	Apr–May 1994	196			Bhattathiri et al. (1996)
Coastal NE AS	Apr–May 1994	294			Bhattathiri et al. (1996)
Central AS	Apr–May 1994	166			Prasanna Kumar et al. (2001)
Central AS	Apr–May 1994	165.5			Gauns et al. (2005)
Coastal NE AS	Apr–May 1994	199			Gauns et al. (2005)
Central AS	Feb–Mar 1995	516			Bhattathiri et al. (1996)
Coastal NE AS	Feb–Mar 1995	504			Bhattathiri et al. (1996)

(continued)

Table 7.1 (continued)

Region	Period	^{14}C based	^{13}C based	^{15}N based	Reference
Off Oman to central AS	Mar 1995	1204			Barber et al. (2001)
Oman coast	Mar–Apr 1995			1444.2	Sambrotto (2001)
West central AS	Mar–Apr 1995			2376.0	Sambrotto (2001)
North central AS	Mar–Apr 1995			1372.8	Sambrotto (2001)
Central AS	May 1995	156–240			Capone et al. (1998)
NE AS	Apr 2000	2711.6			Matondkar et al. (2006)
NE AS	Mar 2003	436.6			Matondkar et al. (2006)
NE AS	Apr 2006			82.1	Gandhi et al. (2010)
Coastal NE AS	Apr–May 2009		552		Gandhi et al. (2011)
Coastal NE AS	May 2010		896.4		Kumar et al. (2017)
Central AS	Apr–May 2014		1860		Subha Anand et al. (2018)
Central AS	Apr–May 2014		1752.7		Subha Anand et al. (2018)
Central AS	May 2014		1483		Dalabehara and Sarma (2021)
Summer monsoon					
Central AS	Sep–Oct 1986	560.4			Owens et al. (1993)
Oman coast	Sep–Oct 1986	2668			Owens et al. (1993)
Central AS	Sep–Oct 1986			3231.4	Owens et al. (1993)
Oman coast	Sep–Oct 1986			7658.6	Owens et al. (1993)
Somali basin	Jul–Aug 1992	215.4			Veldhuis et al. (1997)
Central AS	Aug–Oct 1994	1167			Savidge and Gilpin (1999)
Off Oman to central AS	Aug–Oct 1994			482.4	Watts et al. (1999)
Central AS	Jul–Aug 1995	770			Bhattathiri et al. (1996)
Coastal NE AS	Jul–Aug 1995	953			Bhattathiri et al. (1996)
Off Oman to central AS	Jul–Aug 1995	1890			Barber et al. (2001)
Oman coast	Jul–Aug 1995			1728.0	Sambrotto (2001)
West central AS	Jul–Aug 1995			3528.0	Sambrotto (2001)
South central AS	Jul–Aug 1995			4455.0	Sambrotto (2001)
North central AS	Jul–Aug 1995			3405.6	Sambrotto (2001)
Central AS	Jul–Aug 1995	1306			Gauns et al. (2005)
Coastal NE AS	Jul–Aug 1995	953			Gauns et al. (2005)
Off Oman to central AS	Aug–Sep 1995	1540			Barber et al. (2001)
Central AS	Jul–Aug 1996	1041			Prasanna Kumar et al. (2001)
NE AS	Sep–Oct 2003	383.0			Habeebrehman et al. (2008)
NE AS	Aug–Sep 2005	420.0			Habeebrehman et al. (2008)
NE AS	Sep–Nov 2015		244.6		Sarma and Dalabehera (2019)
Off Oman to central AS	Sep–Nov 2015		1509.1		Sarma and Dalabehera (2019)

Table 7.2 Historical record of water column-integrated primary productivity (mg C m^{-2} day^{-1}) in the Bay of Bengal (Bay). (NW, Northwest)

Region	Period	^{14}C based	^{13}C based	^{15}N based	Reference
Winter monsoon					
Coastal NW Bay	Dec 1991	440			Gomes et al. (2000)
Central bay	Dec 1991	300			Gomes et al. (2000)
West bay	Nov 1999	699			Madhu et al. (2002)
Coastal NW bay	Dec 2001	252			Madhu et al. (2006)
Central bay	Dec 2001	231			Madhu et al. (2006)
NW bay	Nov–Dec 2001	133.2			Balachandran et al. (2008)
NW bay	Nov–Dec 2002	117			Jyothibabu et al. (2004)
NW and central bay	Nov–Dec 2007		310.8		Singh et al. (2015)
NW and central bay	Nov–Dec 2007			4126.32	Singh et al. (2015)
Inter-monsoon					
Coastal NW bay	Mar–Apr 1991	1050			Gomes et al. (2000)
Central bay	Mar–Apr 1991	160			Gomes et al. (2000)
Coastal NW bay	Apr 2001	308			Madhu et al. (2006)
Central bay	Apr 2001	303			Madhu et al. (2006)
Coastal NW bay	Apr–May 2003	365.8			Prasanna Kumar et al. (2007)
Central bay	Apr–May 2003	240.8			Prasanna Kumar et al. (2007)
Coastal NW and central bay	Apr–May 2003			575	Kumar et al. (2004)[a]
Central bay	May 2007			601.1	Gandhi et al. (2010)
Central bay	Apr–May 2010	199–367			Liu et al. (2011)
Central bay	Mar–Apr 2014		764.7		Subha Anand et al. (2017)
Central bay	Apr 2014		878		Dalabehara and Sarma (2021)
NW bay	Mar–Apr 2018		758		Sarma et al. (2019)
Summer monsoon					
Coastal NW bay	Jul–Aug 1989	550			Gomes et al. (2000)
Central bay	Jul–Aug 1989	300			Gomes et al. (2000)
West bay	Jul–Aug 1999	262			Madhu et al. (2002)
Central bay	Jul–Aug 2001	149			Gauns et al. (2005)
Coastal NW bay	Jul–Aug 2001	325			Gauns et al. (2005)
Coastal NW bay	Jul–Aug 2001	39.7–502.0			Madhupratap et al. (2003)

(continued)

Table 7.2 (continued)

Region	Period	^{14}C based	^{13}C based	^{15}N based	Reference
Central bay	Jul–Aug 2001	89.4–220.7			Madhupratap et al. (2003)
Coastal NW bay	Jul–Aug 2002	350			Madhu et al. (2006)
Central bay	Jul–Aug 2002	251			Madhu et al. (2006)
Coastal NW and central bay	Sep–Oct 2002			316	Kumar et al. (2004)[a]
Central bay	Sep–Oct 2002	344			Gauns et al. (2005)
Coastal NW bay	Sep–Oct 2002	264			Gauns et al. (2005)
Coastal NW bay	Sep–Oct 2002	281.2			Prasanna Kumar et al. (2007)
Central bay	Sep–Oct 2002	306.2			Prasanna Kumar et al. (2007)
Central bay	Jul–Aug 2018		649.5		Saxena et al. (2020)
NW and central bay	Jun 2019		190–390		Sarma et al. (2020)

[a]N-based primary productivity was given in their study, i.e., not calculated by us

Table 7.3 Seasonal average of water column-integrated primary productivity (mg C m^{-2} day^{-1})

Season	Arabian Sea	Bay of Bengal
Annual	1268	514
Winter monsoon	1048	734
Inter-monsoon	921	546
Summer monsoon	1823	334

that of the Arabian Sea ~0.06 Tg N $year^{-1}$ through rivers (Singh & Ramesh, 2011). The atmospheric dry-deposition flux of N_r to the Arabian Sea (1.7 Tg N $year^{-1}$) is relatively higher than in the Bay of Bengal (0.9 Tg N $year^{-1}$) (Singh et al., 2012; Sarma et al., 2022). In contrast, the atmospheric dry-deposition input (μmol m^{-2} day^{-1}) of PO_4^{3-} and Fe in the Arabian Sea (PO_4^{3-}, 0.3–0.9; Fe, 0.001–0.015) is substantially lower than in the Bay of Bengal (PO_4^{3-}, 0.5–4.8, and Fe, 0.02–1.2) (Srinivas & Sarin, 2013). Both the basins are among the high Fe regions of the global ocean, where the surface-dissolved Fe concentrations in the

Arabian Sea (0.68 ± 0.03 nmol L^{-1}, Chinni et al., 2019) and the Bay of Bengal (0.44 ± 0.11 nmol L^{-1}, Chinni et al., 2019) are similar to that of tropical north Atlantic Ocean (0.55 ± 0.29 nmol kg^{-1}, Fitzsimmons et al., 2013). Yet, the Arabian Sea is substantially more productive than the Bay of Bengal (Table 7.3), but the new production is comparable in both basins (Singh & Ramesh, 2015).

Differences in physical forcings explain why the Bay of Bengal is less productive than the Arabian Sea. The Bay of Bengal receives a large influx of freshwater from some of the world's largest rivers Ganges and Brahmaputra (Milliman & Meade, 1983), along with Irrawaddy, Mahanadi, Godavari, and Krishna (Fig. 7.2). The Ganges and Brahmaputra River system is the world's largest riverine sediment discharge system to the ocean (Milliman & Meade, 1983). The lithogenic flux (comprising of aeolian dust and riverine input) in the Bay of Bengal (8.6–28.0 g m^{-2}) is about five times of the Arabian Sea (2.6–5.4 g m^{-2}) (Ramaswamy, 1993). The Bay of Bengal receives heavy precipitation (2 m $year^{-1}$), where precipitation exceeds evaporation by 0.80 m $year^{-1}$, unlike the Arabian Sea, which loses ~1 m $year^{-1}$ freshwater through evaporation (Prasad, 1997). This intense freshwater input in the Bay of Bengal causes a considerable decrease in sea surface salinity over the whole basin during and after the monsoons that results in strong stratification of the surface layer (Prasanna Kumar et al., 2002; Vinayachandran et al., 2002). The stratification impedes the vertical transfer of nutrients, and thus, upwelling in the Bay of Bengal remains confined within ~40 km of the coastal region along the southwestern boundary during the summer monsoon (Shetye et al., 1991; Prasanna Kumar et al., 2002; Vinayachandran et al., 2021). Furthermore, the winds in the Bay of Bengal are weaker than in the Arabian Sea (Prasanna Kumar et al., 2009), resulting in weaker upwelling along India's east coast than along Somalia and Oman. Therefore, the oligotrophic surface layer caused by stratification, combined with light inhibition due to dense cloud cover and turbid water driven by sediment-laden river runoff that restricts the light penetrating depths, limits the biological productivity in the Bay of Bengal (Gomes et al., 2000; Prasanna Kumar et al., 2010). In contrast, the copious riverine discharge of nutrient-rich waters in the upwelling-dominated region of the southeastern Arabian Sea, which is prominent during summer monsoon due to heavy precipitation, facilitates the proliferation of phytoplankton biomass and primary production. A decrease in precipitation even when the upwelling was very strong has been proved as a cause for the decrease in phytoplankton biomass for the period 2003–2012 in the southeastern Arabian Sea (Shafeeque et al., 2019), revealing not only upwelling enhances biological productivity but also riverine input in coastal waters. Nevertheless, physical processes such as eddies and cyclones (which are frequent in the Bay of Bengal) are able to erode stratification and upwell nutrients, which result in the localized intense blooms of phytoplankton in the Bay of Bengal (Vinayachandran & Yamagata, 1998; Gomes et al., 2000; Vinayachandran & Mathew, 2003; Prasanna Kumar et al., 2004, 2007; Phillips et al., 2021). Evidently, eddies have been reported for enhanced new production and primary productivity in the Bay of Bengal (Prasanna Kumar et al., 2007; Singh et al., 2015). Conclusively, the Arabian Sea and the Bay of Bengal are biogeochemically different twin basins as a response of distinct seasonal changes in physicochemical parameters.

4 Future Research Directions

It has been long believed that the biological pump is driven by photosynthetic organisms only, which prevail within the sunlit layer of the ocean. However, in reality, C fixation may occur in the entire aphotic zone of the global ocean, predominantly by chemoautotrophs. Chemosynthetic organisms are also capable of assimilating CO_2 gas into their organic matter. The aphotic zone harbors a diverse and rich assemblage of light-independent chemoautotrophs. Within the aphotic zone, the oxygen minimum zones are a potential and preferential niche for chemosynthetic C fixation (Saxena et al., 2022), because it is energetically inexpensive to reduce CO_2 to organic C in anaerobic environments in comparison to aerobic environments (McCollom & Amend, 2005; Hügler & Sievert, 2011). The northern Indian Ocean possesses two of the most intense and largest oxygen minimum zones of the global ocean and is well recognized for the active presence of anammox bacteria, nitrifying organisms, and other chemoautotrophs (Jayakumar et al., 2009; Villanueva et al., 2014; Lüke et al., 2016). Evidently, it has already been revealed that chemoautotrophic C fixation could contribute up to 7.4 Pg C $year^{-1}$, amounting to ∼15% of the global ocean primary production (Saxena et al., 2022). Yet, the potential of aphotic zone C fixation in driving the biological pump remains unrecognized unlike the well-lit layer of the ocean. Additionally and perhaps most importantly, assessment and monitoring the microbial community, diversity, and potential of key microorganisms in CO_2 assimilation are critical for predicting future oceanic productivity.

5 Conclusions

Synthesis of the primary productivity database for the northern Indian Ocean for the period 1986–2021 evidences that primary productivity is more than a fold higher in the Arabian Sea than in the Bay of Bengal, where a huge difference in productivity occurs during the summer monsoon between these twin basins. While coastal upwelling and winter convection replenish the Arabian Sea with nutrients by bringing nutrient-rich subsurface waters to the surface layers, which results in intense and long-lasting phytoplankton blooms and higher primary productivity in the Arabian Sea, the seawater stratification caused by copious riverine discharge and the inability of weaker winds to break the stratification limits productivity in the Bay of Bengal. Nevertheless, the Bay of Bengal occasionally experiences productivity plumes due to eddy-mediated stratification breakage. Conclusively, the physical processes govern the primary productivity in the northern Indian Ocean.

References

Ahmed, A., Gauns, M., Kurian, S., Bardhan, P., Pratihary, A., Naik, H., Shenoy, D. M., & Naqvi, S. W. A. (2017). Nitrogen fixation rates in the eastern Arabian Sea. *Estuarine, Coastal and Shelf Science, 191*, 74–83. https://doi.org/10.1016/j.ecss.2017.04.005

Balachandran, K. K., Laluraj, C. M., Jyothibabu, R., et al. (2008). Hydrography and biogeochemistry of the north western Bay of Bengal and the north eastern Arabian Sea during winter monsoon. *Journal of Marine Systems, 73*, 76–86. https://doi.org/10.1016/j.jmarsys.2007.09.002

Barber, R. T., Marra, J., Bidigare, R. C., et al. (2001). Primary productivity and its regulation in the Arabian Sea during 1995. *Deep Sea Research Part II: Topical Studies in Oceanography, 48*, 1127–1172. https://doi.org/10.1016/S0967-0645(00)00134-X

Bauer, S., Hitchcock, G. L., & Olson, D. B. (1991). Influence of monsoonally-forced Ekman dynamics upon surface layer depth and plankton biomass distribution in the Arabian Sea. *Deep Sea Research Part A. Oceanographic Research Papers, 38*, 531–553. https://doi.org/10.1016/0198-0149(91)90062-K

Behrenfeld, M. J., & Falkowski, P. (1997). Photosynthetic rates derived from satellite-based chlorophyll concentration. *Limnology and Oceanography, 42*, 1–20. https://doi.org/10.4319/lo.1997.42.1.0001

Bhattathiri, P. M. A., Pant, A., Sawant, S. S., Gauns, M., Matondkar, S. G. P., & Mahanraju, R. (1996). Phytoplankton production and chlorophyll distribution in the eastern and central Arabian Sea in 1994–1995. *Current Science, 71*, 857–862.

Brock, J. C., McClain, C. R., Luther, M. E., & Hay, W. W. (1991). The phytoplankton bloom in the northwestern Arabian Sea during the southwest monsoon of 1979. *Journal of Geophysical Research: Oceans, 96*, 20623–20642. https://doi.org/10.1029/91JC01711

Capone, D. G., Subramaniam, A., Montoya, J. P., Voss, M., Humborg, C., Johansen, A. M., Siefert, R. L., & Carpenter, E. J. (1998). An extensive bloom of the N_2-fixing cyanobacterium *Trichodesmium erythraeum* in the central Arabian Sea. *Marine Ecology Progress Series, 172*, 281–292.

Chinni, V., Singh, S. K., Bhushan, R., Rengarajan, R., & Sarma, V. V. S. S. (2019). Spatial variability in dissolved iron concentrations in the marginal and open waters of the Indian Ocean. *Marine Chemistry, 208*, 11–28. https://doi.org/10.1016/j.marchem.2018.11.007

Dalabehara, H. B., & Sarma, V. V. S. S. (2021). Physical forcing controls spatial variability in primary production in the Indian Ocean. *Deep Sea Research Part II: Topical Studies in Oceanography, 183*, 104906. https://doi.org/10.1016/j.dsr2.2020.104906

DeVries, T. (2022). Atmospheric CO_2 and sea surface temperature variability cannot explain recent decadal variability of the ocean CO_2 sink. *Geophysical Research Letters, 49*, e2021GL096018. https://doi.org/10.1029/2021GL096018

DeVries, T., Primeau, F., & Deutsch, C. (2012). The sequestration efficiency of the biological pump. *Geophysical Research Letters, 39*. https://doi.org/10.1029/2012GL051963

Dinauer, A., Laufkötter, C., Doney, S. C., & Joos, F. (2022). What controls the large-scale efficiency of carbon transfer through the ocean's mesopelagic zone? Insights from a new, mechanistic model (MSPACMAM). *Global Biogeochemical Cycles, 36*, e2021GB007131. https://doi.org/10.1029/2021GB007131

Dlugokencky, E., & Tans, P. (2018). *Trends in atmospheric carbon dioxide*. National Oceanic & Atmospheric Administration, Earth System Research Laboratory (NOAA/ESRL).

Eppley, R. W., & Peterson, B. J. (1979). Particulate organic matter flux and planktonic new production in the deep ocean. *Nature, 282*, 677–680. https://doi.org/10.1038/282677a0

Falkowski, P. (1997). Evolution of the nitrogen cycle and its influence on the biological sequestration of CO_2 in the ocean. *Nature, 387*, 272–275. https://doi.org/10.1038/387272a0

Falkowski, P., Barber, R., & Smetacek, V. (1998). Biogeochemical controls and feedbacks on ocean primary production. *Science (New York, N.Y.), 281*, 200–207.

Field, C., Behrenfeld, M., Randerson, J., & Falkowski, P. (1998). Primary production of the biosphere: Integrating terrestrial and oceanic components. *Science, 281*, 237–240. https://doi.org/10.1126/science.281.5374.237

Findlater, J. (1969). A major low-level air current near the Indian Ocean during the northern summer. *Quarterly Journal of the Royal Meteorological Society, 95*, 362–380. https://doi.org/10.1002/qj.49709540409

Fitzsimmons, J. N., Zhang, R., & Boyle, E. A. (2013). Dissolved iron in the tropical North Atlantic Ocean. *Marine Chemistry, 154*, 87–99. https://doi.org/10.1016/j.marchem.2013.05.009

Friedlingstein, P., O'Sullivan, M., Jones, M. W., et al. (2020). Global carbon budget 2020. *Earth System Science Data, 12*, 3269–3340. https://doi.org/10.5194/essd-12-3269-2020

Gandhi, N., Singh, A., Ramesh, R., & Sreeman, S. (2010). Nitrogen sources for new production in the NE Indian Ocean. *Advances in Geosciences, 24*, 55–67. https://doi.org/10.1142/9789814355353_0004

Gandhi, N., Singh, A., Prakash, S., Ramesh, R., Raman, M., Sheshshayee, M. S., & Shetye, S. (2011). First direct measurements of N_2 fixation during a *Trichodesmium* bloom in the eastern Arabian Sea. *Global Biogeochemical Cycles, 25*. https://doi.org/10.1029/2010GB003970

Gauns, M., Madhupratap, M., Ramaiah, N., Jyothibabu, R., Fernandes, V., Paul, J. T., & Kumar, S. P. (2005). Comparative accounts of biological productivity characteristics and estimates of carbon fluxes in the Arabian Sea and the Bay of Bengal. *Deep Sea Research Part II: Topical Studies in Oceanography, 52*, 2003–2017. https://doi.org/10.1016/j.dsr2.2005.05.009

Gomes, H., Goes, J., & Saino, T. (2000). Influence of physical processes and freshwater discharge on the seasonality of phytoplankton regime in the Bay of Bengal. *Continental Shelf Research, 20*, 313–330. https://doi.org/10.1016/S0278-4343(99)00072-2

Gruber, N., Clement, D., Carter, B. R., et al. (2019). The oceanic sink for anthropogenic CO_2 from 1994 to 2007. *Science, 363*, 1193–1199. https://doi.org/10.1126/science.aau5153

Habeebrehman, H., Prabhakaran, M. P., Jacob, J., Sabu, P., Jayalakshmi, K. J., Achuthankutty, C. T., & Revichandran, C. (2008). Variability in biological responses influenced by upwelling events in the Eastern Arabian Sea. *Journal of Marine Systems, 74*, 545–560. https://doi.org/10.1016/j.jmarsys.2008.04.002

Hönisch, B., Hemming, N. G., Archer, D., Siddall, M., & McManus, J. F. (2009). Atmospheric carbon dioxide concentration across the mid-Pleistocene transition. *Science, 324*, 1551–1554. https://doi.org/10.1126/science.1171477

Hügler, M., & Sievert, S. (2011). Beyond the Calvin cycle: Autotrophic carbon fixation in the ocean. *Annual Review of Marine Science, 3*, 261–289. https://doi.org/10.1146/annurev-marine-120709-142712

Jayakumar, A., Naqvi, S. W. A., & Ward, B. B. (2009). Distribution and relative quantification of key genes involved in fixed nitrogen loss from the Arabian Sea oxygen minimum zone. In *Indian Ocean biogeochemical processes and ecological variability* (pp. 187–203). American Geophysical Union (AGU).

Joos, F., & Spahni, R. (2008). Rates of change in natural and anthropogenic radiative forcing over the past 20,000 years. *Proceedings of the National Academy of Sciences, 105*, 1425–1430. https://doi.org/10.1073/pnas.0707386105

Jyothibabu, R., Maheswaran, P. A., Madhu, N. V., et al. (2004). Differential response of winter cooling on biological production in the northeastern Arabian Sea and northwestern Bay of Bengal. *Current Science, 87*, 783–791.

Karl, D., Letelier, R., Tupas, L., Dore, J. E., Christian, J. R., & Hebel, D. V. (1997). The role of nitrogen fixation in biogeochemical cycling in the subtropical North Pacific Ocean. *Nature, 388*, 533–538. https://doi.org/10.1038/41474

Kumar, S., Ramesh, R., Sardesai, S., & Sheshshayee, M. S. (2004). High new production in the Bay of Bengal: Possible causes and implications. *Geophysical Research Letters, 31*. https://doi.org/10.1029/2004GL021005

Kumar, S., Ramesh, R., Dwivedi, R. M., Raman, M., Sheshshayee, M. S., & D'Souza, W. (2010). Nitrogen uptake in the northeastern Arabian Sea during winter cooling. *International Journal of Oceanography, 2010*, 819029. https://doi.org/10.1155/2010/819029. W. Smith [ed.].

Kumar, P. K., Singh, A., Ramesh, R., & Nallathambi, T. (2017). N_2 fixation in the Eastern Arabian Sea: Probable role of heterotrophic diazotrophs. *Frontiers in Marine Science, 4*, 80. https://doi.org/10.3389/fmars.2017.00080

Liu, H., Ke, Z., Song, X., Tan, Y., Huang, L., & Lin, Q. (2011). Primary production in the Bay of Bengal during spring intermonsoon period. *Acta Ecologica Sinica, 31*, 7007–7012.

Lüke, C., Speth, D., Kox, M., Villanueva, L., & Jetten, M. S. M. (2016). Metagenomic analysis of nitrogen and methane cycling in the Arabian Sea oxygen minimum zone. *PeerJ, 4*, e1924. https://doi.org/10.7717/peerj.1924

Madhu, N. V., Maheswaran, P. A., Jyothibabu, R., Sunil, V., Revichandran, C., Balasubramanian, T., Gopalakrishnan, T. C., & Nair, K. K. C. (2002). Enhanced biological production off Chennai triggered by October 1999 super cyclone (Orissa). *Indian Academy of Sciences, 82*, 1472–1479.

Madhu, N. V., Jyothibabu, R., Maheswaran, P. A., Gerson, V. J., Gopalakrishnan, T. C., & Nair, K. K. C. (2006). Lack of seasonality in phytoplankton standing stock (chlorophyll a) and production in the western Bay of Bengal. *Continental Shelf Research, 26*, 1868–1883. https://doi.org/10.1016/j.csr.2006.06.004

Madhupratap, M., PrasannaKumar, S., Bhattathiri, P. M. A., Dileepkumar, M., Raghukumar, S., Nair, K. K. C., & Nagappa, R. (1996). Mechanism of the biological response to winter cooling in the northeastern Arabian Sea. *Nature, 384*. https://doi.org/10.1038/384549a0

Madhupratap, M., Gauns, M., Ramaiah, N., Kumar, S. P., Muraleedharan, P. M., de Sousa, S. N., Sardessai, S., & Muraleedharan, U. (2003). Biogeochemistry of the Bay of Bengal: Physical, chemical and primary productivity characteristics of the central and western Bay of Bengal during summer monsoon 2001. *Deep Sea Research Part II: Topical Studies in Oceanography, 50*, 881–896. https://doi.org/10.1016/S0967-0645(02)00611-2

Matondkar, S. P., Dwivedi, R., Parab, S., Pednekar, S., Desa, E., Mascarenhas, A., Raman, M., & Singh, S. (2006). Satellite and ship studies of phytoplankton in the northeastern Arabian during 2000–2006 period. *Remote Sensing of the Marine Environment. SPIE*, *6406,* 368–377.

McCarthy, J. J., Garside, C., & Nevins, J. L. (1999). Nitrogen dynamics during the Arabian Sea northeast monsoon. *Deep Sea Research Part II: Topical Studies in Oceanography, 46*, 1623–1664. https://doi.org/10.1016/S0967-0645(99)00038-7

McCollom, T. M., & Amend, J. P. (2005). A thermodynamic assessment of energy requirements for biomass synthesis by chemolithoautotrophic micro-organisms in oxic and anoxic environments. *Geobiology, 3*, 135–144. https://doi.org/10.1111/j.1472-4669.2005.00045.x

McCreary, J. P., & Kundu, P. K. (1985). Western boundary circulation driven by an alongshore wind: With application to the Somali current system. *Journal of Marine Research, 43*, 493–516. https://doi.org/10.1357/002224085788440385

McCreary, J. P., Kohler, K. E., Hood, R. R., & Olson, D. B. (1996). A four-component ecosystem model of biological activity in the Arabian Sea. *Progress in Oceanography, 37*, 193–240. https://doi.org/10.1016/S0079-6611(96)00005-5

Milliman, J. D., & Meade, R. H. (1983). World-wide delivery of river sediment to the oceans. *The Journal of Geology, 91*, 1–21. https://doi.org/10.1086/628741

Moore, C. M., Mills, M. M., Arrigo, K. R., et al. (2013). Processes and patterns of oceanic nutrient limitation. *Nature Geoscience, 6*, 701.

Naqvi, S. W. A., Sarma, V. V. S. S., & Jayakumar, D. A. (2002). Carbon cycling in the northern Arabian Sea during the northeast monsoon: Significance of salps. *Marine Ecology Progress Series, 226*, 35–44. https://doi.org/10.3354/MEPS226035

Owens, N. J. P., Burkill, P. H., Mantoura, R. F. C., Woodward, E. M. S., Bellan, I. E., Aiken, J., Howland, R. J. M., & Llewellyn, C. A. (1993). Size-fractionated primary production and nitrogen assimilation in the northwestern Indian Ocean. *Deep Sea Research Part II: Topical Studies in Oceanography, 40*, 697–709. https://doi.org/10.1016/0967-0645(93)90053-P

Parab, S. G., & Matondkar, S. G. P. (2012). Primary productivity and nitrogen fixation by *Trichodesmium* spp. in the Arabian Sea. *Journal of Marine Systems, 105–108*, 82–95. https://doi.org/10.1016/j.jmarsys.2012.06.003

Phillips, H. E., Tandon, A., Furue, R., et al. (2021). Progress in understanding of Indian Ocean circulation, variability, air–sea exchange, and impacts on biogeochemistry. *Ocean Science, 17*, 1677–1751. https://doi.org/10.5194/os-17-1677-2021

Prakash, S., Ramesh, R., Sheshshayee, M. S., Dwivedi, R. M., & Raman, M. (2008). Quantification of new production during a winter *Noctiluca scintillans* bloom in the Arabian Sea. *Geophysical Research Letters, 35*. https://doi.org/10.1029/2008GL033819

Prasad, T. G. (1997). Annual and seasonal mean buoyancy fluxes for the tropical Indian Ocean. *Current Science, 73*, 667–674.

Prasanna Kumar, S., Madhupratap, M., Dileepkumar, M., Muraleedharan, P., Souza, S., Gauns, M., & Vvss, S. (2001). High biological productivity in the central Arabian Sea during the summer monsoon driven by Ekman pumping and lateral advection. *Current Science, 81*, 1633–1638.

Prasanna Kumar, S., Muraleedharan, P. M., Prasad, T. G., Gauns, M., Ramaiah, N., de Souza, S. N., Sardesai, S., & Madhupratap, M. (2002). Why is the Bay of Bengal less productive during summer monsoon compared to the Arabian Sea? *Geophysical Research Letters, 29*, 88-1–88-4. https://doi.org/10.1029/2002GL016013

Prasanna Kumar, S., Nuncio, M., Narvekar, J., et al. (2004). Are eddies nature's trigger to enhance biological productivity in the Bay of Bengal? *Geophysical Research Letters, 31*. https://doi.org/10.1029/2003GL019274

Prasanna Kumar, S., Nuncio, M., Ramaiah, N., Sardesai, S., Narvekar, J., Fernandes, V., & Paul, J. T. (2007). Eddy-mediated biological productivity in the Bay of Bengal during fall and spring intermonsoons. *Deep Sea Research Part I: Oceanographic Research Papers, 54*, 1619–1640. https://doi.org/10.1016/j.dsr.2007.06.002

Prasanna Kumar, S., Narvekar, J., Nuncio, M., Gauns, M., & Sardesai, S. (2009). What drives the biological productivity of the northern Indian Ocean? In *Indian Ocean biogeochemical processes and ecological variability* (pp. 33–56). American Geophysical Union (AGU).

Prasanna Kumar, S., Narvekar, J., Murukesh, N., et al. (2010). Is the biological productivity in the Bay of Bengal light limited? *Current Science, 98*, 1331.

Ramaswamy, V. (1993). *Lithogenic fluxes to the northern Indian Ocean – An overview* (pp. 97–111). University of Hamburg.

Redfield, A. (1958). The biological control of chemical factors in the environment. *Science Progress, 11*, 150–170.

Rocha, C. L. D. L., & Passow, U. (2007). Factors influencing the sinking of POC and the efficiency of the biological carbon pump. *Deep Sea Research Part II: Topical Studies in Oceanography, 54*, 639–658. https://doi.org/10.1016/j.dsr2.2007.01.004

Sambrotto, R. N. (2001). Nitrogen production in the northern Arabian Sea during the Spring Intermonsoon and Southwest Monsoon seasons. *Deep Sea Research Part II: Topical Studies in Oceanography, 48*, 1173–1198. https://doi.org/10.1016/S0967-0645(00)00135-1

Sarma, V. V. S. S., & Dalabehera, H. B. (2019). New and primary production in the western Indian Ocean during fall monsoon. *Marine Chemistry, 215*, 103687. https://doi.org/10.1016/j.marchem.2019.103687

Sarma, V. V. S. S., Rao, D. N., Rajula, G. R., Dalabehera, H. B., & Yadav, K. (2019). Organic nutrients support high primary production in the Bay of Bengal. *Geophysical Research Letters, 46*, 6706–6715. https://doi.org/10.1029/2019GL082262

Sarma, V. V. S. S., Chopra, M., Rao, D. N., Priya, M. M. R., Rajula, G. R., Lakshmi, D. S. R., & Rao, V. D. (2020). Role of eddies on controlling total and size-fractionated primary production in the Bay of Bengal. *Continental Shelf Research, 204*, 104186. https://doi.org/10.1016/j.csr.2020.104186

Sarma, V. V. S. S., Sridevi, B., Kumar, A., Bikkina, S., Kumari, V. R., Bikkina, P., Yadav, K., & Rao, V. D. (2022). Impact of atmospheric anthropogenic nitrogen on new production in the northern Indian Ocean: Constrained based on satellite aerosol optical depth and particulate nitrogen levels. *Environmental Science: Processes & Impacts*. https://doi.org/10.1039/D2EM00234E

Savidge, G., & Gilpin, L. (1999). Seasonal influences on size-fractionated chlorophyll a concentrations and primary production in the north-west Indian Ocean. *Deep Sea Research Part II: Topical Studies in Oceanography, 46*, 701–723. https://doi.org/10.1016/S0967-0645(98)00124-6

Saxena, H., Sahoo, D., Khan, M. A., Kumar, S., Sudheer, A. K., & Singh, A. (2020). Dinitrogen fixation rates in the Bay of Bengal during summer monsoon. *Environmental Research Communications, 2*, 051007. https://doi.org/10.1088/2515-7620/ab89fa

Saxena, H., Sahoo, D., Nazirahmed, S., Rai, D. K., Khan, M. A., Sharma, N., Kumar, S., & Singh, A. (2022). Contribution of carbon fixation toward carbon sink in the ocean twilight zone. *Geophysical Research Letters, 49*, e2022GL099044. https://doi.org/10.1029/2022GL099044

Schindler, D. W. (1975). Broecker, W. S. 1974. Chemical oceanography. Harcourt, Brace, Jovanovich, Inc., New York. 214 p. $7.95. *Limnology and Oceanography, 20*, 299–300. https://doi.org/10.4319/lo.1975.20.2.0299

Shafeeque, M., Shah, P., Platt, T., Sathyendranath, S., Menon, N. N., Balchand, A. N., & George, G. (2019). Effect of precipitation on chlorophyll-a in an upwelling dominated region along the west coast of India. *Journal of Coastal Research, 86*, 218–224. https://doi.org/10.2112/SI86-032.1

Shah, P., Sajeev, R., Santhosh, K., Thara, K., Shafeeque, M., John, K., & George, G. (2018). Observed signals of upwelling and downwelling along the west coast of India. *Indian Journal of Geo-Marine Sciences, 47*, 604–612.

Shah, P., Sajeev, R., Thara, K. J., George, G., Shafeeque, M., Akash, S., & Platt, T. (2019). A holistic approach to upwelling and downwelling along the south-west coast of India. *Marine Geodesy, 42*, 64–84. https://doi.org/10.1080/01490419.2018.1553805

Shetye, S. R., Shenoi, S. S. C., Gouveia, A. D., Michael, G. S., Sundar, D., & Nampoothiri, G. (1991). Wind-driven coastal upwelling along the western boundary of the Bay of Bengal during the southwest monsoon. *Continental Shelf Research, 11*, 1397–1408. https://doi.org/10.1016/0278-4343(91)90042-5

Shiozaki, T., Ijichi, M., Kodama, T., Takeda, S., & Furuya, K. (2014). Heterotrophic bacteria as major nitrogen fixers in the euphotic zone of the Indian Ocean. *Global Biogeochemical Cycles, 28*. https://doi.org/10.1002/2014GB004886

Siegenthaler, U., & Sarmiento, J. L. (1993). Atmospheric carbon dioxide and the ocean. *Nature, 365*, 119–125.

Sigman, D. M., & Boyle, E. A. (2000). Glacial/interglacial variations in atmospheric carbon dioxide. *Nature, 407*, 859–869. https://doi.org/10.1038/35038000

Singh, A., & Ramesh, R. (2011). Contribution of riverine dissolved inorganic nitrogen flux to new production in the coastal northern Indian Ocean: An assessment. *International Journal of Oceanography, 2011*. https://doi.org/10.1155/2011/983561

Singh, A., & Ramesh, R. (2015). Environmental controls on new and primary production in the northern Indian Ocean. *Progress in Oceanography, 131*, 138–145. https://doi.org/10.1016/j.pocean.2014.12.006

Singh, A., Gandhi, N., & Ramesh, R. (2012). Contribution of atmospheric nitrogen deposition to new production in the nitrogen limited photic zone of the northern Indian Ocean. *Journal of Geophysical Research: Oceans, 117*. https://doi.org/10.1029/2011JC007737

Singh, A., Gandhi, N., Ramesh, R., & Prakash, S. (2015). Role of cyclonic eddy in enhancing primary and new production in the Bay of Bengal. *Journal of Sea Research, 97*, 5–13. https://doi.org/10.1016/j.seares.2014.12.002

Singh, A., Gandhi, N., & Ramesh, R. (2019). Surplus supply of bioavailable nitrogen through N_2 fixation to primary producers in the eastern Arabian Sea during autumn. *Continental Shelf Research, 181*. https://doi.org/10.1016/j.csr.2019.05.012

Smith, S. V. (1984). Phosphorus versus nitrogen limitation in the marine environment. *Limnology and Oceanography, 29*, 1149–1160. https://doi.org/10.4319/lo.1984.29.6.1149

Smith, S. L., Codispoti, L., Morrison, J. M., & Barber, R. T. (1998). The 1994–1996 Arabian Sea expedition: An integrated, interdisciplinary investigation of the response of the northwestern Indian Ocean to monsoonal forcing. *Deep-Sea Research Part II: Topical Studies in Oceanography, 45*, 1905–1915. https://doi.org/10.1016/S0967-0645(98)00058-7

Smitha, B. R., Sanjeevan, V. N., Vimalkumar, K. G., & Revichandran, C. (2008). On the upwelling off the southern tip and along the west coast of India. *Journal of Coastal Research, 24*, 95–102. https://doi.org/10.2112/06-0779.1

Srinivas, B., & Sarin, M. M. (2013). Atmospheric deposition of N, P and Fe to the northern Indian Ocean: Implications to C- and N-fixation. *Science of the Total Environment, 456–457*, 104–114. https://doi.org/10.1016/j.scitotenv.2013.03.068

Sterner, R. W., & Elser, J. J. (2002). *The biology of elements from molecules to the biosphere*. Princeton University Press.

Subha Anand, S., Rengarajan, R., Sarma, V. V. S. S., Sudheer, A. K., Bhushan, R., & Singh, S. K. (2017). Spatial variability of upper ocean POC export in the Bay of Bengal and the Indian Ocean determined using particle-reactive ^{234}Th. *Journal of Geophysical Research: Oceans, 122*, 3753–3770. https://doi.org/10.1002/2016JC012639

Subha Anand, S., Rengarajan, R., & Sarma, V. V. S. S. (2018). ^{234}Th-based carbon export flux along the Indian GEOTRACES GI02 section in the Arabian Sea and the Indian Ocean. *Global Biogeochemical Cycles, 32*, 417–436. https://doi.org/10.1002/2017GB005847

Subramanian, V. (1993). Sediment load of Indian rivers. *Current Science, 64*, 928–930.

Turner, J. T. (2015). Zooplankton fecal pellets, marine snow, phytodetritus and the ocean's biological pump. *Progress in Oceanography, 130*, 205–248. https://doi.org/10.1016/j.pocean.2014.08.005

Tyrrell, T. (1999). The relative influence of nitrogen and phosphorus in oceanic primary productivity. *Nature, 400*, 529–531.

Veldhuis, M. J. W., Kraay, G. W., Bleijswijk, J. D. L. V., & Baars, M. A. (1997). Seasonal and spatial variability in phytoplankton biomass, productivity and growth in the northwestern Indian Ocean: The southwest and northeast monsoon, 1992–1993. *Deep Sea Research Part I: Oceanographic Research Papers, 44*, 425–449. https://doi.org/10.1016/S0967-0637(96)00116-1

Villanueva, L., Speth, D. R., van Alen, T., Hoischen, A., & Jetten, M. S. M. (2014). Shotgun metagenomic data reveals significant abundance but low diversity of "*Candidatus Scalindua*" marine anammox bacteria in the Arabian Sea oxygen minimum zone. *Frontiers in Microbiology, 5*, 31. https://doi.org/10.3389/fmicb.2014.00031

Vimal Kumar, K. G., Dinesh Kumar, P. K., Smitha, B. R., Habeeb Rahman, H., Josia, J., Muraleedharan, K. R., Sanjeevan, V. N., & Achuthankutty, C. T. (2008). Hydrographic characterization of southeast Arabian Sea during the wane of southwest monsoon and spring intermonsoon. *Environmental Monitoring and Assessment, 140*, 231–247. https://doi.org/10.1007/s10661-007-9863-3

Vinayachandran, P. N., & Mathew, S. (2003). Phytoplankton bloom in the Bay of Bengal during the northeast monsoon and its intensification by cyclones. *Geophysical Research Letters, 30*. https://doi.org/10.1029/2002GL016717

Vinayachandran, P. N., & Yamagata, T. (1998). Monsoon response of the sea around Sri Lanka: Generation of thermal domesand anticyclonic vortices. *Journal of Physical Oceanography, 28*, 1946–1960. https://doi.org/10.1175/1520-0485(1998)028<1946:MROTSA>2.0.CO;2

Vinayachandran, P. N., Murty, V. S. N., & Ramesh Babu, V. (2002). Observations of barrier layer formation in the Bay of Bengal during summer monsoon. *Journal of Geophysical Research: Oceans, 107*, SRF 19-1–SRF 19-9. https://doi.org/10.1029/2001JC000831

Vinayachandran, P. N., Masumoto, Y., Roberts, M. J., et al. (2021). Reviews and syntheses: Physical and biogeochemical processes associated with upwelling in the Indian Ocean. *Biogeosciences, 18*, 5967–6029. https://doi.org/10.5194/bg-18-5967-2021

Watts, L. J., & Owens, N. J. P. (1999). Nitrogen assimilation and the f-ratio in the northwestern Indian Ocean during an intermonsoon period. *Deep Sea Research Part II: Topical Studies in Oceanography, 46*, 725–743. https://doi.org/10.1016/S0967-0645(98)00125-8

Watts, L. J., Sathyendranath, S., Caverhill, C., Maass, H., Platt, T., & Owens, N. J. P. (1999). Modelling new production in the northwest Indian Ocean region. *Marine Ecology Progress Series, 183*, 1–12. https://doi.org/10.3354/meps183001

Wyrtki, K. (1973). Physical oceanography of the Indian Ocean. In B. Zeitzschel & S. A. Gerlach (Eds.), *The biology of the Indian Ocean* (pp. 18–36). Springer Berlin Heidelberg.

Zehr, J. P., & Capone, D. G. (2020). Changing perspectives in marine nitrogen fixation. *Science, 368*. https://doi.org/10.1126/science.aay9514

Chapter 8
Primary Productivity Dynamics in the Northern Indian Ocean: An Ecosystem Modeling Perspective

Kunal Chakraborty, Linta Rose, Trishneeta Bhattacharya, Jayashree Ghosh, Prasanna Kanti Ghoshal, and Anirban Akhand

Abstract Primary productivity is the basic building block of the marine food web, and phytoplankton is the main primary producer in the ocean. The assimilation and fixation of dissolved inorganic carbon and other inorganic nutrients into organic matter by phytoplankton are known as primary production. The oceanic primary production is essential in regulating the ocean carbon cycle. Phytoplankton consumes atmospheric carbon dioxide and subsequently transfers it to the sediment of the deeper ocean in a process called biological pump. Although the Indian Ocean covers less than 5% of the total area of world oceans, its unique geomorphological settings make it a globally significant ecosystem from the perspective of primary productivity and other related biogeochemical processes. The twin basins of the Indian Ocean, namely, the Arabian Sea (AS) and the Bay of Bengal (BoB), are known to have contrasting characteristics regulating primary productivity. The Bay of Bengal is generally considered to be less productive than the Arabian Sea. The drivers controlling the primary productivity in the northern Indian Ocean include

K. Chakraborty (✉) · P. K. Ghoshal
Indian National Centre for Ocean Information Services, Ministry of Earth Sciences, Hyderabad, India
e-mail: kunal.c@incois.gov.in

L. Rose
Indian National Centre for Ocean Information Services, Ministry of Earth Sciences, Hyderabad, India

School of Ocean and Earth Science and Technology, Cooperative Institute for Marine and Atmospheric Research, University of Hawai'i at Mānoa, Honolulu, USA

T. Bhattacharya · J. Ghosh
Indian National Centre for Ocean Information Services, Ministry of Earth Sciences, Hyderabad, India

School of Ocean Science and Technology, Kerala University of Fisheries and Ocean Studies, Kochi, India

A. Akhand
Department of Ocean Science, Hong Kong University of Science and Technology, Kowloon, Hong Kong, SAR, China

S. C. Tripathy, A. Singh (eds.), *Dynamics of Planktonic Primary Productivity in the Indian Ocean*, https://doi.org/10.1007/978-3-031-34467-1_8

physical factors like sea surface temperature, sea surface salinity, and upwelling, geochemical factors like nutrients (nitrates, phosphate, and silicate), and biological factors like phytoplankton species composition. There are several crucial physical processes associated with the phytoplankton bloom dynamics and primary production, like vertical and horizontal advection, dynamics of the mixed layer depth, and turbulent diffusion. Productivity measurements and physiological rate parameters of phytoplankton suggest that it is not strongly limited by nutrient supply or irradiance in this region. On the contrary, a reduction in primary productivity has been reported due to increased warming of the tropical Indian Ocean. A major shift in the phytoplankton species composition has also been reported in the Indian Ocean and its two basins. State-of-the-art observations on primary productivity suggest that irrespective of its regulating factors, the primary productivity of the Indian Ocean region can efficiently export carbon to the deeper ocean. The Indian Ocean is one of the most significant regions in the global ocean carbon cycle considering its long-term carbon sequestration process in a changing environment. The availability of observations in the northern Indian Ocean is limited, especially with respect to biogeochemical variables, hindering the explication of the dynamics of the marine system. The ecosystem models prove to be an incredible tool that can reinforce satellite and ship-borne observations to explicate the dynamics of the marine system. The modeling studies on primary productivity that has been carried out on the northern Indian Ocean have resulted in major advances in our understanding. Improved model resolution and better understanding and modeling of the fundamental processes involved in the interactions between the physical and biological states of the ocean can further improve our understanding of primary productivity. Keeping in mind the future climatic projections, the Indian Ocean along with the global ocean needs to be monitored closely on the aspects of physical-biogeochemical interactions.

Keywords Indian Ocean productivity · Satellite chlorophyll-a · Vertically generalized productivity model · Mixed layer depth

1 Introduction

The unique characteristics of the northern Indian Ocean (IO) basin have significant control on the primary productivity (PP) dynamics of the region. One of the prominent features of the region is the northern land boundary extending up to 26° N. The Indian subcontinent divides the northern IO into the Arabian Sea (AS) in the west and the Bay of Bengal (BoB) in the east. Another aspect is the annual monsoons characterized by seasonally reversing surface winds leading to intense rainfall over the northern part of the basin during summer. The circulation pattern driven by the seasonal reversal of monsoonal winds and the distributions of resultant upwelling phenomenon provides the physical forcing that controls the distinct biogeochemical (BGC) variability throughout the region. The convective mixing caused by cool and dry northeasterly winds results in winter blooms of phytoplankton over the northern

and central AS during the northeast monsoon (Wiggert et al., 2005; Lévy et al., 2007). However, during the southwest monsoon, a combination of Ekman pumping, horizontal advection, and coastal upwelling result in abundant phytoplankton blooms off the coast of Oman that can propagate more than 500 km away from the coast (Brock & McClain, 1992). Upwelling and entrainment around the Great Whirl give rise to the summer bloom off the coast of Somalia (Schott, 1983; Fischer et al., 1996). In the BoB, the evolution of the cyclonic gyre known as Sri Lanka Dome, recurring annually during the southwest monsoon, is initiated by Ekman pumping (Vinayachandran & Yamagata, 1998). The advection of nutrients upwelled south of the Indian Peninsula to the sea east of Sri Lanka by the intruding Southwest Monsoon Current leads to an enhanced PP at sea east of Sri Lanka (Vinayachandran et al., 2004). In the northern BoB, PP is regulated by the freshwater discharge and also by mesoscale activity (Prasanna Kumar et al., 2004).

In the early stages, the BGC modeling studies of the IO focused mostly on the AS but later it expanded to the whole basin. In an earlier study by Young and Kindle (1994), simple biological formulations were utilized to highlight the significance of horizontal advection of the upwelled water along the Omani coast during the southwest monsoon. This upwelled water supplies nutrients to the open ocean through currents. The first large-scale model for studying coupled ecosystem dynamics of the AS was configured by McCreary Jr et al. (1996) and Fasham et al. (1998). Although the BGC models used in these works were different, both were implemented at relatively a lower horizontal resolution and forced with climatological data. These models also utilized similar mixed layer parameterization, based on Kraus and Turner (1967). Owing to their comparable treatment of the physical processes, the results of the above studies are quite comparable. The studies revealed pronounced phytoplankton blooms during the monsoon season with distinct spatial changes in the bloom dynamics. The classification of the growth response of phytoplankton with respect to physical processes is indicated in these studies. These processes, together with the horizontal advection of nutrient-rich water from the coastal region into the central AS, are the physical drivers of the observed phytoplankton variability. However, the bloom dynamics in these models were simpler and, in several cases inaccurate, compared to observations. Both the models exhibited relatively lower phytoplankton biomass during the monsoon season. Another study by Ryabchenko et al. (1998) discussed similar outcomes based on modeling. But, these studies failed to represent the phytoplankton bloom in the northeastern AS and attributed the reason for this failure to excessive grazing.

Later studies on BGC modeling confirmed the significance of southwest monsoon period nutrient advection in nourishing offshore blooms observed in the ocean color data (Kawamiya, 2001). The first fully coupled biophysical modeling study of the IO was described in Wiggert et al. (2006). Their model successfully captured the basin-wide distinction in phytoplankton abundance during the southwest monsoon. Kone et al. (2009) coupled a 3D primitive equation model to an ecosystem model to understand the biological productivity through BGC cycles of carbon and other key nutrients like phosphate, nitrate, silicate, and iron. Their model reproduced the

seasonal phytoplankton bloom well in association with nutrient limitations and highlighted the role of physical processes like turbulent diffusion, horizontal and vertical advection, and mixed layer bloom dynamics.

The main focus of this chapter is delineating the phytoplankton variability in the IO. In the next few sections, a more comprehensive overview of different approaches to estimating PP, modeling PP, and the drivers of PP is elaborated.

2 Different Approaches of Measuring and Estimating Primary Productivity

Primary production is the process of fixation and assimilation of inorganic carbon and other inorganic nutrients into organic matter by autotrophic organisms. PP is defined as "the rate of change of biomass through photosynthesis per unit area (or volume) per unit time." There are two types of primary production: (a) gross productivity, which is "the amount of carbon fixed per unit space per unit time," and (b) net productivity, "the amount of carbon remaining after losses through respiration and decay." Phytoplankton is the main photosynthesizer in the ocean and the base of the marine food web. Hence, measuring in situ phytoplankton PP is a key domain for understanding the marine food web as well as carbon sequestration potential via a biological pump in the ocean. Different approaches have been taken to measure or estimate PP in the IO region. These methods include in situ methods, laboratory measurements, and estimation through remotely sensed data. Stable isotopic and radioisotopic methods are also notable among in situ and laboratory measurements, whereas different kinds of remote sensing and numerical modeling are also widely used for determining the variability of PP on large scales, spatially and temporally. These have been elucidated further in the next subsections.

2.1 Primary Production Measurement and Estimation Methods Implemented in the Indian Ocean Region

PP was mainly studied by in situ and laboratory measurements in the IO region. The concentration of chlorophyll-a (Chl-a) is the primary requirement for the estimation of PP since variations in primary production directly follow the changes in Chl-a concentration (Kulk et al., 2020). Different expedition cruises were conducted for measurement of PP. The concentration of Chl-a was also measured extensively in those cruises (Hanson et al., 2007). For example, during the AS expedition, which was part of the US Joint Global Ocean Flux Studies (US JGOFS), Chl-a and other pigments were measured using both fluorometer and high-performance liquid chromatography (Barber et al., 2001). Along with the measurement of Chl-a as an indispensable part of the PP measurement, the methods for the estimation and

enumeration of phytoplankton cell density using the Sedgewick rafter counting chamber were also used, as adopted by Chowdhury et al. (2021) for the IO region. A summary of the studies on PP in the IO, sequentially categorized in the order of time period of data measurement, is listed in Table 8.1.

Radioisotopes for estimating in situ PP were also used during the last few decades. In situ estimation of PP included ^{14}C incubation and clean techniques which was a part of in situ data collection during 1992–1997, as part of the Indian program of Joint Global Ocean Flux Study (JGOFS) (Kumar et al., 2000). A combination of in situ measurements and remotely sensed data as a part of the BoB process studies program was used to analyze the seasonal variability of the upper ocean and associated BGC response (Kumar et al., 2007). They used monthly mean Chl-a pigment concentration data derived from Sea-viewing Wide Field-of-view Sensor (SeaWiFS) global 9 km monthly imagery along with in situ Chl-a and radioactive estimation of PP. Marra and Barber (2005) estimated PP in the AS using surface irradiance (Weller et al., 1998) and in situ observations of Chl-a (Kinkade et al., 2001). They measured productivity from ^{14}C assimilation and used nitrogen-based productivity measurements and heterotrophic processes to explicate changes in the biomass of phytoplankton and productivity in the AS.

Madhupratap et al. (2003) also used the ^{14}C incubation and radioactivity measurement using a scintillation counter, to estimate PP values ranging from 40 to 502 mg C m^{-2} d^{-1} in the BoB, during the summer monsoon, which was lower than that reported in the AS values for the same season. Sarma et al. (2020) computed the total primary production in the BoB, using enriched sodium bicarbonate tracer, following Hama et al. (1983), which involved measurement of particulate organic carbon concentration and the atomic ratio of $^{13}C/^{12}C$. Sherin et al. (2018) measured the isotopic compositions of carbon and nitrogen in suspended matter using an elemental analyzer together with an isotopic ratio mass spectrometer and expressed the results relative to conventional standards for carbon and atmospheric nitrogen. They also grouped pigment biomarkers in the BoB, to understand the influence of different size classes in total phytoplankton biomass following Uitz et al. (2006).

Singh and Ramesh (2015) used the ^{15}N tracer technique, to estimate new (based on nitrate uptake) and regenerated production (based on urea and ammonium uptake) (Dugdale & Goering, 1967), in addition to estimation of primary production in the northern IO. This technique computes PP using uptake rates of nitrate, ammonium, and urea, integrated over the photic zone. This technique was first used in the AS during the JGOFS program (Watts et al., 1999; Watts & Owens, 1999). Wei et al. (2019) proposed a fast repetition rate fluorometry-based approach, with the introduction of a non-photochemical quenching proxy, to derive carbon uptake rates in the BoB.

Remotely sensed data based on Moderate Resolution Imaging Spectroradiometer (MODIS) utilizes two global models for the computation of net primary production, (a) vertically generalized productivity model (VGPM) (Behrenfeld & Falkowski, 1997) and (b) mixed layer depth production model (MLPM) (Howard, 1995). Two other available models are the Antoine and Morel absorption-based model (Antoine & Morel, 1996) and Platt and Sathyendranath numerical integration of spectral

Table 8.1 Studies on PP in the IO, sorted by time period of data measurement

Region of study	Range of estimated PP (mg C m^{-2} d^{-1})	Time period for measurement of data	Method adopted for calculation	Reference
AS	163–1782	1992–1997	In situ incubation protocol	Kumar et al. (2000)
AS	1800–3000	1994–1995	^{14}C assimilation	Marra and Barber (2005)
Central AS (65°E)	1032–1476	1995	^{14}C assimilation	Barber et al. (2001)
Northern IO	24–5976	1994–2007	^{15}N tracer technique	Singh and Ramesh (2015)
Coastal eastern IO (21–30°S, 111°E)	110–530	2000	Double integration of photosynthesis through depth and time using trapezoidal method	Hanson et al. (2007)
BoB	400–1400	2001	Light and dark bottle method	Rao et al. (2003)
BoB	40–502	2001	^{14}C incubation	Madhupratap et al. (2003)
BoB	115–513	2002–2003	In situ incubation protocol	Kumar et al. (2007)
BoB	845–1088	2013	Vertically generalized productivity model	Lakshmi et al. (2014)
Southwestern tropical IO	176–268	2014	Vertically generalized productivity model	Tripathy et al. (2020)
BoB		2016 (Nov–Dec)	Fast repetition Fluorometry	Wei et al. (2019)
BoB	60–160	2019 (June)	Enriched sodium bicarbonate tracer	Sarma et al. (2020)

model (Platt & Sathyendranath, 1988). Bhattacharya and Mishra (2005) detailed and compared these models while studying the PP in case 2 waters of northeastern BoB and found that the VGPM gives better results than the MLPM, in their study region.

A study reporting decline in oceanic PP (by 20%) due to increased warming over the tropical IO (Roxy et al., 2016) computed net primary production based on SeaWiFS chlorophyll data, advanced very high-resolution radiometer SST, and photosynthetically active radiation. The above mentioned remotely sensed data were employed by several researchers in a commonly used model (VGPM) for computing PP in the IO (Lakshmi et al., 2014; Tripathy et al., 2020; Roxy et al., 2016; Sarma & Dalabehera, 2019; Rao et al., 2003). The results are detailed in the coming sections.

2.2 *Types of Model Estimation of Primary Production*

PP models can be classified depending on euphotic depth (Zeu) and wavelength (400–700 nm). The available models are depth-integrated models, wavelength-integrated models, time-integrated models, and wavelength-resolved models. Behrenfeld and Falkowski (1997) proposed the Behrenfeld-Falkowski vertically generalized productivity model in which surface chlorophyll is connected to depth-integrated PP up to the euphotic zone. Along the east coast of India, Lakshmi et al. (2014) estimated the PP using the depth-integrated (euphotic depth) vertically generalized productivity model. The input variables used for the model are remotely sensed concentration of Chl-a, vertically diffused attenuation coefficient, radiation conducive to photosynthesis (PAR), and sea surface temperature. For the BoB region, they have estimated PP ranging between 845 and 1088 mg C m^{-2} d^{-1}, using Megard (1972) method, and 650–857 mg C m^{-2} d^{-1}, using the method proposed by Ryther and Yentsch (1957). The least PP was observed during April, after which it increased from May to July, reaching a maximum of 757 mg C m^{-2} d^{-1}. PP in the BoB decreases from July through November.

For the AS, seasonal estimates of net PP were computed using a biophysical coupled model for different cases of aerosol deposition, by Guieu et al. (2019). They used the Regional Ocean Modeling System model coupled with an ecosystem model, Pelagic Interaction Scheme for Carbon and Ecosystem Studies (PISCES) v2, to signify the role of aerosols in PP over the AS during 1998–2014. In their model simulations without aerosol depositions, the net PP reduced from 498 to 451 mg C m^{-2} d^{-1} from the northeast monsoon (DJFM) to spring inter-monsoon (AM), while a reduction from 554 to 521 mg C m^{-2} d^{-1} was seen during the southwest monsoon (JJAS) and the fall inter-monsoon (ON) seasons, respectively. The model simulations with all aerosol (P, N, Fe, Si) depositions, however, showed relatively higher values, 607 mg C m^{-2} d^{-1} in DJFM, 449 mg C m^{-2} d^{-1} in AM, 855 mg C m^{-2} d^{-1} in JJAS, and 641 mg C m^{-2} d^{-1} in ON.

Antoine and Morel (1996) introduced an absorption-based model which uses basic variables like irradiation, phytoplanktonic biomass, and the photo-adaptive state of the phytoplankton to determine PP. The use of Chl-a content and photo-

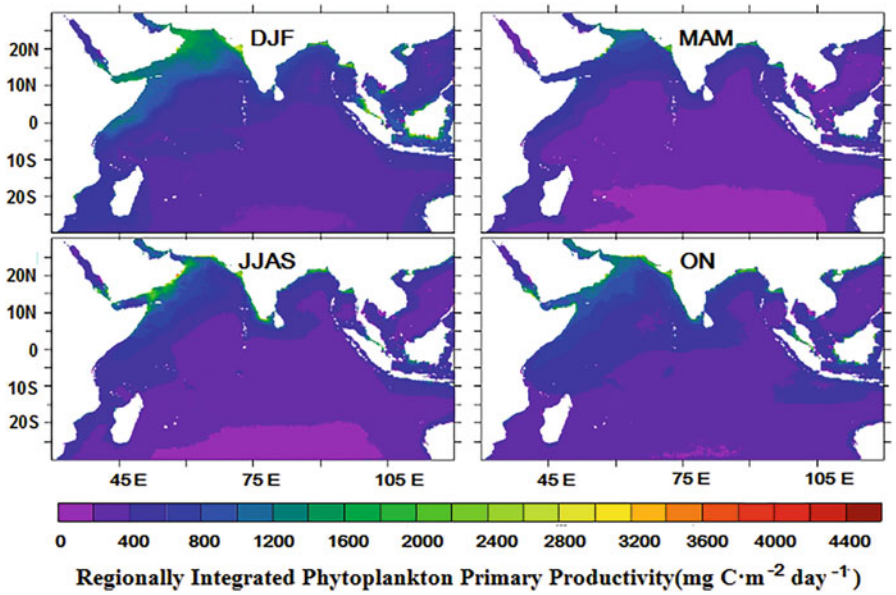

Fig. 8.1 Seasonal variations of PP in the IO. DJF refers to average over the months December, January, and February; MAM refers to March, April, and May; JJAS refers to June, July, August, and September; ON refers to October and November

adoption differentiate this absorption-based model from the depth-integrated model. This model uses column-integrated chlorophyll content, whereas previous models used surface Chl-a. The VGPM is based on an optimal temperature-dependent photo-adoption rate, but the absorption model is based on two basic aspects of the photosynthetic process: the Chl-a-dependent absorption by the photosynthetic apparatus in the phytoplankton and the amount of carbon fixed per mol quanta of absorbed radiation.

Figure 8.1 shows the seasonal variations of PP estimated for the IO region. The estimation is based on a combination of remotely sensed data of Chl-a and light and ship-based measurements on some model parameters. The figure depicts the zones with enhanced biological activity, which is prominent along the northern AS during winter and along the west coast of India during the southwest and northeast monsoons. The monthly data of PP, used to prepare this figure, are available from 1998 to 2010 at 9 km spatial resolution (https://www.oceancolour.org/thredds/catalog/TWAP-PProd/catalog.html; Sathyendranath et al., 2019). PP in this dataset was computed using a spectrally resolved vertical model of light transmission and primary production (Longhurst et al., 1995), using Chl-a, phytoplankton photo-physiology, and surface irradiance. The error estimates for all OC-CCI products are RMSD 0.31 to 0.34, bias −0.006 to −0.04, and R-square 0.73 to 0.81. We have also utilized the same dataset to determine seasonal estimates of PP for regional seas in the IO. These have been detailed in Table 8.2 as regionally integrated values, during 1998–2010.

Table 8.2 Regionally depth-integrated estimates of PP for the IO and its regional seas for different seasons

Seasons	Regionally integrated phytoplankton PP (mg C m^{-2} d^{-1})		
	IO (30°S–30°N, 30°E–120°E)	AS (6°S–30°N, 32°E–78°E)	BoB (5°N–25°N, 80°E–100°E)
DJF	411.0	603.6	488.8
MAM	406.6	588.3	561.7
JJAS	439.9	688.2	546.0
ON	444.4	651.5	526.9

DJF refers to average over the months December, January, and February; MAM refers to March, April, and May; JJAS refers to June, July, August, and September; ON refers to October and November. The error estimates for all OC-CCI products are RMSD (0.31 to 0.34), bias (−0.006 to −0.04), and R-square (0.73 to 0.81)

An extensive review of PP in the BoB is provided in Löscher (2021) with historical values during several seasons. They have also highlighted decreasing rates of primary production in the northern and equatorial IO with a decrease of 9.7% and 17.2% per decade, respectively. This was attributed to a decrease in diatom and chlorophyte primary production, a coinciding increase in cyanobacterial abundance, and decreasing nitrate and silicate concentration. Their estimations based on satellite measurements showed a decrease in PP by 15.4% and 24.8% per decade, for both the BoB and the AS, respectively. They argue that the BoB would be an oceanic basin with a weakened oxygen minimum zone and a marked decrease in primary production unless external inputs of iron, nitrate, and silicate increase.

2.3 Significance of Model Estimation of Primary Production

Changes in ocean primary production control the concentration of atmospheric CO_2 and thereby regulate the global climate. The rising interest in studying the influence of the ocean in controlling the global climate system has pivoted modeling studies for determining PP. Mathematical models of primary production range from simple functions of Chl-a concentration at surface to complex bio-optical models. Global projections make it essential that model inputs are limited to datasets that can be remotely measured or easily calculated from surface measurements. Ecosystem models implemented in climate research show high variations in simulating trends in primary production. In the latest IPCC report, it was shown that some models presented no significant trends in forecast values while others projected negative trends. Froelicher et al. (2015) were able to report uncertainties in marine PP trends estimated using these ecosystem models. Some of these uncertainties were attributed to incomplete knowledge of the fundamental processes. In this context, it is important to understand the fundamental processes better and to improve existing models for better prediction of future climate.

Ecosystem modeling is an essential scientific pathway to explicate the dynamics of the marine system and predict its evolution at both short and long timescales. There has been much work done in recent years to simulate BGC processes prevalent in the northern IO using different suites of models ranging from simple 1D process and location-specific models to highly complex basin-scale models such as Tracers of Phytoplankton with Allometric Zooplankton (TOPAZ) (McCreary Jr et al., 1996, 2001, 2013; Swathi et al., 2000; Hood et al., 2003; Vinayachandran et al., 2005; Sharada et al., 2008; Resplandy et al., 2012). Regional models were also developed to study the BGC processes regulating the productivity of the IO (Chakraborty et al., 2016, 2018, 2019a).

Several observational studies showed that nutrient enrichment in coastal and open ocean waters triggers the phytoplankton bloom in the AS (Madhupratap, 1999; Banse & English, 2000; Wiggert et al., 2005). Previous research on phytoplankton dynamics in this region envisaged dominance of phytoplankton bloom in the order of diatoms, cyanobacteria, and dinoflagellates (Sawant & Madhupratap, 1996). The ecosystem models prove to be an incredible tool that can reinforce and back satellite and ship-borne observations to provide assessment of PP at greater spatial and temporal timescales for the IO as well as the global ocean. The modeling studies can aid in revealing the role of PP in regulating the carbon cycle of the ocean and atmosphere. The identification of potential fishing zones of the ocean can also be easily done using the outputs of high-resolution coupled ocean-ecosystem models (Chakraborty et al., 2019b).

3 Modeling Primary Production

The carbon cycle in any oceanic ecosystem is known to depend strongly on physical dynamics in that ecosystem. One such example is the process of vertical mixing which can increase phytoplankton growth by bringing in nutrients from the subsurface into the surface, or contrariwise it can decrease photosynthetic activity by carrying down nutrients and phytoplankton away from the photic zone. Whether vertical mixing can enhance the quantity of the marine biota depends on a delicate balance of competing circumstances like nutrient and light availability. The relation between changes in the upper ocean ecosystem and the mixed layer depth (MLD) has been studied previously on the basis of numerical modeling (e.g., Venrick et al., 1987; Polovina et al., 1995). Processes within the MLD have a great influence in controlling PP, and thus, these processes should be replicated in numerical models for better estimation. Hence, most of the model studies that investigate the BGC dynamics include the coupling of carbon and nutrient cycles with these physical mechanisms. Bacastow and Maier-Reimer (1990) developed a coupled ocean-ecosystem general circulation model which reproduced the deep layer distribution of tracers and, for the first time, tried to resolve the global ocean carbon cycle from a modeling perspective. However, this simplified model could not resolve the oceanic

processes in MLD responsible for enhanced biological activities. In the subsequent modeling studies, several improvements were incorporated (e.g., Bacastow & Maier-Reimer, 1991; Najjar et al., 1992; Anderson & Sarmiento, 1995; Yamanaka & Tajika, 1996). In particular, Fasham (1993) and Sarmiento et al. (1993) integrated ecological components such as phytoplankton and zooplankton concentration into an ocean general circulation model as explicit state variables. This was done under the assumption that planktonic variables are controlled by vertical mixing and, therefore, the MLD and ecosystem relation could be improved.

The development of phytoplankton PP models and the fundamental synonymy between nearly all the models developed since the 1960s is well documented in Behrenfeld and Falkowski (1997). All of these models used a single formulation equating depth-integrated primary production (PP_{eu} [mg C m^{-2} d^{-1}]) to surface phytoplankton biomass (Chl_{sat} [mg Chl m^{-3}]), a photo-adaptive variable (P^{b}_{opt} [mg C (mg Chl)$^{-1}$ h^{-1}]), euphotic depth (Z_{eu} [m]), an irradiance-dependent function ($f(E_{par})$), and day length (DL [h d^{-1}]):

$$PP_{eu} = Chl_{sat} Z_{eu} f\left(E_{par}\right) DL\, P^{b}_{opt} \tag{8.1}$$

where PP_{eu} is the daily carbon fixation integrated from the surface to the euphotic depth (Z_{eu}) and P^{b}_{opt} is the maximum chlorophyll-specific carbon fixation rate observed in a water column measured under variable irradiance during incubations lasting several hours.

The modeling of PP for different sectors of the world ocean advanced in the last three to four decades. A summary of the sequential development of models used for the evaluation of PP has been depicted in Fig. 8.2. Earlier, there have been few attempts to model the nutrient and plankton dynamics of the upper ocean. The models then concentrated more on the interaction of phytoplankton and zooplankton only (Fasham et al., 1990). The models described in Pace et al. (1984), Fasham et al. (1985), Moloney et al. (1986), and Parsons and Kessler (1987) integrated all the components of the ecosystem and the flows of materials between these components. The background for a plankton dynamics model incorporating bacteria, protozoans, and dissolved organic matter was provided in Williams (1981). The results from such a model incorporating a large number of groups of organisms were described in Pace et al. (1984).

A realistic model based on plankton and nutrient dynamics of the mixed layer incorporating the major plankton groups (phytoplankton, zooplankton, and bacteria) and the major forms of nitrogen was first described in Fasham et al. (1990). This model tested several hypotheses prevalent for marine biota about food web structure and plankton dynamics and eased the configuration of sub-models which could resolve ocean circulation and biogeochemistry over basin-scale (Sarmiento et al., 1990). The main intention of the authors of Fasham et al. (1990) was to utilize this method to model the plankton dynamics and nutrient cycle over seasonal scales in the global ocean so that greater insight can be attained about the significance of

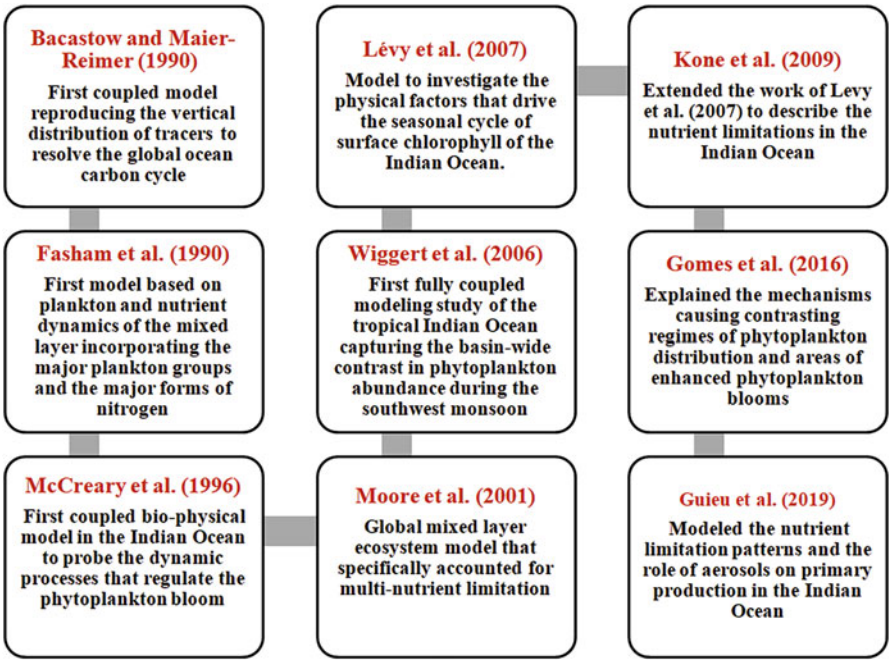

Fig. 8.2 Flowchart on development of models for estimation of PP

marine biology in controlling atmospheric CO_2. Consequentially, a global mixed layer ecosystem model that specifically accounted for multi-nutrient limitation (nitrogen, phosphorus, silica, and iron), diatoms, picoplankton, nitrogen fixation, and calcification was represented in Moore et al. (2001).

One of the earlier works on ecosystem modeling of the IO was chronicled in McCreary Jr et al. (1996), where the authors mainly focused on the biological productivity of the AS. The authors delineated the setup of a coupled biophysical model to probe the dynamic processes that regulate the biological processes and their annual cycles in the AS. They majorly concluded that three types of phytoplankton bloom develop in response to the physical processes like upwelling, entrainment, and detrainment in the AS. The phytoplankton bloom during the upwelling is strong and long-lasting, persisting as long as the upwelling occurs. Mostly, upwelling events in the AS take place during the southwest monsoon off Somalia, Oman, and India. This is in response to alongshore coastal winds. Near the mouth of the Gulf of Aden, bloom is mediated through Ekman pumping. The phytoplankton bloom due to detrainment is intense. However, these are brief events that develop due to abrupt thinning of the mixed layer. Contrary to the before-mentioned phytoplankton bloom events, the entrainment blooms are identified to be weak as entrainment leads to steady thickening of the mixed layer.

A coupled ocean-ecosystem model had been developed by Wiggert et al. (2006) to study the BGC processes over the IO basin. The ecosystem component used in this work has nine functional groups with size classified phytoplankton, zooplankton, and detritus and nutrients like nitrate, ammonium, and iron. The authors projected that the model successfully captured the basin-wide disparity in phytoplankton abundance during the southwest monsoon. The model also exhibited that the circulation pattern of the Somali Current and the spring Wyrtki jet has resulted in a remarkable influence on ecosystem dynamics of the southern BoB during the southwest monsoon.

Lévy et al. (2007) used the outputs from a physical ocean general circulation model to investigate the physical factors that drive the seasonal cycle of surface chlorophyll of the IO. They showed that OGCMs precisely assemble, both spatially and temporally, the bloom along with dynamical factors like the surface currents, the vertical velocity, and the mixed layer depth that most likely modulate productivity. They finally concluded that the physical control on the ocean biology may differ greatly over a short spatial extent. In an extended work of Lévy et al. (2007), Kone et al. (2009) analyzed the major physical and BGC coupled processes in the ocean using a biophysical model. The analysis presented by the authors manifested that at the onset of the bloom periods, the limiting nutrient over most of the IO was nitrogen. However, along the eastern part of the BoB, the ecosystem inclined toward silicate limitation. Their analysis also highlighted the fact that a variety of physical processes (mixed layer depth dynamics, advection in both the horizontal and the vertical, and turbulent diffusion) influence these bloom dynamics. Similar to this, Gomes et al. (2016) used a coupled biophysical ocean model to explain the dynamics behind increased phytoplankton blooms, observed first in remotely sensed datasets, in the oligotrophic regions of the BoB. The model results precisely indicated the contrasting regimes of phytoplankton distribution in the northern and the southern parts of the BoB and the effect of major IO dipole events on the ocean biology of the region.

In another modeling study of BGC processes of the BoB, Chakraborty et al. (2019a) used a coupled biophysical model configured using Regional Ocean Modeling System (ROMS) to study the upper ocean BGC variability of the BoB. The authors culminated that the physical state variables (temperature and salinity), the BGC state variables (nitrate, Chl-a, and dissolved oxygen), barrier layer thickness, and the mixed layer depth have strong seasonal and interannual variability. The variability is primarily controlled by the advection of water mass, local wind stress, and river runoff. Guieu et al. (2019) used ROMS coupled with BGC model, PISCES v2, to study the nutrient limitation patterns and the role of aerosols on primary production. Their study states that PP over the AS would be reduced by half if atmospheric iron inputs through dust deposition during the summer monsoon are absent. Most of the nitrogen fixation over the AS is supported by this atmospheric deposition of iron, while only a negligible fraction of the primary production is fixed by dinitrogen components.

4 Drivers of Primary Productivity in the Indian Ocean Region from Modeling Perspective

In the northern IO, low primary production in the BoB in comparison to the AS is a characteristic feature that is well-known (Prasanna Kumar et al., 2002). Previous studies concluded that low primary production in the BoB on annual timescales results from strong stratification due to freshwater river discharge and direct precipitation onto the sea, which impoverish nutrients in surface layers (Vinayachandran et al., 2002; Madhupratap et al., 2003; Gauns et al., 2005). On the other hand, higher PP in the AS is seen mainly due to the availability of high nutrient concentration in the upper ocean layers associated with wind-driven mixing during winter and coastal upwelling during summer (Schott, 1983; Anderson & Prell, 1992; Madhupratap et al., 1996; Gardner et al., 1999; Kumar et al., 2001; Wiggert et al., 2005). The seasonal and interannual changes in PP in the AS and the BoB result primarily due to changes in nutrient availability in the euphoric zone which in turn is controlled by salinity stratification in the water column. The extent of stratification is controlled by the balance between local evaporation-precipitation, freshwater discharge, wind-driven mixing, and upwelling-related dynamics (Lévy et al., 2001; Vinayachandran et al., 2002; Rao et al., 2011; van de Poll et al., 2013).

Over the global oceans, PP is controlled by many factors. The most commonly known drivers of PP are nutrients, irradiance, and temperature (Watts et al., 1999; Marra et al., 2007; Singh & Ramesh, 2015). A self-explanatory schematic showing the general drivers of PP is depicted in Fig. 8.3. In the IO, the monsoonal winds, circulation patterns, mesoscale features like eddies, and the ocean topography play an important role in controlling PP (Brock et al., 1993; Kumar et al., 2000; Barber et al., 2001; Wiggert et al., 2002; Kantha, 2004; Sherin et al., 2018; Sarma et al., 2020). Growth rates, grazing, and water column stability also cause PP variability in the water column (Sharada & Yajnik, 1997; Goericke, 2002; Wei et al., 2019). High nutrients in the photic zone and optimum irradiance within the spectrum of photosynthetically active radiation (wavelength between 400 and 700 nm) are known conditions that promote higher productivity. However, the interesting factor to note is the collective effect these variables have, along with temperature and salinity, in controlling PP, as seen in the case of the BoB and the AS. Even though productivity, in general, is limited in the BoB, new production is found to be high here, leading to a higher f-ratio (ratio of new production to primary production) in the BoB in contrast to the AS. This is due to sustained N_2 fixation by diazotrophs and eddy-mediated upwelling of nutrients from the below stratified waters (Singh & Ramesh, 2015; Da Silva et al., 2017; Zhou et al., 2020).

The variability of PP was found to be related more to phytoplankton absorption than to Chl-a variation, such that productivity normalized to absorption remains relatively invariant over the world oceans (Marra et al., 2007). Seasonal variability of PP in the IO is driven by the monsoonal circulation. Despite low iron and dust flux, high nutrient flux during the monsoons gives rise to high productivity than the inter-

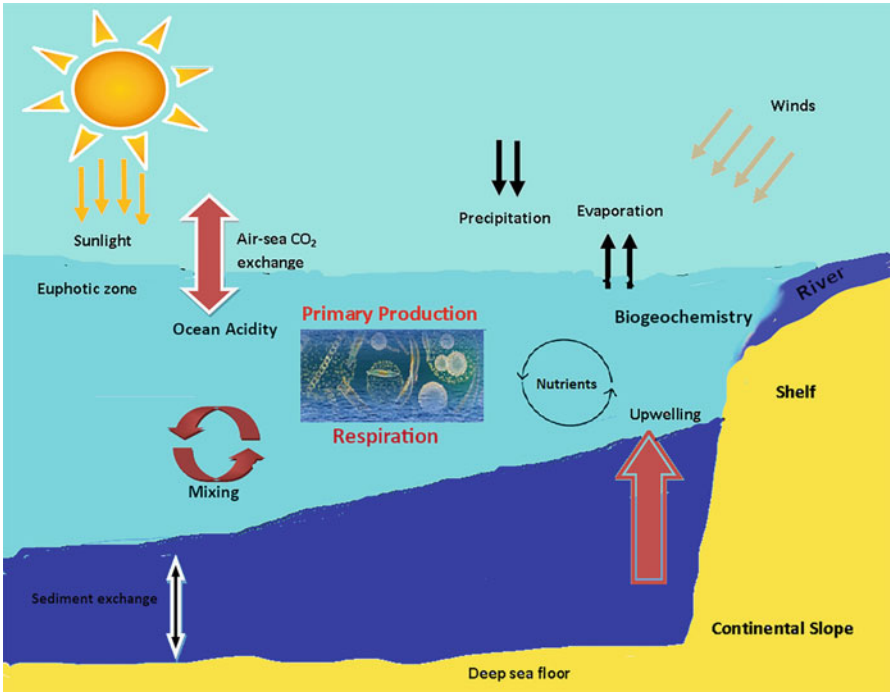

Fig. 8.3 Schematic showing the drivers of PP in the ocean

monsoons in the AS (Brock et al., 1993; Kumar et al., 2000; Barber et al., 2001). Dynamic processes governing circulation and mixing in the upper ocean computed from the mixed layer depth model in a given region were found to have a huge impact on modeling productivity patterns in that region (Kantha, 2004). However, it has been reported that depth-integrated models of PP estimation provide better results than mixed layer depth models of PP estimation (Bhattacharya & Mishra, 2005). Sharada and Yajnik (1997) have modeled the effects of grazing preference of prey densities on the behavior of the ecosystem and shown correlations of PP with Chl-a and sediment fluxes. Wei et al. (2019) applied fast repetition rate fluorometry to an independent field model-derived productivity in the BoB and found that in natural assemblages, light and depth responses to PP are less crucial than the numbers and structure of the phytoplankton communities in the region.

Studies on productivity in the Seychelles-Chagos Thermocline Ridge in the western IO showed how the interactions of currents with the ocean bathymetry may change nutrient supplies to the water column altering PP in the upper ocean. The Seychelles-Chagos Thermocline Ridge acts as a boundary along which the South Equatorial Current is diverted that prevents nutrient enrichment to the east making the western part a region for phytoplankton bloom all the year round

(Dilmahamod, 2014). In the IO region of the Southern Ocean where fronts give rise to characteristic vertical structures in the upper ocean, a pronounced variability in the hydrographic variables can be observed due to variations in the water column stability. The formation of deep chlorophyll maxima in these regions greatly affects rates of PP, making them regions of carbon sequestration and a sink for atmospheric CO_2 (Tripathy et al., 2015).

5 Summary and Future Directions

The availability of observations in the northern IO is limited, especially in terms of BGC variables. This hinders the understanding of the BGC response to physical forcing across the water column at various seasonal and interannual timescales. Improvements in coupled ocean-ecosystem models to accurately simulate the BGC dynamics of the northern IO can overcome these limitations. The modeling studies on PP that has been carried out on both the basins of the northern IO and their subsequent synthesis have resulted in major progress in our understanding. Further, we need to have a better understanding of the spatiotemporal variability of PP of the AS and the BoB. The biophysical models developed to date have successfully described the complex phytoplankton bloom dynamics of the IO along with the seasonal and interannual variability of PP. Improved model resolution and better understanding and modeling of the fundamental processes involved in the interactions between the physical and biological states of the ocean can further improve our understanding of PP.

To have a better understanding of the oceanic variability at wide spatiotemporal scales, it is necessary to have sustained observations spanning over a longer timescale. The lower temporal resolution of in situ and remotely sensed observations has resulted in a hindrance to the time series analysis. The spatial coverage of satellite data is often limited owing to cloud cover. Nevertheless, numerical models overcome these shortcomings, and thus model simulated outputs are extremely useful to assess the long-term changes of the physical and BGC state of the ocean. The influence of nutrients and light in regulating the distribution of phytoplankton, which in turn controls grazing and carbon fluxes to deeper ocean, can be assessed by using the model simulated outputs. There are few studies on the size-fractionated productivity in the BoB and AS region. In the future, size-based studies on phytoplankton can be further emphasized using outputs from high-resolution ecosystem models. The IO is the fastest heating ocean, besides the Arctic Ocean, and in recent investigations, it has been found that the marine productivity of the western IO has decreased by 20% over the past six decades (Roxy et al., 2016). Keeping in mind the future climatic projections, the IO along with the global ocean needs to be monitored closely on the aspects of physical-biological interactions.

References

Anderson, D. M., & Prell, W. L. (1992). The structure of the southwest monsoon winds over the Arabian Sea during the late Quaternary: Observations, simulations, and marine geologic evidence. *Journal of Geophysical Research: Oceans, 97*(C10), 15481–15487.

Anderson, L. A., & Sarmiento, J. L. (1995). Global ocean phosphate and oxygen simulations. *Global Biogeochemical Cycles, 9*(4), 621–636.

Antoine, D., & Morel, A. (1996). Oceanic primary production: 1. Adaptation of a spectral light-photosynthesis model in view of application to satellite chlorophyll observations. *Global Biogeochemical Cycles, 10*(1), 43–55.

Bacastow, R. B. R. B., & Maier-Reimer, E. (1990). Ocean-circulation model of the carbon cycle. *Climate Dynamics, 4*(2), 95–125.

Bacastow, R., & Maier-Reimer, E. (1991). Dissolved organic carbon in modeling oceanic new production. *Global Biogeochemical Cycles, 5*(1), 71–85.

Banse, K., & English, D. C. (2000). Geographical differences in seasonality of CZCS-derived phytoplankton pigment in the Arabian Sea for 1978–1986. *Deep Sea Research Part II: Topical Studies in Oceanography, 47*(7–8), 1623–1677.

Barber, R. T., Marra, J., Bidigare, R. C., Codispoti, L. A., Halpern, D., Johnson, Z., Latasa, M., Goericke, R., & Smith, S. L. (2001). Primary productivity and its regulation in the Arabian Sea during 1995. *Deep Sea Research Part II: Topical Studies in Oceanography, 48*(6–7), 1127–1172.

Behrenfeld, M. J., & Falkowski, P. G. (1997). Photosynthetic rates derived from satellite-based chlorophyll concentration. *Limnology and Oceanography, 42*(1), 1–20.

Bhattacharya, M., & Mishra, A. K. (2005). *Estimation of primary productivity in the case 2 waters of north-eastern Bay of Bengal* [Thesis]. Indian Institute of Remote Sensing, India.

Brock, J. C., & McClain, C. R. (1992). Interannual variability in phytoplankton blooms observed in the northwestern Arabian Sea during the southwest monsoon. *Journal of Geophysical Research: Oceans, 97*(C1), 733–750.

Brock, J., Sathyendranath, S., & Platt, T. (1993). Modelling the seasonality of subsurface light and primary production in the Arabian Sea. *Marine Ecology Progress Series, 101*, 209–221.

Chakraborty, K., Gupta, A., Lotliker, A. A., & Tilstone, G. (2016). Evaluation of model simulated and MODIS-aqua retrieved sea surface chlorophyll in the eastern Arabian Sea. *Estuarine, Coastal and Shelf Science, 181*, 61–69.

Chakraborty, K., Nimit, K., Akhand, A., Prakash, S., Paul, A., Ghosh, J., et al. (2018). Modeling the enhancement of sea surface chlorophyll concentration during the cyclonic events in the Arabian Sea. *Journal of Sea Research, 140*, 22–31.

Chakraborty, K., Lotliker, A. A., Majumder, S., Samanta, A., Baliarsingh, S. K., Ghosh, J., Madhuri, P. P., Saravanakumar, A., Sarma, N. S., Rao, B. S., & Shanmugam, P. (2019a). Assessment of model-simulated upper ocean biogeochemical dynamics of the Bay of Bengal. *Journal of Sea Research, 146*, 63–76.

Chakraborty, K., Maity, S., Lotliker, A. A., Samanta, A., Ghosh, J., Masuluri, N. K., et al. (2019b). Modelling of marine ecosystem in regional scale for short term prediction of satellite-aided operational fishery advisories. *Journal of Operational Oceanography, 12*(sup2), S157–S175.

Chowdhury, K. A., Jiang, W., Liu, G., Ahmed, M. K., & Akhter, S. (2021). Dominant physical-biogeochemical drivers for the seasonal variations in the surface chlorophyll-a and subsurface chlorophyll-a maximum in the Bay of Bengal. *Regional Studies in Marine Science, 48*, 102022.

Da Silva, R., Mazumdar, A., Mapder, T., Peketi, A., Joshi, R. K., Shaji, A., Mahalakshmi, P., Sawant, B., Naik, B. G., Carvalho, M. A., & Molletti, S. K. (2017). Salinity stratification controlled productivity variation over 300 ky in the Bay of Bengal. *Scientific Reports, 7*(1), 1–7.

Dilmahamod, A. F. (2014). *Links between the Seychelles-Chagos thermocline ridge and large scale climate models and primary productivity; and the annual cycle of chlorophyll-a* [Master's thesis, University of Cape Town].

Dugdale, R. C., & Goering, J. J. (1967). Uptake of new and regenerated forms of nitrogen in primary productivity 1. *Limnology and Oceanography, 12*(2), 196–206.

Fasham, M. J. (1993). Modelling the marine biota. In *The global carbon cycle* (pp. 457–504). Springer.

Fasham, M. J. R., Platt, T., Irwin, B., & Jones, K. (1985). Factors affecting the spatial pattern of the deep chlorophyll maximum in the region of the Azores front. *Progress in Oceanography, 14*, 129–165.

Fasham, M. J., Ducklow, H. W., & McKelvie, S. M. (1990). A nitrogen-based model of plankton dynamics in the oceanic mixed layer. *Journal of Marine Research, 48*(3), 591–639.

Fasham, M. J. R., Ryabchenko, V. A., & Gorchakov, V. A. (1998). Seasonal dynamics and biological productivity in the Arabian Sea euphotic zone as simulated by a three-dimensional ecosystem model. *Global Biogeochemical Cycles, 12*(3), 501–530.

Fischer, J., Schott, F., & Stramma, L. (1996). Currents and transports of the Great Whirl-Socotra Gyre system during the summer monsoon, August 1993. *Journal of Geophysical Research: Oceans, 101*(C2), 3573–3587.

Froelicher, T. L., Rodgers, K. B., Stock, C. A., & Cheung, W. W. (2015). Sources of uncertainties in 21st century projections of marine ecosystem drivers. In *AGU Fall Meeting abstracts* (p. B23J-06). American Geophysical Union.

Gardner, W. D., Gundersen, J. S., Richardson, M. J., & Walsh, I. D. (1999). The role of seasonal and diel changes in mixed-layer depth on carbon and chlorophyll distributions in the Arabian Sea. *Deep Sea Research Part II: Topical Studies in Oceanography, 46*(8–9), 1833–1858.

Gauns, M., Madhupratap, M., Ramaiah, N., Jyothibabu, R., Fernandes, V., Paul, J. T., & Kumar, S. P. (2005). Comparative accounts of biological productivity characteristics and estimates of carbon fluxes in the Arabian Sea and the Bay of Bengal. *Deep Sea Research Part II: Topical Studies in Oceanography, 52*(14–15), 2003–2017.

Goericke, R. (2002). Top-down control of phytoplankton biomass and community structure in the monsoonal Arabian Sea. *Limnology and Oceanography, 47*(5), 1307–1323.

Gomes, H. D. R., deRada, S., Goes, J. I., & Chai, F. (2016). Examining features of enhanced phytoplankton biomass in the Bay of Bengal using a coupled physical-biological model. *Journal of Geophysical Research: Oceans, 121*(7), 5112–5133.

Guieu, C., Al Azhar, M., Aumont, O., Mahowald, N., Lévy, M., Éthé, C., & Lachkar, Z. (2019). Major impact of dust deposition on the productivity of the Arabian Sea. *Geophysical Research Letters, 46*(12), 6736–6744.

Hama, T., Miyazaki, T., Ogawa, Y., Iwakuma, T., Takahashi, M., Otsuki, A., & Ichimura, S. (1983). Measurement of photosynthetic production of a marine phytoplankton population using a stable 13C isotope. *Marine Biology, 73*(1), 31–36.

Hanson, C. E., Pesant, S., Waite, A. M., & Pattiaratchi, C. B. (2007). Assessing the magnitude and significance of deep chlorophyll maxima of the coastal eastern Indian Ocean. *Deep Sea Research Part II: Topical Studies in Oceanography, 54*(8–10), 884–901.

Hood, R. R., Kohler, K. E., McCreary, J. P., & Smith, S. L. (2003). A four-dimensional validation of a coupled physical–biological model of the Arabian Sea. *Deep Sea Research Part II: Topical Studies in Oceanography, 50*(22–26), 2917–2945.

Howard, K. L. (1995). *Estimating global ocean primary production using satellite-derived data* [Doctoral dissertation, University of Rhode Island].

Kantha, L. H. (2004). A general ecosystem model for applications to primary productivity and carbon cycle studies in the global oceans. *Ocean Modelling, 6*(3–4), 285–334.

Kawamiya, M. (2001). Mechanism of offshore nutrient supply in the western Arabian Sea. *Journal of Marine Research, 59*(5), 675–696.

Kinkade, C. S., Marra, J., Dickey, T. D., & Weller, R. (2001). An annual cycle of phytoplankton biomass in the Arabian Sea, 1994–1995, as determined by moored optical sensors. *Deep Sea Research Part II: Topical Studies in Oceanography, 48*(6–7), 1285–1301.

Kone, V., Aumont, O., Levy, M., & Resplandy, L. (2009). Physical and biogeochemical controls of the phytoplankton seasonal cycle in the Indian Ocean: A modeling study. In J. D. Wiggert et al. (Eds.), *Indian Ocean biogeochemical processes and ecological variability* (pp. 147–166). AGU.

Kraus, E. B., & Turner, J. S. (1967). A one-dimensional model of the seasonal thermocline II. The general theory and its consequences. *Tellus, 19*(1), 98–106.

Kulk, G., Platt, T., Dingle, J., Jackson, T., Jönsson, B. F., Bouman, H. A., & Sathyendranath, S. (2020). Primary production, an index of climate change in the ocean: Satellite-based estimates over two decades. *Remote Sensing, 12*(5), 826.

Kumar, S. P., Madhupratap, M., Kumar, M. D., Gauns, M., Muraleedharan, P. M., Sarma, V. V. S. S., & De Souza, S. N. (2000). Physical control of primary productivity on a seasonal scale in central and eastern Arabian Sea. *Journal of Earth System Science, 109*(4), 433–441.

Kumar, S. P., Ramaiah, N., Gauns, M., Sarma, V. V. S. S., Muraleedharan, P. M., Raghukumar, S., Kumar, M. D., & Madhupratap, M. (2001). Physical forcing of biological productivity in the Northern Arabian Sea during the Northeast Monsoon. *Deep Sea Research Part II: Topical Studies in Oceanography, 48*(6–7), 1115–1126.

Kumar, S. P., Nuncio, M., Ramaiah, N., Sardesai, S., Narvekar, J., Fernandes, V., & Paul, J. T. (2007). Eddy-mediated biological productivity in the Bay of Bengal during fall and spring intermonsoons. *Deep Sea Research Part I: Oceanographic Research Papers, 54*(9), 1619–1640.

Lakshmi, E., Pratap, D., Nagamani, P. V., Rao, K. H., Latha, T. P., & Choudhury, S. B. (2014). Time series analysis of primary productivity along the east coast of India using Oceansat-2 ocean colour monitor (O cm). *The International Archives of Photogrammetry, Remote Sensing and Spatial Information Sciences, 40*(8), 1049.

Lévy, M., Klein, P., & Treguier, A. M. (2001). Impact of sub-mesoscale physics on production and subduction of phytoplankton in an oligotrophic regime. *Journal of Marine Research, 59*(4), 535–565.

Lévy, M., Shankar, D., André, J.-M., Shenoi, S. S. C., Durand, F., & de Boyer Montégut, C. (2007). Basin-wide seasonal evolution of the Indian Ocean's phytoplankton blooms. *Journal of Geophysical Research, 112*, C12014.

Longhurst, A., Sathyendranath, S., Platt, T., & Caverhill, C. (1995). An estimate of global primary production in the ocean from satellite radiometer data. *Journal of Plankton Research, 17*(6), 1245–1271.

Löscher, C. R. (2021). Reviews and syntheses: Trends in primary production in the Bay of Bengal–is it at a tipping point? *Biogeosciences, 18*(17), 4953–4963.

Madhupratap, M. (1999). Free-living copepods of the Arabian Sea: Distributions and research perspectives. *Indian Journal of Marine Sciences, 28*(2), 146–149.

Madhupratap, M., Kumar, S. P., Bhattathiri, P. M. A., Kumar, M. D., Raghukumar, S., Nair, K. K. C., & Ramaiah, N. (1996). Mechanism of the biological response to winter cooling in the northeastern Arabian Sea. *Nature, 384*(6609), 549.

Madhupratap, M., Gauns, M., Ramaiah, N., Kumar, S. P., Muraleedharan, P. M., De Sousa, S. N., Sardessai, S., & Muraleedharan, U. (2003). Biogeochemistry of the Bay of Bengal: Physical, chemical and primary productivity characteristics of the central and western Bay of Bengal during summer monsoon 2001. *Deep Sea Research Part II: Topical Studies in Oceanography, 50*(5), 881–896.

Marra, J., & Barber, R. T. (2005). Primary productivity in the Arabian Sea: A synthesis of JGOFS data. *Progress in Oceanography, 65*(2–4), 159–175.

Marra, J., Trees, C. C., & O'Reilly, J. E. (2007). Phytoplankton pigment absorption: A strong predictor of primary productivity in the surface ocean. *Deep Sea Research Part I: Oceanographic Research Papers, 54*(2), 155–163.

McCreary, J. P., Jr., Kohler, K. E., Hood, R. R., & Olson, D. B. (1996). A four-component ecosystem model of biological activity in the Arabian Sea. *Progress in Oceanography, 37*(3–4), 193–240.

McCreary, J. P., Jr., Kohler, K. E., Hood, R. R., Smith, S., Kindle, J., Fischer, A. S., & Weller, R. A. (2001). Influences of diurnal and intraseasonal forcing on mixed-layer and biological variability in the central Arabian Sea. *Journal of Geophysical Research: Oceans, 106*(C4), 7139–7155.

McCreary, J. P., Jr., Yu, Z., Hood, R. R., Vinaychandran, P. N., Furue, R., Ishida, A., & Richards, K. J. (2013). Dynamics of the Indian-Ocean oxygen minimum zones. *Progress in Oceanography, 112*, 15–37.

Megard, R. O. (1972). Phytoplankton, photosynthesis, and phosphorus in Lake Minnetonka, Minnesota. *Limnology and Oceanography, 17*(1), 68–87.

Moloney, C. L., Bergh, M. O., Field, J. G., & Newell, R. C. (1986). The effect of sedimentation and microbial nitrogen regeneration in a plankton community: A simulation investigation. *Journal of Plankton Research, 8*(3), 427–445.

Moore, J. K., Doney, S. C., Glover, D. M., & Fung, I. Y. (2001). Iron cycling and nutrient-limitation patterns in surface waters of the World Ocean. *Deep Sea Research Part II: Topical Studies in Oceanography, 49*(1–3), 463–507.

Najjar, R. G., Sarmiento, J. L., & Toggweiler, J. R. (1992). Downward transport and fate of organic matter in the ocean: Simulations with a general circulation model. *Global Biogeochemical Cycles, 6*(1), 45–76.

Pace, M. L., Glasser, J. E., & Pomeroy, L. R. (1984). A simulation analysis of continental shelf food webs. *Marine Biology, 82*(1), 47–63.

Parsons, T. R., & Kessler, T. A. (1987). An ecosystem model for the assessment of plankton production in relation to the survival of young fish. *Journal of Plankton Research, 9*(1), 125–137.

Platt, T., & Sathyendranath, S. (1988). Oceanic primary production: Estimation by remote sensing at local and regional scales. *Science, 241*(4873), 1613–1620.

Polovina, J. J., Mitchum, G. T., & Evans, G. T. (1995). Decadal and basin-scale variation in mixed layer depth and the impact on biological production in the Central and North Pacific, 1960-88. *Deep Sea Research Part I: Oceanographic Research Papers, 42*(10), 1701–1716.

Prasanna Kumar, S., Muraleedharan, P. M., Prasad, T. G., Gauns, M., Ramaiah, N., De Souza, S. N., Sardesai, S., & Madhupratap, M. (2002). Why is the Bay of Bengal less productive during summer monsoon compared to the Arabian Sea? *Geophysical Research Letters, 29*(24), 88–81.

Prasanna Kumar, S., Nuncio, M., Narvekar, J., Kumar, A., Sardesai, D. S., De Souza, S. N., Gauns, M., Ramaiah, N., & Madhupratap, M. (2004). Are eddies nature's trigger to enhance biological productivity in the Bay of Bengal? *Geophysical Research Letters, 31*(7), L07309.

Rao, K. H., Choudhury, S. B., Dash, S. K., Mishra, R. K., & Shaw, B. P. (2003). Evaluation of VGPM model for estimation of primary productivity along Paradeep coast, east coast of India. *International Archives of Photogrammetry Remote Sensing and Spatial Information Sciences, 34*(7/B), 1413–1417.

Rao, R. R., Girishkumar, M. S., Ravichandran, M., Gopalakrishna, V. V., & Thadathil, P. (2011). Do cold, low salinity waters pass through the Indo-Sri Lanka Channel during winter? *International Journal of Remote Sensing, 32*(22), 7383–7398.

Resplandy, L., Lévy, M., Bopp, L., Echevin, V., Pous, S. V. V. S. S., Sarma, V. V. S. S., & Kumar, D. (2012). Controlling factors of the oxygen balance in the Arabian Sea's OMZ. *Biogeosciences, 9*(12), 5095–5109.

Roxy, M. K., Modi, A., Murtugudde, R., Valsala, V., Panickal, S., Prasanna Kumar, S., Ravichandran, M., Vichi, M., & Lévy, M. (2016). A reduction in marine primary productivity driven by rapid warming over the tropical Indian Ocean. *Geophysical Research Letters, 43*, 826–833. https://doi.org/10.1002/2015GL066979

Ryabchenko, V. A., Gorchakov, V. A., & Fasham, M. J. R. (1998). Seasonal dynamics and biological productivity in the Arabian Sea euphotic zone as simulated by a three-dimensional ecosystem model. *Global Biogeochemical Cycles, 12*(3), 501–530.

Ryther, J. H., & Yentsch, C. S. (1957). The estimation of phytoplankton production in the ocean from chlorophyll and light data. *Limnology and Oceanography, 2*(3), 281–286.

Sarma, V. V. S. S., & Dalabehera, H. B. (2019). New and primary production in the western Indian Ocean during fall monsoon. *Marine Chemistry, 215*, 103687.

Sarma, V. V. S. S., Chopra, M., Rao, D. N., Priya, M. M. R., Rajula, G. R., Lakshmi, D. S. R., & Rao, V. D. (2020). Role of eddies on controlling total and size-fractionated primary production in the Bay of Bengal. *Continental Shelf Research, 204*, 104186.

Sarmiento, J. L., Fasham, M. J. R., Slater, R., Toggweiler, J. R., & Ducklow, H. W. (1990). The role of biology in the chemistry of CO2 on the ocean. In M. Farrell (Ed.), *Chemistry of the greenhouse effect*. Lewis.

Sarmiento, J. L., Slater, R. D., Fasham, M. J. R., Ducklow, H. W., Toggweiler, J. R., & Evans, G. T. (1993). A seasonal three-dimensional ecosystem model of nitrogen cycling in the North Atlantic euphotic zone. *Global Biogeochemical Cycles, 7*(2), 417–450.

Sathyendranath, S., Brewin, R. J., Brockmann, C., Brotas, V., Calton, B., Chuprin, A., Cipollini, P., Couto, A. B., Dingle, J., Doerffer, R., Donlon, C., Dowell, M., Farman, A., Grant, M., Groom, S., Horseman, A., Jackson, T., Krasemann, H., Lavender, S., Martinez-Vicente, V., Mazeran, C., Mélin, F., Moore, T. S., Müller, D., Regner, P., Roy, S., Steele, C. J., Steinmetz, F., Swinton, J., Taberner, M., Thompson, A., Valente, A., Zühlke, M., Brando, V. E., Feng, H., Feldman, G., Franz, B. A., Frouin, R., Gould, R. W., Jr., Hooker, S. B., Kahru, M., Kratzer, S., Mitchell, B. G., Muller-Karger, F., Sosik, H. M., Voss, K. J., Werdell, J., & Platt, T. (2019). An ocean-colour time series for use in climate studies: The experience of the ocean-colour climate change initiative (OC-CCI). *Sensors, 19*(19), 4285.

Sawant, S. S., & Madhupratap, M. (1996). *Seasonality and composition of phytoplankton in the Arabian Sea*. Current Science Association.

Schott, F. (1983). Monsoon response of the Somali Current and associated upwelling. *Progress in Oceanography, 12*(3), 357–381.

Sharada, M. K., & Yajnik, K. S. (1997). Seasonal variation of chlorophyll and primary productivity in central Arabian Sea: A macrocalibrated upper ocean ecosystem model. *Proceedings of the Indian Academy of Sciences, Earth and Planetary Sciences, 106*(1), 33–42.

Sharada, M. K., Swathi, P. S., Yajnik, K. S., & Kalyani, C. D. (2008). Role of biology in the air–sea carbon flux in the Bay of Bengal and Arabian Sea. *Journal of Earth System Science, 117*(4), 429–447.

Sherin, C. K., Sarma, V. V. S. S., Rao, G. D., Viswanadham, R., Omand, M. M., & Murty, V. S. N. (2018). New to total primary production ratio (f-ratio) in the Bay of Bengal using isotopic composition of suspended particulate organic carbon and nitrogen. *Deep Sea Research Part I: Oceanographic Research Papers, 139*, 43–54.

Singh, A., & Ramesh, R. (2015). Environmental controls on new and primary production in the northern Indian Ocean. *Progress in Oceanography, 131*, 138–145.

Swathi, P. S., Sharada, M. K., & Yajnik, K. S. (2000). A coupled physical-biological-chemical model for the Indian Ocean. *Journal of Earth System Science, 109*, 503–537. https://doi.org/10.1007/BF02708337

Tripathy, S. C., Pavithran, S., Sabu, P., Pillai, H. U., Dessai, D. R., & Anilkumar, N. (2015). Deep chlorophyll maximum and primary productivity in Indian Ocean sector of the Southern Ocean: Case study in the Subtropical and Polar Front during austral summer 2011. *Deep Sea Research Part II: Topical Studies in Oceanography, 118*, 240–249.

Tripathy, S. C., Sabu, P., Patra, S., Naik, R. K., Sarkar, A., Venkataramana, V., Kerkar, A. U., & Sudarsanarao, P. (2020). Biophysical control on variability in phytoplankton production and composition in the south-western tropical Indian Ocean during monsoon 2014. *Frontiers in Marine Science, 7*, 515.

Uitz, J., Claustre, H., Morel, A., & Hooker, S. B. (2006). Vertical distribution of phytoplankton communities in open ocean: An assessment based on surface chlorophyll. *Journal of Geophysical Research: Oceans, 111*(C8), C08005.

van de Poll, W. H., Kulk, G., Timmermans, K. R., Brussaard, C. P., van der Woerd, H. J., Kehoe, M. J., Mojica, K. D., Visser, R. J., Rozema, P. D., & Buma, A. G. (2013). Phytoplankton chlorophyll a biomass, composition, and productivity along a temperature and stratification gradient in the northeast Atlantic Ocean. *Biogeosciences, 10*(6), 4227–4240.

Venrick, E. L., McGowan, J. A., Cayan, D. R., & Hayward, T. L. (1987). Climate and chlorophyll a: Long-term trends in the central North Pacific Ocean. *Science, 238*(4823), 70–72.

Vinayachandran, P. N., & Yamagata, T. (1998). Monsoon response of the sea around Sri Lanka: Generation of thermal domes and anticyclonic vortices. *Journal of Physical Oceanography, 28*(10), 1946–1960.

Vinayachandran, P. N., Murty, V. S. N., & Ramesh Babu, V. (2002). Observations of barrier layer formation in the Bay of Bengal during summer monsoon. *Journal of Geophysical Research: Oceans, 107*(C12), SRF-19.

Vinayachandran, P. N., Chauhan, P., Mohan, M., & Nayak, S. (2004). Biological response of the sea around Sri Lanka to summer monsoon. *Geophysical Research Letters, 31*(1), L01302.

Vinayachandran, P. N., McCreary, J. P., Jr., Hood, R. R., & Kohler, K. E. (2005). A numerical investigation of the phytoplankton bloom in the Bay of Bengal during Northeast Monsoon. *Journal of Geophysical Research: Oceans, 110*(C12), C12001.

Watts, L. J., & Owens, N. J. P. (1999). Nitrogen assimilation and the f-ratio in the northwestern Indian Ocean during an intermonsoon period. *Deep Sea Research Part II: Topical Studies in Oceanography, 46*(3–4), 725–743.

Watts, L. J., Sathyendranath, S., Caverhill, C., Maass, H., Platt, T., & Owens, N. J. P. (1999). Modelling new production in the northwest Indian Ocean region. *Marine Ecology Progress Series, 183*, 1–12.

Wei, Y., Zhao, X., Sun, J., & Liu, H. (2019). Fast repetition rate fluorometry (FRRF) derived phytoplankton primary productivity in the Bay of Bengal. *Frontiers in Microbiology, 10*, 1164.

Weller, R. A., Baumgartner, M. F., Josey, S. A., Fischer, A. S., & Kindle, J. C. (1998). Atmospheric forcing in the Arabian Sea during 1994–1995: Observations and comparisons with climatology and models. *Deep Sea Research Part II: Topical Studies in Oceanography, 45*(10–11), 1961–1999.

Wiggert, J. D., Murtugudde, R. G., & McClain, C. R. (2002). Processes controlling interannual variations in wintertime (Northeast Monsoon) primary productivity in the central Arabian Sea. *Deep Sea Research Part II: Topical Studies in Oceanography, 49*(12), 2319–2343.

Wiggert, J. D., Hood, R. R., Banse, K., & Kindle, J. C. (2005). Monsoon-driven biogeochemical processes in the Arabian Sea. *Progress in Oceanography, 65*(2–4), 176–213.

Wiggert, J. D., Murtugudde, R. G., & Christian, J. R. (2006). Annual ecosystem variability in the tropical Indian Ocean: Results of a coupled bio-physical ocean general circulation model. *Deep Sea Research Part II: Topical Studies in Oceanography, 53*, 644–676.

Williams, P. J. L. (1981). Incorporation of microheterotrophic processes into the classical paradigm of the planktonic food web. *Kiel Meeresforschungen Sonderheft, 4*, 1–28.

Yamanaka, Y., & Tajika, E. (1996). The role of the vertical fluxes of particulate organic matter and calcite in the oceanic carbon cycle: Studies using an ocean biogeochemical general circulation model. *Global Biogeochemical Cycles, 10*(2), 361–382.

Young, D. K., & Kindle, J. C. (1994). Physical processes affecting availability of dissolved silicate for diatom production in the Arabian Sea. *Journal of Geophysical Research: Oceans, 99*(C11), 22619–22632.

Zhou, X., Duchamp-Alphonse, S., Kageyama, M., Bassinot, F., Beaufort, L., & Colin, C. (2020). Dynamics of primary productivity in the northeastern Bay of Bengal over the last 26 000 years. *Climate of the Past, 16*(5), 1969–1986.

Chapter 9
Past Trends and Future Projections of Marine Primary Productivity in the Tropical Indian Ocean

Aditi Modi and Mathew Koll Roxy

Abstract Changes in marine phytoplankton are crucial to understand the complex but significant climate change impacts on the marine ecosystem and fisheries. Detecting the climatic response in phytoplankton has been a challenge due to the unavailability of long-term observed data and biases and inadequacies in representing the ocean biogeochemistry in ocean models. Research has been indicating that long-term SST warming stratifies the low-latitude waters, impacting nutrient mixing and phytoplankton production. Now, with extended satellite datasets and improved Earth system models, we find that the marine primary productivity in the tropical Indian Ocean, particularly the Arabian Sea and the coastal regions of the Bay of Bengal, shows a significant declining trend during 1998–2022. Future simulations from the Coupled Model Intercomparison Project phase 6 (CMIP6) further project that the decreasing trend will continue in the Arabian Sea, Bay of Bengal, and Sri Lankan coast. Meanwhile, an increasing trend is projected along the coast of Sumatra and Java and coastal regions of the northeast Arabian Sea and northwest Bay of Bengal. Gaps in in situ and satellite data still prevent us from gaining clarity on regional trends at fine temporal scales, particularly in terms of shifts in the timings of phytoplankton blooms. Future response of phytoplankton changes is poorly constrained in the Earth system models since they typically include only 2–3 phytoplankton types and are inadequate to assess the changes in

The original version of this chapter was revised. The correction to this chapter is available at https://doi.org/10.1007/978-3-031-34467-1_15

A. Modi (✉)
Centre for Climate Change Research, Indian Institute of Tropical Meteorology, Ministry of Earth Sciences, Pune, India

IDP in Climate Studies, Indian Institute of Technology, Bombay, India
e-mail: aditi.modi@tropmet.res.in

M. K. Roxy
Centre for Climate Change Research, Indian Institute of Tropical Meteorology, Ministry of Earth Sciences, Pune, India

S. C. Tripathy, A. Singh (eds.), *Dynamics of Planktonic Primary Productivity in the Indian Ocean*, https://doi.org/10.1007/978-3-031-34467-1_9

phytoplankton community structure. Regardless, the observed trends and future projections give a clear signal of a steady and rapid decline in phytoplankton production in the Indian Ocean. These changes need to be closely monitored for phytoplankton community reorganization and abrupt shifts and collapses in the marine ecosystem.

Keywords Chlorophyll · Net primary productivity · Tropical Indian Ocean · Earth system model · Phytoplankton trends · Future projections · CMIP6

1 Introduction

Phytoplankton are single-celled aquatic photoautotrophs that serve as the primary food source for marine species. They regulate the availability of food for higher trophic levels of the marine ecosystem and drive the ocean carbon cycle by converting inorganic carbon into organic carbon through photosynthesis (Cabré et al., 2015; Falkowski et al., 2004; Laufkötter et al., 2015; Smetacek, 1999). Net primary productivity (NPP) is the net organic carbon produced by phytoplankton after subtracting the costs of its metabolic processes from the total organic carbon produced (Falkowski et al., 2003). This NPP is the most critical element in assessing organic carbon export from the ocean surface to the deep ocean (Sarmiento et al., 2007). As a result, variations in the marine NPP can be used to deduce global carbon budget trends (Wernand et al., 2013).

Primary production exhibits variability on timescales ranging from months to years. The tropical Indian Ocean is typically characterized by two annual blooms of phytoplankton – primary bloom during summer (June–September) and a secondary bloom during winter (December–February) (Banse, 1987; Kumar et al., 2013). Changes in physical forcing, especially related to the southwest (summer) and northeast (winter) monsoons, are linked to these seasonal bloom episodes (Kumar et al., 2001; Schott & McCreary, 2001; Wiggert et al., 2005). Due to the various physical mechanisms driving primary production in the Indian Ocean, these seasonal blooms also exhibit spatial diversity (Beal et al., 2019; Kumar et al., 2013). Apart from seasonal fluctuations, the principal climatic modes – El Niño Southern Oscillation (ENSO) and Indian Ocean Dipole (IOD) – influence interannual variations in primary productivity in the Indian Ocean (Currie et al., 2013; Murtugudde & Busalacchi, 1999). These climatic modes also have the potential for ocean rearrangement such as demonstrated by the strongest El Niño of the twentieth century, the 1998/1999 El Niño. It led to a dramatic collapse of mackerels, resulting in the recruitment of oil sardines along India's Malabar coast (Krishnakumar & Bhat, 2007).

In the past, in situ data on indices of ocean primary production in the Indian Ocean were scarce, as opposed to the Pacific and Atlantic Oceans. This is one of the main reasons why the Indian Ocean is the least studied of all the tropical basins. Only since the satellite era has it become able to discern the impact of anthropogenic climate change on the ocean (Henson et al., 2010; Werdell et al., 2009). Satellites collect a uniform spatiotemporal sample of the surface ocean, resulting in an ocean color dataset that spans more than two decades, allowing us to better understand

ocean biophysical interactions (Sathyendranath et al., 2019). Remote-sensed ocean color provides measurements of chlorophyll – the phytoplankton pigment that undergoes photosynthesis and is a proxy for marine phytoplankton. Chlorophyll concentrations are generally employed to discern trends in aggregate plankton types because data on different taxonomic categories of phytoplankton is relatively few as compared to satellite-derived primary production records. At the same time, there are in situ records and model data relating to individual phytoplankton kinds that have been utilized to examine trends and are discussed in this chapter.

Observations over the past century have reported a consistent rise in sea surface temperatures (SST) in the tropical Indian Ocean, particularly in recent decades (Beal et al., 2019; Rao et al., 2012; Roxy et al., 2020; Webster et al., 2006). This rate of warming (0.15 °C/decade) in the tropical Indian Ocean is the fastest among tropical oceans and accounts for about one-quarter of the increase in global oceanic heat content over the last two decades despite being the smallest of the tropical oceans (representing only 13% of the global ocean surface) (Beal et al., 2019; Gnanaseelan et al., 2017). Moreover, the Indian Ocean warm pool has substantially expanded during recent decades (Roxy et al., 2019; Dalpadado et al., 2021). In the low-latitude regions, which are primarily nutrient limited as sunlight is abundant, an increase in ocean surface temperature is projected to enhance upper water column stratification, resulting in less mixing and lesser flow of nutrients from the subsurface into the surface (Behrenfeld et al., 2006; Boyce et al., 2011; Roxy et al., 2016). This increased stratification might affect the phytoplankton growth and species distribution and spread across the region's food web, eventually leading to the restructuring of marine biomes (Cheung et al., 2011; Pörtner et al., 2014). It is, therefore, critical to have a clear understanding of productivity trends in this highly productive ocean basin, particularly since it has been witnessing one of the most significant warming trends, which is the objective of this chapter. Hence, this chapter reviews the historical changes in marine primary productivity in the Indian Ocean as a whole and in the subregions of the Indian Ocean that serve as biodiversity hotspots. This chapter also discusses on the future long-term projections of marine primary productivity based on simulations from Coupled Model Intercomparison Project (CMIP) phase 5 (CMIP5) and available phase 6 (CMIP6).

2 Past Trends in Marine Primary Productivity

The Arabian Sea is one of the largest hotspots for biodiversity and one of the most economically significant, thus forming a unique ecosystem within the Indian Ocean basin (Alexander, 1993; Piontkovski & Queste, 2016). Due to the upwelling of cold nutrient-rich water and enhanced vertical mixing provided by the periodically reversing monsoon winds, this region experiences enormous phytoplankton blooms in the summer and a smaller bloom in the winter, owing to convective vertical mixing (Kumar et al., 2001; Ryther & Menzel, 1965; Wiggert et al., 2005). Behrenfeld et al. (2006) reported a decrease in net primary production (NPP) due

to surface thermal stratification in most of the tropics but an increase in NPP in response to rising SSTs across the western Indian Ocean from 1998 to 2004. Other research (Goes et al., 2005; Gregg et al., 2005) found similar results during the same time period, showing that the western Indian Ocean saw the second biggest rise in chlorophyll concentrations (a phytoplankton biomass indicator) among open-ocean regions. Goes et al. (2005) found a 350% increase in marine phytoplankton in this region, which they attributed to the strengthening of summer monsoon winds in the western Indian Ocean. The increasing trend during the short data period appears to be corresponding to the initial year (1998) with a strong El Niño and a positive Indian Ocean Dipole, which results in warmer SST anomalies in the western Indian Ocean and a corresponding reduction in chlorophyll concentrations (Currie et al., 2013; Murtugudde et al., 1999; Roxy et al., 2016).

Extending the dataset over a 16-year (1998–2013) period, Roxy et al. (2016) report a 30% decline in chlorophyll in the western Indian Ocean. Their study also assessed CMIP5 models, which simulated a 20% decrease in long-term chlorophyll in the western Indian Ocean from 1950 to 2015, thus agreeing with the observations. The increased stratification of the oceanic water column in response to the strong warming of the ocean surface is linked to these declining phytoplankton trends. Another study by Prakash et al. (2012) used SeaWiFS sensor chlorophyll data and found that chlorophyll increased during 1998–2002 and declined since 2003 in the western Arabian Sea. The study suggests that the observed chlorophyll response is not governed by global warming but rather is a result of the decadal oscillations in sea-level anomaly and the thermocline. Diatoms, which are the predominant phytoplankton group in the Arabian Sea, have been reported to be declining in the region (Garrison et al., 2000; do Rosário Gomes et al., 2014). As a result, changes in the trophic interactions of the aquatic food web are to be expected.

We analyze the changes in summer marine primary production during 1998–2022 in the western Indian Ocean remote-sensed chlorophyll concentrations provided by European Space Agency's Ocean Color-Climate Change Initiative (OC-CCI) v6.0 (Henson et al., 2010; Hollmann et al., 2013; Sathyendranath et al., 2019). The chlorophyll-a time series (chl-a) obtained from OC-CCI is a multi-mission product derived by merging data from the SeaWiFS, MODIS, MERIS, and VIIRS sensors. The level-3 data from different sensors were band-shifted to SeaWiFS wavebands and bias-corrected for the signal-to-noise ratio, thus resulting in a climate-quality dataset. The analysis suggests that chlorophyll has declined in the western Indian Ocean during the past 25 years (inset box in Fig. 9.1a). The time series of chlorophyll anomalies indicate a high year-to-year variability with a linear downward trend (red dashed line in Fig. 9.1b). A major decrease in chlorophyll concentrations is seen in the north Indian Ocean, particularly in the north-western Arabian Sea and along the coasts of Bay of Bengal (Fig. 9.1a). However, patches of increased chlorophyll in some of the coastal areas, such as the eastern Indian Ocean off the coasts of Sumatra and Java and the Sri Lankan upwelling dome, are observed. The local biophysical processes need further examination to understand the spatial variability in the observed chlorophyll trends.

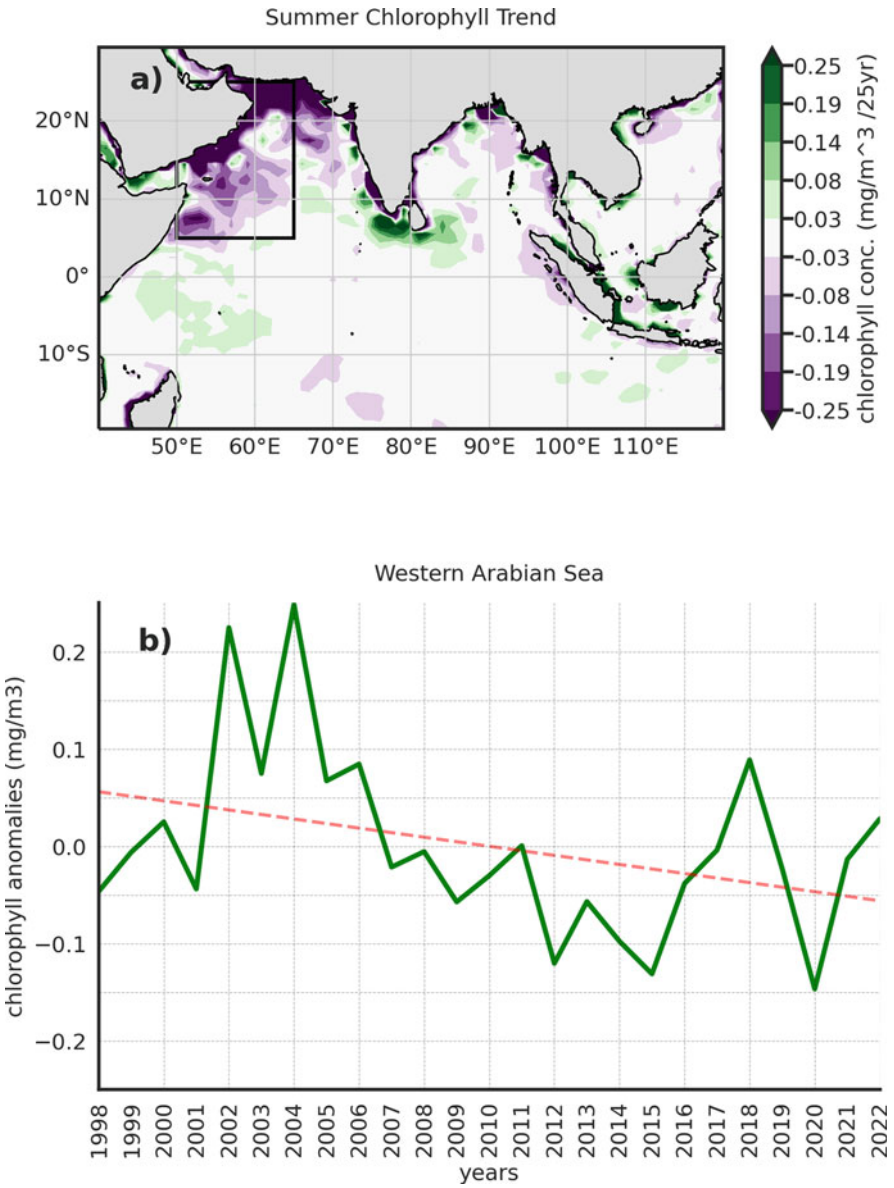

Fig. 9.1 (**a**) Summer (June–September) chlorophyll trend (mg/m^3/25 year) in the tropical Indian Ocean in OC-CCI remote-sensed observations during 1998–2022. The inset box (50–65°E, 5–25°N) indicates the region with the largest trends in chlorophyll concentrations. (**b**) Mean summer anomalies of chlorophyll (mg/m^3) in the western Indian Ocean (50–65°E, 5–25°N; inset box in (**a**)). Dashed line (red) in the chlorophyll time series indicates the trend line. (Data used is from European Space Agency Ocean Color-Climate Change Initiative (OC-CCI) version 6.0 (https://climate.esa.int/en/projects/ocean-colour/))

In comparison to the Arabian Sea, the Bay of Bengal is characterized as a region of low primary productivity. This low primary production in the Bay of Bengal is a result of upper water column stratification caused by high ocean surface temperatures, combined with lower surface water salinity caused by excess precipitation from the southwest monsoon and river discharge (Kumar et al., 2004; Mahadevan et al., 2016). However, despite the low productivity, on longer timescales, the high new production (production by nitrate) in the Bay of Bengal makes it more efficient in removing the atmospheric CO_2 (Kumar et al., 2004). A decrease in primary productivity in the Bay of Bengal has been seen consistently across the observed records, including proxy data, Earth system models, and satellite imagery (Behrenfeld et al., 2006; Gregg & Rousseaux, 2019; Roxy et al., 2016; Shetye et al., 2014). However, the factors underlying this apparent decline differ among datasets. According to evidence from the oldest geological records dating back over 5000 years, the availability of iron on the ocean surface is linked to a decline in primary production over millennial timescales. The current satellite and climate simulations ascribe the recent decline to upper ocean stratification linked to significant temperature rise over the past half-century. Historically available records show that diatoms, eukaryotic plankton, and cyanobacteria are the dominant primary producers in the Bay of Bengal (Bhaskar et al., 2007; Gauns et al., 2005; Lin et al., 2012; Madhupratap et al., 2003; Pujari et al., 2019). The rate of decline of diatoms and chlorophytes has been 16% per decade and can be linked to the declining rate of primary production in the Bay of Bengal. Concurrently, cyanobacteria have grown at a rate of 17% per decade (Gregg & Rousseaux, 2019). Each of these phytoplankton species has a potential community shift, but the evidence is inconclusive because of the high spatial and temporal variability. Löscher (2021) provides a detailed review of the changes in various phytoplankton types.

The subtropical gyre dominates the southern hemisphere of the tropical Indian Ocean. Despite being classified as oligotrophic regions with low nutrient concentrations and consequently having lower biomass and net primary production year-round, the subtropical gyres' enormous size (about 40% of the Earth's surface) makes their overall contribution to biological productivity significant (Jones et al., 1996; refer to Fig. 9.1. in McClain et al., 2004). Despite a significant variation in growth rates, the phytoplankton biomass of the subtropical gyres is relatively stable (Laws et al., 1987; Maranon et al., 2003). Hence, an expansion in the gyre is associated with more oligotrophic waters and reduced biomass. According to satellite data, the southern Indian Ocean gyre grew marginally between 1997 and 2003 (McClain et al., 2004). A growth in the south Indian Ocean gyre and significant falling trends in the chlorophyll and net primary production are also seen in the most recent satellite data records (>10 years) (Polovina et al., 2008). Using multi-sensor satellite observations for the period 1998–2010, an estimation of a decline of 12% in the Indian Ocean subtropical gyre and an SST increase of 0.42 °C has been made (Signorini & McClain, 2012). This decrease in primary productivity is ascribed to the stratification of the upper ocean, less mixing, and warming of the gyres (increase in SST), as well as a shallower mixed layer (MLD). This shift in the gyre-specific

ecosystem indicators is a strong sign of how biological processes have responded to the different forms of climate variability (Karl et al., 2001; Oschlies, 2001). However, further research is required to fully understand how climate modes affect ecosystem variability within the southern Indian Ocean gyre.

The north and equatorial Indian Oceans have been demonstrated to have seen a rapid drop in phytoplankton of 0.16 and 0.69 PgC year^{1} decade^{-1} since 1998 to 2015, respectively, which accounts for the majority of the contributions to the global NPP decline (−0.8 PgC year^{1}decade^{-1}). The fall in diatoms and chlorophytes, as indicated by an ocean biogeochemical model, is indicative of a significant reduction in productivity (Gregg & Rousseaux, 2019). In the Indian Ocean basin, the concentrations of nitrate and silicate have decreased by 32% and 23%, respectively, during 1998–2015. These lower nutrient contents are a sign that the thermocline's supply of nutrients into the mixed layer may be decreasing (Steinacher et al., 2010). The reported loss in the main phytoplankton group, diatoms, reflects the fall in these important nutrients. This suggests that a shift in phytoplankton composition has begun in these tropical and subtropical Indian basins. If SSTs in tropical basins continue to rise, there is a greater chance of a gradual shift of fish stocks to higher latitudes (Solanki et al., 1998).

Chlorophyll levels in the Indian Ocean continued to fall from 0.37 to 0.18 mg/m^3 between 1898 and 1993, according to in situ ocean color observations that have been recorded since 1890 in various expeditions. The observations are filtered into two datasets, one for the open-ocean region 100 km away from coasts and the other located 500 km away from coasts. Figure 9.2a, b depicts the results for the Indian Ocean, which show a blueing ocean for both datasets, with an average decay of −0.0021 mg/m^3 per year. In contrast, we observe a growing tendency in the Atlantic and Pacific Oceans between 1898 and 1993 (Wernand et al., 2013). The "lost" Forel-

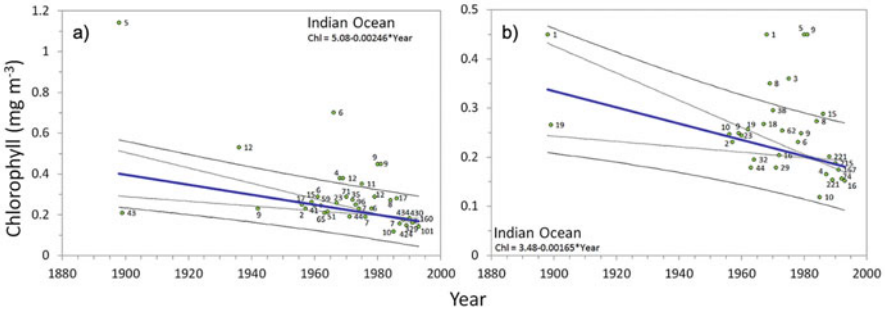

Fig. 9.2 Chlorophyll trend (blue line) in (**a**) open-ocean observations at a distance of more than 100 km off coast. It is chosen to avoid anthropogenic pressure's effects on water coloration in coastal zones, such as locally increased nutrient loading (eutrophication), which tends to increase phytoplankton biomass, or high sediment loading brought on by changes in land use or erosion. (**b**) Open-ocean observations at a distance of more than 500 km from the shore. This region is chosen in order to incorporate the oceans, while also avoiding the effects of mixing with the variously colored water of surrounding seas. All trend lines shown are statistically significant ($P < 0.05$). Regression coefficients are indicated in each graph. (Figure adopted from Wernand et al. (2013))

Ule scale, which was the "then" simplest method of getting the geophysical properties of the natural waters, was used in these observations, making this one of the earliest oceanographic archives. This is the oldest long-term ocean color dataset yet created, thanks to the recent mapping of these observations. More information on the Forel-Ule scale can be found in Wernand and Woerd (2010).

3 Future Projections of Marine Primary Production

Indian Ocean rim nations are dependent on the pelagic ecosystem for their food and livelihood; hence managing it is becoming increasingly challenging than ever. The stressors impacting the marine environment and the corresponding challenges are expected to intensify further as ocean surface warming is projected to continue rapidly in response to an unabated increase in greenhouse gas emissions into the future (Goddard & Groeneveld, 2008; Guillotreau et al., 2012; Houghton et al., 1996; Lee et al., 2005; Levitus et al., 2000; Piontkovski et al., 2015). A majority of Earth system models project a mean global decline in phytoplankton growth during the twenty-first century, which will lower the global NPP thus signaling a net reduction in carbon export into the deeper ocean (Behrenfeld et al., 2006; Bopp et al., 2001; Boyce et al., 2010; Fung et al., 2005).

According to Bopp et al. (2013), all the CMIP5 models, under different emission scenarios, forecast a decrease in NPP in the tropical Indian Ocean. This drop might be as high as 30% under the highest carbon emission scenario (RCP8.5), thus proving detrimental to the basin's marine biodiversity. These NPP and phosphate levels in the ocean's surface and subsurface are expected to keep declining by the year 2300 (Moore et al., 2018). The majority of the CMIP5 models (7 out of 9) project a decrease in NPP, though the mechanism for this reduction varies among the models (Laufkötter et al., 2015). According to simulations from four coupled carbon cycle models of increasing complexity, the primary production in the Indian Ocean is expected to fall relative to preindustrial levels under the earlier set of IPCC emission scenarios (IPCC SRES A2) (Steinacher et al., 2010). A minor rise in net primary productivity is anticipated in some regions of the Indian Ocean close to Australia, nevertheless. This rise is potentially due to the increased upwelling that has improved the flow of nutrients into the mixed layer. In response to the ocean surface freshening and global warming, Cabré et al. (2015) assessed all 16 CMIP5 models that were available and reported a consistent estimate of a decline in marine primary productivity during the twenty-first century across all models.

Diatoms, which make up the majority of marine phytoplankton and represent more than 40% of the biological pump for CO_2 (Tréguer & Pondaven, 2000), are also predicted to experience a rapid decline in the Indian Ocean relative to other phytoplankton types due to a stronger nitrate stress (Bopp et al., 2005; Cermeño et al., 2008). Contrary to other studies, Sarmiento et al. (2004) predict a net rise in global primary production in 2050 and 2090 relative to the preindustrial climate; nevertheless, the low-latitude oceans are expected to experience a loss. According to

the CMIP5 Earth system models' high emission scenarios (RCP 8.5), marine primary production in the Indian Ocean is expected to fall, with the western and equatorial Indian Oceans expected to experience the greatest declines (Seelanki & Pant, 2021). However, it is projected that the northern Arabian Sea would experience an increase in chlorophyll levels (Seelanki & Pant, 2021).

The majority of the studies argues that the model predictions of a fall in marine production in the twenty-first century (both near and far future) in the low and mid-latitudes are due to the decrease in upwelling resulting in a reduced nutrient supply from bottom layers of the ocean. Reduced stratification and a more stable (less-mixed) ocean will result from the ocean's continued monotonous warming; these changes will prevent cold, nutrient-rich deep waters from mixing with the surface. Consequently, there would be a net adverse effect on marine output in the tropical Indian Ocean (Marinov et al., 2010). In striking contrast, the anticipated ocean warming could help the phytoplankton development in high-latitude locations, where growth is limited by the availability of light and other environmental factors (Bopp et al., 2001; Doney, 2006; Moore et al., 2018; Steinacher et al., 2010).

The CMIP6 ensemble mean analysed under medium-to-high emission scenarios projects a further reduction in the phytoplankton stocks in both the near future (2041–2070) and far future (2071–2100), with respect to the recent period (1976–2005) in most parts of the tropical Indian Ocean, (Fig. 9.3) (Roxy et al., 2022). By the end of the twenty-first century, the western Arabian Sea region

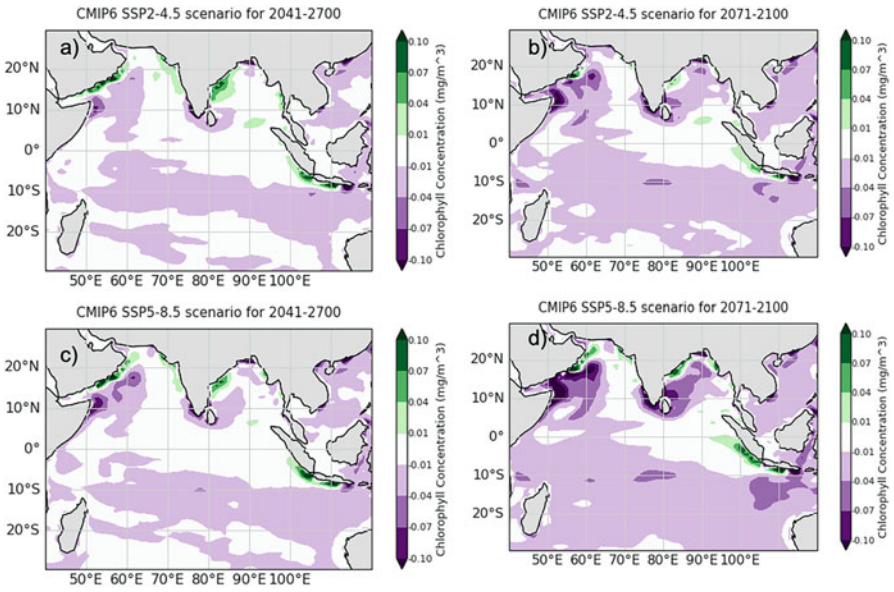

Fig. 9.3 Projected changes in ocean surface chlorophyll (in mg m^{-3}) during the summer monsoon (June–September) in (**a**) SSP2-4.5 for 2041–2070, (**b**) SSP2-4.5 for 2071–2100, (**c**) SSP5-8.5 for 2041–2070, and (**d**) SSP5-8.5 for 2071–2100, with respect to the reference period 1976–2005, in CMIP6 (ensemble mean) simulations. (Figure adopted from Roxy et al. (2022))

(50–65°E, 5–25°N) is projected to have an 8–10% decline in surface chlorophyll under medium-to-high emission scenarios (Fig. 9.3). However, the models project a slight increase in chlorophyll in the southeast Indian Ocean near the shores of Sumatra and Java, as well as along the majority of the northern Indian Ocean's coastal regions (Oman, western and eastern India, Myanmar).

Notably, the inter-model differences and uncertainties in NPP projections are inducted into projected risk assessments under varied climate change scenarios. According to a recent study (Tagliabue et al., 2021), the Indian Ocean is one of the basins with the greatest inter-model spread in the projected changes in NPP. These large inter-model uncertainties are due to the model representation of physical and biogeochemical processes (Whitt & Jansen, 2020). Even though the representation of ocean biogeochemistry in the current generation of Earth system models has improved, further representation of biophysical and biogeochemical feedback is required (Séférian et al., 2020). This necessitates a larger variety of observational datasets so that we can better comprehend the process underlying these ocean emissions.

4 Summary and Future Research Direction

Remote-sensed ocean color observations have made it feasible to examine the trends on regional and global scales. Over the past two decades, satellite records of ocean color have shown a decline in the marine primary production in the western Indian Ocean. This decrease in phytoplankton biomass is attributed to the increased stratification associated with the surface warming of the ocean. However, in other areas, such as along the Java and Sumatra coasts, primary production has increased slightly. To explain these changes, a greater comprehension of the local biophysical processes is required. The Earth system models ensemble also projects a net decline in marine primary production in both the near and far future. The continued warming of the ocean is projected to be the cause of the decline.

Historically, the Indian Ocean has been under-sampled in terms of biogeochemistry and ocean productivity when compared to the Pacific and Atlantic. The vertically generalized productivity model (VGPM; Behrenfeld & Falkowski, 1997), for example, was created with the help of a global database of 1698 primary productivity stations. None of these data are sourced from the Indian Ocean. The absence of any validation data for this satellite productivity algorithm in the Indian Ocean casts doubt on its accuracy despite the fact that it has become the global industry standard for estimating ocean primary productivity and its change over time (Beal et al., 2019; Beal et al., 2020). Recent research has shown that trend detection using satellite ocean color records is extremely sensitive to data processing and drift corrections (Gregg & Rousseaux, 2014; Gregg & Rousseaux, 2019). Assimilation of in situ data with models is needed to reduce this disparity in chlorophyll measurements obtained from different satellites.

Another major limitation of the satellite data is the presence of missing values due to the presence of cloud cover over the north Indian Ocean during the summer monsoon. This renders the data unsuitable for examining the trends in phytoplankton phenology in the Indian Ocean. If chlorophyll in situ records are consistently available, it can be used to fill in the gaps in satellite data. The gaps in the satellite data, however, cannot be filled by the current distribution of in situ observations (Modi et al., 2022). The population of the Indian Ocean rim, which is heavily dependent on fisheries for its sustenance, needs ecological forecasting; therefore, this calls for rapid attention. With the recent launch of the sustained Indian Ocean Observing System (IndOOS) program and similar ongoing observational programs (IOGOOS and SIBER, IIOE2), which aim to improve observations in the tropical Indian Ocean's surface and subsurface by implementing more observing networks like Argo floats, RAMA moorings, satellites, and drifters, we are optimistic that improved observations will be available for the Indian Ocean. While this is a significant collaborative step forward, more global participation is required to sustain the observational networks.

References

Alexander, L. M. (1993). Large marine ecosystems: A new focus for marine resources management. *Marine Policy, 17*(3), 186–198. https://doi.org/10.1016/0308-597X(93)90076-F

Banse, K. (1987). Seasonality of phytoplankton chlorophyll in the central and northern Arabian sea. *Deep Sea Research Part A. Oceanographic Research Papers, 34*(5), 713–723. https://doi.org/10.1016/0198-0149(87)90032-X

Beal, L., Vialard, J., Koll, R., Ravichandran, M., McPhaden, M., Feng, M., et al. (2019). *IndOOS-2: A roadmap to sustained observations of the Indian Ocean for 2020–2030*. https://doi.org/10.36071/clivar.rp.4.2019

Beal, L. M., Vialard, J., Roxy, M. K., Li, J., Andres, M., Annamalai, H., et al. (2020). A road map to IndOOS-2: Better observations of the rapidly warming Indian Ocean. *Bulletin of the American Meteorological Society, 101*(11), E1891–E1913. https://doi.org/10.1175/BAMS-D-19-0209.1

Behrenfeld, M. J., & Falkowski, P. G. (1997). Photosynthetic rates derived from satellite-based chlorophyll concentration. *Limnology and Oceanography*. https://doi.org/10.4319/lo.1997.42.1.0001

Behrenfeld, M. J., O'Malley, R. T., Siegel, D. A., McClain, C. R., Sarmiento, J. L., Feldman, G. C., et al. (2006). Climate-driven trends in contemporary ocean productivity. *Nature, 444*(7120), 752–755. Retrieved from https://doi.org/10.1038/nature05317

Bhaskar, J., Nagappa, R., Gauns, M., & Fernandes, V. (2007). Preponderance of a few diatom species among the highly diverse microphytoplankton assemblages in the Bay of Bengal. *Marine Biology, 152*, 63–75. https://doi.org/10.1007/s00227-007-0657-5

Bopp, L., Monfray, P., Aumont, O., Dufresne, J.-L., Treut, H. L., Madec, G., et al. (2001). Potential impact of climate change on marine export production. *Global Biogeochemical Cycles, 15*(1), 81–99. https://doi.org/10.1029/1999GB001256

Bopp, L., Aumont, O., Cadule, P., Alvain, S., & Gehlen, M. (2005). Response of diatoms distribution to global warming and potential implications: A global model study. *Geophysical Research Letters, 32*(19). https://doi.org/10.1029/2005GL023653

Bopp, L., Resplandy, L., Orr, J. C., Doney, S. C., Dunne, J. P., Gehlen, M., et al. (2013). Multiple stressors of ocean ecosystems in the 21st century: Projections with CMIP5 models. *Biogeosciences, 10*(10), 6225–6245. https://doi.org/10.5194/bg-10-6225-2013

Boyce, D. G., Lewis, M. R., & Worm, B. (2010). Global phytoplankton decline over the past century. *Nature, 466*(7306), 591–596. https://doi.org/10.1038/nature09268

Boyce, D. G., Lewis, M. R., & Worm, B. (2011). Boyce et al. reply. *Nature, 472*(7342). https://doi.org/10.1038/nature09953

Cabré, A., Marinov, I., & Leung, S. (2015). Consistent global responses of marine ecosystems to future climate change across the IPCC AR5 earth system models. *Climate Dynamics, 45*(5), 1253–1280. https://doi.org/10.1007/s00382-014-2374-3

Cermeño, P., Dutkiewicz, S., Harris, R. P., Follows, M., Schofield, O., & Falkowski, P. G. (2008). The role of nutricline depth in regulating the ocean carbon cycle. *Proceedings of the National Academy of Sciences, 105*(51), 20344–20349. https://doi.org/10.1073/pnas.0811302106

Cheung, W. W. L., Dunne, J., Sarmiento, J. L., & Pauly, D. (2011). Integrating ecophysiology and plankton dynamics into projected maximum fisheries catch potential under climate change in the Northeast Atlantic. *ICES Journal of Marine Science, 68*(6), 1008–1018. https://doi.org/10.1093/icesjms/fsr012

Currie, J. C., Lengaigne, M., Vialard, J., Kaplan, D. M., Aumont, O., Naqvi, S. W. A., & Maury, O. (2013). Indian Ocean Dipole and El Niño/Southern Oscillation impacts on regional chlorophyll anomalies in the Indian Ocean. *Biogeosciences, 10*(10), 6677–6698. https://doi.org/10.5194/bg-10-6677-2013

do Rosário Gomes, H., Goes, J. I., Matondkar, S. G. P., Buskey, E. J., Basu, S., Parab, S., & Thoppil, P. (2014). Massive outbreaks of Noctiluca scintillans blooms in the Arabian Sea due to spread of hypoxia. *Nature Communications, 5*(1), 4862. https://doi.org/10.1038/ncomms5862

Dalpadado, P., Arrigo, K. R., van Dijken, G. L., Gunasekara, S. S., Ostrowski, M., Bianchi, G., & Sperfeld, E. (2021). Warming of the Indian Ocean and its impact on temporal and spatial dynamics of primary production. *Progress in Oceanography, 198*, 102688. https://doi.org/10.1016/j.pocean.2021.102688

Doney, S. C. (2006). Plankton in a warmer world. *Nature, 444*(7120), 695–696. https://doi.org/10.1038/444695a

Falkowski, P. G., Laws, E. A., Barber, R. T., & Murray, J. W. (2003). Phytoplankton and their role in primary, new, and export production. In M. J. R. Fasham (Ed.), *Ocean biogeochemistry* (pp. 99–121). Springer Berlin Heidelberg. https://doi.org/10.1007/978-3-642-55844-3_5

Falkowski, P. G., Katz, M. E., Knoll, A. H., Quigg, A., Raven, J. A., Schofield, O., & Taylor, F. J. R. (2004). The evolution of modern eukaryotic phytoplankton. *Science, 305*(5682), 354. https://doi.org/10.1126/science.1095964

Fung, I. Y., Doney, S. C., Lindsay, K., & John, J. (2005). Evolution of carbon sinks in a changing climate. *Proceedings of the National Academy of Sciences, 102*(32), 11201–11206. https://doi.org/10.1073/pnas.0504949102

Garrison, D. L., Gowing, M. M., Hughes, M. P., Campbell, L., Caron, D. A., Dennett, M. R., et al. (2000). Microbial food web structure in the Arabian Sea: A US JGOFS study. *Deep Sea Research Part II: Topical Studies in Oceanography, 47*(7), 1387–1422. https://doi.org/10.1016/S0967-0645(99)00148-4

Gauns, M., Madhupratap, M., Ramaiah, N., Jyothibabu, R., Fernandes, V., Paul, J. T., & Prasanna Kumar, S. (2005). Comparative accounts of biological productivity characteristics and estimates of carbon fluxes in the Arabian Sea and the Bay of Bengal. *Deep Sea Research Part II: Topical Studies in Oceanography, 52*(14), 2003–2017. https://doi.org/10.1016/j.dsr2.2005.05.009

Gnanaseelan, C., Koll, R., & Deshpande, A. (2017). Variability and trends of sea surface temperature and circulation in the Indian Ocean. In *Observed climate variability and change over the Indian region. Springer geology* (pp. 165–179). https://doi.org/10.1007/978-981-10-2531-0_10

Goddard, S., & Groeneveld, J. (2008). Special issue: Peer-reviewed papers written by scientists working at the marine science and fisheries centre of the ministry of fisheries wealth. *Sultan*

Qaboos University Research Journal – Agricultural and Marine Sciences, 13(Special Issue), 1–83. Retrieved from https://www.cabdirect.org/cabdirect/abstract/20113181077

Goes, J., Thoppil, P., Gomes, H., & Fasullo, J. (2005). Warming of the Eurasian landmass is making the Arabian Sea more productive. *Science (New York, N.Y.), 308*, 545–547. https://doi.org/10.1126/science.1106610

Gregg, W., & Rousseaux, C. (2014). Decadal trends in global pelagic ocean chlorophyll: A new assessment integrating multiple satellites, in situ data, and models. *Journal of Geophysical Research: Oceans, 119*. https://doi.org/10.1002/2014JC010158

Gregg, W. W., & Rousseaux, C. S. (2019). Global ocean primary production trends in the modern ocean color satellite record (1998–2015). *Environmental Research Letters, 14*(12), 124011. https://doi.org/10.1088/1748-9326/ab4667

Gregg, W. W., Casey, N. W., & Mcclain, C. R. (2005). Recent trends in global ocean chlorophyll. *Geophysical Research Letters, 32*, 1–5. https://doi.org/10.1029/2004GL021808

Guillotreau, P., Campling, L., & Robinson, J. (2012). Vulnerability of small Island fishery economies to climate and institutional changes. *Current Opinion in Environmental Sustainability, 4*(3), 287–291. https://doi.org/10.1016/j.cosust.2012.06.003

Henson, S. A., Sarmiento, J. L., Dunne, J. P., Bopp, L., Lima, I., Doney, S. C., et al. (2010). Detection of anthropogenic climate change in satellite records of ocean chlorophyll and productivity. *Biogeosciences, 7*(2), 621–640. https://doi.org/10.5194/bg-7-621-2010

Hollmann, R., Merchant, C. J., Saunders, R., Downy, C., Buchwitz, M., Cazenave, A., et al. (2013). The ESA climate change initiative: Satellite data records for essential climate variables. *Bulletin of the American Meteorological Society, 94*(10), 1541–1552. https://doi.org/10.1175/BAMS-D-11-00254.1

Houghton, J. T., Meira Filho, L. G., Callander, B. A., Harris, N. (Neil), Katternberg, A., Maskell, K. (Kathy), et al. (1996). *Climate change 1995*. Cambridge University Press, for the Intergovernmental Panel on Climate Change. Retrieved from https://digitallibrary.un.org/record/223181

Jones, D. R., Karl, D. M., & Laws, E. A. (1996). Growth rates and production of heterotrophic bacteria and phytoplankton in the North Pacific subtropical gyre. *Deep Sea Research Part I: Oceanographic Research Papers, 43*(10), 1567–1580. https://doi.org/10.1016/S0967-0637(96)00079-9

Karl, D. M., Bidigare, R. R., & Letelier, R. M. (2001). Long-term changes in plankton community structure and productivity in the North Pacific Subtropical Gyre: The domain shift hypothesis. *Deep Sea Research Part II: Topical Studies in Oceanography, 48*(8), 1449–1470. https://doi.org/10.1016/S0967-0645(00)00149-1

Krishnakumar, P. K., & Bhat, G. S. (2007). Seasonal and interannual variations of oceanographic conditions off Mangalore coast (Karnataka, India) in the Malabar upwelling system during 1995–2004 and their influences on the pelagic fishery: Oceanographic conditions off Mangalore coast (India) and their influences on pelagic fishery. *Fisheries Oceanography, 17*(1), 45–60. https://doi.org/10.1111/j.1365-2419.2007.00455.x

Kumar, S. P., Ramaiah, N., Gauns, M., Sarma, V. V. S. S., Muraleedharan, P. M., Raghukumar, S., et al. (2001). Physical forcing of biological productivity in the Northern Arabian Sea during the Northeast Monsoon. *Deep Sea Research Part II: Topical Studies in Oceanography, 48*(6), 1115–1126. https://doi.org/10.1016/S0967-0645(00)00133-8

Kumar, S., Ramesh, R., Sardessai, S., & Sreeman, S. (2004). High new production in the Bay of Bengal: Possible causes and implications. *Geophysical Research Letters, 31*. https://doi.org/10.1029/2004GL021005

Kumar, S. P., Narvekar, J., Nuncio, M., Gauns, M., & Sardesai, S. (2013). What drives the biological productivity of the northern Indian Ocean? In *Indian Ocean biogeochemical processes and ecological variability* (pp. 33–56). American Geophysical Union (AGU). https://doi.org/10.1029/2008GM000757

Laufkötter, C., Vogt, M., Gruber, N., Aita-Noguchi, M., Aumont, O., Bopp, L., et al. (2015). Drivers and uncertainties of future global marine primary production in marine ecosystem models. *Biogeosciences, 12*(23), 6955–6984. https://doi.org/10.5194/bg-12-6955-2015

Laws, E. A., DiTullio, G. R., & Redalje, D. G. (1987). High phytoplankton growth and production rates in the North Pacific subtropical gyre1,2. *Limnology and Oceanography, 32*(4), 905–918. https://doi.org/10.4319/lo.1987.32.4.0905

Lee, P.-F., Chen, I.-C., & Tzeng, W.-N. (2005). Spatial and temporal distribution patterns of Bigeye Tuna (Thunnus obesus) in the Indian Ocean. *Zoological Studies, 44*(2), 260–270.

Levitus, S., Antonov, J. I., Boyer, T. P., & Stephens, C. (2000). Warming of the World Ocean. *Science, 287*(5461), 2225–2229. https://doi.org/10.1126/science.287.5461.2225

Lin, Q., Ni, G., Shen, P.-P., Fan, Y., Huang, L., & Tan, Y. (2012). Vertical patterns of early summer chlorophyll a concentration in the indian ocean with special reference to the variation of deep chlorophyll maximum. *Journal of Marine Biology, 2012*. https://doi.org/10.1155/2012/801248

Löscher, C. R. (2021). Reviews and syntheses: Trends in primary production in the Bay of Bengal – Is it at a tipping point? *Biogeosciences, 18*(17), 4953–4963. https://doi.org/10.5194/bg-18-4953-2021

Madhupratap, M., Gauns, M., Nagappa, R., PrasannaKumar, S., Muraleedharan, P. M., DeSousa, S. N., et al. (2003). Biogeochemistry of the Bay of Bengal: Physical, chemical and primary productivity characteristics of the central and western Bay of Bengal during summer monsoon 2001. *Deep Sea Research Part II Topical Studies in Oceanography, 50*. https://doi.org/10.1016/S0967-0645(02)00611-2

Mahadevan, A., Jaeger, G., Freilich, M., Omand, M., Shroyer, E., & Sengupta, D. (2016). *Freshwater in the Bay of Bengal: Its fate and role in air-sea heat exchange*. Graduate School of Oceanography Faculty Publications. https://doi.org/10.5670/oceanog.2016.40

Maranon, E., Behrenfeld, M. J., González-Benítez, N., Mourino, B., & Zubkov, M. (2003). High variability of primary production in oligotrophic waters of the Atlantic Ocean: Uncoupling from phytoplankton biomass and size structure. *Marine Ecology Progress Series, 257*, 1–11. https://doi.org/10.3354/meps257001

Marinov, I., Doney, S. C., & Lima, I. D. (2010). Response of ocean phytoplankton community structure to climate change over the 21st century: Partitioning the effects of nutrients, temperature and light. *Biogeosciences, 7*(12), 3941–3959. https://doi.org/10.5194/bg-7-3941-2010

McClain, C. R., Signorini, S. R., & Christian, J. R. (2004). Subtropical gyre variability observed by ocean-color satellites. *Deep Sea Research Part II: Topical Studies in Oceanography, 51*(1), 281–301. https://doi.org/10.1016/j.dsr2.2003.08.002

Modi, A., Roxy, M. K., & Ghosh, S. (2022). Gapfilling of ocean color over the tropical Indian Ocean using Monte-Carlo method. *Scientific Reports, 12*, 18395. https://doi.org/10.1038/s41598-022-22087-2

Moore, J. K., Fu, W., Primeau, F., Britten, G. L., Lindsay, K., Long, M., et al. (2018). Sustained climate warming drives declining marine biological productivity. *Science, 359*(6380), 1139–1143. https://doi.org/10.1126/science.aao6379

Murtugudde, R., & Busalacchi, A. J. (1999). Interannual variability of the dynamics and thermodynamics of the tropical Indian Ocean. *Journal of Climate, 12*(8), 2300–2326. https://doi.org/10.1175/1520-0442(1999)012<2300:IVOTDA>2.0.CO;2

Murtugudde, R. G., Signorini, S. R., Christian, J. R., Busalacchi, A. J., McClain, C. R., & Picaut, J. (1999). Ocean color variability of the tropical Indo-Pacific basin observed by SeaWiFS during 1997–1998. *Journal of Geophysical Research: Oceans, 104*(C8), 18351–18366. https://doi.org/10.1029/1999JC900135

Oschlies, A. (2001). NAO-induced long-term changes in nutrient supply to the surface waters of the North Atlantic. *Geophysical Research Letters, 28*, 1751–1757. https://doi.org/10.1029/2000GL012328

Piontkovski, S. A., & Queste, B. Y. (2016). Decadal changes of the Western Arabian sea ecosystem. *International Aquatic Research, 8*(1), 49–64. https://doi.org/10.1007/s40071-016-0124-3

Piontkovski, S., Al-Oufi, H., & Al-Jufaili, S. (2015). Seasonal and interannual changes of Indian oil sardine, Sardinella longiceps landings in the governorate of Muscat (the Sea of Oman). https://doi.org/10.7755/MFR.76.3.3

Polovina, J. J., Howell, E. A., & Abecassis, M. (2008). Ocean's least productive waters are expanding. *Geophysical Research Letters, 35*(3). https://doi.org/10.1029/2007GL031745

Pörtner, H. O., Karl, D. M., Boyd, P. W., Cheung, W., Lluch-Cota, S. E., Nojiri, Y., Schmidt, D. N., Zavialov, P. O., Alheit, J., Aristegui, J., Armstrong, C., Beaugrand, G., Belkovich, V., Bowler, C., Brewer, P., Church, M., Cooley, S. R., del Monte-Luna, P., Edwards, M., Flint, M., Follows, M. J., Frölicher, T., Fulton, E. A., Gattuso, J. P., Hoegh-Guldberg, O., Hofmann, E. E., Knoll, A. H., Levin, L. A., Menzel, L., Moloney, C. L., Perry, R. I.,Poloczanska, E. S., Roberts, J. M., Rost, B., Sarmiento, J. L., Sedlacek, J., Storch, D., Wiencke, C., & Wittmann, A. C. (2014). Ocean systems. In C. Field, V. Barros, D. Dokken, K. Mach, M. Mastrandrea, T. Bilir, M. Chatterjee, K. Ebi, Y. Estrada, R. Genova, B. Girma, E. Kissel, A. Levy, S. MacCracken, P. Mastrandrea, & L. White (Eds.), *Climate Change 2014: Impacts, adaptation, and vulnerability. Part A: Global and sectoral aspects. Contribution of Working Group II to the Fifth Assessment Report of the Intergovernmental Panel on Climate Change*. Cambridge University Press. ISBN: 9781107641655.

Prakash, P., Prakash, S., Rahaman, H., Ravichandran, M., & Nayak, S. (2012). Is the trend in chlorophyll- a in the Arabian Sea decreasing? *Geophysical Research Letters*, *39*(23), n/a-n/a. https://doi.org/10.1029/2012GL054187.

Pujari, L., Wu, C., Kan, J., Li, N., Wang, X., Zhang, G., et al. (2019). Diversity and spatial distribution of chromophytic phytoplankton in the Bay of Bengal revealed by RuBisCO genes (rbcL). *Frontiers in Microbiology, 10*, 1501. https://doi.org/10.3389/fmicb.2019.01501

Rao, S., Dhakate, A., Saha, S., Mahapatra, S., Chaudhari, H., Pokhrel, S., & Sahu, S. (2012). Why is Indian Ocean warming consistently? *Climatic Change, 110*, 709–719. https://doi.org/10.1007/s10584-011-0121-x

Roxy, M. K., Modi, A., Murtugudde, R., Valsala, V., Panickal, S., Prasanna Kumar, S., et al. (2016). A reduction in marine primary productivity driven by rapid warming over the tropical Indian Ocean. *Geophysical Research Letters, 43*(2), 826–833. https://doi.org/10.1002/2015GL066979

Roxy, M. K., Gnanaseelan, C., Parekh, A., Chowdary, J. S., Singh, S., Modi, A., et al. (2020). Indian ocean warming. In *Assessment of climate change over the Indian region* (pp. 191–206). https://doi.org/10.1007/978-981-15-4327-2_10

Roxy, M. K., Dasgupta, P., McPhaden, M. J. et al. (2019) Twofold expansion of the Indo-Pacific warm pool warps the MJO life cycle. *Nature, 575*, 647–651. https://doi.org/10.1038/s41586-019-1764-4

Roxy, M. K., Saranya J. S., A. Modi, Anusree A., Cai, W., Resplandy, L., Vialard, J., Frölicher, T. (2022). Future projections for the tropical Indian Ocean, in The Indian Ocean and its Role in the Global Climate System, Eds. Caroline Ummenhofer and Raleigh Hood, Elsevier, ISBN: 9780128226988 [Revised].

Ryther, J. H., & Menzel, D. W. (1965). On the production, composition, and distribution of organic matter in the Western Arabian Sea. *Deep Sea Research and Oceanographic Abstracts, 12*(2), 199–209. https://doi.org/10.1016/0011-7471(65)90025-2

Sarmiento, J. L., Slater, R., Barber, R., Bopp, L., Doney, S. C., Hirst, A. C., et al. (2004). Response of ocean ecosystems to climate warming. *Global Biogeochemical Cycles, 18*(3). https://doi.org/10.1029/2003GB002134

Sarmiento, J., Gruber, N., & McElroy, M. (2007). Ocean biogeochemical dynamics. *Physics Today, 60*, 65. https://doi.org/10.1063/1.2754608

Sathyendranath, S., Brewin, R. J. W., Brockmann, C., Brotas, V., Calton, B., Chuprin, A., et al. (2019). An ocean-colour time series for use in climate studies: The experience of the ocean-colour climate change initiative (OC-CCI). *Sensors, 19*(19), 4285. https://doi.org/10.3390/s19194285

Schott, F. A., & McCreary, J. P. (2001). The monsoon circulation of the Indian Ocean. *Progress in Oceanography, 51*(1), 1–123. https://doi.org/10.1016/S0079-6611(01)00083-0

Seelanki, V., & Pant, V. (2021). Diversity in the simulation of chlorophyll concentration by CMIP5 Earth System Models over the Indian Ocean. *Marine Geodesy*, 1–18. https://doi.org/10.1080/01490419.2021.1909193

Séférian, R., Berthet, S., Yool, A., Palmiéri, J., Bopp, L., Tagliabue, A., et al. (2020). Tracking improvement in simulated marine biogeochemistry between CMIP5 and CMIP6. *Current Climate Change Reports, 6*(3), 95–119. https://doi.org/10.1007/s40641-020-00160-0

Shetye, S. S., Sudhakar, M., Mohan, R., & Jena, B. (2014). Contrasting productivity and redox potential in Arabian Sea and Bay of Bengal. *Journal of Earth Science, 25*(2), 366–370. https://doi.org/10.1007/s12583-014-0415-9

Signorini, S. R., & McClain, C. R. (2012). Subtropical gyre variability as seen from satellites. *Remote Sensing Letters, 3*(6), 471–479. https://doi.org/10.1080/01431161.2011.625053

Smetacek, V. (1999). Diatoms and the ocean carbon cycle. *Protist, 150*(1), 25–32. https://doi.org/10.1016/S1434-4610(99)70006-4

Solanki, H., Raman, M., Kumari, B., Dwivedi, R. M., & Narain, A. (1998). Seasonal trends in the fishery resources off Gujarat: Salient observation using NOAA AVHRR. *Indian Journal of Marine Sciences, 27*, 438–442.

Steinacher, M., Joos, F., Frölicher, T. L., Bopp, L., Cadule, P., Cocco, V., et al. (2010). Projected 21st century decrease in marine productivity: A multi-model analysis. *Biogeosciences, 7*(3), 979–1005. https://doi.org/10.5194/bg-7-979-2010

Tagliabue, A., Kwiatkowski, L., Bopp, L., Butenschön, M., Cheung, W., Lengaigne, M., & Vialard, J. (2021). Persistent uncertainties in ocean net primary production climate change projections at regional scales raise challenges for assessing impacts on ecosystem services. *Frontiers in Climate, 3*. Retrieved from https://www.frontiersin.org/articles/10.3389/fclim.2021.738224

The Indian Ocean and Its Role in the Global Climate System – 1st Edition. (n.d.). Retrieved 30 June 2022, from https://www.elsevier.com/books/the-indian-ocean-and-its-role-in-the-global-climate-system/ummenhofer/978-0-12-822698-8

Tréguer, P., & Pondaven, P. (2000). Silica control of carbon dioxide. *Nature, 406*(6794), 358–359. https://doi.org/10.1038/35019236

Webster, P., Gulledge, J., & Curry, J. (2006). *Expanding tropical warm pool: Increased tropical cyclone season length and storm duration*. American Geophysical Union, Fall Meeting 2006, abstract #U51C-05.

Werdell, P. J., Bailey, S. W., Franz, B. A., Harding, L. W., Feldman, G. C., & McClain, C. R. (2009). Regional and seasonal variability of chlorophyll-a in Chesapeake Bay as observed by SeaWiFS and MODIS-Aqua. *Remote Sensing of Environment, 113*(6), 1319–1330. https://doi.org/10.1016/j.rse.2009.02.012

Wernand, M., & Woerd, H. (2010). Spectral analysis of the Forel-Ule Ocean colour comparator scale. *Journal of the European Optical Society-Rapid Publications, 5*, 10014s. https://doi.org/10.2971/jeos.2010.10014s

Wernand, M. R., van der Woerd, H. J., & Gieskes, W. W. C. (2013). Trends in ocean colour and chlorophyll concentration from 1889 to 2000, worldwide. *PLoS One, 8*(6), e63766. https://doi.org/10.1371/journal.pone.0063766

Whitt, D. B., & Jansen, M. F. (2020). Slower nutrient stream suppresses Subarctic Atlantic Ocean biological productivity in global warming. *Proceedings of the National Academy of Sciences, 117*(27), 15504–15510. https://doi.org/10.1073/pnas.2000851117

Wiggert, J. D., Hood, R. R., Banse, K., & Kindle, J. C. (2005). Monsoon-driven biogeochemical processes in the Arabian Sea. *Progress in Oceanography, 65*(2–4), 176–213. https://doi.org/10.1016/J.POCEAN.2005.03.008

Chapter 10
Understanding Primary Productivity in the Indian Ocean Using Bio-Optics and Remote Sensing

Surya Prakash Tiwari and Srinivas Kolluru

Abstract Phytoplankton are primary producers in the marine food web and optically sensitive aquatic constituents modulating the light in the euphotic zone. These are microscopic organisms capable of converting inorganic matter into organic matter through photosynthesis. Thus, marine phytoplankton primary production plays a key role in biogeochemical cycles, food web dynamics, and fisheries on regional and global scales. Sensors onboard satellites acquire remote sensing imagery in different wavelengths of the electromagnetic spectrum covering a wide spatial area of the aquatic body. Various empirical, semi-analytical, analytical, and ensemble algorithms are developed to derive optical properties and biogeochemical constituents from remote sensing imagery. This chapter begins with a brief introduction to optical properties and their significance for comprehending ocean productivity. The advances in deriving various physical, optical, and biogeochemical parameters are closely associated with ocean productivity, such as chlorophyll-a, downwelling diffuse attenuation coefficient, phytoplankton absorption coefficient, sea surface temperature, euphotic zone depth, backscattering coefficient, etc., across optically complex aquatic environments of the Indian Ocean are then presented and discussed. The discussion is further extended to understand how productivity models utilize remote sensing-based optical parameters. Finally, the difficulties and constraints associated with deriving the optical parameters from remote sensing and approaches to enhance the productivity models are briefly covered.

Keywords Primary productivity · Phytoplankton · Remote sensing · Bio-optics · Indian Ocean

S. P. Tiwari (✉)
Applied Research Center for Environment and Marine Studies, Research Institute, King Fahd University of Petroleum and Minerals, Dhahran, Saudi Arabia
e-mail: surya.tiwari@kfupm.edu.sa

S. Kolluru
Harbor Branch Oceanographic Institute, Florida Atlantic University, Boca Raton, FL, USA

S. C. Tripathy, A. Singh (eds.), *Dynamics of Planktonic Primary Productivity in the Indian Ocean*, https://doi.org/10.1007/978-3-031-34467-1_10

1 Introduction

Remote sensing of ocean color yields information on the seawater constituents, such as the concentration of phytoplankton pigments, suspended sediments, detritus matter, and colored dissolved organic matter (Kirk, 2011). The methods to detect and monitor seawater constituents from aircraft and spaceborne platforms have been successfully developed in the last four decades. Routine monitoring of the abovementioned oceanic constituents and relevant proxy parameters, such as chlorophyll-a (a proxy for phytoplankton abundance; Huot et al., 2007) at regional and global scales, is necessary to study the biogeochemical cycles, primary production, dynamics, and distribution of the marine mineral particles and suspended sediments (Gordon & Morel, 1983; IOCCG, 2006; Morel & Prieur, 1977).

The Indian Ocean (IO) is one of the most highly productive regions in the world. Due to the presence of different hydrological and biogeochemical regimes, phytoplankton primary productivity (PP) in IO exhibits large spatial variability (Bhattathiri et al., 1996; Gauns et al., 2005; Madhu et al., 2006). PP is defined as the rate of production of organic matter per unit area per unit time (Balch et al., 2021). Although having in situ measurements for quantifying the models' skill is ultimately desired, traditional ship-based in situ measurements are limited in their ability to capture the large-scale spatiotemporal dynamics of marine phytoplankton productivity and are time-consuming and expensive. Satellite ocean color remote sensing can address these shortcomings through their routine observations of the dynamics of the ocean surface, providing fundamental means for estimating marine phytoplankton primary productivity on large spatiotemporal scales. Such observations help in accurately assessing the PP, which quantifies the amount of fixed carbon from photosynthesis processes (Lee et al., 2015a, b).

This chapter initially provides concise information on bio-optics, remote sensing, parameters used in PP models derivable from satellite remote sensing data, widely used PP models, global PP products derived from satellite remote sensing data, and trends and studies of PP conducted in the Indian Ocean with remote sensing data. In the following section of this chapter, light interaction with the atmosphere and the ocean as well as optical properties are presented in detail.

1.1 Light Interaction with Atmosphere and Ocean and Remote Sensing

When electromagnetic radiation interacts with the ocean surface, it is reflected, absorbed, scattered, and transmitted. Seawater and its various dissolved and particulate constituents interact with incoming sunlight in different ways (IOCCG, 2006). When the surface is smooth, it gets reflected in the forward direction called specular reflection. When the surface is rough, it is reflected uniformly in all directions, which is referred to as diffused reflection (Mobley, 2008). It may be noted that the surface may appear rough for a particular wavelength region and smooth in another region.

Each feature has a unique spectral signature by which it can be identified. Generally, the ocean color signal, which is reflected and detected by the sensor, is known as ocean color signature. Thus, it plays a vital role in identifying the optically active water constituents based on the amount of light detected by the detector. There are four ways through which information on significant ocean color features are discriminated, namely, spectral, spatial, temporal, and radiometric variations.

1.2 Optical Properties of Ocean Waters

Accurate and synoptic estimates of bio-optical variables (e.g., chlorophyll-a concentration, colored dissolved organic matter (CDOM), and non-algal particulate (NAP) matter) from space are critical for biogeochemical studies (IOCCG, 2006). The connection between the optical properties and biological, geochemical constituents of the natural water and physical environment defines the significant role of optics in oceanographic research. The optical properties of water are conveniently divided into two mutually exclusive classes: inherent and apparent optical properties. Shifrin (1998) stated that the inherent properties define the conditions for the propagation of light in the sea. They provide information on the particles suspended in the water and the organic matter dissolved in it. Apparent properties depend on the properties of the light field in an aquatic medium and inherent optical properties. More information about IOPs can be found in books written by Kirk (2011), Mobley (2004), and Shifrin (1998).

1.2.1 IOPs and AOPs

Inherent optical properties (IOPs) are those properties which are only dependent upon the composition and concentrations of the particulate and dissolved substances and the water itself (Shifrin, 1998). In other words, IOPs are properties of the water and its constituents that are independent of the structure of the ambient light field.

Basically, absorption (a) and scattering (b) are two fundamental IOPs.

The spectral absorption coefficient *a* is defined as the spectral absorbance per unit distance of photon travel in a dielectric medium.

The spectral scattering coefficient *b* is defined as the spectral scatterance per unit distance of photon travel in a dielectric medium.

The spectral beam attenuation coefficient *c* is the sum of the total seawater absorption combined with the rate of the photon losses due to scattering in the water column. For simplicity, it can be defined as $c = a + b$.

Apparent optical properties are those properties that:

1. Depend on the medium (the IOPs) as well as on the geometric (directional) structure of the radiance distribution
2. Display enough regular features and stability to be useful descriptors of a water body

Irradiance Reflectance, *R*

Ocean reflectance (R), the irradiance ratio of upwelling ($E_u(\lambda)$) to downwelling ($E_d(\lambda)$), is an apparent optical property (AOP), which depends not only on seawater constituents but also on the ambient light environment (sky light, cloud, sea surface roughness, sea bottom conditions, etc.) (Gordon & Morel, 1983; Morel & Prieur, 1977). Here, λ is wavelength. However, the reflectance changes primarily with variations in water constituents. Hence, ocean reflectance contains all the essential information concerning the qualitative and quantitative properties of seawater constituents.

$$R(z,\lambda) = \frac{E_u(z,\lambda)}{E_d(z,\lambda)} \tag{10.1}$$

It is a unitless quantity and plays an essential role in describing the in-water optical properties of water. The list of symbols for various parameters with corresponding units are presented in Table 10.1.

Remote Sensing Reflectance, R_{rs}

Remote sensing reflectance is a measure of how much of the downwelling irradiance that occurred onto the water surface in any direction is eventually returned through the water surface into a small solid angle centered on a particular direction (Mobley et al., 2005; O'Reilly et al., 1998). Remote sensing reflectance R_{rs} is defined as the ratio of normalized water-leaving radiance (nL_w) to downwelling irradiance (E_d)

$$R_{rs}(\lambda) = \frac{nL_w(\lambda)}{E_d(\lambda)} \left(\mathrm{sr}^{-1}\right) \tag{10.2}$$

Diffuse Attenuation Coefficient for Downwelling Irradiance, K_d

The diffuse attenuation coefficient for downwelling irradiance, K_d, is an apparent optical property related to light penetration and availability in aquatic ecosystems (Gordon, 1989; Gordon & Clark, 1980). It can also be used to study the clarity and transparency of the water column. The spectral diffuse attenuation coefficient for downwelling irradiance $K_d(\lambda, z)$ can be defined as follows:

$$K_d(\lambda,z) = -\frac{d[\ln E_d(\lambda,z)]}{dz} \left(\mathrm{m}^{-1}\right) \tag{10.3}$$

where $E_d(\lambda, z)$ is the downwelling irradiance at depth z and wavelength λ. K_d varies with the angular distribution of the light field, and as light distribution varies with depth, K_d also varies with depth before reaching an asymptotic value at greater depths (Gordon et al., 1975; Zaneveld, 1989). Owing to the difficulty in collecting accurate and reliable measurements across an infinitesimal range of depths, a general practice is to collect E_d measurements at two depths z_1 and z_2 and calculate K_d according to the following relation. Note that z_1 and z_2 need to be far enough to ensure that reliable change in E_d is observable (Lee et al., 2005a):

Table 10.1 List of symbols and parameters with corresponding units

Symbol	Parameter	Units
a	Total absorption coefficient	m^{-1}
A	Albedo of cloud-surface system	Nondimensional
A_s	Albedo of surface	Nondimensional
a_{ph}	Phytoplankton absorption	m^{-1}
a^*_{ph}	Chlorophyll-normalized phytoplankton-specific absorption coefficient	$m^2 g^{-1}$
a_{dg}	Absorption due to colored dissolved organic matter and non-algal particulate matter	m^{-1}
b_{bp}	Particulate backscattering coefficient	m^{-1}
b_{bps}	Slope of the particulate backscattering	Nondimensional
b	Total scattering coefficient	m^{-1}
c	Beam attenuation coefficient	m^{-1}
C	Carbon biomass	–
Chl	Chlorophyll-a	mg/m^3 or μg/l
D_{irr}	Photoperiod in decimal hours	Hours
E	Incoming solar flux to sea surface	$W\ m^{-2}\ nm^{-1}$
E_{clear}	Solar flux reaching earth surface in a nonreflecting and nonabsorbing cloud/surface system	$W\ m^{-2}\ nm^{-1}$
E_{par}	Incoming solar flux to the sea surface in 400 to 700 nm range	$W\ m^{-2}\ nm^{-1}$
E_u	Upwelling irradiance	$W\ m^{-2}\ nm^{-1}$
E_d	Downwelling irradiance	$W\ m^{-2}\ nm^{-1}$
K_d	Diffuse attenuation coefficient of downwelling irradiance	m^{-1}
λ	Wavelength	nm
μ	Growth rate	–
$\overline{\mu}_d$	Average cosine of E_d	Nondimensional
nL_w	Normalized water-leaving radiance	$W\ m^{-2}\ sr^{-1}\ nm^{-1}$
ϕ	Photosynthetic quantum yield	–
P_B^{opt}	Maximum carbon fixation rate within a water column	$mg\ C\ (mg\ Chl^{-1})h^{-1}$
R	Ocean reflectance	Nondimensional
R_{rs}	Remote sensing reflectance	sr^{-1}
θ_{sza}	Solar Zenith angle	Degrees or radians
θ_v	Viewing angle	Degrees or radians
ϕ_a	Azimuth angle	Degrees or radians
φ	Biomass or chlorophyll normalized photosynthesis rate	–
T, $T_{x\mu m}$	Brightness temperature, T at x μm channel	°C
T_{sfc}	Reference sea surface temperature	°C
z	Depth	m
Z_{eu}	Euphotic zone depth	m

$$\overline{K_{\mathrm{d}}}(z_1 \textit{ to } z_2) = \frac{1}{z_2 - z_1} \ln\left(\frac{E_{\mathrm{d}}(z_1)}{E_{\mathrm{d}}(z_2)}\right) \tag{10.4}$$

The above-mentioned $\overline{K_{\mathrm{d}}}$ is more useful than the K_{d}, as it can be used to calculate E_{d} at different depths. For the rest of the chapter, we use K_{d} for diffuse attenuation of downwelling irradiance instead of $\overline{K_{\mathrm{d}}}$.

1.3 Goals

The goal of this chapter is to provide information on advancements in deriving key biogeochemical and optical parameters used in primary productivity models. Since the focus is ocean color remote sensing, studies using ship-board primary productivity measurements, bio-argo measurements, and inland water studies are not considered and discussed in detail.

2 Materials and Methods

The following subsections briefly describe major methods for deriving the biogeochemical and optical properties from ocean color remote sensing data. The challenges associated with measurements, uncertainties arising in modelling, methods, and limitations will be discussed.

2.1 Processing of Remote Sensing Data

The past and present ocean color sensors launched on various satellites differ in design, calibration, and data produced in terms of instantaneous field of view or spatial resolution, spectral resolution, swath, and temporal resolution (Table 10.2). Spatial resolution is the smallest possible area on the Earth's surface viewed by the sensor. Swath corresponds to the area imaged by the sensor on the Earth's surface. Spectral resolution is the sampling rate and bandwidth in which the sensor collects energy in the electromagnetic spectrum or range of wavelengths in the EM spectrum in which the sensor operates. Temporal resolution is defined as the amount of time required by the sensor/satellite to revisit a location to acquire data (Lillesand et al., 2015). The widely used ocean color remote sensing data for primary productivity models are from Sea-viewing Wide Field-of-view Sensor (SeaWiFS), Moderate Resolution Imaging Spectroradiometer (MODIS), and Visible Infrared Imaging Radiometer Suite (VIIRS).

Table 10.2 Spatial and spectral resolution of remote sensors widely used in primary productivity studies

Sensor/satellite	Parameter	Data availability	Number of spectral channels with range	Spatial resolution and swath
AVHRR (multiple satellites)	SST	1978–[a]	6 in 0.6–12 μm	1.1 km × 1.1 km; ± 1446.58 km
CZCS/Nimbus-7[b]	*Chl-a*	1978–1986	6 in 443–1020 nm	825 m; 1556 km
MODIS/Aqua	*Chl-a*, PAR	2002–[a]	36 in 405–14,385 nm	250/500/1000 m; 2330 km
SeaWiFS/ObrView-2[b]	*Chl-a*, PAR	1997–2010	8 in 402–885 nm	1100 m; 2806 km
VIIRS/Suomi VIIRS/JPSS-1	*Chl-a*	2011–[a] 2017–[a]	22 in 402–11,800 nm	375/750; 3000 km
OCTS/ADEOS[b]	*Chl-a*	1996–1997	12 in 402–12,500 nm	700 m; 1400 km
TMI/TRMM[b]	SST	1997–2015	9 in 10–85 GHz	0.25°; 759 km

AVHRR advanced very-high resolution radiometer, *CZCS* coastal zone color scanner, *JPSS* joint polar satellite system, *OCTS* ocean color and temperature scanner, *ADEOS* advanced earth observing satellite, *TRMM* tropical rainfall measuring mission, *TMI* TRMM microwave imager
[a]Till date
[b]Past sensors

At present, a two-step process is implemented in processing satellite imagery to generate spectral remote-sensing reflectance, which is subsequently used to derive the biogeochemical parameters and IOPs. The first term is called atmospheric correction that converts top-of-the-atmosphere radiance, to exact normalized water-leaving radiance and its equivalent spectral R_{rs} (Gordon, 2021; IOCCG, 2010; Mobley et al., 2016; Wang, 1999). Briefly, atmospheric correction involves calculation of solar radiance scattered by atmospheric molecules and aerosols, Sun and sky radiance reflected by sea surface (sunglint or from white caps), and water-leaving radiance. For a measured water-leaving radiance (L_w), the effect of solar zenith angle, atmospheric attenuation, and Earth-Sun distance are removed in the calculation of $R_{rs}(\theta_v, \phi_{azi})$, where θ_v and ϕ_{azi} correspond to viewing and azimuth angles.

Level 1 radiance products can be atmospherically corrected using "l2gen" tool in National Aeronautical Space Agency's SeaWiFS Data Analysis System (SeaDAS), openly available (NASA SeaDAS). SeaDAS is NASA's software to analyze Earth-viewing satellite data. The default atmospheric correction algorithm implemented in NASA's SeaDAS processing system is an iterative scheme that calculates R_{rs} in near-infrared (NIR) using bio-optical empirical models (Bailey et al., 2010; Mobley et al., 2016). To overcome the limitation of this scheme in turbid waters, short-wave infrared (SWIR) bands present in a few ocean color sensors are used (Bailey et al., 2010; Frouin et al., 2019; Ibrahim et al., 2019; Pahlevan et al., 2017; Wang et al., 2022; Wang & Shi, 2007). A step-by-step implementation of NASA's Ocean Biology and Processing Group (OBPG) to process ocean color data from satellite imagery like MODIS and VIIRS can be found in Mobley et al. (2016). Other

atmospheric correction algorithms used to process ocean color satellite imagery include (1) POLYnomial-based algorithm applied to MERIS (POLYMER) atmospheric correction, a spectral matching method developed to estimate the atmospheric and sunglint contributions. This algorithm uses all the available spectral bands in the visible region and is based on a polynomial to estimate the atmospheric and sunglint reflectance and a water reflectance model (Steinmetz et al., 2011; Waters et al., 2019) (2) ACOLITE (Vanhellemont & Ruddick, 2015, 2016) by Royal Belgian Institute of Natural Sciences (RBINS) originally developed for Landsat-8 satellite's Ocean and land Imaging sensor (OLI). ACOLITE is later adapted to ocean color sensors. ACOLITE assumes that in SWIR bands, 1.6 μm and 2.2 μm, due to extremely high pure-water absorption, the signal in SWIR bands after rayleigh correction is due to aerosol scattering. A simple extrapolation is performed to estimate the aerosol reflectance in visible and near-infrared bands from SWIR bands. ACOLITE provides water-leaving radiance reflectances as output. ACOLITE also provides turbidity, chlorophyll, and other parameters of user interest. Recently, another version of ACOLITE implementing a dark spectrum fitting technique was proposed to mitigate the issues with SWIR-based exponential extrapolation approach (Caballero & Stumpf, 2020; Vanhellemont, 2019). The present state-of-the-art and recent developments pertaining to atmospheric corrections and subroutines can be found in Frouin et al. (2019).

The remote sensing reflectance corrected for atmospheric effects, $R_{rs}(\theta_v, \phi_{azi})$, is still dependent on viewing and azimuth angles. For intercomparison of reflectances acquired from different sensors, R_{rs} need to be converted to a single configuration of geometry. The bidirectional reflectance distribution function (BRDF) describes the relationship between $R_{rs}(\theta_v, \phi_{azi})$ viewed at different geometries and solar zenith angles and R_{rs} at nadir-viewing and sun at zenith geometrical configuration (Morel & Gentili, 1996). At present, NASA implements the BRDF model proposed by Morel et al. (2002) that uses Look-Up-Tables to transform a measurement made at a particular solar zenith angle (SZA), viewing direction, wind speed, atmospheric conditions, and water IOPs to a measurement that corresponds to the sun at zenith and nadir-viewing for a marine atmosphere over Case 1 waters with a chlorophyll value. Apart from the operational BRDF algorithm, other BRDF models were also proposed (Gleason et al., 2012; Lee et al., 2011a, b; Park & Ruddick, 2005; Twardowski & Tonizzo, 2018). A comparative study of Morel's algorithm with Lee's BRDF model (Lee et al., 2011a, b) indicated that Morel's algorithm works better than other models in Case 1 waters and Lee's BRDF model is suggested for Case 2 waters (Gleason et al., 2012; Zhai et al., 2015). Seasonal biases in R_{rs} and subsequently derived ocean color products were identified with incomplete BRDF correction being the possible source of bias (Bisson et al., 2021). Presently, the efforts of the ocean color community is toward generation of accurate BRDF models across various geometries and water types (Tonizzo et al., 2022). Recent advances in the remote sensing data assimilated from multiple satellites lead to generation of Ocean Color Climate Change Initiative (OC-CCI) data (Sect. 2.3).

2.2 Retrieval of Parameters Related to Primary Productivity from Satellite Remote Sensing

Understanding the relationship between the IOP and AOPs, which are dependent on the various oceanic constituents, is critical to carry out the inversion of R_{rs} into IOPs and biogeochemical properties subsequently.

Chlorophyll-a

For decades, *Chl-a* concentration has been derived from empirical ocean color algorithms implementing R_{rs} band ratios in the blue-green region (O'Reilly et al., 1998; O'Reilly & Werdell, 2019). Multiband ratio (MBR) algorithm uses R_{rs} at multiple wavelengths (depending on sensor) in blue-green region and takes the following form (O'Reilly et al., 1998; O'Reilly & Werdell, 2019):

$$\log_{10}(\mathrm{Chl}-a) = a_0 + \sum_{i=1}^{4} a_i \left(\log 10 \left(\max \left(\frac{R_{rs}(\lambda_{blue})}{R_{rs}(\lambda_{green})} \right) \right) \right)^i \tag{10.5}$$

where a_0 to a_4 are sensor-dependent coefficients and $R_{rs}(\lambda_{blue})$ is the maximum of R_{rs} in the blue region, e.g., 443, 490, and 510 nm for OC4 algorithm, and $R_{rs}(\lambda_{green})$ is at single wavelength in 547–565 nm. NASA's operational algorithm to derive *Chl-a* combines the MBR with the Color Index (CI, Hu et al., 2012, 2019) algorithm of the following form

$$\mathrm{CI} = R_{rs}(\lambda_{green}) - \left[R_{rs}(\lambda_{blue}) + \left(\frac{\lambda_{green} - \lambda_{blue}}{\lambda_{red} - \lambda_{blue}} \right) * \left(R_{rs}(\lambda_{red}) - R_{rs}(\lambda_{blue}) \right) \right] \tag{10.6}$$

with λ_{blue}, λ_{green},and λ_{red} close to 443, 555, and 670 nm, respectively. CI algorithm demonstrated higher accuracy in derived *Chl-a* concentrations in oligotrophic waters compared to OCx algorithms. More details about CI and switching between CI and MBR are presented by Hu et al. (2012). For the Indian Space Research Organization's (ISRO) Oceansat-2 Ocean Color Monitor sensor, the tuned MBR-derived *Chl-a* concentrations have higher accuracy compared to previous OCx algorithms (Nagamani et al., 2008). In the case of optically complex waters such as coastal, estuarine, CDOM, and sediment-dominated waters, OC algorithm derived tend to produce *Chl-a* concentrations with higher error; hence, regional algorithms implementing various band combinations of R_{rs} in red-NIR region are developed for more than a decade over different productive waters of the world (Gitelson, 1992; Menon & Adhikari, 2018; Moses et al., 2019). Advancements in the estimation of *Chl-a* from simple to more advanced machine learning models in both open ocean and optically complex waters (Hu et al., 2020; Ioannou et al., 2013; Pahlevan et al., 2021, 2022) have also been carried out. Few studies concentrating on *Chl-a* algorithms from either a single or combination of ocean color sensors like SeaWiFS, MODIS, MERIS, VIIRS, Ocean and Land Color Imager (OLCI)/Sentinel-3, and Geostationary Ocean Color Imager (GOCI) and from high-resolution sensors like

Multispectral Instrument (MSI)/Sentinel-2 and OLI/Landsat-8 (Smith et al., 2021). Previous studies focusing on using *Chl-a* products from ocean color sensors used global monthly 4 km or 9 km datasets; more recently, OC-CCI datasets generated from the use of multiple sensors have been used (Roxy et al., 2016).

Diffuse Attenuation Coefficient (K_d)

Currently, K_d products for various sensors are generated at 490 nm wavelength using a fourth-order polynomial similar to *Chl-a*. Instead of an MBR-type ratio, the K_d algorithm is generated using a ratio of two R_{rs} bands in blue-green region (O'Reilly et al., 2000a; Werdell & Bailey, 2005; Zhang & Fell, 2007). For ISRO's Ocean Color Monitor, K_d algorithm is derived based on ratio of normalized water-leaving radiance (Chauhan et al., 2003). Two-step algorithms (Morel & Loisel, 1998; Morel & Maritorena, 2001) used K_d versus *Chl-a* relationships to calculate K_d at any wavelength using empirical equation. The *Chl-a* required as input for these two-step algorithms are derived using OCx empirical relation. Based on the optical properties of oceanic constituents, Gordon (1989) proposed a K_d algorithm using the bulk IOPs, a and b_b and $\overline{\mu}_d$, the average cosine of E_d dependent on solar elevation, λ, and *Chl-a* (Morel et al., 2007a, b). A semi-analytical model based on a radiative transfer equation with model parameters derived from hydrolight resulted in lower errors for K_d at 490 nm from R_{rs} (Lee et al., 2005b). This semi-analytical model uses bulk IOPs, derived from R_{rs} using quasi-analytical algorithm (QAA, Lee et al., 2002) as inputs to derive K_d. Spectral K_d models (Austin & Petzold, 1986) generating K_d at specified wavelength (based on $K_d(490)$) are used in updated carbon-based net primary productivity (NPP) models (Westberry et al., 2008). An improvement to this, Lee's semi-analytical algorithm included derivation of spectral K_d along with changes in phase function in different wavelength range (Lee et al., 2013). Apart from empirical and semi-analytical models, spectral K_d in open and coastal waters from R_{rs} is derived using a neural network machine learning model (Jamet et al., 2012).

PAR

Photosynthetically available radiation (PAR, Einstein m^{-2} day^{-1}) is one of the inputs used in marine primary productivity models and is defined as the available solar quantum energy flux in 400–700 nm at the ocean surface. The generally used PAR product in PP models is the PAR reaching the Earth's surface over 24-hour period and is different from instantaneous PAR (Frouin et al., 2002, 2012; Frouin & Pinker, 1995). PAR algorithm implements a plane parallel theory and assumes that clouds and clear atmosphere can be decoupled. Surface PAR is the product of the clear-sky component (modelled as positioned above cloud layer) and cloud transmittance. As the PAR algorithm models the atmosphere into layers, clouds and clear regions in satellite pixels need not be carried out. Briefly, the solar flux reaching the ocean surface is computed as

$$E = \frac{E_{clear}(1-A)}{(1-A_s)} \tag{10.7}$$

where A_s and A correspond to the albedo of the surface and cloud-surface system. Albedo or reflectivity of a surface is defined as the ratio of radiative flux reflected by the surface to the incident radiative flux (Hooker et al., 2003). E_{clear} is the solar flux that would reach the ocean surface in a nonreflecting and nonabsorbing cloud/surface system. A is expressed as a function of radiance measured by the sensor in the PAR spectral range (Frouin et al., 2012). The root-mean-square differences for weekly and monthly PAR estimates for SeaWiFS and MODIS sensors are in the range of 2.85–3.30 Einstein m^{-2} day^{-1}. A detailed description of the PAR algorithm implemented in NASA's processing chain is described in Frouin et al. (2002, 2012), Frouin and Pinker (1995), and Hooker et al. (2003) (Fig. 10.1).

Euphotic Zone Depth

Euphotic zone depth (Z_{eu}) is the depth where PAR is 1% of the PAR at the ocean surface and is a measure of water clarity. Z_{eu} is also derived from the *Chl-a* concentration, which itself is derived from an empirical OC4 type algorithm using band ratio of R_{rs} in blue-green region. Empirical approach involving the calculation of Z_{eu} directly based on $K_d(490)$ was also developed for specific regions and specific temporal scales by Mueller and Lange (1989). Owing to the similarity between the vertical distribution of E_d to PAR, analytical algorithm to estimate Z_{eu} from bulk IOPs was developed (Lee et al., 2007).

Backscattering Coefficient and Phytoplankton Absorption Coefficient

Particulate backscattering coefficient $b_{bp}(\lambda)$ and phytoplankton absorption coefficient $a_{ph}(\lambda)$ are subcomponent of IOPs, derivable from R_{rs} either through empirical or semi-analytical methods (IOCCG, 2006). A plethora of models exist to derive $b_{bp}(\lambda)$ and $a_{ph}(\lambda)$ from $R_{rs}(\lambda)$ using empirical or semi-analytical methods. The inversion algorithms involve the use of semi-analytical model involving spectral shape models for the subcomponent IOPs to generate bulk IOPs and relate to R_{rs}. Briefly, various solution methods use one of the following methods: nonlinear spectral optimization methods, linear inversion, spectral deconvolution, stepwise algebraic, ensemble inversion, and hybrid inversion methods (Boss & Roesler, 2006; Brando et al., 2012; Kolluru et al., 2021; Lee et al., 2002; Loisel et al., 2018; Maritorena et al., 2002; Roesler & Perry, 1995; Werdell et al., 2013). A summary of various semi-analytical methods implementing different methodologies is presented by Werdell et al. (2018). In the inversion algorithms (except bulk inversion), $b_{bp}(\lambda)$ is expressed as a power-law model with the slope value (b_{bps}) specified as a constant, varied dynamically. Few studies proposed b_{bp} models using in situ ancillary data *Chl-a* or based on beam-attenuation coefficient and particulate absorption coefficients (Ciotti et al., 1999; Gordon et al., 1988; Lee et al., 2002; Morel & Antoine, 2011; Morel & Maritorena, 2001; Roesler & Boss, 2003). In the case of $a_{ph}(\lambda)$, single-shape models or models involving multiple shapes are used to model $a^*_{ph}(\lambda)$, the phytoplankton specific-absorption coefficient (Bricaud et al., 1995; Ciotti et al., 2002; Roesler & Perry, 1995; Uitz et al., 2008). In some cases, the inversion models provide *Chl-a* as a product, whereas in some models, $a_{ph}(\lambda)$ is directly provided as the product. In case of phytoplankton absorption-based models (Marra

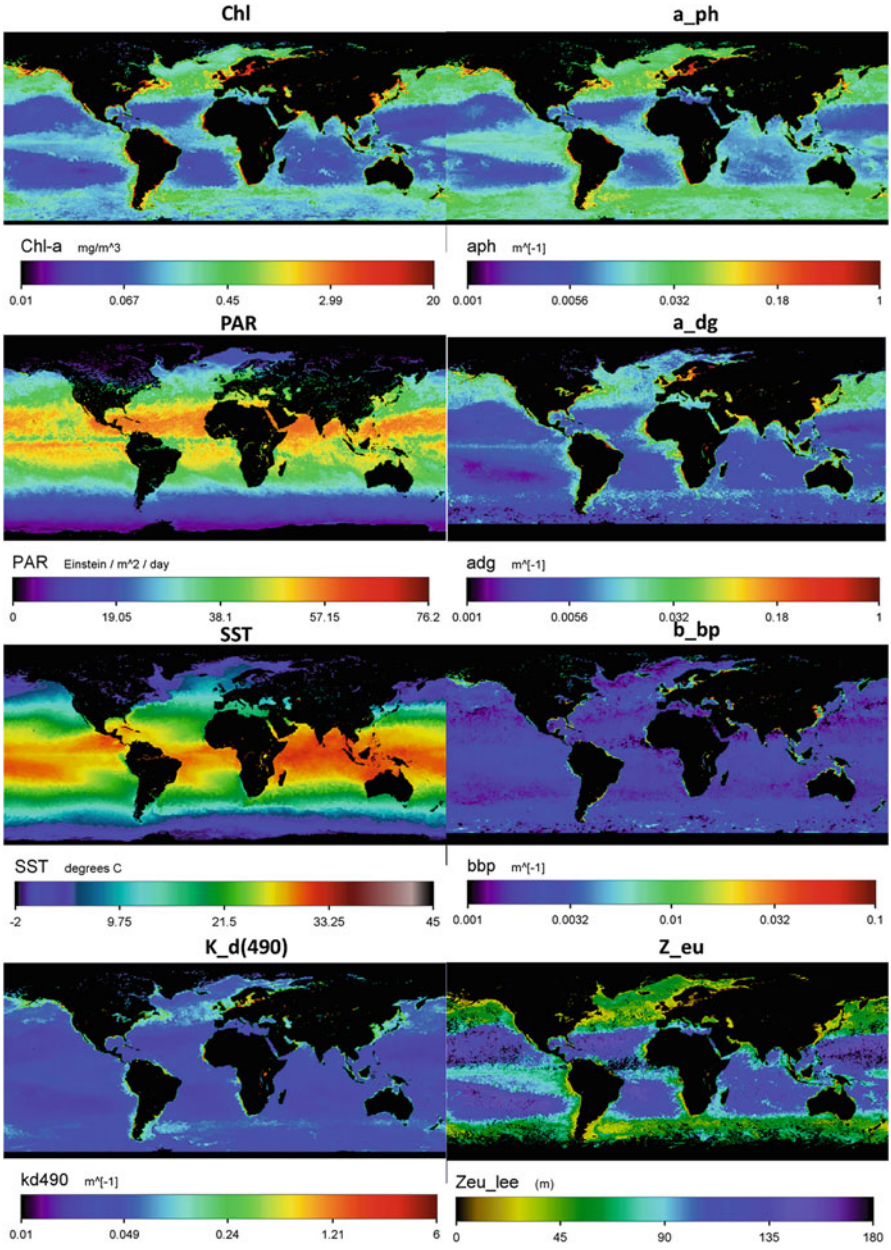

Fig. 10.1 Ocean parameters derivable from remote sensing data in connection with existing PP models. Chl is derived using OCI algorithm using R_{rs} in the visible region, IOPs (a_{ph}, a_{dg}, b_{bp}) are derived using R_{rs} in visible region with generalized inherent optical property (GIOP) algorithm, SST using brightness temperature channels with SST4 algorithm, Z_{eu} using Lee's euphotic zone depth algorithm (Lee et al., 2007), K_d490 using Lee's Kd algorithm (Lee et al., 2005b), PAR from Frouin's algorithm (Frouin et al., 2002, 2012)

et al., 2003), $a^*_{ph}(\lambda)$ is used as input to derive spectrally averaged absorption coefficient in visible range (400–700 nm). Semi-analytical algorithms like GIOP also provide a_{dg}, combined absorption due to NAP and CDOM, and *Chl-a, a*, and b_b as outputs along with a_{ph} and b_{bp}.

Sea Surface Temperature

The SST products (°C) will be generated with mid- and long-wave infrared bands. The Group for High-Resolution Sea Surface Temperature (GHRSST) defines different temperature products owing to the complexity of its measurement in the upper ocean. SST varies widely and dynamically in the upper ocean both horizontally and vertically and changes with ocean turbulence, air-sea heat fluxes, and moisture. In the upper ~10 m of the ocean, GHRSST provides the definition of the following SST products, interface, sea surface skin, sea surface sub-skin, sea water temperature at a depth, and sea surface foundation temperature. The SST triple algorithm was developed for NOAA's polar-orbiting AVHRR satellite to generate night-time NOAA AVHRR SST product (Walton et al., 1998).

$$\mathrm{SST}_{\mathrm{triple}} = a_{ij0} + a_{ij1} T_{11\ \mu\mathrm{m}} + a_{ij2}\left(T_{3.7\ \mu\mathrm{m}} - T_{12\ \mu\mathrm{m}}\right) T_{\mathrm{sfc}} + a_{ij3}\left(\sec(\theta_{\mathrm{sza}}) - 1\right) + a_{ij} \tag{10.8}$$

where $a_{ij0\ -\ 3}$ are algorithm coefficients set for the month of year and latitude ij, θ_{sza} is solar zenith angle, T_{sfc} is reference SST, and $T_{3.7,\ 11,\ 12}$ correspond to brightness temperature channels at 3.7, 11, and 12 μm, respectively. The empirical coefficients are determined by continuous match-ups between satellite measurements and in situ measurements of SST. For MODIS, the SST4 algorithm utilizing the 3.9 and 4 μm spectral bands is used for the SST product. MODIS was the first and only sensor to date to use SWIR channels solely to determine SST.

$$\begin{aligned}\mathrm{SST4} = {} & a_{ij0} + a_{ij1} * T_{3.9\ \mu\mathrm{m}} + a_{ij2}\left(T_{3.9\ \mu\mathrm{m}} - T_{4.0\ \mu\mathrm{m}}\right) + a_{ij3}\left(\sec\theta_{\mathrm{sza}} - 1\right) \\ & + a_{ij4}(\mathrm{mirror}) + a_{ij5}\left(\theta^*_{\mathrm{sza}}\right) + a_{ij6}\left(\theta^2_{\mathrm{sza}}\right)\end{aligned} \tag{10.9}$$

where mirror corresponds to mirror side number (0 or 1), θ^*_{sza} is SZA made negative for pixels in the first half of the scan line, and $T_{3.9,\ 4\ \mu\mathrm{m}}$ correspond to brightness temperature at 3.959 and 4.050 μm, in °C, respectively. The latest version of MODIS SST product, i.e., R2019, uses a cloud mask generated based on cloud classification algorithm implementing (ADtree). The SST products correspond to the skin temperature of the ocean ~1 mm thick surface thermal skin layer (Donlon et al., 2002; Hanafin, 2002; Minnett, 2010; Minnett & Corlett, 2012; Vincent et al., 2008; Walton et al., 1998; Wong & Minnett, 2016, 2018). The SST products are skin temperatures as the radiance measured by infrared radiometers originates from the surface thermal skin layer of the ocean and not from the body of water below as measured by in situ thermometers (Donlon et al., 2007).

Phytoplankton Size Classes (PSC)
Models to infer phytoplankton size classes from remote sensing data can be broadly categorized into radiance, abundance, and absorption-based approaches. PSC algorithms are categorized as a subgroup under phytoplankton functional type algorithms (Mouw et al., 2017). PSC output is generally categorized into pico (0.2–2 μm), nano (2–20 μm), and micro (>20 μm), a size classification proposed by Sieburth (1978). The PSC algorithms fall into abundance-based (Brewin et al., 2011; Uitz et al., 2006), radiance-based (Li et al., 2013), and absorption-based approaches (Bricaud et al., 2012; Ciotti & Bricaud, 2006; Devred et al., 2011; Fujiwara et al., 2011; Hirata et al., 2008; Mouw & Yoder, 2010; Roy et al., 2013). The approaches based on chlorophyll, absorption, and pigment abundance are dependent on $R_{rs}(\lambda)$ and the accuracy of the semi-analytical and empirical models used to derive relevant parameters such as Chl. On the other hand, few algorithms utilize top of the atmosphere satellite reflectance as input such as Phytoplankton Differential Optical Absorption Spectroscopy (PhytoDOAS) (Bracher et al., 2009; Sadeghi et al., 2012).

2.3 Merged Satellite Data Products

The OC-CCI project started in 2010 in ESA's Climate Change Initiative program to generate a set of validated, error-characterized Essential Climate Variables (ECVs) from satellite observations. The latest version of OC-CCI data v5.0 dataset (and previous versions) provides ocean color ECV data focused on case 1 waters, to be used for climate change prediction and assessment models (Sathyendranath et al., 2019, 2021). The OC-CCI v5.0 database provides the ocean color variables at daily, weekly, monthly, and climatology timescales from 1997 to 2020 at 4 km resolution. OC-CCI v5.0 is created by bias-correcting and band-shifting data of SeaWiFS, MODIS, VIIRS, and OLCI sensors to match wavelengths of MERIS data along with uncertainty estimates for each pixel. The merged R_{rs} data along with uncertainty estimates (from in situ and satellite matchups) are used to derive the ocean color variables. The input datasets used are MERIS L1b 3rd reprocessing, MODIS and VIIRS level 1 R2018.0, SeaWiFS level 2 LAC, and GAC R2018.0 and OLCI 3A. The level 1 data from MODIS, VIIRS, MERIS, and OLCI are processed with POLYMER algorithm (v4.1, Steinmetz et al., 2011) to level 2. SeaWiFS level 2 data from NASA processed with l2gen of SeaDAS are used. Data from all satellites are binned to a sinusoidal grid with 4 km spatial resolution. Finally, the individual sensor data, after bias correction and band shifting, are merged using a simple average. The variables present in OC-CCI v5.0 dataset are remote sensing reflectances, a, a_{dg}, and b_{bp} at 412, 443, 490, 510, 560, and 665 nm, Chl, $K_d(490)$, and 15 water classes. A water class membership is assigned to each R_{rs} based on water classes computed using fuzzy logic approach by Moore et al. (2009). For generating Chl, a blended merge of OCI, OCI2, and OCx algorithms (Hu et al., 2012; O'Reilly et al., 2000b; O'Reilly & Werdell, 2019), with weights calculated by the relative levels of membership from specific water classes. The IOP products are generated

using QAA (Lee et al., 2002). K_d is generated using Lee's algorithm (Lee et al., 2005b). Finally, level 3 binned products are generated by accumulating L2 products of a specific sensor onto a well-defined spatial grid for a specified time period. L3 products are stored in global, equal-area grid, with standard sizes of 4 km or 9 km. A detailed description of the procedure for binning, summary, specifications corresponding to spatial and temporal resolutions, day definition, flag criteria, quality levels, etc. are specified in Campbell et al. (1995), Hooker et al. (1995), and (NASA ATBD level-3 Binned Data Products, n.d.)

2.4 Primary Productivity Models

The widely used NPP models and the parameters used as inputs are presented in Table 10.3. The PP models are grouped based on depth resolved (DR) and/or depth integrated (DI), wavelength resolved (WR) and/or wavelength integrated (WI), and time integrated (TI) (Behrenfeld & Falkowski, 1997a, b; Everett & Doblin, 2015), and the complexity increases from simple DI & WI to DI & WR to complex DR & WR models. WR models calculate PP at discrete depths, with light energy illuminating the water body expressed as a function of wavelength. WR models are the most fully expanded productive models that convert the spectral E_d into net photosynthesis utilizing a suite of empirical relations. WI models remove the wavelength dependence and uses PAR, i.e., light energy integrated across wavelengths. TI models removes the time-dependent resolution in solar irradiance. Finally, DI

Table 10.3 A subset of existing optical models and modelling of primary productivity

Model	Parameters used	References
VGPM and Eppley-VGPM (Chlorophyll based)	*Chl-a*, SST, PAR, Z_{eu}	Antoine and Morel (1996), Behrenfeld and Falkowski (1997a, b), Eppley (1972), and Saba et al. (2011)
Carbon-based model	b_{bp}, PAR, $K_d(490)$, Chl, MLD	Behrenfeld et al. (2005) and Westberry et al. (2008)
Phytoplankton absorption-based model (Southern Ocean)	a_{ph}, SST, *Chl-a*, PAR, Z_{eu}	Hirawake et al. (2011), Lee et al. (2011a, b) and Marra et al. (2007)
Phytoplankton class-specific primary productivity model (can be grouped into phytoplankton absorption based model)	a_{ph}, Z_{eu}, PAR, K_d, *Chl-a*, SST, size types	Tao et al. (2017)
CAFÉ (carbon, absorption, and fluorescence euphotic-resolving)	*Chl-a*, PAR, SST, a_{dg}, a_{ph}, b_{bp}, MLD, bbp_s	Silsbe et al. (2016)
Machine learning-based approaches		Li et al. (2022) and Tang et al. (2008)

Most of the existing NPP models with depth integration, depth-resolved, wavelength-integrated, and wavelength-resolved types are compared in Table 10.2 of Saba et al. (2011)

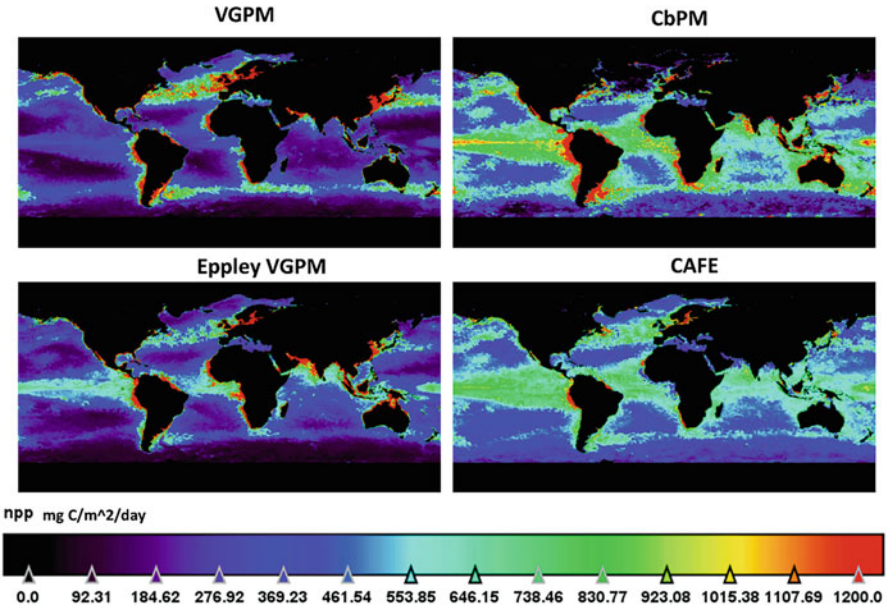

Fig. 10.2 Primary productivity estimates from VGPM, Eppley VGPM, CbPM, and CAFÉ models. (Source: Ocean Productivity: Template (oregonstate.edu) for April 2020)

models lack description of vertically resolved components of the TI, WI, and WR models (Behrenfeld & Falkowski, 1997a, b). The existing PP models can also be divided into four broad categories: (a) Chl-based models, (b) carbon-based models, (c) phytoplankton-absorption-based models, and (d) combined absorption and carbon-based models and hybrid models combining physics-based models and machine learning. A few examples of the PP models falling into the five categories, along with the parameters used as input, are provided in Table 10.3. A variation of the above five broad categories were also proposed and evaluated in many comparison studies (Saba et al., 2011). A visual comparison of the PP derived from four PP models, Vertically Generalized Production Model (VGPM), Eppley's VGPM, carbon-based productivity model (CbPM), and carbon, absorption, and fluorescence euphotic-resolving (CAFÉ) model, indicates the contrasting PP values in many regions (Fig. 10.2). These global PP estimates are derived from various ocean color satellite sensor data (described in the next section).

2.4.1 Chlorophyll-Based Models

Primary productivity quantifies the carbon fixed by phytoplankton from photosynthesis, which represents a transfer of energy from absorbed photons to fixed organic carbon. Chlorophyll, an omnipresent pigment in almost all the phytoplankton species, plays a crucial role in photosynthesis, and hence, a conceptual PP model

(Behrenfeld & Falkowski, 1997a, b; Eppley et al., 1985; Platt & Sathyendranath, 1988) is described as follows:

$$\mathrm{PP} = \phi * a^{*}_{\mathrm{ph}} * \mathrm{Chl} * E_{\mathrm{par}} \tag{10.10}$$

where the E_{par} is the available photon energy representing photosynthetically available radiation, PAR, in 400–700 nm range in quanta/m^2. The photon energy absorbed by phytoplankton is obtained as a product of a^{*}_{ph}, Chl, and E_{par}. Photosynthetic quantum yield, ϕ, indicates the efficiency of the phytoplankton to convert the absorbed photon energy into organic carbon. The light entering below the sea surface changes with depth and wavelength; hence, the impact of depth and wavelength must be included in the PP model. Based on these considerations, a generalized chlorophyll-based model (Behrenfeld & Falkowski, 1997a, b; Platt & Sathyendranath, 1988) is developed and expressed as

$$\mathrm{PP}(z) = \int \varphi(z) * \mathrm{Chl}(z) * E(\lambda, z) d\lambda \tag{10.11}$$

where PP(z) represents primary productivity at depth z, and integration of PP(z) over depth results in photosynthesis of the whole water column. φ is the biomass-normalized or chlorophyll-normalized photosynthesis rate, calculated as the product of ϕ and a^{*}_{ph}. The light propagation in the water column is expressed as

$$E(\lambda, z) = E(\lambda, 0) e^{-K_{\mathrm{d}}(\lambda) * z} \tag{10.12}$$

where $E(\lambda, 0)$ and $E(\lambda, z)$ correspond to spectral light energy at surface and depth z. The VGPM (Behrenfeld & Falkowski, 1997a, b) is a depth-integrated and wavelength-integrated-type chlorophyll-based model expressing photosynthetic rate in terms of PAR and water depth. The water column integrated primary productivity in the euphotic zone by the VGPM model is calculated as

$$\mathrm{PP}_{\mathrm{eu}} = 0.66125 * P^{B}_{\mathrm{opt}} * \left(\frac{E_0}{E_0 + 4.1} \right) * Z_{\mathrm{eu}} * \mathrm{Chla} * D_{\mathrm{irr}} \tag{10.13}$$

With D_{irr}, the photoperiod in decimal hours, E_0 is surface irradiance, and P^{opt}_{B} is the maximum carbon fixation rate within a water column in mg C (mg Chl^{-1})h^{-1}. P^{opt}_{B} is calculated using a 7th-order polynomial of sea surface temperature (SST) for a range of −1 to 29 °C (Behrenfeld & Falkowski, 1997a, b). Eppley's VGPM model is the same as VGPM model except; P^{opt}_{B} is calculated using the following exponential function (Eppley et al., 1985):

$$P^{\mathrm{opt}}_{B} = 1.54 * 10^{0.0275 * \mathrm{SST} - 0.07} \tag{10.14}$$

Some variations of the VGPM model were formulated and compared with other NPP models in Saba et al. (2011); for example, a version of the VGPM model uses the euphotic zone depth estimated using the equations proposed by Morel and Maritorena (2001). The chlorophyll-based PP model has been widely used to estimate PP for more than two decades (Behrenfeld & Falkowski, 1997a, b; Dalpadado et al., 2021; Friedrichs et al., 2009; Kerkar et al., 2020; Kulk et al., 2020; Kumari et al., 2021; Li et al., 2020; Saba et al., 2010, 2011).

2.4.2 Carbon-Based Models

Carbon-based models are developed as a simple proxy of phytoplankton, i.e., Chl does not completely account for changes in phytoplankton species, growth irradiance, nutrient status, light acclimation, photoacclimation, etc. (Behrenfeld et al., 2005; Westberry et al., 2008). The carbon-based model uses phytoplankton carbon biomass (C) that has a tight relationship to algal stocks and is related to NPP, which is the rate of carbon fixed by phytoplankton. The total particulate organic carbon (POC) in the ocean is known to exhibit a tight relationship with the particulate backscattering coefficient (b_{bp}), which is derivable from R_{rs} (Evers-King et al., 2017; IOCCG, 2006; Loisel et al., 2001; Maritorena et al., 2002; Stramski et al., 1999, 2004; Werdell et al., 2013, 2018). Based on this relationship, the PP through C-based model is estimated as

$$\mathrm{PP}_{eu} = C * \mu * Z_{eu} * f(E) \tag{10.15}$$

where μ is the growth rate, and $f(E)$ is the light-adjusted physiology parameter (Behrenfeld et al., 2005).

Initial equations relating the phytoplankton absorption to primary productivity at a depth z of the following form were proposed by Bannister (1974), Kiefer and Mitchell (1983), and Lee et al. (1996)

$$\mathrm{PP}(z) = \phi * a_{ph} * E(z) \tag{10.16}$$

The above equation is modified to accommodate *Chl-a*, as it was measured in previous experiments and $E(z)$ is replaced with $E_{par}(z)$ as

$$\mathrm{PP}(z) = \phi * a^{*}_{ph} * \mathrm{Chla} * E_{par}(z) \tag{10.17}$$

2.4.3 Phytoplankton Absorption-Based Models

In subsequent years, phytoplankton absorption ($a_{ph}(\lambda)$) was found to be highly correlated to primary productivity in initial test studies (Marra et al., 2007), leading

to the development of phytoplankton absorption-based primary productivity models, hereafter referred to as AbPM (Hirawake et al., 2011; Lee et al., 2011a, b) to estimate PP. The AbPM estimates NPP using the following form (Lee et al., 2015a, b)

$$\mathrm{NPP}(z) = \int \phi(z) * a_{\mathrm{ph}}(\lambda, z) * E(\lambda, z) d\lambda \tag{10.18}$$

A model of the above form eliminates the need for using Chl concentration, which is reported to contain high errors in optically complex waters. Further, AbPM uses $a_{\mathrm{ph}}(\lambda)$ that is derivable from R_{rs} using algorithms developed over the past couple of decades (Kolluru et al., 2021; Lee et al., 2002; Loisel et al., 2018; Loisel & Stramski, 2000; Maritorena et al., 2002; Werdell et al., 2013, 2018). The AbPMs are sensitive to seasonal variations, especially in the Southern Ocean, leading to an overestimation of NPP (Ma et al., 2014). As ϕ is known to vary with available light and nutrients and with phytoplankton of different sizes, the AbPM was extended to include phytoplankton size class (PSC) specific ϕ in estimation of NPP (Tao et al., 2017), leading to the development of Phytoplankton Class-Specific Marine Primary Productivity model, hereafter referred to as PCSMPP. The PCSMPP model uses a three-component model of PSC (Brewin et al., 2010) to obtain fractional contributions of nano-, pico-, and micro-plankton from the total *Chl-a*. Then, ϕ_{maximum} for different PSCs is calculated according to methodology provided in Uitz et al. (2008). The PCSMPP model uses the same equations as in AbPM for each size class and adds them to obtain total NPP. Over different sites (including Southern Ocean) exhibiting varying optical properties, NPP estimates from PCSMPP model are better than AbPM (Tao et al., 2017). As PCSMPP also uses *Chl-a* that exhibits higher errors in coastal waters, the derived PSCs might also contain error, and hence, the performance of this model requires further validation and studies in different optically complex waters.

2.4.4 Hybrid and Combined Models

More recently, a new NPP model called CAFÉ (Silsbe et al., 2016) was developed with an aim to utilize global ocean color observations and address physiological and ecological phytoplankton attributes. CAFÉ model combines the fundamental definitions of absorption and chlorophyll-based models. In comparison with three other existing widely used NPP models, CAFÉ model explained the greatest variance in NPP with a low bias for direct field measurements. Finally, machine learning models like support vector machines and enhanced random forest regression to estimate NPP either directly or derive parameters incorporated in other NPP models (Li et al., 2022; Tang et al., 2008).

2.5 Global Scale Primary Productivity Products from Remote Sensing Data

Currently, most studies using ocean color remote sensing-derived products use level-3 data at either 4 km or 9 km resolution with 8-day or monthly products. Net primary productivity products (level 4) from VGPM, Eppley-VPGM, CbPM (standard and updated), CAFÉ for MODIS, SeaWiFS, and VIIRS (based on applicability) are readily available at different time spans (8 days and monthly) and grid sizes (Ocean Productivity – Oregon State University, 2022). A summary of a few studies conducted either in the entire Indian Ocean or parts along with the satellite data used is presented in Table 10.4. It can be observed that for the past couple of decades, satellite data from SeaWiFS, MODIS, VIIRS, AVHRR, and OCTS were used to infer various physical processes in the Indian Ocean.

3 Results and Discussions

3.1 Trends and Rates of Satellite Remote Sensing-Based PP in the Indian Ocean

Based on CZCS climatological data between 1978 and 1986, Longhurst et al. (1995) estimated PP at a global scale. The estimated mean daily and mean annual PP rates from Longhurst's study for the Indian Ocean were 0.4 g C m^{-2} day^{-1} and 6.5 Gt C $year^{-1}$. Similarly, for the monsoon biogeochemical province in the Indian Ocean (comprising mostly Arabian Sea, Bay of Bengal, and Equatorial Indian Ocean), the estimated rates were 0.29 g C m^{-2} day^{-1} and 1.49 Gt C $year^{-1}$, respectively (Longhurst et al., 1995). Utilizing the same CZCS data, Antoine et al. (1996) estimated PP using Antoine and Morel (1996)'s method at a monthly time scale. Antoine's analysis indicated that the northeastern Indian Ocean was the most extended high productive region during the summer monsoon, as well as the most productive one relative to its area. Monthly integrated PP values decreased from January to April, were consistent between April and June, and increased from June to August and decreased toward the end of the year. The estimated PP rate for the Indian Ocean using CZCS from Antoine's study was 6.57 Gt C $year^{-1}$ (18% of total global ocean PP), similar to the values reported in Longhurst's study. Behrenfeld and Falkowski (1997a, b) introduced the VGPM model and calculated PP globally using monthly climatological CZCS data. VGPM model estimated PP rate for the Indian Ocean is 6.2 Pg C $year^{-1}$ (i.e., petagrams C $year^{-1}$ = Gt C $year^{-1}$), similar to the values reported in previous studies. The third primary productivity round-robin algorithm (PPARR3) comparison involved 31 primary productivity algorithms by Carr et al. (2006) to estimate PP at 1% light level. Most of the algorithms in PPARR3 study used SeaWiFS monthly Chlorophyll, AVHRR Pathfinder SST, and PAR from SeaWiFS data and resulted in a model mean of 9.9 Gt C $year^{-1}$ (mean of all models).

Table 10.4 Few studies utilizing satellite remote sensing data to study trends in Chl-a, SST, PAR, and NPP

Study	Time span	Parameters	Source	PP model	Region
Wiggert et al. (2002)	1997–2000	*Chl-a*	SeaWiFS	–	Arabian Sea
Goes et al. (2005)	1997–2004	*Chl-a* SST	ADEOS-1/ OCTS AVHRR	–	Arabian Sea
Wiggert et al. (2005)		SST *Chl-a*	AVHRR SeaWiFS & CZCS		Arabian Sea
Prakash and Ramesh (2007)	1997–2005	*Chl-a* SST	SeaWiFS AVHRR & MODIS	–	Arabian Sea
Henson et al. (2010)	September – December, 2007	*Chl-a* SST PAR	MODIS/ AQUA	VGPM AbPM	Global
Rao et al. (2012)	1950–2009	SST	NOAA NCDC ERSST	–	Indian Ocean
Prakash et al. (2012)	1997–2010	*Chl-a* SST	SeaWiFS TRMM/TMI	–	Arabian Sea
Roxy et al. (2016)	1998–2007	*Chl-a* SST PAR	OC-CCI, SeaWiFS AVHRR SeaWiFS	VGPM	Western Indian Ocean
Kumar et al. (2016)	2002–2012	*Chl-a* SST	MODIS AQUA TRMM	–	Central Equitorial Indian Ocean
Hood et al. (2017)	–	*Chl-a* SST	SeaWiFS, MODIS Aqua GHRSST	VGPM	Indian Ocean
Sreeush et al. (2018)	1990–2010	NPP	SeaWiFS	–	Western Arabian Sea, SCTR, SLD, SC
Kong et al. (2019)	1998–2016	NPP *Chl-a* SST	SeaWiFS/ MODIS OC-CCI V3.1 OI SST V2	VGPM	Tropical eastern Indian and western Pacific Ocean
Dalabehara and Sarma (2021)	April – May, 2014	SST SSS NPP	CMEMS CMEMS VGPM, CbPM (OSU)[a]	VGMP, CbPM	Indian Ocean
Dalpadado et al. (2021)	1998–2019	SST *Chl-a* NPP	OISST V2.1 SeaWiFS and MODIS A VGPM (OSU)[a]	VGPM	Indian Ocean
Löscher (2021)	1998–2014	*Chl-a*	SeaWiFS, MODIS AQUA, VIIRS	–	Bay of Bengal

[a]https://sites.science.oregonstate.edu/ocean.productivity & In these studies, model data is also used; thereby, the span extends beyond satellite observations

Using SeaWiFS chlorophyll data and several empirical relationships, Uitz et al. (2010) estimated class-specific primary productivity at a global scale between January 1998 and December 2007. The contribution of the Indian Ocean was estimated to be around 9 GtC $year^{-1}$, i.e., 20% of global PP, out of which around 2.8 Gt C $year^{-1}$ accounted for the Northern Indian Ocean and the rest to south. Uitz's study indicated that their estimates of PP were about 15% and 20% less compared to Anotoine's study (Antoine et al., 1996) owing to differences in model formulation, particularly in terms of photosynthesis dependence on temperature. Using a global coupled-physical three-dimensional model assimilated with 18-year satellite data between 1998 and 2015, Gregg and Rousseaux (2019) showed a decline in global primary productivity, with a larger contribution from the North (Arabian Sea and Bay of Bengal) and Equatorial Indian Ocean. Gregg and Rousseaux's study indicated that the decline in global PP is associated with shallowing surface mixed layer depth and decreasing nitrate concentrations. Using OC-CCI data and photosynthesis-irradiance (P-I) curves gathered from an extensive database, Kulk et al. (2020) used a spectrally resolved model along with the vertical structure of *Chl-a* to estimate primary productivity at a global scale (Platt & Sathyendranath, 1988; Sathyendranath et al., 2020; Sathyendranath & Platt, 1989). Kulk's study showed that PP in the Indian Ocean increased between 1998 and 2003, stable between 2003 and 2005, decreased between 2005 and 2015 (except for a peak in 2011), and increased after 2015. Kulk's monthly analysis indicated the presence of two monthly PP peaks in spring and autumn and the lowest rates in summer for the Indian Ocean, significantly deviating from the trend observed globally. It should be noted that such a trend was also observed in a study conducted with CZCS data between 1978 and 1986 (Antoine et al., 1996). Kulk's study highlighted the sensitivity of marine primary productivity to potential changes in the photosynthetic response of phytoplankton cells under varying environmental conditions. Further, Kulk's study concluded that the interannual changes in global PP are not linear, and regional differences in the magnitude and direction of PP are observed. Implementation of dynamic assignment of the photosynthetic rates in global PP estimates using empirical relationships between the assimilation number of the P-I curve and temperature is suggested (Kulk et al., 2020).

Numerous studies have been conducted to compare the model performance across different timescales and geographical regions. Although the following studies do not include data collected from the Indian Ocean, they will provide guidance to carryout similar studies for the Indian Ocean. A study encompassing high-quality PP measurements (~1000) compared ~30 PP models in tropical Pacific Ocean (Friedrichs et al., 2009) concluded that nearly half of the difference between measured and modelled PP estimates arise from the uncertainties in input parameters. Subsequent comparison studies (Saba et al., 2010, 2011) included the PP data collected from coastal, oligotrophic, and Southern Ocean, and results indicate the low skill of existing ocean color models in coastal waters by overestimation of NPP. In another comparison study focused on the Arctic Ocean (Lee et al., 2015a, b), the NPP models performed better with the use of in situ measured parameters like Chl

derived from high-performance liquid chromatography (instead of satellite-derived Chl), and model performance is less sensitive to variations in PAR, SST, and mixed layer depth (MLD).

3.2 *Trends Observed in Satellite-Derived Parameter Estimates with Linkage to PP Estimates*

Sea surface temperature and chlorophyll-a concentration estimates from the satellites are widely used for studying the trends in marine phytoplankton primary production. The Indian Ocean Warm Pool (IOWP) is a part of the Indian region with SST >28 °C and is observed to be growing since the last decade (Krishnan et al., 2020; Rao et al., 2012; Roxy et al., 2016). Several studies have explored the effects of Indian Ocean warming on phytoplankton primary production in different temporal and spatial scales (Henson et al., 2010; Roxy et al., 2016). While some studies indicate an increase in PP with warming (Henson et al., 2010), other studies show a decrease in both PP and chlorophyll (Kumar et al., 2016; Prakash et al., 2012; Roxy et al., 2016). In a recent study, an analysis of 22 years (1998–2019) of satellite records of the Indian Ocean indicated an expansion of the IOWP (Dalpadado et al., 2021). The highest increase in SST (0.7 °C) is observed in the southern-central region, and in other regions, an increase of 0.4–0.5 °C is observed. Northern and Central regions of the Indian Ocean exhibited large interannual variability, with slightly decreasing trends in the Northern region. In the first decade of observations (1998–2008), cooler temperatures, and higher productivity, except for a few years. In the later decade (2009–2019), warmer SST and lower productivity are observed. Again, in recent years (2017–2019), the productivity was high (Dalpadado et al., 2021). In Northwest regions, the northeast monsoon resulted in an increase in the *Chl-a* concentration in the last decade, indicating a highly productive region for the upcoming years during the December–March period (Dalpadado et al., 2021). In the case of major upwelling areas, an increase in SST has been observed in the last two decades, and interannual variability was observed in the case of *Chl-a* with no significant trend (Dalpadado et al., 2021).

Following is the summary of a few studies carried out in the Indian Ocean with satellite remote sensing-derived parameters. This summary is provided to indicate the advantage of using satellite data in studying basin-scale processes and variations in environmental parameters. Chaturvedi (2005) studied the variability in *Chl-a* using OC4 generated from SeaWiFS R_{rs} data from 1997 to 2000 and the interrelationship with SST data from AVHRR data. Basin-scale processes controlling the dynamics of mixed layer depth in the Bay of Bengal were studied along with its association with *Chl-a* using SeaWiFS data between 1997 and 2007 (Narvekar & Prasanna Kumar, 2014). Phytoplankton size classes phenology in the Arabian Sea (Shunmugapandi et al., 2020, 2022) was studied for a period of 16 years using MODIS-Aqua 8-day composite *Chl-a* and SST data at 4 km resolution. The PSC phenology is observed to vary with SST, MLD, and seasonal cycle, i.e., Indian Monsoon.

3.3 Uncertainties in Measurements

Uncertainties in the derived satellite products may arise from many factors, and their exhaustive review is out of the scope. A detailed review of the uncertainties in ocean color remote sensing and their propagation to various products is presented in IOCCG (2019). Here, a glimpse of uncertainties arising from BRDF algorithms, IOP-AOP relationships, subcomponent IOP model shapes, and binning methods, uncertainty propagation to products is presented.

Presently, the default BRDF correction algorithm in the NASA processing scheme is based on the lookup-table method proposed by Morel et al. (2002), hereafter referred to as MAG2002. The MAG2002 algorithm uses a particle phase function varied as a function of *Chl-a*, thereby having limited applicability in case 2 waters (Gleason et al., 2012). Gleason's study studied the performance of MAG2002, Lee20011 (Lee et al., 2011b), and their own RT implementation involving different phase functions in case 1 and case 2 waters with thousands of NuRADS images. Gleason's study concluded that (1) for case 1 waters, MAG2002 is better than Lee et al.'s (2011b) algorithm; (2) for case 2 waters, Lee et al.'s (2011b) model was superior to MAG2002 at smaller azimuth angles and for *Chl-a* concentration greater than 10 mg/m^3; and (3) in case 1 waters, at larger azimuth angles, the use of Sullivan and Twardowski's (Sullivan & Twardowski, 2009) particulate volume scattering function in the radiative transfer model resulted in lower errors compared to other models. Uncertainties arising from the IOP assumptions in the MAG2002 model (Zhai et al., 2015) are assessed. More recent developments include the development of a fully analytical ocean color forward model (Twardowski et al., 2018), with explicit phase function parameterization.

After derivation of R_{rs}, different semi-analytical algorithms are used to derive the bulk and subcomponent IOPs. Uncertainties pertaining to the IOP subcomponent model assumptions affect the accuracy of the IOPs derived from R_{rs} (Wang et al., 2005). The choice of method used for the collection of in situ R_{rs} also impacts the accuracy of the radiances acquired using different sensors (Ruddick et al., 2019). Similarly, the collection of absorption measurements for phytoplankton, both in situ and filter pad measurements, has their respective uncertainties (Twardowski et al., 2018). Validation of SST measurements is usually conducted with nighttime measurements owing to higher stability between skin temperature and subsurface. The relationship can, however, vary with low windspeeds, high insolation, and reduced subsurface turbulence. A description of challenges to validating SST for climate records and suggested method of validation with shipboard radiometers can be found in Minnett (2010) and Minnett and Corlett (2012).

4 Summary/Conclusions

We looked at several primary productivity models based on ocean color satellite-derived algorithms and observations that can be used to estimate the global primary productivity of the marine environment in this chapter. Trends in satellite-derived parameter estimates and linkage PP estimates were also studied and discussed in the Indian Ocean. This provided analytical formulas for the components, which were then used to construct PP models for retrieving PP on a global scale. These indirect productivity estimates, on the other hand, show significant model-specific variances. More precise in situ measurements can provide surface and subsurface data on primary production, and their role in the application and calibration of numerical models is growing in importance. Understanding the dynamics and factors governing the spatial and temporal distribution of primary production is critical for higher trophic levels in aquatic systems. Therefore, the various components of the PP models were described using ocean color remote sensing and bio-optics in optically complex aquatic environments of the Indian Ocean. It is being researched further to determine how productivity models relate to ocean color remote sensing in the Indian Ocean. Finally, we briefly discussed the uncertainty associated with parameters derived from ocean color remote sensing used in primary productivity models.

5 Future Research Directions/Outlook

1. Accurate BRDF models need to be developed to correct for seasonal biases present in remote sensing reflectance data. The effect of the seasonal bias observed in global R_{rs} data on the derived IOPs and subsequently derived PP estimates needs to be assessed.
2. Independent global and regional studies with multiple types of measurement methods (Argo, LiDAR, Buoy, underway flowthrough, mooring, etc.) of parameters (R_{rs}, b_{bp}, and Chl) need to be conducted to assess the accuracy of the remote-sensing derived parameters.
3. Integration of analytical models with machine learning models (Li et al., 2022) and assimilation of data from multiple sources like Argo, Buoys, and moorings may further improve the global primary productivity estimates.

More research is carried out toward in situ PP estimates; however, ocean color remote sensing-based approaches require more studies.

Acknowledgments We would like to thank the King Fahd University of Petroleum and Minerals, Dhahran, Saudi Arabia, and the Harbor Branch Oceanographic Institute, Florida, Atlantic University, USA. The authors would also like to extend their thanks to Oregon State University for making available of the Ocean Productivity Estimates from VGPM, Eppley VGPM, CbPM, and CAFÉ models.

References

Antoine, D., & Morel, A. (1996). Oceanic primary production: 1. Adaptation of a spectral light-photosynthesis model in view of application to satellite chlorophyll observations. *Global Biogeochemical Cycles, 10*, 43–55. https://doi.org/10.1029/95GB02831

Antoine, D., Andre, J.-M., & Morel, A. (1996). Oceanic primary production 2. Estimation at global scale from satellite (coastal zone color scanner). *Global Biogeochemical Cycles, 10*, 57–69.

Austin, R., & Petzold, T. J. (1986). Spectral dependence of the diffuse attenuation coefficient of light in ocean waters. *Optical Engineering, 25*. https://doi.org/10.1117/12.7973845

Bailey, S. W., Franz, B. A., & Werdell, P. J. (2010). Estimation of near-infrared water-leaving reflectance for satellite ocean color data processing. *Optics Express, 18*, 7521. https://doi.org/10.1364/oe.18.007521

Balch, W. M., Carranza, M. M., Erickson, Z. K., Fassbender, A. J., Fernández-Carrera, A., Ferrón, S., García-Martín, E. E., & Langdon, C. (2021). Ocean optics & biogeochemistry protocols for satellite ocean colour sensor validation IOCCG protocol series volume 7.0, 2021 aquatic primary productivity field protocols for satellite validation and model synthesis (DRAFT) report of a NASA-sponsored 7.

Bannister, T. T. (1974). Production equations in terms of chlorophyll concentration, quantum yield, and upper limit to production. *Limnology and Oceanography, 19*.

Behrenfeld, M. J., & Falkowski, P. G. (1997a). A consumer's guide to phytoplankton primary productivity models. *Limnology and Oceanography, 42*, 1479–1491. https://doi.org/10.4319/lo.1997.42.7.1479

Behrenfeld, M. J., & Falkowski, P. G. (1997b). Photosynthetic rates derived from satellite-based chlorophyll concentration. *Limnology and Oceanography, 42*, 1–20.

Behrenfeld, M. J., Boss, E., Siegel, D. A., & Shea, D. M. (2005). Carbon-based ocean productivity and phytoplankton physiology from space. *Global Biogeochemical Cycles, 19*, 1–14. https://doi.org/10.1029/2004GB002299

Bhattathiri, P. M. A., Pant, A., Sawant, S., Gauns, M., Matondkar, S. G. P., & Mohanraju, R. (1996). Phytoplankton production and chlorophyll distribution in the eastern and central Arabian Sea in 1994–1995. *Current Science, 71*, 857–862.

Bisson, K. M., Boss, E., Werdell, P. J., Ibrahim, A., Frouin, R., & Behrenfeld, M. J. (2021). Seasonal bias in global ocean color observations. *Applied Optics, 60*, 6978. https://doi.org/10.1364/ao.426137

Boss, E., & Roesler, C. (2006). Chapter 8. Over constrained linear matrix inversion with statistical selection. In *IOCCG 2006 report on remote sensing of inherent optical properties: Fundamentals, tests of algorithms, and applications*.

Bracher, A., Vountas, M., Dinter, T., Burrows, J. P., Röttgers, R., & Peeken, I. (2009). Quantitative observation of cyanobacteria and diatoms from space using PhytoDOAS on SCIAMACHY data. *Biogeosciences, 6*, 751–764.

Brando, V. E., Dekker, A. G., Park, Y. J., & Schroeder, T. (2012). Adaptive semianalytical inversion of ocean color radiometry in optically complex waters. *Applied Optics, 51*, 2808. https://doi.org/10.1364/AO.51.002808

Brewin, R. J. W., Sathyendranath, S., Hirata, T., Lavender, S. J., Barciela, R. M., & Hardman-Mountford, N. J. (2010). A three-component model of phytoplankton size class for the Atlantic Ocean. *Ecological Modelling, 221*, 1472–1483. https://doi.org/10.1016/J.ECOLMODEL.2010.02.014

Brewin, R. J. W., Hardman-Mountford, N. J., Lavender, S. J., Raitsos, D. E., Hirata, T., Uitz, J., Devred, E., Bricaud, A., Ciotti, A., & Gentili, B. (2011). An intercomparison of bio-optical techniques for detecting dominant phytoplankton size class from satellite remote sensing. *Remote Sensing of Environment, 115*, 325–339. https://doi.org/10.1016/j.rse.2010.09.004

Bricaud, A., Babin, M., Morel, A., & Claustre, H. (1995). Variability in the chlorophyll-specific absorption coefficients of natural phytoplankton: Analysis and parameterization phytoplankton. *Journal of Geophysical Research, 100*, 13321–13332. https://doi.org/10.1029/95JC00463

Bricaud, A., Ciotti, A. M., & Gentili, B. (2012). Spatial-temporal variations in phytoplankton size and colored detrital matter absorption at global and regional scales, as derived from twelve years of SeaWiFS data (1998–2009). *Global Biogeochemical Cycles, 26*, 1–17. https://doi.org/10.1029/2010GB003952

Caballero, I., & Stumpf, R. P. (2020). Atmospheric correction for satellite-derived bathymetry in the Caribbean waters: From a single image to multi-temporal approaches using Sentinel-2A/B. *Optics Express, 28*, 11742. https://doi.org/10.1364/oe.390316

Campbell, J. W., Blaisdell, J. M., & Darzi, M. (1995). Level-3 SeaWiFS data products: Spatial and temporal binning algorithms. *NASA Technical Memorandum – SeaWiFS Technical Report Series, 32*, 104566.

Carr, M. E., Friedrichs, M. A. M., Schmeltz, M., Noguchi Aita, M., Antoine, D., Arrigo, K. R., Asanuma, I., Aumont, O., Barber, R., Behrenfeld, M., Bidigare, R., Buitenhuis, E. T., Campbell, J., Ciotti, A., Dierssen, H., Dowell, M., Dunne, J., Esaias, W., Gentili, B., Gregg, W., Groom, S., Hoepffner, N., Ishizaka, J., Kameda, T., Le Quéré, C., Lohrenz, S., Marra, J., Mélin, F., Moore, K., Morel, A., Reddy, T. E., Ryan, J., Scardi, M., Smyth, T., Turpie, K., Tilstone, G., Waters, K., & Yamanaka, Y. (2006). A comparison of global estimates of marine primary production from ocean color. *Deep Sea Research Part II: Topical Studies in Oceanography, 53*, 741–770. https://doi.org/10.1016/j.dsr2.2006.01.028

Chaturvedi, N. (2005). Variability of chlorophyll concentration in the Arabian Sea and Bay of Bengal as observed from SeaWiFS data from 1997–2000 and its interrelationship with Sea Surface Temperature (SST) derived from NOAA AVHRR. *International Journal of Remote Sensing, 26*, 3695–3706. https://doi.org/10.1080/01431160500159818

Chauhan, P., Sahay, A., Rajawat, A. S., & Nayak, S. (2003). Remote sensing of diffuse attenuation coefficient (K490) using IRS-P4 Ocean Colour Monitor (OCM) sensor. *Indian Journal of Marine Sciences, 32*, 279–284.

Ciotti, A. M., & Bricaud, A. (2006). Retrievals of a size parameter for phytoplankton and spectral light absorption by colored detrital matter from water-leaving radiances at SeaWiFS channels in a continental shelf region off Brazil. *Limnology and Oceanography: Methods, 4*, 237–253. https://doi.org/10.4319/lom.2006.4.237

Ciotti, A. M., Cullen, J. J., & Lewis, M. R. (1999). A semi-analytical model of the influence of phytoplankton community structure on the relationship between light attenuation and ocean color. *Journal of Geophysical Research, 104*, 1559–1578. https://doi.org/10.1029/1998JC900021

Ciotti, M., Lewis, M. R., & Cullen, J. J. (2002). Assessment of the relationships between dominant cell size in natural phytoplankton communities and the spectral shape of the absorption coefficient. *Limnology and Oceanography, 47*, 404–417. https://doi.org/10.4319/lo.2002.47.2.0404

Dalabehara, H. B., & Sarma, V. V. S. S. (2021). Physical forcing controls spatial variability in primary production in the Indian Ocean. *Deep Sea Research Part II: Topical Studies in Oceanography, 183*, 104906. https://doi.org/10.1016/j.dsr2.2020.104906

Dalpadado, P., Arrigo, K. R., van Dijken, G. L., Gunasekara, S. S., Ostrowski, M., Bianchi, G., & Sperfeld, E. (2021). Warming of the Indian Ocean and its impact on temporal and spatial dynamics of primary production. *Progress in Oceanography, 198*, 102688. https://doi.org/10.1016/j.pocean.2021.102688

Devred, E., Sathyendranath, S., Stuart, V., & Platt, T. (2011). A three component classification of phytoplankton absorption spectra: Application to ocean-color data. *Remote Sensing of Environment, 115*, 2255–2266. https://doi.org/10.1016/J.RSE.2011.04.025

Donlon, C. J., Minnett, P. J., Gentemann, C., Nightingale, T. J., Barton, I. J., Ward, B., & Murray, M. J. (2002). Toward improved validation of satellite sea surface skin temperature measurements for climate research. *Journal of Climate, 15*, 353–369. https://doi.org/10.1175/1520-0442(2002)015<0353:TIVOSS>2.0.CO;2

Donlon, C., Robinson, I., Casey, K. S., Vazquez-Cuervo, J., Armstrong, E., Arino, O., Gentemann, C., May, D., LeBorgne, P., Piolle, J., Barton, I., Beggs, H., Poulter, D. J. S., Merchant, C. J., Bingham, A., Heinz, S., Harris, A., Wick, G., Emery, B., Minnett, P., Evans, R., Llewellyn-Jones, D., Mutlow, C., Reynolds, R. W., Kawamura, H., & Rayner, N. (2007). The global ocean data assimilation experiment high-resolution sea surface temperature pilot project. *Bulletin of the American Meteorological Society, 88*, 1197–1213. https://doi.org/10.1175/BAMS-88-8-1197

Eppley, R. W. (1972). Temperature and phytoplankton growth in the sea. *Fishery Bulletin, 70*, 1063–1085.

Eppley, R. W., Stewart, E., Abbott, M. R., & Heyman, U. (1985). Estimating ocean primary production from satellite chlorophyll. Introduction to regional differences and statistics for the Southern California Bight. *Journal of Plankton Research, 7*, 57–70.

Everett, J. D., & Doblin, M. A. (2015). Characterising primary productivity measurements across a dynamic western boundary current region. *Deep Sea Research Part I: Oceanographic Research Papers, 100*, 105–116. https://doi.org/10.1016/j.dsr.2015.02.010

Evers-King, H. et al. (2017). Validation and intercomparison of ocean color algorithms for estimating particulate organic carbon in the oceans. *Frontiers in Marine Science, 4*, 251.

Friedrichs, M. A. M., Carr, M. E., Barber, R. T., Scardi, M., Antoine, D., Armstrong, R. A., Asanuma, I., Behrenfeld, M. J., Buitenhuis, E. T., Chai, F., Christian, J. R., Ciotti, A. M., Doney, S. C., Dowell, M., Dunne, J., Gentili, B., Gregg, W., Hoepffner, N., Ishizaka, J., Kameda, T., Lima, I., Marra, J., Mélin, F., Moore, J. K., Morel, A., O'Malley, R. T., O'Reilly, J., Saba, V. S., Schmeltz, M., Smyth, T. J., Tjiputra, J., Waters, K., Westberry, T. K., & Winguth, A. (2009). Assessing the uncertainties of model estimates of primary productivity in the tropical Pacific Ocean. *Journal of Marine Systems, 76*, 113–133. https://doi.org/10.1016/J.JMARSYS.2008.05.010

Frouin, R., & Pinker, R. T. (1995). Estimating photosynthetically active radiation (PAR) at the earth's surface from satellite observations. *Remote Sensing of Environment, 51*, 98–107.

Frouin, R., Franz, B. A., & Werdell, P. J. (2002). The SeaWiFS PAR product. In S. B. Hooker, & E. R. Firestone (Eds.), *Algorithm updates for the Fourth SeaWiFS Data Reprocessing, NASA Tech. Memo. 2003-206892* (Vol. 22). Greenbelt, MD, USA.

Frouin, R., McPherson, J., Ueyoshi, K., & Franz, B. A. (2012). A time series of photosynthetically available radiation at the ocean surface from SeaWiFS and MODIS data. In R. J. Frouin, N. Ebuchi, D. Pan, & T. Saino (Eds.), *Remote sensing of the marine environment II* (pp. 234–245). SPIE. https://doi.org/10.1117/12.981264

Frouin, R. J., Franz, B. A., Ibrahim, A., Knobelspiesse, K., Ahmad, Z., Cairns, B., Chowdhary, J., Dierssen, H. M., Tan, J., Dubovik, O., Huang, X., Davis, A. B., Kalashnikova, O., Thompson, D. R., Remer, L. A., Boss, E., Coddington, O., Deschamps, P. Y., Gao, B. C., Gross, L., Hasekamp, O., Omar, A., Pelletier, B., Ramon, D., Steinmetz, F., & Zhai, P. W. (2019). Atmospheric correction of satellite ocean-color imagery during the PACE era. *Frontiers in Earth Science, 7*, 1–43. https://doi.org/10.3389/feart.2019.00145

Fujiwara, A., Hirawake, T., Suzuki, K., & Saitoh, S.-I. (2011). Remote sensing of size structure of phytoplankton communities using optical properties of the Chukchi and Bering Sea shelf region. *Biogeosciences, 8*, 3567–3580. https://doi.org/10.5194/bg-8-3567-2011

Gauns, M., Madhupratap, M., Ramaiah, N., Jyothibabu, R., Fernandes, V., Paul, J. T., & Prasanna Kumar, S. (2005). Comparative accounts of biological productivity characteristics and estimates of carbon fluxes in the Arabian Sea and the Bay of Bengal. *Deep Sea Research Part II: Topical Studies in Oceanography, 52*, 2003–2017. https://doi.org/10.1016/j.dsr2.2005.05.009

Gitelson, A. (1992). The peak near 700 nm on radiance spectra of algae and water: Relationships of its magnitude and position with chlorophyll concentration. *International Journal of Remote Sensing, 13*, 3367–3373.

Gleason, A. C. R., Voss, K. J., Gordon, H. R., Twardowski, M., Sullivan, J., Trees, C., Weidemann, A., Berthon, J.-F., Clark, D., & Lee, Z.-P. (2012). Detailed validation of the bidirectional effect in various case I and case II waters. *Optics Express, 20*, 7630. https://doi.org/10.1364/oe.20.007630

Goes, J. I., Thoppil, P. G., Gomes, H. D. R., & Fasullo, J. T. (2005). Warming of the Eurasian landmass is making the Arabian Sea more productive. *Science (80-.), 308*, 545–547. https://doi.org/10.1126/science.1106610

Gordon, H. R. (1989). Theoretical aspects of hydrologic optics. *Limnology and Oceanography, 34*, 1389–1409.

Gordon, H. R. (2021). Evolution of ocean color atmospheric correction: 1970–2005. *Remote Sensing, 13*, 1970–2005. https://doi.org/10.3390/rs13245051

Gordon, H. R., & Clark, D. K. (1980). Remote sensing optical properties of a stratified ocean: An improved interpretation. *Applied Optics, 19*, 3428. https://doi.org/10.1364/ao.19.003428

Gordon, H. R., & Morel, A. Y. (1983). *Remote assessment of ocean color for interpretation of satellite visible imagery: A review (Coastal and Estuarine Studies)*. Springer.

Gordon, H. R., Brown, O. B., & Jacobs, M. M. (1975). Computed relationships between the inherent and apparent optical properties of a flat homogeneous ocean. *Applied Optics, 14*, 417–427.

Gordon, H. R., Brown, O. B., Evans, R. H., Brown, J. W., Smith, R. C., Baker, K. S., & Clark, D. K. (1988). A semianalytic radiance model of ocean color. *Journal of Geophysical Research, 93*, 10909–10924. https://doi.org/10.1029/JD093iD09p10909

Gregg, W. W., & Rousseaux, C. S. (2019). Global ocean primary production trends in the modern ocean color satellite record (1998–2015). *Environmental Research Letters, 14*, 124011. https://doi.org/10.1088/1748-9326/ab4667

Hanafin, J. A. (2002). *On sea surface properties and characteristics in the infrared*. University of Miami.

Henson, S. A., Sarmiento, J. L., Dunne, J. P., Bopp, L., Lima, I., Doney, S. C., John, J., & Beaulieu, C. (2010). Detection of anthropogenic climate change in satellite records of ocean chlorophyll and productivity. *Biogeosciences, 7*, 621–640. https://doi.org/10.5194/bg-7-621-2010

Hirata, T., Aiken, J., Hardman-Mountford, N., Smyth, T. J., & Barlow, R. G. (2008). An absorption model to determine phytoplankton size classes from satellite ocean colour. *Remote Sensing of Environment, 112*, 3153–3159. https://doi.org/10.1016/J.RSE.2008.03.011

Hirawake, T., Takao, S., Horimoto, N., Ishimaru, T., Yamaguchi, Y., & Fukuchi, M. (2011). A phytoplankton absorption-based primary productivity model for remote sensing in the Southern Ocean. *Polar Biology, 34*, 291–302. https://doi.org/10.1007/s00300-010-0949-y

Hood, R. R., Beckley, L. E., & Wiggert, J. D. (2017). Biogeochemical and ecological impacts of boundary currents in the Indian Ocean. *Progress in Oceanography, 156*, 290–325. https://doi.org/10.1016/j.pocean.2017.04.011

Hooker, S. B., Firestone, E. R., Acker, J. G., Mueller, J. L., Fraser, R. S., Biggar, S. F., Thome, K. J., Slater, P. N., Holmes, A. W., Barnes, R. A., Weir, C. T., Siegel, D. A., Menzies, D. W., Michaels, A. F., & Podesta, G. (1995). SeaWiFS technical report series volume 27, Case studies for SeaWiFS calibration and validation, Part 3 Volume 27, Case studies for SeaWiFS calibration 27.

Hooker, S. B., Firestone, E. R., Patt, F. S., Barnes, R. A., Eplee, R. E., Franz, B. A., Robinson, W. D., Feldman, G. C., Bailey, S. W., Gales, J., Werdell, P. J., Wang, M., Frouin, R., Stumpf, R. P., Arnone, R. A., Gould, R. W., Martinolich, P. M., Ransibrahmanakul, V., O'Reilly, J. E., & Yoder, J. A. (2003). SeaWiFS postlaunch technical report series volume 22, Algorithm updates for the fourth SeaWiFS data reprocessing 22.

Hu, C., Lee, Z., & Franz, B. (2012). Chlorophyll a algorithms for oligotrophic oceans: A novel approach based on three-band reflectance difference. *Journal of Geophysical Research: Oceans, 117*, 1–25. https://doi.org/10.1029/2011JC007395

Hu, C., Feng, L., Lee, Z., Franz, B. A., Bailey, S. W., Werdell, P. J., & Proctor, C. W. (2019). Improving satellite global chlorophyll a data products through algorithm refinement and data recovery. *Journal of Geophysical Research: Oceans, 124*, 1524–1543. https://doi.org/10.1029/2019JC014941

Hu, C., Feng, L., & Guan, Q. (2020). A machine learning approach to estimate surface chlorophyll a concentrations in global oceans from satellite measurements. *IEEE Transactions on Geoscience and Remote Sensing, 59*, 1–18. https://doi.org/10.1109/tgrs.2020.3016473

Huot, Y., Babin, M., Bruyant, F., Grob, C., Twardowski, M. S., Claustre, H., Huot, Y., Babin, M., Bruyant, F., Grob, C., & Twardowski, M. S. (2007). Does chlorophyll a provide the best index of phytoplankton biomass for primary productivity studies? *Biogeosciences Discussions, 4*, 707–745.

Ibrahim, A., Franz, B. A., Ahmad, Z., & Bailey, S. W. (2019). Multiband atmospheric correction algorithm for ocean color retrievals. *Frontiers in Earth Science, 7*, 1–15. https://doi.org/10.3389/feart.2019.00116

Ioannou, I., Foster, R., Gilerson, A., Gross, B., Moshary, F., & Ahmed, S. (2013). Neural network approach for the derivation of chlorophyll concentration from ocean color. *Ocean Sensing and Monitoring V, 8724*, 87240P. https://doi.org/10.1117/12.2018143

IOCCG. (2006). *Remote sensing of inherent optical properties: Fundamentals, tests of algorithms, and applications, reports of the International Ocean Colour Coordinating Group*. IOCCG. https://doi.org/10.25607/OBP-96

IOCCG. (2010). *Atmospheric correction for remotely-sensed ocean-colour products, reports of the International Ocean Colour Coordinating Group*. IOCCG. https://doi.org/10.25607/OBP-101

IOCCG. (2019). *Uncertainties in ocean colour remote sensing, reports of the International Ocean Colour Coordinating Group*. IOCCG. https://doi.org/10.25607/OBP-696

Jamet, C., Loisel, H., & Dessailly, D. (2012). Retrieval of the spectral diffuse attenuation coefficient Kd(l) in open and coastal ocean waters using a neural network inversion. *Journal of Geophysical Research, 117*, 1–14. https://doi.org/10.1029/2012JC008076

Kerkar, A. U., Tripathy, S. C., Minu, P., Baranval, N., Sabu, P., Patra, S., Mishra, R. K., & Sarkar, A. (2020). Variability in primary productivity and bio-optical properties in the Indian sector of the Southern Ocean during an austral summer. *Polar Biology, 43*, 1469–1492. https://doi.org/10.1007/s00300-020-02722-2

Kiefer, D. A., & Mitchell, B. G. (1983). A simple, steady state description of phytoplankton growth based on absorption cross section and quantum efficiency. *Limnology and Oceanography, 28*, 770–776. https://doi.org/10.4319/lo.1983.28.4.0770

Kirk, J. T. O. (2011). *Light and photosynthesis in aquatic ecosystems* (3rd ed.). Cambridge University Press.

Kolluru, S., Tiwari, S. P., & Gedam, S. S. (2021). Hybrid inversion algorithms for retrieval of absorption subcomponents from ocean colour remote sensing reflectance. *Remote Sensing, 13*, 1726. https://doi.org/10.3390/RS13091726

Kong, F., Dong, Q., Xiang, K., Yin, Z., Li, Y., & Liu, J. (2019). Spatiotemporal variability of remote sensing ocean net primary production and major forcing factors in the tropical eastern Indian and Western Pacific Ocean. *Remote Sensing, 11*, 1–18. https://doi.org/10.3390/rs11040391

Krishnan, R., Sanjay, J., Gnanaseelan, C., Mujumdar, M., Kulkarni, A., & Chakraborty, S. (2020). *Assessment of climate change over the Indian region*: *A report of the Ministry of Earth Sciences* (*MOES*), *Government of India*. https://doi.org/10.1007/978-981-15-4327-2

Kulk, G., Platt, T., Dingle, J., Jackson, T., Jönsson, B. F., Bouman, H. A., Babin, M., Brewin, R. J. W., Doblin, M., Estrada, M., Figueiras, F. G., Furuya, K., González-Benítez, N., Gudfinnsson, H. G., Gudmundsson, K., Huang, B., Isada, T., Kovač, Ž., Lutz, V. A., Marañón, E., Raman, M., Richardson, K., Rozema, P. D., van de Poll, W. H., Segura, V., Tilstone, G. H., Uitz, J., van Dongen-Vogels, V., Yoshikawa, T., & Sathyendranath, S. (2020). Primary production, an index of climate change in the ocean: Satellite-based estimates over two decades. *Remote Sensing, 12*, 1–26. https://doi.org/10.3390/rs12050826

Kumar, G. S., Prakash, S., Ravichandran, M., & Narayana, A. C. (2016). Trends and relationship between chlorophyll-a and sea surface temperature in the central equatorial Indian Ocean. *Remote Sensing Letters, 7*, 1093–1101. https://doi.org/10.1080/2150704X.2016.1210835

Kumari, P. V., Thomas, S., Mohanty, P. C., Jayappa, K. S., Mahendra, R. S., & Gupta, A. (2021). Effect of sea surface temperature variation on productivity and fisheries off Karnataka, West Coast of India. *Journal of the Indian Society of Remote Sensing*. https://doi.org/10.1007/s12524-021-01447-x

Lee, Z. P., Carder, K. L., Peacock, T. G., Davis, C. O., & Mueller, J. L. (1996). Method to derive ocean absorption coefficients from remote-sensing reflectance. *Applied Optics, 35*, 453–462. https://doi.org/10.1364/AO.35.000453

Lee, Z., Carder, K. L., & Arnone, R. A. (2002). Deriving inherent optical properties from water color: A multiband quasi-analytical algorithm for optically deep waters. *Applied Optics, 41*, 5755–5772. https://doi.org/10.1364/AO.41.005755

Lee, Z. P., Darecki, M., Carder, K. L., Davis, C. O., Stramski, D., & Rhea, W. J. (2005a). Diffuse attenuation coefficient of downwelling irradiance: An evaluation of remote sensing methods. *Journal of Geophysical Research: Oceans, 110*. https://doi.org/10.1029/2004JC002573

Lee, Z. P., Du, K. P., & Arnone, R. (2005b). A model for the diffuse attenuation coefficient of downwelling irradiance. *Journal of Geophysical Research – C: Oceans, 110*, 1–10. https://doi.org/10.1029/2004JC002275

Lee, Z., Weidemann, A., Kindle, J., Arnone, R., Kendall, L., Davis, C., Amone, R., & Carder, K. L. (2007). Euphotic zone depth: Its derivation and implication to ocean – color remote sensing. *Journal of Geophysical Research, 112*, 1–11. https://doi.org/10.1029/2006JC003802

Lee, Z., Lance, V. P., Shang, S., Vaillancourt, R., Freeman, S., Lubac, B., Hargreaves, B. R., Del Castillo, C., Miller, R., Twardowski, M., & Wei, G. (2011a). An assessment of optical properties and primary production derived from remote sensing in the Southern Ocean (SO GasEx). *Journal of Geophysical Research, 116*, 0–03. https://doi.org/10.1029/2010JC006747

Lee, Z. P., Du, K., Voss, K. J., Zibordi, G., Lubac, B., Arnone, R., & Weidemann, A. (2011b). An inherent-optical-property-centered approach to correct the angular effects in water-leaving radiance. *Applied Optics, 50*(19), 3155. https://doi.org/10.1364/AO.50.003155

Lee, Z., Hu, C., Shang, S., Du, K., Lewis, M., Arnone, R., & Brewin, R. (2013). Penetration of UV-visible solar radiation in the global oceans: Insights from ocean color remote sensing. *Journal of Geophysical Research: Oceans, 118*, 4241–4255. https://doi.org/10.1002/jgrc.20308

Lee, Y. J., Matrai, P. A., Friedrichs, M. A. M., Saba, V. S., Antoine, D., Ardyna, M., Asanuma, I., Babin, M., Bélanger, S., Benoît-Gagné, M., Devred, E., Fernández-Méndez, M., Gentili, B., Hirawake, T., Kang, S. H., Kameda, T., Katlein, C., Lee, S. H., Lee, Z., Mélin, F., Scardi, M., Smyth, T. J., Tang, S., Turpie, K. R., Waters, K. J., & Westberry, T. K. (2015a). An assessment of phytoplankton primary productivity in the Arctic Ocean from satellite ocean color/in situ chlorophyll-a based models. *Journal of Geophysical Research: Oceans, 120*, 6508–6541. https://doi.org/10.1002/2015JC011018

Lee, Z., Marra, J., Perry, M. J., & Kahru, M. (2015b). Estimating oceanic primary productivity from ocean color remote sensing: A strategic assessment. *Journal of Marine Systems, 149*, 50–59. https://doi.org/10.1016/j.jmarsys.2014.11.015

Li, Z., Li, L., Song, K., & Cassar, N. (2013). Estimation of phytoplankton size fractions based on spectral features of remote sensing ocean color data. *Journal of Geophysical Research: Oceans, 118*, 1445–1458. https://doi.org/10.1002/JGRC.20137

Li, W., Tiwari, S. P., El-Askary, H. M., Qurban, M. A., Amiridis, V., Manikandan, K. P., Garay, M. J., Kalashnikova, O. V., Piechota, T. C., & Struppa, D. C. (2020). Synergistic use of remote sensing and modeling for estimating net primary productivity in the Red Sea with VGPM, Eppley-VGPM, and CbPM models intercomparison. *IEEE Transactions on Geoscience and Remote Sensing, 58*, 8717–8734. https://doi.org/10.1109/TGRS.2020.2990373

Li, Z., Yang, W., Matsushita, B., & Kondoh, A. (2022). Remote estimation of phytoplankton primary production in clear to turbid waters by integrating a semi-analytical model with a machine learning algorithm. *Remote Sensing of Environment, 275*, 113027. https://doi.org/10.1016/J.RSE.2022.113027

Lillesand, T., Kiefer, R. W., & Chipman, J. (2015). *Remote sensing and image interpretation*. John Wiley & Sons, Ltd.

Loisel, H., & Stramski, D. (2000). Estimation of the inherent optical properties of natural waters from the irradiance attenuation coefficient and reflectance in the presence of Raman scattering. *Applied Optics, 39*, 3001–3011.

Loisel, H., Bosc, E., Stramski, D., & Oubelkheir, K. (2001). Seasonal variability of the backscattering coefficient in the Mediterranean Sea based on Satellite SeaWiFS imagery. *Geophysical Research Letters, 28*, 4203–4206.

Loisel, H., Stramski, D., Dessailly, D., Jamet, C., Li, L., & Reynolds, R. A. (2018). An inverse model for estimating the optical absorption and backscattering coefficients of seawater from remote-sensing reflectance over a broad range of oceanic and coastal marine environments. *Journal of Geophysical Research: Oceans, 123*, 2141–2171. https://doi.org/10.1002/2017JC013632

Longhurst, A., Sathyendranath, S., Platt, T., & Caverhill, C. (1995). An estimate of global primary production in the ocean from satellite radiometer data. *Journal of Plankton Research, 17*, 1245–1271. https://doi.org/10.1093/plankt/17.6.1245

Löscher, C. R. (2021). Reviews and syntheses: Trends in primary production in the Bay of Bengal-Is it at a tipping point? *Biogeosciences, 18*, 4953–4963. https://doi.org/10.5194/bg-18-4953-2021

Ma, S., Tao, Z., Yang, X., Yu, Y., Zhou, X., Ma, W., & Li, Z. (2014). Estimation of marine primary productivity from satellite-derived phytoplankton absorption data. *IEEE Journal of Selected Topics in Applied Earth Observations and Remote Sensing, 7*, 3084–3092. https://doi.org/10.1109/JSTARS.2014.2298863

Madhu, N. V., Jyothibabu, R., Maheswaran, P. A., John Gerson, V., Gopalakrishnan, T. C., & Nair, K. K. C. (2006). Lack of seasonality in phytoplankton standing stock (chlorophyll a) and production in the western Bay of Bengal. *Continental Shelf Research, 26*, 1868–1883. https://doi.org/10.1016/j.csr.2006.06.004

Maritorena, S., Siegel, D. A., & Peterson, A. R. (2002). Optimization of a semianalytical ocean color model for global-scale application. *Applied Optics, 41*, 2705–2714. https://doi.org/10.1364/AO.41.002705

Marra, J., Ho, C., & Trees, C. C. (2003). An alternative algorithm for the calculation of primary productivity from remote sensing data. LDEO Tech. Rep. 1, pp. 1–27.

Marra, J., Trees, C. C., & O'Reilly, J. E. (2007). Phytoplankton pigment absorption: A strong predictor of primary productivity in the surface ocean. *Deep Sea Research Part I: Oceanographic Research Papers, 54*, 155–163. https://doi.org/10.1016/J.DSR.2006.12.001

Menon, H. B., & Adhikari, A. (2018). Remote sensing of chlorophyll-a in case II waters: A novel approach with improved accuracy over widely implemented turbid water indices. *Journal of Geophysical Research: Oceans, 123*, 8138–8158. https://doi.org/10.1029/2018JC014052

Minnett, P. J. (2010). The validation of sea surface temperature retrievals from spaceborne infrared radiometers. In V. Barale, J. F. R. Gower, & L. Alberotanza (Eds.), *Oceanography from space*. Springer. (Revisited).

Minnett, P. J., & Corlett, G. K. (2012). A pathway to generating Climate Data Records of sea-surface temperature from satellite measurements. *Deep Sea Research Part II: Topical Studies in Oceanography, 77–80*, 44–51. https://doi.org/10.1016/J.DSR2.2012.04.003

Mobley, C. D. (2004). *Light and water: Radiative transfer in natural waters*. Academic Press.

Mobley, C. D. (2008). Radiative transfer in the ocean. In *Encyclopedia of ocean sciences* (2nd ed., pp. 619–628). https://doi.org/10.1016/B978-012374473-9.00469-0

Mobley, C. D., Sundman, L. K., Davis, C. O., Bowles, J. H., Downes, T. V., Leathers, R. A., Montes, M. J., Bissett, W. P., Kohler, D. D. R., Reid, R. P., Louchard, E. M., & Gleason, A. (2005). Interpretation of hyperspectral remote-sensing imagery by spectrum matching and look-up tables. *Applied Optics, 44*, 3576. https://doi.org/10.1364/AO.44.003576

Mobley, C. D., Werdell, J., Franz, B., Ahmad, Z., & Bailey, S. (2016). Atmospheric correction for satellite ocean color radiometry. A tutor. Doc. NASA Ocean Biol. Process. Gr. 1–73.

Moore, T. S., Campbell, J. W., & Dowell, M. D. (2009). A class-based approach to characterizing and mapping the uncertainty of the MODIS ocean chlorophyll product. *Remote Sensing of Environment, 113*, 2424–2430. https://doi.org/10.1016/j.rse.2009.07.016

Morel, A., & Antoine, D. (2011). ATBD 2.9: Pigment index retrieval in case 1 waters. ESA Doc (2007).

Morel, A., & Gentili, B. (1996). Diffuse reflectance of oceanic waters. III. Implication of bidirectionality for the remote-sensing problem. *Applied Optics, 35*, 4850–4862. https://doi.org/10.1364/AO.35.004850

Morel, A., & Loisel, H. (1998). Apparent optical properties of oceanic water: Dependence on the molecular scattering contribution. *Applied Optics, 37*, 4765. https://doi.org/10.1364/AO.37.004765

Morel, A., & Maritorena, S. (2001). Bio-optical properties of oceanic waters: A reappraisal. *Journal of Geophysical Research: Oceans, 106*, 7163–7180. https://doi.org/10.1029/2000JC000319

Morel, A., & Prieur, L. (1977). Analysis of variations in ocean color. *Limnology and Oceanography, 22*, 709–722. https://doi.org/10.4319/lo.1977.22.4.0709

Morel, A., Antoine, D., & Gentili, B. (2002). Bidirectional reflectance of oceanic waters: Accounting for Raman emission and varying particle scattering phase function. *Applied Optics, 41*, 6289. https://doi.org/10.1364/AO.41.006289

Morel, A., Claustre, H., Antoine, D., & Gentili, B. (2007a). Natural variability of bio-optical properties in Case 1 waters: Attenuation and reflectance within the visible and near-UV spectral domains, as observed in South Pacific and Mediterranean waters. *Biogeosciences, 4*, 913–925. https://doi.org/10.5194/bg-4-913-2007

Morel, A., Huot, Y., Gentili, B., Werdell, P. J., Hooker, S. B., & Franz, B. A. (2007b). Examining the consistency of products derived from various ocean color sensors in open ocean (Case 1) waters in the perspective of a multi-sensor approach. *Remote Sensing of Environment, 111*, 69–88. https://doi.org/10.1016/j.rse.2007.03.012

Moses, W. J., Saprygin, V., Gerasyuk, V., Povazhnyy, V., Berdnikov, S., & Gitelson, A. A. (2019). OLCI-based NIR-red models for estimating chlorophyll-a concentration in productive coastal waters—A preliminary evaluation. *Environmental Research Communications, 1*, 011002. https://doi.org/10.1088/2515-7620/aaf53c

Mouw, C. B., & Yoder, J. A. (2010). Optical determination of phytoplankton size composition from global SeaWiFS imagery. *Journal of Geophysical Research, 115*, 12018. https://doi.org/10.1029/2010JC006337

Mouw, C. B., Hardman-Mountford, N. J., Alvain, S., Bracher, A., Brewin, R. J. W., Bricaud, A., Ciotti, A. M., Devred, E., Fujiwara, A., Hirata, T., Hirawake, T., Kostadinov, T. S., Roy, S., & Uitz, J. (2017). A consumer's guide to satellite remote sensing of multiple phytoplankton groups in the global ocean. *Frontiers in Marine Science, 4*, 41. https://doi.org/10.3389/FMARS.2017.00041/BIBTEX

Mueller, J. L., & Lange, R. E. (1989). Bio-optical provinces of the Northeast Pacific Ocean: A provisional analysis. *Limnology and Oceanography, 34*, 1572–1586. https://doi.org/10.4319/LO.1989.34.8.1572

Nagamani, P. V., Chauhan, P., & Dwivedi, R. M. (2008). Development of chlorophyll-a algorithm for ocean colour monitor onboard OCEANSAT-2 satellite. *IEEE Geoscience and Remote Sensing Letters, 5*, 527–531. https://doi.org/10.1109/LGRS.2008.923213

Narvekar, J., & Prasanna Kumar, S. (2014). Mixed layer variability and chlorophyllabiomass in the bay of bengal. *Biogeosciences, 11*, 3819–3843. https://doi.org/10.5194/bg-11-3819-2014

NASA ATBD Level-3 Binned Data Products. (n.d.). Ocean Level-3 binned data products NASA ATBD – NASA GSFC Ocean Data Processing System.

O'Reilly, J. E., & Werdell, P. J. (2019). Chlorophyll algorithms for ocean color sensors – OC4, OC5 & OC6. *Remote Sensing of Environment, 229*, 32–47. https://doi.org/10.1016/j.rse.2019.04.021

O'Reilly, J. E., Maritorena, S., Mitchell, B. G., Siegel, D. A., Carder, K. L., Garver, S. A., Kahru, M., & McClain, C. R. (1998). Ocean color chlorophyll algorighms for SeaWiFS. *Journal of Geophysical Research, 103*, 24937–24953. https://doi.org/10.1029/98JC02160

O'Reilly, J. E., Maritorena, S., O'Brien, M., Siegel, D., Toole, D., Menzies, D., Smith, R., Mueller, J. L., Mitchell, G., Kahru, M., Chavez, F., Strutton, P., Cota, G., McClain, C., Carder, K., Muller-Karger, F., Harding, L., Magnuson, A., Phinney, D., Moore, G., Aiken, J., Arrigo, K., Letelier, R., & Culver, M. (2000a). SeaWiFS postlaunch technical report series. *NASA, 11*, 1–49.

O'Reilly, J. E., Maritorena, S., O'Brien, M. C., Siegel, D. A, Toole, D., Menzies, D., Smith, R. C., Mueller, J. L., Mitchell, B. G., Kahru, M., Chavez, F. P., Strutton, P., Cota, G. F., Hooker, S. B., Mcclain, C. R., Carder, K. L., Müller-Karger, F. E., Harding, L., Magnuson, A., Phinney, D., Moore, G. F., Aiken, J., Arrigo, K. R., Letelier, R., & Culver, M. (2000b). SeaWiFS postlaunch calibration and validation analyses, part 3. SeaWiFS Postlaunch Tech. Rep. Ser. 11, p. 51.

Ocean Productivity – Oregon State University [WWW Document]. (2022). http://sites.science.oregonstate.edu/ocean.productivity/index.php

Pahlevan, N., Roger, J.-C., & Ahmad, Z. (2017). Revisiting short-wave-infrared (SWIR) bands for atmospheric correction in coastal waters. *Optics Express, 25*, 6015. https://doi.org/10.1364/oe.25.006015

Pahlevan, N., Smith, B., Binding, C., Gurlin, D., Li, L., Bresciani, M., & Giardino, C. (2021). Hyperspectral retrievals of phytoplankton absorption and chlorophyll-a in inland and nearshore coastal waters. *Remote Sensing of Environment, 253*. https://doi.org/10.1016/j.rse.2020.112200

Pahlevan, N., Smith, B., Alikas, K., Anstee, J., Barbosa, C., Binding, C., Bresciani, M., Cremella, B., Giardino, C., Gurlin, D., Fernandez, V., Jamet, C., Kangro, K., Lehmann, M. K., Loisel, H., Matsushita, B., Hà, N., Olmanson, L., Potvin, G., Simis, S. G. H., VanderWoude, A., Vantrepotte, V., & Ruiz-Verdù, A. (2022). Simultaneous retrieval of selected optical water quality indicators from Landsat-8, Sentinel-2, and Sentinel-3. *Remote Sensing of Environment, 270*, 112860. https://doi.org/10.1016/J.RSE.2021.112860

Park, Y.-J., & Ruddick, K. (2005). Model of remote-sensing reflectance including bidirectional effects for case 1 and case 2 waters. *Applied Optics, 44*, 1236–1249. https://doi.org/10.1364/ao.44.001236

Platt, T., & Sathyendranath, S. (1988). Oceanic primary production: Estimation by remote sensing at local and regional scales. *Science (80-.), 241*, 1613–1620. https://doi.org/10.1126/SCIENCE.241.4873.1613

Prakash, S., & Ramesh, R. (2007). Is the Arabian Sea getting more productive? *Current Science, 92*, 667–671.

Prakash, P., Prakash, S., Rahaman, H., Ravichandran, M., & Nayak, S. (2012). Is the trend in chlorophyll-a in the Arabian Sea decreasing? *Geophysical Research Letters, 39*. https://doi.org/10.1029/2012GL054187

Rao, S. A., Dhakate, A. R., Saha, S. K., Mahapatra, S., Chaudhari, H. S., Pokhrel, S., & Sahu, S. K. (2012). Why is Indian Ocean warming consistently? *Climatic Change, 110*, 709–719. https://doi.org/10.1007/S10584-011-0121-X

Roesler, C. S., & Boss, E. (2003). Spectral beam attenuation coefficient retrieved from ocean color inversion. *Geophysical Research Letters, 30*, 1–4. https://doi.org/10.1029/2002GL016185

Roesler, C. S., & Perry, M. J. (1995). In situ phytoplankton absorption, fluorescence emission and particulate backscattering spectra determined from reflectance. *Journal of Geophysical Research, 100*, 279–294. https://doi.org/10.1029/95JC02176

Roxy, M. K., Modi, A., Murtugudde, R., Valsala, V., Panickal, S., Prasanna Kumar, S., Ravichandran, M., Vichi, M., & Lévy, M. (2016). A reduction in marine primary productivity driven by rapid warming over the tropical Indian Ocean. *Geophysical Research Letters, 43*, 826–833. https://doi.org/10.1002/2015GL066979

Roy, S., Sathyendranath, S., Bouman, H., & Platt, T. (2013). The global distribution of phytoplankton size spectrum and size classes from their light-absorption spectra derived from satellite data. *Remote Sensing of Environment, 139*, 185–197. https://doi.org/10.1016/j.rse.2013.08.004

Ruddick, K. G., Voss, K., Boss, E., Castagna, A., Frouin, R., Gilerson, A., Hieronymi, M., Carol Johnson, B., Kuusk, J., Lee, Z., Ondrusek, M., Vabson, V., & Vendt, R. (2019). A review of protocols for fiducial reference measurements of water-leaving radiance for validation of satellite remote-sensing data over water. *Remote Sensing, 11*. https://doi.org/10.3390/rs11192198

Saba, V. S., Friedrichs, M. A. M., Carr, M. E., Antoine, D., Armstrong, R. A., Asanuma, I., Aumont, O., Bates, N. R., Behrenfeld, M. J., Bennington, V., Bopp, L., Bruggeman, J., Buitenhuis, E. T., Church, M. J., Ciotti, A. M., Doney, S. C., Dowell, M., Dunne, J., Dutkiewicz, S., Gregg, W., Hoepffner, N., Hyde, K. J. W., Ishizaka, J., Kameda, T., Karl, D. M., Lima, I., Lomas, M. W., Marra, J., McKinley, G. A., Melin, F., Moore, J. K., Morel, A., O'Reilly, J., Salihoglu, B., Scardi, M., Smyth, T. J., Tang, S., Tjiputra, J., Uitz, J., Vichi, M., Waters, K., Westberry, T. K., & Yool, A. (2010). Challenges of modeling depth-integrated marine primary productivity over multiple decades: A case study at BATS and HOT. *Global Biogeochemical Cycles, 24*. https://doi.org/10.1029/2009GB003655

Saba, V. S., Friedrichs, M. A. M., Antoine, D., Armstrong, R. A., Asanuma, I., Behrenfeld, M. J., Ciotti, A. M., Dowell, M., Hoepffner, N., Hyde, K. J. W., Ishizaka, J., Kameda, T., Marra, J., Mlin, F., Morel, A., O'Reilly, J., Scardi, M., Smith, W. O., Smyth, T. J., Tang, S., Uitz, J., Waters, K., & Westberry, T. K. (2011). An evaluation of ocean color model estimates of marine primary productivity in coastal and pelagic regions across the globe. *Biogeosciences, 8*, 489–503. https://doi.org/10.5194/bg-8-489-2011

Sadeghi, A., Dinter, T., Vountas, M., Taylor, B. B., Altenburg-Soppa, M., Peeken, I., & Bracher, A. (2012). Improvement to the PhytoDOAS method for identification of coccolithophores using hyper-spectral satellite data. *Ocean Science, 8*, 1055–1070. https://doi.org/10.5194/os-8-1055-2012

Sathyendranath, S., & Platt, T. (1989). Computation of aquatic primary production: Extended formalism to include effect of angular and spectral distribution of light. *Limnology and Oceanography, 34*, 188–198.

Sathyendranath, S., Brewin, R. J., Brockmann, C., Brotas, V., Calton, B., Chuprin, A., Cipollini, P., Couto, A. B., Dingle, J., Doerffer, R., Donlon, C., Dowell, M., Farman, A., Grant, M., Groom, S., Horseman, A., Jackson, T., Krasemann, H., Lavender, S., Martinez-Vicente, V., Mazeran, C., Mélin, F., Moore, T. S., Müller, D., Regner, P., Roy, S., Steele, C. J., Steinmetz, F., Swinton, J., Taberner, M., Thompson, A., Valente, A., Zühlke, M., Brando, V. E., Feng, H., Feldman, G., Franz, B. A., Frouin, R., Gould, R. W., Hooker, S. B., Kahru, M., Kratzer, S., Greg Mitchell, B., Muller-Karger, F. E., Sosik, H. M., Voss, K. J., Werdell, J., & Platt, T. (2019). An ocean-colour time series for use in climate studies: The experience of the ocean-colour climate change initiative (OC-CCI). *Sensors, 19*, 4285. https://doi.org/10.3390/s19194285

Sathyendranath, S., Platt, T., Kovač, Ž., Dingle, J., Jackson, T., Brewin, R. J. W., Franks, P., Marañón, E., Kulk, G., & Bouman, H. A. (2020). Reconciling models of primary production and photoacclimation [Invited]. *Applied Optics, 59*, C100. https://doi.org/10.1364/ao.386252

Sathyendranath, S., Jackson, T., Brockmann, C., Brotas, V., Calton, B., Chuprin, A., Clements, O., Cipollini, P., Danne, O., Dingle, J., Donlon, C., Grant, M., Groom, S., Krasemann, H., Lavender, S., Mazeran, C., Mélin, F., Müller, D., Steinmetz, F., Valente, A., Zuhlke, M., Feldman, G., Franz, B., Frouin, R., Werdell, J., & Platt, T. (2021). *ESA Ocean Colour Climate Change Initiative (Ocean_Colour_cci): Version 5.0 Data*. NERC EDS Centre for Environmental Data Analysis.

Shifrin, K. S. (1998). *Physical optics of ocean water, AIP translation series*. American Institute of Physics.

Shunmugapandi, R., Inamdar, A. B., & Gedam, S. K. (2020). Long-time-scale investigation of phytoplankton communities based on their size in the Arabian Sea. *International Journal of Remote Sensing, 41*, 5992–6009. https://doi.org/10.1080/01431161.2020.1714785

Shunmugapandi, R., Gedam, S., & Inamdar, A. B. (2022). Phenology of phytoplankton size classes in the Arabian Sea. *IEEE Geoscience and Remote Sensing Letters, 19*. https://doi.org/10.1109/LGRS.2021.3132660

Sieburth, J. M. (1978). Pelagic ecosystem structure: Heterotrophic compartments of the plankton and their relationship to plankton size fractions. *Limnology and Oceanography, 23*, 1256–1263.

Silsbe, G. M., Behrenfeld, M. J., Halsey, K. H., Milligan, A. J., & Westberry, T. K. (2016). The CAFE model: A net production model for global ocean phytoplankton. *Global Biogeochemical Cycles, 30*, 1756–1777. https://doi.org/10.1002/2016GB005521

Smith, B., Pahlevan, N., Schalles, J., Ruberg, S., Errera, R., Ma, R., Giardino, C., Bresciani, M., Barbosa, C., Moore, T., Fernandez, V., Alikas, K., & Kangro, K. (2021). A chlorophyll-a algorithm for Landsat-8 based on mixture density networks. *Frontiers in Remote Sensing, 0*, 5. https://doi.org/10.3389/FRSEN.2020.623678

Sreeush, M. G., Valsala, V., Pentakota, S., Prasad, K. V. S. R., & Murtugudde, R. (2018). Biological production in the Indian Ocean upwelling zones – Part 1: Refined estimation via the use of a variable compensation depth in ocean carbon models. *Biogeosciences, 15*, 1895–1918. https://doi.org/10.5194/bg-15-1895-2018

Steinmetz, F., Deschamps, P.-Y., & Ramon, D. (2011). Atmospheric correction in presence of sun glint: Application to MERIS. *Optics Express, 19*, 9783. https://doi.org/10.1364/oe.19.009783

Stramski, D., Reynolds, R. A., Kahru, M., & Mitchell, B. G. (1999). Estimation of particulate organic carbon in the ocean from satellite remote sensing. *Science (80-.), 285*, 239–242.

Stramski, D., Boss, E., Bogucki, D., & Voss, K. J. (2004). The role of seawater constituents in light backscattering in the ocean. *Progress in Oceanography, 61*, 27–56. https://doi.org/10.1016/j.pocean.2004.07.001

Sullivan, J. M., & Twardowski, M. S. (2009). Angular shape of the oceanic particulate volume scattering function in the backward direction. *Applied Optics, 48*, 6811–6819.

Tang, S., Chen, C., Zhan, H., & Zhang, T. (2008). Determination of ocean primary productivity using support vector machines. *International Journal of Remote Sensing, 29*, 6227–6236. https://doi.org/10.1080/01431160802175355

Tao, Z., Wang, Y., Ma, S., Lv, T., & Zhou, X. (2017). A phytoplankton class-specific marine primary productivity model using MODIS data. *IEEE Journal of Selected Topics in Applied Earth Observations and Remote Sensing, 10*, 5519–5528. https://doi.org/10.1109/JSTARS.2017.2747770

Tonizzo, A., Kolluru, S., & Twardowski, M. S. (2022). Evaluating the BRDF correction for a new semi-analytical model using field measurements. In *Interanational radiation symposium*.

Twardowski, M., & Alberto T. (2018). Ocean color analytical model explicitly dependent on the volume scattering function. *Applied Sciences, 8*(12), 2684. https://doi.org/10.3390/app8122684

Twardowski, M. S., Rottgers, R., & Stramski, D. (2018). Chapter 1: The absorption coefficient, an overview. In *Ocean optics & biogeochemistry protocols for satellite ocean colour sensor validation* (pp. 1–15). International Color Coordinating Group (IOCCG), Bedford Institute of Oceanography.

Uitz, J., Claustre, H., Morel, A., & Hooker, S. B. (2006). Vertical distribution of phytoplankton communities in open ocean: An assessment based on surface chlorophyll. *Journal of Geophysical Research: Oceans, 111*. https://doi.org/10.1029/2005JC003207

Uitz, J., Huot, Y., Bruyant, F., Babin, M., & Claustre, H. (2008). Relating phytoplankton photophysiological properties to community structure on large scales. *Limnology and Oceanography, 53*, 614–630. https://doi.org/10.4319/lo.2008.53.2.0614

Uitz, J., Claustre, H., Gentili, B., & Stramski, D. (2010). Phytoplankton class-specific primary production in the world's oceans: Seasonal and interannual variability from satellite observations. *Global Biogeochemical Cycles, 24*, 1–19. https://doi.org/10.1029/2009GB003680

Vanhellemont, Q. (2019). Adaptation of the dark spectrum fitting atmospheric correction for aquatic applications of the Landsat and Sentinel-2 archives. *Remote Sensing of Environment, 225*. https://doi.org/10.1016/j.rse.2019.03.010

Vanhellemont, Q., & Ruddick, K. (2015). Advantages of high quality SWIR bands for ocean colour processing: Examples from Landsat-8. *Remote Sensing of Environment, 161*, 89–106. https://doi.org/10.1016/j.rse.2015.02.007

Vanhellemont, Q., & Ruddick, K. (2016). *ACOLITE processing for Sentinel-2 and Landsat-8: Atmospheric correction and aquatic applications*. Living Planet Symp.

Vincent, R. F., Marsden, R. F., Minnett, P. J., Creber, K. A. M., & Buckley, J. R. (2008). Arctic waters and marginal ice zones: A composite Arctic Sea surface temperature algorithm using satellite thermal data. *Journal of Geophysical Research: Oceans, 113*. https://doi.org/10.1029/2007JC004353

Walton, C. C., Pichel, W. G., Sapper, J. F., & May, D. A. (1998). The development and operational application of nonlinear algorithms for the measurement of sea surface temperatures with the NOAA polar-orbiting environmental satellites. *Journal of Geophysical Research*. https://doi.org/10.1029/98JC02370

Wang, M. (1999). Atmospheric correction of ocean color sensors: Computing atmospheric diffuse transmittance. *Applied Optics, 38*, 451. https://doi.org/10.1364/ao.38.000451

Wang, M., & Shi, W. (2007). The NIR-SWIR combined atmospheric correction approach for MODIS ocean color data processing. *Optics Express, 15*, 15722–15733. https://doi.org/10.1029/2004JD004950

Wang, P., Boss, E. S., & Roesler, C. (2005). Uncertainties of inherent optical properties obtained from semianalytical inversions of ocean color. *Applied Optics, 44*, 4074–4085. https://doi.org/10.1364/AO.44.004074

Wang, J., Wang, Y., Lee, Z., Wang, D., & Chen, S. (2022). A revision of NASA SeaDAS atmospheric correction algorithm over turbid waters with artificial Neural Networks estimated remote-sensing reflectance in the near-infrared. *ISPRS Journal of Photogrammetry and Remote Sensing, 194*, 235–249. https://doi.org/10.1016/j.isprsjprs.2022.10.014

Waters, C., Ocean, S. O., Sensor, C., Mograne, M. A., Jamet, C., & Loisel, H. (2019). *Evaluation of five atmospheric correction algorithms over French optically-evaluation of five atmospheric correction algorithms over French optically-complex waters for the Sentinel-3A OLCI ocean color sensor*. https://doi.org/10.3390/rs11060668.

Werdell, P. J., & Bailey, S. W. (2005). An improved in-situ bio-optical data set for ocean color algorithm development and satellite data product validation. *Remote Sensing of Environment, 98*, 122–140. https://doi.org/10.1016/j.rse.2005.07.001

Werdell, P. J., Franz, B. A., Bailey, S. W., Feldman, G. C., Boss, E., Brando, V. E., Dowell, M., Hirata, T., Lavender, S. J., Lee, Z., Loisel, H., Maritorena, S., Mélin, F., Moore, T. S., Smyth, T. J., Antoine, D., Devred, E., D'Andon, O. H. F., & Mangin, A. (2013). Generalized ocean color inversion model for retrieving marine inherent optical properties. *Applied Optics, 52*, 2019–2037. https://doi.org/10.1364/AO.52.002019

Werdell, P. J., McKinna, L. I. W., Boss, E., Ackleson, S. G., Craig, S. E., Gregg, W. W., Lee, Z., Maritorena, S., Roesler, C. S., Rousseaux, C. S., Stramski, D., Sullivan, J. M., Twardowski, M. S., Tzortziou, M., & Zhang, X. (2018). An overview of approaches and challenges for retrieving marine inherent optical properties from ocean color remote sensing. *Progress in Oceanography, 160*, 186–212. https://doi.org/10.1016/j.pocean.2018.01.001

Westberry, T., Behrenfeld, M. J., Siegel, D. A., & Boss, E. (2008). Carbon-based primary productivity modeling with vertically resolved photoacclimation. *Global Biogeochemical Cycles, 22*. https://doi.org/10.1029/2007GB003078

Wiggert, J. D., Murtugudde, R. G., & McClain, C. R. (2002). Processes controlling interannual variations in wintertime (Northeast Monsoon) primary productivity in the central Arabian Sea. *Deep Sea Research Part II: Topical Studies in Oceanography, 49*, 2319–2343. https://doi.org/10.1016/S0967-0645(02)00039-5

Wiggert, J. D., Hood, R. R., Banse, K., & Kindle, J. C. (2005). Monsoon-driven biogeochemical processes in the Arabian Sea. *Progress in Oceanography, 65*, 176–213. https://doi.org/10.1016/j.pocean.2005.03.008

Wong, E. W., & Minnett, P. J. (2016). Retrieval of the ocean skin temperature profiles from measurements of infrared hyperspectral radiometers-part I: Derivation of an algorithm. *IEEE Transactions on Geoscience and Remote Sensing, 54*, 1879. https://doi.org/10.1109/TGRS.2015.2483746

Wong, E. W., & Minnett, P. J. (2018). The response of the ocean thermal skin layer to variations in incident infrared radiation. *Journal of Geophysical Research: Oceans, 123*, 2475–2493. https://doi.org/10.1002/2017JC013351

Zaneveld, J. R. V. (1989). An asymptotic closure theory for irradiance in the sea and its inversion to obtain the inherent optical properties. *Limnology and Oceanography, 34*, 1442–1452. https://doi.org/10.4319/lo.1989.34.8.1442

Zhai, P.-W., Hu, Y., Trepte, C. R., Winker, D. M., Lucker, P. L., Lee, Z., & Josset, D. B. (2015). Uncertainty in the bidirectional reflectance model for oceanic waters. *Applied Optics, 54*, 4061. https://doi.org/10.1364/ao.54.004061

Zhang, T., & Fell, F. (2007). An empirical algorithm for determining the diffuse attenuation coefficient Kd in clear and turbid waters from spectral remote sensing reflectance. *Limnology and Oceanography: Methods, 5*, 457–462. https://doi.org/10.4319/lom.2007.5.457

Chapter 11
Remote Sensing-Based Estimation of Primary Production in the Arabian Sea

Mini Raman and Shailesh Nayak

Abstract The key element in regulating the carbon dynamics of the oceans through biological processes is the microscopic free-floating autotrophic phytoplankton and associated rates of primary production. Accurate assessment of large-scale spatio-temporal dynamics of primary production by traditional platforms is frustrating due to limited spatial resolution and undersampling. By the virtue of its broad, synoptic coverage, ocean color imagery provides a two-dimensional window onto the dynamic state of phytoplankton biomass fields indexed as chlorophyll-a concentration. An important application of remotely sensed ocean data is the estimation of oceanic primary production. Compared with high seas, regional seas such as Arabian Sea are characterized by definite geographical boundaries encompassing coastal regions, continental shelves, and current systems. Estimation of primary production in the Arabian Sea from the Indian Ocean color monitor OCM-1 involved the use of a depth-integrated nonspectral model to compute the daily rate of euphotic zone primary production. The model driven by OCM-1derived chlorophyll data was operated with additional information on surface irradiance, light transmission in the water column, day length, and photosynthetic rate parameters, which accounts for the light capture and utilization by the phytoplankton. Euphotic zone primary production maps were generated covering the broad continental shelf, slope, and open ocean waters of the Arabian Sea, and computed values were validated with in situ measured rates of primary production. Statistical analysis indicated that the model explained 70% variance in the in situ dataset with a low negative bias of 3% and an overall uncertainity of 41.8% in the euphotic zone primary production estimates that was within the desired accuracy goal of 45% set by ocean color missions. The optimum performance of the model was due to region-specific chlorophyll algorithm (OC-OCM) for Arabian Sea as input compared to global chlorophyll algorithms such as OC2 and OC4.

M. Raman (✉)
Marine Ecosystems Division, Space Applications Centre (ISRO), Ahmedabad, India
e-mail: mraman@sac.isro.gov.in

S. Nayak
National Institute of Advanced Studies, Indian Institute of Science Campus, Bengaluru, India

S. C. Tripathy, A. Singh (eds.), *Dynamics of Planktonic Primary Productivity in the Indian Ocean*, https://doi.org/10.1007/978-3-031-34467-1_11

Keywords Arabian Sea · Modelling · Ocean color · Phytoplankton production · Satellite

1 Introduction

Global warming induced climate change in recent years due to carbon dioxide (CO_2), and other gases released into the atmosphere through anthropogenic activity has renewed scientific interest in the role of the ocean in the global carbon (C) cycle. Approximately 95% of the carbon that circulates actively in the biosphere is stored by the ocean, and the carbon inventory of the ocean is ~40 gigatonnes. This is about 65 times larger than the CO_2 inventory of the atmosphere and ~20 times larger than the quantity of carbon tied up in the terrestrial biosphere. Observational and modelling estimates indicate carbon inventory of the ocean to be increasing at a rate of two gigatonnes C per year. This amount is equivalent to the absorption of ~40% of the excess CO_2 release annually to the atmosphere from human activities (Sarmiento et al., 1992).

The Arabian Sea has been described as a natural laboratory for studying the upper ocean's response to atmospheric forcing due to the asymmetry caused by the existence of the Asian subcontinent in the north which profoundly influences the regional climate, ocean circulation, and biogeochemical processes. This unusual geographical asymmetry results in two phases of seasonally reversing monsoonal winds and surface currents with two transition periods in between (Dietrich, 1973; Wyrtki, 1973). Rates of primary production and carbon fluxes are strongly regulated by the magnitude of nutrient inputs resulting from wind-driven upwelling during the southwest monsoon (June-September) and deep winter-convective mixing during the northeast monsoon (November-mid March). The transition periods are marked by oligotrophic conditions (Babenerd & Krey, 1974). Very high rates of new production sustained by upwelling and vertical mixing during both monsoons leads to the export of large quantities of organic matter to the deep sea, depleting dissolved oxygen within a large body of intermediate waters, a marked feature of the Arabian Sea (Naqvi, 1991; SenGupta et al., 1976). In addition to these characteristics, interannual anomalies in the magnitude of primary production of the Arabian Sea are also affected by continental influences such as fluvial discharge, atmospheric inputs like dust events, cyclones, large-scale climatic events (El Niño-La Niña events, Indian Ocean Dipole, Eurasian snow cover), eddies, and frontal features (Parthasarathy et al., 1995; Saji et al., 1999; Goés et al., 2005).

As regards the biogeochemistry of the Arabian Sea, several key variables and parameters of carbon cycle remains unknown or poorly understood. Large uncertainities exist as to whether this basin is a sink due to its high rates of primary production and large export flux or source (outgassing of deep CO_2-rich waters brought to the surface by upwelling) for atmospheric CO_2 (Somasunder et al., 1990; Sarma et al., 1998; Goyet et al., 1998).

Time-series observations are the most valuable data for climate change and biogeochemical studies (Brewer et al., 1986). Measurements by traditional platforms (ship surveys and moorings) are expensive, laborious, and intrinsically limited to small space and timescales, and many parts of the oceans remain grossly undersampled. In the Arabian Sea, a major impediment has been the lack of time-series observations. Most time-series datasets collected by shipboard methods are spatially isolated and discontinuous over long timescales, making any meaningful assessments of the variation in the biogeochemical properties difficult. Fortunately, rapid technological advances in ocean observations achieved during the last decade, particularly with respect to satellite ocean color remote sensing, provide a unique opportunity to obtain information directly related to ecological and biogeochemical processes.

Remote sensing is a generic term covering a variety of non intrusive monitoring techniques that measure energy-matter interactions to determine the characteristics of a target medium or surface (Colwell, 1983). Over the past three decades, a wide range of Earth-orbiting satellite systems and sensors have evolved, from the proof of concept to operational missions, which have totally revolutionized our understanding of land-ocean-atmospheric interactions. Although remote sensing includes a wide variety of instruments and methods, it is most often associated with overhead imaging techniques, such as aerial photography and satellite imagery, that record energy in the electromagnetic spectrum between 400 and 2500 nm wavelengths absorbed or scattered by objects on the Earth. The spectral reflectance pattern constitutes a characteristic signature enabling satellite sensors to retrieve information about the target object under view.

Prior to the use of ocean color data, inference on the spatial and temporal distribution of phytoplankton biomass in the vast stretches of the Arabian Sea was solely dependent on data collected from ship cruises conducted during various expeditions and exploration programmes (Subrahmanyan, 1959; Subrahmanyan & Sarma, 1960; Raman & Prakash, 1989). However, these data were from point locations and were extrapolated over large areas of the ocean to give an overall picture of phytoplankton distribution either seasonally or annually. Inevitably, maps produced from such data failed to capture the spatial and temporal dynamics of phytoplankton biomass. By the virtue of its broad, synoptic coverage, ocean color imagery provides a two-dimensional window into the dynamic state of pelagic ecosystem. With the help of simple band-ratio algorithms, CZCS was able to capture the intrinsic variability of phytoplankton biomass of the Arabian Sea (Gordon & Morel, 1983). Subsequently, ocean color sensors such as SeaWiFS, MODIS-AQUA, Oceansat- OCM 1 and 2, NPP-VIIRS, etc., used a maximum band ratio algorithm (OC4) to map phytoplankton biomass or chlorophyll-a concentration in the Arabian Sea.

Information on the oceanic primary production is important for carbon biogeochemistry, the influence of anthropogenic carbon on the ocean, understanding the limits to marine production and the management of sustainability of marine resources. It could be stated that apart from the amount of phytoplankton biomass, the rate of carbon fixation is also dependent on factors such as nutrients, temperature,

light, and the physiological response of phytoplankton biomass to these factors. Classical methods of primary production estimation depend on ship-based observations and in situ incubation experiments. Though successful in determining the scales of production, the methodology is intrinsically limited to small space and timescales and many regions in the oceans are grossly undersampled. Lack of synoptic observations means that episodic events and spatiotemporal extremes of seasonal dynamics are frequently not sampled sufficiently, which could have a bearing on our understanding of the ecosystem. In this context, remotely sensed images of chlorophyll-a concentration at daily and longer timescales offer the possibility of providing the estimates of primary production at the basin to global scales. Initial efforts were based on empirical models, which exploited the relationship between primary production integrated to euphotic depth (depth at which the sun light reaches 1% of its surface value) and surface phytoplankton concentration (Ryther & Yentsch, 1957; Eppley et al., 1985; Joint & Groom, 2000). The advantages of these models are that they are simple and remotely sensed chlorophyll-a can be easily used to interpolate between the data in space and time. However, these models are region-specific, empirical relationships valid only for a range of data from which they were derived and therefore, may not be extrapolated to other locations.

Subsequently, analytical or semiempirical models were adopted to estimate primary production, which are based on the first principles of plant physiology and ocean optics. These models involve the use of photosynthesis-light relationships characterizing the functional response of phytoplankton photosynthesis to available light. Production is estimated by combining remotely sensed biomass concentration with information of day-length, incident solar irradiance at the sea surface, modeled distribution of light field within the water column, vertical structure of phytoplankton biomass, and photosynthetic rate parameters (Platt et al., 1988; Sathyendranath & Platt, 1989; Morel, 1991; Behrenfeld & Falkowski, 1997b). Primary production models may be spectral, where influence of individual wavelengths on transmission and absorption of light is considered, or nonspectral, where spectral dependencies in light transmission are ignored (Platt & Sathyendranath, 1993; Antoine et al., 1996). Further, they may be depth-integrated models where the vertical structure of phytoplankton biomass is ignored, and total or average euphotic zone biomass is considered for computing light within the water column, or depth-resolved models where the vertical structure of the local biomass profile is parameterized up to euphotic depth to allow for the computation of light field as a function of depth (Sathyendranath & Platt, 1993, 2007; Behrenfeld & Falkowski, 1997a).

A critical aspect of these models is the determination of photosynthetic rate parameters, which cannot be retrieved directly from satellite data. The rate parameters, which account for the light capture and utilization are neither spatially uniform nor constant throughout the year (Platt & Sathyendranath, 1999). This is because the rate parameters vary for different phytoplankton assemblages, which are characterized by unique pigment compositions, pigment packaging, and size structure (Sathyendranath et al., 1987). The spatial and temporal variability of phytoplankton assemblages, in turn, are dependent on the light history and nutrient regimes of a

given region that vary seasonally and spatially due to dynamics of atmospheric and oceanographic processes (Longhurst, 2006). This implies a partition of ocean regions into a suite of provinces within which the phytoplankton assemblages will be similar in their requirement of environmental factors conducive for their growth and will experience common physical forcing (light, nutrients) (Platt et al., 1995). The provinces can form a template upon which the photosynthetic rate parameters could be assigned for regional scale modeling of primary production (Longhurst et al., 1995; Bouman et al., 2005). Spatiotemporal variability of biogeochemical processes and biological properties in a province is more pronounced in regional seas compared with provinces in open ocean due to changes in the regional characteristics of physicochemical processes such as coastal upwelling, frontal dynamics, topographic effects, and many more. The provinces embedded in a regional sea, therefore, will have variable spatial and temporal dynamic boundaries that can be delineated using ocean color imagery (Devred et al., 2007).

2 Materials and Methods

2.1 Modelling Column Primary Production

2.1.1 Water-Column Primary Production Model Formulation

Primary production (P) and phytoplankton biomass (B) are local variables subjected to changes in their magnitudes on short scales of time and space. Variations in biomass are the primary cause of variation in rates of primary production. Therefore, to estimate P, given information on irradiance (I), it is important to account for the effects of variations in B (Banse & Yong, 1990). This is the premise to define a variable known as normalized primary production, P^B (primary production divided by biomass), which is more informative than absolute P because its variation between regions and seasons can be analyzed without the difficulty that might arise from random fluctuations in the local biomass (Platt & Sathyendranath, 1993). In other words, P^B is an intrinsic property of a sample or of a hydrographic station from which it was sampled. Its magnitude will be stable against local variations of the biomass, and its value at a particular station can be considered more representative of the region in which the station is embedded than the station values with either P or B. Thus,

$$P^B = \frac{P}{B} \tag{11.1}$$

If required, the absolute production P can be recovered by inversion of Eq. 11.1

$$P = B \times P^B \tag{11.2}$$

The pigment biomass usually depends on depth (z), so that Eq. 11.2 can be written as

$$P(z) = B(z) \times P^B(z) \tag{11.3}$$

The normalized production is a function of available irradiance, and in aquatic systems, irradiance is always a function of depth (Jerlov, 1976; Kirk, 1983). Therefore, the dependence of normalized production at depth $P^B(z)$ on irradiance or photon flux may be stated formally as

$$P^B(z) = p^B(I(z)) \tag{11.4}$$

where $I(z)$ may be given as a function of surface irradiance I_0

$$I(z) = I_0 e^{-kz} \tag{11.5}$$

From Eqs. 11.3 and 11.4,

$$P(z) = B(z) \times p^B(I(z)) \tag{11.6}$$

$I(z)$ in the above equation is a time-dependent variable. Therefore, the above equation can be rewritten as

$$P(z,t) = B(z,t) \times p^B(I(z,t)) \tag{11.7}$$

The above equation computes production at discrete depths. To compute the production of a water column, the above equation has to be integrated over depth. Thus, water-column production P_z can be computed as

$$P_z = \int_z P(z,t)dz = \int_0^\infty B(z,t) \times p^B(I(z,t))dz \tag{11.8}$$

The upper limit of integration over depth is set to infinity because contributions to the integral at this limit will be insignificantly small due to the exponential decay of irradiance with depth (Platt & Sathyendranath, 1993). It is also necessary to integrate the above equation, which gives the instantaneous water-column rates through time to compute primary production for the day. Thus,

$$P_{ZT} = \int_0^\infty \int_0^{D_L} B(z,t) \times p^B(I(z,t))dzdt \tag{11.9}$$

where time (t) is measured from sunrise and the day length (D_L) is in hours. For integration through time, it is assumed that diurnal changes in B are sufficiently slow to be significant, i.e., the time dependence of B in the above equation is suppressed to give

$$P_{ZT} = \int_0^{\infty} \int_0^{D_L} B(z) \times p^B(I(z,t))dzdt \tag{11.10}$$

This is the basic formalism for the computation of water-column primary production.

For a finite depth (such as mixed-layer depth (MLD) or euphotic depth), water-column production in Eq. 11.10 becomes

$$P_{ZT} = \int_0^{X} \int_0^{D_L} B(z) \times p^B(I(z,t))dzdt \tag{11.11}$$

where X is either MLD or euphotic depth or any other arbitrary depth, P_{ZT} is the total integrated primary production, $B_{(Z)}$ is biomass at depth, $p^B(I(z,t))$ is the normalized production as a function of irradiance, specified in terms of PI parameters, and D_L is day length or photoperiod.

2.1.2 Variables and Parameters of Primary Production Model

Production (P) and Biomass (B)

The rate of conversion of inorganic carbon into organic carbon (or carbon fixation) is called photosynthetic rate or rate of primary production denoted by the symbol P with dimensions [ML^{-3} T^{-1}] and units as mass of C (g or mg) m^{-3} day^{-1} or, generally, per unit time. The photosynthetic biomass engaged in primary production is denoted as B, with dimensions [ML^{-3}] and units as mg or g m^{-3}. The magnitudes of both P and B change with time and space and, therefore, are local variables. There are several possibilities for biomass index B, which includes phytoplankton carbon (Westberry et al., 2008), total carbon (Stramski et al., 1999), and total pigment mass (Morel & Berthon, 1989). However, chlorophyll-a concentration is the most preferred one because of its central role in the photosynthetic process. Also it is a variable that can easily be measured in the field and also derived from satellite data. A suite of bio-optical algorithms is currently available to estimate chlorophyll-a concentration from the atmospherically corrected water-leaving radiances with reasonable accuracy (Morel & Prieur, 1977; Gordon & Morel, 1983; Platt & Sathyendranath, 1988; O'Reilly et al., 2000; Chauhan et al., 2002; Chauhan, 2005).

Irradiance (I or E) and Photoperiod (D_L)

The next input variables are the irradiance designated as I or E and photoperiod or day length (D_L). Irradiance is expressed either as the flux of energy per unit area per unit time [MT^{-3}] or as the flux of photons per unit square area per unit time [L^{-2} T^{-1}]. The fundamental aspects of irradiance are quantity and quality (Kirk,

1983). Both these properties of irradiance vary strongly in the sea depending on time (daily, seasonally, and annually), space (different locations on the earth and depth), weather conditions, and angular distribution (including direction of maximum flux and degree of diffusion and polarization). The control on the quality and quantity of light originates not only in the atmosphere above or at the surface (e.g., the change in flux due to the rising and setting of the sun) but also within the water itself, such as changes in diffusion due to suspended matter and spectral changes due to selective absorption (Kirk, 1984; Sathyendranath & Platt, 1989).

Light energy required by algal photosynthesis to carry out the basic photochemical reactions is restricted to the range from UV through the visible spectrum or between 300 and 720 nm. Total radiation at this wavelength is called "photosynthetically available radiation." In the aquatic environment, PAR is taken operationally to be in the range of 400 and 700 nm (Smith & Tyler, 1967). Important properties of the irradiance field include wavelength (λ) and angular distribution (zenith and azimuth angles θ, ϕ). However, in simple models, the wavelength and angular distribution of the irradiance field may be suppressed.

Irradiance reaching the surface may be computed, for clear-sky conditions, given latitude, day number, and local time. The local time is generally noon when the sun is at its zenith. Latitude, day number, and local time are used to calculate solar angles and photoperiod or $D_L[T]$, which describes the sunshine hours for phytoplankton photosynthesis. The solar angles can then be coupled to a clear-sky model such as Bird's (1984) for the computation of surface irradiance over visible wavelengths throughout the day.

Vertical Diffuse Attenuation Coefficient (K_d)

As seen from Eqs. 11.4, 11.5, and 11.6, photosynthesis is dependent on the available irradiance, and therefore, photosynthesis at depth is also dependent upon the irradiance available at that depth. In aquatic systems, irradiance is always a function of depth. To estimate light reaching a particular depth, an important parameter called the downward vertical diffuse attenuation coefficient or $K_d[\mathrm{L}^{-1}]$ is used. $K_d(\lambda)$ defines the propagation of spectral downwelling irradiance from the surface to the interior of the ocean and controls the availability of light within the water column for photosynthesis and other biological processes (Platt et al., 1988; Marra et al., 1995). Given the surface irradiance field, the flux at any depth in the ocean can be computed by knowing the diffuse attenuation coefficient K_d (Sathyendranath & Platt, 1988). $K_d(\lambda)$ is an apparent optical property and therefore varies with solar zenith angle, sky, and surface conditions. The K_d can be computed either directly from satellite data (Mueller & Trees, 1994) or indirectly using biomass data. The vertically averaged value of $K_d(\lambda)$ in the surface mixed layer is the commonly used quantity in ocean color remote sensing. For case-1 waters, K_d can be computed from biomass since phytoplankton biomass is considered the most important factor responsible for changes in the optical properties of seawater (Morel, 1988).

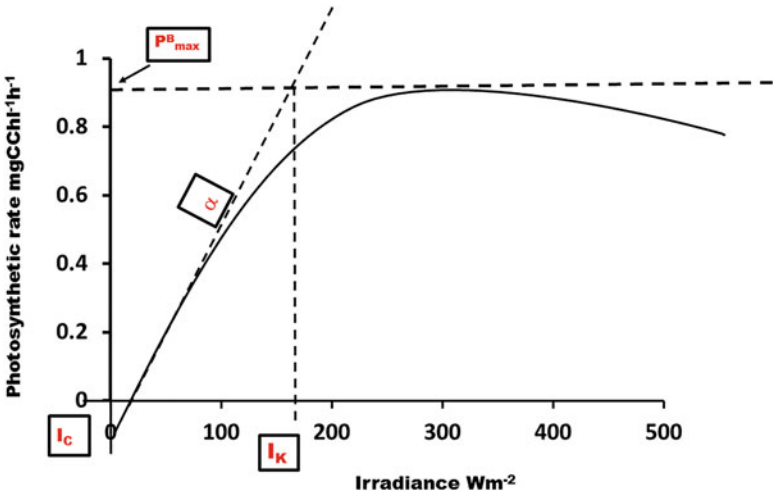

Fig. 11.1 A typical curve of the photosynthetic rate as a function of irradiance (*PI* curve)

Parameters (α, $P_{\max}$) of Photosynthesis-Irradiance (*PI*) Curve

Since photosynthesis is a photochemical process, the functional response of phytoplankton photosynthesis to available light is studied through the use of photosynthesis-light experiments (called either *PI* or *PE* experiments). The relationship between light and photosynthesis (Fig. 11.1) is called the light-saturation curve (*PI* or *PE* curve), and the *PI* curves provide a basic tool to understand the photosynthesis-light process (Kirk, 1994). The parameters describing the *PI* curves are known as *PI* parameters, which are used as inputs to the mathematical models, formulated to compute primary production over larger space and timescales (Platt & Sathyendranath, 1988; Longhurst et al., 1995,). Much of the variability in the PI relationship observed in nature can be characterized through changes in its initial slope (α) and maximal value ($P_{\max}$) (Fig. 11.1). In nature, $P_{\max}$ and α are slowly varying properties that can be obtained only from in situ observations.

The photosynthesis-light curve is a manifestation of environmental effects (nutrients, temperature) on photosynthesis (Cullen et al., 1992) and can be used to diagnose certain properties of algal species (community structure) or natural samples of phytoplankton (Bouman et al., 2005). It can be seen (Fig. 11.1) that the rate of photosynthesis increases with increasing light intensity up to some asymptotic value where the photosynthetic process becomes light saturated.

The point where the curve cuts the abscissa is the compensation point (I_C) defined as the irradiance for which the photosynthesis just balances the dark respiration. The curve is quasi-linear close to the abscissa with a slope ($\Delta P/\Delta I$) known as α^B or initial slope. The initial slope characterizes the light reactions of photosynthesis and has units ([mgC [mgChl.a]$^{-1}$ h^{-1}][E m^{-2} h^{-1}]$^{-1}$). At higher irradiances, the slope of the curve decreases progressively until the curve reaches a plateau of amplitude $P^{B\max}$ or P^{Bm}, called the assimilation number or biomass-specific

primary production at saturating irradiance (Platt et al., 1980). The units are mgC [mgChl.a]$^{-1}$ h^{-1}. The photo-adaptation parameter is the projection of the intersection of the initial slope with the plateau onto the abscissa or the ratio of P^{Bm} to α^B, and it is designated as I_k (μE m^{-2} h^{-1}). It has the same dimensions of irradiance, and it is therefore used as a scale to normalize the irradiance and render it dimensionless, i.e.,

$$I^* = \frac{I}{I_K} = \frac{\alpha^B}{P^B_m} \tag{11.12}$$

The curves are divided into two regimes around the value of I_* and equals 1 (corresponding to $I = I_k$). For I_* less than or equal to 1, photosynthesis depends strongly on irradiance. For I_* greater than 1, photosynthesis depends less strongly on irradiance, eventually becoming independent of it. Sometimes, the curve, after reaching the maximum amplitude, may drop down at higher irradiances, as in the case of tropical seas during the peak summer season. This is due to photoinhibition, where photosynthesis decreases as irradiance increases. This may be characterized by another parameter β^{B-} (Platt & Sathyendranath, 1993). However, in general, and for most cases, the curve can be characterized by two parameters α and P^m assuming that the curve passes through the origin and can be written as

$$P(I) = p^B\left(I; \alpha^B, P^B_m\right) \tag{11.13}$$

In other words, photosynthesis-light curve is a function of one variable; irradiance, and two parameters. This function p^B defines a family of curves, and the individual members are identified by the value or magnitude of parameters α^B and P^{Bm}. Since α^B and P^{Bm} vary for different areas and seasons, it is necessary to know the local magnitude of α^B and P^{Bm} to compute primary production. The slope α^B may also be depth dependent. In the ocean, light decays exponentially with depth, and phytoplankton species adapted to the lower light levels at depth may have a higher efficiency of photosynthesis (higher alpha conditions). Slope of the P versus I curve is also spectral in nature, a consequence mainly due to the spectral absorption of light by phytoplankton. Because the spectral composition of the submarine light field changes with depth, depth-dependent changes in α^B can be expected (Sathyendranath et al., 1989a). As a result, photosynthesis models may be based on spectral or nonspectral formulations. In spectral models, the spectral effects of light transmission and spectral dependence of α are taken into consideration. In nonspectral models, the spectral dependencies are ignored.

Depth of the Water Column for Integral Production: Mixed-Layer Depth (MLD) or Euphotic Depth (Z_{eu})

In the mixed-layer primary production model, the mixed-layer depth (MLD) is obtained as a function of the temperature or density profiles of a given hydrographic

station. MLD depth is taken to be the depth, where surface temperature decreases to 0.5 °C or density reduces to 0.125 sigma units. For a spatial data such as satellites, MLD (m) can be obtained as a daily product of the Ocean General Circulation Model (OGCM various versions) at a specified spatial resolution (0.5°, 0.25°, 0.125° latitude × 0.5°, 0.25°, 0.125° longitude grid) or from climatology (http://www.nodc.noaa.gov).

Euphotic depth is the depth of 1% isolume or the depth where surface irradiance falls to 1% of its intensity and is often taken to be the lower limit for photosynthesis. It can be obtained from radiometric profiles for a single hydrographic station or can be estimated from vertical diffuse attenuation coefficient K_d as $4.6/K_d$.

Vertical Structure of Phytoplankton Biomass and Integrated Biomass

In open ocean, phytoplankton biomass is not uniform throughout the water column. The vertical profile of phytoplankton biomass is characterized by a deep chlorophyll maximum (DCM) (Longhurst & Harrison, 1989). Ocean color satellites provide information only on the near-surface layer of the water column, i.e., 90% of the signal detected by the satellite originates from the top optical depth ($1/K$) of the euphotic zone. The first optical depth is approximately one-fifth of the productive part of the water column, such that the satellite may not detect much of the phytoplankton in the euphotic zone. This brings in an additional requirement of defining the vertical structure of the local biomass concentration $B(z)$ in the productive zone. This is important for two reasons: firstly, because it determines the transmittance of surface irradiance flux through the water column and thereby the euphotic depth (Sathyendranath & Platt, 1991), and secondly, it determines the amount of absorption of transmitted energy by the phytoplankton (Antoine & Morel, 1996). The vertical distribution of B may be specified as a series of discrete values or as a smooth curve following some standard shape (Platt et al., 1988, 1994) and integrated to determine the total biomass of the productive column (Morel & Berthon, 1989).

2.2 *Algorithm for Computation of Primary Production*

Evaluation of biomass $B_{(Z)}$, PI paramters $p^B(I)$, and light field within the water column $I(z)$ under various assumptions have resulted in empirical, semi-analytical, and analytical algorithms. Accordingly, computation of primary production may be from chlorophyll-a or carbon-based $B_{(Z)}$, spectral or nonspectral $I(z)$, and light absorbed or light available for parameters of $p^B(I)$ (Bannister, 1974; Morel, 1978; Falkowski, 1981; Eppley et al., 1985; Platt, 1986; Sakshaug et al., 1989; Sathyendranath et al., 1989b; Dubinsky, 1992; Behrenfeld et al., 2005; Sathyendranath & Platt, 2007; Westberry et al., 2008; Hirawake et al., 2012). Chlorophyll-based, light available, and depth-integrated nonspectral model is

described in the following section. Depth-integrated models (DIMs) use vertically integrated functions to relate variables measurable at the sea surface for estimating column production. Chlorophyll-based light available DIMs incorporate estimates of surface biomass indexed as chlorophyll-a concentration, vertical diffuse attenuation coefficient, day length, and photosynthetic rate parameters based on available surface irradiance and irradiance-dependent functions.

2.2.1 Analytical Algorithm for Depth-Integrated Primary Production

Based on dimensional analysis, Platt and Sathyendranath (1993) have shown that analytical solutions are possible with certain assumptions for the evaluation of Eqs. 11.10 and 11.11. The assumptions for a finite layer computation were uniform biomass throughout the layer, uniform diffuse attenuation coefficient K_d, and a sinusoidal variation of surface irradiance throughout the day.

A fifth-order polynomial was found to provide an approximation to the analytical solution for the daily rate of primary production as a function of surface irradiance at local noon. For a finite layer such as MLD, the solution has the form

$$P_{ZT} \sim \frac{BP_m D_L}{k} f\left(I_*^m\right) \tag{11.14}$$

where $I^m{}_*$ is the dimensionless irradiance obtained by normalizing irradiance at noon I^m to photo-adaptative parameter I_k of the P vs I curve.

2.2.2 Computation of Mixed-Layer Primary Production

Mixed-layer models are appropriate when the phytoplankton biomass can be assumed reasonably to be vertically homogeneous throughout the layer. The areas for which mixed-layer primary production computations can be carried out are (a) mixed-layer water column in the open ocean, shelf, or slope, (b) during the seasons of upwelling and convective mixing, when euphotic depth lies within the mixed-layer column and phytoplankton biomass are more or less uniform, (c) in shallow coastal areas where tidal currents and waves ensure vertical mixing of bulk properties of temperature, nutrients, and biomass. The algorithm for computing daily rate mixed-layer primary production (Platt et al., 1990) is given as

$$P_{(Zm,D)} = A \sum_{X=1}^{5} \Omega_X \left(I_*^m\right)^X - A \sum_{x=1}^{5} \Omega_X \left(MI_*^m\right)^X \tag{11.15}$$

where

$P_{Zm\ D}$ = daily water-column production
$A = \mathrm{BDP_m{}^B/K}$

B = phytoplankton biomass given as the concentration of chlorophyll-a (mg chl m^{-3}) from in situ or satellite
D_L = day length (h)
$P_m{}^B$ = assimilation number (mg C mg chl^{-1} h^{-1}) from PI curve
K = vertical diffuse attenuation coefficient (m^{-1})
Ω = weights for fifth-order polynomial fit ($x = 5$)
I_* = dimensionless irradiance calculated as $I_o{}^m/I_k$ ($I_k = P_m{}^B/\alpha^B$)
$M = \exp^{-KZm}$ is the optical transmittance of mixed layer of thickness Z_m

2.2.3 Computation of Euphotic Zone Primary Production

Euphotic zone production is the total column-integrated primary production up to 1% light depth. Generally, this depth is considered to be the lower limit of production. Below this depth, respiration increases, and depth above this is characterized by net photosynthesis. Tropical seas are usually characterized by a pronounced vertical structure of phytoplankton biomass and production as shown by various in situ observations. Typically, this is known as subsurface chlorophyll maxima (SCM) or deep chlorophyll maxima (DCM) due to the accumulation of biomass as a result of higher primary production. To compute production of a water column with a vertical biomass structure or nonuniform biomass, there exist two possibilities.One approach is to characterize the vertical structure and calculate the production of a profile at each depth, followed by numerical integration. Another approach is to determine the integrated chlorophyll and relate it with the observed euphotic depth. The integrated chlorophyll can be empirically related to surface chlorophyll, and euphotic depth can be determined. The total euphotic column divided into five to eight uniform sublayers depending on the depth of the euphotic column is used to compute primary production for each sublayer, and daily production for the euphotic depth is estimated by summing over all sublayers (Platt & Sathyendranath, 1991). The algorithm for euphotic-column production is given as

$$P_{(Z_{eu},D)} = \sum_{S=1}^{S} \left\{ \begin{array}{l} \left(\dfrac{BP_m D_L}{\langle K(Z_0, Z_{eu}, B) \rangle} \right) \\ * \left(\sum\limits_{X=1}^{5} \Omega_X \left(I_0^m \exp^{-KZ_0 \frac{\alpha B}{P_m^B}} \right) - \sum\limits_{X=1}^{5} \Omega_X \left(I_0^m \exp^{-KZ_{eu}} \dfrac{\alpha}{P_m^B} \right) \right) \end{array} \right\} \quad (11.16)$$

where

Daily euphotic zone primary production = $P_{Zeu,\ D}$
Chlorophyll = B
Photosynthetic parameters from ship measurements = $P^B{}_m$, α^B
Surface irradiance at noon from light transmission model = $I_0{}^m$
Dimensionless irradiance = $I^* = I_o{}^m/I_k$. $I_k = P^B{}_m/\alpha^B$Day length from standard astronomical calculations = D_L
Average vertical diffuse attenuation coefficient = $<K>$

Euphotic depth as a function of total integrated chlorophyll $= Z_{eu}$
Weights for fifth-order polynomial fit $(x = 5) = \Omega_x$
Optical transmittance of the euphotic depth of thickness $Z_{eu} = \exp -kZ_{eu}$
Number of layers for integration $= S$

3 Remote Sensing-Based Estimation of Primary Production

3.1 Methodology for Remote Estimation of Water-Column Primary Production

Estimation of primary production at large horizontal scales involves the application of the local algorithm to several points in the spatial domain, as in the case of satellite data, to obtain spatially resolved primary production. Satellite techniques and optical models provide information on light and biomass, the two important variables necessary for the computation of primary production. Biomass indexed as chlorophyll-a concentration can be estimated from ocean color data using bio-optical algorithms. The parameter of light transmission (K_d490, K_{dPAR}) of an underwater light field for a uniformly distributed water-column biomass can also be obtained from satellite data. However, the parameters that define the functional relationship between the light and biomass can be obtained only from shipborne observations. Also, information on the vertical structure of the biomass profile cannot be obtained from ocean color data since satellites can detect signals only from one attenuation length or first optical depth. Although the rate parameters and shape parameters of biomass profile are neither spatially constant nor uniform throughout the year, they vary slowly and can be considered quasi-stable (Sathyendranath et al., 1989a). Thus, a protocol for estimating primary production using remote sensing involves combining satellite inputs of biomass and light transmission to provide information on the rapidly changing variables (biomass and light) with ship-based information on the more stable parameters (α^B and $P^B{}_m$) of photosynthesis-light curves and vertical profile $B(z)$ (Platt & Sathyendranath, 1988). Since rate parameters and shape parameters are ship-based measurements, one approach to assign these parameters to each pixel involves partitioning the geographical domain into a number of biogeochemical provinces, each province having its own set of PI parameters and parameters of vertical biomass structure. The other method consists of determining the typical shape of biomass structure and empirically relating depth-integrated biomass concentration and that at the surface, which in turn is accessible from satellite data.

3.2 Estimation of Primary Production in Arabian Sea Using Oceansat-1 Ocean Color Monitor (OCM-1)

Ocean color monitor (OCM-1) on-board the Indian Remote Sensing Satellite IRS-P4 (OCEANSAT-1) was the first in the series of the Indian satellites to address directly

the oceanographic applications of visible spectral radiometry (Navalgund & Kiran Kumar, 1999). OCEANSAT-1 was launched by Indian Space Research Organisation (ISRO) on May 26, 1999. The sensor had provision for along track tilt (±20°) to minimize the effects of sun glint. It had eight spectral bands in the visible region similar to SeaWiFS, a high spatial resolution of 360 m with a swath of 1420 km, and temporal resolution of 2 days. The launch of IRS-P4 OCM-1 in May 1999 paved way for various research and operational applications and provided excellent opportunity to monitor and study optical and biogeochemical properties of seas around India (Chauhan & Raman, 2017). OCM-1 provided data until August 2010 for various operational applications to Indian oceanographic community. Following the success of OCM-1 and to provide continuity of ocean color data, OCM-2 sensor, onboard OCEANSAT-2 satellite was launched on September 23, 2009, and continued to provide data till 1 May 2023. OCM-2 is almost identical to OCEANSAT-1 OCM-1 but has a minor spectral shift for bands 6 and 7 from OCEANSAT-1 OCM-1 configuration. The spectral band 6, which was located at 670 nm in OCEANSAT-1 OCM-1 has been shifted to 620 nm for better quantification of suspended sediments. The spectral band 7, which was located at 765 nm in OCEANSAT-1 OCM-1, has been shifted to 740 nm to avoid oxygen absorption in case of OCEANSAT-2 OCM. With the launch of the OCM-1 and OCM-2, the potential use of remotely sensed ocean color data to applications gained momentum.

3.3 Estimation of Inputs for Production Algorithm Using OCM–1

3.3.1 Phytoplankton Biomass Indexed as Chlorophyll-a Concentration (Chl-a)

Retrieval techniques and algorithms for derivation of bio-optical variables for generating chlorophyll maps from OCM-1are documented in Chauhan et al. (2002), Sanwlani et al. (2011), and Raman M. (2013). Chlorophyll-a map generation involves two major steps. The first step requires atmospheric correction of visible channels to remove the effects of the atmospheric contribution by air molecules, ozone, atmospheric gasses, sun glint, clouds, and aerosols and retrieve normalized water-leaving radiances. The second step involves the estimation of chlorophyll-a concentration from the retrieved spectral water-leaving radiances by the application of suitable bio-optical algorithms. A regional empirical algorithm OC-OCM was applied to OCM-1 retrieved water-leaving radiances to derive Chl-a concentrations in the Arabian Sea (Sanwlani et al., 2011; Raman, 2013). The regional algorithm fitted to local bio-optical characteristics of the region performed better than global algorithms (OC2 and OC4) for accurately estimating chlorophyll-a concentrations in the Arabian Sea (Raman, 2013).

3.3.2 Vertical Diffuse Attenuation Coefficient (K_d)

The parameter of underwater light transmission K_d controls the light available for photosynthesis within the water column. As in the case of chlorophyll, a regional empirical algorithm was developed by merging Arabian Sea datasets with the global NASA bio-optical marine algorithm datasets (NOMAD) to improve the accuracy of the derived $Kd_{(490)}$ in the Arabian Sea (Chauhan et al., 2003; Raman, 2013). For uniform biomass within the water column, such as in mixed-layer primary production and for case-1 waters, K_d was estimated by implementing the algorithm to OCM-1 water-leaving radiances in blue (490 nm) and green bands (555 nm). K_d for euphotic zone primary production was estimated as average $<K_d>$ of the water column and computed from the depth-averaged concentration of euphotic zone biomass $<B>$ in terms of Chl-a as given by Morel (1988)

$$\langle K_{z_{\mathrm{eu}}} \rangle = 0.121 \langle B \rangle^{0.428} \tag{11.17}$$

The above equation is valid for case-1 waters where phytoplankton are principal attenuators of submarine light field and dissolved organic matter absorption co-varies with phytoplankton concentration.

3.3.3 Photosynthetically Available Radiation (PAR)

The PAR available at the sea surface under cloud-free conditions was estimated using a clear-sky spectral irradiance model (Bird, 1984). Briefly, the model involves the computation of direct and diffuse irradiance. The total irradiance I (watts m^{-2}) is the combination of direct light and diffused light at the sea surface as a function of time t(h), location (latitude), and date and is given as

$$I_{\mathrm{T}}(\lambda) = I_{\mathrm{D}}(\lambda) + I_{\mathrm{S}}(\lambda) \tag{11.18}$$

where $I_{\mathrm{T}}(\lambda)$ is total irradiance, $I_{\mathrm{D}}(\lambda)$ is direct irradiance, and $I_{\mathrm{s}}(\lambda)$ is diffused irradiance. Direct irradiance on a surface normal to the direction of the sun at surface level for a wavelength λ is given as

$$I_D(\lambda) = F_0(\lambda) * T_{\mathrm{R}}(\lambda) * T_{\mathrm{A}}(\lambda) * T_{\mathrm{O}}(\lambda) * T_{\mathrm{WV}}(\lambda) * T_{\mathrm{G}}(\lambda) * \cos(\vartheta) \tag{11.19}$$

where $T_{\mathrm{R}}(\lambda)$, $T_{\mathrm{A}}(\lambda)$, $T_{\mathrm{O}}(\lambda)$, $T_{\mathrm{WV}}(\lambda)$, and $T_{\mathrm{G}}(\lambda)$ are the transmittance functions for Rayleigh scattering, aerosol scattering, ozone absorption, water vapor absorption, and absorption by uniformly mixed gases (O_2 and CO_2). $F_0(\lambda)$ is the extraterrestrial solar irradiance. Variability in mean extraterrestrial solar flux for seasonal variation of the Earth-Sun distance was calculated by using equations 3.9, 3.10, and 3.11 given in Raman (2013). A total of 24 wavelengths between 400 and 700 nm at 10 nm spectral resolution, along with absorption coefficients of water vapor, ozone, and

uniformly mixed gases, were taken from Bird (1984). Cos(θ) is the zenith angle, which gives the direct irradiance at the horizontal surface. Computation for ozone absorption, Rayleigh phase function, Rayleigh scattering, Rayleigh radiances and transmittance, aerosol phase function, and aerosol radiances using a marine aerosol model and single-scattering approximation is explained in Raman, M. (2013). Values for transmittance due to water vapor and uniformly mixed gases were obtained from equations 7 and 10 of Bird (1984).

The diffuse irradiance was calculated for wavelength λ as

$$I_S(\lambda) = (I_R(\lambda) + I_A(\lambda)) * C(\lambda) + I_G(\lambda) \tag{11.20}$$

where $I_R(\lambda)$ is the Rayleigh scattered irradiance on a horizontal surface at the wavelength (λ), and $I_A(\lambda)$ is aerosol scattered component on a horizontal surface at λ, $I_G(\lambda)$ is the ground/air reflected irradiance on a horizontal surface at λ, and $C(\lambda)$ is a correction factor that is wavelength and zenith dependent. The values of correction factor $C(\lambda)$ was taken from Tables 4–7 of Bird (1984) and linearly interpolated to obtain the correction factor between tabulated wavelengths.

The total irradiance at each wavelength is the sum of the direct irradiance (Eq. 11.19) and diffuse irradiance (Eq. 11.20). Total irradiance was integrated over 400–700 nm to estimate PAR (I_0) as

$$I_0 = \int_{400}^{700} I(\lambda) d\lambda \tag{11.21}$$

PAR was further integrated over sunshine hours or photoperiod, assuming a sinusoidal approximation of light throughout the day to obtain total daily irradiance in Wm^{-2}

$$I_T = \int_0^{D_L} I_0(t) dt \tag{11.22}$$

The analytical solution for the daily rate of primary production is a function of surface irradiance at local noon (Platt & Sathyendranath, 1993). To obtain irradiance at local noon, the function I_0 is assumed to be symmetric about noon ($t = D/2$), which allows Eq. 11.22 to be expressed as

$$I_T = \int_0^{D_L/2} I_0(t) dt + \int_{D_L/2}^{D_L} I_0(t) dt \tag{11.23}$$

$$I_T = 2 \int_0^{D_L/2} I_0(t)dt \tag{11.24}$$

Evaluating the above equation gives irradiance at noon $I^m{}_0$ as

$$I_T = \int I_0^m \sin(\pi t/D_L) \tag{11.25}$$

$$I_0^m = I_T \pi / 2D_L \tag{11.26}$$

Irradiance at noon was estimated for 1° × 1° grid for the entire Arabian Sea ranging from 0°–32° N to 32°–80° E for each day using the abovementioned clear-sky irradiance model. For each OCM-1 image, the PAR values were interpolated using a triangular interpolation technique (available in the Image Processing Software) to correspond to the pixel resolution and image size of OCM-1 data.

3.3.4 Photoperiod or Day Length (D_L)

Day length was calculated as a function of day number (d), latitude (γ), solar declination angle (γ), and solar elevation (β). Solar declination angle is given as (Kirk, 1983)

$$\delta - 0.39647 - 22.9133 \ \cos\psi + 4.02543 \ \sin\psi - 0.3872 \ \cos\ 2\psi + 0.052 \ \sin\ 2\psi \tag{11.27}$$

where ψ is the day number expressed as an angle (ψ =360° * d/365). Day number ranges from 0 on January 1 to 364 on December 31.

Solar elevation (β) at any given latitude (γ) varies with the time of the day (τ) and is given as

$$\sin\beta = \sin\gamma \sin\delta - \cos\gamma \cos\delta * \cos\tau \tag{11.28}$$

$$\tau = 360^0 * t/_{24} \tag{11.29}$$

where (τ) is expressed as an angle and t is hours elapsed since 00.00 h. If time at sunrise is τ_s, then at any time of the year

$$\cos\tau_S = (-\tan\gamma \tan\delta) \tag{11.30}$$

(since sin β = 0 at sunrise)

Day length expressed as angle is given as $360° - 2\tau_S$, which is equal to

$$2\cos^{-1}(-\tan\gamma\tan\delta) \tag{11.31}$$

Day length expressed in hours is given by

$$D_L = 0.133\cos^{-1}(-\tan\gamma\tan\delta) \tag{11.32}$$

The value 0.133 is obtained by 2/15° as the sun moves 15° every hour.

Day length was computed for 1° latitude × 1° longitude grid for the entire Arabian Sea ranging from 0°–32° N to 32°–80° E for each day using the abovementioned steps. The values were then interpolated in the same way as PAR to correspond to the pixel resolution and image size of OCM-1 data.

3.3.5 Mixed-Layer Depth (MLD)

Climatological data of mixed-layer depth was used to define the monthly mixed-layer thickness. The MLD-depth data is available from http://www.nodc.noaa.gov as climatological monthly mean profiles of potential temperature or potential density based on two different criteria: a temperature change from the ocean surface of 0.5 °C or a density change from the ocean surface of 0.125 (sigma units), and a variable density change from the ocean surface corresponding to a temperature change of 0.5 °C. The MLD depths for mixed-layer primary production were computed from climatological monthly mean profiles of potential temperature. MLD fields obtained for 1° × 1° grid resolution was interpolated to correspond to the pixel resolution and image size of OCM-1 data (Fig. 11.6e). Interpolated MLD fields deeper than bathymetry in the coastal region (<20 m) were replaced by the bathymetry values using a bathymetry image of the same size as that of the OCM-1 image.

3.3.6 Determination of Photosynthetic Parameters from *PI* Data

Approach for Generation of *P* Versus *I* Parameters

Two basic methodological approaches are available to construct *PI* curves. The first method uses the measurement of oxygen concentration over time to quantify the photosynthetic rate. The rate measurements are made at defined light levels over periods from 1 to 2 minutes under constant temperature. This approach has the advantage that the *PI* curve is generated in real-time, oxygen rate measurements measure net photosynthesis, and the same sample is used for all points on the curve. However, the major disadvantages of this approach are that (a) prior measurement of light levels can significantly influence the observed photosynthetic rates and (b) the oxygen evolution technique is not sensitive enough to measure *PI* curves in oligotrophic waters with low biomass (Falkowski & Raven, 1997). The second general

approach to generating PI curves is to use the tracer technique (Steemann Nielsen, 1952). For field measurements, known amounts [^{14}C] or [^{13}C] bicarbonate are added to bottles containing water samples with the natural phytoplankton population, which are suspended at a series of depths throughout the euphotic zone, generally for a few hours in the middle of the day. The amount of ^{14}C or ^{13}C fixed in cells, collected on a filter, and treated with acid is determined. This type of measurement requires adequate ship support for mooring and retrieval of bottles in the open ocean.

A more convenient method is to adopt a laboratory-based procedure (but still on board an oceanographic vessel) to measure photosynthesis using a photosynthetron (Fig. 11.2). Briefly, the methodology involves incubation of the phytoplankton samples with tracer, as mentioned above, in a chamber at a series of irradiance values (i.e., different light intensities ranging from near surface to zero) provided by an artificial light source, intended to correspond to different depths in the euphotic zone for a certain period of time. The samples are kept at the same temperature as that in the water body. The photosynthetron-based approach is the conventional technique for measuring PI curves in most aquatic environments (Cleveland et al., 1989; Hiscock et al., 2003). The addition of tracer allows the average rate of photosynthesis to be determined for the incubation duration. For estimating PI parameters, a photosynthetron-based approach has been adopted in this study.

Measurement of *P* Versus *I* Parameters

Description of a Photosynthetron

A photosynthetron was designed and fabricated at Space Applications Centre, Ahmedabad, and was used for PI measurements (Fig. 11.2). The watertight incubation chamber of flat acrylic material is designed to contain a stack of thirteen 300 ml flat rectangular bottles. The bottles are made of acrylic material with a black

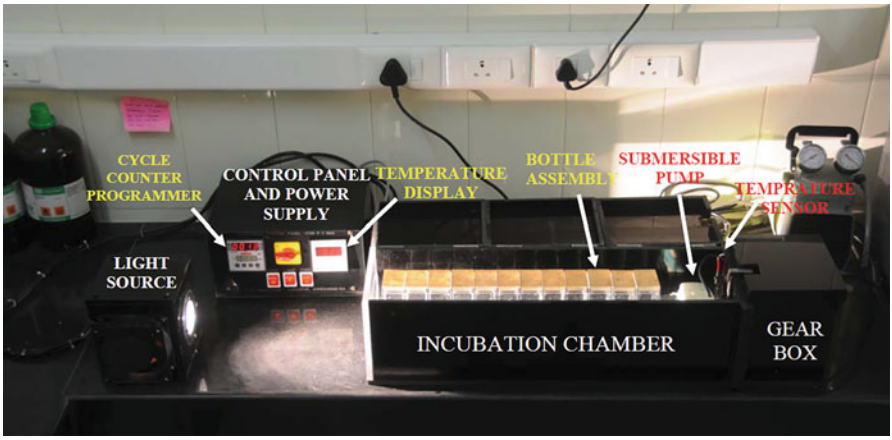

Fig. 11.2 Photosynthetron for determining photosynthetic parameters (*PI* curve) as a function of irradiance

rectangular lid. All the walls of the incubator, including the cover, are black, but the one facing the light source is made from transparent diffusing acrylic material. The photosynthetron is illuminated from one end by a 250 W quartz-halogen lamp housed separately in a small square chamber made of acrylic material in black and can be attached to the main body of the photosynthetron if required. Exhaust fans are fixed on two walls to prevent heating of the lamp-housing chamber. The incubation chamber has a rack to tightly stack 12 bottles and is attached to a gearbox unit with a motor to move the rack sideways at a predetermined frequency (5 cycles/minute). This arrangement keeps the algal cells inside the bottle well mixed, prevents their settlement at the bottom of the bottle, and dissipates the heat produced by the source lamp. A submersible pump is used at the other end of the chamber to circulate water inside the chamber and flow it around the rack of bottles. A temperature sensor is provided to measure the temperature of the circulating water inside the chamber. A control panel and a transformer are provided separately to regulate the intensity of lamp output through voltage-regulated variation, monitor the temperature variation, and set the time required for the incubation of water samples.

P *Versus* I *Experiments*

PI experiments were carried out for selected hydrographic stations with the fabricated incubation box. Water samples were taken using CTD for *PI* experiments and chlorophyll-a measurements. Surface water samples from 2 and 5 m depth were mixed together, and 3 l of the sample were inoculated with a radiocarbon tracer ($NaH^{14}CO_3$). The added activity of the tracer was 5 μCi per 100 ml. The inoculated samples were dispensed into 10 light and one dark bottle (as a control) and incubated for 3 h inside the incubation box maintained at a temperature close to the sea surface. A set of neutral supple plastic filters was inserted between the bottles to provide a regular gradient of light from the diffusing source. Prior to the start of the experiment, two sample bottles with added tracers were filtered and put into a scintillation vial (20 ml) to determine the initial activity. After the incubation, each sample was filtered onto a pre-combusted Whatman GF/F glass fiber filters, rinsed with filtered seawater, placed into 20 ml scintillation vials, wetted with 1.0 N HCl, and placed under a fume hood for 1–1.5 h to remove the excess carbon and stored dry. The second set of bottles with the same sample was placed in the same way as before but without adding the tracer. Photon flux within each bottle was measured with a 4π collector (Biospherical Instruments) to determine the light available in each bottle during the experiment. In the laboratory, radioactivity present in each sample after incubation was measured using a liquid scintillation counter. Chlorophyll-a concentrations for the samples were measured fluorometrically using 90% acetone extracts. Production was computed according to the equations in JGOFS protocols and normalized to the respective chlorophyll-a concentrations (Fig. 11.3, Table 11.1).

The chlorophyll-a-specific initial slope (α^B) and maximum photosynthesis at saturation light level ($P^B{}_m$) of the P vs I curves were derived by fitting to the experimental data points a hyperbolic tangent function as given by Platt and Jassby (1976) as

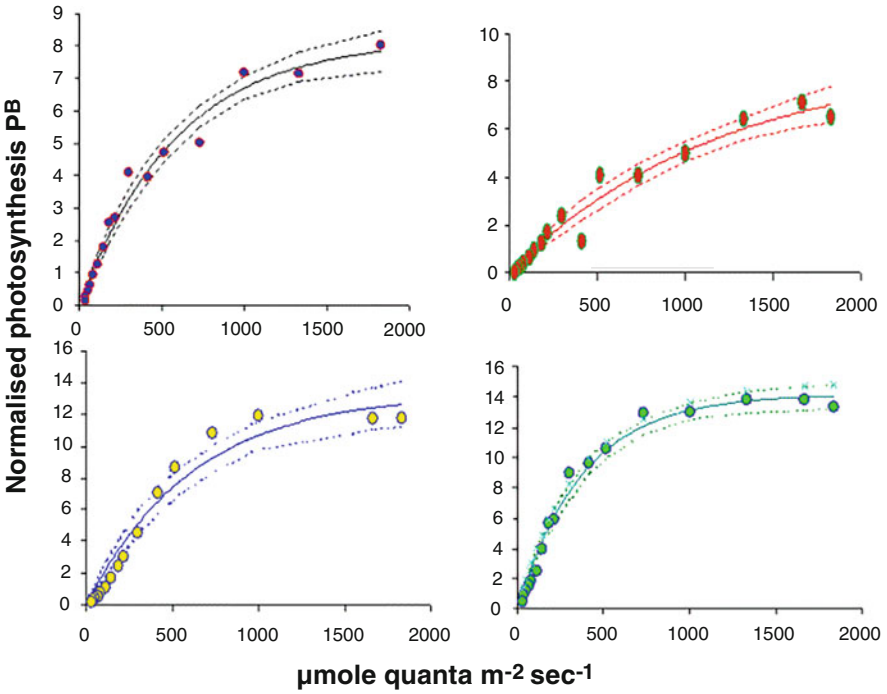

Fig. 11.3 The *P* vs *I* curves (for surface water samples) generated using the experimental setup and Table 11.1 presents as an example the values of the *P* vs *I* curves for various surface water samples during the cruise FORV 257 (March, 2007)

Table 11.1 *P* vs *I* parameters α^B, $P^B{}_m$, and I_k for different water samples

PI curves	Initial slope (α^B)	Maximum photosynthesis $P^B{}_m$	I_K	r^2	S.E
a	0.014	8.196	589.67	0.977	0.39
b	0.007	9.016	1210.35	0.958	0.508
c	0.0215	13.32	619.53	0.955	0.985
d	0.0371	14.124	380.71	0.983	0.664
e	0.606	31.7102	52.327	0.809	4.3536

$$P^B = P^B_m \left[1 - \exp\left(-\frac{\alpha^B I}{P^B_m}\right)\right] \tag{11.33}$$

3.3.7 Column-Integrated Phytoplankton Biomass (Chl_{tot}) and Euphotic Depth (Z_{eu})

Tropical seas such as the Arabian Sea are characterized by stratified water columns for most part of the year, having a pronounced vertical structure of nutrients and phytoplankton biomass (Herbland & Voituriez, 1979; Longhurst & Harrison, 1989).

Typically, ocean color sensors do not sense this depth since the signal detected by the satellite originates from the top optical depth of the euphotic zone (Gordon & Mcclune, 1975). The vertical structure of the phytoplankton biomass is usually characterized by a deep chlorophyll maximum (DCM), varies with the season for a given area, and may be different for different regions of the ocean as a function of its light and nutrient history (Cullen, 1982; Platt et al., 1992). However, the shape and magnitude of the vertical profiles are slowly varying and can be considered quasi-stable over large horizontal distances and in time (Longhurst et al., 1995; Platt et al., 1995). Sathyendranath and Platt (1989) have shown that ignoring the vertical structure of the phytoplankton biomass and assuming a uniform biomass (equal to surface biomass concentration) distribution throughout the euphotic column can lead to significant errors in estimated integral production. This error is large (of the order of 70%) for waters with low surface biomass and reduces as the biomass concentration increases. In order to account for the effect of nonuniformity of biomass profile on daily water column primary production, a primary requisite is to characterize the shape of the biomass profile from biomass concentration available at discrete depths.

Characterization of Vertical Biomass (Chlorophyll-a) Profile

The vertical structure of biomass up to euphoticdepth was characterized by in situ measurements of chlorophyll-a concentration at discrete depths during various ship cruises carried out in the northeastern Arabian Sea. Chl-a concentrations (mg m^{-3}) at each depth were determined fluorometrically following Holm-Hansen method (Holm-Hansen et al., 1965). Chl-a concentrations were also determined for few samples in each cruise from the HPLC method to convert fluorometric chlorophyll-a to HPLC Chl-a concentrations before being subjected to further analysis. The vertical structure of phytoplankton biomass (Chl-a) as a function of depth was characterized by a shifted Gaussian model (Platt et al., 1988) and is given as (Fig. 11.4)

$$B_Z = B_0 + \frac{h}{\sigma\sqrt{2\pi}} \exp - \left[\frac{(Z - Z_m)^2}{2\sigma^2}\right] \tag{11.34}$$

where B_Z is chlorophyll biomass as a function of depth z, B_0 is initial biomass or background biomass, and Z_m is center of the Gaussian peak corresponding to the depth of deep chlorophyll maxima (DCM); σ is thickness of DCM or spread; and H is height of peak given as $h/\sigma\sqrt{2\pi}$, and h is total biomass under the peak.

The shifted Gaussian model allows the structure of the vertical profile to match with the surface values, unlike a Gaussian model, where the surface concentrations would tend toward zero (Platt et al., 1988). The shifted Gaussian model was applied to chlorophyll concentrations at discrete depths of several hydrographic stations to obtain the four parameters (B_0, Z_m, σ and h) of the shifted Gaussian curve. The

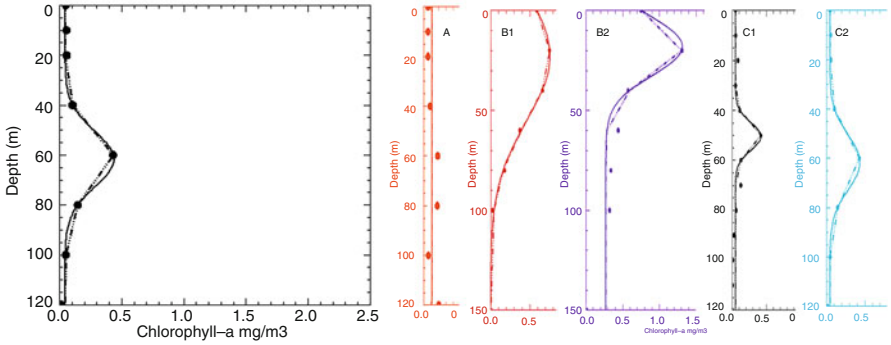

Fig. 11.4 (**a**) Shifted Gaussian curve fitted to in situ discrete-depth chlorophyll measurements. (**b**) Categories of vertical biomass profile from the eastern Arabian Sea. (A) Uniform Chl profile. (B1) Subsurface Chl maximum (broad width). (B2) Subsurface Chl maximum (narrow width). (C1) Deep Chl maximum (broad width). (C2) Deep Chl maximum (narrow width)

individual parameters were then used to recover the continuous profile of the phytoplankton biomass structure as a function of depth for each hydrographic station (Fig. 11.4a). Based on the shape of the biomass profile and the four parameters of the shifted Gaussian curve, all the hydrographic stations ($n = 140$) of various cruises were grouped into three main categories (Fig. 11.4b), (1) uniform profile, (2) subsurface maximum, and (3) deep-chlorophyll maximum.

Integrated Biomass and Euphotic Depth

Column-integrated primary production for a given hydrographic station can be estimated with the model of primary production using the local PI parameters and parameters of the pigment profile. However, the application of the model to satellite observations requires a method to be devised for extrapolating these parameters to large spatial scales where no measurements exist. One method proposed by Platt and Sathyendranath (1988) consists of partitioning the spatial domain (regional seas, global oceans) into a number of biogeochemical provinces, each province having its own set of PI parameters and parameters of vertical biomass structure. This approach relies on the assumption that the shape of the biomass profile and photosynthetic rate parameters obtained from PI curves are slowly varying properties for a given province and are manifestations of the light and nutrient history of that province. The other method proposed by Morel and Berthon (1989) consists of defining typical shapes of vertical biomass profile according to the trophic state of the region, which in turn is accessible to satellite observations through an empirical relationship between depth-integrated biomass concentration and that at the surface. The empirical relationship allows the estimation on a pixel-by-pixel basis. A primary requisite of implementing biogeochemical-based provinces scheme is knowledge of the average values of biomass profile and *PI* parameters for each province. This requires

at least one set of in situ observations for *PI* and profile parameters in each province. The second method proposed by Morel and Berthon (1989), relating surface biomass to column-integrated biomass, was adopted to determine the euphotic depth. Using the shifted Gaussian model, continuous profiles of biomass indexed as chlorophyll-a concentration was estimated using the shape parameters and integrated for each station as

$$\mathrm{Chl}_{\mathrm{tot}} = \int_{0}^{4.6/k} \mathrm{Chl}(z)dz \tag{11.35}$$

Integrated biomass was then averaged as

$$\langle \mathrm{Chl} \rangle = \frac{\int_{0}^{4.6/k} \mathrm{Chl}(z)dz}{\int_{0}^{4.6/k} zdz} \tag{11.36}$$

For chlorophyll-a concentration, less than 1.0 mg m^{-1}, the relationship between $\mathrm{Chl}_{\mathrm{SAT}}$ and $\mathrm{Chl}_{\mathrm{tot}}$ was fitted with a polynomial expression ($n = 140$; $r^2 = 0.904$) and was given as

$$\begin{aligned}\mathrm{Chl}_{\mathrm{tot}} &= 10.645 + 48.455 * \mathrm{Chl}_{\mathrm{SAT}} - 34.359 * (\mathrm{Chl}_{\mathrm{SAT}})^2 \\ &+ 18.02^{*}(\mathrm{Chl}_{\mathrm{SAT}})^3 - 4.844^{*}(\mathrm{Chl}_{\mathrm{SAT}})^4\end{aligned} \tag{11.37}$$

For chlorophyll-a concentrations 1.0 mg m^{-1} and greater than 1.0 mg m^{-1}, the relationship between $\mathrm{Chl}_{\mathrm{SAT}}$ and $\mathrm{Chl}_{\mathrm{tot}}$ was fitted with a polynomial expression ($n = 80$; $r^2 = 0.95$) and was given as

$$\begin{aligned}\mathrm{Chl}_{\mathrm{tot}} &= 28.972 + 15.506^{*}\mathrm{Chl}_{\mathrm{SAT}} + 0.6477^{*}(\mathrm{Chl}_{\mathrm{SAT}})^2 \\ &- 0.014^{*}(\mathrm{Chl}_{\mathrm{SAT}})^3 - 0.9^{*}10^{-5}(\mathrm{Chl}_{\mathrm{SAT}})^4\end{aligned} \tag{11.38}$$

Euphotic depth was calculated on a pixel-to-pixel basis as a function of total integrated biomass as (Morel & Berthon, 1989)

$$Z_{\mathrm{eu}} = X * \mathrm{Chl}_{\mathrm{tot}}{}^{Y} \tag{11.39}$$

where x and y are 200 and -0.293 for $Z_{\mathrm{eu}} > 102$ m; x and y are 568 and -0.746 for $Z_{\mathrm{eu}} < 102$ m.

3.4 Results

3.4.1 Generation of Mixed-Layer Primary Production and Euphotic Zone Primary Production Images from OCM-1 Data

Many OCM-1 data corresponding to various ship campaigns from November 2001 to March 2007 have been processed to derive chlorophyll-a and $K_d(490)$. These spatial data were further used as inputs along with other input variables for generating daily primary production maps using the algorithms and procedure mentioned in the above sections. The flow diagram for the generation of primary production images is shown in Fig. 11.5. Using commercially available image processing software, the derived outputs were further processed for image projection, color coding, histogram generation, overlaying masks for clouds and land, and flags for coastal and shallow waters.

For generating weekly and monthly composites of ocean primary production, cloud correction procedure was implemented as described in Raman (2013) to generate weekly and monthly averaged primary production fields corrected for cloud effects. Figure 11.6a–f show examples of various inputs used for generating daily mixed-layer primary production. Euphotic zone primary production images (Fig. 11.7) for various cruise dates and monthly climatology of mixed-layer primary production (Fig. 11.8) were generated for the year (1999–2000) for the eastern Arabian Sea.

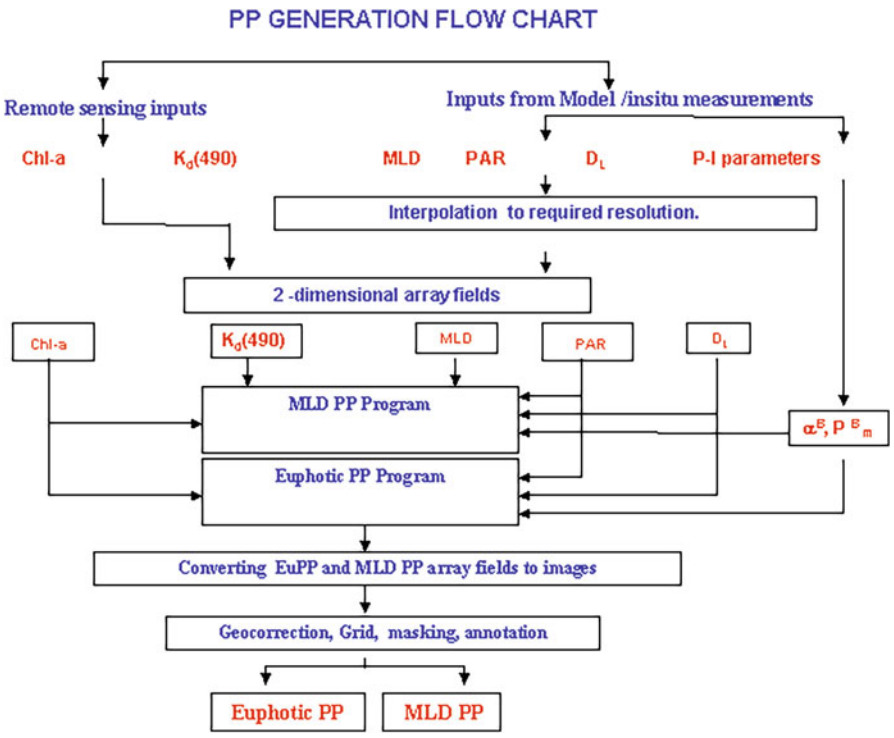

Fig. 11.5 Flow diagram for generation of primary production images on an operational basis

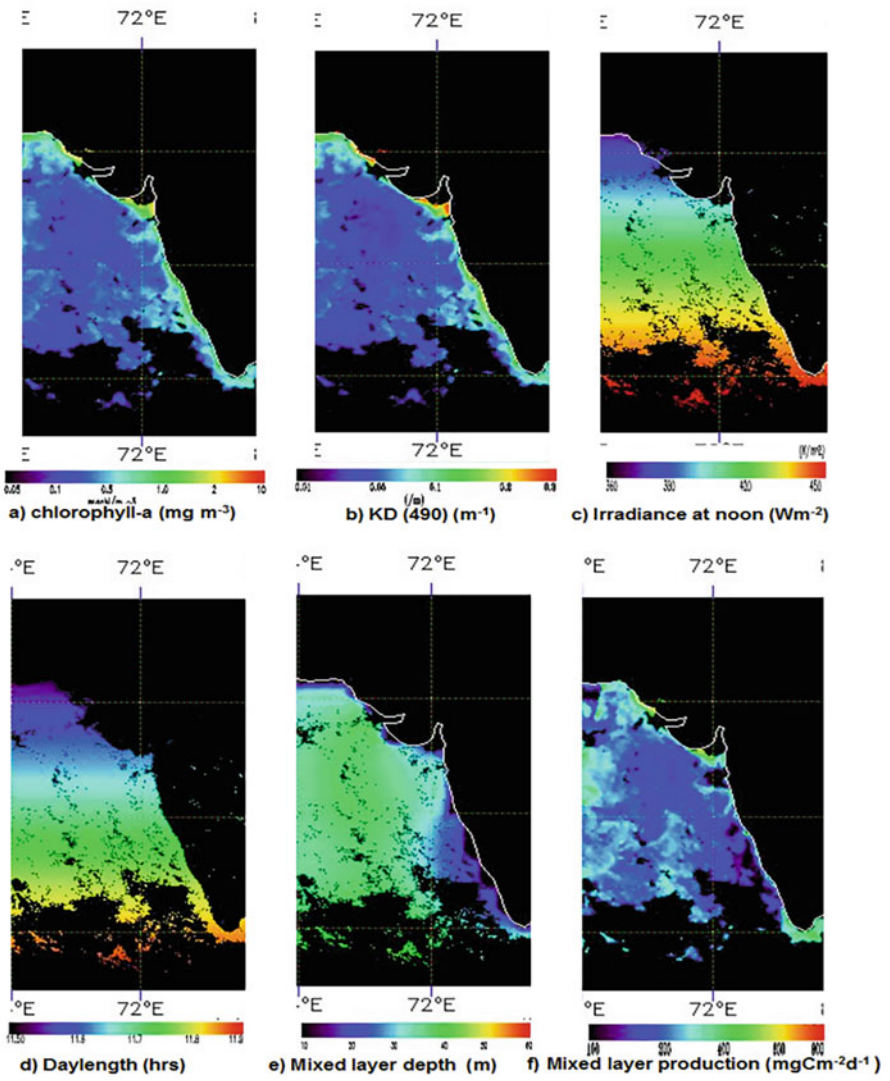

Fig. 11.6 (**a–e**) Inputs and (**f**) output for daily mixed-layer production (October 13, 1999)

3.5 Discussion

The routine way to assess primary production in the field is through in situ or simulated in situ incubations using either the radioactive ^{14}C, or stable isotope ^{13}C methods (Steemann Nielsen, 1952; Dugdale & Goering, 1967). This method gives a vertical profile of primary production throughout the photic zone. The profile can be integrated over depth and adjusted for incubation time to give an estimate of daily

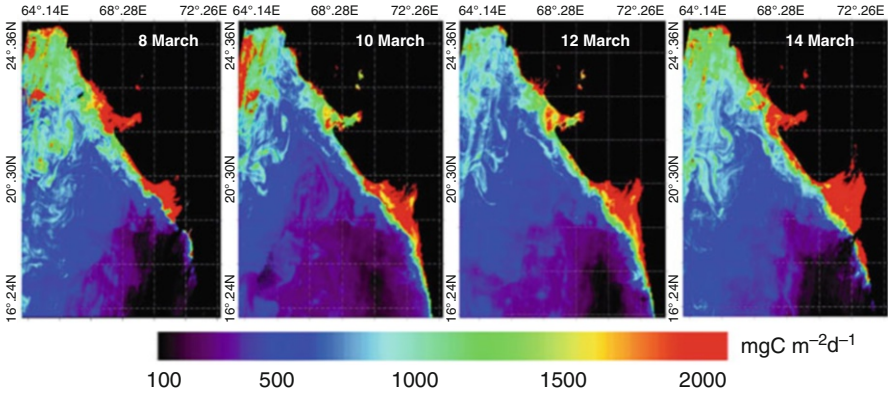

Fig. 11.7 Daily euphotic zone production (March, 2011)

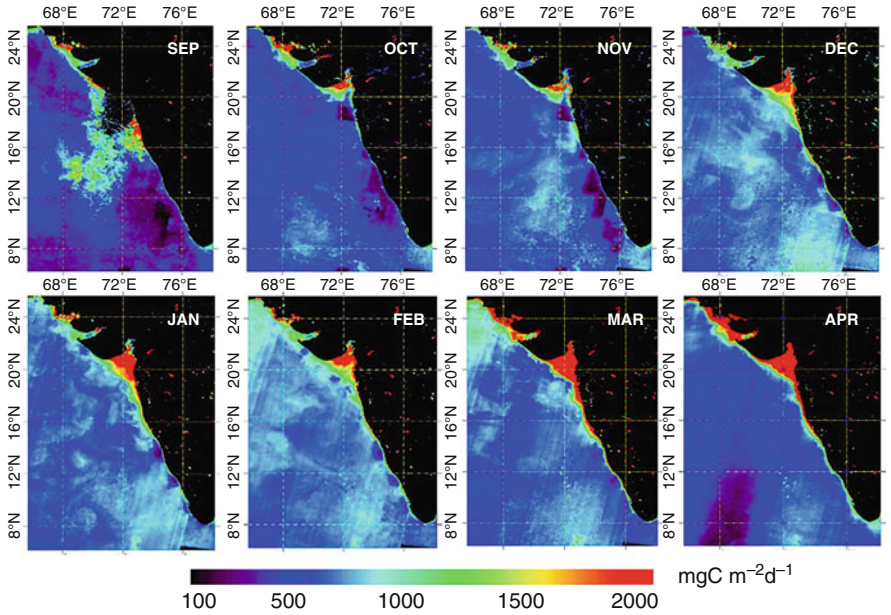

Fig. 11.8 Climatology of monthly mixed-layer production for the year (September 1999–April 2000)

water-column production. Based on the cruise track and the position of the predetermined hydrographic station, primary productivity measurements were carried out in the early morning hours between 7:00 and 8:00 h to allow maximum hours of the sunshine period (6 h) symmetric around noon for on-deck incubation of samples. It is assumed that diurnal changes in phytoplankton biomass of the sample

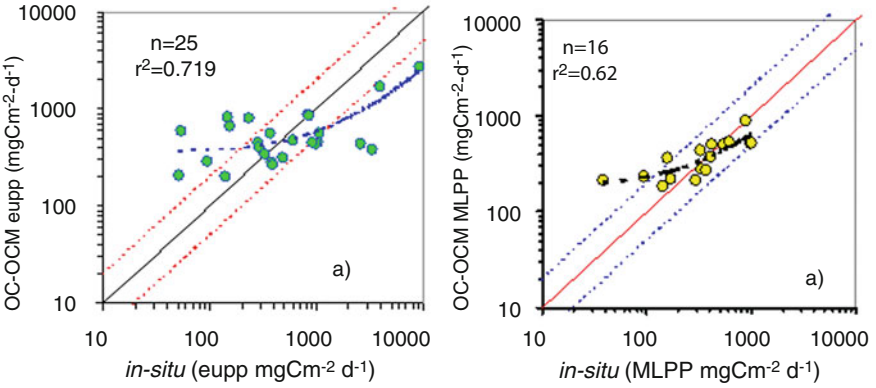

Fig. 11.9 Validation of daily rate of euphotic zone primary production (euPP)and mixed-layer primary production MLPP against concurrent in situ measured primary productivity data

stations are not significant. The method followed by JGOFS India (1994–1995) was adapted to measure in situ primary production (Bhattathiri et al., 1996). Primary production values estimated for individual depths of a station were integrated up to euphotic depth using a five-point Newton-Cotes integration formula. Twenty-five matchup points of euphotic integrated primary production were available for comparison with satellite-estimated primary production. Statistical and graphical criteria were used to assess the uncertainty in satellite-derived estimates.

In situ matchup dataset of daily column-integrated euphotic zone primary production showed a wide variation of values. Maximum values (>1800 mgC m^{-2} day^{-1}) were measured during winter monsoon cruises, whereas minimum values (~450 mgC m^{-2} day^{-1}) were recorded during inter-monsoon period. The results of the validation of euphotic zone primary production estimates (euPP) compared with the in situ data set are shown in Fig. 11.9. The scatterplot shows the distribution of matching points around the 1:1, 2:1, and 1:2 lines. Euphotic zone primary production (euPP) product showed a distinct tendency to underestimate and overestimate the in situ dataset for low and high values of euphotic-column integrated production. The squared correlation coefficients (r^2) of the satellite estimated versus in situ dataset was 0.72, and the mean absolute percentage difference (MAPD) was 99.43%. The overall uncertainty in the comparison between the satellite-derived and in situ euPP estimates, expressed in terms of RMSE log error was 41.87% with a low negative bias of 3.2%. The RMSE log error was within the accuracy goal of 45% set by ocean color missions (IOCCG, 2000). Euphotic zone primary production estimates generated using OCM-derived inputs were able to capture 72% of the variance in the in situ dataset.

Individual-depth measurements of daily primary production were also integrated into MLD for validation with mixed-layer primary production (MLPP). A stepwise linear interpolation technique was used for calculating production at MLD for those stations where water samples were not collected at MLD, followed by integration up to MLD. Sixteen matchup points of mixed-layer primary production were available

for comparison with satellite-estimated values. A result similar to euPP product comparison was obtained for MLPP. The bias in log space was positive indicating overestimation of mixed-layer primary production compared with in situ values. A RMSE of 26.38% with an overestimation as indicated by positive bias (5.27%) and low MAPD (65.70%) was observed when compared with euphotic zone production values. However, the coefficient of determination (r^2) for OCM-MLPP was only 62% indicating an unexplained variance of about 38% compared with 28% of unexplained variance in OCM-euPP estimate. The principal source of uncertainty in the primary production estimates is the accurate determination of phytoplankton biomass indexed as Chl-a concentration for space-based primary production models (Platt & Sathyendranath, 1988). Further, the accurate quantification of Chl-a concentration depends on the bio-optical state of the phytoplankton community structure of a given region, and a regional algorithm such as OC-OCM tuned to local bio-optical characteristics is better suited to quantify column primary production estimates.

A series of round-robin experiments have been carried out to evaluate and compare models, which estimate primary productivity from ocean color. In these experiments, in situ measurements of column-integrated primary production were used to test the ability of the participating models to predict depth-integrated primary production based on remote sensing data and other inputs. A comparison of the models revealed that most of the models, notwithstanding the complexity, were within a factor of 2.4 (based on one standard deviation in log-difference errors) of the ^{14}C measurements (Campbell et al., 2002). Further progress in space-based primary production modeling requires an improved understanding of the effect of temperature and other factors on photosynthesis and better parameterization of the PI parameters (Carr et al., 2006; Kulk et al., 2020, 2021).

Decadal primary production (Fig. 11.10) of the Arabian Sea computed from the 10-year averaged (1998–2007) SeaWiFS data using the abovementioned nonspectral, depth-integrated analytical model ranged from 0.15 to 1.6 g Cm^{-2}. The south-central Arabian Sea near the equatorial region showed very low values of production ranging from 0.2 to 0.3 gC m^{-2} with a mean value of 0.22 gC m^{-2} (SD $\pm$ 0.054). Such regions are characterized as low chlorophyll low-nutrient areas (LNLC) of the ocean and can be the potential sites for artificial enrichment and carbon capture and sequestration (Raman et al., 2016).

4 Future Research Direction

Accurate assessment of spatiotemporal dynamics of primary production in regional seas such as the Arabian Sea from ocean color necessitates information on the bio-optical properties of phytoplankton populations living under regional environmental conditions of light and nutrients. Such information can be used to develop region-specific algorithms that are most suited to estimate primary production from remote sensing using mathematical models. However, the rate parameters (*PI*

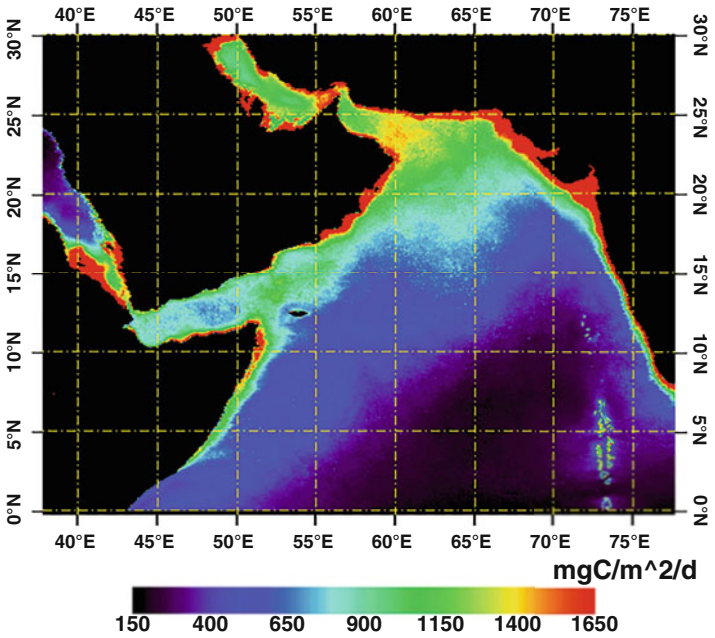

Fig. 11.10 Decadal primary production in the northern Indian Ocean (1998–2007). The yellow region has minimum primary production

curves) and the vertical structure of biomass have to be measured and modeled from in situ data using sea-truth campaigns since they cannot be directly estimated from ocean color data. In situ data of *PI* parameters in Arabain Sea is very sparse and limited to few locations and season. Knowledge on vertical structure of phytoplankton biomass is mainly limited to north eastern Arabian Sea while many other areas remain undersampled. Future direction would be to establish a network of stations in Arabian Sea for sampling according to biogeochemical provinces at carefully chosen times, to produce a comprehensive database of parameters that would provide the basis for future estimation of regional primary production from ocean color in operational mode.

5 Conclusions

Phytoplankton biomass and its rate of production are two fundamental properties of the pelagic ecosystem. They are required for a wide range of applications, such as research on ocean's carbon inventory and biogeochemical pathways, climate change, fluctuations in the exploited fish stocks, etc. Traditional methods of survey using ships and moorings do not provide a synoptic picture of spatiotemporal dynamics of these important properties. Fortunately, the advent of ocean color

sensors with enhanced spatial and spectral resolution capabilities have paved the way for time-series observations related to phytoplankton biomass and the associated production of the marine ecosystem. Algorithms developed for global scale estimation of phytoplankton biomass indexed as chlorophyll-a concentration are not representative of regional bio-optical characteristics. Therefore, regional algorithm similar to the one described in this chapter (OC-OCM) performs with better accuracy since they are fitted to local bio-optics characteristics of the region, such as the Arabian Sea. A protocol for estimating primary production from remote sensing is described which combines ocean color inputs of chlorophyll and euphotic depth with in situ measured PI parameters and shape parameters of phytoplankton biomass (chlorophyll) profile in a depth-integrated nonspectral analytical model.

References

Antoine, D., & Morel, A. (1996). Oceanic primary production: I. Adaptation of a spectral light-photosynthesis model in view of application to satellite chlorophyll observations. *Global Biogeochemical Cycles, 10*, 43–55.

Antoine, D., André, J.-M., & Morel, A. (1996). Oceanic primary production 2. Estimation at global scale from satellite (coastal zone color scanner) chlorophyll. *Global Biogeochemical Cycles, 10*, 57–69.

Babenerd, B., & Krey, J. (1974). *Indian Ocean: Collected data on primary production, phytoplankton pigments, and some related factors*. Institut for Meerskunde an der Universitat Kiel.

Bannister, T. T. (1974). A general theory of steady state phytoplankton growth in a nutrient saturated mixed layer. *Limnology and Oceanography, 19*, 13–30.

Banse, K., & Yong, M. (1990). Sources of variability in satellite-derived estimates of phytoplankton production in the Eastern Tropical Pacific. *Journal of Geophysical Research, 95*, 7201–7215.

Behrenfeld, M. J., & Falkowski, P. G. (1997a). Photosynthetic rates derived from satellite-based chlorophyll concentration. *Limnology and Oceanography, 42*(1), 1–20.

Behrenfeld, M. J., & Falkowski, P. G. (1997b). A consumer's guide to phytoplankton primary productivity models. *Limnology and Oceanography, 42*(7), 1479–1491.

Behrenfeld, M. J., Boss, E., Siegel, D., & Shea, D. M. (2005). Carbon-based ocean productivity and phytoplankton physiology from space. *Global Biogeochemical Cycles, 19*, GB1006. https://doi.org/10.1029/2004GB002299

Bhattathiri, P. M. A., Pant, A., Sawant, S., Gauns, M., Matondkar, S. G. P., & Mohanraju, R. (1996). Phytoplankton production and chlorophyll distribution in the eastern and central Arabian Sea in 1994–95. *Current Science, 71*, 857–862.

Bird, R. E. (1984). A simple, solar spectral model for direct normal and diffuse horizontal irradiance. *Solar Energy, 32*, 461–471.

Bouman, H., Platt, T., Sathyendranath, S., & Stuart, V. (2005). Dependence of light- saturated photosynthesis on temperature and community structure. *Deep Sea Research, 52*, 1284–1299.

Brewer, P. G., Bruland, K. W., Eppley, R. W., & Mccarthy, J. J. (1986). The Global Ocean Flux Study (GOFS): Status of the U.S. JGOFS Program. *EOS, 67*, 44.

Campbell, J. W., Antoine, D., Armstrong, R., Arrigo, K., Balch, W., Barber, R., Behrenfeld, M., Bidigare, R., Bishop, J., et al. (2002). Comparison of algorithms for estimating ocean primary productivity from surface chlorophyll, temperature, and irradiance. *Global Biogeochemical Cycles, 16*(3). https://doi.org/10.1029/2001GB001444

Carr, M.-E., Friedrichs, A. M., Schmeltz, M., Aita, M. N., Antoine, D., Arrigo, K. R., et al. (2006). A comparison of global estimates of marine primary production from ocean color. *Deep Sea Research Part II: Topical Studies in Oceanography, 53*, 741–770.

Chauhan, P. (2005). *Interpretation of spectral radiance over open ocean and turbid coastal waters using contemporary ocean colour satellite sensors*. PhD. Dissertation, Gujarat University, p. 170.

Chauhan, P., & Raman, M. (2017). Satellite remote sensing for ocean biology: An Indian perspective. *Proceedings of the National Academy of Sciences, India Section A: Physical Sciences, 87*(4), 629–640. https://doi.org/10.1007/s40010-017-0439-5

Chauhan, P., Mohan, M., Sarangi, R. K., Kumari, B., Nayak, S. R., & Matondkar, S. G. P. (2002). Surface chlorophyll-a estimation using IRS-P4 OCM data in the Arabian Sea. *International Journal of Remote Sensing, 23*(8), 1663–1676.

Chauhan, P., Sahay, A., Rajawat, A. S., & Nayak, S. R. (2003). Remote sensing of diffuse attenuation coefficient (K490) using IRS P4 Ocean Colour Monitor (OCM) sensor. *Indian Journal of Marine Sciences, 32*(4), 279–284.

Cleveland, J. S., Perry, M. J., Kiefer, D. A., & Talbot, M. C. (1989). Maximal quantum yield of photosynthesis in the north western Sargasso Sea. *Journal of Marine Research, 47*, 869–886.

Colwell, R. N. (1983). *Manual of remote sensing* (Vol. 1, pp. 19–44). American Society of Photogrammetry.

Cullen, J. J. (1982). The deep chlorophyll maximum: Comparing vertical profiles of chlorophyll-a. *Canadian Journal of Fisheries and Aquatic Sciences, 39*, 791–803.

Cullen, J. J., Neale, P. J., & Lesser, M. (1992). Biological weighting function for the inhibition of phytoplankton photosynthesis by ultraviolet radiation. *Science, 258*, 646–650.

Devred, E., Sathyendranath, S., & Platt, T. (2007). Delineation of ecological provinces using ocean colour radiometry. *Marine Ecology Progress Series, 346*, 1–13.

Dietrich, G. (1973). The unique situation in the environment of the Indian Ocean. In B. Zeizschel (Ed.), *B* (The biology of the Indian Ocean) (pp. 1–6). Springer-Verlag.

Dubinsky, Z. (1992). The functional and optical cross sections of phytoplankton photosynthesis. In P. G. Falkowski & A. Woodhead (Eds.), *Primary productivity and biogeochemical cycles in the sea* (pp. 31–46). Plenum Press.

Dugdale, R. C., & Goering, J. J. (1967). Uptake of new and regenerated forms of nitrogen in primary productivity. *Limnology and Oceanography, 12*, 196–206.

Eppley, R. W., Stewart, E., Abbott, M. R., & Heyman, U. (1985). Estimating ocean primary production from satellite chlorophyll: Introduction to regional differences and statistics for the Southern California-Bight. *Journal of Plankton Research, 7*, 57–70.

Falkowski, P. G. (1981). Light-shade adaptation and assimilation numbers. *Journal of Plankton Research, 3*, 203–216.

Falkowski, P. G., & Raven, J. A. (1997). *Aquatic photosynthesis* (p. 375). Blackwell Science.

Goés, J. I., Thoppil, P. G., Gomes, H., Do, R., & Fasullo, J. T. (2005). Warming of the Eurasian landmass is making the Arabian Sea more productive. *Science, 308*(5721), 545–547.

Gordon, H. R., & Mcclune, W. R. (1975). Estimation of depth of sunlight penetration in the sea for remote sensing. *Applied Optics, 4*, 413–416.

Gordon, H. R., & Morel, A. (1983). Remote assessment of ocean colour for interpretation of satellite visible imagery: A review. In R. T. Barber, N. K. Mooers, M. J. Bowman, & B. Zeitzschel (Eds.), *Lecture notes on coastal and esturine studies* (p. 114). Springer-Verlag.

Goyet, C., Millero, F. J., O'sullivan, D. W., Eischeid, G., Mccue, S. J., & Bellerby, R. G. J. (1998). Temporal variations of pCO2 in surface seawater of the Arabian Sea in 1995. *Deep-Sea Research Part II, 45*, 609–624.

Herbland, A., & Voituriez, B. (1979). Hydrological structure analysis for estimating the primary production in the tropical Atlantic Ocean. *Journal of Marine Research, 37*, 87–101.

Hiscock, M. R., Marra, J., Smith, W. O., Jr., Goercke, R., Measures, C., Vink, S., Olson, R. J., Sosik, H. M., & Barber, R. T. (2003). Primary productivity and its regulation in the Pacific Sector of the Southern Ocean. *Deep Sea Research Part II: Topical Studies in Oceanography, 50*, 533–558.

Hirawake, T., Shinmyo, K., Fujiwara, A., & Saitoh, S. (2012). Satellite remote sensing of primary productivity in the Bering and Chukchi Seas using an absorption-based approach. *ICES Journal of Marine Science, 112*, 175–188.

Holm-Hansen, O., Lorenzen, C. J., Holmes, R. W., & Strickland, J. D. H. (1965). Fluorometric determination of chlorophyll. *Journal du conseil. Conseil Permanent International Pour l'Exploration de la Mer, 30*, 3–15.

IOCCG. (2000). Remote sensing of ocean colour in coastal, and other optically-complex, waters. In S. Sathyendranath (Ed.), *Reports of the International Ocean-Colour Coordinating Group*, No. 3. IOCCG, Dartmouth, Canada.

Jerlov, N. G. (1976). *Marine optics* (2nd ed.). Elsevier Press.

Joint, I., & Groom, S. B. (2000). Estimation of phytoplankton production from space: Current status and future potential of satellite remote sensing. *Journal of Experimental Marine Biology and Ecology, 250*, 233–255.

Kirk, J. T. O. (1983). *Light and photosynthesis in aquatic ecosystems*. Cambridge University Press.

Kirk, J. T. O. (1984). Dependence of relationship between inherent and apparent optical properties of water on solar altitude. *Limnology and Oceanography, 29*, 350–356.

Kirk, J. T. O. (1994). *Light and photosynthesis in aquatic ecosystems* (2nd ed.). Cambridge University Press.

Kulk, G., Platt, T., Dingle, J., Jackson, T., Jönsson, B. F., Bouman, H. A., Babin, M., Brewin, R. J. W., Doblin, M., Estrada, M., et al. (2020, 2021). Primary production, an index of climate change in the ocean: Satellite-based estimates over two decades. *Remote Sensing, 12*, 826. 2021 *Remote Sensing, 13*, 3462.

Longhurst, A. R. (2006). *Ecological geography of the sea* (p. 560). Academic Press.

Longhurst, A. R., & Harrison, W. G. (1989). The biological pump: Profiles of plankton production and consumption in the upper ocean. *Progress in Oceanography, 22*, 47–123.

Longhurst, A., Sathyendranath, S., Platt, T., & Caverhill, C. (1995). An estimate of global primary production in the ocean from satellite radiometer data. *Journal of Plankton Research, 17*, 1245–1271.

Marra, J., Langdon, C., & Knudson, C. (1995). Primary production, water column changes and the demise of a Phaeocystis bloom at the ML-ML site in the Northeast Atlantic Ocean. *Journal of Geophysical Research, 100*, 6645–6653.

Morel, A. (1978). Available, usable, and stored radiant energy in relation to marine photosynthesis. *Deep-Sea Research Part I, 25*, 673–688.

Morel, A. (1988). Optical modeling of the upper ocean in relation to its biogenous matter content (case-I waters). *Journal of Geophysical Research, 93*(C9), 10749–10768.

Morel, A. (1991). Light and marine photosynthesis: A spectral model with geochemical and climatological implications. *Progress in Oceanography, 26*, 263–306.

Morel, A., & Berthon, J. F. (1989). Surface pigments, algal biomass profiles, and potential production of the euphotic layer: Relationships reinvestigated in review of remote-sensing applications. *Limnology and Oceanography, 34*, 1545–1562.

Morel, A., & Prieur, L. (1977). Analysis of variations in ocean color. *Limnology and Oceanography, 22*(4), 709–722.

Mueller, J. L., & Trees, C. C. (1994). Revised SeaWiFS prelaunch algorithm for the diffuse attenuation coefficient K (490). In *Case studies for SeaWiFS calibration and validation, Part 4. NASA Tech. Memo. 104566* (Vol. 28).

Naqvi, S. W. A. (1991). Geographical extent of denitrification in the Arabian Sea in relation to some physical processes. *Oceanologica Acta, 14*, 281–290.

Navalgund, R. R., & Kiran Kumar A. S. (1999). Ocean Colour Monitor (OCM) IRS-P4, IOCCG web site, http://www.ioccg.org/generate/ocm/ocm.html

O'Reilly, J. E., Maritorena, S., Siegel, D., O'Brien, M., Toole, D., Mitchell, B. G., Kahru, M., Chavez, F., Strutton, P., Cota, G., Hooker, S., Mcclain, C., Carder, K., Muller-Karger, F., Harding, L., Magnuson, A., Phinney, D., Moore, G., Aiken, J., Arrigo, K., Letelier, R., & Culver, M. (2000). Ocean color chlorophyll a algorithms for SeaWiFS, OC2, and OC4: Version

4. In S. B. Hooker & E. R. Firestone (Eds.), *SeaWiFS postlaunch calibration and validation analyses, part 3. NASA Tech. Memo. 2000-206892* (Vol. 11, pp. 9–23). NASA GSFC Greenbelt, MD.

Parthasarathy, B., Munot, A. A., & Kothawale, D. R. (1995). *Monthly and seasonal rainfall series for all-india homogeneous regions and meteorological subdivisions, 1871–1994*. Indian Institute of Tropical Meteorology.

Platt, T. (1986). Primary production of the ocean water column as a function of surface light intensity, algorithms for remote sensing. *Deep Sea Research Part A. Oceanographic Research Papers, 33*, 149–163.

Platt, T., & Jassby, A. D. (1976). The relationship between photosynthesis and light for natural assemblages of coastal marine phytoplankton. *Journal of Phycology, 12*, 421–430.

Platt, T., & Sathyendranath, S. (1988). Oceanic primary production: Estimation by remote sensing at local and regional scales. *Science, 241*, 1613–1620.

Platt, T., & Sathyendranath, S. (1991). Biological production models as elements of coupled, atmosphere-ocean models for climate research. *Journal of Geophysical Research, 96*, 2585–2592.

Platt, T., & Sathyendranath, S. (1993). Estimators of primary production for interpretation of remotely sensed data on ocean color. *Journal of Geophysical Research, 98*, 14561–14576.

Platt, T., & Sathyendranath, S. (1999). Spatial structure of pelagic ecosystem processes in the global ocean. *Ecosystems, 2*, 384–394.

Platt, T., Gallegos, C. L., & Harrison, W. G. (1980). Photo inhibition of photo synthesis in natural assemblages of marine phytoplankton. *Journal of Marine Research, 38*, 687–701.

Platt, T., Sathyendranath, S., Caverhill, C., & Lewis, M. R. (1988). Ocean primary production and available light: Further algorithms for remote sensing. *Deep Sea Research, 35*, 855–879.

Platt, T., Sathyendranath, S., & Ravindran, P. (1990). Primary production by phytoplankton: Analytic solutions for daily rates per unit area of water surface. *Proceedings of the Royal Society of London. Series B, 241*, 101–111.

Platt, T., Sathyendranath, S., & Ulloa, O. (1992). Nutrient control of phytoplankton photosynthesis in the Western North Atlantic. *Nature, 356*, 229–231.

Platt, T., Sathyendranath, S., White, G. N., III, & Ravindran, P. (1994). Attenuation of visible light by phytoplankton in a vertically-structured ocean: Solutions and applications. *Journal of Plankton Research, 16*, 1461–1487.

Platt, T., Sathyendranath, S., & Longhurst, A. (1995). Remote sensing of primary production in the ocean: Promise and fulfillment. *Philosophical Transactions of the Royal Society of London. Series B, Biological Sciences, 348*, 191–202.

Raman, M. (2013). *Estimating primary production in the Arabian Sea using satellite derived data*. PhD. Dissertation, Mangalore University, p. 223.

Raman, A. V., & Prakash, K. P. (1989). Phytoplankton in relation to pollution in Visakhapatnam harbour, east coast of India. *Indian Journal of Marine Sciences, 18*, 33–36.

Raman, M., Rajan, R., & Ajai. (2016). Identification and mapping of ocean biological deserts using satellite data. *Indian Journal of Marine Sciences, 6*(50), 1–9.

Ryther, J. H., & Yentsch, C. S. (1957). The estimation of phytoplankton production in the ocean from chlorophyll and light data. *Limnology and Oceanography, 2*, 281–286.

Saji, N. H., Goswami, B. N., Vinayachandran, P. N., & Yamagata, T. (1999). A dipole mode in the tropical Indian Ocean. *Nature, 401*, 360–363.

Sakshaug, E., Andresen, K., & Kiefer, D. A. (1989). A steady state description of growth and light absorption in the marine planktonic diatom, Skeletonema costatum. *Limnology and Oceanography, 34*, 198–205.

Sanwlani, N., Chauhan, P., & Navalgund, R. R. (2011). Atmospheric correction using 1240 and 2130 nm combination of MODIS SWIR channels. *Asian Journal of Geoinformatics, 11*, 1–10.

Sarma, V. V. S. S., Kumar, M. D., & George, M. D. (1998). The central and eastern Arabian Sea as a perennial source for atmospheric carbon dioxide. *Tellus B: Chemical and Physical Meteorology, 50*, 179–184.

Sarmiento, J. L., Orr, J. C., & Siegenthaler, U. (1992). A perturbation simulationof CO2 uptake in an ocean general circulation model. *Journal of Geophysical Research, 97*, 3621–3645.

Sathyendranath, S., & Platt, T. (1988). The spectral irradiance field at the surface and in the interior of the ocean: A model for applications in oceanography and remote sensing. *Journal of Geophysical Research, 93*(C8), 9270–9280.

Sathyendranath, S., & Platt, T. (1989). Remote sensing of ocean chlorophyll: Consequence of non-uniform pigment profile. *Applied Optics, 28*, 490–495.

Sathyendranath, S., & Platt, T. (1991). Angular distribution of the submarine light: Modification by multiple scattering. *Proceedings of the Royal Society of London. Series A, 433*, 287–297.

Sathyendranath, S., & Platt, T. (1993). Remote sensing of water-column primary production. In W. K. W. Li & S. Y. Maestrini (Eds.), *Measurement of primary production from the molecular to the global scale* (Vol. 197, pp. 236–243). ICES Marine Science Symposia.

Sathyendranath, S., & Platt, T. (2007). Spectral effects in bio-optical control on the ocean system. *Oceanologia, 49*(1), 5–39.

Sathyendranath, S., Lazzara, L., & Prieur, L. (1987). Variations in the spectral values of specific absorption of phytoplankton. *Limnology and Oceanography, 32*, 403–415.

Sathyendranath, S., Platt, T., Caverhill, C. M., Warnock, R. E., & Lewis, M. R. (1989a). Remote sensing of oceanic primary production: Computations using a spectral model. *Deep Sea Research Part A. Oceanographic Research Papers, 36*, 431–453.

Sathyendranath, S., Prieur, L., & Morel, A. (1989b). A three-component model of ocean colour and its application to remote sensing of phytoplankton pigments in coastal waters. *International Journal of Remote Sensing, 10*, 1373–1394.

Sengupta, R., Rajagopal, M. D., & Qasim, S. Z. (1976). Relationship between dissolved oxygen and nutrients in the Northwest Indian Ocean. *Indian Journal of Marine Sciences, 5*, 201–211.

Smith, R. C., & Tyler, J. E. (1967). Optical properties of clear natural water. *Journal of the Optical Society of America, 57*, 589–595.

Somasunder, K., Rajendran, A., Kumar, M. D., & Sen Gupta, R. (1990). Carbon and nitrogen budgets of the Arabian Sea. *Marine Chemistry, 30*, 363–377.

Steemann Nielsen, E. (1952). The use of radio-active carbon (14C) for measuring organic production in the sea. *Journal du Conseil/Conseil Permanent International pour l'Exploration de la Mer, 18*(2), 117–140.

Stramski, D., Reynolds, R. A., Kahru, M., & Mitchell, B. G. (1999). Estimation of particulate organic carbon in the ocean from satellite remote sensing. *Science, 285*, 239–242.

Subrahmanyan, R. (1959). Studies on phytoplankton of the west coast of India. *Proceedings of the Indian Academy of Sciences, L (3) Section B, 50*, 113–187.

Subrahmanyan, R., & Sarma, A. H. V. (1960). Studies on phytoplankton of the west coast of India III. Seasonal variations of the phytoplankters and environmental factors. *Indian Journal of Fisheries, 7*, 307–336.

Westberry, T., Behrenfeld, M. J., Siegel, D. A., & Boss, E. (2008). Carbon-based primary productivity modeling with vertically resolved photoacclimation. *Global Biogeochemical Cycles, 22*(GB2024), 1–18.

Wyrtki, K. (1973). Physical oceanography of the Indian Ocean. In B. Zeitzschel (Ed.), *The biology of the Indian Ocean* (pp. 18–36). Springer Verlag.

Chapter 12
Monitoring Phytoplankton Bloom, Ocean Productivity, and Associated Features Around the Southern Peninsular Indian Water Using Oceansat-2 Ocean Color Monitor and Scatterometer Data

Ranjit Kumar Sarangi

Abstract Oceansat-2 ocean color monitor (OCM) data analysis was carried out to study phytoplankton bloom in the Indian water over the southern peninsula. Chlorophyll-*a* product processing and analysis are carried out during September–October 2011 for studying the upwelling enhanced bloom and its phases in the southwest Bay of Bengal and the adjoining Arabian Sea. Oceansat-2/OCM-derived chlorophyll-*a* images off the Tamilnadu, Kerala, and Srilankan regions were retrieved using 21 dates with less-cloudy OCM scenes, covering path 10 and row 14 passes. The satellite images were geometrically corrected. The high chlorophyll-*a* concentration (1.0–3.0 mg m^{-3}) patches were seen along the coastline. Algal bloom features were seen with the effect of southwest monsoon upwelling around the Kerala coast during August–September and progressed. Oceansat-2 scatterometer (OSCAT) level-2 datasets (18 scenes) have been archived from the National Remote Sensing Centre (NRSC) server and processed to generate wind speed maps from September–October 2011. The wind speed was observed in the range of 1–10 m/s. High wind speed (~6–10 m/s) features are observed around the upwelling region along the Kerala coast and in the southwest Bay of Bengal. There has been an observation of algal bloom patches with high chlorophyll-*a* concentration (~2.0 mg m^{-3}), which coincidentally matched with the high wind speed (~7–8 m/s) zones during the 1st week of October. The reported upwelling during the southwest monsoon has been interpreted to be the causative factor for high chlorophyll-*a* concentration. There were similar high chlorophyll-*a* concentration patches during the same period of 2010–2012 observed using MODIS datasets. So, the study portrays the wind-induced enhancement in ocean productivity in the southern peninsular Indian water during the southwest and inter-monsoon phases. The study will be useful for correlating with physical oceanographic processes like upwelling, currents, and wind patterns. The biogeochemical cycling and flux patterns can also be studied

R. K. Sarangi (✉)
Marine Ecosystem Division, Space Applications Centre (ISRO), Ahmedabad, India
e-mail: sarangi@sac.isro.gov.in

S. C. Tripathy, A. Singh (eds.), *Dynamics of Planktonic Primary Productivity in the Indian Ocean*, https://doi.org/10.1007/978-3-031-34467-1_12

during the seasons like southwest and northeast monsoons. This is a unique study and attempts to encompass both the Indian satellite sensors OCM and scatterometer data from a single space platform for the ocean color applications in Indian water to assess ocean productivity.

Keywords Oceansat-2 OCM · Scatterometer/oscat · Chlorophyll-*a* · Wind speed · Phytoplankton bloom · Upwelling

1 Introduction

Ocean color remote sensing provides information on the quality and constituents of seawater, which includes the concentration of phytoplankton pigments, suspended sediments, and yellow substances. There has been successful detection and mapping of seawater constituents with the survey utilizing aircrafts and spaceborne platforms, over the last three decades (Clarke et al., 1970; Gordon & Morel, 1983; Evans & Gordon, 1994). Satellite measurements have been applied successfully to measure and map surface ocean pigment concentrations (Gordon et al., 1980; Baker & Smith, 1982; Morel, 1988). Ocean color observations based on satellite datasets have been able to provide large-scale, repeated coverage sampling of global ocean chlorophyll-*a* that is essential to help understand the role of phytoplankton on biogeochemical cycling, climate change, and fisheries (Gregg & Conkright, 2001). Large areas need to be covered rapidly and frequently to determine the spatial extent of bloom in near real time by satellite-based monitoring methods, which would essentially cater to the effective means to detect and monitor bloom-forming stages (Sarangi et al., 2001). Satellite-based detection and monitoring of harmful algal blooms (HABs) need methods/algorithms that are developed mostly based on a huge set of in situ bio-optical data from optically less complex oceanic waters and modeled optical properties (Ahn & Shanmugam, 2006). The monsoonal climate is well known for its dominance over the north Indian Ocean, and its effects have been on record far into the subtropics of the southern hemisphere (Fein & Stephens, 1987). Sea-viewing Wide Field-of-view Sensor (SeaWiFS images of the summer monsoon of 1998 (Murtugudde et al., 1999) have indicated seasonal blooms in southern Sri Lanka and in the northern Indian Ocean. The chlorophyll-*a*-rich waters from the Indian coast and their advection with the southwest monsoon current (SMC) move toward Sri Lanka from the Indian southern peninsula and in the northern Indian Ocean around the Indian tip (Vinayachandran et al., 2004).

The physical forces alter the water column nutrients vertically and regulate the biological production, which happens in the mixed layer (Banse & English, 2000). The northeasterly trade winds and their impact on the winter blooms have been studied in the northern Arabian Sea (Dwivedi et al., 2006). The changes in the ocean surface chlorophyll-*a* along with physical parameters are studied in the northeast Arabian Sea (Singh et al., 2001). The bloom formation gets intensified due to anticyclonic activity-induced nutrient injection (Vinayachandran & Mathew, 2003). The Bay of Bengal is known to be a unique and dynamic study area as it

experiences many distinguished oceanic features. But the Arabian Sea basin at the west has been studied extensively, which experiences monsoon with season reversal patterns (Shetye et al., 1993). The Bay of Bengal is well known due to the large amount of freshwater fluxes from multiple rivers. The water column in the Bay of Bengal is strongly influenced by freshwater flux along with monsoonal winds, its impact on water column stratification, and on the surface water currents in the Bay of Bengal. Generally, the Bay of Bengal has been of concern as less productive compared with Arabian Sea. It has been observed that a large amount of nutrients are brought into the sea by many major rivers; still, the Bay of Bengal productivity was found to be low, which is due to narrow shelves, excess cloud cover round the year, and low insolation conditions at sea. Like the Somali current and the West India Coastal Current (WICC) in the Arabian Sea, the East India Coastal Current (EICC) shows a reversal pattern in its flow twice every year, flows northeastward from February to September with a strong peak during March–April and southeastward from October to January with the strongest flow during November (Hellerman & Rosenstein, 1983; Potemra et al., 1991; Shetye et al., 1993; McCreary et al., 1996). The seas around the Indian subcontinent experience winter monsoon, and topography variation-based gap wind events (Dey & Singh, 2003). The gap winds are experienced with high wind stress and high turbulent heat loss in the Gulf of Mannar around the north of 10°N. Hence, this influence is linked to hydrospheric and atmospheric changes and the monsoon wind reversal happens semiannually and has been noteworthy (Luis & Kuwamura, 2000). The nutrient concentration and circulation pattern connected to ocean water have remarkable importance in understanding various processes of oceans (Dey & Singh, 2003). Hence, the observations on ocean productivity in different timescales in relation to physical parameters have been of utmost importance.

There have been observations of phytoplankton blooms in different parts of the world's oceans. The red tide blooms appeared as an extreme incubator in the northeast Monterey Bay inner shelf water along the California coast. Within the California current upwelling system, the bloom dynamics have been on record with the influence of strong wind and their reversal pattern, which enhances the upwelling cycle (Ryan et al., 2009). Along the western Santa Barbara channel, the cyclonic circulation on ocean surface along with coastal upwelling results in increased phytoplankton concentration and productivity. This happens with the enrichment of nutrients in the water column and in the ocean surface, observed during an interannual study (Brzezinski & Washburn, 2011). There has been an example of a bloom study in the southern ocean region, using the ocean color and wind speed data. In the marginal ice zone (MIZ), the bloom and algal biomass have been observed to be diminished and suppressed with high wind speed and high blooms at low wind speed (~5 m/s). This acted in reverse order in the MIZ region in the southern ocean (Fitch & Moore, 2007). Another study along the Kerala coast and Indian west coast showed the increase in fish catch based on landing data from coastal areas which showed the linkage to phytoplankton bloom condition (George et al., 2012). There has been a study on the harmful algal bloom with the effect of upwelling-enhanced productivity (Tweddle et al., 2010). So, the current study glimpses the ocean color-based features' observation, its variability and dynamics

with the effect of wind, upwelling, and linkage to productivity. This has been discussed in relation to the ocean ecosystem, like the cases of several algal blooms observation.

2 Objectives

(i) To analyse the Indian satellite Oceansat-2 OCM and scatterometer (OSCAT) day-wise data over the southern peninsula of India (the Bay of Bengal and the Arabian Sea) during the period September–October 2011 to generate chlorophyll-*a* images and wind speed maps.
(ii) To interpret the daily and weekly variability of chlorophyll-*a* and phytoplankton bloom features and their link to wind speed data.
(iii) To study and understand the link of the phytoplankton bloom to weekly chlorophyll-*a* variability trend during the upwelling season.

3 Materials and Methodology

3.1 Oceansat-2 OCM

The Indian Remote Sensing satellite Oceansat-2 OCM-derived chlorophyll-*a* images have been processed from September to October 2011 over the southwest Bay of Bengal and the southeast Arabian Sea. The study area covers latitude 5.0–15.0°N and longitude 75.0–85.0°E observed by OCM path 10 and row 14 satellite pass based on its orbit calendar. Station datasets have been retrieved for the bloom and non-bloom locations.

Oceansat-2 OCM Instrument and Applications
Ocean color monitor (OCM-2) on board Oceansat-2 with the continuity from Oceansat-1 mission of the Indian Space Research Organization (ISRO) was launched on September 23, 2009. Earlier the Oceansat-1 was launched in May 1999. The objective of the OCM-2 mission was to retrieve chlorophyll-*a* concentration, suspended sediment concentration, aerosol optical depth, and colored dissolved organic matter in different types of coastal and offshore waters. The detailed technical specifications of OCM-2 are mentioned in Tables 12.1 and 12.2.

3.2 Oceansat-2 OCM Data Processing

The OCM-2 data processing is required to undergo two steps. These are the atmospheric correction of optical channels using different wavelengths to retrieve normalized water-leaving radiances. The next step is to retrieve different bio-optical parameters by applying different algorithms.

Table 12.1 Central wavelengths, bandwidth, and applications of oceansat-2 OCM

Band No.	Central λ (nm)	Bandwidth (nm)	Potential applications
1	412	20	Yellow substance absorption
2	443	20	Low chlorophyll-*a* concentration
3	490	20	Mid chlorophyll-*a* concentration
4	510	20	High chlorophyll-*a* concentration
5	555	20	Chlorophyll-*a* reference
6	620	20	Total suspended matter (TSM)
7	740	30	Atmospheric correction
8	865	40	Atmospheric correction

Table 12.2 Technical characteristics of the oceansat-2 OCM sensor

IGFOV	360 m × 236 m (720 km altitude @ nadir)
SWATH	1420 km (FOV ± 43°)
Repeativity	2 days
MTF at Nyquist	>0.26
SNR @ ref radiance	C1 C2 C3 C4 C5 C6 C7 C8 356 386 380 324 311 240 286 141
Quantization (bits)	12
Equatorial crossing time	12 noon
Along track steering	±20°
No of bands	8

3.3 *Atmospheric Correction of the OCM-2 Imagery*

As we know, only 8–10% of signal contributed from the ocean surface to the total atmospheric radiance received by the satellite sensors. Hence, the rest of about 90% signal is only from the atmosphere and needs to be eliminated from the total sensor detected radiance. Hence, the role of atmospheric correction is vital to studying the oceans through optical remote sensing. The long-wavelength approach takes care of atmospheric correction in removing the Rayleigh and aerosol scattering. The infrared channels (740 and 865 nm) were used to perform atmospheric correction for the visible channels (Gordon & Wang, 1994; Chauhan et al., 2002). Then the atmospherically corrected channels/bands are used to retrieve chlorophyll-*a* and other bio-optical parameters.

3.4 *Chlorophyll-a Algorithm*

Various regression-based algorithms have been developed over global waters and in Indian waters as well using empirical and semiempirical methods, as shown in Table 12.3.

Table 12.3 Oceansat-2 OCM chlorophyll-*a* retrieval algorithm

Model	Input bands	Coefficients	r^2	RMSE
Modified cubic polynomial $\log_{10}(C) = (a + b * R + c * R^2 + d * R^3) + e$	$R = \log_{10}(R_{rs}443 > R_{rs}490 > R_{rs}510/R_{rs}555)$	$a = 0.48$; $b = -3.03$ $c = 2.24$; $d = -1.25$ $e = -0.03$	0.96	0.118

The algorithms used in Indian waters obtained an accuracy of ±30% error in the southwest Bay of Bengal (Shanthi et al., 2013). Several steps are taken up to improve the accuracy of geophysical parameters retrieval; hence, vicarious calibration has been performed over Indian water to minimize the error by ±30%.

3.5 Oceansat-2 Scatterometer (OSCAT) Data

The Indian Oceansat-2 scatterometer mission was accomplished by configuring with 13.5 GHz Ku-band microwave channel (Gohil et al., 2008). The OSCAT was built-in 1-meter parabolic antenna that generated two beams. It observed continuous swaths for 1400 km for both inner and outer beams, respectively. There have been ascending and descending daily passes. The goal of the mission was to retrieve wind speed/direction with an accuracy of 2 m/s and 20°, respectively. The wind speed range is targeted to be 4–24 m/s. These wind speed data have been received online from the National Remote Sensing Centre (NRSC), India (http://www.nrsc.gov.in/), server for the study area covering the duration of September–October 2011.

3.6 MODIS Data Archival

The chlorophyll-*a* images were archived from the MODIS-Aqua 8-day averaged composite data during September–October 2010, 2011, and 2012. MODIS-Aqua binned data of 9-km resolutions over the selected study area (latitude 5–15°N and longitude 75–87°E) in the southern peninsular India water covering the Bay of Bengal and Arabian Sea (source: http://modis.gsfc.nasa.gov/Oceancolor).

MODIS-Aqua Chlorophyll-a Algorithm

The MODIS-Aqua satellite sensor used the OC-3 (Ocean Chlorophyll-3) algorithm for global observation (Morel & Maritorena, 2001). The algorithm has been able to retrieve a broad range of chlorophyll covering 0.01–100 mg m^{-3}. The algorithm has been estimated to have error accuracy within ±35% over global waters. The algorithm is shown with the following mathematical form:

$$C = 10^{(0.283 - 2.753*R + 1.457*R2 - 0.659*R3 - 1.403*R4)},$$

where $R = \log_{10}[(R_{rs}443 > R_{rs}488)/R_{rs}551]$ and R_{rs} is remote sensing reflectance.

4 Results and Discussion

4.1 Intraseasonal Variability of Phytoplankton Bloom

A total of 21 dates of Oceansat-2 OCM chlorophyll-*a* data has been retrieved from September to October 2011. The processed images have been used for

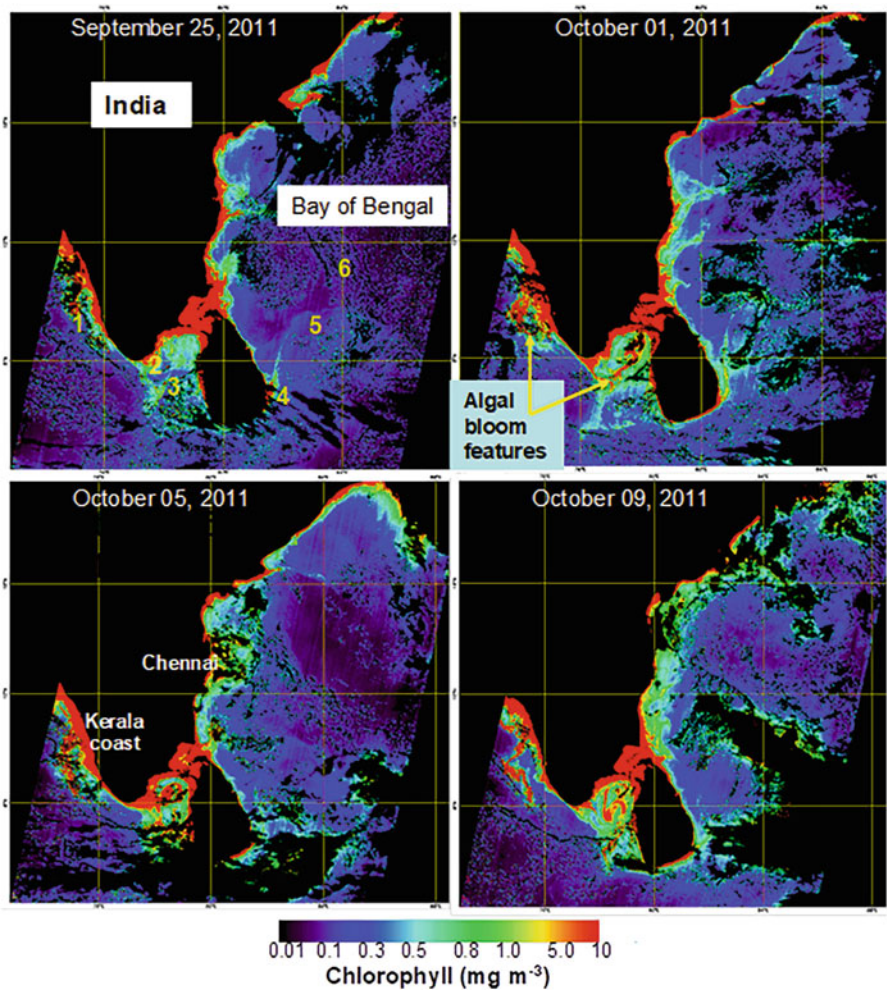

Fig. 12.1 Indian Oceansat-2 ocean color monitor (OCM) sensor-derived chlorophyll-*a* images indicating massive algal bloom off Kerala and Tamilnadu coast

studying upwelling-based ocean productivity in the southwest Bay of Bengal and the southeast Arabian Sea separately. Limited numbers (15 scenes) of cloud-free and less cloudy images were interpreted. The high chlorophyll-*a* concentration (1.0–3.0 mg m^{-3}) patches were seen along the coastline. Algal bloom features were seen with the effect of southwest monsoon upwelling around the Kerala coast during the September–October months (Figs. 12.1 and 12.2). Several coastal/riverine plumes (off Godavari, Krishna, and Kaveri rivers) with high chlorophyll-*a* concentrations (~2.0 mg m^{-3}) were seen during October on the east coast of India. Oceansat-2 scatterometer (OSCAT) level-2 datasets (18 scenes) have been

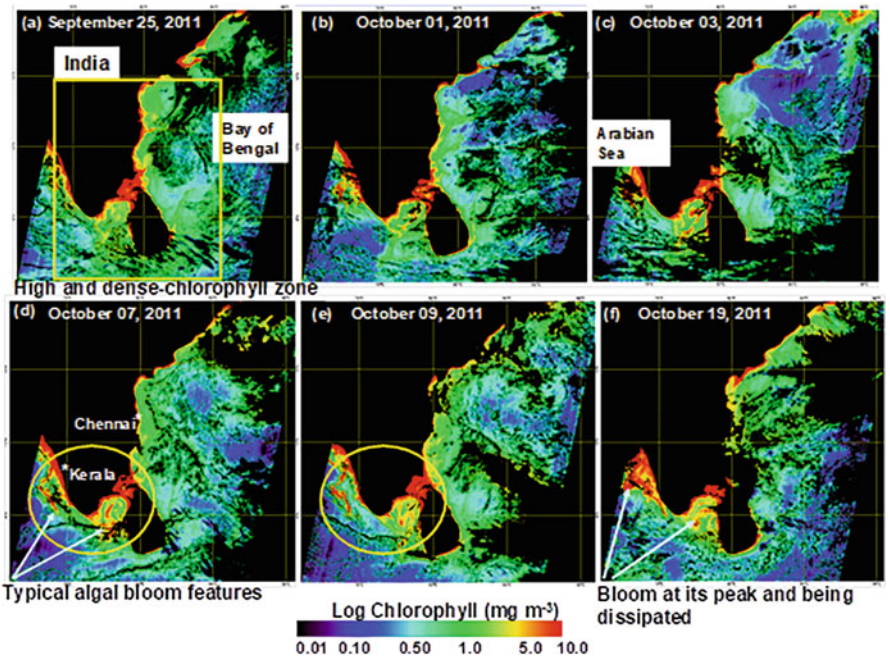

Fig. 12.2 Oceansat-2 OCM derived chlorophyll-*a* images showing algal bloom stages over the southwest Bay of Bengal and southeast of the Arabian Sea

archived from NRSC server and processed to generate wind speed maps, from September to October 2011 (Figs. 12.3 and 12.4). Algal bloom observations based on Oceansat-2 OCM and scatterometer and MODIS-Aqua chlorophyll-*a* data in southern Indian water have been interpreted. The high wind speed of ~7–8 m/s has been seen around the upwelling region around the Kerala coast and in the SW Bay of Bengal. The wind speed ranged between 2 and 10 m/s. The high wind speed (6–10 m/s) features have been observed around the Sri Lankan coast and off the Kerala coast, exhibiting evidence of upwelling and jetlike features. The OCM-2-derived chlorophyll-*a* images were generated for the same period and showed high chlorophyll-*a* biomass (1.0–1.5 mg m^{-3}) around the region. So, it shows the wind-induced enhanced ocean productivity in the southern peninsular Indian water during the southwest and inter-monsoon phases. The wind direction information (white arrows) is also visible along with wind speed maps (Figs. 12.3 and 12.4); even with its low resolution, it shows that the wind blows in an easterly direction (alongshore wind) moving toward the Kerala coast and the southern tip of India, which diverges the ocean surface water and causes upwelling.

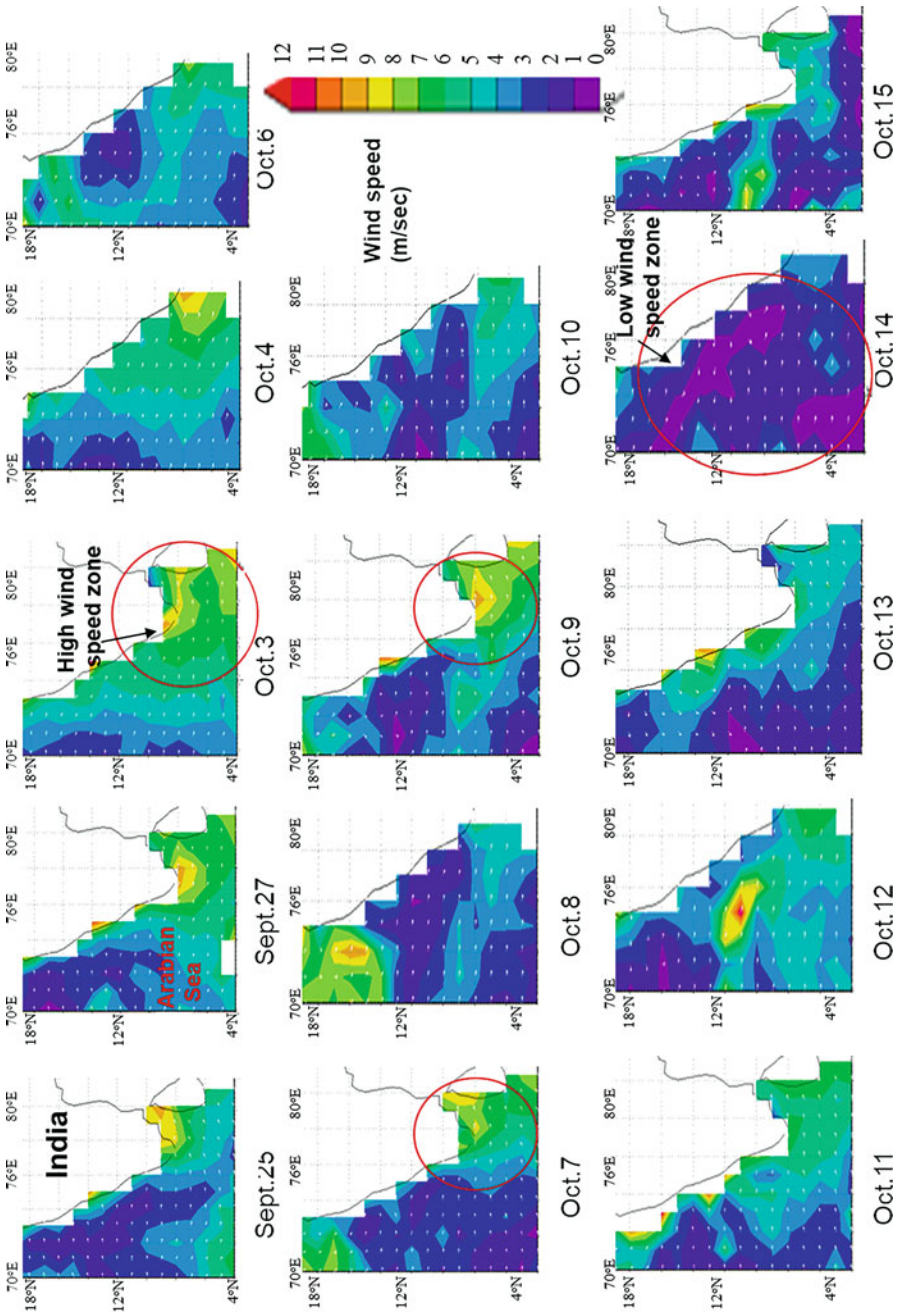

Fig. 12.3 Oceansat-2 scatterometer-derived wind speed and wind vector maps over southeast Arabian Sea (September–October 2011)

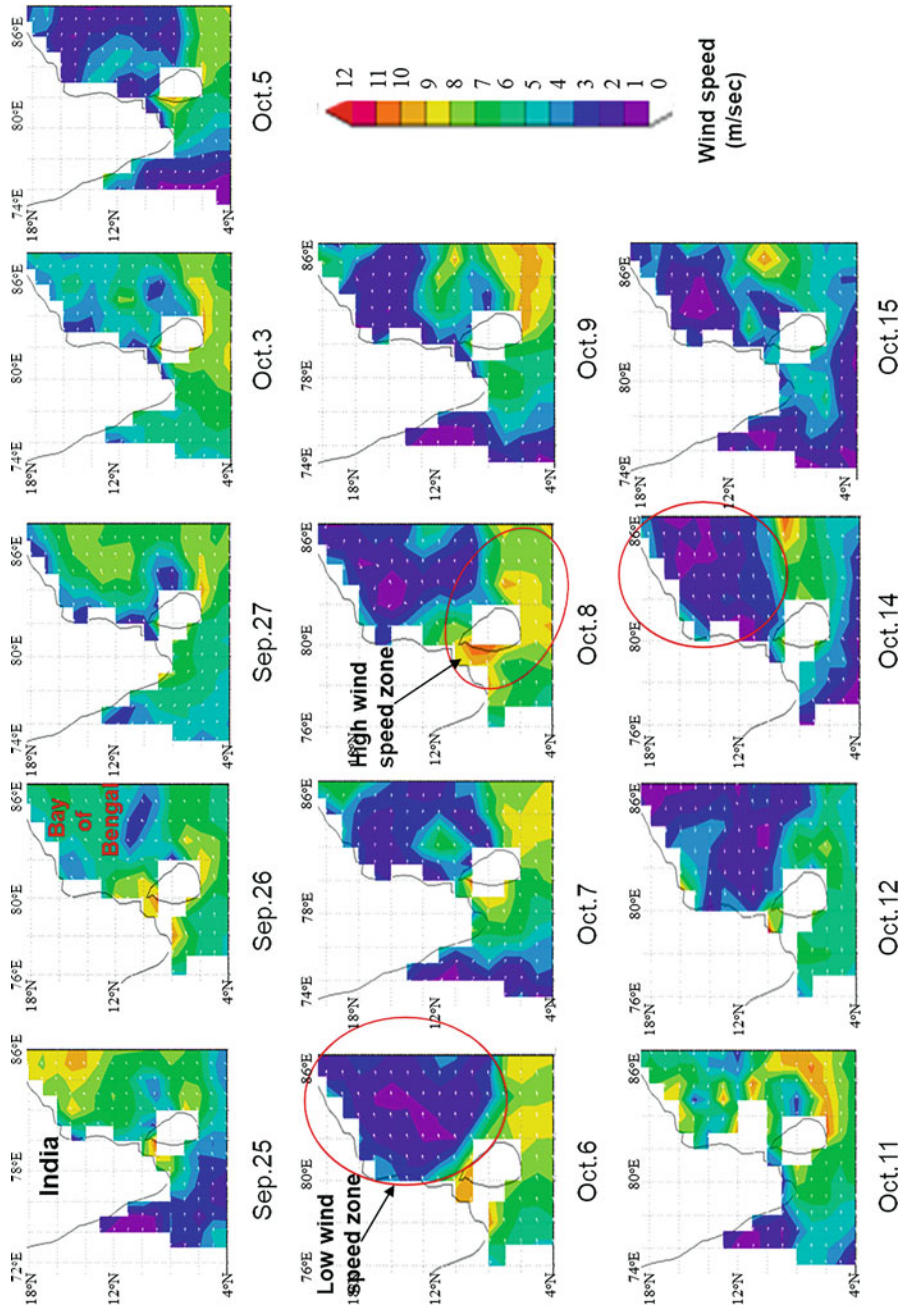

Fig. 12.4 Oceansat-2 scatterometer derived wind speed and wind vector maps over southwest Bay of Bengal (September–October 2011)

4.2 Location-Based Variability of Phytoplankton Bloom

There has been an observation of chlorophyll-*a* variability along six points during September–October 2011 for 11 dates. Latitude and longitude for six points (bloom points 1, 2, 3, & 4) and non-bloom location points (5 and 6). Point 1 at 9°N and 75°E, point 2 at 8°N and 77.5°E, point 3 at 7°N and 78°E, point 4 at 6.5°N and 82°E, point 5 at 9°N and 83°E, and point 6 at 11°N and 84°E were selected to retrieve chlorophyll-*a* and wind speed values. The chlorophyll-*a* peak was seen on October 7, 2011, which was around 10–12 mg m^{-3} for all points. Similarly, the wind speed was high, mostly around 7–11 m/s for the bloom points/locations (points 2, 3, & 4). Even the high chlorophyll-*a* (~2–4.5 mg m^{-3}) was seen on October 1 when the wind speed range was high (4–9 m/s) for the bloom points (1–3). The chlorophyll-*a* variability plot shows a distinct pattern (Fig. 12.5a), but the wind speed plot pattern is seen as scattered (Fig. 12.5b). Still, the bloom points portray the high wind speed pattern and the non-bloom points show the low wind speed pattern (Fig. 12.5b). So, the existing relationship between chlorophyll-*a* and wind speed has been regressed and correlated (Fig. 12.6). The chlorophyll-*a* and wind speed points for the same data show the relationship, $R = 0.33$, and the 2-day lag phase relationship shows $R = 0.26$ (Fig. 12.6a, b). It shows that the same-day and concurrent time wind speed and instant chlorophyll-*a* show a little better relationship than with the wind speed with a 2-day lag phase chlorophyll-*a* concentration relationship. There have been cases of upwelling along the southern peninsular Indian water. Coastal upwelling has been effective due to the alongshore wind stress component round the year along this coast with the monthly mean alongshore wind stress component directed toward the equator (Shetye et al., 1985). The International Indian Ocean Expedition (IIOE) and other cruises carried out in the southeast Arabian Sea mentioned the occurrence of upwelling during southwest monsoon as evidenced by Banse (1959, 1968), Darbyshire (1967), and Sharma (1973). The upwelling phenomenon between 8 and 15°N latitude along the Indian coast has been observed in water temperature and Ekman transport data (Shetye, 1984). Upwelling indices have been measured for the southeast Arabian Sea based on temperature and Ekman transport data (Smitha, 2010; Jayaram et al., 2010). The southwest coast of India and around the southern Indian tip experience upwelling by the end of May/early June and propagate northward with time. This upwelling phenomenon is known to be effective with the influence of southwesterly winds (Madhupratap et al., 2001). The upwelling process lasts up to September and progressively gets reduced. The diverging current is portrayed to be the main cause inducing upwelling (Rao & Jayaraman, 1966). Hence, this region is of interest in the upwelling event occurrence and prevails due to the joint effect of alongshore wind and conducive ocean circulation pattern.

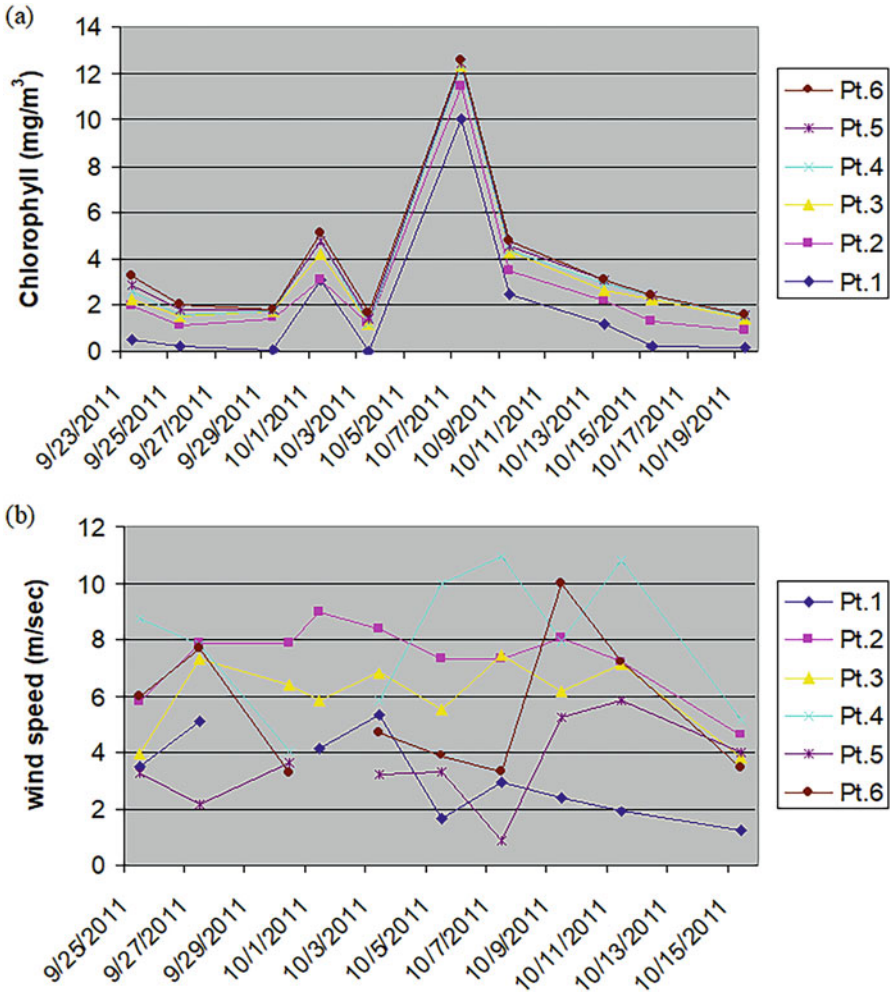

Fig. 12.5 Oceansat-2 (**a**) OCM sensor-derived chlorophyll-*a* concentration variability for 6 locations (Fig. 12.1) covering coastal and offshore waters around southern peninsular Indian water and (**b**) OSCAT scatterometer-derived wind speed variability for respective locations

4.3 Linkages of the Bloom Phenomenon with Earlier Studies

The above works confirm the occurrence of upwelling along the Kerala coast during the southwest monsoon. Upwelling is a well-known process in the redistribution of nutrients in oceanic regions (Vinayachandran & Mathew, 2003). The nutrient concentrations increase due to the upwelling process and enhance the euphotic productivity. With its effect, the cooler and nutrient-enriched waters are brought up from the bottom of the water column, and warm waters get dissipated. These

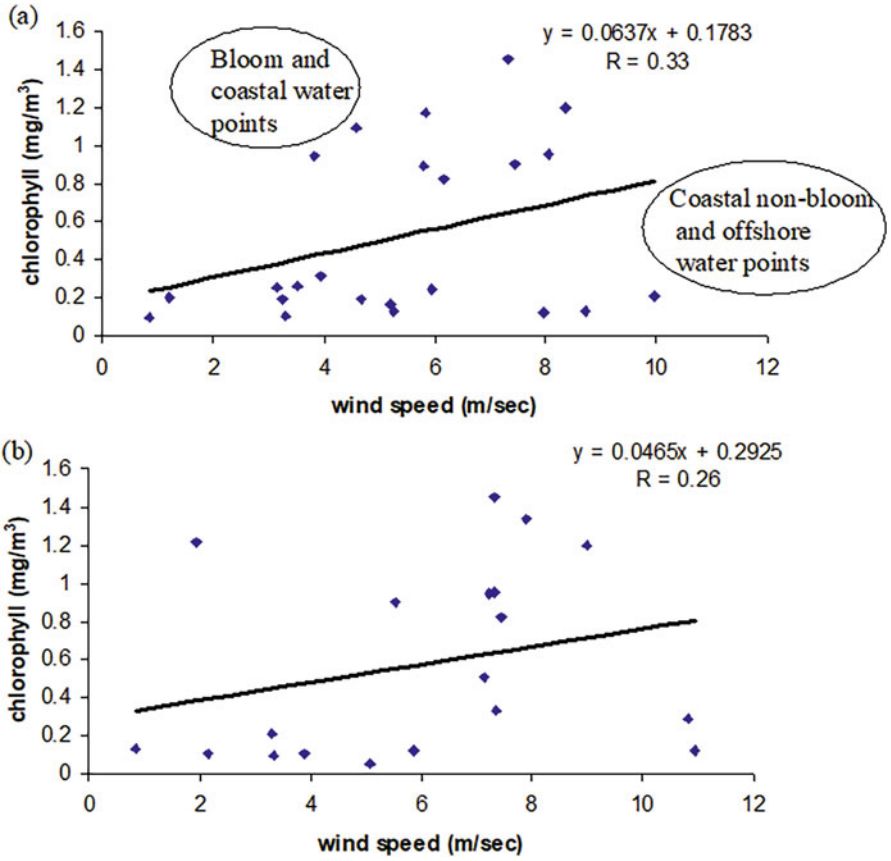

Fig. 12.6 (**a**) Oceansat-2 scatterometer (OSCAT) wind speed with synchronous OCM-2 chlorophyll-*a* and (**b**) with 2-day lag period OCM-2 chlorophyll-*a* concentration relationship during September–October 2011 around southern peninsular Indian water

regions are the locations to have the occurrence of algal blooms and the increase in fishery resources as well (Madhupratap et al., 2001). The coastal areas of the Arabian Sea are important upwelling zones during the southwest monsoon. The Arabian Sea shows the maximum abundance of phytoplankton and zooplankton (Rao & Griffiths, 1998). A strong upwelling is regularly observed here during summer (Prasannakumar et al., 2001) and the whole southwest monsoon season, largely confined to the shelf (Banse, 1959). The hydrographic data depicts the upwelling phase from March to September, occurring along the Kerala coast (Johannessen et al., 1981). The current study is a piece of work to demonstrate the upwelling-induced algal bloom and ocean productivity.

Earlier algal bloom was observed using Indian Remote Sensing (IRS)-P4 (Oceansat-1) OCM and in situ data during September 2002 and 2003 around the Kerala coastal waters. The algal bloom features were detected and monitored via the

total radiance, remote sensing reflectance, chlorophyll-*a*, and diffuse attenuation coefficient images (Sarangi & Mohammed, 2011). In situ observations noted the dominance of dinoflagellate *Noctiluca scintillensis* in the 1st, 2nd, and 3rd weeks of September 2002. Along the Kerala coast, in southern Calicut water, there was mass mortality of fishes, which hints at the harmful impact of algal bloom diminishing the food chain. The water color appeared greenish due to toxic microalgae *Hornelia marina (green tide)*. The fishermen reported the red coloration of water even up to 30–35 km from the coastline, and this appeared as strong reflectance in OCM-derived chlorophyll-*a* images with the dense algal bloom features. The red color of the water was due to the dinoflagellate *Noctiluca scintillans*, which caused red tide with a very high chlorophyll-*a* concentration (20–50 mg m^{-3}). The water currents have moved dense blooms offshore and near the coast (Sarangi & Mohammed, 2011). The discoloration was observed due to algal bloom. Massive death of green mussel, *Perna viridis*, was observed during September 2002, 3rd week around Calicut. The bloom was then reported in the coastal waters of Calicut and Kannur (Sarangi & Mohammed, 2011). So, this study period somehow coincides with the earlier study period and would be of interest to correlate with the environmental impact assessment in the future.

There have been similar high chlorophyll-*a* concentration phytoplankton bloom features seen consistently during the 3-year study period (2010–2012) during the study period of September–October using the MODIS-Aqua 8-day composite maps (Fig. 12.7). It indicates the specific type/dominant species of algal blooms in the study area and might be a causative effect due to a particular nutrient, which acts as a limiting factor. So, the upwelling-enhanced nutrient enrichment is also the major concern and inference from the current study. It can be also cited that the bloom has a strong resemblance to the species observed during the 2002–2003 period from in situ and satellite monitoring approaches. So, this study could be a precursor for ecological impact assessment and ecological management if the bloom becomes severe and harmful. So, like Oceansat-1, the Oceansat-2 OCM and OSCAT sensors have been proven to provide vital inputs and information for ocean biological and ecological assessment.

4.4 Phytoplankton Bloom Induced by Wind Speed

Monitoring of phytoplankton bloom and dense chlorophyll-*a* features using Oceansat-2 OCM and scatterometer datasets has been carried out successfully during September–October 2011. The bloom-forming features were nicely picked up during the September–October months along the Tamilnadu and Kerala coasts and off Sri Lankan water. The densification of features and their movement were very well seen in the chlorophyll-*a* images. The bloom features are resembling the features seen during a previous study along the Kerala coast depicting the Chlorophyceae *Hornelia marina* bloom (Sarangi & Mohammed, 2011). As mentioned earlier, the bloom was observed for 2 consecutive years (2002 and 2003) and caused fish kill

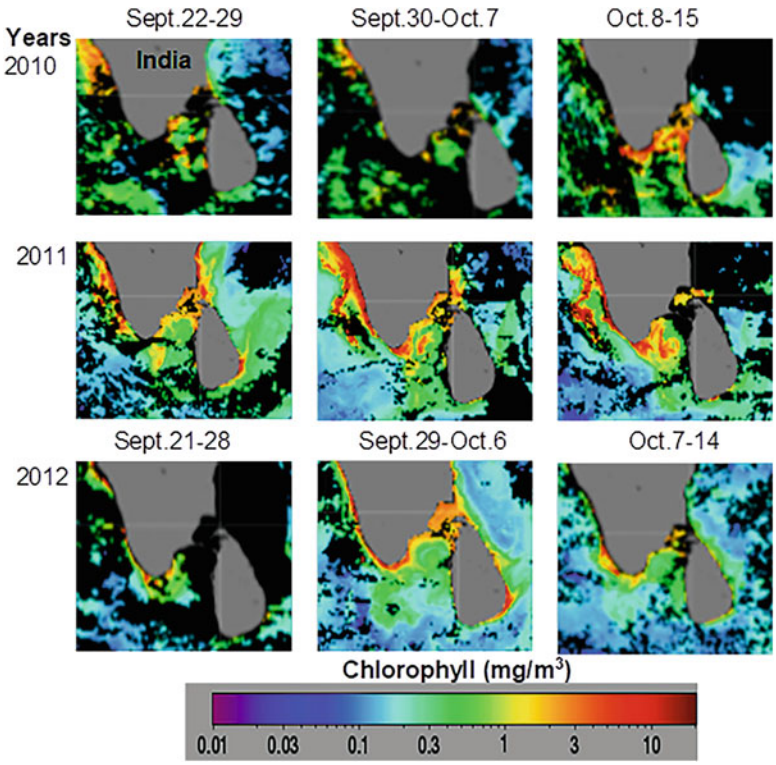

Fig. 12.7 MODIS-Aqua retrieved 8-day composite chlorophyll-*a* concentration maps showing the interannual trend of algal bloom during September–October

due to harmful algal toxins. So, the current bloom seen around the Kerala coast with typical curly and branching features would be of interest to refer to the taxonomy of species and its impact study. This study can be a precursor for the interested researchers to correlate and pursue in-depth analysis at in situ and remote sensing levels. The OSCAT-derived wind maps have been displayed and showed the locations and patterns of wind stress over the study area. The wind speed was seen high around the coastal region (around 100 km distance), which has acted as a triggering force to enhance the bloom event. The study will be useful for further research into correlating the physical oceanographic processes like upwelling, currents, and wind patterns to biological productivity. The biogeochemical cycling can also be studied during the seasons like southwest and northeast monsoons.

4.5 Phytoplankton Bloom and Ocean Productivity

Phytoplankton are the floating pastures of the world's oceans, and they are the autotrophic component of the world ocean. The marine processes that contribute to the ocean biological pump begin with phytoplankton that soak up carbon dioxide

from the atmosphere as they grow, and when phytoplankton diminishes or perishes, they collectively sink the carbon into the ocean water column and ocean floor. During the algal bloom events, the absorption of carbon dioxide efficiency increases drastically and the carbon sequestration effect is more; hence, the phytoplankton bloom has a proven role in primary productivity in the ocean. Most of the carbon that sinks beneath plankton blooms is dissolved and remineralized well above the seafloor and eventually (days to centuries) returns to the atmosphere, negating the original benefit (Sarmiento & Gruber, 2006). Hence, the location of algal blooms and their carbon sequestration process and overall understanding of the biological pump is the essence of the researchers working on marine biogeochemistry using the in situ, satellite data, and models as well. The current study provides a synoptic glimpse of the phytoplankton bloom features and zone monitoring using satellite ocean color datasets using NASA and ISRO satellite datasets and eventfully observed the phytoplankton bloom zones in the southern peninsular Indian water, which is the source of upwelling process and the induction of essential nutrients and minerals to add up to successive bloom events every year during the southwest monsoon and post-monsoon season. Hence, the study is important from the point of understanding ocean productivity based on pigment concentration variability and their synoptic-scale variability and accumulation.

5 Future Research and Direction

More exclusive works are needed to know different phytoplankton species distribution and productivity quantum and fluxes due to those species and phytoplankton types. The impact of different species on the ecosystem, food chain, and in a nutshell on primary, secondary, and tertiary productivity needs to be studied on local, regional, and global scales. From a satellite remote sensing point of view, more frequent observations are needed with a variety of higher-resolution datasets and with different hyper-spectral and narrow bandwidth channels based on reflectance datasets and pigment algorithms and their linkages to ocean productivity, so that more accurate models would be established with concurrent validations.

6 Conclusion

Oceansat-2 OCM has been observed to detect and monitor the phytoplankton bloom features successfully. The OSCAT scatterometer wind speed maps have been interpreted, and the high and low wind speed gradient zones have been identified. Understanding the possible link of wind speed to dense and sparse chlorophyll-*a* zones has been attempted using the datasets from a single space platform on board Oceansat-2 OCM and scatterometer, which is the first of such attempt complying with the upwelling phenomenon's impact on Ocean biology using day-to-day basis

satellite data. The chlorophyll-*a* and wind correlation show a linear trend, which means with an increase in wind speed, there is an increase in chlorophyll-*a* concentration, even if there is a vast difference as far as the resolution of the two sensors is concerned, which is about 30 times and more. The same-day wind speed and chlorophyll-*a* concentration for respective points/pixels were observed to match better than the 2-day lag phase data correlation with limited points. It shows that there is rich nutrient availability due to the upwelling occurring season. So, the time lag is not much needed for nutrient enrichment-based phytoplankton production. The study is also being referred to the previous study of algal bloom incidences due to two species: *Hornelia marina* (green tide) and *Noctiluca scintillans* (red tide) bloom phenomenon causing harmful algal blooms (HABs); the similarity with the current study may not be ruled out, and a seasonal trend based on an interannual study of MODIS-Aqua chlorophyll-*a* maps shows that bloom features occur during the months of September–October. So the study is interesting from the ecological aspect as well. So, the Oceansat-2 OCM-derived chlorophyll-*a* and oscat wind speed information are vital to linking the biological features with physical oceanography.

Acknowledgment The author is thankful to Dr. Raj Kumar, former Deputy Director, EPSA, and to former Director Shri A. S. Kiran Kumar and Shri Nilesh Desai, Director, Space Applications Centre for their support and encouragement in utilizing Oceansat-2 data and to perform relevant application-oriented works. The supporting chlorophyll-*a* maps retrieved from the NASA website (http://oceancolor.gsfc.nasa.gov) have been acknowledged.

References

Ahn, Y.-H., & Shanmugam, P. (2006). Detecting the red tide algal blooms from satellite ocean color observations in optically complex Northeast-Asia Coastal waters. *Remote Sensing of Environment, 103*, 419–437.

Baker, K. S., & Smith, R. C. (1982). Bio-optical classification and model of natural waters. *Limnology and Oceanography, 27*, 500–509.

Banse, K. (1959). On upwelling and bottom – Trawling off the southwest coast of India. *Journal of Marine Biological Association of India, 1*, 33–49.

Banse, K. (1968). Hydrography of the Arabian Sea shelf of India and Pakistan and effects on demersal fishes. *Deep Sea Research, 15*, 45–79.

Banse, K., & English, D. C. (2000). Geographical differences in seasonality of CZCS-derived phytoplankton pigment in the Arabian Sea for 1978–1986. *Deep Sea Research, 47*, 1623–1677.

Brzezinski, M. A., & Washburn, L. (2011). Phytoplankton primary productivity in the Santa Barbara Channel: Effects of wind-driven upwelling and mesoscale eddies. *Journal of Geophysical Research, 116*, C12013. https://doi.org/10.1029/2011JC007397

Chauhan, P., Mohan, M., Sarangi, R. K., Kumari, B., Nayak, S. R., & Matondkar, S. G. P. (2002). Surface chlorophyll-*a* estimation in the Arabian Sea using IRS-P4 Ocean Colour Monitor (OCM) satellite data. *International Journal of Remote Sensing, 23*(8), 1663–1676.

Clarke, G. L., Ewing, G. C., & Lorenzen, C. J. (1970). Spectral of backscatterd light from the sea obtained from aircraft as a measurement of chlorophyll concentration. *Science, 167*, 1119–1121.

Darbyshire, M. (1967). The surface waters off the coast of Kerala, southwest India. *Deep Sea Research, 14*, 295–320.

Dey, S., & Singh, R. P. (2003). Comparison of chlorophyll distributions in the northeastern Arabian Sea and southern Bay of Bengal using IRS-P4 Ocean Color Monitor data. *Remote Sensing of Environment, 85*, 424–428.

Dwivedi, R. M., Raman, M., Parab, S., Matondkar, S. G. P., & Nayak, S. (2006). Influence of northeasterly trade winds on intensity of winter bloom in the northern Arabian Sea. *Current Science, 90*(10), 1397–1406.

Evans, R. H., & Gordon, H. R. (1994). Coastal zone colour scanner 'system calibration': A retrospective examination. *Journal of Geophysical Research, 99*, 7293–7307.

Fein, J. S., & Stephens, P. L. (1987). *Monsoons*. Wiley.

Fitch, D. T., & Moore, J. K. (2007). Wind speed influence on phytoplankton bloom dynamics in the Southern Ocean Marginal Ice Zone. *Journal of Geophysical Research, 112*, C08006. https://doi.org/10.1029/2006JC004061

George, G., Meenakumari, B., Raman, M., Kumar, S., Vethamony, P., Babu, M. T., & Verlecar, X. (2012). Remotely sensed chlorophyll: A putative trophic link for explaining variability in Indian oil sardine stocks. *Journal of Coastal Research, 28*(1A), 105–113.

Gohil, B. S., Sarkar, A., & Agarwal, V. K. (2008). A new algorithm for wind vector retrieval from scatterometer. *IEEE Geoscience and Remote Sensing Letters, 5*(3), 387–391.

Gordon, H. R., & Morel, A. (1983). *Remote assessment of ocean color for interpretation of satellite visible imagery: A review*. Springer.

Gordon, H. R., & Wang, M. (1994). Retrieval of water-leaving radiance and aerosol optical thickness over the oceans with SeaWiFS: A preliminary algorithm. *Applied Optics, 33*, 443–452.

Gordon, H. R., Clark, D. K., Mueller, J. L., & Hovis, W. A. (1980). Nimbus-7 coastal zone color scanner: System description and initial imagery. *Science, 210*, 60–66.

Gregg, W. W., & Conkright, M. E. (2001). Global seasonal climatologies of ocean chlorophyll: Blending in situ and satellite data for the CZCS era. *Journal of Geophysical Research, 106*, 2499–2515.

Hellerman, S., & Rosenstein, M. (1983). Normal monthly wind stress over the World Ocean with error estimates. *Journal of Physical Oceanography, 13*, 1093–1104.

Jayaram, C., Chacko, N., Joseph, K. A., & Balchand, A. N. (2010). Interannual variability of upwelling indices in the Southeastern Arabian Sea: A satellite based study. *Ocean Science Journal, 45*(1), 27–40.

Johannessen, O. M., Subbaraju, G., & Blindheim, J. (1981). Seasonal variations of the oceanographic conditions of the southwest coast of India during 1971–1975. *Fisk Dir Skr Ser Hav Unders, 18*, 247–261.

Luis, A. J., & Kuwamura, H. (2000). Wintertime wind forcing and sea surface cooling near the south India tip observed using NSCAT and AVHRR. *Remote Sensing of Environment, 73*, 55–64.

Madhupratap, M., Nair, K. N. V., Gopalakrishnan, T. C., Haridas, P., Nair, K. K. C., Venugopal, P., & Gauns, M. (2001). Arabian Sea oceanography and fisheries off the west coast of India. *Current Science, 81*, 355–361.

McCreary, J. P., Han, W., Shankar, D., & Shetye, S. R. (1996). Dynamics of East India Coastal Current, numerical solutions, Part 2. *Journal of Geophysical Research, 101*, 13,993–14,010.

Morel, A. (1988). Optical modeling of the upper ocean in relation to its biogenous matter content (case I waters). *Journal of Geophysical Research: Oceans, 93*, 10749–10768.

Morel, A., & Maritorena, S. (2001). Bio-optical properties of oceanic waters: A reappraisal. *Journal of Geophysical Research, 106*, 7163–7180.

Murtugudde, R. G., Signorini, S. R., Christian, J. R., Busalachhi, A. J., McClain, C. R., & Picaut, J. (1999). Ocean color variability of the tropical Indo-Pacific basin observed by the SeaWIFS. *Journal of Geophysical Research, 104*, 18,351–18,366.

Potemra, J. T., Luther, M. E., & Brien, J. J. (1991). The seasonal circulation of the upper ocean in the Bay of Bengal. *Journal of Geophysical Research, 96*, 12667–12683.

Prasannakumar, S., Madhupratap, M., Dileep Kumar, M., Gauns, M., Muraleedharan, P. M., Sarma, V. V., & DeSouza, S. N. (2001). Physical control of primary productivity on a seasonal scale in central and eastern Arabian Sea. *Proceedings of the Indian Academy of Sciences (Earth and Planetary Sciences), 109*, 433–441.

Rao, T. S. S., & Griffiths, R. C. (1998). *Understanding the Indian Ocean-perspectives on oceanography* (p. 187). UNESCO.

Rao, L. V. G., & Jayaraman, R. (1966). Upwelling in the Minicoy region of Arabian Sea. *Current Science, 35*, 378–380.

Ryan, J. P., Fischer, A. M., Kudela, R. M., Gower, J. F. R., King, S. A., Marin, R., & Chavez, F. P. (2009). Influences of upwelling and downwelling winds on red tide bloom dynamics in Monterey Bay, California. *Continental Shelf Research, 29*, 785–795.

Sarangi, R. K., & Mohammed, G. (2011). Seasonal algal bloom and water quality around the coastal Kerala during southwest monsoon using *in situ* and satellite data. *Indian Journal of Geo-Marine Sciences (IJMS), 40*(2), 1–9.

Sarangi, R. K., Chauhan, P., & Nayak, S. R. (2001). Phytoplankton bloom monitoring in the offshore water of Northern Arabian Sea using IRS-P4 OCM Satellite data. *Indian Journal of Marine Science, 30*(4), 214–221.

Sarmiento, J. L., & Gruber, N. (2006). *Ocean biogeochemical dynamics, geological magazine* (Vol. 144, p. 1034). Princeton University Press. https://doi.org/10.1017/S0016756807003755

Shanthi, R., Poornima, D., Raja, S., Sethubathi, G. V., Thangaradjou, T., Balasubramanian, T., Babu, K. N., & Shukla, A. K. (2013). Validation of OCM-2 sensor performance in retrieving chlorophyll and TSM along the southwest Bay of Bengal coast. *Journal of Earth System Sciences, 122*(2), 1–7.

Sharma, G. S. (1973). Upwelling off the southwest coast of India. *Indian Journal of Marine Science, 7*, 209–218.

Shetye, S. R. (1984). Seasonal variability of the temperature field off the southwest coast of India. *Proceedings of Indian Academy of Sciences (Earth and Planetary Sciences), 93*, 399–411.

Shetye, S. R., Shenoi, S. S. C., Antony, M. K., & Kumar, V. K. (1985). Monthly-mean wind stress along the coast of the north Indian Ocean. *Proceedings of Indian Academy of Sciences (Earth and Planetary Sciences), 94*, 129–137.

Shetye, S. R., Gouveia, A. D., Shenoi, S. S. C., Sundar, D., Michael, G. S., & Nampoothiri, G. (1993). The western boundary current of the seasonal subtropical gyre in the Bay of Bengal. *Journal of Geophysical Research, 98*(C1), 945–954.

Singh, R. P., Bhoi, S., & Sahoo, A. K. (2001). Significant changes in the ocean parameters after the Gujarat earthquake. *Current Science, 80*(11), 1376–1377.

Smitha, B. R. (2010). *Coastal upwelling of the south eastern Arabian Sea – An integrated approach* (Ph.D thesis). Cochin Univeristy of Science & Technology, India.

Tweddle, J. F., Strutton, P. G., Foley, D. G., O'Higgins, L., Wood, A. M., Scott, B., Everroad, R. C., Peterson, W. T., Cannon, D., Hunter, M., & Forster, Z. (2010). Relationships among upwelling, phytoplankton blooms, and phycotoxins in coastal Oregon shellfish. *Marine Ecological Progress Series, 405*, 131–145.

Vinayachandran, P. N., & Mathew, S. (2003). Phytoplankton bloom in the Bay of Bengal during the northeast monsoon and its intensification by cyclones. *Geophysical Research Letters, 30*(11), 1572. https://doi.org/10.1029/2002GL016717

Vinayachandran, P. N., Chauhan, P., Mohan, M., & Nayak, S. R. (2004). Biological response of the sea around Sri Lanka to summer monsoon. *Geophysical Research Letters, 31*, L01302. https://doi.org/10.1029/2003GL018533

Chapter 13
Harmful Algal Blooms: An Ecological Perspective and Its Implications to Productivity Patterns in Tropical Oceans

Lathika Cicily Thomas, Twinkle Sathish, and K. B. Padmakumar

Abstract Microalgae or phytoplankton are the primary energy harvesters in the marine ecosystems forming the base of the marine food chain as the primary producers and fixing nearly 40% of the total atmospheric carbon globally. Additionally, microalgae account for more than 50% of the available planetary oxygen through the process of photosynthesis. Even though microalgae generally follow a logarithmic growth curve in certain conditions, their population undergoes an outburst when favorable or altered environmental conditions arise like physical, chemical, or biological changes. An exponential growth pattern of microalgae with the rapid proliferation of cells followed by a population crash occurs. This phenomenon, referred to as harmful algal blooms (HABs), represents several ecosystem reverberations. At times, this can be beneficial as it increases the primary standing stock of the area, but in many cases, HABs produce serious ecological implications that are reflected in the overall ecosystem health. In marine systems, HABs affect both coastal and open-ocean systems by either affecting the water quality through oxygen depletion, a mechanical hindrance to other aquatic organisms like clogging of gills in fishes and invertebrates, or through the production of potent toxins that can cause serious neurological or physiological disorders in other organisms including human beings. HABs have long-standing effects on the marine ecosystems, including disruption and shortening of the food chain, decreasing biodiversity and productivity, reducing the fishery stock, and affecting the aesthetics. According to the recent analytics, there is an increase in the frequency of HABs globally, which is reflected in the Indian EEZ also. Decadal studies on HABs in the Indian EEZ have observed an increase in the number of HAB events, and several HAB hotspots have been identified along the region. Indian EEZ caressed by the Arabian Sea on the west and Bay of Bengal on the east witness algal blooms habitually in tune with altering monsoon patterns and related nutrient influx. HAB monitoring programs perceived more frequent events in the Arabian sea; however, this does not read out the Bay of Bengal from HAB events. Physical forcings like upwelling and winter cooling-

L. C. Thomas · T. Sathish · K. B. Padmakumar (✉)
Department of Marine Biology, Microbiology & Biochemistry, School of Marine Sciences, Cochin University of Science and Technology, Kochi, Kerala, India

S. C. Tripathy, A. Singh (eds.), *Dynamics of Planktonic Primary Productivity in the Indian Ocean*, https://doi.org/10.1007/978-3-031-34467-1_13

related bloom events are a regular phenomenon in the Arabian sea of which upwelling relaxation phases witness short-term dinoflagellate blooms. Regular monitoring of HAB for nearly two decades spotlights several hotspots along the Indian EEZ with a persistent increase in the frequency of events. Major blooms in the Indian EEZ is caused by diatoms, dinoflagellates, or cyanophytes with sporadic blooms of flagellates. *Noctiluca scintillans*, the dinoflagellate, are reckoned to be a major bloom species on both the coasts of India, which include open-ocean HAB events. The cyanophyte *Trichodesmium erythraeum* blooms are also frequently observed mainly in oligotrophic status. Blooms caused by certain dinoflagellates can produce potent toxins related to several shellfish poisoning causalities in the country. This chapter discusses the marine HAB status in the tropical oceans pertaining to Indian EEZ, including its ecological and socioeconomic influences. An exertion has been made to depict major algal blooms and their repercussions on productivity patterns and marine trophic structure.

Keywords HABs · Microalgae · Productivity · Toxins · Shellfish poisoning · Indian EEZ

1 Phytoplankton: The Productive and Harmful Linkages to the Marine Ecosystem

Photosynthesis forms the primary process of autotrophic energy fixation in world oceans and is executed mainly by microscopic algal groups generally referred to as phytoplankton. Phytoplanktons are the components of the plankton community inhabiting the surface waters (photic zones) of the oceanic and coastal environment. Provided with the light-harvesting pigments like chlorophyll, they fix organic carbon from inorganic substrates like carbon dioxide utilizing dissolved nutrients such as mineral salts containing nitrogen, phosphorus, etc., in the water column. These microscopic algae represent less than 1% of the Earth's photosynthetic biomass but are responsible for about half of annual global net primary production (Field et al., 1998). These photosynthetic groups play a significant role in carbon sequestration and, thus, in controlling the climatic changes. The phytoplankton occupies a pivotal status in determining global climate and bio coupling of air-sea interactions (Finkel et al., 2010; Van de Waal et al., 2010). More importantly, phytoplankton forms the base of the marine and freshwater food chain and energy transfer in aquatic trophodynamics.

The population size of phytoplankton often appears to be nonlinear that cannot be closely fixed with time and space. These are dynamic, particularly along coastal waters with continual variations in physicochemical characteristics. Even though microalgae generally follow a logarithmic growth curve in absolute conditions, their population undergoes an outburst when favorable or altered environmental conditions arise like physical, chemical, or biological changes (Glibert et al., 2005). An exponential growth pattern of microalgae with the rapid proliferation of cells

followed by a population crash occurs. Such an occurrence is often referred to as "blooms." Phytoplankton blooms are natural events and are often harmless or beneficial in the functioning of marine and freshwater ecosystems as it increases the primary standing stock of the area. However, in some cases, the abundance of cells can be so high that it becomes visible discoloration of the surface water giving rise to red, mahogany, brown, or green tides, as floating scums or covering beaches with biomass or exudates (foam), and depleting oxygen levels through excessive respiration or decomposition. Such blooms are commonly termed as "red tides" or "harmful algal blooms (HABs)."

Alternatively, certain species in harmful algal blooms (HABs) can produce potent toxins that interfere with other organisms' physiological and morphological activities, from plankton to humans. The most severe, and therefore memorable, effects of HABs include fish, bird, and mammal mortalities, respiratory or digestive tract problems, memory loss, seizures, lesions, and skin irritation, as well as losses of coastal resources such as submerged aquatic vegetation and benthic epi- and in-fauna. Microalgae groups capable of producing toxins include representatives from dinoflagellates, cyanophytes, raphidophytes, and very few representatives from diatoms. The primary groupings of HAB toxins according to syndrome include paralytic shellfish poisons (PSP), neurotoxic shellfish poisons (NSP), amnesic shellfish poisons (ASP), diarrhetic shellfish poisons (DSP), azaspiracid shellfish poisoning (AZP), ciguatera fish poisoning (CFP), and cyanobacteria toxin poisoning (CTP) (Richardson, 1997). Several recent reviews have come up with new toxins, producer organisms, and toxic syndromes. For example, yessotoxins (YTXs; by the dinoflagellates *Lingulodinium polyedrum*, *Gonyaulax spinifera*, and *Protoceratium reticulatum*) were previously under DSP toxins and have now been reclassified because of a different toxicological mechanism (Tubaro et al., 2010). A new toxin called "karlotoxins" produced by toxic dinoflagellate *Karlodinium veneficum* is supposed to be associated with *Pfisteria* spp. that causes poisoning in fishes and humans termed as "estuary-associated syndrome" (Place et al., 2008; Peng et al., 2010). The toxin prymnesin is observed to be produced by Prymnesiophytes, and similarly, several other dinoflagellates are observed to produce toxins (e.g., *Cochlodinium polykrikoides*) that need further characterization (Kudela et al., 2008; Manning & La Claire, 2010).

Over the years, the frequency of HABs has been on the rise globally with its repercussions in Indian EEZ also. Decadal studies on HABs in the Indian EEZ have observed an increase in the number of HAB events, and several HAB hotspots have been identified along the region. The present rising state of HABs along Indian waters can lead to severe constraints, as the resources from India's marine environment provide a livelihood to more than 3.5 million people and an estimated income worth $7 billion in a year through recreation, fishing, and other economic activities (Saxena, 2012; Singh, 2003). This chapter discusses the marine HAB status in the tropical oceans pertaining to Indian EEZ, including its ecological and socioeconomic influences. An exertion has been made to depict major algal blooms and their repercussions on productivity patterns and marine trophic structure.

2 Methods of Analysis

To create a comprehensive review of HAB occurrences along Indian Peninsular, research publications from 1908 to the most recent studies published in 2021 were assessed. Information regarding the bloom period, location, and causative organisms were retrieved. Besides this, an in situ observation was carried out along the southwest coast of India, as a part of various HAB monitoring programs (UGC-BSR-Startup grant program; Seed Money for New Research Initiatives-CUSAT; UGC-Women PDF) are included to understand the trends in frequency and expansion of events. Monthly phytoplankton samples were collected by filtering ~50 L of surface waters through a 20 μm net material. The concentrate was preserved in 3% formaldehyde solution for further analysis. Quantitative and qualitative analyses of phytoplankton were done using a Sedgewick Rafter counting cell under a Leica DM2000 microscope following standard identification keys (Tomas, 1997). Sea surface temperature (SST) and salinity were analyzed using a precision mercury thermometer with an accuracy of ±0.01 °C and a handheld refractometer (RHS-10 ATC), respectively. Dissolved oxygen was estimated using modified Winkler's method (Winkler, 1888). Nutrients such as nitrate, phosphate, and silicate were estimated using standard procedures (Grasshoff et al., 1983). Chlorophyll *a* was measured spectrophotometrically using a Hitachi U-2900 UV/VIS Spectrophotometer following the acetone extraction method (Parsons et al., 1984).

In order to obtain the spatial distribution of blooms, the retrieved latitude and longitude data were represented graphically using suitable software. From the collected environmental parameters (SST, salinity, dissolved oxygen, NO_3-N, PO_4-P, and SiO_4-Si) and cell density of the bloom events, average, standard deviation, and range values for each taxon and individual species were estimated. Principal component analysis (PCA) was carried out to establish the correlation between blooms formed by different taxa and abiotic factors by correlating the ordination scores using PRIMER v.6 software. When one or more physicochemical parameter(s) was not available in the source article, the entire data was excluded from the PCA analysis.

3 Overview of HAB Occurrences Around the Indian Peninsula: Spatiotemporal Analysis

The analysis of the bloom reports from 1908 to 2021 from the Indian EEZ accounted for nearly 59 phytoplankton species, which included 31 diatoms, 18 dinoflagellates, 7 cyanobacteria, 2 haptophytes, and 1 raphidophyte. Among these, 29 species were regarded as harmful and were responsible for 162 HAB events around the Indian peninsula from 1908 to 2020 (Fig. 13.1). Of the 162 HAB events, 93 blooms were formed by dinoflagellates, cyanobacteria formed 59, raphidophytes formed 4, and haptophytes and diatoms formed 3 blooms each. The contributing groups toward HAB events in the Indian EEZ for the period 1908 to 2020 are depicted in Fig. 13.2.

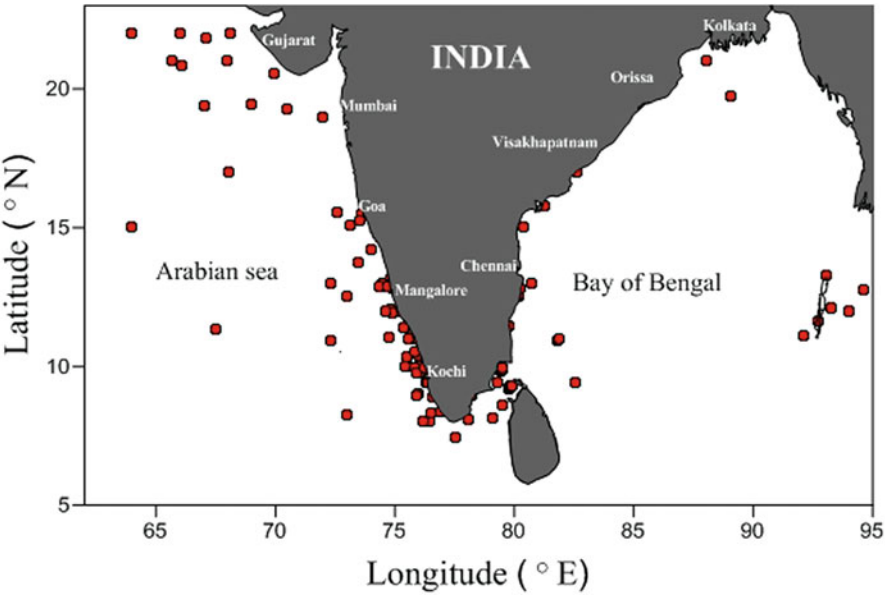

Fig. 13.1 Schematic representation of harmful algal bloom reports along the Indian EEZ from 1908 to 2020

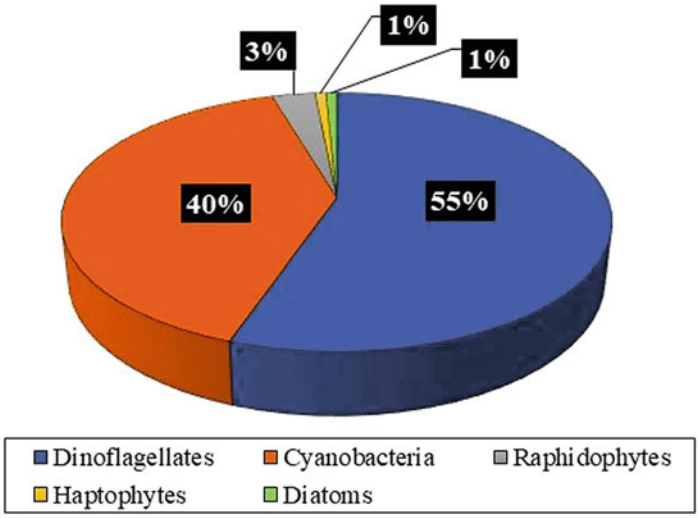

Fig. 13.2 Groups of phytoplankton in percentage, contributing to the HAB events from 1908 to 2020

A summary of all the HAB events that have been recorded from the Indian EEZ since 1908 is given in Table 13.1.

For the first three decades (1900–1940), the HABs were mainly reported from the taxonomic group class – dinophyceae. However, over time, additions from other taxa such as Bacillariophyceae, Cyanophyceae, Raphidophyceae, and Haptophyceae

Table 13.1 Details and sources of HAB events along the Indian EEZ from 1908 to 2020

Date	Location	Causative Organisms	Effect	Cell Density	Area	References
November 1908	Malabar Coast to Laccadive Islands	*Noctiluca*, *Hornellia marina* (= *Chattonella marina*)	Greenish grey discoloration, fish mortality	–	15 miles	Hornell (1917)
June 1935	Madras coast	*Noctiluca scintillans*	Pink discoloration, massive fish kills	–	–	Aiyar (1936)
May 1942	Krusadai Island, Gulf of Mannar	*Trichodesmium erythraeum*	Greenish yellow discoloration, mortality of holothurians, fishes, and other bottom-dwelling fauna	–	–	Chacko (1942)
October 1948	Malabar and Kanara coast	*Noctiluca scintillans*, *Gymnodinium* sp. *Dinophysis* sp.	Red discoloration, abrupt reduction in fish catch	0.5×10^5 cells L^{-1}	–	Bhimachar and George (1950)
August 1949	West Hill-off Calicut	*Hornellia marina* (= *Chattonella marina*)	Brownish green discoloration, total exclusion of other planktonic species	–	4–6 fathom area	Subrahmanyan (1954)
April 1952	Off Mandapam	*Noctiluca scintillans*	Bright green discoloration	3300 cc	–	Raghu Prasad (1953)
July 1952	Virudhunagar-Madras	*Microcystis* and rotifer	Green discoloration	13×10^3 cells ml^{-1}	–	Chacko and Srinivasan (1954)
December 1952	Off Calicut	*Noctiluca scintillans*	Green discoloration	–	–	Subrahmanyan (1954)
March–November 1952	Palk Bay and Gulf of Mannar	*Noctiluca scintillans*	–	18×10^4 cc	–	Raghu Prasad and Jayaraman (1954)
March 1953	Off Calicut	*Noctiluca scintillans*	Green discoloration	–	8 miles from the shore to about 10 mile out	Subrahmanyan (1954)
1959	West coast	*Gymnodinium* sp.	–	–	–	Subrahmanyan (1959)

July 1963	Anthakarai estuary, Mandapam	*Noctiluca scintillans*	Mortality of fishes and other benthic fauna	–	–	Durve and Alagarswami (1964)
November 1963	Off Cochin	*Gonyaulax polygramma*	Red discoloration	1.08×10^7 cells L^{-1}	8 miles from Cochin harbor	Prakash and Sarma (1964)
November 1963	Off Mt. Dalley, Arabian Sea	*Gonyaulax polygramma*	Red discoloration (Tomato soup-like)	5.5×10^5 cells L^{-1}	4 sq miles	Lewis (1965)
March 1964	Off Ullal, Mangalore	*Trichodesmium erythraeum* and *T. hildebrandtii*	Greenish yellow patch	1.03×10^5 cells L^{-1}; 7.5×10^4 cells L^{-1}	12–25 meters	Prabhu et al. (1965)
March 1965	Porto Novo, Tamil Nadu	*Trichodesmium erythraeum*	Red discoloration	412 cells ml^{-1}	–	Ramanamurthy and Seshadri (1966)
June 1965	Minicoy Island	*Trichodesmium erythraeum*	Deep brownish discoloration	–	35 miles	Nagabhushanam (1968)
May 1968	Gulf off Mannar	*Trichodesmium thiebautii*	Pale yellow discoloration	1204 cells ml^{-1}	–	James (1972)
April 1968	Laccadives	*Trichodesmium erythraeum*	Yellow discoloration	8540 clumps m^{-3}	100 miles	Qasim (1970)
February–March 1968	Off Mangalore	*Trichodesmium*	Brownish scums	6.3×10^5 cells L^{-1}	–	Prabhu et al. (1971)
March 1970	Porto Nova, Tamil Nadu	*Trichodesmium erythraeum*	–	15–25 filaments L^{-1}	–	Ramamurthy (1973)
March 1972	Central west coast	*Trichodesmium erythraeum*	–	–	–	Ramamurthy et al. (1972)
March 1973	Off Kochi	*Trichodesmium erythraeum*	Dense brownish patches	20×10^3 cells L^{-1}	40 miles	Sakthivel and Harida (1974)

(continued)

Table 13.1 (continued)

Date	Location	Causative Organisms	Effect	Cell Density	Area	References
March, April, September, 1973	Off Veppalodai-Gulf of Mannar	*Trichodesmium thiebautii*	Dense patch-brownish shade	10–15 filaments L^{-1}	–	Chellham and Alagarswami (1978)
March–May 1975	Off Goa	*Trichodesmium erythraeum*	Yellowish discoloration	–	–	Pant and Devassy (1976)
August 1976, 1977	South Kerala coast	*Noctiluca scintillans*	Red discoloration	7.7×10^3 cells m^{-3}	–	Venugopal et al. (1979)
March 1977	South west coast	*Trichodesmium erythraeum*	Brownish patches	–	–	Verlancar (1978)
August 1982	Parangipettai	*Hemidiscus hardmanianus*	–	4.9×10^4 cells L^{-1}	10 km in seas	Subramanian and Purushothaman (1985)
January 1987	Someswar to Surathkal-off Mangalore	*Noctiluca scintillans*	Green discoloration	1.6×10^4 to 7.55×10^9 cells m^{-3}	–	Katti and Gupta (1988)
February–April 1987	Mandovi and Zuari estuaries-Goa	*Noctiluca scintillans*	Green discoloration	51×10^3 cells L^{-1}	–	Devassy and Nair (1987)
Pre-monsoon	Arabian Sea	*Trichodesmium*	Dense patch	–	–	Devassy (1987)
October 1988	Kalpakkam coastal waters	*Noctiluca scintillans*	Green discoloration	38×10^3 cells L^{-1}	–	Sasikumar et al. (1989)
March 1989	Tuticorin Bay	*Trichodesmium*	–	0.01 to 17.5×10^6 filaments L^{-1}	–	Santhanam et al. (1994)
December 1989	Off Someswar, West coast	*Gymnodinium nagasakiense*	Red discoloration	–	–	Karunasagar and Karunasagar (1992)

May 1993	Mangalore	*Noctiluca scintillans*	–	1.56×10^6 cells m^{-3}	60 km	Nayak et al. (2000)
May 1993	Kalpakkam coastal waters	*Asterionella japonica*	Brownish discoloration	5.45×10^{10} cells m^{-3}	–	Satpathy and Nair (1996)
April 1996	Lakshadweep Sea	*Trichodesmium erythraeum*	Thick yellow patch	–	–	Koya and Kaladharan (1997)
July–August 1996	Arabian Sea	*Phaeocystis globosa*	Thick green patch	3750×10^6 cells m^{-3}	240 nautical miles	Madhupratap et al. (1999)
1996	Tuticorin Bay	*Dinophysis caudata*	–	–	–	Santhanam and Srinivasan (1996)
September 1997	Vizhinjam, Thiruvananthapuram	*Gymnodinium catenatum*	–	–	–	Karunasagar et al. (1998)
August 1998	Off Cochin	*Noctiluca scintillans*	Red discoloration	–	28 km off Cochin, 700 m long and 5–10 m wide	Naqvi et al. (1998)
November 1998	Off Mangalore	*Noctiluca scintillans*	Red discoloration	1.63×10^6 cells L^{-1}	4000 m long and 500 m wide	Nayar et al. (2001)
June 1998	Off Mumbai	*Trichodesmium thiebautii*	Straw yellow patch	1.58×10^7 cells L^{-1}	–	TAB-Final Report
October 1998	Off Kannur	*Noctiluca scintillans*	–	1.1×10^3 cells L^{-1}	–	TAB-Final Report
August 1999	Off Kochi	*Gymnodinium veneficum*	Pale red discoloration	2.84×10^5 cells L^{-1}	–	TAB-Final Report
June–July 2000	Port Blair Bay-Andaman	*Noctiluca scintillans*	Green discoloration	$1.5–2.3 \times 10^4$ cells L^{-1}	–	Eashwar et al. (2001)

(continued)

Table 13.1 (continued)

Date	Location	Causative Organisms	Effect	Cell Density	Area	References
March 2000	Off Ratnagiri	*Noctiluca scintillans*	–	1.8×10^2 cells L^{-1}	–	TAB-Final Report
March 2000	Northern Arabian Sea	*Noctiluca scintillans*	Green discoloration	1.7×10^2 cells L^{-1}	–	TAB-Final Report
March 2000	Off Kochi	*Trichodesmium thiebautii*	Straw yellow	–	–	TAB-Final Report
April 2000	Off Tarapur, Maharashtra	*Trichodesmium thiebautii*	Straw yellow	1.9×10^2 cells L^{-1}	–	TAB-Final Report
May 2000	Off Kochi	*Trichodesmium thiebautii*	–	2.1×10^2 cells L^{-1}	–	TAB-Final Report
May 2000	Inlet of Kochi estuary	*Anabaena spiroides*	–	–	–	TAB-Final Report
June 2000	Off Singarayakonda, Andhra Pradesh	*Trichodesmium erythraeum*	Straw yellow	3×10^6 cells L^{-1}	–	TAB-Final Report
June 2000	Off Singarayakonda, Andhra Pradesh	*Trichodesmium erythraeum*	Straw yellow	1×10^7 cells L^{-1}	–	TAB-Final Report
October 2000	Off Kochi	*Gymnodinium veneficum*	–	–	–	TAB-Final Report
April 2001	Off Karaikal, off Calicut	*Trichodesmium erythraeum*	Brownish yellow discoloration	–	–	Jyothibabu et al. (2003)
April 2001	Off Cuddalore	*Trichodesmium erythraeum*	Straw yellow	2×10^7 cells L^{-1}	–	TAB-Final Report
April 2001	Off Chennai	*Trichodesmium erythraeum*	Straw yellow	11.5×10^7 cells L^{-1}	–	TAB-Final Report
April 2001	Off Satapada, Odisha	*Trichodesmium erythraeum*	Straw yellow	29.8×10^7 cells L^{-1}	–	TAB-Final Report
July 2001	Off Kannur	*Trichodesmium erythraeum*	–	–	–	TAB-Final Report

July 2001	Off Kannur	*Noctiluca scintillans*	Red discoloration	10.4×10^5 cells L^{-1}	–	TAB-Final Report
August 2001	Off Calicut	*Noctiluca scintillans*	Red discoloration	3.2×10^4 cells L^{-1}	–	TAB-Final Report
September 2001	Off Kannur, off Mangalore	*Gymnodinium* and *Noctiluca*	–	–	–	TAB-Final Report
April–May 2002	Saurashtra coast, Gujarat	*Trichodesmium erythraeum*	Dark brown discoloration	–	–	Sarangi et al. (2004)
May 2002	Off Mumbai	*Trichodesmium erythraeum*	Straw yellow	4.3×10^3 cells L^{-1}	–	TAB-Final Report
July 2002	Off Calicut	*Trichodesmium thiebautii*	Straw yellow	4.6×10^4 cells L^{-1}	–	TAB-Final Report
September 2002	Andaman Sea	*Trichodesmium thiebautii*	Straw yellow	5×10^4 cells L^{-1}	–	TAB-Final Report
December 2002	Minnie Bay- Port Blair- Andaman	*Noctiluca scintillans*	Green discoloration	17×10^3 cells L^{-1}	2 m wide	Dharani et al. (2004)
August 2003	Off Vizhinjam	*Noctiluca scintillans*	Golden yellow discoloration with a frothy appearance; low fish landings	1.02×10^5 cells L^{-1}	–	Jugnu and Kripa (2006)
September 2003	Thangassery Bay, Arabian Sea	*Noctiluca scintillans*	Deep orange discoloration, Fish mortality, and complete exclusion of other phytoplankton	9.8×10^4 cells L^{-1}	–	Jugnu and Kripa (2006)
September 2003	Chombala-Calicut	*Chattonella marina*	Muddy green discoloration, *Mactra violacea* with decayed meat washed ashore	135×10^5 cells L^{-1}	50 km	Jugnu and Kripa (2006)
September 2004	Off Kollam and Thiruvananthapuram	*Noctiluca* sp., *Cochlodinium* sp., *Karenia mikimotoi*	Red discoloration	–	–	TAB-Final Report
August 2006	Off Alappuzha	*Noctiluca scintillans*	Red discoloration	7.3×10^4 cells L^{-1}	–	Padmakumar (2010b)
March 2007	Northern Arabian Sea	*Noctiluca scintillans*	Green discoloration	4×10^6 cells L^{-1}	30 km^2	Padmakumar et al. (2008)

(continued)

Table 13.1 (continued)

Date	Location	Causative Organisms	Effect	Cell Density	Area	References
March 2007	Kalpakkam	*Trichodesmium erythraeum*	Yellowish green colored streaks	4.14×10^6 cells L^{-1}	4 to 5 m wide	Satpathy et al. (2007)
April 2007	Candolim-off Goa	*Trichodesmium*	Yellow patch	–	–	Roy et al. (2011)
August 2008	Off Kochi	*Noctiluca scintillans*	Brick red discoloration	8.1×10^8 cells L^{-1}	5 km^2	Padmakumar et al. (2010)
October 2008	Off Goa	*Noctiluca scintillans*	Pale red discoloration	2×10^3 cells L^{-1}	–	HAB CMLRE – Annual Report
October 2008	Off Mangalore	*Gonyaulax polygramma*	Brownish red discoloration	5×10^8 cells L^{-1}	–	HAB CMLRE – Annual Report
October 2008	Gulf of Mannar	*Noctiluca scintillans*	Greenish discoloration	13.5×10^5 cells L^{-1}	–	HAB CMLRE – Annual Report
December 2008	Off Kakinada, Andhra Pradesh	*Trichodesmium erythraeum*	Straw yellow discoloration	3×10^5 cells L^{-1}	–	HAB CMLRE – Annual Report
February–March 2009	Northern Arabian Sea	*Noctiluca scintillans*	Greenish discoloration	24×10^3 cells L^{-1}	–	HAB CMLRE – Annual Report
April 2009	Off Mangalore and off Goa	*Trichodesmium erythraeum*	Straw yellow discoloration	–	–	HAB CMLRE – Annual Report
June 2009	Off Kollam	*Trichodesmium erythraeum*	Pale brown discoloration	1.14×10^6 cells L^{-1}	10 km^2	Padmakumar et al. (2010)
June 2009	Off Kochi	*Trichodesmium erythraeum*	Straw Yellow discoloration	1.968×10^6 cells L^{-1}	–	HAB CMLRE – Annual Report 2009–10
June 2009	Off Kannur	*Trichodesmium erythraeum*	Pink reddish discoloration	1.51×10^6 cells L^{-1}	20 km^2	HAB CMLRE – Annual Report 2009–10
August 2009	Off Cape Comorin	*Noctiluca scintillans*	Reddish orange discoloration	8×10^4 cells L^{-1}	–	HAB CMLRE – Annual Report 2009–10

August 2009	Off Azhikode	*Prymnesium parvum*	Brownish discoloration	8×10^7 cells L^{-1}	–	HAB CMLRE – Annual Report 2009–10
September 2009	Off Kochi	*Chattonella marina*	Rusty brownish red discoloration	1.59×10^7 cells L^{-1}		Padmakumar et al. (2011)
October 2009	Off Mangalore	*Pyrophacus steinii*	Light greenish discoloration	7.75×10^5 cells L^{-1}	–	HAB CMLRE – Annual Report 2009–10
October 2009	Cochin Bar mouth	*Karenia mikimotoi*	Intense brownish discoloration	701.3×10^4 to 1550×10^4 cells L^{-1}	Few kilometers toward the coast	Madhu et al. (2011)
December 2009	Vellar estuary	*Microcystis aeruginosa*	Green discoloration	3.76×10^4 cells L^{-1}	–	Santhosh Kumar et al. (2010)
March 2010	Northern Arabian Sea	*Noctiluca scintillans*	Greenish discoloration	180–220 cells L^{-1-}	–	HAB CMLRE – Annual Report 2009–10
March 2010	Off Kundapura, Karnataka	*Trichodesmium erythraeum*	Straw yellow discoloration	3.28×10^6 cells L^{-1}	–	HAB CMLRE – Annual Report 2009–10
May 2010	Off Goa	*Trichodesmium erythraeum*	Straw yellow discoloration	2.93×10^6 cells L^{-1}	–	HAB CMLRE – Annual Report 2009–10
August 2010	Off Kochi	*Noctiluca scintillans*	Yellowish orange discoloration	6.27×10^6 cells L^{-1}	–	HAB CMLRE – Annual Report 2010–11
January – February 2011	Northern Arabian Sea	*Noctiluca scintillans*	Greenish discoloration	1.4×10^3 cells L^{-1}	–	HAB CMLRE – Annual Report 2010–11
June 2011	Andaman Sea	*Phaeocystis* spp.	–	2.6×10^4 cells L^{-1}	–	Sachithanandam et al. (2013)

(continued)

Table 13.1 (continued)

Date	Location	Causative Organisms	Effect	Cell Density	Area	References
September 2011	Off Kollam	Multi species bloom dominated by *Protoperidinium pyriforme, Noctiluca scintillans* and *Phaeocystis* sp.	–	4.4×10^5 cells L^{-1}	–	HAB CMLRE – Annual Report 2011–12
October 2011	Mahe coastal waters	*Chattonella marina*	Brownish discoloration	4.5×10^6 cells L^{-1}	1 km in width	Sanilkumar et al. (2012)
March 2012	Northern Arabian Sea	*Noctiluca scintillans*	Yellowish green discoloration	3.7×10^6 cells L^{-1}	–	HAB CMLRE – Annual Report 2011–12
April 2012	Northern Arabian Sea	*Noctiluca scintillans*	Yellowish green discoloration	4.8×10^6 cells L^{-1}	–	HAB CMLRE – Annual Report 2011–12
June 2012	Muttukadu backwater	*Microcystis aeruginosa*	Green color, slimy nature with foul smell, Massive number of fishes washed ashore	6×10^8 cells L^{-1}	–	Prasanth et al. (2014)
March 2013	Northern Arabian Sea	*Noctiluca scintillans*	Yellowish green discoloration	5.8×10^6 cells L^{-1}	–	HAB CMLRE – Annual Report 2012–13
March 2013	Andaman coast	*Trichodesmium erythraeum*	Inhibited growth of other phyto-plankton and zooplankton	14.65×10^6 trichomes L^{-1}	3–5 m in width	Narayana et al. (2014)
March 2013	Off Kochi	*Trichodesmium erythraeum*	Straw yellow discoloration	3.9×10^6 cells L^{-1}	–	HAB CMLRE – Annual Report 2012–13
April 2013	Andaman sea	*Trichodesmium erythraeum*	Less fish catch	7×10^3 fila-ments L^{-1}	–	HAB CMLRE – Annual Report 2012–13
July 2013	Off Valappad-Thrissur	*Noctiluca scintillans*	Red discoloration	2.5×10^4 cells L^{-1}	–	HAB CMLRE – Annual Report 2013–14

July 2013	Off Kochi	*Pseudo-nitzschia* sp.	No discoloration	1.56×10^4 cells L^{-1}	–	HAB CMLRE – Annual Report 2013–14
September 2013	Off Kollam	*Gonyaulax polygramma*	Brownish red discoloration	7.8×10^5 cells L^{-1}	–	HAB CMLRE – Annual Report 2013–14
July 2015	Alappuzha	*Noctiluca scintillans*	Red color patches, foul smell	3.1×10^5 cells L^{-1}	4000 m long and 500 m wide	Peter et al. (2016)
August 2015	Off Kappad-Calicut	*Noctiluca scintillans*	Red tomato soup like consistency, low fish catch, and shoreward drifting of moribund crabs	5.3×10^6 cells L^{-1}	–	Padmakumar et al. (2016a)
July–August 2016	Off Cochin	*Noctiluca scintillans*	Reddish discoloration	4.73×10^5 cells L^{-1}	–	Shaju et al. (2018)
September 2016	Alappuzha	*Prorocentrum shikokuense*	Dark brownish discoloration	7.5×10^5 cells L^{-1}	2–3 km along shore, 1–2 km offshore	Madhu et al. (2020b)
September 2016	Chavakkad	*Noctiluca scintillans*	Reddish discoloration	7.5×10^5 cells L^{-1}	15 km coastal sea	Vijayalakshmy et al. (2018)
March 2018	Bangaram Lagoon, Lakshadweep	*Prorocentrum rhathymum*	Reddish brown discoloration	7.6×10^5 cells L^{-1}	5 km^2	Thomas et al. (2021)
November 2018	Cochin estuary, Southwest coast of India	*Noctiluca scintillans*	Greenish discoloration	1.7×10^6 cells L^{-1}	10–50 m long and 3–5 m wide	HAB monitoring Program CUSAT
November 2018	Cochin estuary, Southwest coast of India	*Peridinium quadridentatum*	Brownish discoloration	6.2×10^6 cells L^{-1}	50–100 m long and 10–20 m wide	HAB monitoring Program CUSAT
December 2018	Cochin estuary, Southwest coast of India	*Akashiwo sanguinea*	Brownish discoloration	3.6×10^4 cells L^{-1}	5–10 m long and 2–3 m wide	HAB monitoring Program CUSAT

(continued)

Table 13.1 (continued)

Date	Location	Causative Organisms	Effect	Cell Density	Area	References
April 2019	Cochin estuary, Southwest coast of India	*Akashiwo sanguinea*	Brownish discoloration	2×10^4 cells L^{-1}	3–5 m long and 1–2 m wide	HAB monitoring Program CUSAT
June 2019	Chal Beach, Kannur	*Noctiluca scintillans*	Greenish discoloration	3×10^4 cells L^{-1}	1–3 km along shore	HAB monitoring Program CUSAT
June 2019	Cochin estuary, Southwest coast of India	*Akashiwo sanguinea*	Brownish discoloration	28×10^4 cells L^{-1}	50–100 m long and 10–20 m wide	HAB monitoring Program CUSAT
January 2020	Off Goa	*Trichodesmium erythraeum*	Straw yellow discoloration	10×10^4 cells L^{-1}	5–10 m wide and extended to several meter	HAB monitoring Program CUSAT
January 2020	Bhatkal coast	*Trichodesmium erythraeum*	Straw yellow discoloration	29×10^4 cells L^{-1}	10 km long and 5 km wide	HAB monitoring Program CUSAT
January 2020	Ponnani coast	*Trichodesmium erythraeum*	Straw yellow discoloration	28×10^4 cells L^{-1}	7 km long and 2 km wide	HAB monitoring Program CUSAT
January 2020	Valappad coast	*Trichodesmium erythraeum*	Straw yellow discoloration	20×10^4 cells L^{-1}	2–3 m wide and extended to several meters	HAB monitoring Program CUSAT
January 2020	Kochi coast	*Trichodesmium erythraeum*	Straw yellow discoloration	24×10^4 cells L^{-1}	5 km long and 1–2 km wide	HAB monitoring Program CUSAT
November 2020	Cochin estuary, Southwest coast of India	*Peridinium quadridentatum*	Brownish discoloration	66×10^3 cells L^{-1}	2–3 m long and 1–2 m wide	HAB monitoring Program CUSAT
December 2020	Cochin estuary, Southwest coast of India	*Tripos furca*	No discoloration	9.1×10^4 cells L^{-1}	3–4 m long and 1–2 m wide	HAB monitoring Program CUSAT
January 2021	Cochin estuary, Southwest coast of India	*Akashiwo sanguinea*	Brownish discoloration	45×10^3 cells L^{-1}	2–3 m long and 1 m wide	HAB monitoring Program CUSAT

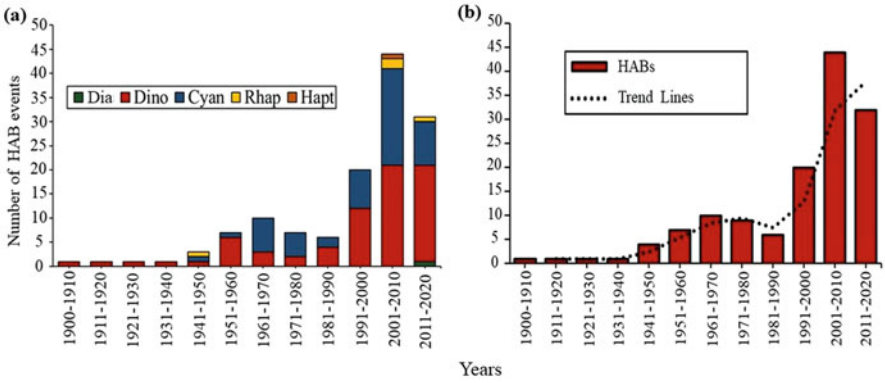

Fig. 13.3 Incidence of HABs around the Indian EEZ from 1908 to 2020. (**a**) Occurrences by different phytoplankton groups (Dia, diatoms; Dino, dinoflagellates; Cyan, cyanobacteria; Rhap, raphidophytes; Hapt, haptophytes). (**b**) Frequency of HAB events along the Indian waters

were observed (Fig. 13.3a). A remarkable increase in the frequency of HABs along the Indian EEZ has also been recorded from 1950 to 2020. Two HAB incidents were documented from 1900 to 1940, 27 incidents from 1941 to 1980, and 133 incidents from 1981 to 2020 (Fig. 13.3b).

3.1 Seasonality in the HAB Events

The occurrence and progression of HAB events rely on various climatic factors, and hence, there appears significant influence on such events by the Indian monsoon system. The biannually reversing monsoon seasons with southwest (summer monsoon, SM) and northeast (winter monsoon, WM) and intervening spring inter-monsoon (SIM) and fall inter-monsoon (FIM) have a pivotal role in the HAB events of the Indian EEZ. An account of the HAB events on both west and east coast of the Indian subcontinent clearly shows seasonality in occurrence. Seasonally, occurrences of HABs were more pronounced during spring inter-monsoon (SIM), followed by summer monsoon (SM). Considering the entire Indian EEZ, blooms of dinoflagellates dominated fall inter-monsoon (FIM) and following winter monsoon (WM) seasons, while those of cyanobacteria dominated SIM season. Events attributed to raphidophytes were most pronounced during the FIM and SM seasons, while those associated with the diatoms and haptophytes occurred majorly during SM (Fig. 13.4).

Harmful algal blooms were a recurrent phenomenon along the west coast, with the majority of the blooms occurring during March–May (SIM), August (SM), and September–October (FIM). Seasonality in the occurrence of HABs was also observed, with dinoflagellate blooms mainly occurring during SM (August) and FIM (September–October), whereas cyanobacteria blooms were more frequent

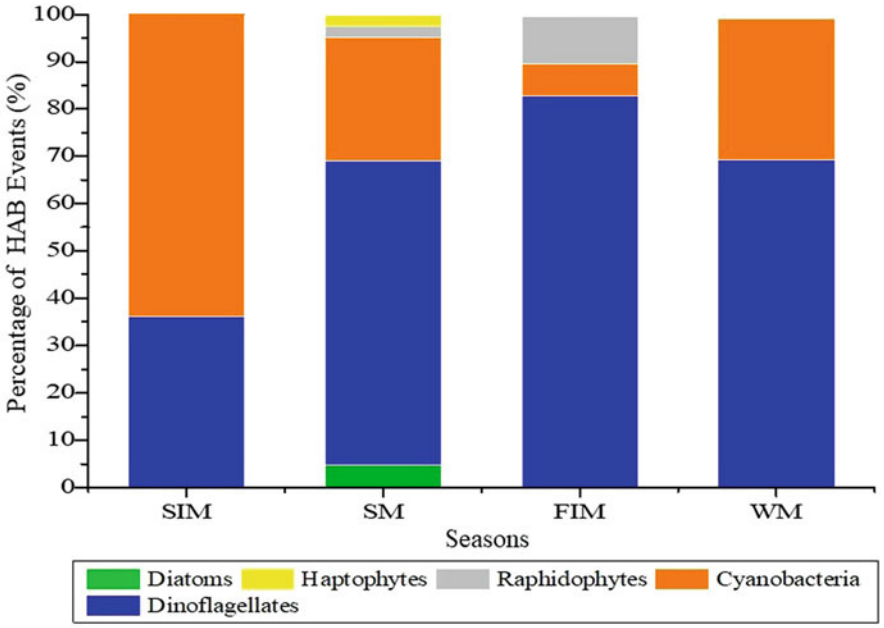

Fig. 13.4 Seasonal occurrences of HAB events along the Indian waters from 1908 to 2020. SIM spring inter-monsoon, SM summer monsoon, FIM fall inter-monsoon, WM winter monsoon

during SIM (March–May). *C. marina* blooms occurred only during SM (August) and FIM (September–October) period. While diatom (*Pseudo-nitzschia* sp.) and haptophyte (*Prymnesium parvum* and *Phaeocystis* sp.) blooms occurred only during the SM (July and August, respectively) (Fig. 13.5). Along the east coast of India, most HABs occurred during the SIM period from March to April. Most of the cyanobacteria blooms occurred during SIM (March–April), whereas dinoflagellate blooms occurred during SM (June–August) and FIM (September–October) period (Fig. 13.6).

3.2 Spatial Variability in HAB Events

Analyzing the spatial variability in the HAB occurrences, from 162 harmful algal blooms recorded, 111 were accredited from the west coast and 51 from the east coast of India. Also, higher numerical incidences were observed in the southern region on both the east and west coast than in the northern region (Fig. 13.1).

A total of 111 cases of HAB occurrences were reported along the west coast and 51 from the east coast of India during the observational period. Considering the west coast, the blooms were caused by diatoms, dinoflagellates, cyanobacteria,

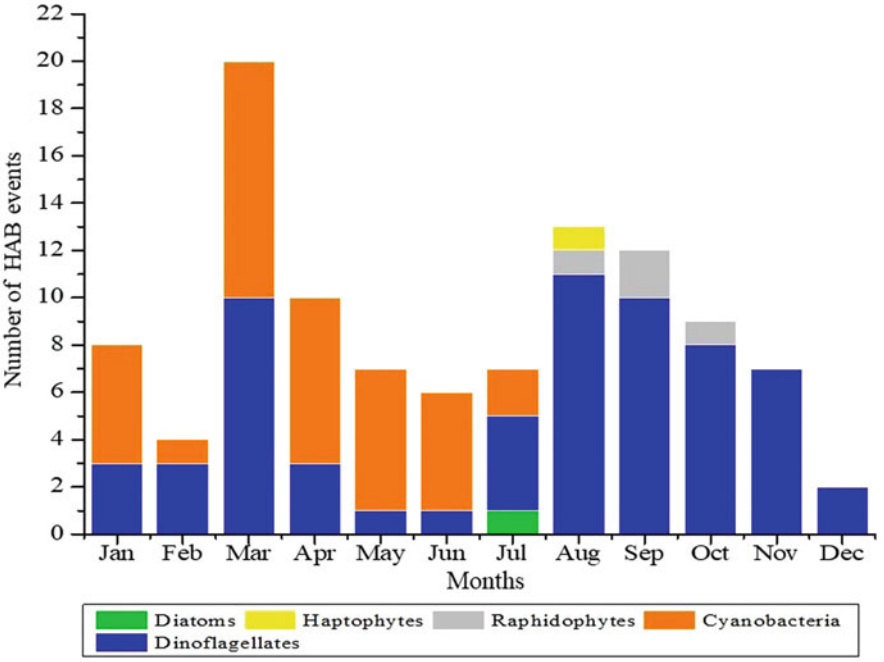

Fig. 13.5 Seasonal variation of HAB events by different groups of phytoplankton during different time period of a year along the west coast of India

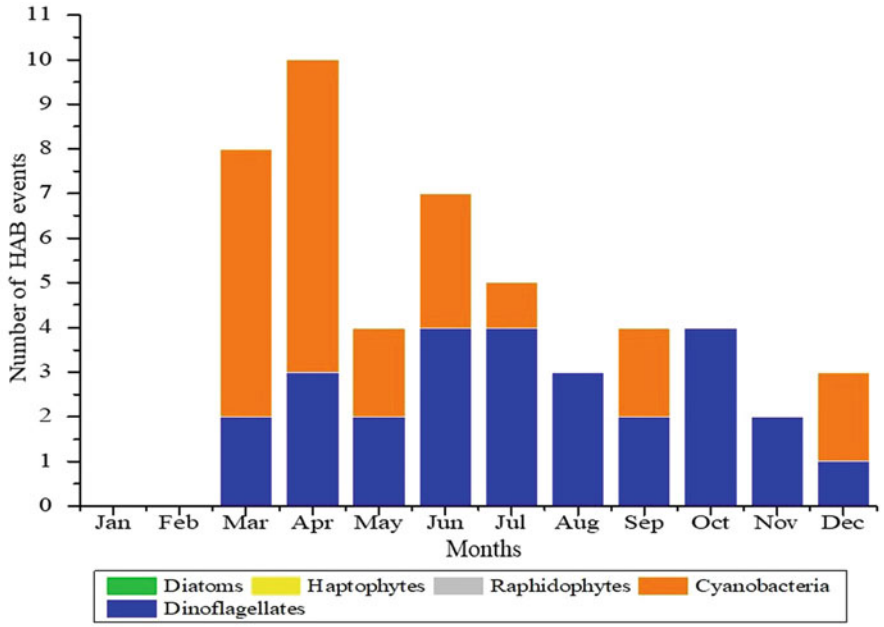

Fig. 13.6 Seasonal variation of HAB events by different groups of phytoplankton during different time period of a year along the east coast of India

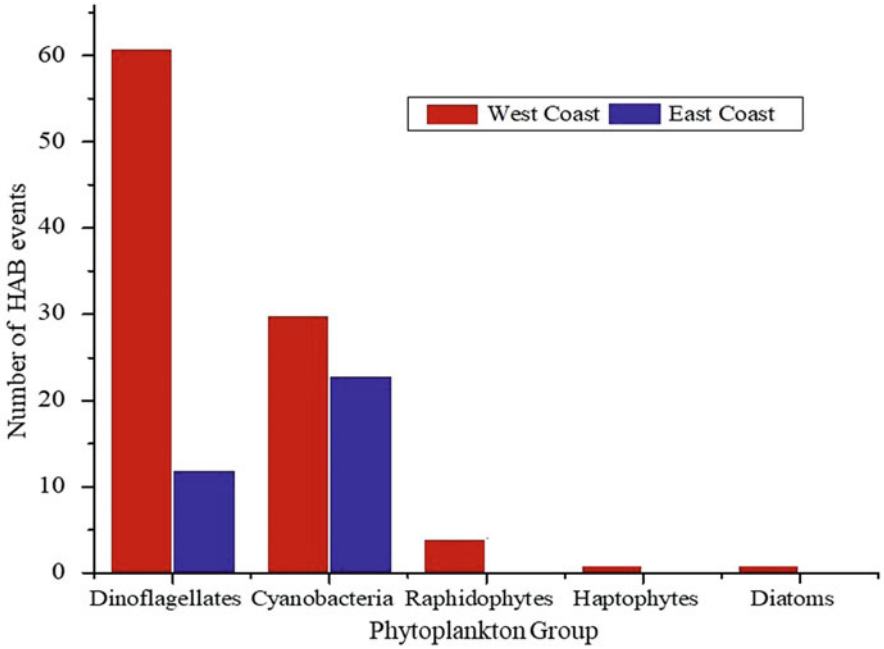

Fig. 13.7 Comparison on the frequency of HAB events caused by various groups along the west and east coast of India

raphidophytes, and haptophytes (Fig. 13.7). Dinoflagellate constituted the dominant bloom-forming group which included potentially toxic representatives. Of the 21 causative species reported along the west coast, *N. scintillans* (dinoflagellate) and *Trichodesmium erythraeum* (cyanobacteria) formed a significant constituent. The coastal waters of Kerala, Karnataka, and Goa recorded maximum bloom events (Fig. 13.8). The coastal waters of Kerala reported maximum bloom species, which included mainly dinoflagellates (*Noctiluca scintillans*, *Akashiwo sanguinea*, *Cochlodinium* sp., *Gonyaulax polygramma*, *Gymnodinium* sp., *Gymnodinium catenatum*, *Gymnodinium veneficum*, *Gymnodinium nagasakiense*, *Prorocentrum shikokuense*, *Protoperidinium pyriforme,* and *Tripos tripos*). While cyanobacterial blooms (*Trichodesmium erythraeum*) increased along Lakshadweep, Goa, and Mumbai-Ratnagiri coast. Harmful blooms of raphidophyte (*Chattonella marina*), haptophyte (*Prymnesium parvum* and *Phaeocystis* sp.), and diatom (*Pseudo-nitzschia* sp.) were only reported from the Kerala coast. Considering the seasonal influences on the dinoflagellate blooms along the west coast, the relaxation phases of summer monsoon upwelling observed maximum and recurrent occurrences along the southern part, whereas mid and late winter monsoon (February–March) observed extensive and intense bloom of heterotrophic dinoflagellate *Noctiluca scintillans*.

The HAB events along the east coast of India were caused by cyanophytes (*T. erythraeum)* and dinoflagellates (*N. scintillans)* (Fig. 13.7). However, short-

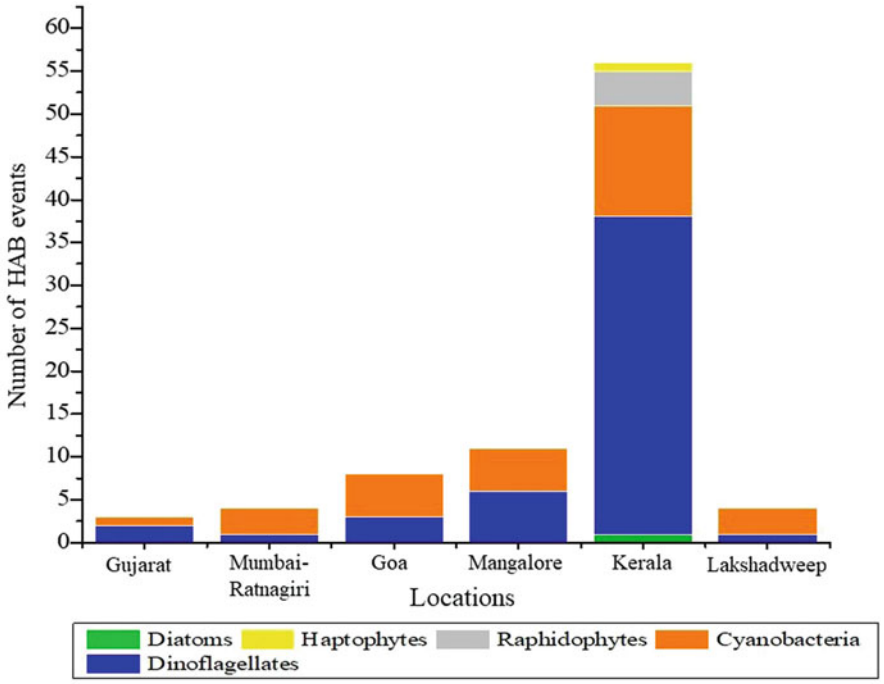

Fig. 13.8 Spatial variation of total HAB events by different groups of phytoplankton along the west coast of India

term multispecies diatom blooms that occur along the coast are generally conserved harmless and add to the basin's productivity. These blooms were mainly caused by dinoflagellates and cyanobacteria. Among these, dinoflagellates were the predominant group, with the maximum number of bloom cases reported. Spatial distribution of HAB occurrences indicated their prevalence more toward the south, including Tamil Nadu, followed by the Andaman Sea (Fig. 13.9).

4 Physicochemical Drivers of Indian Marine HABs

The prevalence of HAB in any aquatic ecosystem is subjected to the ambient environmental status that covers the physical settings of the water column, nutrient availability, physiology of the algal species, atmospheric interactions with the water column, etc. Indian EEZ records both coastal and open-ocean blooms and are closely linked with the monsoon-influenced biogeochemistry. Biophysical coupling that also includes air-sea interactions influences the bloom ecophysiology. Analyzing the environmental setting of the pooled data from various published resources on the different HAB events from the Indian EEZ provided information on the strong

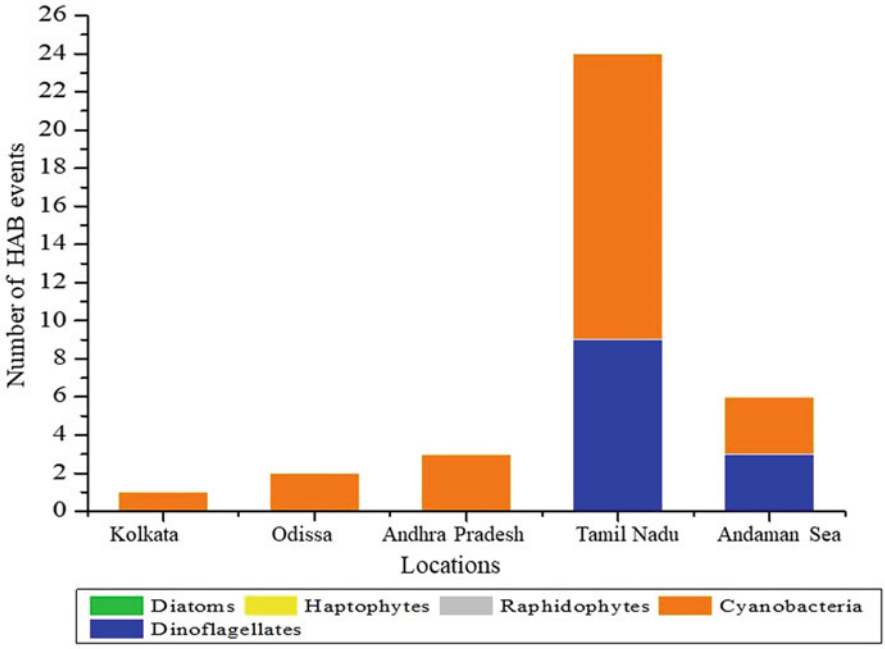

Fig. 13.9 Spatial variation of total HAB events by different groups of phytoplankton along the east coast of India

interconnection between the algal blooms and environmental conditions in the Indian marine ecosystems. Predictive models using exploratory data analysis like principal component analysis (PCA) were carried out to delineate the environmental correlations with the accounts of HAB events.

PCA recognized three principal components (PC1, PC2, and PC3), explaining a cumulative variation of 85% between the environmental conditions of various blooms recorded. PC1 accounted for 48.6% (eigenvalue = 2.92) of the total variance, with a high positive loading on NO_3-N (0.54), PO_4-P (0.53), and SiO_4-Si (0.41). SST and SSS observed negative loading (−0.11 and −0.50), indicating water eutrophication as a significant condition explained by this component. Axis PC2 and PC3 signified a variance of 21.3% (eigenvalue = 1.28) and 15.4% (eigenvalue = 0.93), respectively, and showed maximum loading on SSS and SST (Tables 13.2 and 13.3). The observations on the eigenvalues indicated the relationship of the frequency of HAB events with higher nutrient concentrations and low surface water temperature (SST). A detailed observation of the environmental setting of different groups of HAB formation are discussed below.

Table 13.2 Eigenvalues of the correlation matrix

PC	Eigenvalues	Percentage of variance	Cumulative percentage of variance
1	2.92	48.6	48.6
2	1.28	21.3	69.9
3	0.927	15.4	85.4

Table 13.3 Factor loading matrix of total variance explained by each vector of the principal component analysis (PCA)

	Coefficients of PC1	Coefficients of PC2
SST	−0.11	0.527
Salinity	−0.50	0.202
DO	0.048	−0.692
NO_3-N	0.544	−0.013
PO_4-P	0.525	0.090
SiO_4-Si	0.41	0.048

4.1 Dinoflagellate: A Major Causative Group of HABs in Indian EEZ

Dinoflagellates and unicellular protists occupy a wide range of environmental conditions (pelagic to benthic) and differ in the types of nutrition, varying from autotrophic to heterotrophic and even mixotrophic modes. In the marine ecosystem, they occupy the trophic role as primary producers and consumers. In some instances, the population outburst of dinoflagellates produces toxic substances, resulting in various toxicity events to the aquatic ecosystem. The existence, proliferation, and toxin production in dinoflagellates rely on environmental conditions. The stability of the water column or the turbulence measure, temperature, salinity, and nutrient characteristics directly or indirectly influences the dinoflagellate community dynamics and thereby the bloom prevalence and ecophysiology. Various models and strategies have been adopted to describe the population ecology and community dynamics of microalgae, including dinoflagellates. *Margalef's Mandala* (describing the phytoplankton assemblage from r to k strategist in response to physicochemical tolerances) (Margalef, 1978), C (colony forming and dominating in chemically disturbed habitats), S (nutrient stress-tolerant species), and R (physical stress like turbulent-tolerant species) strategist based on their preferences to physicochemical factors (Smayda & Reynolds, 2003) are some references to such attempts.

From the analysis of the reported HAB events along the Indian EEZ, the blooms of dinoflagellates were observed in varying environmental circumstances depending on the causative species. Dinoflagellate blooms were recorded under a wide range of SST (24.1–32 °C) and surface salinity (12–35.9 psu); however, there was a preference for low surface temperature and higher salinity. Dinoflagellate blooms were

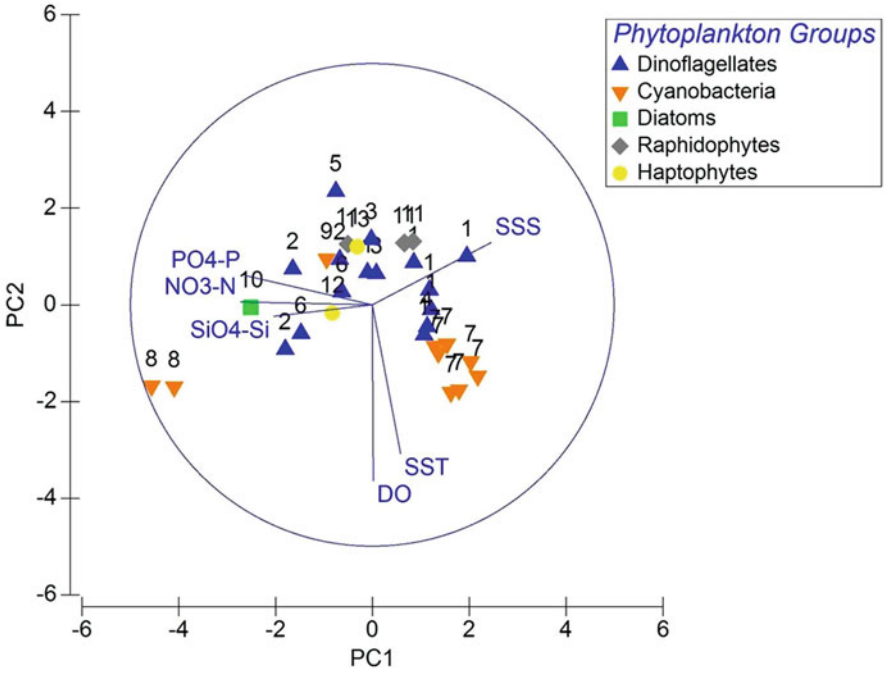

Fig. 13.10 PCA plot showing the relationship between the blooms of various phytoplankton with environmental variables. 1–6 Dinoflagellates (1. *Noctiluca*, 2. *Protoperidinium*, 3. *Akashiwo*, 4. *Prorocentrum*, 5. *Gonyaulax*, 6. *Karenia*), 7–9 Cyanobacteria (7. *Trichodesmium*, 8. *Microcystis*, 9. *Anabaena*), 10. Diatom (*Pseudo-nitzschia*), 11. Raphidophytes (*Chattonella*), 12–13 Haptophytes (12. *Phaeocystis*, 13. *Prymnesium*)

observed to prefer eutrophic waters, but there were variations between the species. Blooms of *Karenia* sp., *Cochlodinium* sp., *Protoperidinium* spp., and *Akashiwo* sp. were mostly observed in waters with high NO_3-N and PO_4-P conditions than the blooms of *Noctiluca scintillans*, *Prorocentrum* spp., and *Gonyaulax* sp. that records comparatively low values (Fig. 13.10). This might be due to the variability in nutrient requirement or shifting in the mode of nutrition (Jeong et al., 2005; Gribble et al., 2007; Turkoglu, 2013; Gomes et al., 2014; Kopuz et al., 2014; Zhang et al., 2016; Stoecker et al., 2017). As mentioned above, most blooms of these dinoflagellates have been from the southwest part of India, proceeding the SM season with an upwelling process (Thomas et al., 2013; Rai & Rajashekhar, 2014; Ahmed et al., 2016). The highest bloom occurrences of red *Noctiluca scintillans* (without endosymbiont *Pedinomonas noctilucae*) have been reported significantly from the southwest coast during the summer monsoon period. The green *N. scintillans* (with endosymbiont *Pedinomonas noctilucae*) dominated the northwest coast of India, characterized by winter convective mixing and resultant ocean dynamics. *Noctiluca scintillans* prefer water temperature and salinity between 10–30 °C and 28–36 psu, respectively (Huang & Qi, 1997; Tada et al., 2004; Miyaguchi et al., 2006; Harrison

et al., 2011). However, from the present observations as part of HAB monitoring programs, *Noctiluca* blooms were observed to occur within the range of temperature (25.02–32.13 °C) and salinity (25.00–40.00 psu), suggesting that the species in Indian waters exceeded their optimum level and are adapted to high temperature and salinity. Hence, eutrophication, the rising temperature, and salinity gradients could be supplementing blooms of the dinoflagellates along the Indian waters.

4.2 Cyanobacteria Blooms and Environmental Characteristics

The blooms caused by cyanobacteria is a growing concern around the globe in both marine and freshwater ecosystems. Several studies have attributed this increasing frequency to the rising temperature or global warming and climatic changes. The toxicity effect of cyanotoxins is also raising threats to coastal water and freshwater aquaculture activities. In addition to the toxicity effects, their high biomass and resulting oxygen depletion also result in deleterious effects on the aquatic systems. Cyanobacterial blooms are favored by various environmental factors that involve increased temperature, stable water column, illumination, low-nitrate and high phosphate conditions, low N/P ratio, etc.

In the Indian coastal waters, Cyanobacteria blooms were recorded mainly during inter-monsoon period predominantly in SIM, with high SST (30.1 ± 1.12 °C) and salinity (35.28 ± 1.12 psu), together with low NO_3-N (1.5 ± 2.03 μmol L^{-1}) and PO_4-P (1.09 ± 1.63 μmol L^{-1}). The PCA analysis shows a strong positive correlation between cyanobacterial blooms with high SST and salinity and low nutrients in the water column (Fig. 13.10). Photosynthetic nitrogen-fixing cyanobacterium *Trichodesmium erythraeum* was the most common bloom-forming cyanophycean member from Indian marine waters, particularly from January to June (Panikkar, 1959; Nagabhushanam, 1968; Qasim, 1970; Sarangi et al., 2004; Krishnan et al., 2007; Padmakumar et al., 2010a). The blooms of these filamentous algae were usually reported when the temperature was high with brilliant sunlight, and high salinity, and the water column was somewhat stable (Sellner, 1997; Jyothibabu et al., 2003). The low NO_3-N concentrations observed during most of the blooms of *Trichodesmium* sp. is linked to its diazotrophic nature, where the NO_3-N limited conditions could probably trigger diazotrophy in *Trichodesmium* sp. (D'Silva et al., 2012). Also, the low wind speed, water mixing, and high stratification prevalent during the SIM season could have promoted the buoyancy of the organism and its ability to form extensive blooms (Capone et al., 1997).

Recently, the proliferation of toxin (microcystin) producing cyanophyceae, *Microcystis,* was reported from the estuarine brackish ecosystems of the Indian EEZ. Both the west and east coast of India observe such bloom and are mainly toward the southern part. The scum formation and associated deleterious effects on water column characteristics are the primary concern, whereas the toxin production

and associated biological consequences cannot be neglected. Blooms of *Microcystis* were formerly reported from the east coast of India (Chacko & Srinivasan, 1954; Santhosh Kumar et al., 2010; Prasanth et al., 2014), but from 2008, bloom incidents of *Microcystis* were reported along the west coast, especially along the Kerala coast (Padmakumar et al., 2008; Mohan et al., 2020). High SST and elevation in the nitrate and phosphate concentrations were regarded as the main factors behind the rising *Microcystis* blooms in these regions (Padmakumar et al., 2008; Mohan et al., 2020).

4.3 Blooms of Diatoms, Haptophytes, and Raphidophytes: Environmental Preferences

The mixing process of the water column in the coastal and open-ocean waters of Indian EEZ associated with reversing monsoon winds aids the nutrient replenishment of surface waters and thereby promotes primary production. Summer monsoon and associated mixed diatom blooms are a regular phenomenon along the southwest coast of India (Thomas et al., 2013). Upwelling-induced nutrient influx supports the luxurious growth of diatoms, which are usually multispecies in composition. This type of diatom proliferation can also be observed in the northern Arabian Sea associated with winter convective mixing (Lathika, 2015). Such mixed diatom blooms are generally considered beneficial as they provide necessary food supplements for the higher trophic level organisms, particularly supporting the major fishery of the region. Apart from the beneficial diatom blooms, this diatom proliferation can sometimes have harmful effects on the aquatic ecosystem either by impairing water quality, physical stress, and mainly mechanical clogging of gills like that of *Asterionellopsis glacialis, Thalassiosira* spp., etc. (Villac et al., 2010) or by toxin production (certain species of pennate diatom *Pseudo-nitzschia* spp. that produce potent neurotoxin called domoic acid) (Trainer et al., 2008). Blooms caused by raphidophytes (mainly *Chattonella marina* and haptophytes (*Prymnesium parvum* and *Phaeocystis* sp.) are also observed to prefer nutrient-rich, comparatively stable water columns with low surface waters that promote their aggregation in surface waters.

The physicochemical characteristics observed during the blooms of diatoms, raphidophytes, and haptophytes clearly showed their preference for cold, nutrient-rich waters (Fig. 13.10). Blooms of diatoms, haptophytes, and raphidophytes during the SM season are ascribed to the high-nutrient conditions resulting from upwelling and inputs from runoffs during the period. Nutrient levels in the water during the initial phases of these blooms (diatoms, haptophytes, and raphidophytes) are recorded to be much higher. The PCA clearly indicated these preferences. Hence, the monsoonal influences in water column mixing and eutrophication substantially stimulate the diatoms as well as the raphidophyte and haptophyte blooms in Indian marine ecosystems.

5 HABs and Its Impacts on Indian Marine Ecosystems

5.1 Algal Blooms and Productivity

The effects of any algal proliferation on an aquatic ecosystem vary depending on the type of species, intensity, expansion, the time duration of its existence (residence time), water column characteristics, and the geographical settings of the bloom-forming region. However, not all algal blooms are troublesome. Seasonal or regular algal blooms in coastal waters help sustain the primary productivity that supports secondary and tertiary production and the fishery of the region. They act as a natural component of the ecosystem and support the food chain and, thereby, trophodynamics. Indian coastal ecosystems, especially the southwest coast of India, which harbors the major fish landing centers of the country, are favored by the summer monsoon upwelling and associated primary production. Extensive blooms of various size-fractioned diatoms occur during the season associated with upwelling-associated nutrient flux which supports the major fishery of herbivorous and carnivorous fishes. The winter blooms in the northern part of the Arabian Sea during the winter monsoon observe the blooms of dinoflagellate *Noctiluca scintillans* and alternating blooms of diatoms. Even though massive blooms of the dinoflagellate can result in many harmful effects, the increase in primary productivity through the extensive diatom blooms in the early and mid-phases of winter cooling (December–February) and thereby secondary production cannot be considered substandard. Similarly, along the east coast of India, there are reports of blooms of diatoms, predominantly multispecies that can support the fishery of the coast. These blooms along the east coast of India augmented by the northeast monsoonal influences and cyclonic events efficiently increase the productivity of the basin. Hence, all algal blooms cannot be considered harmful but can be very beneficial, especially in the case of diatom blooms that cater as a food source to many herbivorous aquatic dwellers. Moreover, algal blooms and associated organic carbon production play a vital role in carbon sequestration and augmenting blue carbon. The major role they can play in export flux and thereby channeling to bacterial and other microbial community sustenance often remains underestimated.

5.2 Ecological Consequences of HAB Events in the Indian Peninsular Region

Algal blooms that can cause undesirable alterations to the habitat are generally considered harmful. These alterations can be physical, chemical, or biological and include discoloration, change in smell, and increased turbidity of water (e.g., red tides). So, habitat loss can be considered a major consequence of algal blooms. Oxygen depletion, accumulation of ammonia in the water column, and more importantly, toxin production are the major aftermaths reported by the outbreaks of algae

in the Indian waters. Mechanical clogging of the gills of fishes by proliferating algae and the destruction of habitat can cause various stress effects in aquatic organisms. The outcomes include mass mortality of fishes and shellfishes, cases of human intoxication and death reports, loss of beach aesthetics, and its adverse impacts on tourism and recreational activities.

Along the Indian marine ecosystem, the occurrence of HAB events is reported to be on the rise (Padmakumar et al., 2012; D'Silva et al., 2012; Oyeku & Mandal, 2020). In recent years, HAB reports also corroborate the rising trend of HAB events in the Indian EEZ (Fig. 13.3). These increasing events have far-reaching consequences on the marine ecosystem. The red tides and green tides caused by dinoflagellate *Noctiluca scintillans* is a remarkable bloom phenomenon that strikes the coastal and open-ocean waters of the Indian EEZ. Regular episodic events of both green and red *N. scintillans* occur throughout the Indian coast. Winter blooms of the green variant of *N. scintillans* and summer blooms of red *N. scintillans* are well studied from the Indian waters. Extensive open-ocean blooms of green *N. scintillans* during the northeast monsoon and associated winter water column mixing increase the carbon sequestration and export flux of open-ocean ecosystems. These blooms are observed to occur in between the episodes of diatom blooms that increase the productivity of the open-ocean basin (Lathika, 2015). However, they are recently occurring in massive volumes, resulting in oxygen depletion, ammonia production, and food chain disruptions. Studies have shown an interrelationship between the recurrent blooms of *Noctiluca scintillans* and spreading hypoxia in the open-ocean waters (Gomes et al., 2014; Goes et al., 2020).

The coastal water blooms of *Noctiluca scintillans* and oxygen depletion seriously affect marine organisms. Some instances include the phenomenon of "crab jubilee" reported from India's southwest coast. During the event, many crabs, mainly blue swimming crab *Portunus pelagicus* and bottom-dwelling flatfishes in a moribund state, massively moved toward shore. This event was later linked to the oxygen depletion and related stress caused by *Noctiluca scintillans* red tide (Padmakumar et al. 2016a, b). Similar incidence by other invertebrates like bivalves was also reported from the southwest coastal waters in connection with red tides (Thomas et al., 2020a).

The ecological consequences become more conspicuous when we consider such intensive and expanding blooms in the coastal waters where the water column flushing is comparatively less. Significant dietary interrelationship has been suggested with the increasing gelatinous zooplankton swarms in the Arabian Sea ecosystems (Thomas et al., 2020b). Due to their sloppy feeding nature, gelatinous zooplankton filter off the mesozooplankton community, thereby reducing the competitive pressure for *Noctiluca scintillans* that feed on diatoms. This can support the bloom formation of *Noctiluca scintillans* which also depends on several other environmental parameters. On the other hand, the increasing *Noctiluca* blooms can cater to gelatinous zooplankton and support their population. However, this dietary interrelationship can alter the food chain in marine ecosystems and can cause a reduction in biodiversity and sustainability (Fig. 13.11).

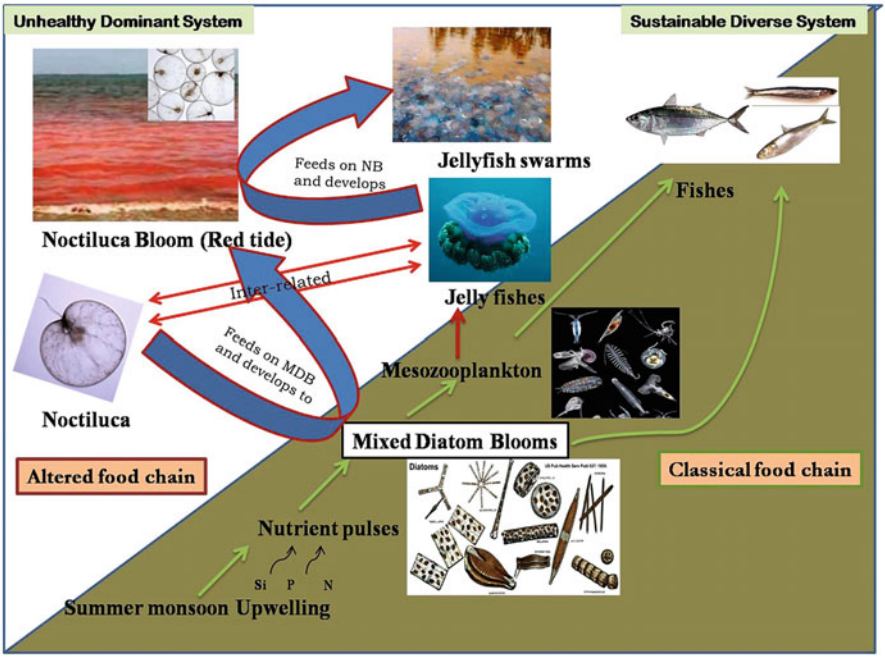

Fig. 13.11 The schematic representation of the interrelationship of *Noctiluca scintillans* and jellyfishes and its influence on the marine food chain. (Courtesy Thomas et al. (2020a))

The increasing algal blooms can affect the aesthetic and recreational value of the beaches. Production of huge volumes of "sea foam" occurs in the beach areas following intense algal blooms. In most circumstances, it is harmless and an indication of productive waters with the organic load. However, this can cause an unpleasant experience for the beachgoers with the fishy smell, pungency, and murky nature. These foams can produce aerosols that are released into the atmosphere, and if the bloom-forming algae contain any toxic molecules, the chances of the release of the same to air are high and can also affect the air quality. From Indian marine ecosystems, the reports on seafoam are less, but recently, a huge volume of seafoam production was reported from the Kollam coast off the southwest coast of India during the early summer monsoon season of 2019 (Fig. 13.12). These foam were reported to have been caused by Haptophyte *Phaeocystis globosa* (Madhu et al., 2020a). The phenomenon lasted for a few hours and might be due to the post-bloom phase of the haptophyte supported by wind factors. Even though the locals did not experience any harmful effects from the phenomenon, such events are warning signals of eutrophication in the coastal waters.

Fig. 13.12 File picture of seafoam event at Kollam Beach during the summer monsoon of 2019 (ref: https://www.deccanchronicle.com/nation/current-affairs/190619/algal-bloom-behind-sea-foam-in-kollam.html)

5.3 HAB-Related Mortalities in Aquatic Organisms and Allied Health Issues in Human Beings

When we analyze the HAB-associated aquatic health consequences to date, several species, majorly dinoflagellates followed by cyanophyceans and raphidophytes, were responsible for the mass mortality of aquatic organisms in the Indian peninsular region. The earliest record of an algal bloom event was in 1908 which described surface water discoloration and massive fish mortality from the Malabar coast of southwest India that extended to the Laccadive Sea (Hornell, 1908). This was supposed to be caused by flagellate species and was later identified to be *Hornellia marina* (Subrahmanyan, 1954) which was reclassified as the raphidophyte *Chattonella marina* by Hara and Chihara (1982). Since its first report, there were several documented cases of HAB-associated fish and shellfish mortalities (Table 13.1). The majority of them were related to habitat destruction through oxygen depletion that resulted from bulky biomass formation as that of dinoflagellate *Noctiluca scintillans* and cyanobacterium *Trichodesmium* spp. Paralytic shellfish poisoning (PSP) was one among those with fish kills and hospitalization of 85 people and three reported deaths after the consumption of contaminated clam, *Meretrix casta,* along the coast of Tamil Nadu (Silas et al., 1982). Similar incidents with human causalities or deaths were reported from both the east and west coast of India which include PSP outbreak in Mangalore by the consumption of contaminated clams (Karunasagar et al., 1984; Segar et al., 1989), in Vizhinjam in 1997, where seven people died, and over 500 were hospitalized after consumption of

affected mussels *Perna indica* (Karunasagar et al., 1998). Even then, the causative algal species for these events remain in ambiguity. Similar outbreaks observed along the coastal waters of Malaysia and the Philippines were identified to be caused by *Alexandrium tamiyavanichii* and *Pyrodinium bahamense* (Ching et al., 2015; Suleiman et al., 2017; Mohammad-Noor et al., 2018). Mass mortality of fishes was also reported from the coastal waters of Kerala that were linked to the blooms of dinoflagellates *Karenia mikimotoi, Cochlodinium citron,* and *Gonyaulax diegensis.* Several economically important fishes were killed or stressed following these bloom events (Iyer et al., 2008; Robin et al., 2013). The bloom caused by the noxious raphidophyte *Chattonella marina* was also observed to cause several fish kills and human causalities, especially on the southwest coast of India (Jugnu & Kripa, 2009; Padmakumar et al., 2011; Sarangi & Mohammed, 2011; Sanilkumar et al., 2012). Mass mortalities of bivalves, demersal fishes, and shrimps were reported in such blooms and were due to the presence of hemolytic compounds and oxygen depletion.

Extensive stench events were reported along the Kerala coast during September 2004, causing mass mortalities of fishes and shellfishes. The consumption of stench-related seafood resulted in several health effects that mainly included children (The New Indian Express, 2004; The Hindu, 2004). *Cochlodinium polykrikoides* and *Karenia brevis* were identified as the causative organism, but further studies proved the occurrence of holococcolithopore and *N. scintillans* (Ramaiah et al., 2005; Sahayak et al., 2005).

The filamentous cyanobacteria *Trichodesmium erythraeum* bloom was reported to occur all along peninsular India, especially during oligotrophic, stable inter-monsoon seasons. Oxygen depletion is the significant consequence of these red tides caused by *T. erythraeum.* Water column deterioration, mechanical gill clogging, and oxygen depletion-related mortalities in connection with *T. erythraeum* are mainly reported from the east coast of India, and one severe among those was at the Krusadai Island from the Gulf of Mannar region (Chacko, 1942; Chidambaram & Unny, 1944; Ramamurthy, 1970). Around 756 holothurians, 250 fishes belonging to 16 genera, and other bottom fauna like crabs, sea urchins, and mollusks along a shoreline of about 2.4 km were killed in one day. The death of animals was due to asphyxiation caused during blooms' decay. *T. erythraeum* blooms elsewhere caused water discoloration, noxious smell production, and low fish catch (Verlancar, 1978; Krishnan et al., 2007; Mohanty et al., 2010; Karthik & Padmavati, 2017).

The stress and mortalities in connection with the bloom of dinoflagellate *N. scintillans* were observed mainly through oxygen depletion, turbidity, mechanical clogging of gills, etc. (Aiyar, 1936). Intense bloom and its decay can also result in ammonia accumulation in the water and cause allied toxic effects in aquatic organisms (Okaichi & Nishio, 1976). Several cases of massive death in aquatic fauna, as well as reduction of fish catch associated with *N. scintillans* blooms, were reported from Indian waters (Aiyar, 1936; Bhimachar & George, 1950; Devassy & Nair, 1987; Naqvi et al., 1998; Mohammed, 2003; Sahayak et al., 2005; Jugnu & Kripa, 2006; Mohamed et al., 2007; Anantharaman et al., 2010; Padmakumar et al., 2010b, 2016a, b). The asphyxiation by intense algal blooms is reported to kill fast-growing

corals in the Gulf of Mannar. The blooms of *N. scintillans* were the causative species for these incidents and is observed to have recurred along the region (Raj et al., 2020).

Diatom blooms are generally considered harmless unless they result in massive decay and oxygen depletion. However, some reports on the consequences of diatom blooms negatively affect the fishery. The blooms of centric diatom *Hemidiscus hardmannianus* and pennate form *Asterionella glacialis* were linked to mortality and reduction of fish catch along the east coast of India (Subramanian & Purushothaman, 1985; Satpathy & Nair, 1996). Globally, there are several reports on the adverse effects of diatom blooms, including toxic events like the domoic acid production and amnesic shellfish poisoning associated with certain species of *Pseudo-nitzschia* spp. (Bates, 1998, 2000). Mortalities of sea birds documented to be connected with oily surface film production by certain diatoms like *Coscinodiscus centralis* and mechanical gill clogging by certain chain-forming, and large-sized diatoms were studied (Villac et al., 2010). However, such type of detailed investigations is lacking from the Indian waters.

5.4 HABs: Socioeconomic Impacts

Socioeconomic status and ecosystem stability are intertwined, and any alteration in one may affect the other system. HABs have far-reaching consequences in marine as well as freshwater ecosystems. Contamination of drinking water is the major concern of freshwater HABs, whereas pollution and fishery impacts form the major outcome of marine events. Indian economy depends significantly on the fishery sector, including capture and culture systems. With an estimated coastline of 8118 km and an EEZ of 2.02 million sq. km, marine fish production is estimated to be 3.72 MMT. The fisheries potential of the country has been estimated at 22.31 million t with 5.31 and 17 million t from marine and inland sectors, respectively, and contributes to 7.28% of the agricultural GDP (Handbook on fisheries statistics, 2020). This sector also plays a pivotal role in food security and employment generation. One major setback of harmful algal blooms is the disruption in the flow of energy transfer in the trophic systems, reduction in biodiversity, and rise of dominance. This can cause profound habitat alterations and result in ecosystem shifts or stress in most fish and other aquatic organisms. With the increase in HAB events, the tolerance threshold will be lost, and ultimately reduction in fishery occurs, which presumably impacts the economic status of the country.

When it comes to the events of toxic episodes with the poisoning of fishes and shellfishes, the upshot might also include illness, seafood contamination, and related issues that may affect the export quality of marine products, reduction in local purchase for consumption, etc., thereby negatively impacting the fishery-related economics of the country (Hoagland et al., 2002; Hoagland & Scatasta, 2006; Adams et al., 2018). The financial loss treating the algal toxin-related human illness and management activities for clearing HAB- associated littering of beaches also

need to be considered. The actual financial losses caused by HABs in the Indian EEZ have not been estimated and reported to date. However, it's noteworthy to mention that the west coast of India, which contributes to more than 68.8% of marine fish landing in the country (Sathianandan, 2017), has become a hotspot for HAB events, and the impacts arising from blooms could increase in the near future. Unwanted algal proliferation can lead to the loss of aesthetic value of beaches and hindrance to tourism and recreation activities. Phenomena like seafoam, jellyfish swarm, aerosols from toxic algal blooms, stench events, etc., can affect the beach tourism activities and closure of beaches. This can reduce the revenue generation from the beach recreational sector.

6 Recommendations and Future Approach

Management and mitigation strategies for HAB events range from extensive field surveys to species level molecular studies. Predictive models based on in situ and remote sensing data form integral components for developing management protocols. Global warming, climate change, and eutrophication are the various factors reckoned to be the contributing factors for the intensification of HAB events worldwide. Increased monitoring programs and awareness among the scientific and local population about the HAB phenomenon can also be considered a factor contributing to the increase in the integer of HAB events. Mitigation, prevention, and control become the thumb rule for managing HAB issues (Anderson, 2009). Mitigation deals with the management of an ongoing bloom event, whereas prevention is the further reduction in the outburst of potential bloom formers present in the water column by various activities that include reduction in pollution load or eutrophication. Control activities may include combating or suppressing HABs and is much more challenging. With emerging technologies like molecular-level analysis of species and toxins, the field of HAB research is refining and can be helpful in developing effective management strategies.

7 Conclusion

Microalgae form the base of the marine food chain and are the ultimate fixers of atmospheric carbon. Their role in the sustainability and trophodynamics of marine ecosystems are invariably pertinent. However, there are instances where this boon became a bane, as in the case of harmful algal blooms (HABs). The HAB aftermaths range from mere discoloration of the water column to significant alteration in the water quality, habitat destruction, and mass mortality of marine organisms or even human casualties and death. In the Indian scenario, HAB events are on the rise due to eutrophication, global warming, and climate change and, in certain instances, due to improved monitoring programs by the scientific community. The west coast of India

reports more bloom events and is mainly by dinoflagellates. The biannually reversing monsoon forcing relates to the HAB events in the Indian EEZ. The scientific attention on Indian marine HABs has increased recently. Apart from the regular monitoring, early warning systems utilizing remote sensing data have been well established in the last few decades. However, with climate change and alien species invasions, novel blooms are increasingly reported in the country. India being a country with high fishery potential and obtaining a good share of its GDP from the fishery, studies on HABs and its ecological and economic impacts are of utmost importance. Intense research needs to be carried out not only on regular monitoring and predicting HABs but also in devising efficient mitigation activities.

References

Adams, C. M., Larkin, S. L., Hoagland, P., & Sancewich, B. (2018). Assessing the economic consequences of Harmful Algal Blooms: A summary of existing literature, research methods, data, and information gaps. In S. E. Shumway, J. M. Burkholder, & S. L. Morton (Eds.), *Harmful Algal Blooms: A compendium desk reference* (pp. 243–336). Wiley. https://doi.org/10.1002/9781118994672.ch8

Ahmed, A., Kurian, S., Gauns, M., Chndrasekhararao, A. V., Mulla, A., Naik, B., Naik, H., & Naqvi, S. W. A. (2016). Spatial variability in phytoplankton community structure along the eastern Arabian Sea during the onset of south-west monsoon. *Continental Shelf Research, 119*, 30–39. https://doi.org/10.1016/j.csr.2016.03.005

Aiyar, R. G. (1936). Mortality of fish of the Madras coast. *Current Science, 4*(7), 488–489. https://doi.org/10.1093/plankt/fbt059

Anantharaman, P., Thirumaran, G., Arumugam, R., Kanna, R. R. R., Hemalatha, A., Kannathasan, A., Sampathkumar, P., & Balasubramanian, T. (2010). Monitoring of *Noctiluca* bloom in Mandapam and Keelakarai coastal waters, Southeast coast of India. *Recent Research in Science and Technology, 2*(10), 51–58.

Anderson, D. M. (2009). Approaches to monitoring, control and management of harmful algal blooms (HABs). *Ocean and Coastal Management, 52*(7), 342. https://doi.org/10.1016/j.ocecoaman.2009.04.006

Bates, S. S. (1998). Ecophysiology and metabolism of ASP toxin production. In D. M. Anderson, A. D. Cembella, & G. M. Hallegraeff (Eds.), *Physiological ecology of harmful algal blooms* (pp. 405–426). Springer-Verlag.

Bates, S. S. (2000). Domoic-acid-producing diatoms: Another genus added. *Journal of Phycology, 36*, 978–983.

Bhimachar, B. S., & George, P. C. (1950). Abrupt set-backs in the fisheries of the Malabar and Kanara coasts and "red water" phenomenon as their probable cause. *Proceedings of Indian Academy of Sciences B, 31*, 339–350. https://doi.org/10.1007/BF03050614

Capone, D. G., Zehr, J. P., Paerl, H. W., & Carpenter, E. J. (1997). *Trichodesmium*, a significant marine cyanobacterium. *Science, 276*, 1221–1229.

Chacko, P. I. (1942). An usual incidence of mortality of marine fauna. *Current Science, 11*(10), 404.

Chacko, P. I., & Srinivasan, R. (1954). Effect of jaggery on fish life. *Journal of the Bombay Natural History Society, 52*(2&3), 629–634.

Chellham, A., & Alagarswami, K. (1978). Blooms of *Trichodesmium thiebautii* and their effects on experimental pearl culture in the Pambau area and its effect on the fauna. *Current Science India, 210*, 263.

Chidambaram, K., & Unny, M. M. (1944). Note on the swarming of the planktonic algae *Trichodesmium erythraeum* in the Pamban area and its effect on the fauna. *Current Science, 13*, 263.

Ching, P. K., Ventura, R. J., de los Reyes, V. C., Sucaldito, M. N., & Tayag, E. (2015). Lethal paralytic shellfish poisoning from consumption of green mussel broth, Western Samar, Philippines, August 2013. *Western Pacific Surveillance and Response Journal, 6*(2), 22–26. https://doi.org/10.5365/wpsar.2015.6.1.004

D'Silva, M. S., Anil, A. C., Naik, R. K., & D'Costa, P. M. (2012). Algal blooms: A perspective from the coasts of India. *Natural Hazards, 63*(2), 1225–1253. https://doi.org/10.1007/s11069-012-0190-9

Dharani, G., Nazar, A. A., Kanagu, L., Venkateshwaran, P., Kumar, T. S., Ratnam, K., Venkatesan, R., & Ravindran, M. (2004). On the recurrence of Noctiluca scintillans bloom in Minnie Bay, Port Blair: Impact on water quality and bioactivity of extracts. *Current Science, 87*, 990–994.

Devassy, V. P. (1987). Trichodesmium- Red tides in the Arabian Sea. In *Contribution in marine sciences, Dr. SZ Qasim Sastyabdapurti felicitation volume* (pp. 61–66). NIO.

Devassy, V. P., & Nair, S. R. S. (1987). Discolouration of water and its effect on fisheries along the Goa coast. *Mahasagar-Bulletin National Institute of Oceanography, 20*, 121–128.

Durve, V. S., & Alagarswami, K. (1964). An incidence of fish mortality in Athankarai estuary near Mandapam. *Journal of the Marine Biological Association of India, 6*(1), 147–151.

Eashwar, M., Nallathambi, T., Kuberaraj, K., & Govindarajan, G. (2001). *Noctiluca* blooms in Port Blair Bay, Andamans. *Current Science, 81*(2), 203–206.

Field, C. B., Behrenfeld, M. J., Randerson, J. T., & Falkowski, P. G. (1998). Primary production of the biosphere: Integrating terrestrial and oceanic components. *Science, 281*, 237–240. https://doi.org/10.1126/science.281.5374.237

Finkel, Z. V., Beardall, J., Flynn, K. J., Quigg, A., Rees, T. A. V., & Raven, J. A. (2010). Phytoplankton in a changing world: Cell size and elemental stoichiometry. *Journal of Plankton Research, 32*, 119–137. https://doi.org/10.1093/plankt/fbp098

Glibert, P. M., Anderson, D. M., Gentien, P., Granéli, E., & Sellner, K. G. (2005). The global, complex phenomena of harmful algal blooms. *Oceanography, 18*(2), 136–147.

Goes, J. I., Tian, H., Gomes, H. R., et al. (2020). Ecosystem state change in the Arabian Sea fuelled by the recent loss of snow over the Himalayan-Tibetan Plateau region. *Scientific Reports, 10*, 7422. https://doi.org/10.1038/s41598-020-64360

Gomes, R. H., Goes, J. I., Matondkar, S. G. P., Buskey, E. J., Basu, S., Parab, S., & Thoppil, P. (2014). Massive outbreaks of *Noctiluca scintillans* blooms in the Arabian Sea due to spread of hypoxia. *Nature Communications, 5*. https://doi.org/10.1038/ncomms5862

Grasshoff, K., Ehrhardt, M., Kremling, K., & Almgren, T. (1983). *Methods of seawater analysis* (p. 419). Verlag Chemie.

Gribble, K. E., Nolan, G., & Anderson, D. M. (2007). Biodiversity, biogeography and potential trophic impact of Protoperidinium spp. (Dinophyceae) off the southwestern coast of Ireland. *Journal of Plankton Research, 29*(11), 931–947. https://doi.org/10.1093/plankt/fbm070

Handbook on fisheries statistics. (2020). Department of Fisheries, Ministry of Fisheries, Animal Husbandry & Dairying, Government of India, New Delhi. pp. 176.

Hara, Y., & Chihara, M. (1982). Ultrastructure and taxonomy of Chattonella (Class Raphidophyceae) in Japan. *Japanese Journal of Phycology, 30*, 47–56.

Harrison, P. J., Furuya, K., Glibert, P. M., Xu, J., Liu, H. B., Yin, K., Lee, J. H., Anderson, D. M., Gowen, R., Al-Azri, A. R., & Ho, A. Y. T. (2011). Geographical distribution of red and green *Noctiluca scintillans*. *Chinese Journal of Oceanology and Limnology, 29*(4), 807–831.

Hoagland, P., Anderson, D. M., Kaoru, Y., & White, A. W. (2002). The economic effects of Harmful Algal Blooms in the United States: Estimates, assessment, issues, and information needs. *Estuaries, 25*, 819–837. https://doi.org/10.1007/BF02804908

Hoagland, P., & Scatasta, S. (2006). The economic effects of harmful algal blooms. In E. Graneli & J. Turner (Eds.), *Ecology of harmful algae. Ecological studies (analysis and synthesis)* (pp. 391–402). Springer.

Hornell, J. (1908). Report of the results of a fishery cruise along the Malabar coast to the Laccadive Islands in 1908. *Madras Fisheries Bulletin, 4*, 71–126.

Hornell, J. (1917). A new protozoan cause of widespread mortality among marine fishes. *Madras Fisheries Bulletin, 11*, 53–66.

Huang, C., & Qi, Y. (1997). The abundance cycle and influence factors on red tide phenomena of *Noctiluca scintillans* (Dinophyceae) in Dapeng Bay, the south. *Journal of Plankton Research, 19*(3), 303–318. https://doi.org/10.1093/plankt/19.3.303

Iyer, C. S. P., Robin, R. S., Sreekala, M. S., & Kumar, S. S. (2008). *Karenia mikimotoi* bloom in Arabian Sea. *Harmful Algae News, 37*, 9–10.

James, P. S. B. R. (1972). On a bloom of *Trichodesmium thiebautii* Gomont in the Gulf of Mannar at Mandapam. *Indian Journal of Fisheries, 19*(1&2), 205–207.

Jeong, H. J., Du Yoo, Y., Seong, K. A., Kim, J. H., Park, J. Y., Kim, S., Lee, S. H., Ha, J. H., & Yih, W. H. (2005). Feeding by the mixotrophic red-tide dinoflagellate: Mechanisms, prey species, effects of prey concentration, and grazing impact. *Aquatic Microbial Ecology, 38*(3), 249–257.

Jugnu, R., & Kripa, V. (2006). *Studies on the prevalence of algal blooms along Kerala coast, India* (Doctoral dissertation, Cochin University of Science and Technology).

Jugnu, R., & Kripa, V. (2009). Effect of *Chattonella marina* [(Subrahmanyan) Haraet Chihara 1982] blooms in the coastal fishery resources along Kerala coast, India. *Indian Journal of Marine Sciences, 38*, 77–88.

Jyothibabu, R., Madhu, N. V., Murukesh, N., Haridas, P. C., Nair, K. K. C., & Venugopal, P. (2003). Intense blooms of *Trichodesmium erythraeum* (Cyanophyta) in the open waters along east coast of India. *Indian Journal of Marine Sciences, 32*, 165–167.

Karthik, R., & Padmavati, G. (2017). Temperature and salinity are the probable causative agent for the *Trichodesmium erythraeum* (Cyanophyceae) algal bloom on the Burmanallah Coastal Waters of South Andaman Island. *World Applied Sciences Journal, 35*(8), 1271–1281. https://doi.org/10.5829/idosi.wasj

Karunasagar, I., Gowda, H. S. V., Subburaj, M., Venugopal, M. N., & Karunasagar, I. (1984). Outbreak of paralytic shellfish poisoning in Mangalore, west coast of India. *Current Science, 53*(5), 247–249.

Karunasagar, I., & Karunasagar, I. (1992). *Gymnodinium nagasakiense* red tide off Someshwar, west coast of India and mussel toxicity. *Journal of Shellfish Research, 11*, 477–478.

Karunasagar, I., Joseph, B., Philipose, K. K., & Karunasagar, I. (1998). Another outbreak of PSP in India. *Harmful Algae News, 17*, 1.

Katti, R. J., & Gupta, C. (1988). On the occurrence of" green tide" in the Arabian Sea off Mangalore. *Current Science. Bangalore, 57*(7), 380–381.

Kopuz, U., Feyzioglu, A. M., & Valente, A. (2014). Seasonal changes of phytoplankton chlorophyll a, primary production and their relation in the continental shelf area of the South Eastern Black Sea. *Turkish Journal of Fisheries and Aquatic Sciences, 14*(3), 261–268. https://doi.org/10.4194/1303-2712-v14

Koya, K. P., & Kaladharan, P. (1997). *Trichodesmium* bloom and mortality of *Canthigaster margaritatus* in the Lakshadweep Sea. *Marine Fisheries Information Service, Technical and Extension Series, 147*, 14–14.

Krishnan, A. A., Krishnakumar, P. K., & Rajagopalan, M. (2007). *Trichodesmium erythraeum* (Ehrenberg) bloom along the southwest coast of India (Arabian Sea) and its impact on trace metal concentrations in seawater. *Estuarine, Coastal and Shelf Science, 71*(3–4), 641–646.

Kudela, R. M., Ryan, J. P., Blakely, M. D., Lane, J. Q., & Peterson, T. D. (2008). Linking the physiology and ecology of Cochlodinium to better understand harmful algal bloom events: A comparative approach. *Harmful Algae, 7*(3), 278–292.

Lathika, C. T. (2015). *Microphytoplankton community structure along the North Eastern Arabian Sea during Winter monsoon*. Ph.D Thesis, Cochin University of Science and Technology, pp. 218.

Lewis, E. J. (1965). *On a Gonyaulax bloom off Mt Dalley, in the Arabian Sea*. Proceedings of the Seminar on Sea, Salt and Plants, pp. 224–226.

Madhu, N. V., Reny, P. D., Paul, M., Ullas, N., & Resmi, P. (2011). Occurrence of red tide caused by *Karenia mikimotoi* (toxic dinoflagellate) in the Southwest coast of India. *Indian Journal of Marine Sciences, 40*(6), 821–825.

Madhu, N. V., Anil, P., Vishal, C. R., Muraleedharan, K. R., Parvathi, A., Gireeshkumar, T. R., Arya, K. S., & Hafza, S. (2020a). Occurrence of white gelatinous foam on the beaches of Kollam (Southwest Coast of India) due to the senescent bloom of *Phaeocystis globosa*. *Current Science, 119*, 1371–1375.

Madhu, N. V., Anil, P., Gireeshkumar, T. R., Muraleedharan, K. R., Kiran, K., & Vishal, C. R. (2020b). Phytoplankton characterisation in the Alappuzha mud banks during the pre−/post phases of a red-tide, *Prorocentrum shikokuense* Hada. *Regional Studies in Marine Science, 40*, 101486. https://doi.org/10.1016/j.rsma.2020.101486

Madhupratap, M., Sawant, S., & Gauns, M. (1999). A first report on a bloom of the marine prymnesiophycean, *Phaeocystis globosa* from the Arabian Sea. *Oceanologica Acta, 23*, 83–90.

Manning, S. R., & La Claire, J. W. (2010). II Multiplex PCR methods for the species-specific detection and quantification of *Prymnesium parvum* (Haptophyta). *Journal of Applied Phycology, 22*, 587–597. https://doi.org/10.1007/s10811-009-9498-6

Margalef, R. (1978). Life-forms of phytoplankton as survival alternatives in an unstable environment. *Oceanologica Acta, 1*, 493–509.

Miyaguchi, H., Fujiki, T., Kikuchi, T., Kuwahara, V. S., & Toda, T. (2006). Relationship between the bloom of *Noctiluca scintillans* and environmental factors in the coastal waters of Sagami. *Journal of Plankton Research, 28*, 313–324. https://doi.org/10.1093/plankt/fbi127

Mohamed, K. S., Kripa, V., Jugnu, R., Radhakrishnan, P., Alloycious, P. S., Sharma, J., Joseph, M., & Velayudhan, T. S. (2007). Mortality of farmed pearl oyster *Pinctada fucata* (Gould, 1850) due to the blooming of *Noctiluca scintillans* and *Cochlodinium* sp. at Kollam Bay, Kerala. *Journal of the Marine Biological Association of India, 49*, 213–218.

Mohammad-Noor, N., Adam, A., Lim, P. T., Leaw, C. P., Lau, W. L. S., Liow, G. R., Muhamad-bunnori, N., Hamdan, N., Md-nor, A., Kemat, N., & Muniandi, D. (2018). First report of paralytic shellfish poisoning (PSP) caused by *Alexandrium tamiyavanichii* in Kuantan Port, Pahang. East Coast of Malaysia. *Phycological Research, 66*, 37–44. https://doi.org/10.1111/pre.12205

Mohammed, G. (2003). Algal bloom and mass mortality of fishes and mussels along Kozhikode coast. *The Marine Fisheries Information Service. Technical and Extension Series, 175*, 7–8.

Mohan, R., Sathish, T., & Padmakumar, K. B. (2020). Occurrence of potentially toxic cyanobacteria *Microcystis aeruginosa* in aquatic ecosystems of central Kerala (south India). *Annals of Limnology - International Journal of Limnology, 56*(18), 1–10. https://doi.org/10.1051/limn/2020015

Mohanty, A. K., Satpathy, K. K., Sahu, G., Hussain, K. J., Prasad, M. V. R., & Sarkar, S. K. (2010). Bloom of *Trichodesmium erythraeum* (Ehr.) and its impact on water quality and plankton community structure in the coastal waters of southeast coast of India. *Indian Journal of Marine Sciences, 39*(3), 323–333.

Nagabhushanam, A. K. (1968). On an unusual dense phytoplankton bloom around Minicoy Island (Arabian Sea), and its effect on the local Tuna fisheries. *Current Science, 36*(22), 611–612.

Naqvi, S. W. A., George, M. D., Narvekar, P. V., Jayakumar, D. A., Shailaja, M. S., Sardesai, S., Sarma, V. V. S. S., Shenoy, D. M., Naik, H., Maheswaran, P. A., Krishnakumari, K., Rajesh, G., Sudhir, A. K., & Binu, M. S. (1998). Severe fish mortality associated with 'red tide' observed in the sea off Cochin. *Current Science, 75*, 543–544.

Narayana, S., Chitra, J., Tapase, S. R., Thamke, V., Karthick, P., Ramesh, C., Murthy, K. N., Ramasamy, M., Kodam, K. M., & Mohanraju, R. (2014). Toxicity studies of *Trichodesmium erythraeum* (Ehrenberg, 1830) bloom extracts, from Phoenix Bay, Port Blair, Andamans. *Harmful Algae, 40*, 34–39. https://doi.org/10.1016/j.hal.2014.10.003

Nayak, B. B., Karunasagar, I., & Karunasagar, I. (2000). Bacteriological and physico-chemical factors associated with *Noctiluca miliaris* bloom along Mangalore south west coast of India. *Indian Journal of Marine Sciences, 29*, 139–143.

Nayar, S., Gupta, T. R. C., & Prabhu, H. V. (2001). Bloom of *Noctiluca scintillans* MaCartney in the Arabian Sea off Mangalore SW India. *Asian Fisheries Science, 14*, 77–82.

Okaichi, T., & Nishio, S. (1976). Identification of ammonia as the toxic principle of red tide of *Noctiluca miliaris*. *Bulletin of the Plankton Society of Japan, 23*, 75–80.

Oyeku, O. G., & Mandal, S. K. (2020). Historical occurrences of marine microalgal blooms in Indian peninsula: Probable causes and implications. *Oceanologia, 63*(1), 51–70. https://doi.org/10.1016/j.oceano.2020.08.008

Padmakumar, K. B., Sanilkumar, M. G., Saramma, A. V., Sanjeevan, V. N., & Menon, N. R. (2008). *Microcystis aeruginosa* bloom on Southwest coast of India. *Harmful Algae News, 37*, 11–12.

Padmakumar, K. B., Smitha, B. R., Thomas, L. C., Fanimol, C. L., SreeRenjima, G., Menon, N. R., & Sanjeevan, V. N. (2010a). Blooms of *Trichodesmium erythraeum* in the South Eastern Arabian Sea during the onset of 2009 summer monsoon. *Ocean Science Journal, 45*(3), 151–157.

Padmakumar, K. B., SreeRenjima, G., Fanimol, C. L., Menon, N. R., & Sanjeevan, V. N. (2010b). Preponderance of heterotrophic *Noctiluca scintillans* during a multi-species diatom bloom along the south-west coast of India. *International Journal of Oceans and Oceanography, 4*(1), 55–63.

Padmakumar, K. B., Thomas, L. C., Salini, T. C., John, E., Menon, N. R., & Sanjeevan, V. N. (2011). Monospecific bloom of noxious raphidophyte Chattonella marina in the coastal waters of South–West coast of India. *International Journal of Biosciences, 1*(1), 57–69.

Padmakumar, K. B., Menon, N. R., & Sanjeevan, V. N. (2012). Is occurrence of Harmful Algal Blooms in the exclusive economic zone of India on the rise? *International Journal of Oceanography, 2012*, Article ID 263946. https://doi.org/10.1155/2012/263946

Padmakumar, K. B., Lathika, C. T., Sudhakar, M., & Bijoy Nandan, S. (2016a). Extensive outbreaks of heterotrophic dinoflagellate *Noctiluca scintillans* blooms along the coastal waters of South Eastern Arabian Sea. *Harmful Algae News, 52*, 11–12.

Padmakumar, K. B., Thomas, L. C., Vijayan, A., & Sudhakar, M. (2016b). "Crab Jubilee" subsequent to red tide of *Noctiluca scintillans* along the central Kerala coast (SW coast of India). *Indian Journal of Marine Sciences, 45*(11), 1549–1551.

Panikkar, N. K. (1959). Indian fisheries. *Current Science, 28*(12), 53–54.

Pant, A., & Devassy, V. P. (1976). Release of extracellular matter during photosynthesis by a *Trichodesmium* bloom. *Current Science*, *45*(13), 487–489.

Parsons, T. R., Maita, Y., & Lalli, C. M. (1984). *A manual of chemical and biological methods for seawater analysis* (p. 173). Pergamon Press.

Peng, J., Place, A. R., Yoshida, W., Anklin, C., & Hamann, M. T. (2010). Structure and absolute configuration of karlotoxin-2, an ichthyotoxin from the marine dinoflagellate *Karlodinium veneficum*. *Journal of the American Chemical Society, 132*, 3277–3279.

Peter, S., Agnes, F., Sreeparvathy, P., Pillai, D., & Kumar, B. M. (2016). *Noctiluca scintillans* (Macartney) Kofoid and Swezy Bloom and its impact on the coastal water quality off Alappuzha, Arabian Sea. *Fishery Technology, 53*(1), 82–85.

Place, A. R., Saito, K., Deeds, J. R., Robledo, J. A. F., & Vasta, G. R. (2008). A decade of research on Pfiesteria spp. and their toxins: Unresolved questions and an alternative hypothesis. In L. M. Botana (Ed.), *Seafood and freshwater toxins: Pharmacology, physiology, and detection* (2nd ed., pp. 717–751). CRC Press.

Prabhu, M. S., Ramamurthy, S., Kuthalingam, M. D. K., & Dhulkhed, M. H. (1965). On an unusual swarming of the planktonic blue-green algae *Trichodesmium* spp., off Mangalore. *Current Science, 34*(3), 95–95.

Prabhu, M. R., Ramamurthy, S., Dhulkhed, M. H., & Radhakrishnan, N. S. (1971). *Trichodesmium* bloom and the failure of oil sardine fishery. *Mahasagar, 4*(2), 62.

Prakash, A., & Sarma, A. V. (1964). On the occurrence of 'red water' phenomenon on the west coast of India. *Current Science, 33*(6), 168–170.

Prasanth, B., Nandakumar, B. R., Jayalakshmi, T., & Santhanam, P. (2014). First report on the intense cyanobacteria *Microcystis aeruginosa* Kützing, 1846 bloom at Muttukkadu Backwater, Southeast coast of India. *Indian Journal of Marine Sciences, 43*(2), 528–262.

Qasim, S. Z. (1970). Some characteristics of a *Trichodesmium* bloom in the Laccadives. *Deep Sea Research and Oceanographic Abstracts, 17*(3), 655–660. https://doi.org/10.1016/0011-7471(70)90077-X

Rai, S. V., & Rajashekhar, M. (2014). Seasonal assessment of hydrographic variables and phytoplankton community in the Arabian Sea. *Brazilian Journal of Oceanography, 62*(4), 279–293. https://doi.org/10.1590/S1679-87592014069906204

Raghu Prasad, R. (1953). Swarming of *Noctiluca* in the Palk Bay and its effect on the 'Choodai' fishery, with a note on the possible use of Noctiluca as an indicator species1. *Proceedings/Indian Academy of Sciences*. Springer India, *38*(1), 40–47.

Raghu Prasad, R., & Jayaraman, R. (1954). Preliminary studies on certain changes in the plankton and hydrological conditions associated with the swarming of *Noctiluca*. *Proceedings/Indian Academy of Sciences*. Springer India, *40(2)*, 49–57.

Raj, K. D., Mathews, G., Obura, D. O., et al. (2020). Low oxygen levels caused by Noctiluca scintillans bloom kills corals in Gulf of Mannar, India. *Scientific Reports, 10*, 22133. https://doi.org/10.1038/s41598-020-79152-x

Ramaiah, N., Paul, J. T., Fernandes, V., Raveendran, T., Raveendran, O., Sundar, D., Revichandran, C., Shenoy, D. M., Mangesh, G., Kurian, S., Gerson, V. J., Shoji, D. T., Madhu, N. V., Kumar, S. S., Lokabharathi, P. A., & Shetye, S. R. (2005). The September 2004 stench off the southern Malabar coast- a consequence of holococcolithophore bloom. *Current Science, 88*(4), 551–554.

Ramanamurthy, V. D., & Seshadri, R. (1966). Phosphorous concentration during *Trichodesmium erythraeum* bloom in near shore waters of Portonovo. *Current Science, 4*, 100–101.

Ramamurthy, V. D. (1970). Antibacterial activity of the marine blue green alga *Trichodesmium erythraeum* in the gastro-intestinal contents of the seagull *Laurus brunicephalus*. *Marine Biology, 6*, 74–76. https://doi.org/10.1007/BF00352610

Ramamurthy, V. D., Selvakumar, R. A., & Bhargava, R. M. S. (1972). Studies on the blooms of *Trichodesmium erythraeum* (Ehr.) in the waters of the central west coast of India. *Current Science India, 41*, 803–805.

Ramamurthy, V. D. (1973). Infra red spectral analysis of antibacterial substance isolated from *Trichodesmium erythraeum* (Marine blue green alga). *Hydrobiologia, 41*(2), 247–250. https://doi.org/10.1007/BF00016449

Richardson, K. (1997). Harmful or exceptional phytoplankton blooms in the marine ecosystem. *Advances in Marine Biology, 31*, 301–385.

Robin, R. S., Kanuri, V. V., Muduli, P. R., Mishra, R. K., Jaikumar, M., Karthikeyan, P., Suresh Kumar, C., & Saravana Kumar, C. (2013). Dinoflagellate bloom of *Karenia mikimotoi* along the Southeast Arabian Sea, Bordering Western India. *Journal of Ecosystem, 2013*, Article ID 463720. https://doi.org/10.1155/2013/463720

Roy, R., Pratihary, A., Narvenkar, G., Mochemadkar, S., Gauns, M., & Naqvi, S. W. A. (2011). The relationship between volatile halocarbons and phytoplankton pigments during a Trichodesmium bloom in the coastal eastern Arabian Sea. *Estuarine, Coastal Shelf Science*, *95*(1), 110–118.

Sachithanandam, V., Mohan, P. M., Karthik, R., Elangovan, S. S., & Padmavathi, G. (2013). Climate changes influence the phytoplankton bloom (Prymnesiophyceae: *Phaeocystis* spp.) in North Andaman coastal region. *Indian Journal of Marine Sciences, 42*(1), 58–66.

Sahayak, S., Jyothibabu, R., Jayalakshmi, K. J., Habeebrehman, H., Sabu, P., Prabhakaran, M. P., Jasmine, P., Shaiju, P., Rejomon, G., Thresiamma, J., & Nair, K. K. C. (2005). Red tide of *Noctiluca miliaris* off south of Thiruvananthapuram subsequent to the 'stench event' at the southern Kerala coast. *Current Science, 89*(9), 1472–1473.

Sakthivel, M., & Harida, P. (1974). Synchronization in the occurrence of *Trichodesmium* bloom and swarming of *Creseis acicula* Rang (Pteropoda) and *Penilia avirostris* Dana (Cladocera) in the area off Cochin. *Mahasagar, 7*(1–2), 61–67.

Sanilkumar, M. G., Thomas, A. M., Vijayalakshmi, K. C., Mohamed, H. A. A., & Saramma, A. V. (2012). *Chattonella marina* bloom in the coastal sea off Mahe, Southwest India. *Current Science, 103*(6), 624–626.

Santhanam, R., Srinivasan, A., Ramadhas, V., & Devaraj, M. (1994). Impact of *Trichodesmium* bloom on the plankton and productivity in the Tuticorin Bay, southeast coast of India. *Indian Journal of Marine Sciences, 23*, 27–30.

Santhanam, R., & Srinivasan, A. (1996). Impact of dinoflagellate *Dinophysis caudata* bloom on the hydrography and fishery potentials of Tuticorin Bay, South India. In T. Yasumoto, Y. Oshima, & Y. Fukuyo (Eds.), *Harmful and toxic algal blooms* (pp. 41–44). IOC UNESCO.

Santhosh Kumar, C., Ashok Prabu, V., Sampathkumar, P., & Anantharaman, P. (2010). Occurrence of algal bloom *Microcystis aeruginosa* in the Vellar estuary, South-East coast of India. *Indian Journal of Marine Sciences, 5*, 52–55.

Sarangi, R. K., & Mohammed, G. (2011). Seasonal algal bloom and water quality around the coastal Kerala during south-west monsoon using in situ and satellite data. *Indian Journal of Marine Sciences, 40*(3), 356–369.

Sarangi, R. K., Prakash, C., & Nayak, S. R. (2004). Detection and monitoring of Trichodesmium bloom in the coastal waters of Sourashtra coast, India using IRS P4 OCM data. *Current Science, 86*, 1636–1841.

Sasikumar, N., Venugopalan, V. P., Azariah, J., & Nair, K. V. K. (1989). After effects of a dinoflagellate bloom on the hard bottom community in Kalpakkam coastal waters. *Mahasagar, 22*(4), 159–164.

Sathianandan, T. V. (2017). Marine fish production in India- present status. In S. Kuriakose, K. Mini, & T. Sathianandan (Eds.), *Summer School on advanced methods for fish stock assessment and fisheries management* (pp. 23–27). Central Marine Fisheries Research Institute.

Satpathy, K. K., & Nair, K. V. K. (1996). Occurrence of phytoplankton bloom and its effect on coastal water quality. *Indian Journal of Marine Sciences, 25*(2), 145–147.

Satpathy, K. K., Mohanty, A. K., Sahu, G., Prasad, M. V. R., Venkatesan, R., Natesan, U., & Rajan, M. (2007). On the occurrence of Trichodesmium erythraeum (Ehr.) bloom in the coastal waters of Kalpakkam east coast of India. *Indian Journal of Science and Technology*, *2*(1), 1–9.

Saxena, A. (2012). *Marine biodiversity in India: Status and issues* (pp. 127–134). International day for Biological Diversity. Available from http://www.upsbdb.org/pdf/Souvenir2012/ch-14.pdf

Segar, K., Karunasagar, I., & Karunasagar, I. (1989). Dinoflagellate toxins in shellfishes along the coast of Karnataka. In M. M. Joseph (Ed.), *The first Indian fisheries forum proceedings* (pp. 389–390). Asian Fisheries Society, Indian Branch.

Sellner, K. G. (1997). Physiology, ecology, and toxic properties of marine cyanobacteria blooms. *Limnology and Oceanography, 45*, 1089–1104.

Shaju, S. S., Akula, R. R., & Jabir, T. (2018). Characterization of light absorption coefficient of red *Noctiluca scintillans* bloom in the South Eastern Arabian Sea. *Oceanologia, 60*(3), 419–425. https://doi.org/10.1016/j.oceano.2017.12.002

Silas, G. S., Alagarswami, K., Narasimham, K. K., Appukuttan, K. K., & Muthiah, P. (1982). Country reports: India. In F. B. Davy & M. Graham (Eds.), *Bivalve culture in Asia and the Pacific. Proc. workshop* (pp. 34–43).

Singh, H. (2003). Marine protected areas in India. *Indian Journal of Marine Sciences, 32*(3), 226–233.

Smayda, T. J., & Reynolds, C. S. (2003). Strategies of marine dinoflagellate survival and some rules of assembly. *Journal of Sea Research, 49*, 95–106.

Stoecker, D. K., Hansen, P. J., Caron, D. A., & Mitra, A. (2017). Mixotrophy in the marine plankton. *Annual Review of Marine Science, 9*, 311–335. https://doi.org/10.1146/annurev-marine-010816-060617

Subrahmanyan, R. (1954). On the life-history and ecology of *Hornellia marina* gen. et sp. nov., (Chloromonadineae), causing green discoloration of the sea and mortality among marine organisms off the Malabar coast. *Indian Journal of Fisheries, 1–2*, 182–203.

Subrahmanyan, R. (1959). Studies on the phytoplankton of the west coast of India. *Proceedings of the Indian Academy of Sciences-Section B*. Springer India*, 50*(4), 189–252.

Subramanian, A., & Purushothaman, A. (1985). Mass mortality of fish and invertebrates associated with a bloom of *Hemidiscus hardmannianus* (Bacillariophyceae) in Parangipettai (southern India). *Limnology and Oceanography, 30*(4), 910–911. https://doi.org/10.4319/lo.1985.30.4.0910

Suleiman, M., Jeep, J., Rundi, C., & Chua, T. H. (2017). Case report: Paralytic Shellfish poisoning in Sabah, Malaysia. *The American Journal of Tropical Medicine and Hygiene, 97*(6), 1731–1736. https://doi.org/10.4269/ajtmh.17-0589

Tada, K., Plthakpol, S., & Montani, S. (2004). Seasonal variation in the abundance of *Noctiluca scintillans* in the Seto Inland Sea Japan. *Plankton Biology and Ecology, 51*(1), 7–14.

The Hindu. (2004). Stench from sea: children hospitalized. *The Hindu*, Kerala Edition, 17 Sept 2004.

The New Indian Express. (2004). Kerala Edition, 17 Sept 2004.

Thomas, L. C., Padmakumar, K. B., Smitha, B. R., Devi, C. R. A., Nandan, S. B., & Sanjeevan, V. N. (2013). Spatio-temporal variation of microphytoplankton in the upwelling system of the southeastern Arabian Sea during the summer monsoon. *Oceanologia, 55*(1), 185–204. https://doi.org/10.5697/oc.55-1.185

Thomas, L. C., Nandan, S. B., & Padmakumar, K. B. (2020a). Understanding the dietary relationship between extensive Noctiluca bloom outbreaks and Jellyfish swarms along the eastern Arabian Sea (West coast of India). *Indian Journal of Marine Sciences, 49*(08), 1389–1394.

Thomas, L. C., Sathish, T., Jeslin, I. J., Sreerag, A., Nandan, S. B., & Padmakumar, K. B. (2020b). Unusual mass shoreward movement of bivalve (Mollusca) *Donax scortum* Linnaeus along the coastal waters off Calicut-South Eastern Arabian Sea. *Indian Journal of Marine Sciences, 49*(01), 67–72.

Thomas, L. C., Nandan, S. B., & Padmakumar, K. B. (2021). First report on an unusual bloom of the potentially toxic epibenthic dinoflagellate *Prorocentrum rhathymum* from Bangaram Lagoon of the Lakshadweep archipelago: Arabian Sea. *Regional Studies in Marine Science, 41*, 101549. https://doi.org/10.1016/j.rsma.2020.101549

Tomas, C. R. (1997). *Identifying marine diatoms and dinoflagellates*. Academic Press.

Trainer, V. L., Hickey, B. M., & Bates, S. S. (2008). Toxic diatoms. In P. J. Walsh, S. L. Smith, L. E. Fleming, H. M. Solo-Gabriele, & W. H. Gerwick (Eds.), *Oceans and human health: Risks and remedies from the seas* (pp. 219–237). Elsevier Science Publishers.

Tubaro, A., Dell'Ovo, V., Sosa, S., & Florio, C. (2010). Yessotoxins: A toxicological overview. *Toxicon, 56*, 163–172.

Turkoglu, M. (2013). Red tides of the dinoflagellate *Noctiluca scintillans* associated with eutrophication in the Sea of Marmara (the Dardanelles, Turkey). *Oceanologia, 55*(3), 709–732. https://doi.org/10.5697/oc.55-3.709

Van de Waal, D. B., Verschoor, A. M., Verspagen, J. M. H., van Donk, E., & Huisman, J. (2010). Climate-driven changes in the ecological stoichiometry of aquatic ecosystems. *Frontiers in Ecology and the Environment, 8*, 45–152.

Venugopal, P., Haridas, P., Madhupratap, M., & Rao, T. S. S. (1979). Incidence of red water along South Kerala coast. *Indian Journal of Marine Sciences, 8*, 94–97.

Verlancar, X. N. (1978). Some observation on the Trichodesmium bloom along south-west coast of India. *Mahasagar-Bulletin of the National Institute of Oceanography, 11*(3–4), 221–224.

Vijayalakshmy, K. C., Abhijith, M., Megha, M. K., Hatha, A. A., & Saramma, A. V. (2018). Incidence of heterotrophic red *Noctiluca scintillans* bloom along Chavakkad, southwest coast of India. *Indian Journal of Marine Sciences, 47*(8), 1648–1651.

Villac, M., Doucette, G., & Kaczmarska, I. (2010). Toxic marine diatoms. In J. Smol & E. Stoermer (Eds.), *The Diatoms: Applications for the environmental and earth sciences* (pp. 540–551). Cambridge University Press. https://doi.org/10.1017/CBO9780511763175.031

Winkler, L. W. (1888). Die Bestimmung des im Wasser gelösten Sauerstoffes. *Berichte der Deutschen Chemischen Gesellschaft, 21*, 2843–2853.

Zhang, S., Liu, H., Guo, C., & Harrison, P. J. (2016). Differential feeding and growth of *Noctiluca scintillans* on monospecific and mixed diets. *Marine Ecology Progress Series, 549*, 27–40. https://doi.org/10.3354/meps11702

Chapter 14
Phytoplankton, Primary Productivity, and Fishery: Case Study from the Northern Indian Ocean

Nimit Kumar, S. Manickavasagam, M. Ponmani, V. R. Madhu, and B. Meenakumari

Abstract Phytoplankton are the base of the food web, and their efficiency to capture carbon in the organic form via the process of photosynthesis determines the rate of primary productivity. Similar to many other species in the higher trophic levels, fish stocks are inherently dependent on primary productivity. This could be in the form of larval survival that determines the success of recruitment or in the form of providing food for adult fishes that takes up long migration to the breeding ground. The dynamics of phytoplankton distribution itself is connected to the met-ocean processes, including teleconnection to the processes far in the Indian Ocean or even in the Pacific Ocean. In this chapter, these linkages are described by using the fish catch landings as well as satellite remote sensing data to provide a holistic view of how fish catch may vary because of the combination of factors, including anthropogenic and natural.

Keywords Primary productivity · Fishery · Trophic level · El Nino Southern Oscillation · Indian Ocean Dipole

N. Kumar (✉)
Indian National Centre for Ocean Information Services (MoES-INCOIS), Hyderabad, Telangana, India
e-mail: nimitkumar.j@incois.gov.in

S. Manickavasagam · M. Ponmani
TNJFU – Fisheries College and Research Institute, Thoothukudi, Tamil Nadu, India

V. R. Madhu
ICAR-Central Institute of Fisheries Technology, Kochi, Kerala, India

B. Meenakumari
ICAR-Central Institute of Fisheries Technology, Kochi, Kerala, India

Indian Council of Agriculture Research, Pusa, Delhi, India

National Biodiversity Authority, Chennai, Tamil Nadu, India

S. C. Tripathy, A. Singh (eds.), *Dynamics of Planktonic Primary Productivity in the Indian Ocean*, https://doi.org/10.1007/978-3-031-34467-1_14

1 Introduction

Upon evolution, humans have increasingly attempted to cater to their food security. Hunter or gatherer populations settled down with time, primarily along the shores of great rivers. These were the same rivers that became the first fishing grounds. Eventually, humans ventured into the sea, and so far, hunting in the form of capture fishery has been the prime mode of marine food resources. With the development of science and resultant conscience, the feeling of responsibility toward the planet has grown parallel. While the United Nations population projections indicate that not before the year 2050, the population of Asia may get stabilize, along with the fact that population explosion in Africa is almost a predictable future. Understanding ecology and its sustainable management is inevitably a vital tool for creating a world that prevails with a culture of cooperation and not of conflict. Marine resources are the answer to the limits of land availability and land-use conflicts. At the same time, due to overexploitation concerns (Pauly et al., 1998), precaution toward conservation requires more weightage than it did ever before. The greater concern is about the Indian Ocean, as the rim countries are underdeveloped or transient economies. The detailed study of the Indian Ocean is not older than a few decades when with the Indian Ocean International Expedition (IIOE), the National Institute of Oceanography (NIO) was established in India. In the scenario where the seas around us are relatively little understood, as a country that has harnessed space technology, it becomes our responsibility to explore it further.

Phytoplankton are single-celled algae in oceans whichhas its own chlorophyll and, thus, like trees on land, play as primary producers in the ocean food web, with each species having its own role in the ecosystem. Chlorophyll concentration and its variation form the basis of discontinuous productivity in the oceans. However, the mere presence of phytoplankton does not always translate to the fertility – to be precise, productivity – of the ocean. Marine phytoplankton faces two constraints for carrying out photosynthesis – light and nutrients. Light is available to a certain depth in the upper waters, which is called the euphotic zone. The euphotic depth is not a constant number as it depends on the clarity of the water and how deep light can penetrate the water column. Often, offshore waters have deeper euphotic depth. Within the euphotic zone, nutrient availability regulates the photosynthesis rates, and coastal waters tend to show relatively high productivity due to the constant mixing of shallow waters, whereas in the open ocean, upwelling zones and cold-core eddies tend to show high productivity. When phytoplankton grows in size and numbers due to nutrients introduced from other than the euphotic zone, it results in new production, whereas in regenerated production, the nutrients come from the degradation of existing organic matter in the euphotic zone. Productive areas provide food for fishes that feed on plankton (planktivorous), which in turn attract carnivore fishes. Productivity in the ocean thus becomes one of the major driving forces for fish to migrate in search of food. Identification of areas with higher chlorophyll content conducive to fish aggregation is one of the most important operational products of satellite oceanography.

2 Plankton and Primary Production Linkages to Fishery

The majority of fish have planktotrophic larvae, and their existence indicates that the adult species that make up the fishery are present as well. They also serve as indicator organisms, like flat fish, which have lengthy larval stages. Nair (1951) and Nair and Subrahmanyan (1955) found a correlation between fluctuations in the abundance of oil sardines and the appearance of a diatom bloom of the species *Fragilaria oceanica* along the Kerala coast. In 1970, Selvakumar discovered a relationship between mackerel fishing and cladocerans (*Evadne and Penilia*). Pteropods have a crucial role to perform as indicators and food for tuna and herring, according to Sakthivel (1972). The presence of *Sagitta decipiens* (arrow worm) and anchovy larvae in the Indian Ocean was documented by Alvarino (1981).

The high larval mortality may be attributed to the enormous number of fish larvae consumed by predators. They grow more quickly and vice versa depending on how much plankton the young fish consume. For juveniles, food is a matter of growth rate rather than survival, and for larvae, feeding is a function of plankton availability. According to Parsons and LeBrasseur (1973), the availability of the right type of food, as well as the absolute abundance of prey items, is the most crucial factor in a fish's ability to grow since the food's composition affects how efficiently it can grow. Leong and O'Connell (1969) observed a change in the rate of feeding by anchovies switching from filter to raptorial prey capturing. The potential production of fish in an area (zone), including both early-stage carnivores (predators) and zooplankton eaters, can be approximated by knowing the primary production and the quantitative transfer across trophic levels.

The primary productivity in the world's oceans is estimated by Platt and Rao (1975) to be roughly 31×10^9 tonnes of carbon annually. Koblentz-Mishke (1970) reported deprived primary productivity over wide oceanic regions and greater productivity, i.e., two to three times more, in close vicinity to land masses. According to Gulland (1970), there is a difference of 4000 times between the annual fish catch and the total annual primary production in the oceans, which is equal to about 20×10^9 tons of carbon synthesized. The annual fish catch is equal to 5×10^8 tons of carbon, or 100×10^6 tons per year of fish. This is due to the fact that the fish being caught have undergone around a 90% decline at various trophic levels and are several trophic levels removed from the main primary production.

Balachandran and Peter (1987) estimated the ecological efficiency to be at 10%. The production of fish at the fifth trophic level increased by an order of magnitude, according to Balachandran and Peter (1987), who took into account ecological efficiency of 10–20%. Recent research indicates that fish production can vary significantly, most likely as a result of changes in the efficiency with which primary production is turned into fish rather than changes in total primary production.

Generally, the first trophic level includes autotrophs and saprophytes; herbivorous animals at the second trophic level include polychaetes, certain benthic mollusk larvae, copepodite stages, nauplii of copepods, and *Oikopleura* sp.; at the third level, omnivorous organisms include *Acartia* sp., *Oithona* sp., and *Centropages* sp., which

are later stages of copepods; at the fourth level, there are primary predators like adult *Oithona* sp., secondary carnivores like Chaetognaths, and a tertiary carnivore called *Pleurobrachia* sp. that consumes all other zooplanktons. It's intriguing to observe how, as they mature, some species move from one level to another.

The number of trophic levels in three communities, such as the oceanic, continental shelf, and upwelled, was examined by Ryther (1969). He proposed that oceanic organisms had lengthy food chains, with low ecological efficiencies determined by the three or four stages of carnivorous feeding, as a result of a continual flow of biomass from phytoplankton to fish. It took five trophic levels to produce fish in the oceanic region, which typically has low annual primary production average values of 50 g C/m^2/year. The second food chain, which is referred to as the coastal or continental shelf and occurs in regions with total annual primary production of roughly 100 g C/m^2/year, is made up of three trophic levels, whether this is done through the benthic or pelagic community. With a primary production of 300 g C/m^2/year, the third chain of upwelling areas represents one and a half trophic levels, with adult anchovies eating directly on phytoplankton and whales feeding on euphausiids.

Ecological efficiency at each trophic level in the aforementioned three communities were thought to be highest when predominantly controlled by phytoplankton/herbivore relationships and lowest when communities of secondary and tertiary carnivores were present. As a result, oceanic, coastal, and upwelling food chains were given respective efficiency ratings of 10%, 15%, and 20%. Ryther (1969) calculated that the upwelling, shelf, and oceanic areas might produce fish at rates of 36,000, 340, and 0.5 mg C/m^2/h, respectively.

A shift in feeding behavior, as with anchovies, which mostly eat phytoplankton but occasionally eat zooplankton, can decrease the overall effectiveness of energy transfer from phytoplankton to zooplankton feeders. Likewise, plaice larvae eating on some large diatoms as *Biddulphia* sp. and *Coscinodiscus* sp., in the earlier nurturing stage, can be seen sharply changing to a zooplankton diet of *Oikopleura* sp. As is the case when herring feed on giant *Calanus* sp. instead of small *Temora* sp. and *Pseudocalanus* sp., the efficiency may change as a result of qualitative changes in the zooplankton that are ingested (Steele, 1965). Despite the fact that there does not appear to be a connection between the total food supply and the larval fish, food supplies, maybe of a specific type at a specific moment, such as when the yolk sac resources are depleted, may still be important.

The ability of a system to retain itself after a minor external perturbation, or stability, is a crucial characteristic of the food web (Hurd et al., 1971). According to MacArthur's (1955) theory, the main factor in creating community stability is the emergence of numerous species (i.e., a high diversity). But because the intricate food system consumes more energy, productivity for unit biomass will be low. Low productivity is a result of the high diversity and stability of tropical plankton groups and the food chain. In contrast, the plankton population in temperate waters exhibits poor stability and diversity, which results in high productivity from one or two species. The distribution of prey was patchy; there was an imposition of a limit on

the predator; it periodically migrated away from its food source; and there was an application of a threshold concentration below which the prey is not consumed by the predator, and these factors all contributed to stabilization.

Examples include the zooplankton's diel migration toward the euphotic zone (McLaren, 1963; Balachandran & Kurian, 1980), euphausiids' capacity to transition from carnivores to herbivores (Parsons & LeBrasseur, 1973), the presence of a threshold prey concentration in phytoplankton/zooplankton associations (Parsons et al., 1967), euphausiids' capacity to transition from carnivores to herbivores (Parsons & LeBrasseur, 1973), the presence of a threshold prey concentration in phytoplankton/zooplankton associations (Parsons et al., 1967), and the ability of zooplankton to convert from carnivores to herbivores; on the other side, time delays can introduce instability into a plankton community (Balachandran & Peter, 1987), as is the case with the barnacle population depending on the timing of the *Skeletonoma* sp. bloom for the release of its larvae (Barnes, 1956).

An aquatic ecosystem would be more affected by a perturbation given to the top of the food chain (such as the elimination of predators) than one applied to the bottom of the food chain, which would result in an increase in biomass fish production. In the marine environment, it is challenging to establish density-dependent correlations between the growth of planktivorous fish and plankton growth rates because the exchange of water may remove organisms from one region to another. Typically, there is a correlation between plankton richness and fish abundance. When a huge number of fish larvae compete for a small amount of food, the dispensatory mechanism can be observed, and the surviving may grow significantly smaller than if fewer larvae were initially present. Gulland (1962) observed a similar, significant slowing of the growth rate of haddock larvae. The scale structure of an aquatic food web is frequently impacted by planktivorous fish predation on the plankton community (Brooks & Dodson, 1965). Smaller zooplankton and phytoplankters grow more rapidly when there are more planktivorous fish present, but larger zooplankton thrives when there are fewer fish present.

3 Case Study: Northeast Arabian Sea

As physicochemical processes are closely interlinked to the biology of the oceans, it is understood that weather and climate mark their impact on the ecology. While air-sea interaction and numerical modeling of the atmosphere and up to a certain extent of the general circulation of oceans is achieved, the next big challenges involve first understanding their influence on ecology and later coupling them with ecological models which can enable us to predict the future course of ecosystem's status. Physical processes in the ocean, such as upper-layer mixing, variation in thermocline, upwelling, and eddy formation, are known to affect regional biogeochemistry. These mainly lead to changes in oxygen levels, nutrient entrainment in the mixed layer, and its advection. Such variations control the productivity of the

area for the time being. It will be impractical if one has to sample vast areas that our oceans have. On the other hand, geo-referenced fish catch data can be an effective tool akin to biological sampling, as the presence and abundance of various species provide a proxy for these processes.

Researchers have often been wondering if a productivity model can help us understand marine resource migration in better ways. A productivity model usually includes the estimation of upwelling index parameters with the help of satellite-born SST and Chlorophyll data. It, in turn, calculates the primary production at a given place, which by theory should support the fishery, and there have been few studies on the same lines. Researchers have found limited success in correlating Vertically Generalized Production Model (VGPM) with fish catch data (Friedland et al., 2012), and such study carried out in geographic vicinity to our study area was at Eastern Great Australian Bight (van Ruth et al., 2010). Numerous studies have attempted to apply GIS tools to understand the fishery in various regions. While most of these studies address the mariculture site suitability indexing, many others focus on a wide variety of issues related to marine capture fishery. Be it addressing artisanal croaker fishery in Uruguay (Horta & Defeo, 2012) or about the removal of lobster trap marine debris to prevent ghost fishing (Martens & Huntington, 2012), or understanding the cephalopod fishery in the northeast Atlantic Ocean (Pierce et al., 2001), GIS has helped researchers in many ways.

Though some studies indicate that the recent relationship between Indian Summer Monsoon (ISM) and El Niño-Southern Oscillation (ENSO) may have weakened (Kumar et al., 1999), there is little doubt about ENSO and IOD (Indian Ocean Dipole) events having linkage with the southwest monsoon (Ashok et al., 2001). ENSO episodes are not only known to influence the weather of the Indian subcontinent but also that of the Arabian Peninsula (Charabi, 2009). It is to be noted that a signal of upwelling in the same region results in bloom that travels further northward in the Arabian Sea and, in turn, feeds to the ecology of the northern-northeastern Arabian Sea, where ultimately it crashes. Therefore, it is important to study these linkages on a bigger scale and to understand the forces that drive ecosystems in our region.

Gujarat is a coastal state of India with a substantial (~40%) contribution to marine fishery production and export of the country. Fish-landing center-wise data collected from the state fishery department have shown that Veraval alone contributes to 20% of marine fish production in Gujarat. Thus, it may be concluded that Veraval alone contributes to about 8% of the nation's marine fish production. The fishing fleet of Veraval is known to explore far seas during their typical multiday voyages. It was known during the data collection phase that collectively this fishing community explores vast areas ranging from off Jakhau (Kachchh) (even till nearby India-Pakistan IBL toward the edge of Indian EEZ) to Bombay High in the southeast on the other hand. It is also common knowledge that fishermen often found these extreme ends in their most frequently visited areas for good fishing. However, due to the unavailability of any prior study, it was unknown whether any pattern exists in fishing behavior.

The first finding of this study was to support the common knowledge that fishermen from this region cover the huge diagonal stretch from off Jakhau in the northwest and off Bombay High in the southeast. Another major finding was understanding the pattern that spans the entire fishing season. It was observed that when fishing season opens post-monsoon, most of the fishing efforts are concentrated toward Bombay High. However, as the season progress, the cluster of majority fishing efforts starts moving toward the northwest. During winter times, it approaches the grounds off Veraval and Mangrol. Toward the end of wintertime, the fishing efforts tend further northwest and, by springtime, settle off Okha and Jakhau, where these dynamics end during pre-monsoon times when seas start getting rougher with high winds and waves. It was also learned from the GIS that fishing efforts were more focused between bathymetry of 50–100 m and between the distance range of 50–100 km from the coastline, except Bombay High, which falls beyond 100 km from most of the shoreline.

The preference of Bombay High in post-monsoon times can be understood considering the presence of major rivers of South Gujarat, bringing a log of nutrients to the region. The same region also experiences the mixing of the water column as the met-ocean signature of leaving the Indian Summer Monsoon. The retreat of the efforts closer to Veraval and Mangrol also accompanies a smaller number of efforts and reflects the winter "lull" in the fishing that is common knowledge. The pull to the fishing efforts toward the northwest is believed to serve the purpose of benefiting from spring bloom-assisted flourishing ecosystem, however, without knowing the science behind it but routinely following the collective experiences of generations. In fact, the spring bloom usually starts from the western side of the northern Arabian Sea (off Somalia or Oman) and follows the eastward currents to ultimately crash off Gujarat in the month of March. Hence, it can be hypothesized that the age-old practice of reaching for harvesting from spring bloom could have habituated fisherfolk to move northwest over the season (Fig. 14.1).

Teleconnections of El Niño-Southern Oscillation (ENSO) have been observed over weather patterns around the globe. Its atmospheric, as well as oceanographic precursors, are being followed very well nowadays. However, how the same alter the ecosystem during these oscillating changes, very little is what we know when it comes to the Indian Ocean. This study attempts to explain a wobble in the fish catch with the background of ENSO. Similarly to Southern Oscillation in the central Pacific Ocean, the Indian Ocean is also believed to have its own counterbalance system. Lesser known earlier, studies on this system – called IOD, i.e., Indian Ocean Dipole – have only started in the late 1990s. During the period of this study, a positive IOD event occurred in the year 2006, and La Niña conditions were in the following year (2007). While positive IOD affected the fish catch in the Spring of 2007, La Niña conditions prevailed during 2007, negatively affecting the post-monsoon fish catch heavily in that year as well as the spring fish catch of the subsequent year.

Fish catch data was collected in kilograms. The data was collected on a daily basis and averaged for a month. This was done for four consecutive fishing seasons from 2004 (post-monsoon) to 2008 (pre-monsoon). The contribution of major

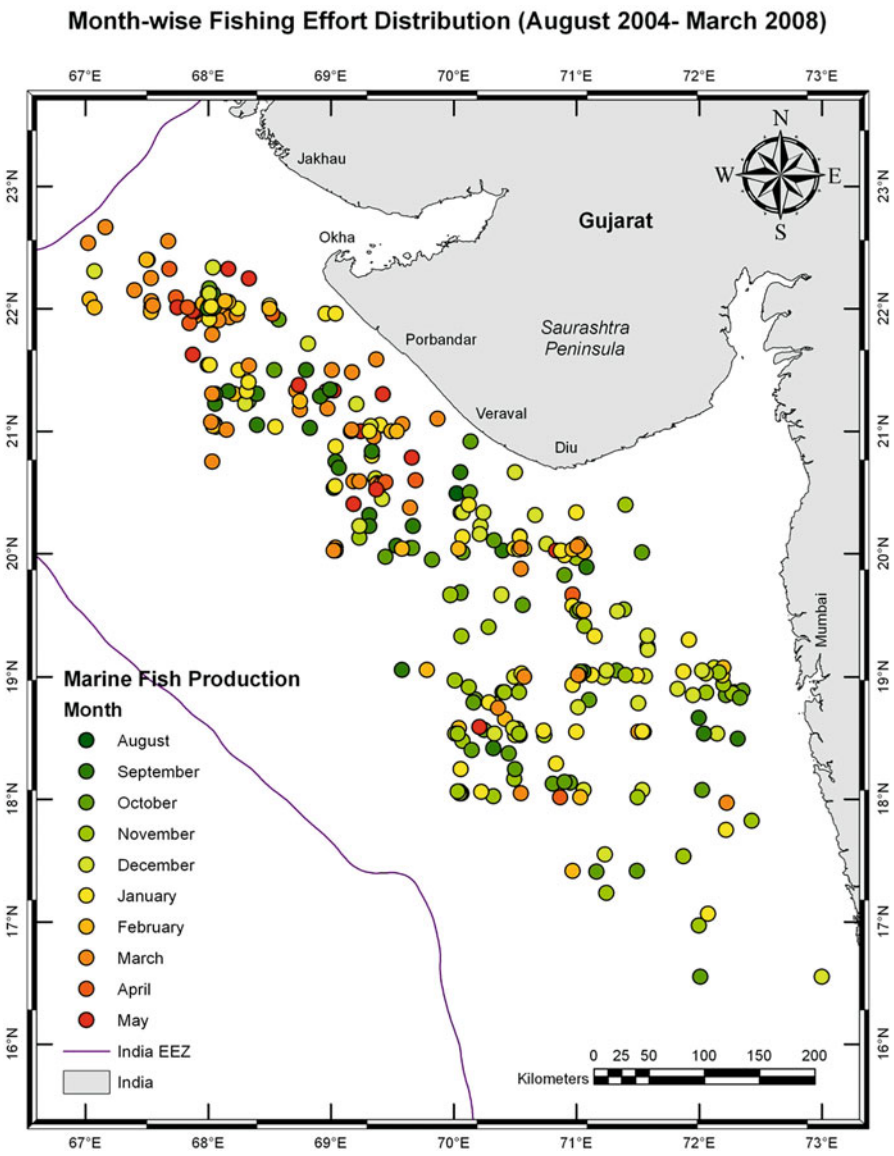

Fig. 14.1 Monthwise dynamics of fishing efforts

commercially important fishes was analyzed. A significant positive correlation between the catch of ribbonfishes (*Trichiurus lepturus* & *Lepturacanthus savala*) and breams (*Nemipterus japonicus*) and ONI (Oceanic Nino Index) values (inverse correlation with SOI) was observed. Both had shown a drastic decline of catch during La Niña of 2007–2008, where ONI values were at their lowest. The first conclusion of this study was that ONI has a significant correlation with the monthly trend of fish catch from the northeast Arabian Sea (Fig. 14.2).

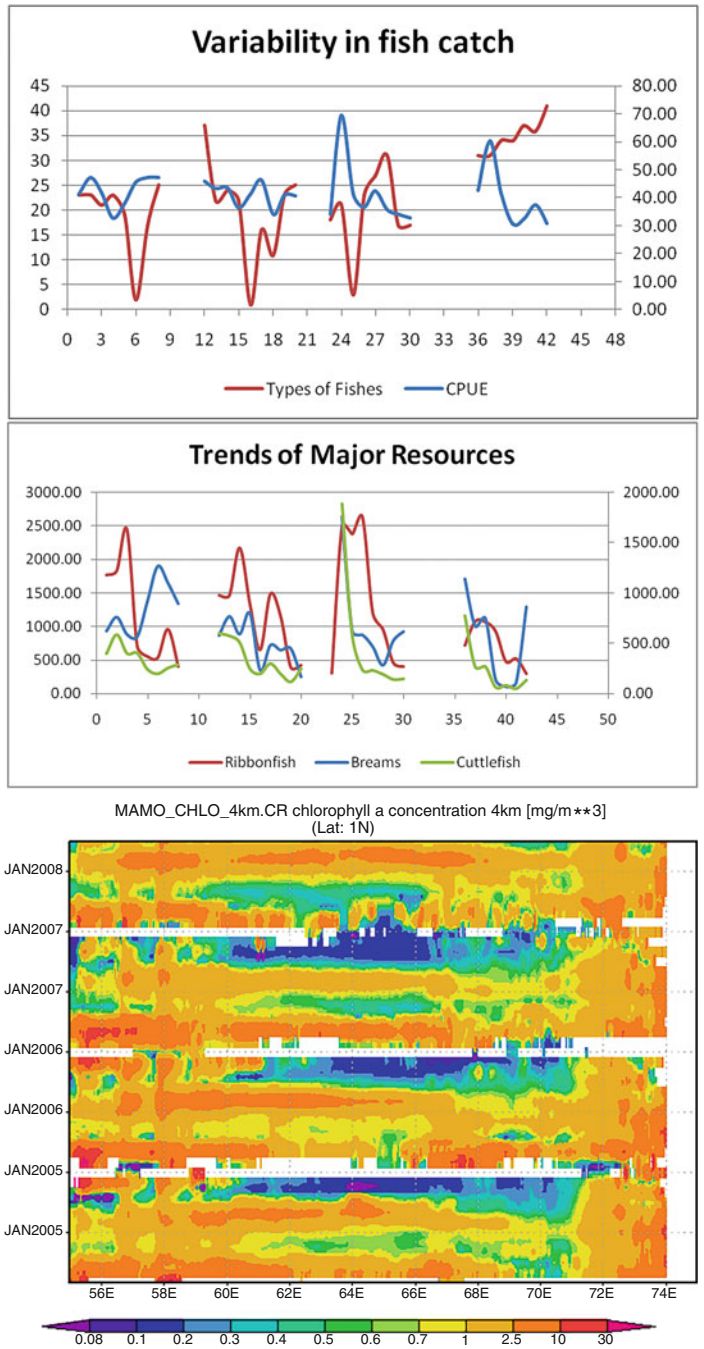

Fig. 14.2 Upper panel, fish catch variability; middle panel, average monthly catch/boat for major resources; and below panel, Hovmöller plot of corresponding chlorophyll-a concentration derived through MODIS-Aqua satellite's ocean color sensor for the northeast Arabian Sea during the years 2004–2008. Note that the fourth fishing season of 2007–2008 is significantly different

4 Future Research Direction

The science of resolving marine primary productivity from space is poised to witness a sea change during the UN Ocean Decade, chiefly with the planned launch of operational hyperspectral mission such as PACE (Plankton, Aerosol, Cloud, ocean Ecosystem) by NASA. Such data will enable the researchers to begin a new era in the OC sciences due to its potential of developing a plethora of applications. This includes but does not limit to better resolving phytoplankton functional types, fishery resource management, and ecosystem health monitoring. The latter is more important especially with the posing challenges such as ballast discharge and invasive species, jellyfish swarming, and plastics in the oceans (Pattiaratchi et al., 2022). Simultaneously, the temporal limitations seem to be negated through various approaches such as using the Day-Night Band (DNB) data or ocean color data from the geostationary orbit (e.g., GOCI, or Geostationary Ocean Color Imager). When ocean color science follows the footsteps of other satellite types, we may also have a "swarm" of nano-satellites or cubesats – further improving temporal and, up to some extent, spatial coverage as well (Nimit et al., 2016). Placement of HICO (Hyperspectral Imager for Coastal Oceans) on the International Space Station (ISS) reminds us that the ocean color science may not limit to satellite remote sensing in the coming decades (Nimit, 2021). All of these are in one or the other way intertwined with the fishery as an important blue economy activity. This will also make the regional primary productivity models an essential requirement for the data-deficient areas such as the northern Indian Ocean.

5 Conclusion

The key finding of this study on the function of plankton in the formation of fisheries is that it provides insight into a fundamental question in biological oceanography: Why are some fish species superabundant in particular regions. We can estimate the overall organic production using plankton biomass, which also aids in identifying possible fishing grounds. Plankton biomass serves as an indicator of the oceans' fertility. Changes in the efficiency with which primary production is transformed into fish, rather than changes in the overall primary production, might affect fish production. Direct inferences about the size of the spawning stock can be made from the survey data on eggs and larvae. The primary food source is plankton, and the variation in its composition has an impact on the eating habits of fish. The influence of plankton on fish spawning was revealed by plankton assemblages. When the right conditions, including a sufficient food supply and a drop in prey density, are present, a fishery can survive. The ability of the resultant year class to survive the larval stage without suffering a disproportionately high death rate is one of the key determinants of the size of the year class. Fisheries and class strength in the following year are

affected by zooplankton predation on fish larvae. The percentage of starved larvae can serve as an indicator for the overall strength of a year class. Fisheries can be detected by specific planktonic species present. The amount of variability in larval and juvenile fishes' survival is influenced by an extensive range of variables.

References

Alvarino, A. (1981). The relation between the distribution of zooplankton predators and anchovy larvae. *Rapports et Proces-verbaux des Réunions. Conseil International pour l'Éxploration de la Mer, 178*, 197–199.

Ashok, K., Guan, Z., & Yamagata, T. (2001). Impact of the Indian Ocean dipole on the relationship between the Indian monsoon rainfall and ENSO. *Geophysical Research Letters, 28*(23), 4499–4502.

Balachandran, T., & Kurian, C. V. (1980). *Studies on meroplankton* [Doctoral dissertation, Cochin University of Science and Technology].

Balachandran, T., & Peter, K. J. (1987). The role of plankton research in fisheries development. In *CMFRI bulletin: National symposium on research and development in marine fisheries sessions I & II 1987* (Vol. 44, pp. 163–173). CMFRI.

Barnes, H. (1956). Balanus balanoides (L.) in the Firth of Clyde: The development and annual variation of the larval population, and the causative factors. *The Journal of Animal Ecology, 25*, 72–84.

Brooks, J. L., & Dodson, S. I. (1965). Predation, body size, and composition of plankton: The effect of a marine planktivore on lake plankton illustrates theory of size, competition, and predation. *Science, 150*(3692), 28–35.

Charabi, Y. (2009). Arabian summer monsoon variability: Teleconexion to ENSO and IOD. *Atmospheric Research, 91*(1), 105–117., ISSN 0169-8095. https://doi.org/10.1016/j.atmosres.2008.07.006

Friedland, K. D., Stock, C., Drinkwater, K. F., Link, J. S., Leaf, R. T., Shank, B. V., Rose, J. M., Pilskaln, C. H., & Fogarty, M. J. (2012). Pathways between primary production and fisheries yields of large marine ecosystems. *PLoS One, 7*(1), e28945.

Gulland, J. A. (1962). The application of mathematical models to fish populations. In E. D. Le Cren & N. W. Holdgate (Eds.), *The exploitation of natural animal populations*. Blackwell Scientific Publications.

Gulland, J. A. (1970). Food chain studies and some problems in world fisheries. In J. H. Steele (Ed.), *Marine food chains* (p. 296). Oliver and Boyd.

Horta, S., & Defeo, O. (2012). The spatial dynamics of the whitemouth croaker artisanal fishery in Uruguay and interdependencies with the industrial fleet. *Fisheries Research, 125*, 121–128.

Hurd, L. E., Mellinger, M. V., Wolf, L. L., & McNaughton, S. J. (1971). Stability and diversity at three trophic levels in terrestrial successional ecosystems. *Science, 173*(4002), 1134–1136.

Koblentz-Mishke, O. J. (1970). Plankton primary production of the world ocean. In W. S. Wooster (Ed.), *Scientific exploration of the South Pacific* (pp. 183–193). National Academy of Sciences.

Kumar, K. K., Rajagopalan, B., & Cane, M. A. (1999). On the weakening relationship between the Indian monsoon and ENSO. *Science, 284*(5423), 2156–2159.

Leong, R. J., & O'Connell, C. P. (1969). A laboratory study of particulate and filter feeding of the northern anchovy (Engraulis mordax). *Journal of the Fisheries Research Board of Canada, 26*(3), 557–582.

MacArthur, R. (1955). Fluctuations of animal populations and a measure of community stability. *Ecology, 36*(3), 533–536.

Martens, J., & Huntington, B. E. (2012). Creating a GIS-based model of marine debris "hot spots" to improve efficiency of a lobster trap debris removal program. *Marine Pollution Bulletin, 64*(5), 949–955.

McLaren, I. A. (1963). Effects of temperature on growth of zooplankton, and the adaptive value of vertical migration. *Journal of the Fisheries Research Board of Canada, 20*(3), 685–727.

Nair, R. V. (1951). Studies on the life-history, bionomics and fishery of the white sardine, Kowala goval (Cuv.). *Proceedings of Indo-Pacific Fisheries Council, 2*, 1–16.

Nair, R. V., & Subrahmanyan, R. (1955). The diatom, Fragilaria oceanica Cleve, an indicator of abundance of the Indian oil sardine, Sardinella longiceps Cuv. and Val. *Current Science, 24*(2), 41–42.

Nimit, K. (2021). Ideas and perspectives: Ushering the Indian Ocean into the UN Decade of Ocean Science for Sustainable Development (UNDOSSD) through marine ecosystem research and operational services–an early career's take. *Biogeosciences, 18*(12), 3631–3635.

Nimit, K., Lotlikar, A., & Srinivasa Kumar, T. (2016). Validation of MERIS sensor's CoastColour algorithm for waters off the west coast of India. *International Journal of Remote Sensing, 37*(9), 2066–2076.

Parsons, T. R., et al. (1967). Some observations on the dependence of zooplankton grazing on cell size and concentration of phytoplankton blooms. *Journal of the Oceanographic Society of Japan, 23*, 10–17.

Parsons, T. R., & LeBrasseur, R. J. (1973). The availability of food to different trophic levels in the marine food chain. In J. H. Steele (Ed.), *Marine food chains*. Oliver and Boyd.

Pattiaratchi, C., van der Mheen, M., Schlundt, C., Narayanaswamy, B. E., Sura, A., Hajbane, S., White, R., Kumar, N., Fernandes, M., & Wijeratne, S. (2022). Plastics in the Indian Ocean–sources, transport, distribution, and impacts. *Ocean Science, 18*(1), 1–28.

Pauly, D., Christensen, V., Dalsgaard, J., Froese, R., & Torres, F., Jr. (1998). Fishing down marine food webs. *Science, 279*(5352), 860–863.

Pierce, G. J., Wang, J., Zheng, X., Bellido, J. M., Boyle, P. R., Denis, V., & Robin, J. P. (2001). A cephalopod fishery GIS for the Northeast Atlantic: Development and application. *International Journal of Geographical Information Science, 15*(8), 763–784.

Platt, T., & Rao, D. S. (1975). 11. Primary production of marine microphytes. In J. P. Cooper (Ed.), *Photosynthesis and productivity in different environments* (p. 249). Cambridge University Press.

Ryther, J. H. (1969). Photosynthesis and fish production in the sea: The production of organic matter and its conversion to higher forms of life vary throughout the world ocean. *Science, 166*(3901), 72–76.

Sakthivel, M. (1972). *Studies on Euthecosomata of the Indian ocean* [Doctoral dissertation, Ph.D. Thesis, Cochin University, India].

Selvakumar, R. A. (1970). Cladoceran swarm in relation to mackerel fishery along the west coast of India. *Curr Sci, 39*, 481–482.

Steele, J. H. (1965). Some problems in the study of marine resources. *Special Publications International Commission for North-West Atlantic Fisheries, 6*, 463–476.

van Ruth, P. D., Ganf, G. G., & Ward, T. M. (2010). Hot-spots of primary productivity: An alternative interpretation to conventional upwelling models. *Estuarine, Coastal and Shelf Science, 90*(3), 142–158.

Correction to: Past Trends and Future Projections of Marine Primary Productivity in the Tropical Indian Ocean

Aditi Modi and Mathew Koll Roxy

Correction to:
Chapter 9 in: S. C. Tripathy, A. Singh (eds.), ***Dynamics of Planktonic Primary Productivity in the Indian Ocean,***
https://doi.org/10.1007/978-3-031-34467-1_9

The original version of Chapter 9 "Past Trends and Future Projections of Marine Primary Productivity in the Tropical Indian Ocean" was inadvertently published with incorrect co-author name. The co-author name has now been updated from "Roxy Mathew Koll" to "Mathew Koll Roxy."

The updated original version of this chapter can be found at
https://doi.org/10.1007/978-3-031-34467-1_9

S. C. Tripathy, A. Singh (eds.), *Dynamics of Planktonic Primary Productivity in the Indian Ocean*, https://doi.org/10.1007/978-3-031-34467-1_15

Index

S. C. Tripathy, A. Singh (eds.), *Dynamics of Planktonic Primary Productivity in the Indian Ocean*, https://doi.org/10.1007/978-3-031-34467-1